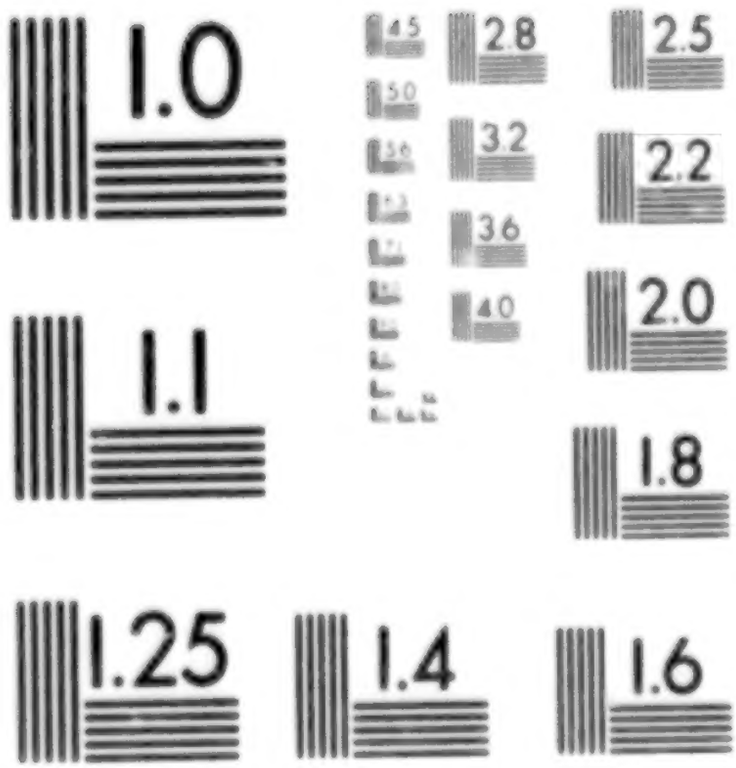

MICROCOPY RESOLUTION TEST CHART
NATIONAL BUREAU OF STANDARDS
STANDARD REFERENCE MATERIAL 1010a
(ANSI and ISO TEST CHART No. 2)

NASA Conference Publication 3077

First International Conference on Laboratory Research for Planetary Atmospheres

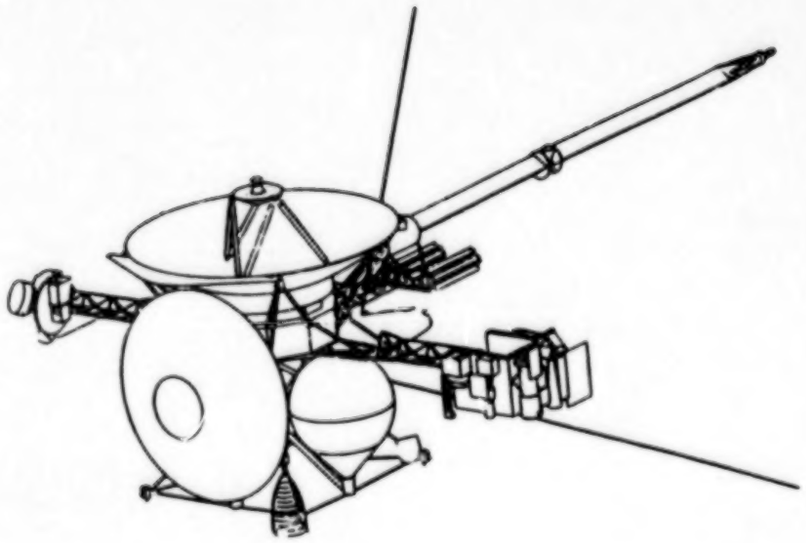

Proceedings of a conference held at
Bowie State University
Bowie, Maryland
October 25–27, 1989

NASA

(NASA-CP-3077) FIRST INTERNATIONAL CONFERENCE ON LABORATORY RESEARCH FOR PLANETARY ATMOSPHERES (NASA) 481 pCSCL 03B

N90-257--
--THRU--
N90-2578
Unclas
H1/91 0269072

NASA Conference Publication 3077

First International Conference on Laboratory Research for Planetary Atmospheres

Edited by
Kenneth Fox
University of Tennessee
Knoxville, Tennessee

John E. Allen, Jr.
and Louis J. Stief
NASA Goddard Space Flight Center
Greenbelt, Maryland

Diana T. Quillen
Bowie State University
Bowie, Maryland

Proceedings of a conference held at
Bowie State University
Bowie, Maryland
October 25–27, 1989

NASA
National Aeronautics and
Space Administration
Office of Management
Scientific and Technical
Information Division
1990

PHOTOGRAPH KEY

1. Allen, Jr., J.E.
2. Fegley, B.
3. Duncan, M.A.
4. Hougen, J.T.
5. Wagener, R.
6. Caldwell, J.J.
7. Judge, D.L.
8. Halthore, R.N.
9. Masterson, C.M.
10. Morgan, T.
11. Nesbitt, F.L.
12. Lovas, F.J.
13. Rice, J.K.
14. Green, J.
15. Bjoraker, G.
16. Steinfeld, J.I.
17. Giver, L.P.
18. Johnsen, R.
19. Steffes, P.G.
20. Ruhl. E
21. Halpern, J.B.
22. Stief, L.J.
23. Weber, A.
24. Lafferty, W.J.
25. Mickelson, M.
26. Barts, S.A.
27. Glaser, F.
28. Trajmar, S.
29. Blass, W.E.
30. Allen, M.
31. Yung, Y.L.
32. Moralejo, C.
33. O'Brien, J.J.
34. Sack, N.J.
35. Lutz, B.L.
36. Menchan, D.
37. Fox, K.
38. Wu, Y.C.R.
39. Frye, J.
40. Payne, W.A.
41. Pickett, H.M.
42. Johnson III, R.D.
43. Fraser, G.T.
44. Spilker, T.R.
45. Suarez, C.B.
46. Chackerian, Jr., C.
47. Guilford, C.A.
48. Bergstralh, J.
49. Arakawa, E.T.
50. Khare, B.N.
51. Urdahl, R.S.
52. Nava, D.F.
53. Cody, R.J.
54. Quillen, D.T.
55. Moore, M.H.
56. Kleiner, I.
57. Yanamandra-Fisher, P.
58. Suenram, R.D.
59. Parent, D.
60. Fahr, A.
61. Babaki, M.
62. Leone, S.R.

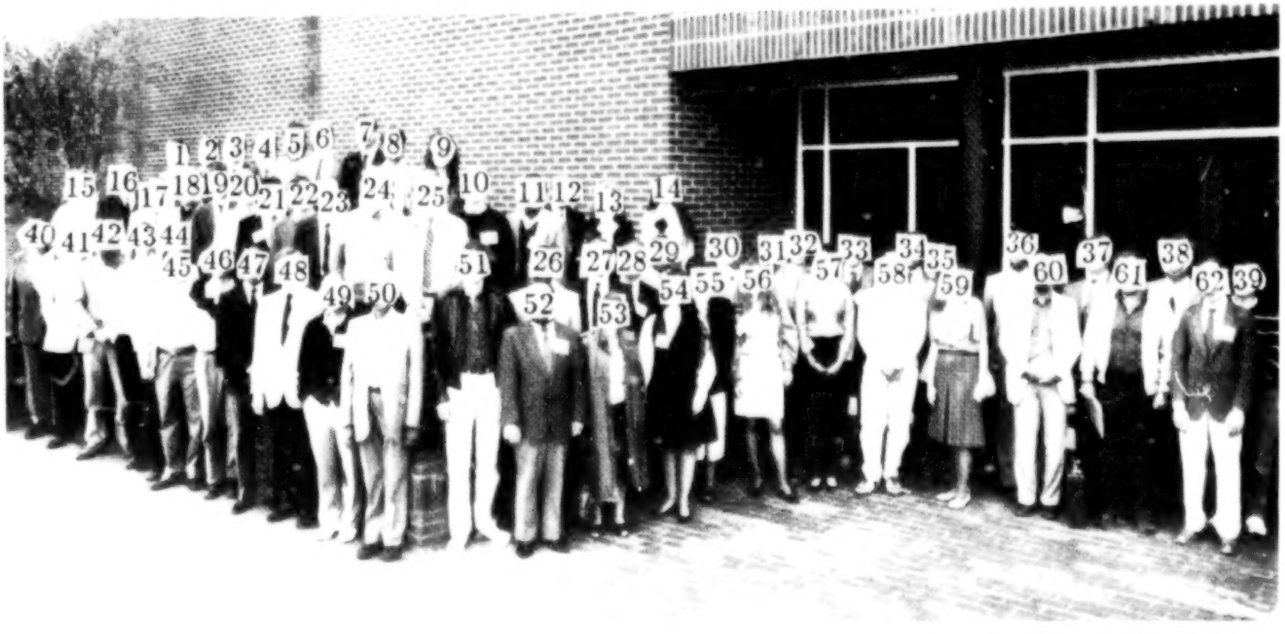

ORIGINAL PAGE
BLACK AND WHITE PHOTOGRAPH

ORIGINAL PAGE
BLACK AND WHITE PHOTOGRAPH

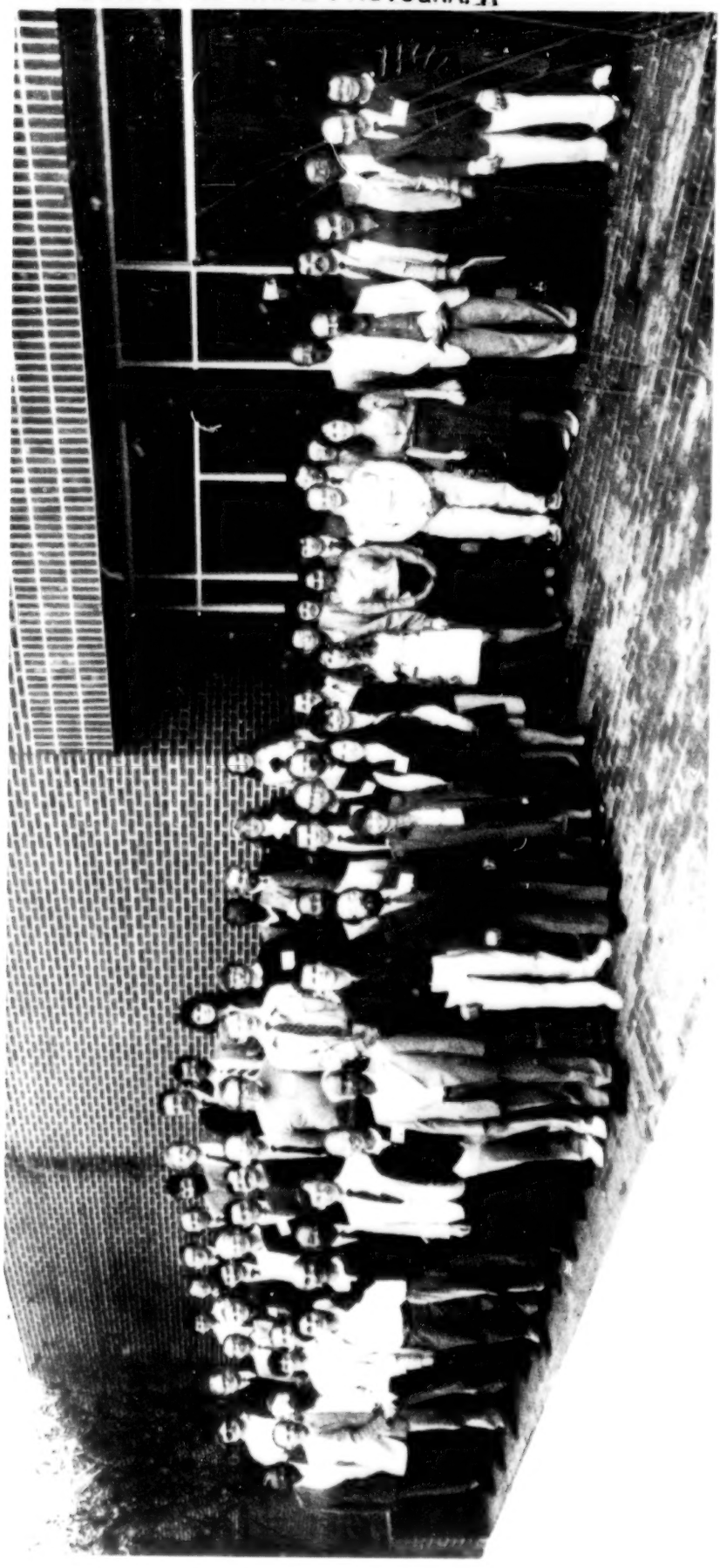

ORIGINAL PAGE
BLACK AND WHITE PHOTOGRAPH

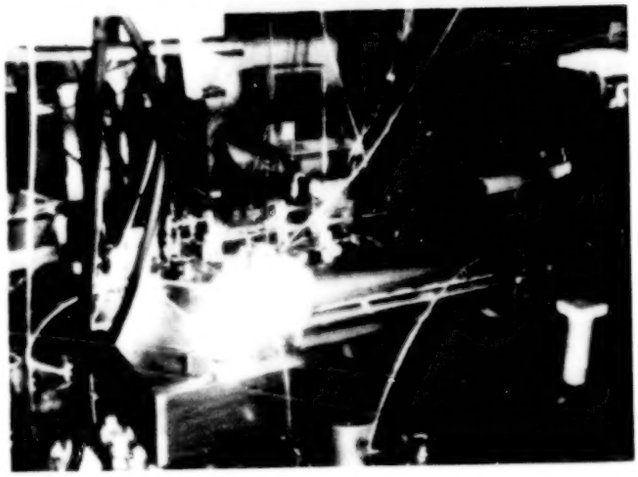

LABORATORY RESEARCH FOR PLANETARY ATMOSPHERES

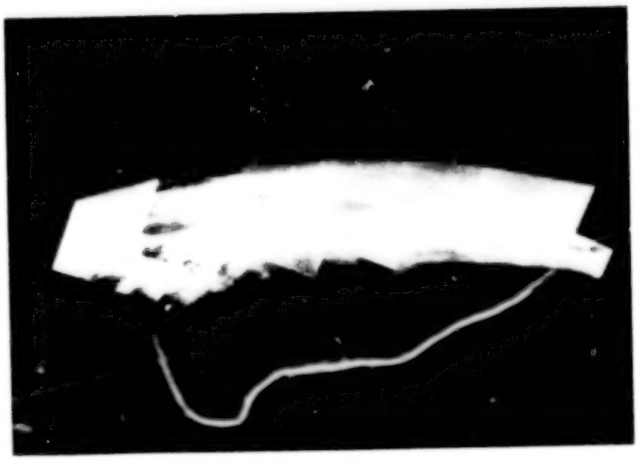

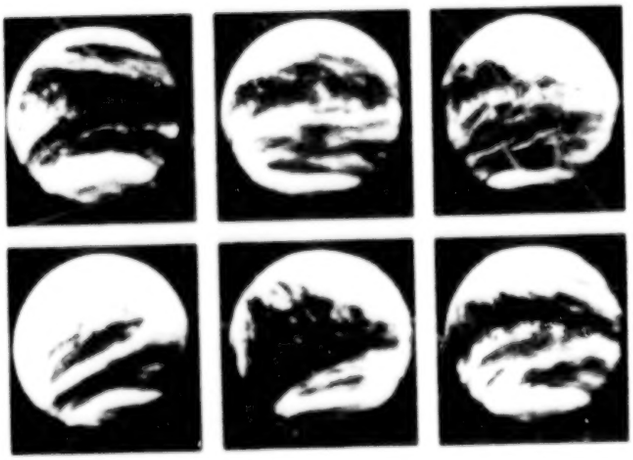

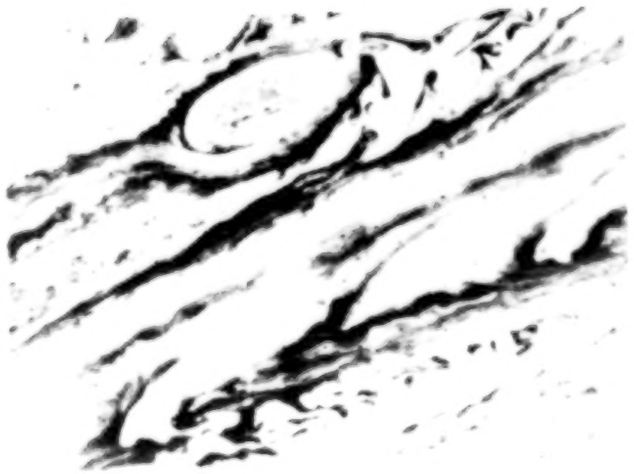

PROLOGUE

I am pleased to be able to join in welcoming you and to offer the best wishes of the NASA Office of Space Science and Applications (OSSA) for a successful conference.

This meeting is particularly timely for several reasons. First, with the launches of Magellan and Galileo and the Voyager flyby of Neptune, all in 1989, we are entering a second golden age in solar system exploration. We can look forward to a 16 year period of uninterrupted activity starting with Magellan at Venus from 1990 to 1992 and continuing with Mars Observer operating in orbit at Mars from 1993 to 1995, Galileo at Jupiter from 1996 to 2000, CRAF in its rendezvous with a comet from 2000 to 2003, and Cassini at Saturn from 2003 to 2006. Laboratory studies of the kind that you will be discussing in this workshop will be critical to the successful interpretation of the data from that extraordinary series of space flight missions.

Second, the highest priority new flight mission in the OSSA strategic plan is the Earth Observing System (EOS). The EOS program will utilize a series of polar orbiting platforms to carry a multidisciplinary complement of instruments to study the interactions of the Earth's oceans, atmosphere, land surface, and biosphere, and to seek an understanding of global change. Here, also, laboratory studies will play a crucial role.

As you begin your discussions, I would ask you to keep two thoughts in mind. Both pertain to the practical issue of helping those of us who worry about budgets and schedules provide support for the best program that we can in an environment of constrained resources. First, look at how the remarkable multidisciplinary character of your topic -- that is, the fact that your laboratory studies are important to astrophysics, planetary science, and Earth science -- can be used to advantage, from the point of view of both science and economics. Second, work hard to identify the critical scientific questions and highest priority scientific problems for the field so that we will have the best possible scientific guidance on where to steer our program.

Once again, best wishes for a vigorous and productive workshop.

Joseph K. Alexander
Assistant Associate Administrator for Space Science
(Science and Applications)
NASA Headquarters

TABLE OF CONTENTS

I. INTRODUCTION 1

II. SPECTROSCOPY

Invited Papers

Laboratory Measurements of Microwave and Millimeter-Wave Properties of Planetary Atmospheric Constituents -- P.G. Steffes 5

High Resolution Spectroscopy in the Microwave and Far Infrared -- H.M. Pickett 27

High Resolution Infrared Spectroscopy of Planetary Molecules Using Diode Lasers and Fourier Transform Spectrometers -- D.E. Jennings 37

Contributed Papers

Laboratory Studies, Analysis, and Interpretation of the Spectra of Hydrocarbons Present in Planetary Atmospheres Including Cyanoacetylene, Acetylene, Propane, and Ethane -- W.E. Blass, S.J. Daunt, A.V. Peters, and M.C. Weber 54

Infrared Spectra of Van Der Waals Complexes of Importance in Planetary Atmospheres -- G.T. Fraser, A.S. Pine, and W.J. Lafferty 64

Laboratory Measurements and Modeling of Microwave Absorption by Ammonia in Gas Mixtures Applicable to Giant Planet Atmospheres -- T.R. Spilker 69

Recent High Resolution Laboratory Determinations of Line Broadening and Intensity Parameters: PH_3, CH_3D, and CO_2 -- C.B. Suarez, C. Chackerian, Jr., F.P.J. Valero, and G. Tarrago 74

Microwave Spectra of Van Der Waals Complexes of Importance in Planetary Atmospheres -- R.D. Suenram and F.J. Lovas 78

Infrared Line Parameters at Low Temperatures Relevant to Planetary Atmospheres -- P. Varanasi 85

III. SPECTROSCOPY AND MOLECULAR DYNAMICS

Invited Papers

Absolute Vacuum Ultraviolet Photoabsorption Cross Section Studies of Atomic and Molecular Species: Techniques and Observational Data -- D.L. Judge and C.Y.R. Wu 93

PRECEDING PAGE BLANK NOT FILMED

TABLE OF CONTENTS

Determination of Molecular Spectroscopic Parameters and Energy-Transfer Rates by Double Resonance Spectroscopy -- J. I. Steinfeld, B. Foy, J. Hetzler, C. Flannery, J. Klaassen, Y. Mizugai, and S. Coy 114

Novel Laser Gain and Time-Resolved FTIR Studies of Photochemistry -- S.R. Leone 129

Contributed Papers

High Resolution, Low Temperature Photoabsortion Cross-Section of C_2H_2, With Application to Saturn's Atmosphere -- J. J. Caldwell, C.Y.R. Wu, T.J. Xia, D.L. Judge, and R. Wagener 142

Gaussian Quadrature Exponential Sum Modeling of Near Infrared Methane Laboratory Spectra Obtained at Temperatures from 106 to 297 K -- L.P. Giver, D.C. Benner, M.G. Tomasko, U. Fink, and D. Kerola 147

Measurements of the Methane Relaxation Times for Application to the Infrared Emission Models of the Upper Atmospheres of Outer Planets and Titan -- R.N. Halthore, J.J. Caldwell, J.E. Allen, Jr., J.A. Burt, K. Yang, and P. Delaney 157

New Electronic States of NH and ND Observed by Resonance Enhanced Multiphoton Ionization Spectroscopy -- R.D. Johnson III and J.W. Hudgens 164

Intracavity Dye-Laser Absorption Spectroscopy (IDLAS) for Application to Planetary Molecules -- T.M. Lang and J.E. Allen, Jr. 168

Methane Overtone Absorption by Intracavity Laser Spectroscopy -- J.J. O'Brien 173

IV. CHEMICAL KINETICS

Invited Papers

Chemical Kinetics and Modeling of Planetary Atmospheres -- Y.L. Yung 181

Kinetics and Thermochemistry of Polyatomic Free Radicals: New Results and New Understandings -- D. Gutman and I.R. Slagle 210

Contributed Papers

The Heat of Formation of CN Radicals and Radiative Lifetimes of the $A^1\Sigma^-$ State of C_2N_2 -- S.A. Barts, K.V. Pinnex, and J.B. Halpern 221

TABLE OF CONTENTS

A Laboratory Investigation of the Production and Properties of Molecular and Radical Species Pertinent to Planetary Atmospheres -- A. Fahr, J. Herron, and A.H. Laufer 227

Dissociative Recombination of Molecular Ions With Electrons -- R. Johnsen 232

Rate Constant for Reaction of Atomic Hydrogen With Germane -- D.F. Nava, W.A. Payne, G. Marston, and L.J. Stief 237

Role of the Methylene Amidogen (H_2CN) Radical in the Atmospheres of Titan and Jupiter -- F.L. Nesbitt, G. Marston, and L.J. Stief 244

Laboratory Measurements and Methane Photochemistry Modeling -- P.N. Romani 249

UV and VUV Spectroscopy and Photochemistry of Small Molecules in a Supersonic Jet -- E. Ruhl and V. Vaida 255

Laboratory Studies of Photodissociation Processes Relevant to the Formation of Cometary Radicals -- R.S. Urdahl, Y. Bao, and W.M. Jackson 260

V. CHEMICAL THERMODYNAMICS

Invited Papers

The Applications of Chemical Thermodynamics and Chemical Kinetics to Planetary Atmospheres Research -- B. Fegley, Jr. 267

Liquid-Vapor Equilibrium of Multicomponent Cryogenic Systems -- W.R. Thompson, J.C.G. Calado, and J.A. Zollweg 303

Contributed Papers

Optical Constants of Solid Methane -- B.N. Khare, W.R. Thompson, C. Sagan, E.T. Arakawa, C. Bruel, J.P. Judish, R.K. Khanna, and J.B. Pollack 327

Optical Constants of Kerogen From 0.15 to 40 μm: Comparison With Meteoritic Organics -- B.N. Khare, W.R. Thompson, C. Sagan, E.T. Arakawa, C. Meisse, and I. Gilmour 340

Vapor Pressures of Acetylene at Low Temperatures -- C.M. Masterson, J.E. Allen, Jr., G.F. Kraus, and R.K. Khanna 357

TABLE OF CONTENTS

VI. CHARGED PARTICLE INTERACTIONS

Invited Papers

Laboratory Studies of the Interaction of Ions With Condensed Gases: Planetary Applications -- J.W. Boring and R.E. Johnson 365

Electron-Impact Spectroscopy -- S. Trajmar 386

Contributed Papers

Optical Signatures of Molecular Particles Via Mass-Selected Cluster Spectroscopy -- M.A. Duncan 399

Study of Polyoxymethylene and its Sputtered Fragments - Implications for Comets -- M.H. Moore and T. Tanabe 405

Proton Irradiation of Simple Gas Mixtures: Influence of Irradiation Parameters -- N.J. Sack, R. Schuster, and A. Hofmann 411

Photon Sputtering of H_2O Ices: A Preliminary Report -- C.Y.R. Wu and D.L. Judge 414

VII. PLENARY REVIEWS

Spectroscopy -- K. Fox 423
Spectroscopy and Molecular Dynamics -- J.E. Allen, Jr. 429
Chemical Kinetics -- M. Allen 443
Chemical Thermodynamics -- B. Fegley, Jr. 451
Charged Particle Interactions -- L. J. Lanzerotti 457

VIII. APPENDIX ONE

SPASE Report 465

IX. APPENDIX TWO

Attendees 481

INTRODUCTION

This First International Conference on Laboratory Research for Planetary Atmospheres has a heritage. Its predecessors included sessions prior to meetings of the Division for Planetary Sciences (DPS) of the American Astronomical Society (AAS) in Pasadena, California and Paris, France during 1987 and 1986, respectively. There was considerable feeling that successor sessions ought to continue in order to present laboratory research which might not be highlighted suitably at the main DPS meetings.

An additional important consideration developed after the Spring of 1987 when the National Aeronautics and Space Administration (NASA) Planetary Atmospheres Management Operations Working Group (MOWG) created a Subgroup on Strategies for Planetary Atmospheres Exploration (SPASE) which was charged with the task of identifying and documenting appropriate areas for augmentation within the Planetary Atmospheres Program. Specifically, SPASE was asked to identify that area of atmospheres research where the need for additional support was particularly urgent, given the status of the field and of current and planned NASA programs in planetary science. After much deliberation, the SPASE group concluded that the area of research most in need of augmented support was that of laboratory measurements. The SPASE Report, included here as an Appendix, documented the kinds of laboratory work which could lead to notable advances in specific areas of planetary atmospheres research.

The SPASE Report recommended that workshops and special meetings should be held to highlight requirements and progress relating to laboratory studies for planetary atmospheres. SPASE noted: "A national meeting involving many members of the Planetary Atmospheres community is planned for calendar 1989; this will serve as an introductory forum for the proposed augmentation ... this would both highlight progress and set the stage for the follow-on option." The 1989 Conference on Laboratory Research for Planetary Atmospheres is indeed this "national meeting" and "introductory forum."

The areas of research principally covered by this Conference, and consequently by these Proceedings, are photon and electron spectroscopy, chemical kinetics, and thermodynamics. Invited papers were presented orally and were followed by extensive

discussions. Contributed papers were displayed as posters throughout the Conference. Plenary reviews were given orally, covering both invited and contributed papers in each subject area, at the concluding session.

This Conference on Laboratory Research for Planetary Atmospheres was well attended, with active participation by more than sixty registrants. Research workers came from across the United States of America and from several foreign nations. Their home institutions included universities, government laboratories, and the private sector.

There was a consensus at the conclusion of this Conference that such activities be encouraged and supported for the future. Specific suggestions included sessions prior to the meetings of the DPS/AAS planned for Charlottesville, Virginia and Munich, Federal Republic of Germany during the Autumn of 1990 and 1992, respectively.

There are many individuals and organizations whose participation and support were essential to a successful Conference, and to whom thanks and appreciation are due: Bowie State University, the NASA Goddard Space Flight Center, NASA Headquarters, and the University of Tennessee coordinated this Conference from its initial stages to its conclusion; the NASA Planetary Atmospheres Program of the Solar System Exploration Division provided fiscal support; the National Organizing Committee provided the rationale and motivation for this enterprise; the Local Organizing Committee handled the seemingly endless details of ensuring that this Conference ran smoothly and effectively; and the Conference Secretary implemented what had to be done - and more - to make it all happen in a timely and outstanding fashion. To these and to the others whose work was essential, thank you.

SPECTROSCOPY

INVITED

AND

CONTRIBUTED

PAPERS

N90-26745

LABORATORY MEASUREMENTS OF MICROWAVE AND MILLIMETER-WAVE PROPERTIES OF PLANETARY ATMOSPHERIC CONSTITUENTS

PAUL G. STEFFES
Georgia Institute of Technology
School of Electrical Engineering
Atlanta, GA 30332-0250

ABSTRACT

Accurate data on microwave and millimeter-wave properties of potential planetary atmospheric constituents is critical for the proper interpretation of radio occultation measurements, and of radio astronomical observations of both continuum and spectral line emissions. Such data is also needed to correct for atmospheric effects on radar studies of surface reflectivity. Since the refractive and absorptive properties of atmospheric constituents often vary drastically from theoretically-predicted profiles, especially under the extreme conditions characteristic of planetary atmospheres, laboratory measurements under simulated planetary conditions are required.

This paper reviews the instrumentation and techniques used for laboratory measurement of the refractivity and absorptivity of atmospheric constituents at wavelengths longward of 1 mm, under simulated planetary conditions (temperature, pressure, and broadening gases). Techniques for measuring both gases and condensates are considered. Also reviewed are the relative accuracies of the various techniques. We conclude by reviewing laboratory measurements which have already been made, and highlight additional measurements which are needed for interpretation of data from Venus and the outer planets.

I. INTRODUCTION

Radio absorptivity data for planetary atmospheres obtained from spacecraft radio occultation experiments and earth-based radio astronomical observations can be used to infer abundances of microwave absorbing atmospheric constituents in those atmospheres, as long as reliable information regarding the microwave absorbing properties of potential constituents is available. The use of theoretically-derived microwave absorption properties for such atmospheric constituents, or laboratory measurements of such properties under environmental conditions which are significantly different than those of the planetary

PRECEDING PAGE BLANK NOT FILMED

atmosphere being studied, often leads to significant misinterpretation of available opacity data. For example, results obtained for the microwave opacity from gaseous H_2SO_4, under simulated Venus conditions showed that not only was the opacity from H_2SO_4 much greater than theoretically predicted, but that its frequency (wavelength) dependence was far different than that theoretically predicted (Steffes, 1985 and Steffes, 1986). Subsequent measurements made by Steffes and Jenkins (1987), showed that the microwave opacity of gaseous ammonia (NH_3) under simulated Jovian conditions did agree with theoretical predictions to within their experimental accuracy at wavelengths longward of 1.3 cm. However, work performed by Joiner et al. (1989) has shown that laboratory measurements of the millimeter-wave opacity of ammonia between 7.5 mm and 9.3 mm and also at the 3.2 mm wavelength require a different lineshape to be used in the theoretical prediction for millimeter-wave ammonia opacity than had been previously used. The recognition of the need to make such laboratory measurements of simulated planetary atmospheres over a range of temperatures and pressures which correspond to the altitudes probed by both radio occultation experiments and radio astronomical observations, and over a range of frequencies which correspond to those used in both radio occultation experiments and radio astronomical observations, has led to the development of facilities at Georgia Tech and at other institutions which are capable of making such measurements.

This paper reviews the instrumentation and techniques used for laboratory measurement of the refractivity and absorptivity of atmospheric constituents at wavelengths longward of 1 mm, under simulated planetary conditions (temperature, pressure, and broadening gases). Techniques for measuring both gases and condensates are considered. Also reviewed are the relative accuracies of the various techniques. We conclude by reviewing laboratory measurements which have already been made, and highlight additional measurements which are needed for interpretation of data from Venus and the outer planets.

II. INSTRUMENTATION AND MEASUREMENT TECHNIQUES

A large number of measurement techniques are used for characterizing the refractivity and absorptivity of gases and condensates at microwave and millimeter-wavelengths. At the shorter millimeter-wavelengths (near 1 mm), the techniques resemble the IR/optical spectroscopic techniques described by other authors. At the longer microwave wavelengths ($\lambda > 1$ cm), techniques involving

RF (radio frequency) components are employed.

A. Absorptivity Measurements at Wavelengths Longward of 1 cm

At wavelengths longward of 1 cm, the two major techniques for inferring planetary atmospheric opacity and refractivity are spacecraft radio occultation experiments and earth-based radio emission measurements. At these wavelengths, the vast majority of measured opacity is due to atmospheric gases at pressures at or above 1 Bar. Measurement of the microwave absorption and refraction properties of such gases is most often accomplished with cylindrical cavity resonators. Figure 1 (from Steffes, 1986) and Figure 2 (from Steffes and Jenkins, 1987) show measurement systems designed to measure microwave absorption and refraction properties of atmospheric gases under simulated conditions for the Venus atmosphere (Figure 1) and the atmospheres of the outer planets (Figure 2).

The approach used to measure the microwave absorptivity of gaseous H_2SO_4 in a CO_2 atmosphere can be seen in Figure 1. The absorptivity is measured by observing the effects of the introduced gas mixture on the Q, or quality factor, of two cavity resonators at particular resonances from 1.34 GHz to 23.6 GHz. The changes in the Q of the resonances which are induced by the introduction of an absorbing gas mixture can be monitored by the high resolution microwave spectrum analyzer, since Q is simply the ratio of the cavity resonant frequency to its half-power bandwidth. For relatively low-loss gas mixtures, the relation between the absorptivity of the gas mixture and its effect on the Q of a resonance is straightforward:

$$\alpha \simeq (Q^{-1}_L - Q^{-1}_C)\ \pi/\lambda \qquad (1)$$

where α is absorptivity of the gas mixture in Nepers km^{-1}. (Note, for example, that an attenuation constant or absorption coefficient or absorptivity of 1 Neper km^{-1} = 2 optical depths per km (or km^{-1}) = 8.686 dB km^{-1}, where the first notation is the natural form used in electrical engineering, the second is the usual form in physics and astronomy, and the third is the common (logarithmic) form. The third form is often used in order to avoid a possible factor-of-two ambiguity in meaning.) Q_L is the quality factor of the cavity resonator when the gas mixture is present, Q_C is the quality factor of the cavity resonator in a vacuum, and λ is the wavelength (in km) of the test signal in the gas mixture.

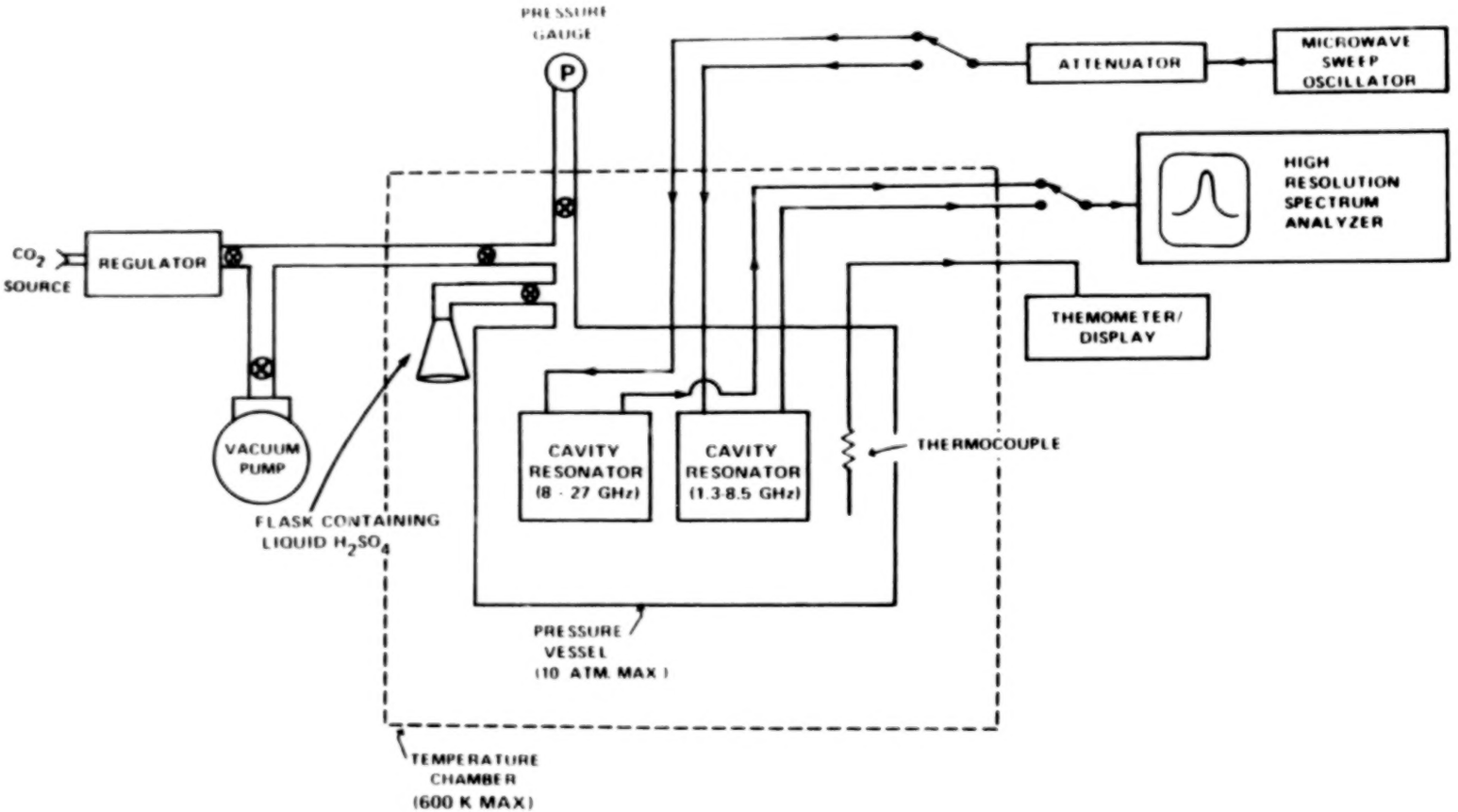

Figure 1: Block diagram of the atmospheric simulator as configured for measurements of the microwave absorption and refraction of gaseous H_2SO_4 under Venus atmospheric conditions over the 1.2-22.3 cm wavelength range.

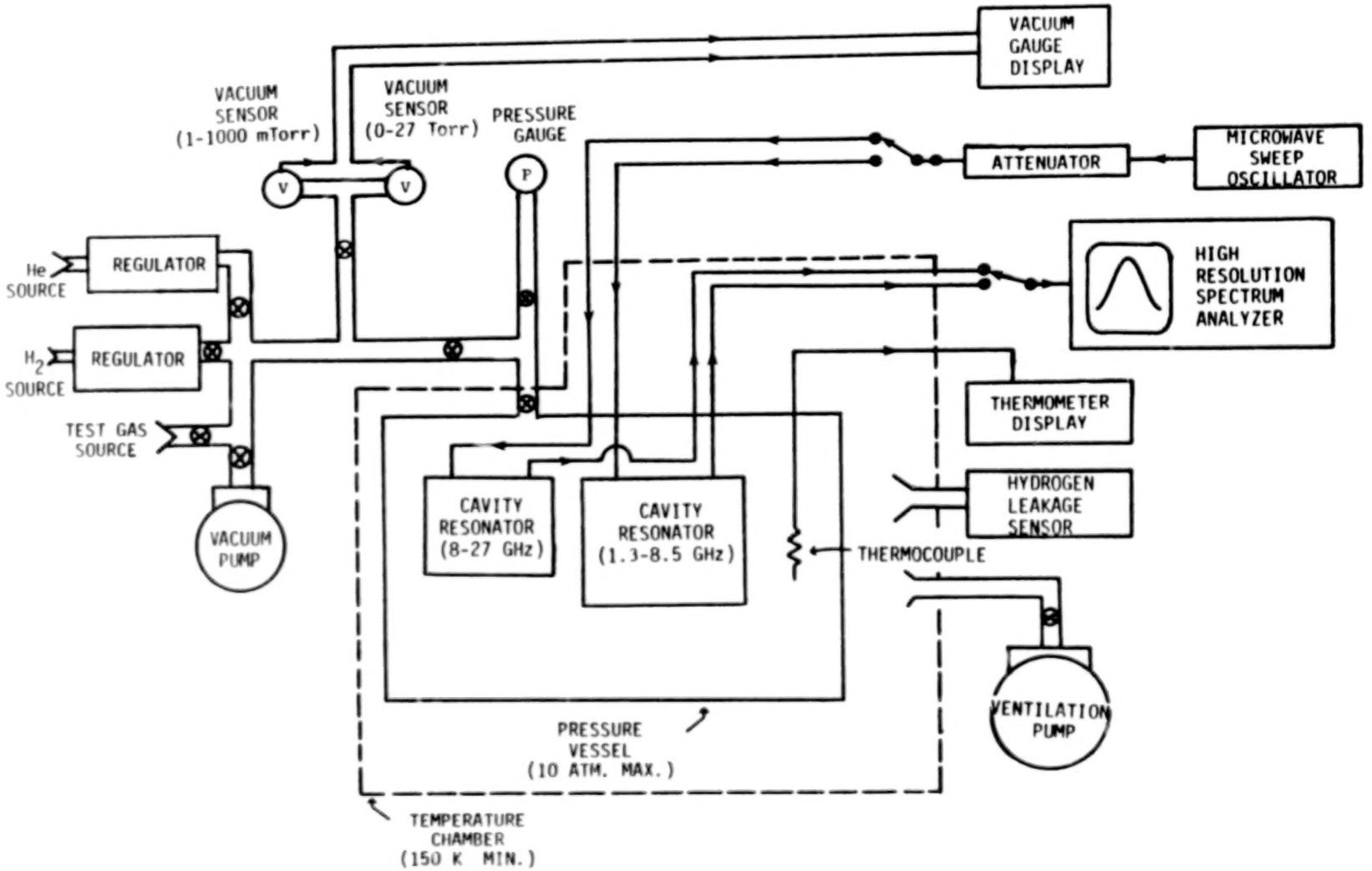

Figure 2: Block diagram of the atmospheric simulator, as configured for measurements of the refraction and microwave absorption of test gases (NH_3, CH_4, and H_2O) under simulated Jovian conditions.

In order to obtain a gas mixture with a sufficient amount of H_2SO_4 vapor so that the microwave absorption is detectable, the system must be operated at temperatures exceeding 450 K. While this is suboptimal in that the temperatures at altitudes from 35 to 50 km (where both radio occultation and radio astronomical experiments have detected microwave opacity) range from 350 to 450 K, temperature dependencies measured for similar gases (such as SO_2) can be used to estimate temperature effects in that range. In order to infer H_2SO_4 vapor pressure, the volume of liquid sulfuric acid which is vaporized to generate the gaseous H_2SO_4 is determined to a high accuracy (up to $\pm$0.005 ml). It is then possible to compute the partial pressure of gaseous H_2SO_4 using the ideal gas equation, the measured change in liquid volume, and published densities for H_2SO_4 liquid. However, since gaseous H_2SO_4 can dissociate to form gaseous H_2O and SO_3 which have relatively low microwave opacity when compared with gaseous H_2SO_4, an accurate estimate of the "dissociation factor" is necessary in order accurately estimate the H_2SO_4 abundance, and therefore the relationship between abundance and absorptivity. Recently, Fahd and Steffes (1989) have measured this dissociation factor. Initially, a vacuum is drawn in the pressure vessel containing the microwave cavity resonator, and the bandwidth and center frequency of the resonances are then measured. For this experiment, resonances at 1.34 GHz (22.3 cm) 2.24 GHz (13.4 cm), 8.42 GHz (3.6 cm), 13.23 GHz (2.26 cm), 21.63 GHz (1.38), and 23.64 GHz (1.27 cm) were used. A valve is then opened which allows the sulfuric acid vapor eluting from the flask to fill the pressure vessel (0.031 cubic meters of open volume with resonator in place) and reach vapor pressure equilibrium with the liquid H_2SO_4.

As H_2SO_4 vapor fills the chamber, changes in the resonance center frequency are observed. These changes are related to the H_2SO_4 vapor abundance. After equilibrium is reached, the valve to the reservoir flask is then closed, and CO_2 is admitted to the chamber containing the H_2SO_4 vapor. For this experiment, a total pressure of 6 atm was used. The bandwidth of each response is then measured and compared with its value when the chamber was evacuated in order to determine the absorptivity of the CO_2/H_2SO_4 gas mixture at 6 atm total pressure. The total pressure is then reduced by venting, and the bandwidths are again measured. Subsequent measurements are likewise made at lower pressures in order to determine absorptivities at those pressures. The pressure vessel is then evacuated and the bandwidths again measured so as to assure no variation (either

due to thermal shift or chemical reaction) of the Q's of the evacuated resonators has occurred. Note that this approach has the advantage that the same gas mixture is used for the absorptivity measurements at the various pressures. Thus, even though some uncertainty may exist as to the mixing ratio of the initial mixtue, the mixing ratios at all pressures are the same, and thus the uncertainty for any derived pressure dependence is due only to the accuracy limits of the absorptivity measurements, and not to uncertainty in the mixing ratio. Similarly, measurements of the frequency dependence of the absorptivity from the gas mixture are likewise immune to mixing ratio uncertainty, as long as foreign-gas broadening predominates.

Measurements have also been made of the absorptive properties of several gases under simulated conditions for the outer planets, using the system in Figure 2. The first experiment involved gaseous NH_3.

In order to obtain a gas mixture with a sufficient amount of gaseous NH_3 so that microwave absorption is detectable using our system, temperatures at or above 170 K must be used. (This limit is set by the saturation vapor pressures for ammonia and by the sensitivity of our measurement system.) While this covers most of the temperature range in the Jupiter atmosphere over which radio occultation and radio astronomical experiments have detected microwave opacity (140-300 K), it is somewhat above the temperature range over which microwave opacity has been detected at Saturn. However, the measured temperature dependencies can be used to extrapolate to those temperatures. In order to conduct the required measurements, the pressure vessel and its microwave resonators must first be cooled to the desired temperature.

After thermal stability is reached, which can be monitored using both the temperature sensors and the resonant frequencies of the system, a vacuum is drawn in the pressure vessel containing the resonators, and the bandwidth and center frequency of each of resonances is then measured. For this experiment (absorption from NH_3), resonances at 1.34 GHz (22.3 cm), 2.25 GHz (13.3 cm), 8.53 GHz (3.52 cm), 13.3 GHz (2.26 cm), and 21.7 GHz (1.38 cm) were used. A valve is then opened which allows the ammonia gas to enter the chamber. Measurements of the gaseous NH_3 pressure were made with the high accuracy thermocouple vacuum gauge tubes which are shown in Figure 2. Next, 5.4 atm of hydrogen (H_2) and 0.6

atm of helium (He) are added. These gases are admitted to the chamber at a sufficiently slow rate so as not to significantly affect the temperature within the chamber. The bandwidth of each resonance is then measured and compared with its value when the chamber was evacuated in order to determine the absorptivity of the gas mixture at 6 atm total pressure. The total pressure is then reduced by venting to 4 atm, and the bandwidths are again measured.

As before, this approach has the advantage that the same gas mixture is used for the absorptivity measurements at the various pressures. Thus, even though some small uncertainty may exist as to the mixing ratio of the initial mixture, the mixing ratios at all pressures are the same.

B. Absorptivity Measurements at Wavelengths Between 1 mm and 1 cm

While the techniques for measuring millimeter-wave absorptivity are similar to those used at longer wavelengths, the cylindrical resonators used at wavelengths longward of 1 cm become ineffective at the shorter wavelengths. Shortward of 1 cm, cylindrical resonators become extremely small, resulting in a very low quality factor (Q) and making it difficult to couple energy in and out of the resonator. An alternative approach is the semi-confocal Fabry-Perot resonator shown in Figure 3. The resonator shown in Figure 3 has several bandpass resonances in the range from 30-40 GHz with quality factors around 8000. A similar resonator which operates at 94 GHz with a Q of over 30,000 is shown in Figure 4. The system used to measure the 94 GHz absorptivity of NH_3 in a H_2/He atmosphere is shown in Figure 5. Note the use of a premixed, constituent analyzed, hydrogen/helium/ammonia atmosphere with a mixing ratio accuracy of better than $\pm$ 2% of its value (e.g., [1.85 $\pm$ 0.04] % of NH_3).

Before the absorption coefficient can be calculated, the effect of the dielectric properties of hydrogen and helium on the system must be known. The dielectric properties of gases with little or no absorption such as hydrogen and helium can cause changes in the apparent bandwidths of resonances. Because the percentage change in bandwidth (on the order of 20%) due to the absorption of NH_3 is relatively small for our system, any changes in bandwidth due to the dielectric effects of hydrogen and helium may lead to significant errors in the absorption measurement.

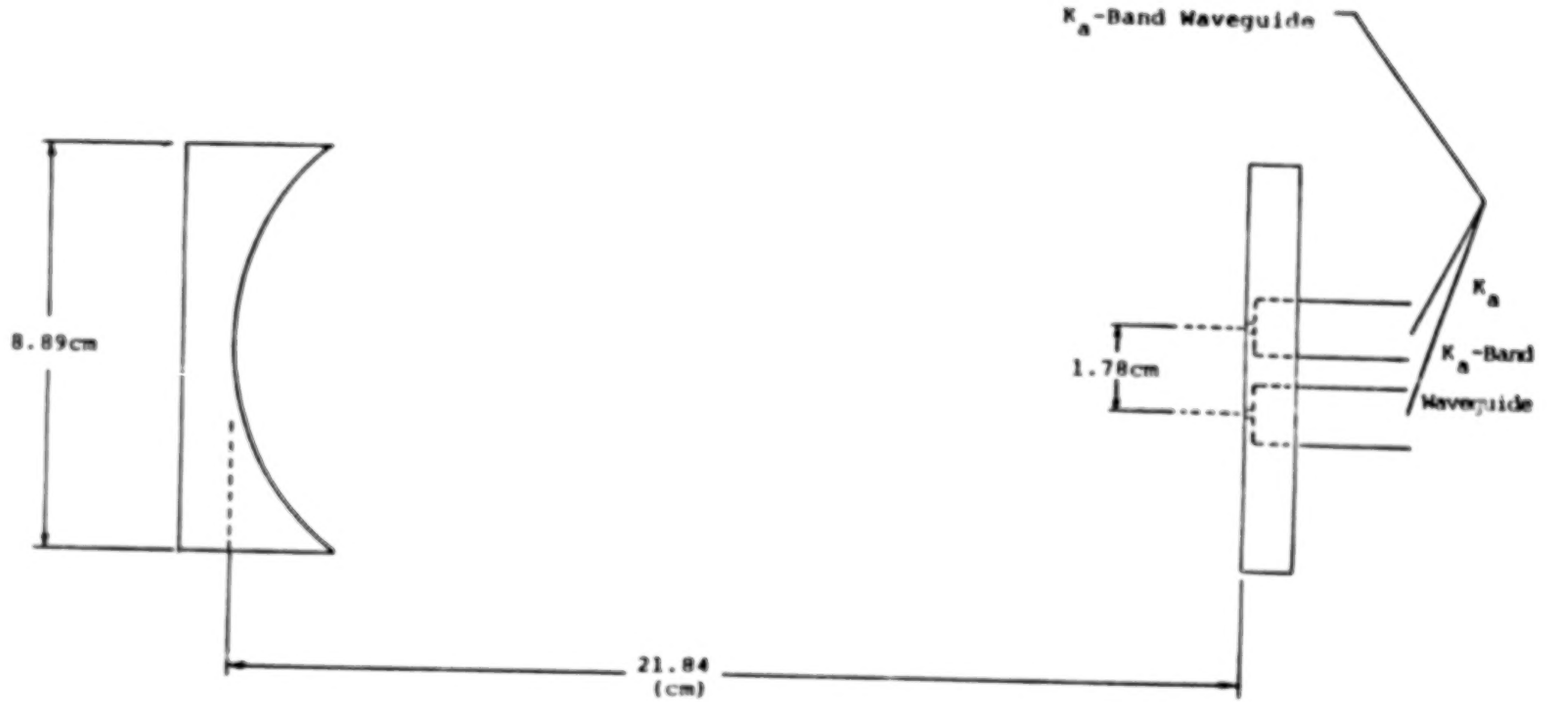

Q = 8000 N = 1.13 EPL = 10m

Figure 3: **Dimensions of Semi-Confocal Fabry-Perot Interferometer** (Resonator) used from 32-40 GHz.

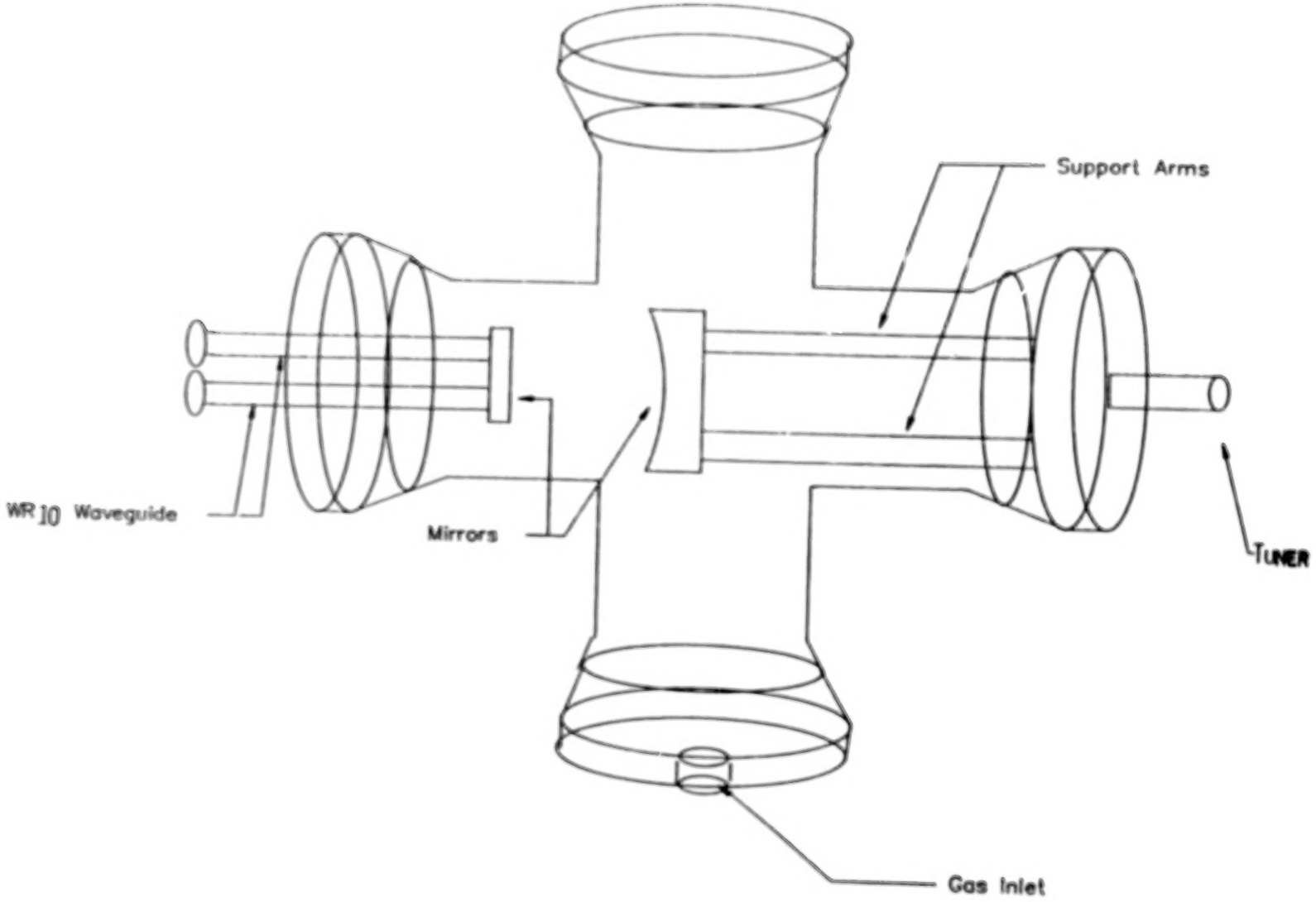

Figure 4: DIAGRAM OF FABRY-PEROT RESONATOR (94GHz)

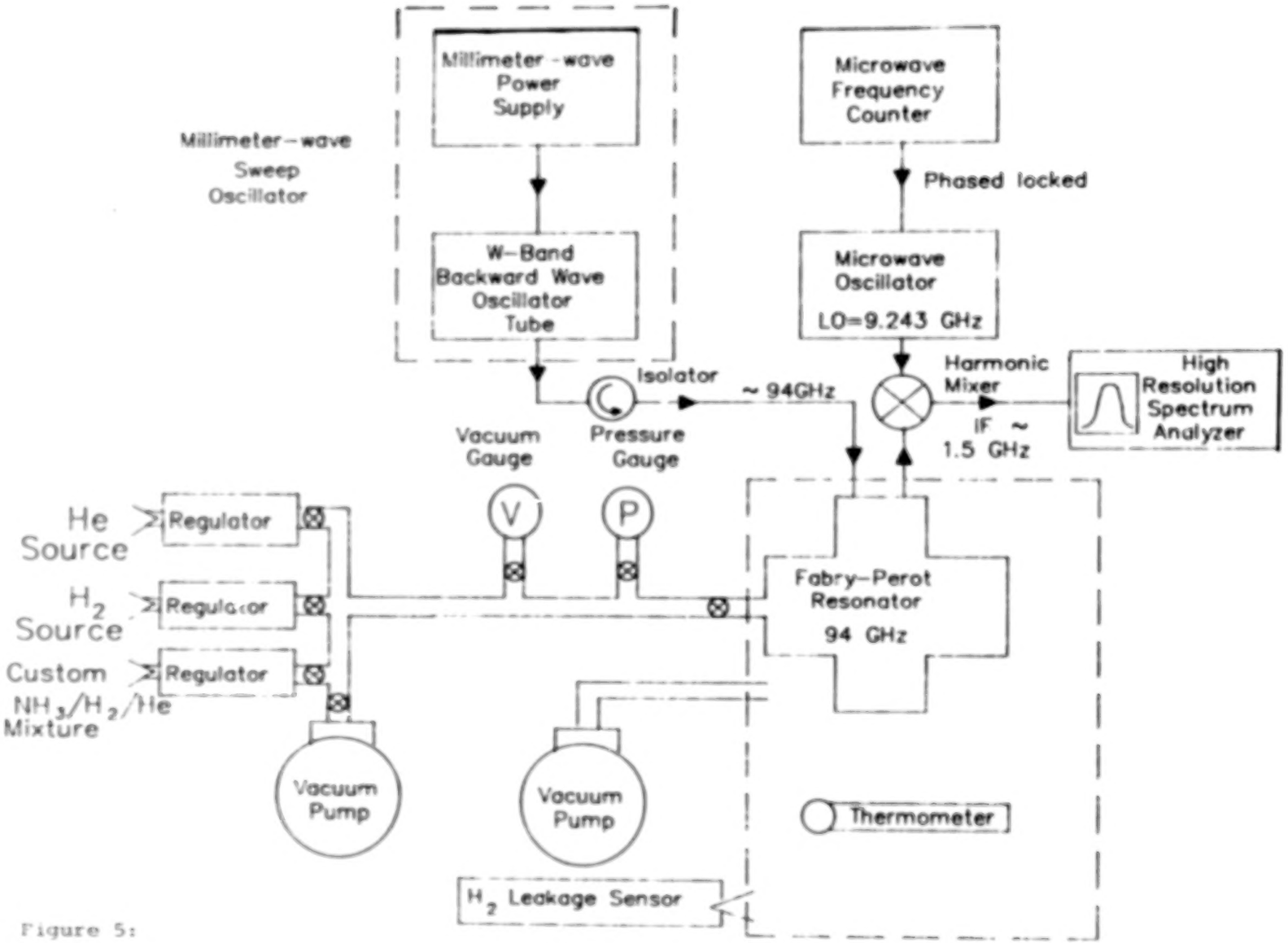

Figure 5:

BLOCK DIAGRAM OF ATMOSPHERIC SIMULATOR (94 GHZ)

The resonator, which operates as a bandpass filter, is connected to a signal source (the sweep oscillator) and to a receiver (the high resolution spectrum analyzer). The Q of the resonator, which is defined as the ratio of the resonant center frequency to the resonance half-power bandwidth, is proportional to the ratio of the energy stored in the resonator to the energy lost per cycle. Therefore, stronger coupling between the resonator and the spectrum analyzer or sweep oscillator causes more energy to be lost per cycle, and thus decreases the Q of the resonance. For this reason, the resonator was designed with minimal coupling, so as to maximize Q and minimize the variations in Q that might result from changes in coupling that occur when gases are introduced into the resonator. These changes in coupling, which we refer to as dielectric loading, are due to the dielectric constant or permittivity of the test gas mixtures and are not related to the absorptivity of the gases. Slight imperfections in the waveguide or irises can make the apparent Q of the resonator appear to vary with the abundance of lossless gases. It is therefore necessary to repeat the absorption measurement <u>without</u> the absorbing gas present. The last step in the experimental procedure is to measure the bandwidth of each resonance in a mixture consisting of 90% hydrogen (H_2) and 10% helium (He) with no ammonia present. Since, for the pressures and wavelengths involved, the H_2/He atmosphere is essentially transparent, no absorption is expected. If any apparent absorption is detected, dielectric loading (or a change in coupling due to the dielectric properties of the gases) is indicated.

We have found that the effects of dielectric loading are additive, in that they add to the apparent changes of resonator bandwidth caused by the absorbing gases. Thus, as long as the effects of dielectric loading are not time variable, they can be removed by using the measured value of the Q of the resonance with the non-absorbing gases present rather than the Q of the resonance in a vacuum for the quantity Q_C in equation (1).

C. Experimental Uncertainties

Uncertainties in the measurement of the absorption coefficient may be classified into two categories: uncertainties due to instrumental error and the uncertainty due to noise. The uncertainties due to instrumental error are caused by the limited resolution and capability of the equipment used to measure pressure, temperature, and resonant bandwidth. These uncertainties have been

significantly reduced so that they are relatively small when compared to the uncertainty due to noise. For instance, proper calibration of the spectrum analyzer has made the uncertainty in the measurement of the resonant bandwidth and center frequency in the absence of noise negligible. Likewise, the limited ability of the temperature chamber to maintain a constant temperature results in variations of only $\pm$ 2.5%. The largest source of uncertainty due to instrumental error in the past has been associated with the mixing ratio of the gas mixture. The uncertainty in the measurement of the amount of ammonia present in the mixture due to the inaccuracy inherent in the thermocouple vacuum gauge is on the order of $\pm$20%, or (1.85 $\pm$ 0.37) % NH_3 volume mixing ratio. Thus, even though measurements at all frequencies are made with the same mixing ratio and the frequency dependence remains intact, a large uncertainty still remains in the relative amplitude of the absorption. We have been able to reduce this uncertainty by repeating the measurements using a pre-mixed, constituent analyzed, hydrogen/helium/ammonia atmosphere with a mixing ratio accuracy of better than $\pm$ 2%, or (1.85 $\pm$ 0.04) % NH_3 volume mixing ratio.

The most significant source of uncertainty in the measurement of the absorption coefficient is due to the effects of noise in the system. This electrical noise is displayed by the spectrum analyzer. As a result, the measurement of the bandwidth of a resonance must be accompanied by an error term which is directly related to the width of the noise on the spectrum analyzer's display.

In order to reduce the effects of noise, the system sensitivity, which is dependent on both the Q of the resonator and the noise present in the system, must be as high as possible. Because the Q is defined as 2λ times the ratio of the average energy stored in the resonator to the energy lost (per cycle) in the resonator, reducing losses in the resonator increases the sensitivity of the system. The losses in a Fabry-Perot type resonator can be attributed to the resistive losses on the surfaces of the mirrors, coupling losses due to energy coupling out of the resonator through the irises on the flat-surfaced mirror, and diffraction losses around the sides of the mirrors (Collin, 1966). (The diffraction losses are, of course, minimal in the cylindrical cavity resonators.)

Computation of the resistive losses from the mirrors of the Fabry-Perot resonators showed that, in the absence of all other losses, the quality factor should have been on the order of 250,000, whereas its actual quality factor was on the order of 10,000. Therefore, the limiting factor in the performance of the resonator must be attributed to either coupling losses or diffraction losses. (As a result, even the introduction of high temperature superconducting material would not significantly improve the sensitivity of the system.) In order to minimize the coupling losses, adjustable irises were developed so that the smallest possible coupling losses would occur, while still allowing sufficient signal coupling in and out of the resonator. However, this yielded only slightly improved results.

The major limiting factor to the system sensitivity is diffraction losses around the edges of the mirrors. One approach used to reduce diffraction losses involves the precise pointing of the mirrors to assure that both mirrors are oriented directly toward each other. This is accomplished by directing the beam of a helium-neon laser through the input waveguide and iris and into the resonator. The parabolic mirror is then adjusted so that the reflected beam focuses precisely on the output iris. This is found to maximize both the signal to noise ratio and the Q of the resonator, and therefore increase the sensitivity of the system. Figure 6 shows the improvement in the sensitivity of the 30-40 GHz system obtained with this approach. Figure 7 shows the sensitivity of the 1.34 - 23.6 GHz system shown in Figure 2.

D. Refractivity Measurements

The refractive index, n, of a gas is the ratio of the velocity of an electromagnetic wave in a vacuum, c, to the velocity of the wave in the presence of the gas, v_g. Since the resonant frequencies of a microwave resonator are directly proportional to the velocity of electromagnetic waves within the resonator, the refractive index of a gas can be determined by comparing the frequency of a particular resonance when a vacuum is present within the resonator, f_v, to the resonant frequency when the gas is present, f_g. That is,

$$n = c/v_g = f_v/f_g \qquad (2)$$

Refractivity, N, is defined as being equal to $(n-1) \times 10^6$. Thus, it can be determined simply by measuring the change in center frequency of a given

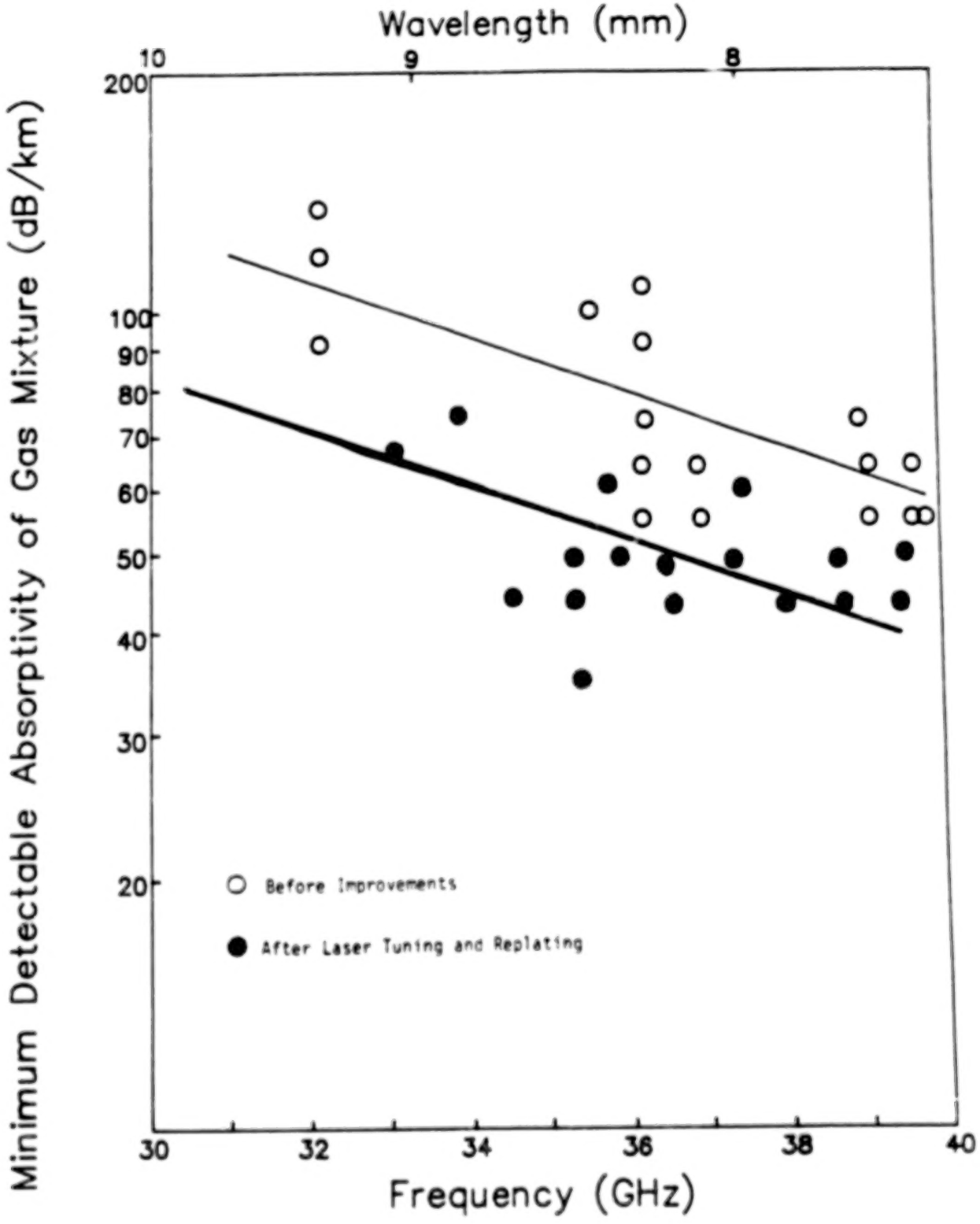

Figure 6: Performance (minimum detectable absorptivities) for the 32-40 GHz resonator system (operating at 200 K). Note improvement in average performance (solid lines) after laser tuning.

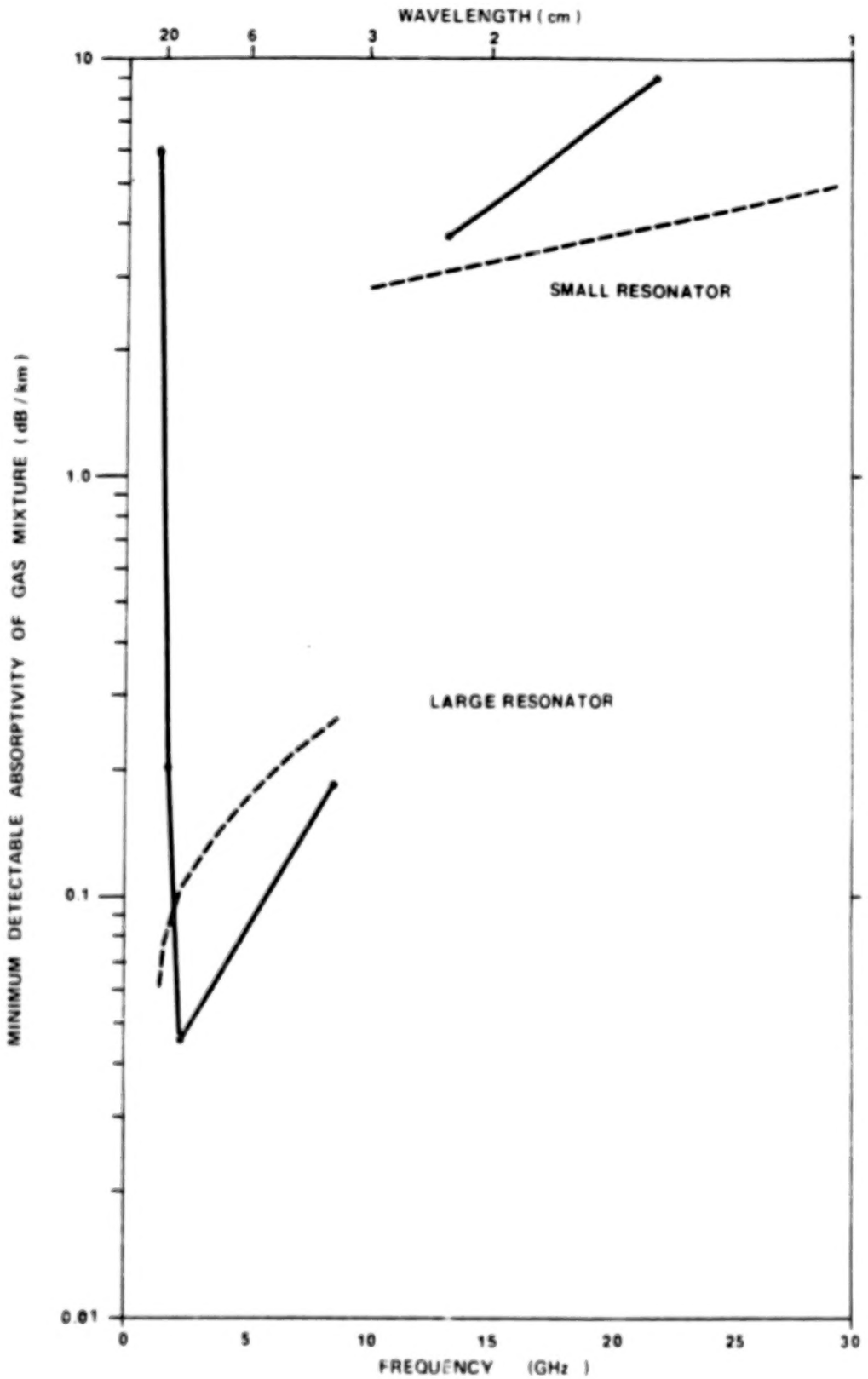

Figure 7: Predicted sensitivity (dashed line) and actual measured sensitivity (solid) of resonator system shown in Figure 2 when operated at 150 K.

resonance after the gas has been introduced. That is,

$$N = (n-1) \times 10^6 = [(f_v - f_g)/f_g] \times 10^6 \quad (3)$$

Since the refractivity of a gas is directly proportional to the molecular density of the gas, ρ, the refractivity is often expressed in a form which is normalized by molecular density in terms of the temperature and pressure of the gas. That is, $\rho = P/RT$ where ρ is density in molecules per cm^3, P is the pressure in atmosphere, R is the ideal gas constant (1.362344×10^{-22} cm^3-atm/molecule/Kelvin), and T is the temperature in Kelvins. Thus, the density-normalized refractivity, N/ρ, can be expressed as NRT/P. It is often assumed that the density-normalized refractivity for a gas is independent of pressure or temperature.

Any of the resonator systems described can be used to measure the density-normalized refractivity of gas mixtures. Knowledge of this quantity is necessary for determining pressure-temperature profiles from radio occultation data, and for proper modeling of microwave and millimeter-wave emission. Initially, a vacuum is drawn in the chamber containing the resonator. The heating or cooling system is then used to bring the chamber to the appropriate planetary temperature. As the temperature is changed, the resonant frequencies change due to thermal contraction. Thus, when thermal stability is reached, the resonant frequencies likewise stabilize. After thermal stability is reached, a vacuum is drawn in the pressure vessel containing the two microwave resonators, and the center frequencies of the resonances of interest are than measured. A valve is then opened which admits the test gas to the chamber. As the gas is added, the shifting of the center frequencies of the various resonances can be observed. Once the desired pressure is reached the total frequency shift can be used to compute the refractivity, N, of the gas under those conditions. It should be noted that while the major source of uncertainty for our refractivity measurements is the frequency measuring capability of our system, two other sources of uncertainty affect the accuracy of our determination of density-normalized refractivity, and those are our abilities to measure pressure and temperature.

E. Measurements of Absorptivity and Refractivity of Solids and Liquids

Measurements of the absorptivity and refractivity (also referred to as the

complex dielectric constants) of condensate materials have been less common at longer wavelengths because of their relatively small effect on observed microwave emission, or measured microwave absorption at the depths to which radio occultation experiments have been able to probe. However, with the upcoming Galileo mission, in which a probe carrying a microwave transmitter will penetrate into the deep Jovian atmosphere, the opportunity to measure the microwave absorption from the dense clouds may be possible. Similarly, radar studies of Titan have suggested the possibility of measuring the properties of surface liquids (Spilker and Eshleman, private communication). Therefore, in order to properly identify surface constituents based on their radar reflectivity, measurements of the complex dielectric constants of potential surface liquids are necessary at the 12.6 and 3.6 cm radar wavelengths.

Three techniques are used for the measurement of complex dielectric constants. The first is essentially identical to that previously described. That is, a system such as that shown in Figure 2 (using cylindrical resonators) is employed, and changes in the bandwidth and center frequencies of the resonances when the resonators are filled with liquid or solid materials are measured to determine refractivity and absorptivity. However, many liquids have such large amounts of refraction and absorption that the resonances are totally attenuated. With these sorts of materials, the most common alternative approach for measuring the complex dielectric constant is to place the material within an open circuited coaxial line (between the conductors), and to measure the complex impedance of the line using a microwave network analyzer. Scott and Smith (1986a) have used this technique at frequencies up to 2 GHz, and expect it to be useful to over 8 GHz. (Note that we have successfully used this technique to measure the properties of aqueous ammonia solutions up to 2 GHz.)

The third method involves placing a monopole antenna in a hemispherical tank containing the material (liquid or crystalline) to be tested. By measuring the change in the complex impedance of the antenna from when it is in air to when it is immersed in the material, it is possible to infer the complex dielectric constant of the material. Scott and Smith (1986b) have used this technique at frequencies up to 10 GHz, and expect it to be useful at much higher frequencies as long as the network analyzers to measure complex impedance are available.

Since the first two techniques described are generally not useful at wavelengths shortward of 1 cm and since the third technique has yet to be tried at millimeter-wavelengths, an alternative approach is frequently employed. Breeden and Langley (1969) developed a technique whereby a slab of solid material or a container of liquid material is placed on the surface of the flat mirror of a semi-confocal Fabry-Perot resonator, such as those shown in Figure 3 and 4. As long as the physical dimensions of the material being tested are well known, it is possible to infer its complex dielectric constant from the measured changes in the resonant frequency and quality factor of the resonator which accompany the introduction of the material. We intend to pursue this technique for future laboratory measurements of the millimeter-wave properties of potential Venus and Jovian cloud constituents.

III. CONCLUSION

In this paper, we have described techniques for laboratory measurement of microwave and millimeter-wave absorption and refraction properties of planetary atmospheric constituents. In Table I, we present a summary of known laboratory measurements of a number of planetary atmospheric constituents. It should be noted that this summary should not be considered to be complete. Similarly, even if multiple measurements are listed for a given constituent, more measurements may be necessary in order to provide a complete spectral analysis and to provide measurements over a complete range of appropriate pressures and temperatures with the necessary accuracy.

ACKNOWLEDGEMENT

This work was supported by the Planetary Atmospheres program of the Solar System Exploration Division (Office of Space Science and Applications) of the National Aeronautics and Space Administration under Grant NAGW-533.

TABLE I: REFERENCES FOR LABORATORY MEASUREMENTS OF MICROWAVE/MILLIMETER-WAVE PROPERTIES OF PLANETARY ATMOSPHERIC CONSTITUENTS

CONSTITUENT	REFERENCE
CH_4	Jenkins and Steffes (1988)
CO	Britt, Tolbert, and Straiton (1961) Waters (1976)
CO_2	Ho, Kaufman, and Thaddeus (1966) Tyler and Howard (1969)
COS	Kolbe, Buscher, and Leskovar (1977)
HCN	Rohart, Derozier, and Legrand (1987)
H_2O (g)	Ho, Kaufman and Thaddeus (1966) Jenkins and Steffes (1988) Liebe and Dillon (1969)
H_2O (ℓ)	Hasted (1973)
H_2CO	Kolbe, Buscher, and Leskovar (1977)
H_2SO_4 (g)	Fahd and Steffes (1989) Kuczkowski, Suenram, and Lovas (1981) Steffes (1985) Steffes (1986) Steffes and Eshleman (1981) Steffes and Eshleman (1982)
H_2SO_4 (ℓ)	Ho and Hall (in Cimino, 1982)
N_2	Ho, Kaufman, and Thaddeus (1966)
NH_3	Birnbaum and Maryott (1953) Bleaney and Loubser (1950) Morris and Parsons (1970) Poynter and Kakar (1975) Steffes and Jenkins (1987) Joiner, Steffes and Jenkins (1989) Spilker and Eshleman (1988)
NO	French and Arnold (1968)
O_2	Liebe and Layton (1969)
SO_2	Steffes and Eshleman (1981)
SO_3	Steffes and Eshleman (1981)

IV. REFERENCES

Bleaney, B. and J.H.N. Loubser (1950). The inversion spectrum of NH_3, CH_3Cl, and CH_3Br at high pressures. Proc. Royal Soc. (London) A63, 483-493.

Britt, C.O., C.W. Tolbert, and A.W. Straiton (1961). Cu line parameters. J. Res. NBS) 65D, 15.

Birnbaum, G. and A.A. Maryott (1953). Absorption in the low-frequency wing of the NH_3 inversion spectrum. J. Chem. Phys. 21, 1774-1777.

Fahd, A.K. and Steffes, P.G. (1989). Laboratory Measurements of the Dissociation Factor of Gaseous Sulfuric Acid (H_2SO_4). Bull. Amer. Astron. Soc. 21, 927.

French, I.P. and T.E. Arnold, Jr. (1968). Nitric oxide absorption coefficients and transitions. J. Chem. Phys. 48, 5720.

Hasted, J.D. (1973). Aqueous Dielectrics, Chapman and Hall, London.

Ho, W. and W.F. Hall (in Cimino, J.B., 1982). The composition and vertical structure of the lower cloud deck on Venus. Icarus 51, 334-357.

Ho, W., I.A. Kaufmann and P. Thaddeus (1966). Laboratory measurements of microwave absorption in models of the atmosphere of Venus, J. Geophys. Res. 21, 5091-5108.

Jenkins, J.M. and P.G. Steffes (1988). Constraints on the microwave opacity of gaseous methane and water vapor in the Jovian atmosphere. Icarus 76, 378-382.

Joiner, J., P.G. Steffes, and J.M. Jenkins (1988). Laboratory measurements of the 7.5 - 9.38 mm absorption of gaseous ammonia (NH_3) under simulated Jovian conditions. Icarus 81, 386-395.

Kolbe, W.F., H. Buscher, and B. Leskovar (1977). Microwave absorption coefficients of atmospheric pollutants and constituents. J. Quant. Spec. Radiat. Transfer 18, 47-64.

Kuczkowski, R.L., R.D. Suenram and F.J. Lovas (1981). The microwave spectrum, structure, and dipole moment of sulfuric acid. J. Amer. Chem. Soc. 103, 2561-2566.

H.J. Liebe and T.A. Dillon (1969). Accurate foreign-gas-broadening parameters of the 22-GH H_2O line from refraction spectroscopy. J. Chem. Phys. 50, 727-732.

H.J. Liebe and D.H. Layton (1987). Millimeter-Wave Properties of the Atmosphere: Laboratory Studies and Propagation Modeling. NTIA Report 87-224, U.S. Dept. of Commerce.

Morris, E.C., and R.W. Parsons (1970). Microwave absorption by gas mixtures at pressures up to several hundred bars. Astron. J. Phys. 23, 335-349.

Poynter, R.L., and R.K. Kakar (1975). The microwave frequencies, line parameters, and spectral constants for NH_3. Astrophys. J. Suppl. 29, 87-96.

Rohart, F., D. Derozier, and J. Legrand (1987). Foreign gas relaxation of the J = 0 → 1 transition of $HC^{15}N$. A study of the temperature dependence by coherent transients. J. Chem. Phys. 87, 5794-5803.

Spilker, T.R. and V.R. Eshleman (1988). A new formalism for predicting microwave absorption by ammonia based on laboratory measurements under varying conditions. Bull. Amer. Astron. Soc. 20, 867.

Steffes, P.G. (1985). Laboratory measurements of the microwave opacity and vapor pressure of sulfuric acid under simulated conditions for the middle atmosphere of Venus. Icarus 64, 576-585.

Steffes, P.G. (1986). Evaluation of the microwave spectrum of Venus in the 1.2 to 22 centimeter wavelength range based on laboratory measurements of constituent gas opacities. Astrophysical Journal 310, 482-489.

Steffes, P.G., and V.R. Eshleman (1981). Laboratory measurements of the microwave opacity of sulfur dioxide and other cloud-related gases under simulated conditions for the middle atmosphere of Venus. Icarus 48, 180-187.

Steffes, P.G. and V.R. Eshleman (1982). Sulfuric acid vapor and other cloud-related gases in the Venus atmosphere: abundances inferred from observed radio opacity. Icarus 51, 322-333.

Steffes, P.G. and J.M. Jenkins (1987). Laboratory measurements of the microwave opacity of gaseous ammonia (NH_3) under simulated conditions for the Jovian atmosphere. Icarus 72, 35-47.

Tyler, G.L., and Howard, H.T. (1969). Refractivity of carbon dioxide under simulated Martian conditions. Radio Sci. 4, 899-904.

Waters, J.W. (1976). Absorption and emission by atmospheric gases. In Methods of Experimental Physics, 12, Atrophysics, Part B. pp. 142-176. Academic Press, New York.

N90-26746

HIGH RESOLUTION SPECTROSCOPY IN THE MICROWAVE AND FAR INFRARED

HERBERT M. PICKETT
Jet Propulsion Laboratory, California Institute of Technology, Pasadena, CA 91109

ABSTRACT

High resolution rotational spectroscopy has long been central to remote sensing techniques in atmospheric sciences and astronomy. As such, laboratory measurements must supply the required data to make direct interpretation of data for instruments which sense atmospheres using rotational spectra. Spectral measurements in the microwave and far infrared regions are also very powerful tools when combined with infrared measurements for characterizing the rotational structure of vibrational spectra. In the past decade new techniques have been developed which have pushed high resolution spectroscopy into the wavelength region between 25 μm and 2 mm. Techniques to be described include: (1) harmonic generation of microwave sources, (2) infrared laser difference frequency generation, (3) laser sideband generation, and (4) ultra high resolution interferometers.

INTRODUCTION

The rotational spectra of molecules provide a very sensitive probe for remote sensing in the atmospheres of planets and the interstellar medium. The rotational lines are very narrow and uniquely characteristic of the species observed. Since the lines can be observed in thermal emission, temperature can can often be determined. In addition, the profiles of the lines can be used to infer pressure and species abundance. When observations are made close to the planet, limb observations can be made with great sensitivity. Weight and power limitations have made limb observations impractical for observations of planets other than the Earth. However, nadir observations are still of great utility provided that there is sufficient contrast between sources of continuum emission (ground and clouds) and the molecular emission. A consequence of this limitation is that observations are most sensitive to areas of planetary atmospheres which are at a different temperature than the ground or the cloud tops.

To interpret the data, or indeed to determine the sensitivity of a potential instrument, it is essential for laboratory spectroscopy to determine the transition frequencies of the lines, their pressure broadening coefficients, and their strengths. It is also important to determine the spectra of all plausible molecules so that interfering lines are avoided. These needs are common to all regions of the spectra where high resolution observations are made. In fact, determinations of rotational spectra and infrared vibrational spectra have been combined in a powerful way to provide more accurate information for use in both spectral regions.[1]

The trend for planetary instruments which observe rotational lines is to evolve to higher frequency. The antenna optics become smaller with smaller wavelength and the absorption

coefficients of molecules generally become larger. Thus, there is both a size premium and a sensitivity premium in moving to higher frequency. In addition, many of the hydride molecules such as NH_3, PH_3, H_2O, HDO, CH_3D, and HCN have their predominant spectra in the far infrared. Other molecules such as CO and SO_2 have strong spectra throughout the far infrared. The difficulty with this region is that water in the Earth's atmosphere absorbs strongly, and so observations are best made from space. Technology for high resolution submillimeter and far infrared instruments is evolving rapidly and will form an important part of planetary observations in the future. In the next decade, application will be found in high altitude observatories, aircraft and balloons. Astrophysics missions such as the Large Deployable Reflector (LDR) and its precursors will provide significant measurement capability in the submillimeter wavelength region. Such measurement capability will be of little use to the planetary community unless an adequate laboratory spectral data base exists.

The emphasis of this paper will be on the new techniques for submillimeter and far infrared laboratory spectroscopy which have appeared in the past decade. With encouragement, these techniques can become important tools for laboratory measurements of planetary molecules.

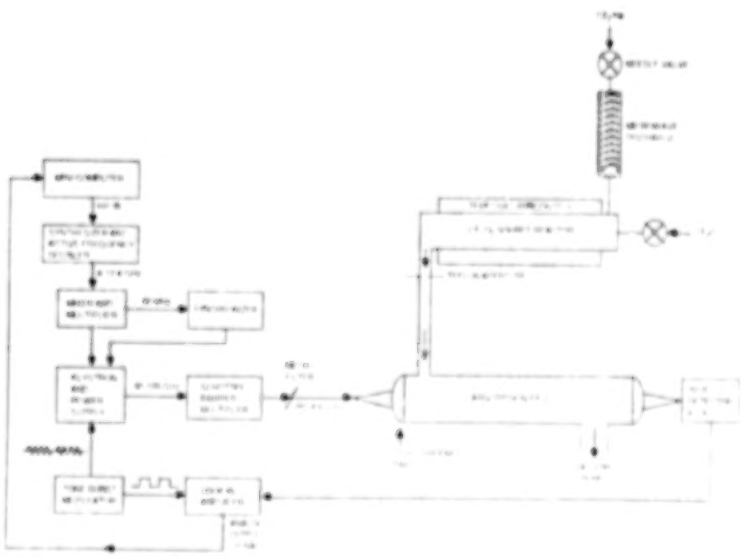

Fig. 1: Submillimeter Spectrometer Using Harmonic Generation

HARMONIC GENERATION

Harmonic generation is one of the oldest of the far infrared spectral techniques, and was developed by Walter Gordy and his students at Duke University.[2] Recently, several developments have made this technique more sensitive for routine measurements. The

method involves illuminating a diode with microwave power and detecting absorption with the harmonics of the microwave source. The general scheme for this is illustrated in Fig. 1.

The first development has been to replace the W-Si point contact diodes with monolithic Schottky diodes. The diodes we have used most successfully for this application have been produced by R. Mattauch at the University of Virginia.[3] Interestingly, the best types have been high frequency mixer diodes. Varactor diodes, while theoretically better for multiplication, suffer from excess diode capacitance. The best mount for high harmonic generation is still the simple crossed waveguide mount originally developed by Gordy. While more efficient mounts can be made for doubling or tripling, the task of terminating all the harmonics and idler frequencies becomes a very difficult design problem at higher multiples. Our experience is that the harmonic power in the simple crossed waveguide mount drops by 6-10 dB per harmonic.

The second development has been the use of sensitive liquid He cooled detectors. The best in the 0.3 - 2 mm region is the InSb hot electron bolometer.[4] Unlike most bolometers, the InSb bolometer has its limiting thermal conductance between the conduction electrons (which are heated by the far infrared radiation) and the lattice. Because of this the InSb bolometer is best mounted in good thermal contact with the liquid He cold surface. The response time is $< 1\mu$sec, making the detector more immune to 1/f noise in the source, but the sensitivity falls off above 20 cm^{-1}.

The third development has been the use of a dichroic plate to filter out the lower harmonics of the harmonic generator. These plates are designed after similar but much larger plates used to separate S and X band at the JPL Deep Space Network. In our application the plates are made of 1-2 mm thick aluminum and have a close-packed array of circular holes. Each of the holes act like a small circular waveguide. The plate reflects frequencies which are below the cut-off frequency of the waveguide. The plates have better than 80% transmission up to about twice the cut-off frequency, where diffraction starts becoming important. The highest frequency cutoff filter we have made has a 500 GHz (16.7 cm^{-1}) cutoff employing about 2000 holes of 0.25 mm diameter.

These developments have allowed us to make many studies of spectra in the 10-30 cm^{-1} region. An untouched example is shown in Fig. 2. It is the J,K = 3,3 inversion transition of ammonia in the $\nu_2 = 1$ excited state at 1073 049.708 MHz (35.79308 cm^{-1}).

LASER DIFFERENCE FREQUENCY GENERATION

Laser difference frequency generation is a technique developed by Ken Evenson and his co-workers at NBS (now NIST) in Boulder, CO.[5] The apparatus for two photon generation is shown in Fig. 3. Central to this technique is the W-NiO-Ni tunnel junction called a MIM diode which provides the non-linearity for mixing the two CO_2 lasers. One of these lasers is fixed in frequency and Lamb dip stabilized to an accuracy of 10 kHz. The second waveguide laser can be tuned over $\sim$ 100 MHz. Its frequency is determined by beating a portion of the output with a Lamb dip stabilized laser, which is lasing on the same CO_2 line, in a HgCdTe high speed detector. By choosing different laser transitions wide

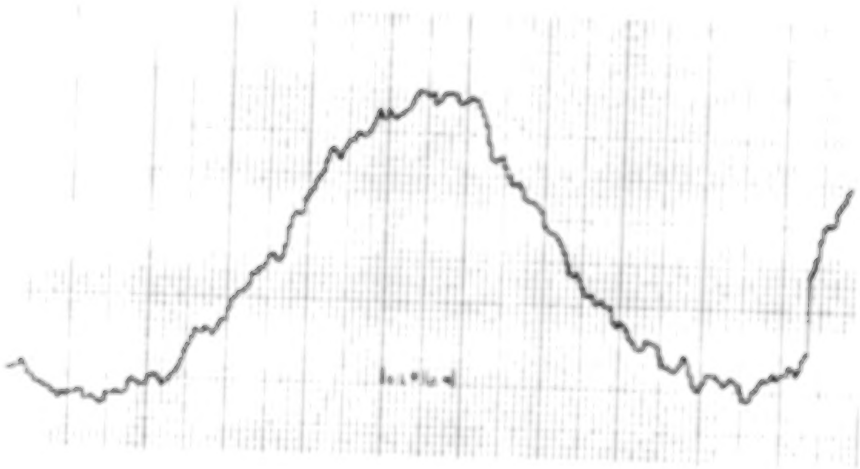

Fig. 2: NH_3 ν_2 inversion line for J.K = 3.3 at 1073 049.708 MHz

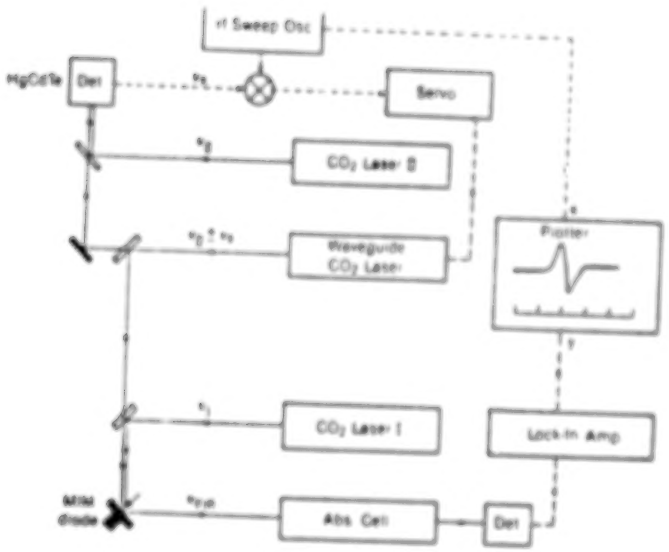

Fig. 3: Two Photon Laser Difference Generation

frequency coverage can be obtained in selected 100 MHz patches. Frequency accuracy is limited by ability to measure the peak position of the far infrared absorptions or $\sim$ 200 kHz.

In order to fill in the frequency coverage, Evenson has developed a three photon method in which two mid-infrared photons are combined with a microwave photon.[6] In this method, the two CO_2 lasers are both Lamb dip stabilized, and the tuning comes from the microwave

source. The optical layout is shown in Fig. 4. Frequency accuracy is comparable to the two photon method, but getting three wave mixing from the MIM diode is much more difficult.

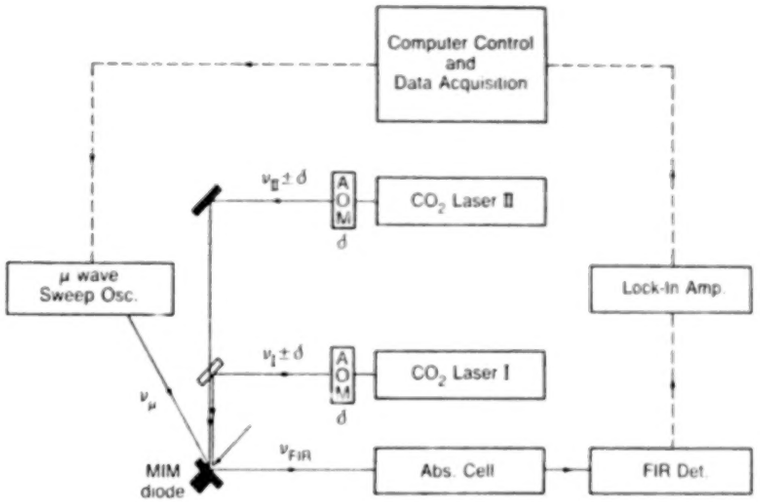

Fig. 4: Three Photon Laser and Microwave Difference Generation

Actually three far infrared frequencies are generated: one from the difference of the two infrared lasers, and two which are above and below the two photon frequency by an amount equal to the microwave frequency. These are readily distinguished by frequency modulating one of the lasers and observing the sense of the first derivative lineshape obtained under phase-sensitive detection while sweeping the microwave source.

LASER SIDEBAND GENERATION

Laser sideband generation involves mixing the output of a fixed-frequency far infrared laser with a microwave source to produce sidebands above and below the laser frequency. Early demonstrations of this technique were made by Dymanus in the Netherlands[7] and by a group at Lincoln Laboratory.[8] Our improvement of the technique at JPL proceeded concurrently with Evenson's work using infrared lasers. The goal of our work was to produce a source which had an accuracy of 100 kHz and had adequate power to make sensitive spectroscopic measurements. The far infrared laser is obtained by pumping a molecule such as methanol with a high power CO_2 laser and observing lasing from rotational transitions in the pumped vibrational state. While the output frequency is nominally at the rotational frequency, cavity and pump pulling effects make the laser frequency uncertain by as much as several MHz. Our strategy was to measure "today's" laser frequency by measuring a transition of known frequency before or after the unknown transition is measured. This required development of a very stable far infrared laser using Invar and active temperature stabilization.[9] A diagram of it is shown in Fig. 5. Interestingly, this laser also turned out

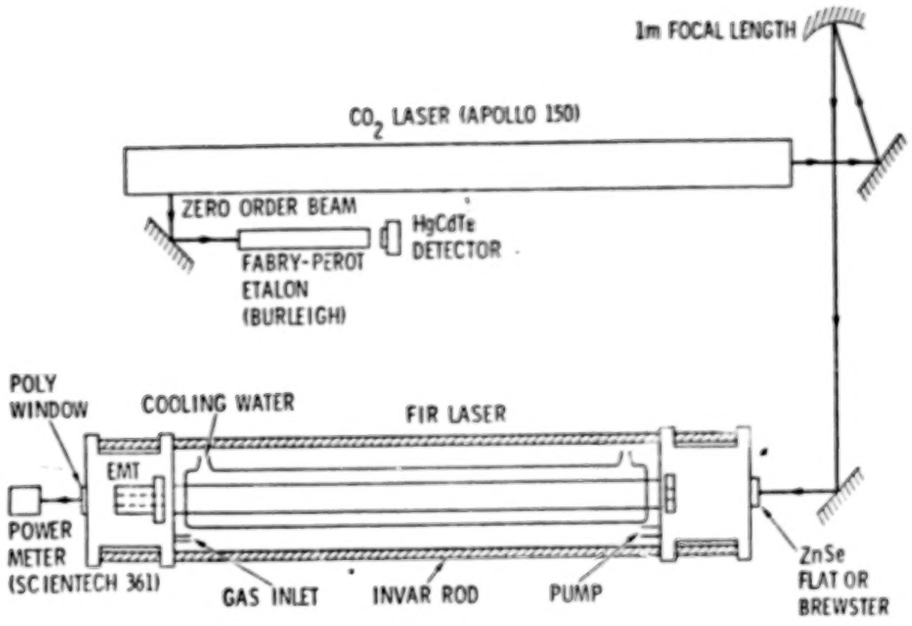

Fig. 5: Far Infrared Laser

to be a very high power laser, and our measured power of 1.25 W at 118 μm wavelength is probably a far infrared world record. More importantly, the frequency stability is < 100 kHz / hour.

In order to have usable sideband output power, it is essential to have a good way of separating sidebands from the laser. The way we chose to do this is shown in Fig. 6.[10] The

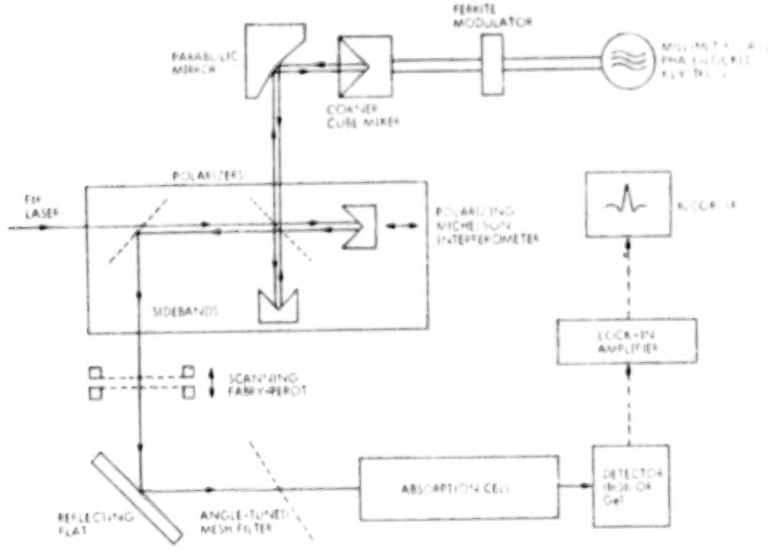

Fig. 6: Laser Sideband Generator

output from the laser passes through the analyzer polarizer and the polarizing Martin-

ORIGINAL PAGE IS
OF POOR QUALITY

Puplett interferometer such that it is not attenuated and arrives at the corner cube diode mount with the correct polarization. At the diode, the laser is mixed with the output of a mm wavelength klystron. The sidebands and the unused laser power are reflected from the corner cube back through the interferometer. If the optical path difference is $\sim \frac{1}{4}\times$ the wavelength of the microwave source, then the sideband polarization is rotated by 90° with respect to the laser. As a consequence, the sidebands are reflected off the analyzer polarizer toward the sample cell and detector. Frequently we use a Fabry-Perot resonator to discriminate between the sidebands and to provide further rejection of the laser. A typical length scan of this Fabry-Perot, shown in Fig. 7, clearly shows the two sidebands and the original laser frequency.

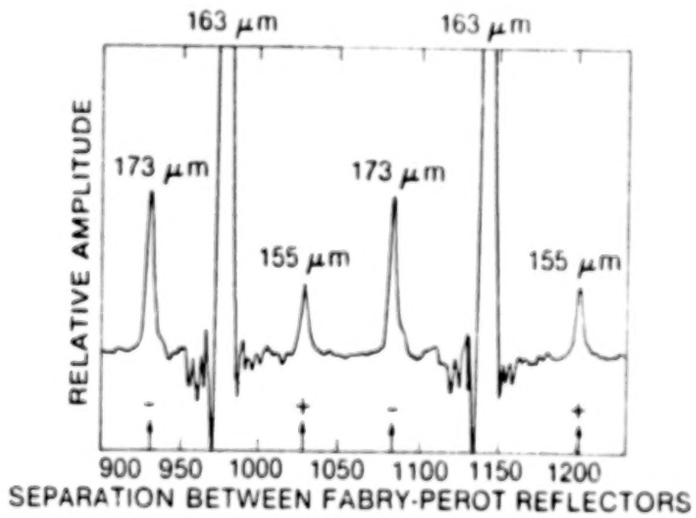

Fig. 7: Fabry-Perot Scan of Laser Sideband Output

Fig. 8 shows spectra obtained of ammonia and HDO using two cells in series. Accurate frequency measurements require a reference gas whose frequencies are known to the 100 kHz level, and whose doppler width facilitates accurate measurements. HDO is not a good reference gas in this sense, but CO is better since extensive laser difference measurements have been made on this gas.[11] An even better choice is a gas like SO_2, which has a narrower doppler width and a denser spectrum. We have calibrated SO_2 against the CO standard, and in addition have made several measurements of two SO_2 lines in the same laser sideband scan. In many cases, for example if the lines are P and R branch lines of different K, the difference in frequency is almost as valuable to the fit as the absolute frequency. The fit combining these far infrared determinations with microwave data is providing a very useful secondary standard for the laser sideband technique which is accurate to the level of our ability to measure the frequencies.

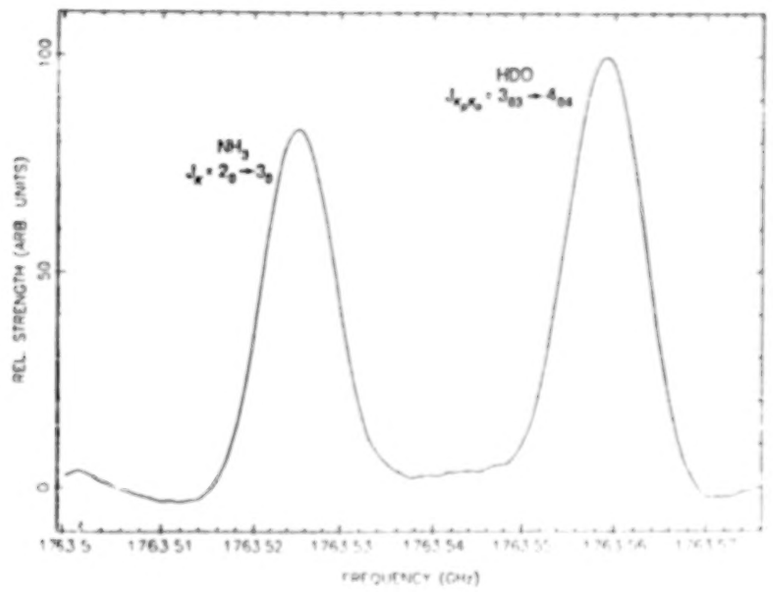

Fig. 8: Laser Sideband Spectrum of NH_3 and HDO

INTERFEROMETERS

There has been a steady improvement of both user-constructed and commercial far infrared interferometers. In the far infrared it is important to have large optics and high throughput so that resolution is not limited by diffraction. In the long wavelength region, the advantages of the polarizing Martin-Puplett design (in which a wire-grid polarizer forms the beam splitter) have been employed by B. Carli at IROE in Italy.[12] More common are the mylar beam splitter Michelson interferometers represented by the Bomem and Bruker instruments. The Bomem instrument in its highest resolution form has an optical path difference of 2.5 m, although J. Johns at the Hertzberg Institute in Canada has a modification to effectively double this difference.[13] The Brucker instrument in its highest resolution form has an optical path difference of 6 m, which represents a resolution of 0.0016 cm^{-1}. Last November JPL received delivery of the first Bruker of this resolution in this country. We are still in the process of characterizing this instrument, but an example of the spectra we have obtained is shown in Fig. 9. Unfortunately, the pressure is too high to display the spectra at the doppler limit, but an indication of the resolution is given by the splitting at 101.6 cm^{-1} which is 0.005 cm^{-1}. While the ultimate resolution of 50 MHz is not comparable to laser-based methods, it is very good for survey work and linewidth measurements.

CONCLUSIONS

The four techniques described here are both complementary and powerful. Harmonic generation is most useful for the millimeter wavelength end of the spectral region. High resolution interferometers are diffraction limited in this region, but are very accurate and

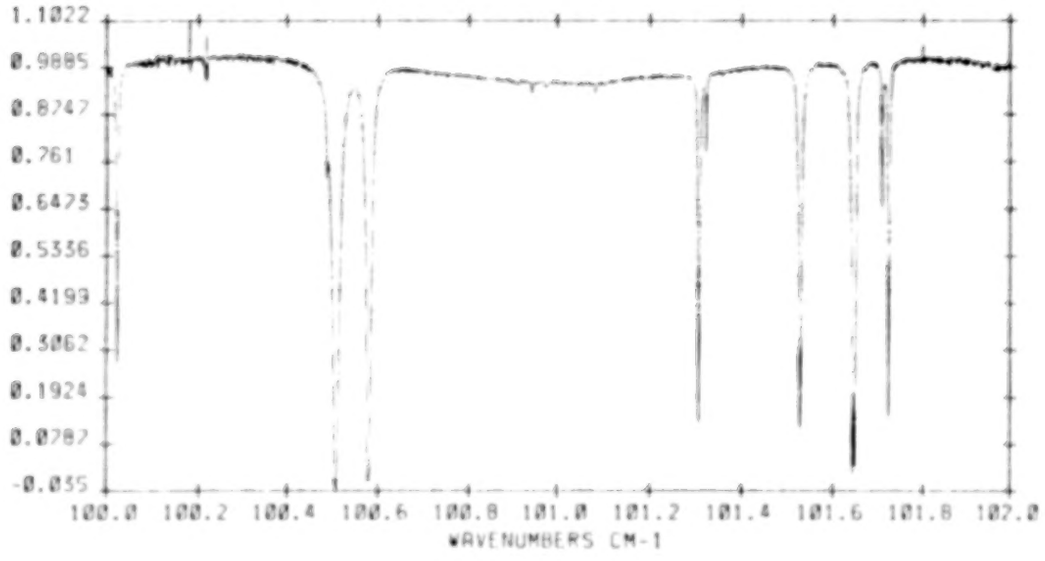

Fig. 9: Bruker Spectrum of HDO at 2 Torr Pressure

sensitive survey instruments at shorter wavelengths. The two methods for laser generation of tunable far infrared radiation are capable of higher resolution measurements on selected lines. Difference frequency generation has high absolute accuracy in frequency, but laser sideband generation is probably easier once suitable standards are available.

ACKNOWLEDGEMENT

Part of the research described in this paper was performed by Jet Propulsion Laboratory, California Institute of Technology, under contract with the National Aeronautics and Space Administration.

REFERENCES

1. H. M. Pickett, E. A. Cohen, L. R. Brown, C. P. Rinsland, M. A. H. Smith, V. Malathy Devi, A. Goldman, A. Barbe, B. Carli, and M. Carlotti, *J. Mol. Spec.* **128,** 151 (1988).

2. W. Gordy, and R. L. Cook, *Microwave Molecular Spectra, Techniques of Chemistry, Wiley, N. Y., Vol. XVIII,* (1984).

3. T. W. Crowe, and R. J. Mattauch, *IEEE Trans. Microwave Theory Tech.* **27,** 159 (1987).

4. M. A. Kinch, and B. V. Rollin, *Brit. J. Appl. Phys.* **14,** 672 (1963).

5. K. M. Evenson, D. A. Jennings, and F. R. Petersen, *Appl. Phys. Lett.* **44,** 576 (1984).

6. K. M. Evenson, D. A. Jennings, L. R. Zink, and K. R. Leopold, *11th Conf. Infrared and Mm. Waves, Pisa, Italy*, 267 (1986).

7. D. D. Bicanic, B. F. J. Zuiberg, and A. Dymanus, *Appl. Phys. Lett.* **32,** 367 (1978).

8. H. R. Fetterman, P. E. Tannenwald, B. J. Clifton, W. D. Fitzgerald, and N. R. Erickson, *Appl. Phys. Lett.* **33,** 151 (1978).

9. J. Farhoomand, and H. M. Pickett, *Int. J. Infrared and Mm. Waves* **8,** 441 (1987).

10. J. Farhoomand, G. A. Blake, M. A. Frerking, and H. M. Pickett, *J. Appl. Phys.* **57,** 1763 (1985).

11. I. G. Nolt, J. V. Radositz, G. DiLonardo, K. M. Evenson, D. A. Jennings, K. R. Leopold, M. D. Vanek, L. R. Zink, A. Hinz, and K. V. Chance, *J. Mol. Spec.* **125,** 274 (1987).

12. M. G. Baldecchi, B. Carli, M. Carlotti, G. DiLonardo, F. Forni, F. Mencaraglia, and A. Trombetti, *Int. J. Infrared and Mm. Waves* **5,** 381 (1984).

13. J. W. C. Johns, and J. Vander Auwera, *submittted to J. Mol. Spec.* , (1989).

N90-26747

HIGH RESOLUTION INFRARED SPECTROSCOPY OF PLANETARY MOLECULES USING DIODE LASERS AND FOURIER TRANSFORM SPECTROMETERS

DONALD E. JENNINGS

Planetary Systems Branch, Code 693, NASA Goddard Space Flight Center, Greenbelt, MD 20771

ABSTRACT

Modern observations of infrared molecular lines in planets are performed at spectral resolutions which are as high as those available in the laboratory. Analysis of such data requires laboratory measurements at the highest possible resolution, which also yield accurate line positions and intensities. For planetary purposes the spectrometer must be coupled to sample cells which can be reduced in temperature and varied in pressure. An approach which produces the full range of required molecular line parameters uses a combination of tunable diode lasers and Fourier transform spectrometers. The FTS provides broad spectral coverage and good calibration accuracy, while the diode laser can be used to study those regions which are not resolved by the FTS.

INTRODUCTION

The number of molecules known to be present in planetary atmospheres has grown tremendously in recent years. Ten planets and moons in the solar system have molecular atmospheres. These atmospheric bodies are listed in Table 1 (from Jennings, 1988). Spectra of the outer planets from the Voyager encounters show many molecular features, with Titan showing the greatest variety. The Voyager Infrared Interferometer Spectrometer (IRIS) has provided high spatial resolution infrared spectra of the Jupiter, Saturn, Uranus, and Neptune systems. With the aid of laboratory spectra from our program, IRIS identified six molecular species in Titan's atmosphere which had not been seen on planets (Maquire et al. 1981, Kunde et al. 1981, Samuelson et al. 1983). Condensed phases of complex organics have also been identified on Titan (Khana et al. 1987).

Ground-based spectrometers now have spectral resolutions high enough to completely resolve molecular line profiles on planets. Several types of high resolution spectrometer are used for ground-based and airborne observations of planets. Infrared laser heterodyne receivers have produced spectra of narrow molecular features on Mars, Venus and Jupiter (Betz et al. 1976, Kostiuk et al. 1983). Fourier transform spectrometers have been operated on large telescopes at Mt. Palomar (Connes and Michel 1975) and Kitt Peak (Hall 1976, Wiedemann et al. 1989), as well as the KAO

TABLE 1. MOLECULES IN THE SOLAR SYSTEM

OBJECT	MAJOR SPECIES	MINOR SPECIES
Venus	CO_2	H_2O, CO, HCl, HF
Earth	N_2, O_2	H_2O, CO_2, CH_4, NO, O_3, N_2O, CO, NH_3, HF, HCl...
Mars	CO_2	N_2, O_2, CO, H_2O, H_2, O_3, NO
Jupiter	H_2	NH_3, PH_3, CH_4, CH_3D, C_2H_6, C_2H_4, C_2H_2, H_2O, GeH_4, CO, HCN, HD
Io		SO_2
Saturn	H_2	NH_3, PH_3, CH_4, CH_3D, C_2H_6, C_2H_2, CO
Titan	N_2	H_2, CH_4, CH_3D, C_2H_2, C_2H_4, C_2H_6, C_3H_4, C_3H_8, C_4H_2, HCN, HC_3N, C_2N_2, CO_2, CO
Uranus	H_2	CH_4
Neptune	H_2	CH_4, C_2H_6
Triton	CH_4 (or N_2)	
Pluto	CH_4	
Sun		CO, C_2, CH, CN, NH, OH, MgH, CaH, TiO, SiH, ZrO, CoH, NiH, H_2O, H_2, SiO
Comets		C_2, C_3, CH, CN, CO, CS, NH, NH_2, OH, H_2O, S_2, HCN, CH_3CN, CO^+, CO_2^+, CH^+, H_2O^+, OH^+, N_2^+, CN^+

(Larson and Fink 1975). A Fabry-Perot spectrometer has observed molecules on Jupiter (Tokunaga et al. 1981, Drossart et al. 1986).

Our laboratory at Goddard Space Flight Center interacts closely with observational astronomers so that important infrared molecular problems can be identified and addressed early. The correct interpretation of a feature occurring in a planetary spectrum follows not only from information about the species which are known to be present, but also from knowledge of possible minor constituents which have spectra in the region of interest. Complete interpretation of planetary spectra requires knowledge of line frequencies and strengths, vibration-rotation constants, and line broadening coefficients (as functions of temperature). Laboratory determinations of these parameters must be continually refined to keep pace with the improving planetary results.

LABORATORY STUDIES RELATED TO PLANETARY OBSERVATIONS

Jovian C_2H_6 and C_2H_2

Our group has an ongoing program of observations of Jupiter in the 12-micron ethane band using our post-disperser coupled to the FTS at the Kitt Peak 4-meter telescope. An observed spectrum is shown in Figure 1. Prior to the observations we recorded a low temperature (140 K) laboratory spectrum of this ethane fundamental band with the 1-meter FTS located at the McMath telescope at Kitt Peak. The Jovian and laboratory spectra are compared in the figure. The features apparent in the Jovian spectrum are due to $^{12}C^{12}CH_6$. Elsewhere in the spectrum we have observed the RQ_0 Q-branch of $^{13}C^{12}CH_6$, which was not expected to be detectable. The detection of C-13 ethane, and the overall interpretation of the ethane spectra were greatly facilitated by the laboratory data.

During the same observations we measured acetylene line intensities near 755 cm^{-1} at various locations on the Jovian disk, including the "hot spot" identified by Caldwell et al. (1980). Our own laboratory spectra of acetylene, recorded with the 1-meter FTS, are being used to supply line strengths for the analysis of the Jovian data.

Support of Heterodyne Observations

Another observing technique which yields very high spectral resolution on planets is infrared heterodyning with CO_2 lasers. The Goddard Space Flight Center heterodyne receiver was used to detect narrow high-altitude emission lines from 12-micron ethane on Jupiter (Kostiuk et al. 1983). Before the search for this emission was begun a list was needed of precise frequencies for ethane transitions in the 12-micron band which would be within 0.1

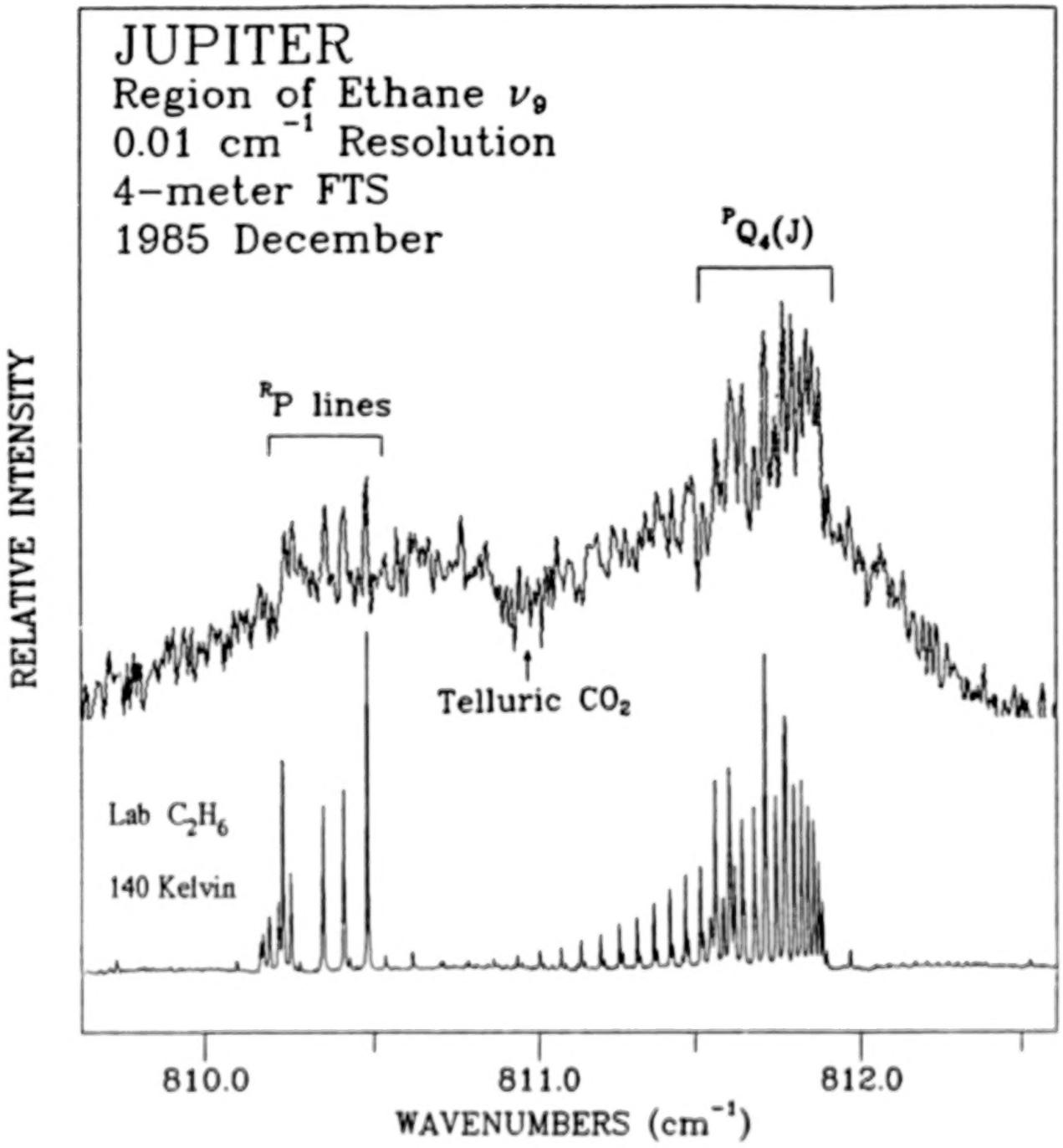

Figure 1. A portion of the high resolution FTS spectrum of ethane in Jupiter compared with a laboratory spectrum taken at 140 Kelvin (Jennings, 1988).

cm^{-1} of $^{14}CO_2$ laser lines at various geocentric source velocities, corresponding to dates on which the observations would take place. Ethane line intensities were also required to aid in choosing the strongest candidates for observation. This spectral information was derived from a combination of diode laser and FTS data for the 12-micron band. Thermal emission features due to the J=16 and 17 doublets, observed in the heterodyne spectra of Jupiter, are compared with diode laser spectra in Figure 2.

The 12-micron band of ethane is a prime candidate for study in the outer planets using high resolution instruments such as FTS and laser heterodyne spectrometers. We have published a laboratory analysis of this band (Susskind et al. 1982, Daunt et al. 1984). In that work Fourier transform spectra and diode laser spectra were combined to produce a complete characterization of the band. This culminated in a line atlas (Atakan et al. 1983) which is generally available to atmospheric modelers. Line broadening of ethane by hydrogen was measured at temperatures from 95 to 300 K (Halsey et al. 1988).

High Resolution Spectra of Hydrocarbons

Complex hydrocarbons gained a new degree of importance in planetary physics with the detection by Voyager of propane, diacetylene and methylacetylene on Titan (Maguire et al. 1981; Kunde et al. 1981). These added to the already known planetary hydrocarbons methane, acetylene, ethylene, and ethane. Because of the high line density in the infrared spectra of these molecules, very high spectral resolution is needed to resolve the rotational structure within bands when performing laboratory studies. It is important to completely resolve the line structure in these studies because only in this way can modeling of planetary spectra be correct in detail. Moreover, weaker hot band features which contribute to planetary spectra can only be studied by resolving the stronger main-band structure. High resolution laboratory spectra is, of course, also needed when individual line parameters (position, strength, broadening) are to be derived for use in high resolution observations of planets. We have devised a technique for double-passing the 1-meter FTS at Kitt Peak to improve its resolution to 0.0025 cm^{-1}. This was done in a simple manner (described in section 5.1) which retained the high quality of the spectra produced by this instrument. Spectra of many hydrocarbons (methane, methane-d, ethylene, ethane, propane, acetylene, methylacetylene, allene, and silane) were recorded for reference purposes, so that band structure and line parameters could be found when needed. These are supplemented with diode laser spectra in regions where doppler-limited resolution is required.

In addition to spectroscopy at mid-IR wavelengths, we have systematically studied the line intensities and pressure broadening parameters in the R-branch of $3\nu_3$ of methane near 1.1

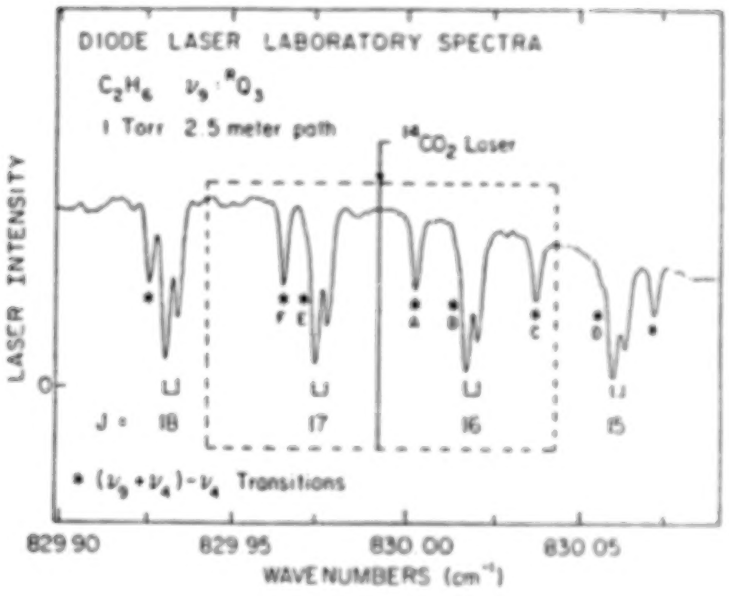

Figure 2a. Diode laser laboratory spectra in the region of $^RQ_3$ of ethane near 12 microns (Kostiuk et al. 1983).

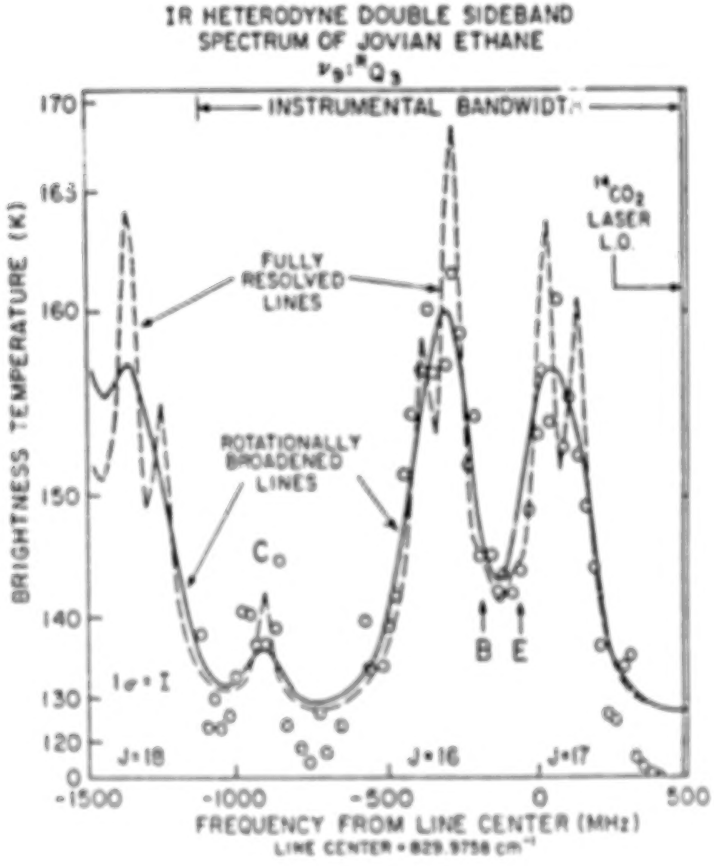

Figure 2b. Jovian stratospheric emission from ethane in the same region as Figure 2a, observed with the CO_2 laser heterodyne receiver (Kostiuk et al. 1983).

micron (Brault et al. 1981, Fox and Jennings 1985, Fox et al. 1988). These lines are important in that they can be observed on the outer planets using ground-based facilities. Broadening by hydrogen, helium, nitrogen and argon have been measured. We are new deriving pressure shifts of these lines, easily visible in the spectra (Fox and Jennings, 1989). This study has recently been extended to the ν_3 band at 3 microns.

Temperature Dependence of Line Broadening

A goal of this laboratory program since its beginning has been to measure the line broadening parameters for planetary molecules as a function of temperature. This temperature dependence is especially important in predicting the profiles of molecular bands in the outer planets where the temperature is well below "room temeprature." Extrapolating broadening parameters from 300 K laboratory results to ~150 K planetary conditions can introduce significant errors.

We have designed and constructed a low temeprature sample cell (described in section 5.3) which can be operated at any temperature between 50 and 300 K. We have completed a diode laser study of line broadening in the 12-micron band of ethane as a function of temperature (Halsey et al. 1988), and the results of this work are shown in Figure 3. The broadening follows a 1/T law, which is a stronger dependence on temperature than was expected from hard-sphere collision theory. We also regularly use the 1-meter FTS at Kitt Peak to record temperature dependent spectra at 0.0025 cm^{-1} resolution. Molecules whose spectra have been recorded at low temperature so far in our program are methane, ethylene, ethane, and propane.

Hot Bands of Acetylene and Ethane

One would expect, at the low temepratures of the outer planets, that hot bands of gases would be absent in observed spectra. Hot bands arise from lower levels which are above the vibrational ground state of a molecule. It is now apparent at high resolution, however, that hot bands do contribute to observed spectra. In heterodyne spectra of the 12-micron ν_9 band of ethane in Jupiter's stratosphere we found weak features due to $(\nu_9 + \nu_4)-\nu_4$. Drossart et al. (1985) detected $(\nu_4 + \nu_5)-\nu_5$ and $2\nu_5-\nu_5$ lines of acetylene near 14 microns in the north "hot spot" region of Jupiter. Molecules such as ethane and acetylene which have low-lying vibrational states can have significant populations in these states even at temperatures around 150 K. Hot band lines are very sensitive probes of atmospheric temperature in regions of line formation.

We have now begun identifying and analyzing hot bands in the 12-micron region of ethane and the 14-micron region of acetylene. Spectra have been recorded of both gases using the 1-meter FTS at

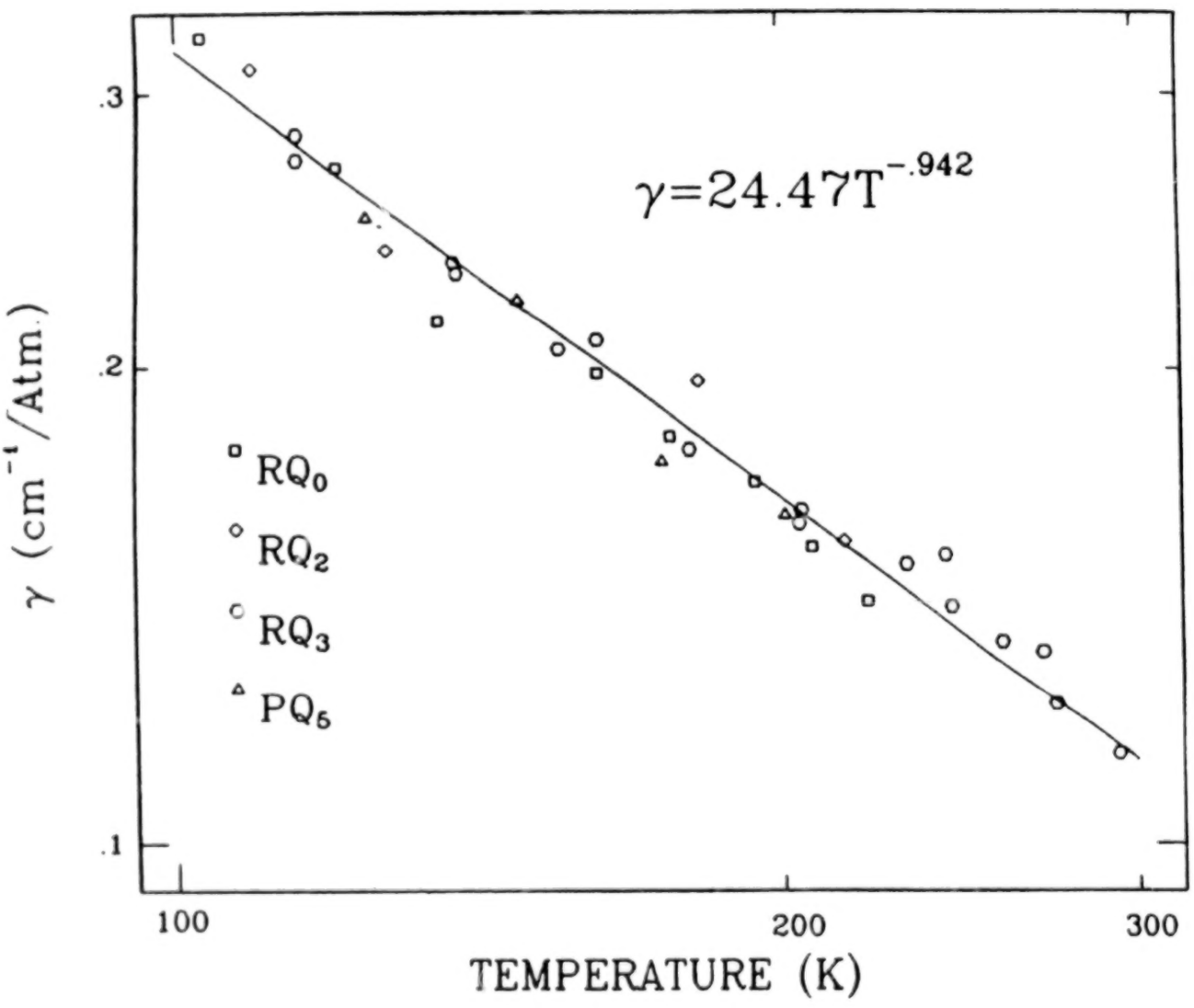

Figure 3. Temperature dependence of line broadening in the 12-micron band of ethane due to hydrogen. Note the log-log plot. (Halsey etal. 1988.)

Kitt Peak. We set the FTS up in double-pass configuration to give 0.0025 cm^{-1} resolution. The spectra were recorded with a variety of gas pressures and path lengths. From these spectra we identified seven hot bands in the ν_5 region of acetylene and have identified the major $(\nu_4 + \nu_9)$-ν_4 lines in ethane.

The 13-micron Spectrum of Propane

The 13-micron band of propane was identified by the Voyager 1 infrared spectrometer in the atmosphere of Titan (Maguire et al. 1981). Low resolution spectra were recorded by us for use in identifying propane in the Voyager spectra, and for deriving a band strength for the abundance determination.

Because of the complexity of the vibration-rotation structure in this band, very little laboratory work has been performed at high spectral resolution. It is important, however, to understand the detailed line structure in this region, because the band profile cannot be accurately modeled otherwise, and because the contributions from hot bands, which vary with temperature, cannot be predicted.

We have been pursuing an analysis of high resolution spectra of the 13-micron ν_{21} band of propane in our laboratory. An assymetric-rotor analysis of this band has produced preliminary rotation-vibration constants. These have been made available to the Voyager IRIS team. The analysis is based on high resolution FTS data (0.0025 cm^{-1}) recorded at Kitt Peak at both room temperature and 175 K (see Figure 4), as well as diode laser spectra. Diode laser spectra have also been used to measure pressure broadening of lines in the 13-micron band due to H_2, N_2, and He (Figure 5).

INSTRUMENTATION

We use two types of spectrometers to perform high resolution spectroscopy. The 1-meter Fourier transform spectrometer of the National Solar Observatory at Kitt Peak is used to provide up to 0.0025 cm^{-1} resolution in the 1-20 micron range. A tunable diode laser spectrometer provides ~10^{-4} cm^{-1} resolution in the regions where the structure is not sufficiently resolved by the FTS.

Fourier Transform Spectroscopy

The high resolution FTS used in this work is operated by the National Solar Observatory and is a facility instrument at the McMath Solar Telescope at Kitt Peak. This 1-meter path difference interferometer can be operated in the single-sided interferogram mode with a resolution 0.005 cm^{-1}. The spectral coverage with several beamsplitters is from the ultraviolet to 20 microns

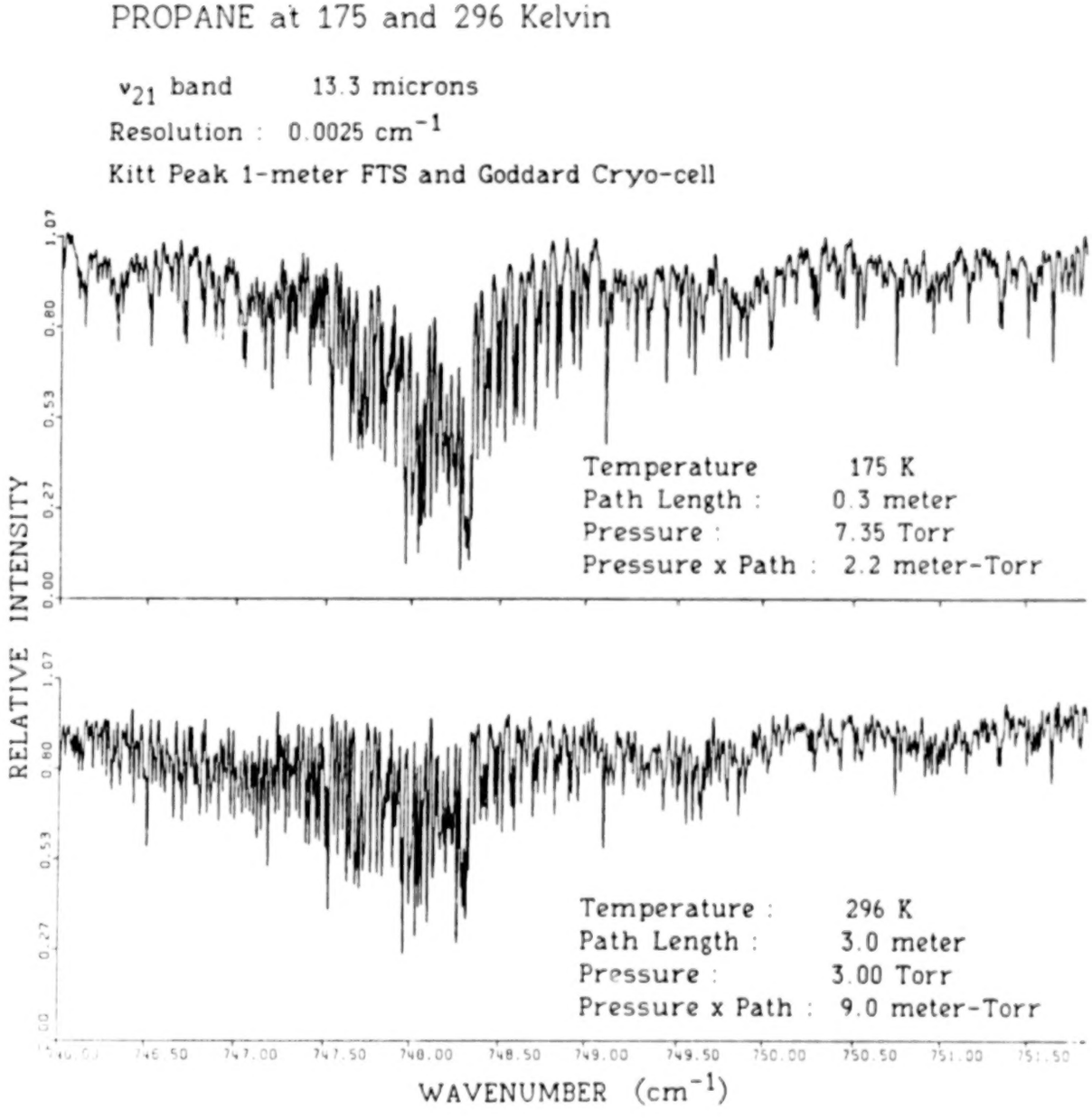

Figure 4. Comparison of the Q-branch region in the 13-micron band of propane at room temperature and at 175 K.

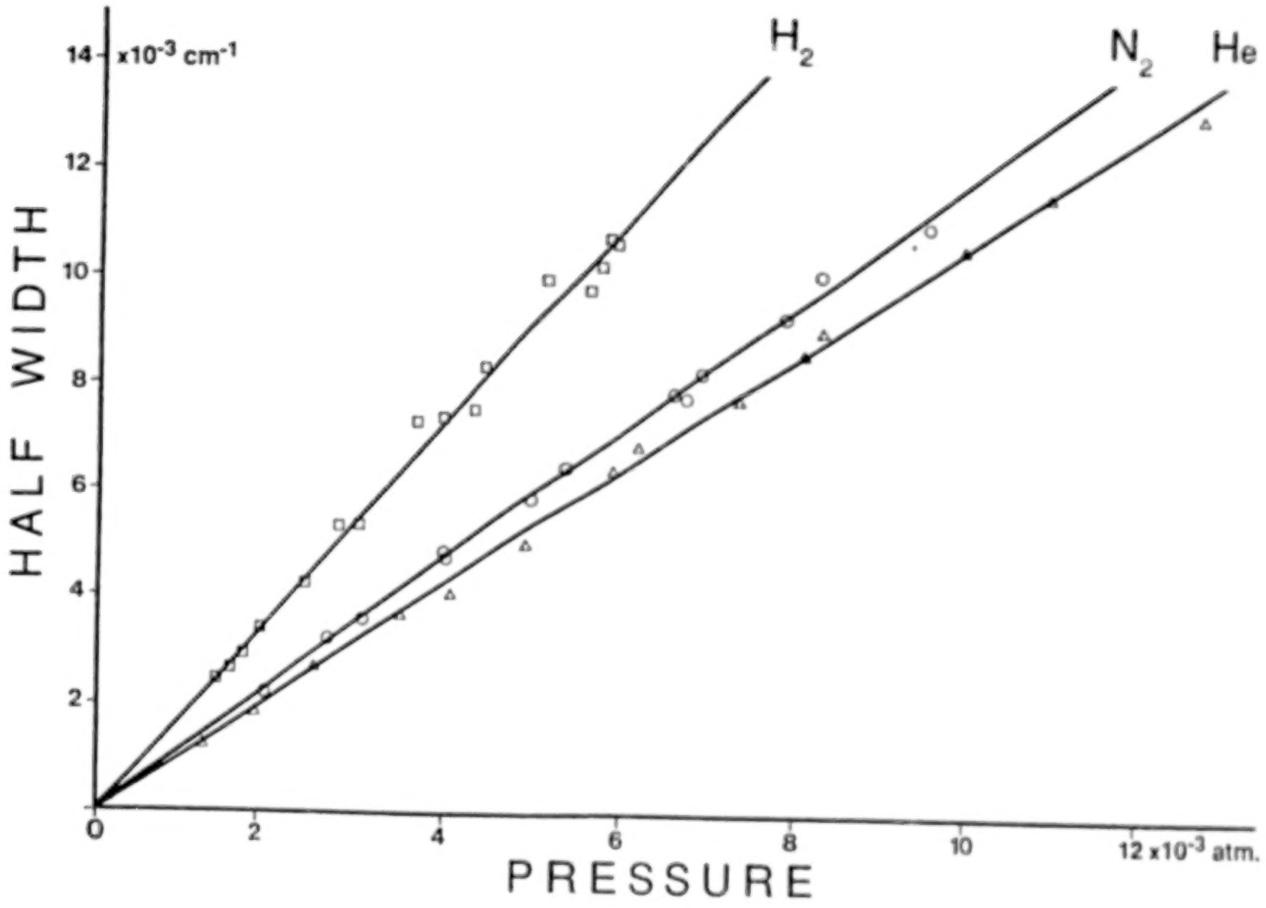

Figure 5. Plots of the foreign-gas broadening widths (HWHM) as functions of pressure for propane broadened by hydrogen, nitrogen, and helium (Nadler and Jennings 1989).

wavelength. Absolute calibration accuracy throughout this range exceeds 10^{-4} cm^{-1}. A variety of auxiliary equipment is available for laboratory spectroscopy using this instrument, including a 6-meter multiple traversal sample cell adjustable to 434 meters path.

The technique for double-passing the 1-meter FTS at Kitt Peak (Jennings, et al. 1985) is described by Figure 6. In conventional operation the instrument uses separated beamsplitter and recombiner, accepting radiation from two input ports and sending it to two output ports. The second input is not normally used for laboratory work with this instrument. To double the optical retardation of the instrument we place two mirrors and a compensator in the beams before the recombiner. These mirrors return the beams through the cat's-eyes to the beamsplitter and the modulated signal is detected at the second input. When single-sided interferograms are run the maximum optical retardation is 2 meters, yielding 0.0025 cm^{-1} resolution.

Diode Laser Spectroscopy

A schematic of the GSFC tunable diode laser spectrometer is shown in Figure 7. Th figure is taken from detailed desciptions of the spectrometer which have appeared in the literature (Jennings 1980, 1988). The instrument uses diode lasers manufactured by Laser Analytics which are mounted in a closed-cycle mechanical helium refrigerator. Coarse tuning of the laser frequency is accomplished by adjusting the refrigerator temperature in the range 9-80 K. The laser frequency is fine-tuned by sweeping the injection current. Devices have been invented in this laboratory for stabilizing the output frequency of diode lasers operated on methanical refrigerators (Jennings and Hillman 1977a,b).

The spectrometer is dual-beam, permitting sample spectra to be recorded simultaneously with either reference spectra or calibration etalon fringes. The optical beam is divided between two paths with either a rotating mirror chopper or wedged beamsplitter. Each path can accommodate a one-meter long absorption cell or combinations of etalons and cells. A multiple-traversal cell (up to 140 meters) can be inserted into one of the beam paths before the detector. The other beam is passed through an etalon to generate calibration fringes. Confocal etalons are used for calibrating the diode spectra; a 50 cm etalon produces fringes with 0.005 cm^{-1} spacing and 0.0001 cm^{-1} widths (Jennings 1984).

Data acquisition and recording is done using signal averaging. The diode laser is modulated at about 50 Hz and successive sweeps are averaged. The two detector signals are accumulated separately. For strong laser outputs the signal-to-noise can approach 10^4 after 30 seconds of accumulation. The advantage of signal averaging in this manner is that the diode mount

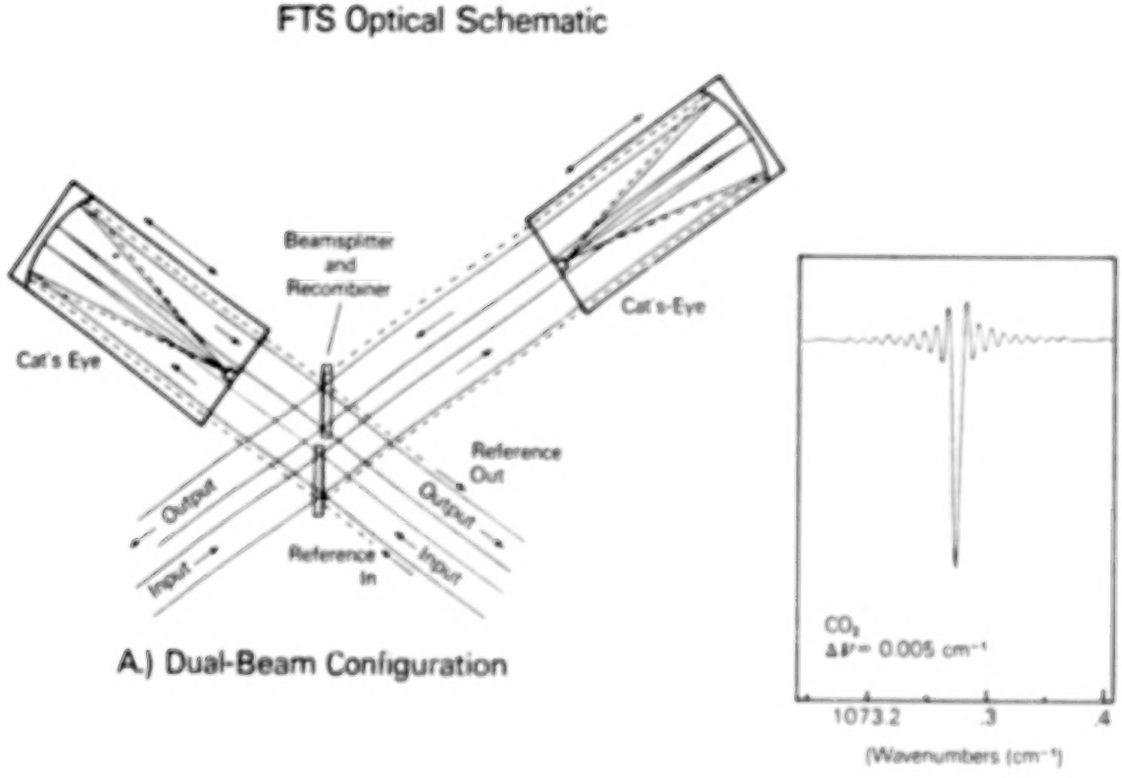

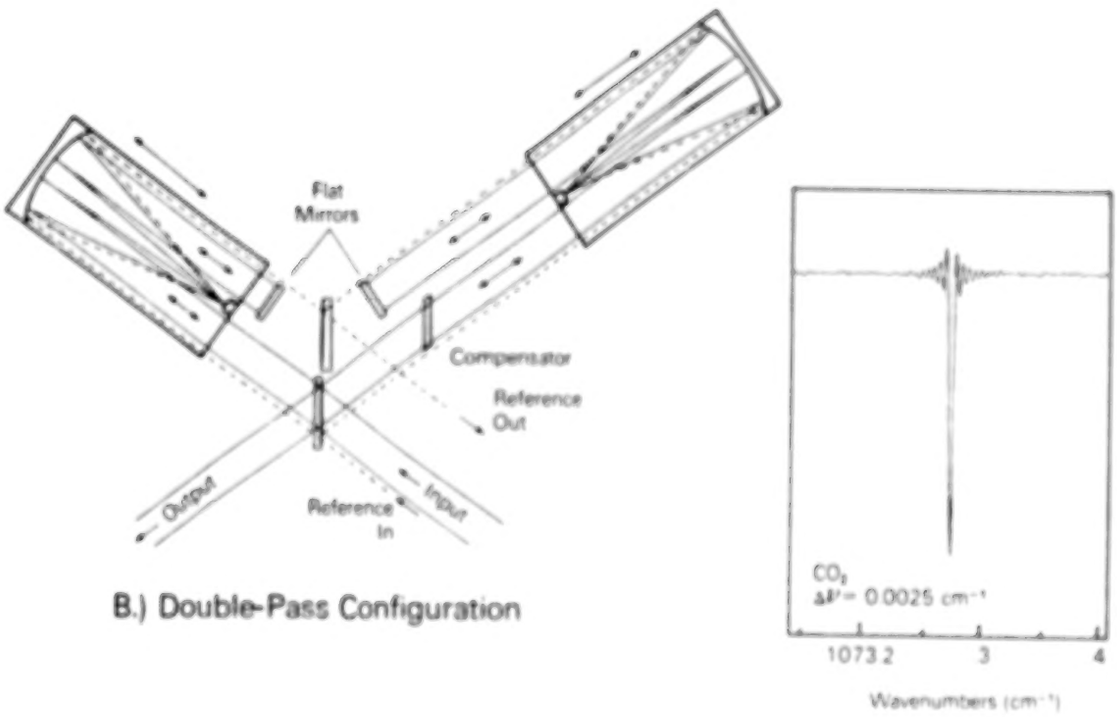

Figure 6. Single-pass (A) and double-pass (B) configurations of the 1-meter FTS at Kitt Peak (Jennings *etal*. 1985).

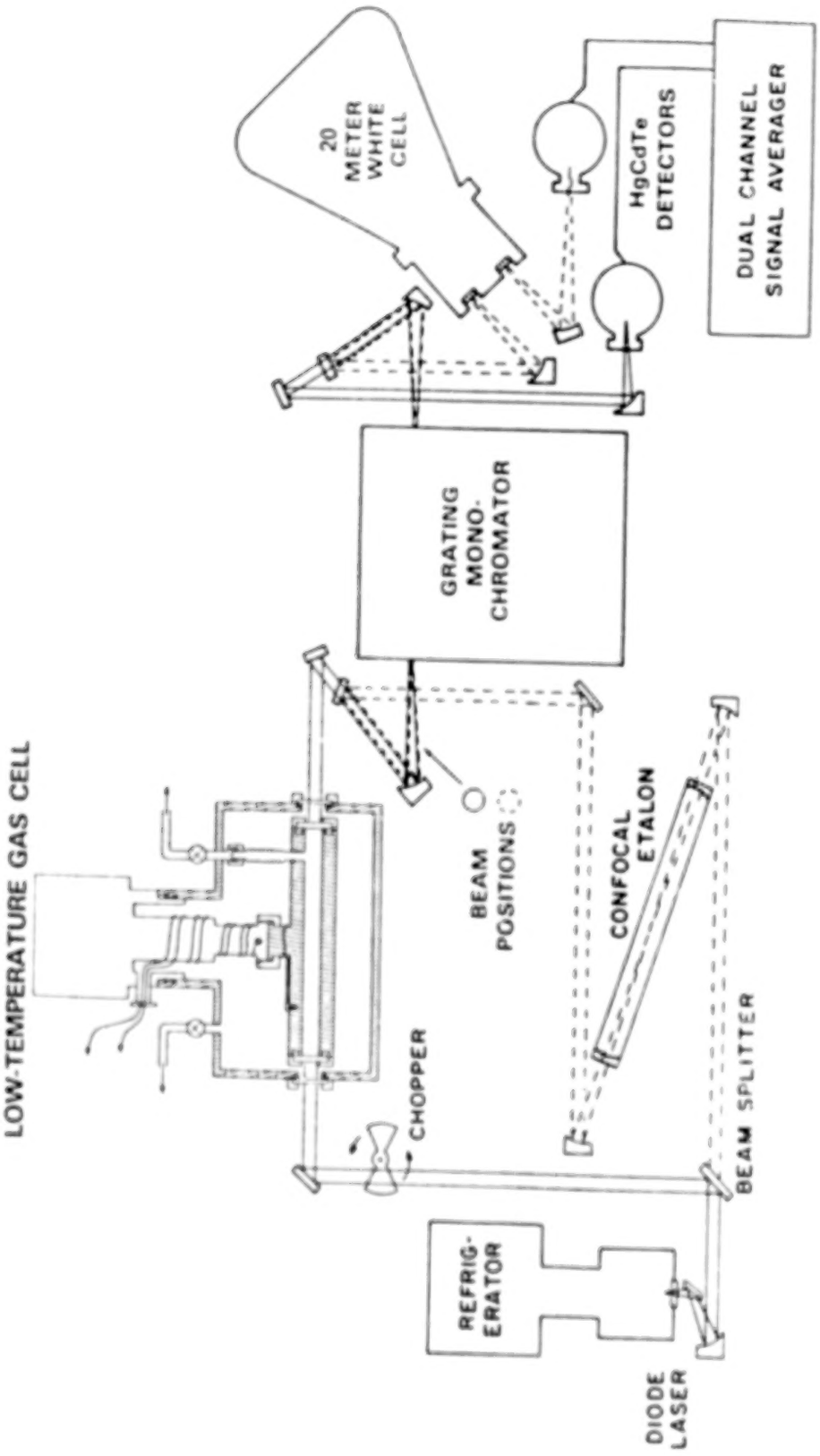

Figure 7. Schematic of the diode laser spectrometer.

temperature reaches equilibrium with the average laser current and does not change during a scan. Temperature dependent variation of frequency sweep rate and laser output structure are thereby eliminated. Moreover, calibration fringe spacings in the spectrum do not vary. This eliminates a common source of calibration error.

We use deconvolution as a method for improving measurements of line positions and intensities when the Doppler linewidth causes blending in diode laser spectra (Halsey et al. 1985). In this manner were are able to remove the Doppler, Lorentz, and laser linewidths, making blended structure more visible. The final linewidth is less than 0.0003 cm^{-1}.

Temperature-Variable Sample Cell

We have constructed a low-temperature absorption cell which can be operated anywhere between 300 and 50 Kelvin. In this design a closed-cycle helium refrigerator is connected directly to a 30-cm long straight-path cell which is mounted inside a vacuum chamber. With ZnSe windows the cell can be used anywhere in the 0.6 to 20 micron range. The cell is described in detail by Halsey et al. (1988) and Jennings (1988). Figure 4 shows a portion of the Q-branch region in the 14-micron band of propane recorded at room temperature and at 175 K. Note the elimination of many lines at low temperature, simplifying the line structure.

REFERENCES

Atakan, A. K., W. W. Blass, J. W. Brault, S. J. Daunt, G. W. Halsey, D. E. Jennings, D. C. Reuter, and J. Susskind 1983, NASA Tech. Memorandum 85108.

Betz, A. L., M. A. Johnson, R. A. McLaren, and E. C. Sutton 1976, Astrophys. J. Letters, 247, L101.

Brault, J. W., K. Fox, D. E. Jennings, and J. W. Margolis 1981, Astrophys. J. Letters, **247**, L101.

Caldwell, J., A. T. Tokunaga, F. C. Gillett 1980, Icarus, **41**, 667.

Connes, P., and G. Michel 1975, Appl. Opt., **14**, 2067.

Daunt, S. J., A. K. Atakan, W. E. Blass, G. W. Halsey, D. E. Jennings, D. C. Reuter, J. Susskind, and J. W. Brault 1984, Astrophys. J., **280**, 921.

Drossart, P., B. Bezard, S. Atreya, J. Lacy, E. Serabyn, A. Tokunaga, and Encrenaz 1986, Icarus, **66**, 610.

Fox, K., and D. E. Jennings, 1985, JOSRT, **33**, 275.

Fox, K,. and D. E. Jennings 1989, JOSRT, **42**, 201.

Fox, K., and D. E. Jennings, E. A. Stern, and R. Hubbard 1988, JOSRT, **39**, 473.

Hall, D. N. B., 1976, J. Opt. Soc. Am., **66**, 1081.

Halsey, G. W., J. J. Hillman, S. Nadler and D. E. Jennings 1988, JOSRT, **39**, 429.

Halsey, G. W., D. E. Jennings, and W. E. Blass 1985, JOSA B, **2**, 837.

Jennings, D. E. and J. J. Hillman 1977a, Rev. Sci Instrum., **48**, 1568.

Jennings, D. E. and J. J. Hillman 1977b, Rev. Sci Instrum., **48**, 1716.

Jennings, D. E.1980, Appl. Optics, **19**, 2695.

Jennings, D. E.1984, Appl. Optics, **23**, 1299.

Jennings, D. E.1988, JOSRT, **40**, 221.

Jennings, D. E., R. Hubbard, and J. W. Brault 1985, Appl. Optics, **24**,3438.

Khana, R. K., M. A. Perera-Jarmer, and M. J. Ospina 1987, Spectrochim. Acta Part A, **43**, 421.

Kostiuk, T., M. J. Mumma, F. Espenak, D. Deming, D. E. Jennings, and W. Maguire, 1983, Astrophys. J., **265**, 564.

Kunde, V. G., A. C. Aikin, R. A. Hanel, D. E. Jennings, W. C. Maguire, and R. E. Samuelson 1981, Nature, **292**, 686.

Larson, H. P. and U. Fink 1975, Appl. Opt., **14**, 2085.

Maguire, W. C., R. A. Hanel, D. E. Jennings, V. G. Kunde, and R. E. Samuelson, 1981, Nature, **292**, 683.

Nadler, S., and D. E. Jennings 1989, JOSRT, **42**, 399.

Samuelson, R. E., W. C. Maguire, R. A. Hanel, V. G. Kunde, D. E. Jennings, Y. L. Yung, and A. C. Aikin 1983, JGR, **88**, 8709.

Susskind, J., D. Reuter, D. Jennings, S. Daunt, W. Halsey, W. Blass 1982, J. Chem. Phys., **77**, 2728.

Tokunaga, A. T., S. C. Beck, T. R. Geballe, J. H. Lacy, and E. Serabyn 1981, Icarus, 48, 283.

Wiedemann, G. R., D. E. Jennings, R. A. Hanel, V. G. Kunde, S. H. Moseley, G. Lamb, M. D. Petroff, and M. G. Stapelbroek 1989, Appl. Opt., 28, 139.

N90-26748

LABORATORY STUDIES, ANALYSIS, AND INTERPRETATION OF THE SPECTRA OF HYDROCARBONS PRESENT IN PLANETARY ATMOSPHERES INCLUDING CYANOACETYLENE, ACETYLENE, PROPANE, AND ETHANE

WILLIAM E. BLASS*, STEPHEN J. DAUNT*,**, ANTONI V. PETERS** and MARK C. WEBER*
*Department of Physics and Astronomy, The University of Tennessee, Knoxville, TN 37996-1200, **Department of Chemistry, Concordia University, Montreal, P.Q. H3G 1M8 Canada

ABSTRACT

Combining broadband FTS data from the McMath facility at NSO and from NRC in Ottawa and narrow band TDL data from our laboratories with novel computational physics techniques has produced a broad range of results for the study of planetary atmospheres.

Motivation for our effort flows from the Voyager/IRIS observations and the needs of Voyager analysis for laboratory results. In addition, anticipation of the Cassini mission adds incentive to pursue studies of observed and potentially observable constituents planetary atmospheres.

Current studies include cyanoacetylene, acetylene, propane, and ethane. Particular attention is devoted to cyanoacetylene (HC_3N) which is observed in the atmosphere of Titan. The results of a high resolution infrared laboratory study of the line positions of the 663, 449, and 222.5 cm^{-1} fundamental bands are presented. Line positions, reproducible to better than 5 MHz for the first two bands, are available for infrared astrophysical searches. Intensity and broadening studies are in progress.

Acetylene is a nearly ubiquitous atmospheric constituent of the outer planets and Titan due to the nature of methane photochemistry. Results of ambient temperature absolute intensity measurements are presented for the fundamental and two two-quantum hotband in the 730 cm^{-1} region. Low temperature hotband intensity and linewidth measurements are planned.

CYANOACETYLENE

The infrared spectra of two of the bending fundamentals of HC_3N have been observed by Voyager/IRIS in the atmosphere of Titan. The results of a high resolution infrared laboratory study of the ν_5, ν_6, and ν_7 fundamental bands are presented. A complimentary study of ν_5 and ν_6 is in progress at Orsay.[1]

Fourier transform spectra were recorded at the Herzberg Institute for Astrophysics in Ottawa on a Bomem DA.003 interferometer. The ν_5 and ν_6

bending fundamentals were recorded at 0.004cm^{-1} while ν_7 was recorded at somewhat lower resolution. Rotational structure has been assigned for J values up to 78. Ground state constants from a global analysis are in excellent agreement with those derived from microwave data.[7] Upper state constants, including ℓ - doubling parameters are obtained. Analysis results, retrieved using the statistically controlled regression system described below, are presented in Tables I-III. Line positions reproducible to better than 0.2 x10^{-3}cm^{-1} (~5MHz) for ν_5 and ν_6 should facilitate infrared astrophysical searches. The positions for ν_7 are estimated to be good to 0.7 x 10^{-3}cm^{-1}.

Improved spectra for the long wavelength region have been acquired and are being prepared for analysis. Upon completion of the analysis of the new data, generation of a spectral atlas including line lists is planned.

ACETYLENE

Understanding of acetylene spectral features observed in the laboratory with high-resolution is a prerequisite for quantitative analyses of acetylene spectra in the planetary atmospheres of Titan, Saturn, and Jupiter. Line-intensity measurements on $^{12}C_2H_2$ near 13.7μm were made using a swept-frequency tunable diode-laser spectrometer[5,6] with resolution of 0.0005 cm^{-1}. Vibrational band intensities S_v^o at 300K which were determined from the line-intensity measurements are 560(17) cm^{-2}atm^{-1} for the ν_5-fundamental band of $^{12}C_2H_2$, 13.5(3) cm^{-2}atm^{-1} for the$(\nu_4+\nu_5)^{0^-}$-$\nu_4^{0^+}$ hotband of $^{12}C_2H_2$, and 13.8(1) cm^{-2}atm^{-1} for the$(\nu_4+\nu_5)^{0^+}$-$\nu_4^{0^-}$ hotband of $^{12}C_2H_2$.

Neglecting the rotation-vibration interaction, the intensity of an individual transition S_J can be directly related to the (vibrational) band intensity S_v^o as[5,6]

$$S_J = S_v^o [g_J \exp(-BJ(J+1)hc/kT)/Q_r] \cdot [1-\exp(-\nu_o hc/kT)] \times$$

$$\times A(J,\Delta J,\ell,\Delta\ell), \qquad (1)$$

where ν_o is the band-center frequency and $A(J,\Delta J,\ell,\Delta\ell)$ is the Honl-London factor.[7]

TABLE I

RESULTS OF THE ANALYSIS OF THE ν_5 BAND OF CYANOACETYLENE[a]

	THIS WORK	IR/MW[b]	IR[c]	MW[d]
ν_0	663.36639(17)	663.361(12)[e]	663.37378(98)[e]	-.-
B_0	0.15173928(209)	-.-	-.-	0.151740238(39)
$\alpha^B(10^5)$	-5.4311(66)	-6.047(37)	-1.143(78)[f] [-1.120(14)[g]]	-5.613(19)
D_0	$1.800(26) \times 10^{-8}$	-.-	-.-	$1.8116(45) \times 10^{-8}$
β^J	$0.659(14) \times 10^{-10}$	$3.56(4.70) \times 10^{-9}$	-.-	$-2.840(3) \times 10^{-9}$
H_0	0.0	-.-	-.-	-.-
δ^J	$-1.37(27) \times 10^{-14}$	-.-	-.-	-.-
q	$8.622(13) \times 10^{-5}$	$8.573(90) \times 10^{-5}$	-.-	$8.4638(37) \times 10^{-5}$
q^J	$1.835(73) \times 10^{-10}$	0.0[h]	-.-	0.0[h]

---

[a] All parameters in units of cm^{-1}. Values in parentheses are error estimates of 3σ.

[b] IR: Mallinson and Fayt, Mol. Phys. 32, 473 (1976); MW: Mallinson and de Zafra, Mol. Phys. 36, 827 (1978).

[c] Yamada and Bürger, Z. Naturforsch. 41a, 1021 (1986).

[d] Yamada and Creswell, J. Mol. Spectrosc. 116, 384 (1986).

[e] Corrected from reported values by $-l^2B_v$ term.

[f] $\alpha^B_{eff} = \alpha^B + \frac{1}{4}q$ for the P and R transitions studied in their work.

[g] Calculated from their α^B_{eff} and our q value.

[h] Assumed value by these workers.

TABLE II

RESULTS FROM THE ANALYSIS OF THE ν_6 BAND OF CYANOACETYLENE[a]

	INFRARED	MICROWAVE[b]
ν_0	498.953 37 (90)	[498.953 66 (1 17)][IR,c]
B_0	0.151 740 21 (1 45)	0.151 740 238 (39)
α^B	$-3.085\ 84\ (59) \times 10^{-4}$	$-3.087\ 55\ (65) \times 10^{-4}$
D_0	$1.810\ 2\ (29\ 4) \times 10^{-8}$	$1.811\ 6\ (4\ 5) \times 10^{-8}$
β^J	$-2.954\ (174) \times 10^{-10}$	$-3.796\ (800) \times 10^{-10}$
q	$1.195\ 6\ (10\ 0) \times 10^{-4}$	$1.194\ 45\ (18) \times 10^{-4}$
q_J	$2.69\ (87) \times 10^{-11}$	0.0[d]

$N/N_0 = 162/166$

$\sigma = 2.35 \times 10^{-4}\ cm^{-1}$

---

[a]All parameters in units of cm^{-1}. Values in parentheses are error estimates of 3σ.

[b]Yamada and Creswell, J. Mol. Spectrosc. 116, 384 (1986).

[c]Yamada and Bürger, Z. Naturforsch. 41a, 1021 (1986).

TABLE III

RESULTS FROM THE ANALYSIS OF THE ν_7 BAND CYANOACETYLENE[a]

	INFRARED	MICROWAVE[b]
ν_0	222.565 347 (329)	222.554 (15) [IR,c]
B_0	0.151 739 74 (52)	0.151 740 238 (39)
α^B	-4.806 53 (1 66) x 10^{-4}	-4.821 68 (59) x 10^{-4}
D_0	1.869 2 (73 8) x 10^{-8}	1.811 6 (4 5) x 10^{-8}
β^J	UD	-8.148 97 (72) x 10^{-10}
q_7	2.170 36 (332) x 10^{-4}	2.180 939 (390) x 10^{-4}

$N/N_0 = 144/144$

$\sigma = 0.81 \times 10^{-4}$ cm^{-1}

---

[a]All parameters in units of cm^{-1}. Values in parentheses are error estimates of 3σ.

[b]Yamada and Creswell, J. Mol. Spectrosc. 116, 384 (1986).

[c]Mallinson and Fayt, Mol. Phys. 32, 473 (1976).

Equation (1) can be used as a linear least squares model for band intensity retrieval using observed line strengths as data. Incorporation of a Herman-Wallis term is particularily simple using this technique. The results below were obtained using this model and are thus least squares estimators of the band intensies.

We used direct width measurements and peak transmittance results for intensity retrieval. The results were verified in a number of cases by direct fitting of a Voigt profile to the observed data. In addition, the equivalent width method[8,9] was applied to several transitions to check the peak transmittance results. The two methods were consistent to better than 4%. Table IV presents the equivalent width/peak transmittance comparison. Table V presents present results for acetylene intensities in the 14μm region.

Table IV. Selected line-intensities from ν_5 determined using the method of equivalent widths. The parameter a is the dimensionless Voigt parameter defined as $a=(b_L/b_D)\sqrt{\ln 2}$. For the Lorentz width b_L the following average self-broadening coefficient γ_L retrieved by P. Varanasi, L.P. Giver and F.P.J. Valero, JQSRT 30, 497(1983a) is assumed: $\gamma_L=0.15 cm^{-1}/atm$. Measurements were carried out at 298K. The averaged line-intensities derived from equivalent width measurements are listed in the sixth column (EQ), and those derived from the peak transmittance determinations (PT) are presented in the last column for comparison.

Line Identification	p [mtorr]	ℓ [cm]	a [10^{-2}]	W equ.wdth [$10^{-3} cm^{-1}$]	S_J $cm^{-2}atm^{-1}$	S_J avg. (EW) $cm^{-2}atm^{-1}$	S_J avg. (PT) $cm^{-2}atm^{-1}$
$Q^{(1)}(3)^+$	71.3	2.54	1.325	2.120	15.805		
	58.5		1.087	1.900	15.876	**15.62**	**15.74**
	48.7		0.905	1.668	15.449		
	39.3		0.730	1.438	15.356	±0.22	±0.117
	29.2		0.542	1.172	15.620		
$Q^{(1)}(6)^+$	96.0	2.54	1.784	1.768	8.516		
	82.5		1.533	1.588	8.408	**8.343**	**7.896**
	69.5		1.292	1.393	8.265		
	55.5		1.031	1.172	8.196	±0.125	±0.082
	45.8		0.851	1.019	8.330		

Table V. Comparison of acetylene vibrational band intensities with previous results in P. Varanasi, L.P. Giver and F.P.J. Valero, JQSRT 30, 497(1983a). S_v^o for *This Work* is stated for natural abundance samples at 300K.

Band Identification	Band Freq. ν_o [cm^{-1}]	Varanasi et al $S_v^{(0)}$ [$cm^{-2}atm^{-1}$]	This Work $S_v^{(0)}$ [$cm^{-2}atm^{-1}$]
ν_5-fundamental	730.33	588	560. ± 17
$(\nu_4+\nu_5)^{0-}-\nu_4^{e,f}$	727.68	18.7	13.5 ± 0.3
$(\nu_4+\nu_5)^{0-}-\nu_4^{e}$	715.20	17.7	13.8 ± 0.1

Figure 1 displays an intensity contour based on the retrieved intensity from our ν_5 observations. Figure 2 indicates the need for inclusion of a Herman-Wallis term in the band intensity model for the hotbands. For both of the $(\nu_4+\nu_5)-\nu_4^1$ hotbands a short-fall of about 50% in observed intensity is indicated. This result agrees with a preliminary analysis by Halsey[10] of KPNO FTS data observed at 0.0025cm^{-1} resolution.[11] In his study a 50% smaller band intensity was observed for all seven two quantum number hotbands involved in the transitions $\nu_4+\nu_5-\nu_4$ and $2\nu_5-\nu_5$ in the 13.7μm region in addition to observed J dependence due to rotation-vibration interaction. Current investigation of other hotband transitions seem to support these observations. Further measurements are indicated and are in progress.

COMPUTATIONAL TECHNIQUES

A number of novel computational techniques have been developed to enhance the retrieval of useful information from spectral data. Our approach is to attempt to obtain maximum information from the data at hand. Compared to time on one of a kind facilities, computer machine cycles are very inexpensive.

The multiple regression system in use has evolved over a twenty year period.[12] The most valuable aspects of this least squares system, apart from its stepwise nature, are the use of bi-weights[13] and a Komolgrov-Smirnov[14] statistical test as a termination indicator. The analysis system uses a version of the stepwise regression analysis system used in Lin *et al.*[15] and Daunt *et al.*[16] Modified bi-weights[16] are used beginning with a width of 6 standard deviations, reducing that width by 80% when the variance stabilizes in the iterative regression-weight correction process. At each

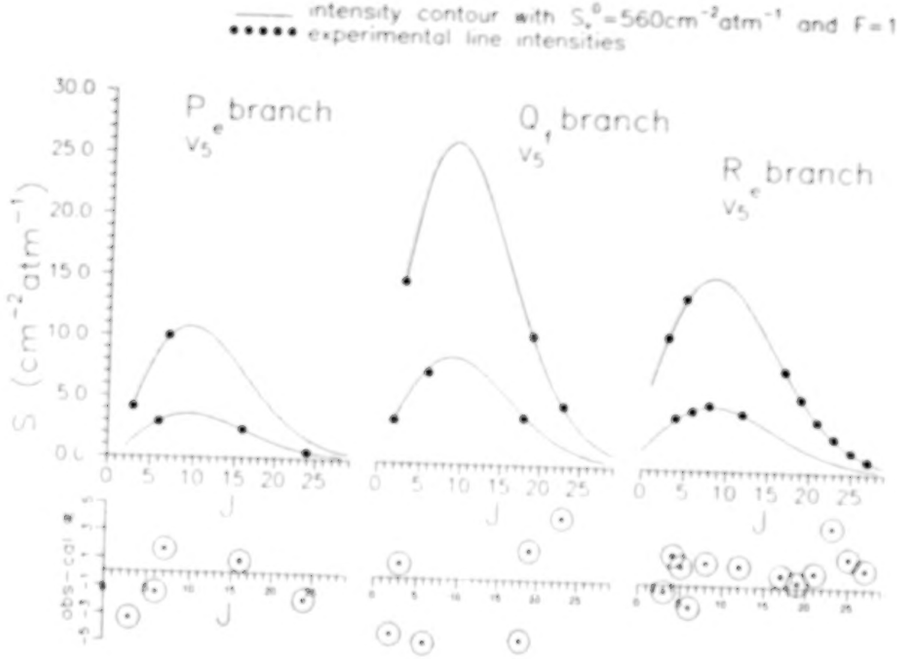

Fig. 1 Intensity contour for ν_5 showing observed strengths.

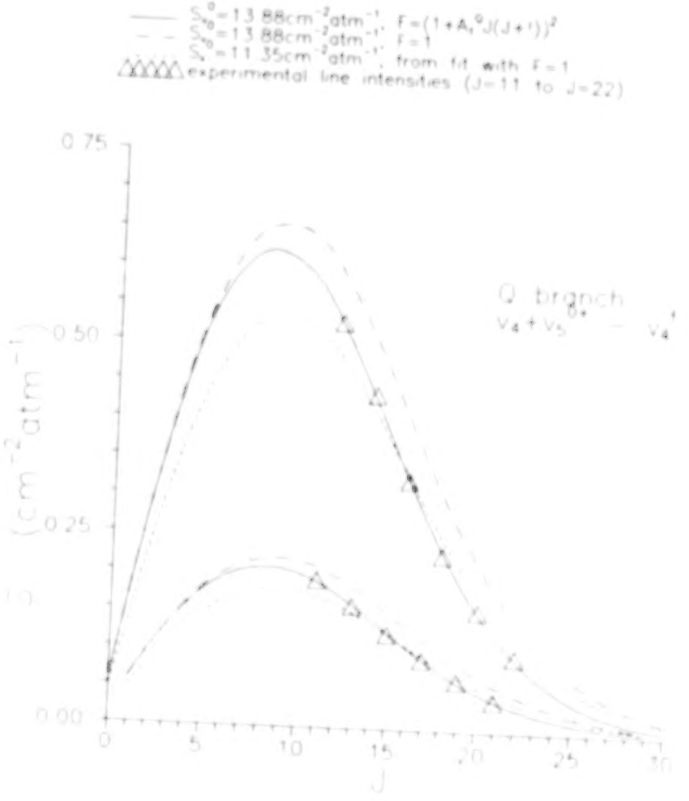

Fig. 2 Intensity contour for the Q-branch of a two quantum hotband showing the sensitivity of the data to the Herman-Wallis model

ORIGINAL PAGE IS
OF POOR QUALITY

step, an iterative Komolgrov-Smirnov (K-S) test[16] is performed on the residuals against a model normal distribution with a variance approximating the expected variance in the data. The iterations in the K-S sequence involve varying the expected variance of the model distribution in order to find the maximum probability that the weighted residuals are drawn from a normal distribution. When a maximum probability is achieved in the bi-weighting iterations, the process is terminated and the maximum probability results retrieved. The maximum probability is often above 90%. This system was used to retrieve intensities, analyze the cyanoacetylene data and to recover lower state rotational constants from the KPNO acetylene data in collaboration with J. J. Hillman et al.[17]

Other novel techniques have been developed and include automatic (two dimensional spline interpolation) strength retrieval using equivalent widths. Accidental resonance analysis systems using Hellman-Feynman derivative generation in the iterative non-linear least squares analysis system have also been developed. This system is being used to analyze the $\nu_9+\nu_4-\nu_4$ hotband of ethane and the two and three quantum hotband data for the 14 μm acetylene data. In both of these cases the data was obtained at KPNO by Donald E. Jennings, et al.

REFERENCES

1. G. Graner, private communication.
2. R. A. G. Creswell, G. Winnewisser, and M. C. L. Gerry, J. Mol. Spectrosc. 65,420(1977).
3. V.W.L. Chin, M.S. Thesis, University of Tennessee, Knoxville, 1985. W.E. Blass and V.W.L. Chin, JQSRT 38, 185(1987).
4. D.E. Jennings, Appl.Opt. 19, 2695(1980).
5. S.S. Penner, Quantitative Molecular Spectroscopy and Gas Emissivities, Addison-Wesley, Reading, Massachusetts, 1959.
6. M.A.H. Smith, C.P. Rinsland, B. Fridovich and K.N. Rao, Chapter 3 in Molecular Spectroscopy: Modern Research. Vol.III, ed. K.N. Rao, Academic Press, New York, 1985.
7. D. Papousek and M.R. Aliev, Molecular Vibrational-Rotational Spectra, Elsevier, Amsterdam, 1982.
8. P.A. Jansson, C.L. Korb, JQSRT 8, 1399(1968).
9. M. C. Weber, W. E. Blass, and Jean-Luc Salanave, JQSRT in press.

10. G.W. Halsey, private communication (1988).
11. G.W. Halsey, J.J. Hillman, and D.E. Jennings, " The 14 Micron Bands of Acetylene -- the Region of the Bending Modes," Technical Report, Laboratory for Extraterrestrial Physics, Goddard Space Flight Center, Greenbelt MD (June 1985).
12. W. E. Blass, Program FILE5, unpublished.
13. A. E. Beaton and J. W. Tukey, in Critical Evaluation of Physical Structural Information, (D. R. Lide and M. A. Paul, Eds.), pp15-35,National Academy of Sciences, Washington, D. C. 1974.
14. W. H. Press, B. P. Flannery, S. A. Teukolsky, and W. T. Vetterling, Numerical Recipes, The Art of Scientific Computing, pp. 472-475, 539, Cambridge University Press, Cambridge, 1986.
15. K. F. Lin, W. E. Blass and N. M. Gailar, J. Mol. Spectrosc. **79**, 151-157 (1980).
16. S. J. Daunt, A. K. Atakan, W. E. Blass, G. W. Halsey, D. E. Jennings, D. C. Reuter, J. Susskind, and J. W. Brault, Ap. J. **280**,921-936 (1984).
17. J. J. Hillman, D. E. Jennings, G. W. Halsey, Sacher Nadler, and W. E. Blass, manuscript in revision.

N90-26749

INFRARED SPECTRA OF VAN DER WAALS COMPLEXES OF IMPORTANCE IN PLANETARY ATMOSPHERES

G.T. FRASER, A.S. PINE, AND W.J. LAFFERTY
Molecular Spectroscopy Division, National Institute of Standards and Technology, Gaithersburg, MD 20899

ABSTRACT

It has been suggested[1] that $(CO_2)_2$ and Ar-CO_2 are important constituents of the planetary atmospheres of Venus and Mars. Here, we present recent results on the laboratory spectroscopy of CO_2-containing van der Waals complexes which may be of use in the modeling of the spectra of planetary atmospheres. Sub-Doppler infrared spectra have been obtained for $(CO_2)_2$, $(CO_2)_3$, and rare-gas-CO_2 complexes in the vicinity of the CO_2 Fermi diad ($\nu_1+\nu_3$, $2\nu_2+\nu_3$) at 2.7 μm using a color-center-laser optothermal spectrometer. From the spectroscopic constants the geometries of the complexes have been determined and van der Waals vibrational frequencies have been estimated. The equilibrium configurations are C_{2h}, C_{3h}, and C_{2v}, for $(CO_2)_2$, $(CO_2)_3$, and the rare-gas-CO_2 complexes, respectively. Most of the homogenous linewidths for the rovibrational transitions range from 0.5 to 22 MHz, indicating that predissociation is as much as four orders of magnitude faster than radiative processes for vibrational relaxation in these complexes.

INTRODUCTION

The spectral observation[2] of $(H_2)_2$ in the atmosphere of Jupiter indicates the presence of weakly bound complexes in planetary atmospheres. Those results led Fox and Kim[1] to estimate the role that other van der Waals complexes play in the spectra of planetary atmospheres. The complexes of $(CO_2)_2$ and Ar-CO_2 were considered due to the large abundances of CO_2 in the atmospheres of Venus and Mars. Attempts were made to model the contributions of $(CO_2)_2$ and Ar-CO_2 to the spectra of these planets. A realistic simulation of these spectra, though, requires a substantial amount of information,

including geometries, binding energies, spectroscopic constants, and transition moments for the complexes, which were not known or only incorrectly known at the time. Accurate spectroscopic data are now becoming available for a number of van der Waals complexes through laboratory measurements of rotationally resolved spectra of these complexes. The complexes are typically produced in adiabatic expansions of suitable gas mixtures and then studied using high-sensitivity microwave and infrared spectroscopy.

Here, we will discuss sub-Doppler infrared spectra that have been obtained for $(CO_2)_2$[3], $(CO_2)_3$[4], and rare-gas-CO_2[5] complexes using a single-mode color-center laser. A molecular beam of the appropriate complex is formed by seeding a few percent of CO_2 in He or Ar/He and expanding the gas through a pinhole nozzle into a vacuum chamber. The molecular beam energy is monitored using a liquid-He cooled bolometer. Between the nozzle and bolometer, the laser beam is multiply crossed through the molecular beam. The laser excites a vibration in the complex correlating to the $\nu_1+\nu_3/2\nu_2{}^0+\nu_3$ Fermi diad in CO_2. In transit to the bolometer (i.e. in less than ~1 ms) the vibrationally excited complex predissociates, leading to a loss of energy detected by the bolometer. In this way a spectrum is recorded by monitoring the bolometer response as a function of laser frequency.

$(CO_2)_2$

The infrared spectra of the two Fermi diad bands of $(CO_2)_2$ were recorded near 3611.5 and 3713.9 cm^{-1}, with band origins red shifted by ~ 1 cm^{-1} from the monomer origins. The observed nuclear-spin statistical weights and inertial defect are interpreted in terms of a planar C_{2h} complex [see Fig. 1], in disagreement with previous low resolution infrared results. The nearest neighbor C···O distance is nearly identical to that found in the CO_2 crystal. A centrifugal distortion analysis yields weak bond stretching and symmetric bending frequencies of 32(2) and 90(1) cm^{-1}, respectively. The measured transition linewidths of ~ 2 MHz give an estimate for the predissociation broadening.

$(CO_2)_3$

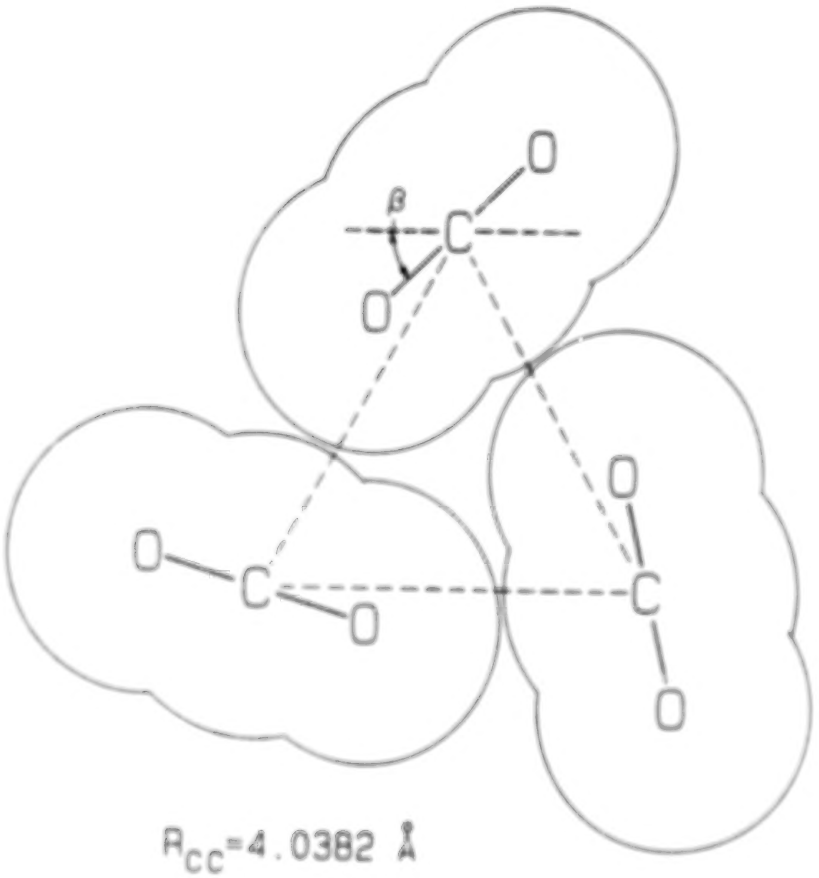

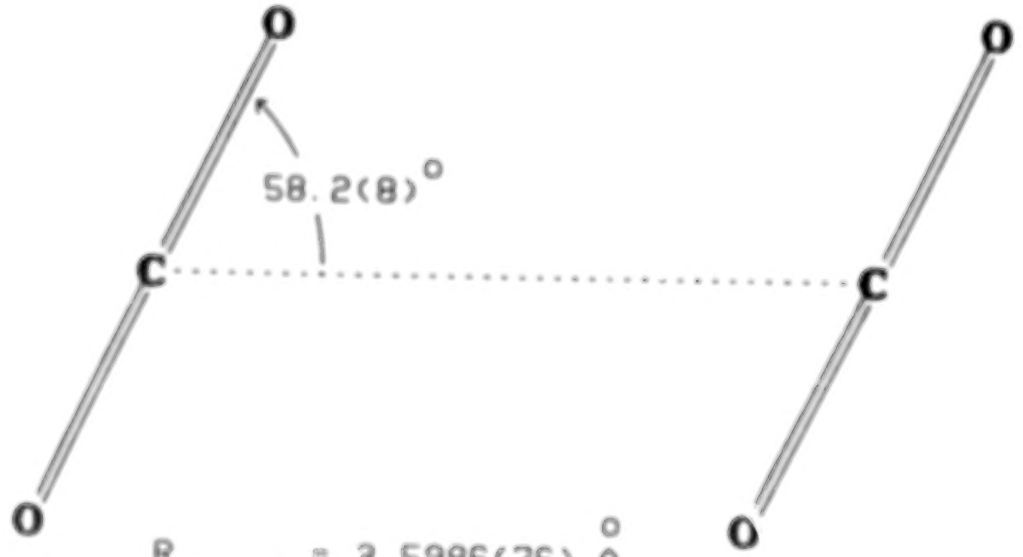

Fig. 1. Structures of CO_2 Dimer and Trimer

The observed spectrum for $(CO_2)_3$ is shown in Fig. 2. Only the lower frequency Fermi diad band was observed, blue shifted by ~ 1 cm^{-1} from the monomer origin. A symmetric top spectrum is seen, with statistical weights depending only on K and a near zero inertial defect, giving a planar C_{3h} structure for the complex [see Fig. 1]. The C--C separation of 4.0382 Å is larger than the 3.599 Å value found in the dimer.

Ne-CO_2, Ar-CO_2, AND Kr-CO_2

Infrared spectra of the C_{2v}[6] Ne-, Ar-, and Kr-CO_2 have been recorded for both Fermi-diad bands of the complex. The band origins for the Ar and Kr complexes are red shifted from that of free CO_2 by 1-2 cm^{-1}, while for Ne-CO_2 they are blue shifted by ~ 0.2 cm^{-1}. The predissociation linewidths range from 0.5 to ≤ 5 MHz except for the upper Fermi-diad band of Ne-CO_2, which shows a broad width of ~ 22 MHz arising from near resonant predissociation of Ne-$CO_2(\nu_1+\nu_3) \rightarrow$ Ne + $CO_2(2\nu_2+\nu_3)$.

CONCLUSION

Here, we have summarized spectral results that have been obtained for weakly bound complexes of CO_2. The present data provide valuable information on the spectroscopy and dynamics of these species which should be useful for modeling their spectra in planetary atmospheres.

REFERENCES

[1]K. Fox and S.J. Kim, J.Quant.Spectrosc.Radiat.Transfer, 40, 177 (1988).
[2]L. Frommhold, R. Samuelson, and G. Birnbaum, Astrophys.J. 283, L79 (1984).
[3]K.W. Jucks, Z.S. Huang, D. Dayton, R.E. Miller, and W. Lafferty, J.Chem.Phys. 86, 4341 (1987);K.W. Jucks, Z.S. Huang, R.E. Miller, G.T. Fraser, A.S. Pine, and W. Lafferty, J.Chem.Phys. 88, 2185 (1988).
[4]G.T. Fraser, A.S. Pine, W.J. Lafferty, R.E. Miller, J.Chem.Phys. 87, 1502 (1987).
[5]G.T. Fraser, A.S. Pine, and R.D. Suenram, J.Chem.Phys. 88, 6157 (1988);A.S. Pine and G.T. Fraser, J.Chem.Phys. 89, 100 (1988).
[6]J.M. Steed, T.A. Dixon, and W. Klemperer, J.Chem.Phys. 70, 4095 (1979).

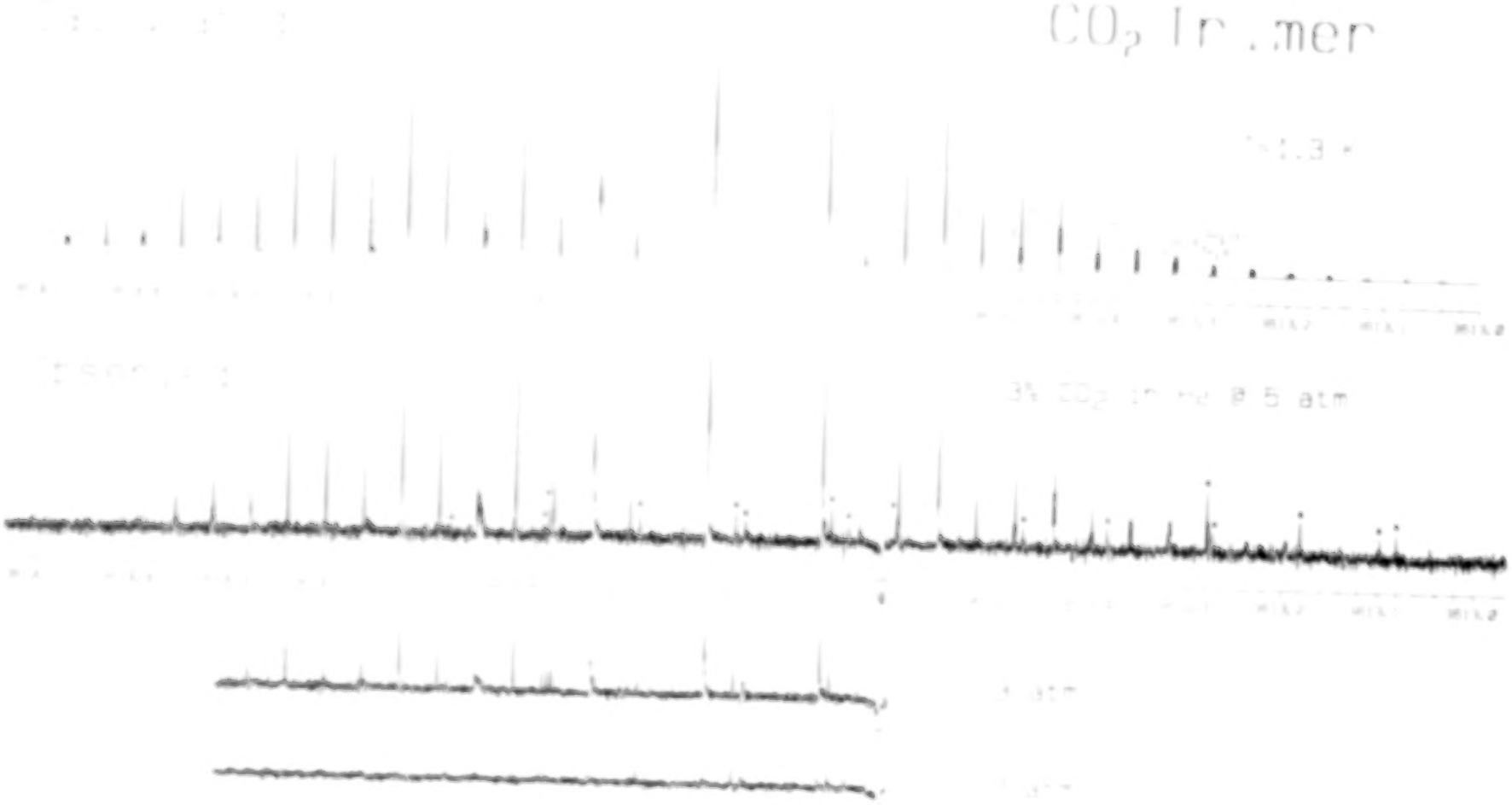

Fig. 2. Observed and calculated infrared spectra of $(CO_2)_3$ near the $2\nu_2+\nu_3$ vibration of CO_2.

N90-26750

LABORATORY MEASUREMENTS AND MODELING OF MICROWAVE ABSORPTION BY AMMONIA IN GAS MIXTURES APPLICABLE TO GIANT PLANET ATMOSPHERES

T.R. SPILKER
Stanford Center for Radar Astronomy, SEL Durand Bldg., Stanford, CA 94305-4055

Accurate knowledge of the microwave absorption behavior of ammonia is critical to the correct interpretation of radio astronomical and radio occultation data from the giant planets. Despite over 50 years of study, however, the microwave spectrum of ammonia has been a problem child in microwave spectroscopy, defying accurate characterization by a single general theory. Van Vleck-Weisskopf (VVW) theory[1] does well at pressures below about half a bar in a Jovian mixture but errs by as much as a factor of two at higher pressures[2]. A quantum mechanical treatment of the problem by Ben-Reuven[3] produced a formalism that worked well for pure gaseous ammonia but fared less well in mixtures[4,5]. Empirical modifications to the original Ben-Reuven formalism by Wrixon *et al.*[2] and Berge and Gulkis[6] improved its performance for mixtures resembling the atmospheres of giant planets, but newer data point to errors in their predictions that are considerably larger than the errors in radio occultation data.

New cavity resonator techniques developed at the Stanford Center for Radar Astronomy have allowed accurate laboratory measurements of the microwave absorptivity and refractivity spectra of gas mixtures containing trace amounts of ammonia in foreign gases, including hydrogen, helium, and a Jovian mixture of hydrogen and helium, over the entire range of temperatures, pressures, and frequencies currently available to our resonator-based spectrometer: 210 to 320 K, 1 to 8 atmospheres total pressure, and 9 to 18 GHz. The data point out sizable ranges of conditions where neither VVW nor modified Ben-Reuven formalisms yield accurate predictions, and strongly suggest that temperature dependences expressed in those formalisms are incorrect. They also indicate that the pressure range near one atmosphere (total pressure) involves fundamental change in the microwave absorption behavior of gaseous ammonia.

A parameterized version of the modified Ben-Reuven formalism of Berge and Gulkis[6] was optimized to fit the new data and that of other researchers[7,8]. Like other ammonia absorptivity prediction schemes this formalism is a summation of absorptivity contributions from individual inversion lines:

$$\alpha(f_0) = C \sum_J \sum_K A(J, K, \mathbf{m})\, F(J, K, \mathbf{m}, f_0) \,, \tag{1}$$

where $\alpha(f_0)$ is the absorption coefficient at frequency f_0, J and K are the rotational quantum numbers specifying individual absorption lines, $A(J, K, \mathbf{m})$ and $F(J, K, \mathbf{m}, f_0)$ are the line intensity and shape factors, respectively, and C is an empirical correction factor used by Berge and Gulkis to force a fit to the high pressure laboratory data of Morris and Parsons[7]. The vector $\mathbf{m}$ is a vector of the macroscopic conditions (*i.e.* temperature and the partial pressures of ammonia and all pertinent foreign gases in the mixture). In the Ben-Reuven line shape factor of Equation 1 these conditions are manifested in three parameters internal to F: γ, ζ, and δ. In the context of a Jovian mixture at

moderate pressures the line shift parameter δ is insignificant[2] and is not treated in this analysis. The other parameters are the line broadening parameter γ and the coupling element ζ.

Using a mix of theoretical results and empirical data Berge and Gulkis give equations for γ and ζ of the forms:

$$\gamma(J, K, m) = G_{H_2}\left(\frac{300}{T}\right)^{\frac{2}{3}} P_{H_2} + G_{He}\left(\frac{300}{T}\right)^{\frac{2}{3}} P_{He} + G_{NH_3}\left(\frac{300}{T}\right)\gamma_0(J, K)\, P_{NH_3} \quad \text{GHz}, \tag{2}$$

$$\zeta(J, K, m) = Z_{H_2}\left(\frac{300}{T}\right)^{\frac{2}{3}} P_{H_2} + Z_{He}\left(\frac{300}{T}\right)^{\frac{2}{3}} P_{He} + Z_{NH_3}\left(\frac{300}{T}\right)\gamma_0(J, K)\, P_{NH_3} \quad \text{GHz}. \tag{3}$$

In these equations T is temperature in Kelvins, $\gamma_0(J, K)$ is the self-broadened line width in MHz/torr, P_i is the partial pressure of the gas species i, and G_i and Z_i are scaling coefficients for species i. In accord with the predictions of Ben-Reuven theory Berge and Gulkis used constants for the scaling coefficients: $G_{H2} = 2.318$, $G_{He} = 0.79$, $G_{NH3} = 0.75$, $Z_{H2} = 1.92$, $Z_{He} = 0.3$, $Z_{NH3} = 0.49$; these worked well with the Morris and Parsons data, taken at a single frequency and temperature. Data from this work, however, taken over a range of temperatures and at lower pressures suggested these coefficient values may not be usable for all temperatures and pressures, an indication that the temperature and pressure dependences expressed in Equations 2 and 3 are not completely correct. The parameterized version of the formalism substituted free parameters for these coefficients and the Berge and Gulkis correction factor C, which is essentially unity for total pressures less than about 100 atmospheres. An optimization routine was implemented that would read the measured absorption spectrum of a specific gas mixture at a constant temperature and pressure, and adjust the values of the parameters to best fit those data. The design of the data set allowed separation of the seven-parameter optimization problem into three much simpler three-parameter problems.

Results of optimizations on data at varying temperatures and pressures allowed (in most cases) characterization of the variation of the parameters with temperature and pressure. Notably, as pressure decreased to one atmosphere the best-fit value of G_{H2} decreased significantly (to about a tenth the high pressure value) while the value of Z_{H2} more than doubled. As temperature decreased, the value of C also decreased, suggesting the temperature dependence of the Ben-Reuven intensity factor A (identical to the VVW intensity factor) is incorrect. Empirical expressions were derived for the variations of the parameters with macroscopic conditions. Incorporating these expressions into the formalism produced a new formalism that quite accurately fit the data.

Pure gaseous ammonia data by Bleaney and Loubser[8] yielded the values $G_{NH3} = 0.74$ and $Z_{NH3} = 0.50$, independent of pressure and in close agreement with Berge and Gulkis' values. Precise details of the pressure dependences of G_{He} and Z_{He} at the lowest pressures could not be characterized from the data of this work, but approximate temperature dependences were derived. Fortunately, like G_{NH3} and Z_{NH3}, these coefficients are relatively insignificant to the ultimate accuracy of the formalism. The critical coefficients are G_{H2} and Z_{H2}, for which more accurate characterizations could be made. An expression yielding G_{H2} directly from macroscopic conditions was derived, but

finding an accurate expression for Z_{H2} was not possible with available data. However it was found that there was a close relation between G_{H2} and Z_{H2}, such that Z_{H2} could be calculated from the value of G_{H2}. The hydrogen broadening coefficient is given by:

$$G_{H_2} = 2.34 \left[1 - \frac{2.157\, e^{-T/116.8}}{\left(e^{(9.022 - T/20.3)} - 1 + P_{tot} \right)^r} \right] \quad , \quad \text{where } r = 8.79\, e^{-T/83} \quad , \tag{4}$$

with P_{tot} the total pressure in atmospheres; the value of Z_{H2} is then calculated from G_{H2}:

$$Z_{H_2} = 5.7465 - 7.7644\, G_{H_2} + 9.1931\, G_{H_2}^2 - 5.6816\, G_{H_2}^3 + 1.2307\, G_{H_2}^4 \, . \tag{5}$$

The expressions for the helium term coefficients are:

$$G_{He} = 0.46 + \frac{T}{3000} \quad , \qquad Z_{He} = 0.28 - \frac{T}{1750} \quad . \tag{6}$$

For P_{tot} less than about 10 bars, C is given by:

$$C = -0.33664 + \frac{T}{110.4} - \frac{T^2}{70{,}600} \quad . \tag{7}$$

The new formalism produced by this method predicts ammonia absorptivity much more accurately than previous formalisms over a significant range of conditions. Figure 1 compares the predictions of three formalisms, Van Vleck-Weisskopf, Berge and Gulkis' Ben-Reuven, and the new formalism of this work, to laboratory data not used in generating the new formalism. Other laboratory data by Joiner *et al.*[9], and Steffes and Jenkins[10], indicate that it is accurate over a frequency range of at least 2 GHz (and possibly much lower) to 40 GHz. Figure 2 is a temperature-pressure diagram showing the relationship of the conditions represented in the data to the conditions observed in the atmospheres of the giant planets by Voyager spacecraft radio occultation experiments. The data are directly applicable to Jupiter at pressures greater than two bars, and to Saturn at pressures greater than about five bars. The Uranian and Neptunian atmospheres require extrapolation at all levels.

Due to the behavior of the expressions for G_{H2} and Z_{H2}, extrapolating this formalism to total pressures less than one bar is not possible. As has been done previously[2] a VVW formalism may be used for the lower pressures, although this will produce a discontinuity at one bar. One matching technique which would eliminate the discontinuity would involve using VVW below half a bar, where it is most accurate; linear interpolation (or a higher-order interpolation scheme) would be used between the VVW value at half a bar and the new formalism's value at one bar. Extrapolation in temperature more than 30 to 40 K beyond the data is considered risky, especially given

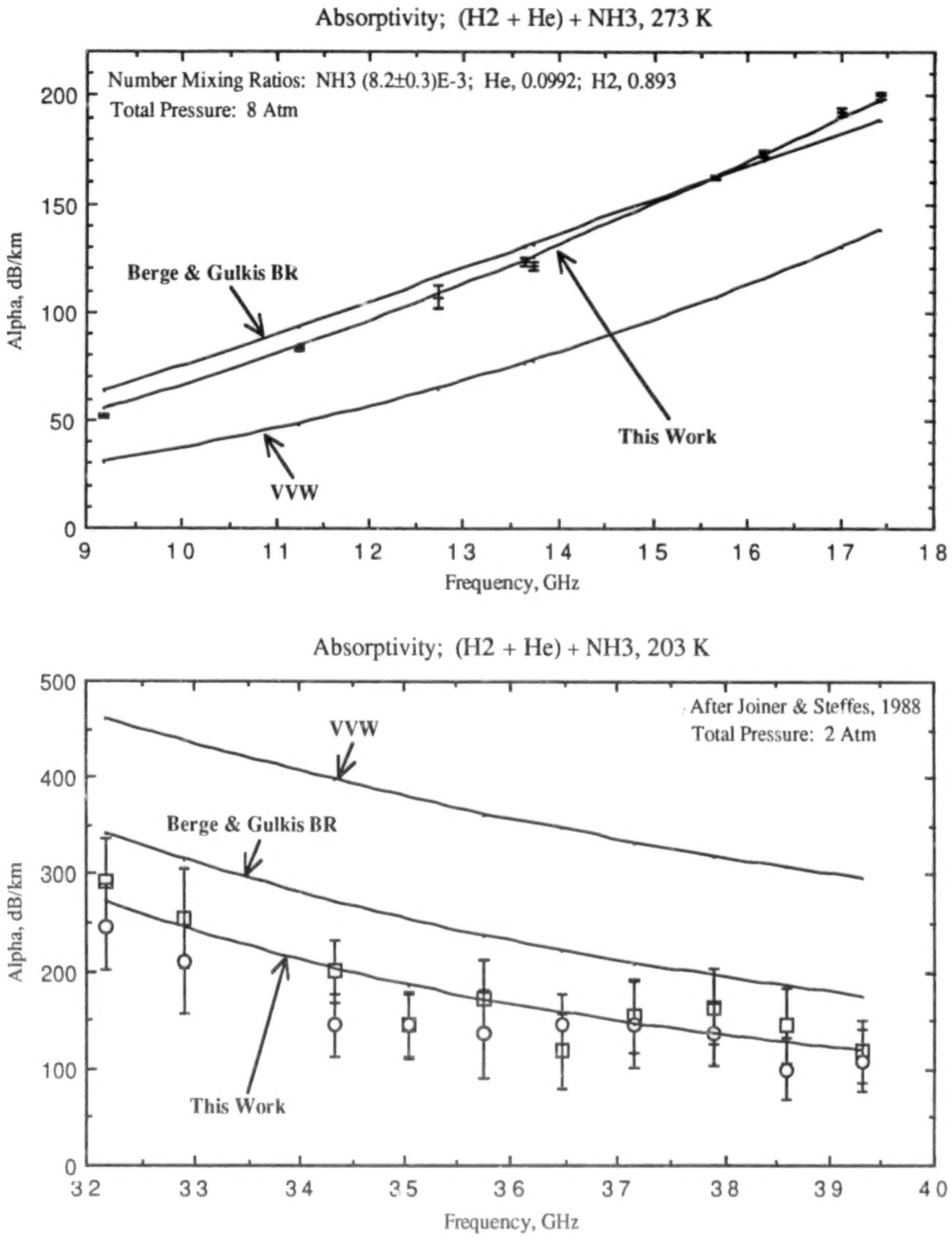

Figure 1: Predictions of the new formalism compared with laboratory data. Data in the upper graph were taken as part of this work but were not used in generating the formalism. Although the Berge and Gulkis formalism is reasonably accurate at this temperature its predicted frequency dependence is incorrect. Data in the lower graph are from Joiner *et al.*[9], and cover a frequency range considerably different from the data used in this work. These and other data indicate the new formalism is accurate over a frequency range of at least 2 to 40 GHz.

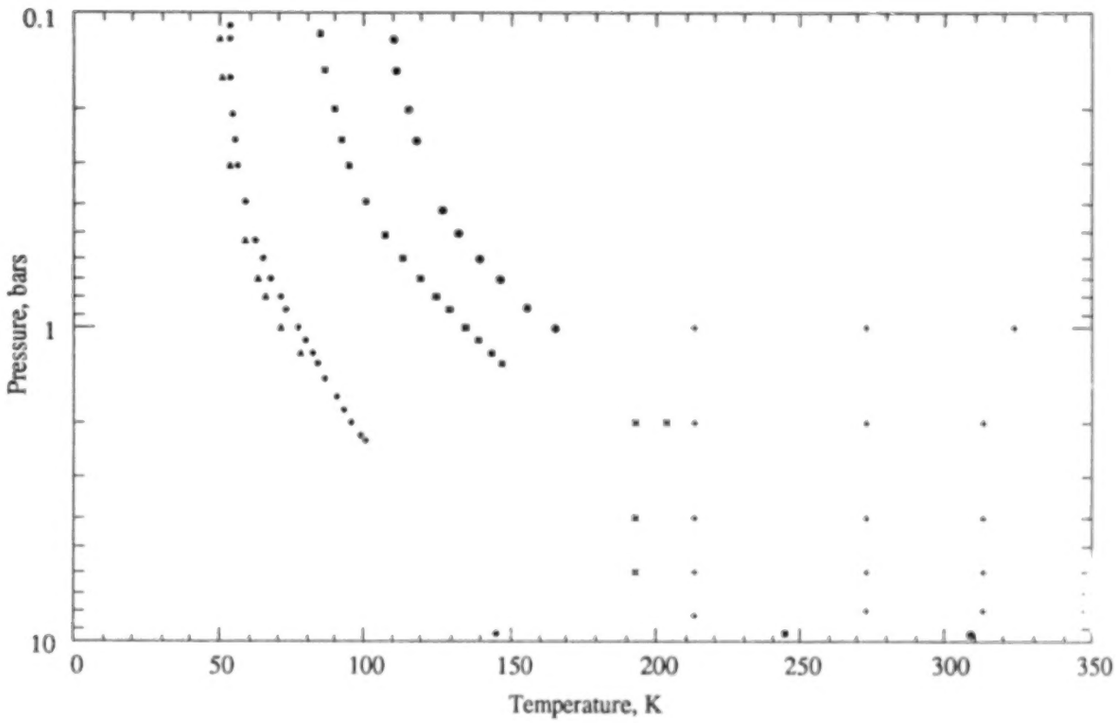

Figure 2: A comparison of the temperature and pressure ranges of laboratory data on microwave absorption by gas mixtures applicable to the atmospheres of giant planets, and conditions measured by the Voyager radio occultation experiments at Jupiter (circles), Saturn (squares), Uranus (diamonds), and Neptune (triangles). Values for Jupiter, Saturn, and Uranus at the bottom of the graph are extrapolations based on work by Lewis and Prinn[11]. The crosses represent data from this work; data from Joiner *et al.*[9], and Steffes and Jenkins[10] are marked with an "x."

the polynomial character of the expression for C, Equation 7. The data do indicate that the temperature dependence of the intensity factor is incorrect, such that absorptivities predicted by previous formalisms will be too high at low temperatures. Since this intensity factor is also used in VVW theory it may be necessary to use a modified VVW formalism in the matching scheme previously suggested.

[1] J.H. Van Vleck and V.F. Weisskopf, Phys. Rev. **44**, 391 (1945).

[2] G.T. Wrixon, W.J. Welch, and D.D. Thornton, Astrophys. J. **169**, 171 (1971).

[3] A. Ben-Reuven, Phys. Rev. **145**, 7 (1966).

[4] G. Birnbaum, personal communication, (1987).

[5] R.L. Poynter, personal communication, (1987).

[6] G.L. Berge and S. Gulkis, in *Jupiter*, T. Gehrels ed. (Univ. of Arizona Press), 621 (1976).

[7] E.C. Morris and R.W. Parsons, Aust. J. Phys. **23**, 335 (1970).

[8] B. Bleaney and J.H.N. Loubser, Proc. Phys. Soc. **A63**, 483 (1950).

[9] J. Joiner, P.G. Steffes, and J.M. Jenkins, Icarus **81**, 386 (1989).

[10] P.G. Steffes and J.M. Jenkins, Icarus **72**, 35 (1987).

[11] R.G. Prinn and J.S. Lewis, *Planets and Their Atmospheres* (Academic Press), (1984).

N90-26751

RECENT HIGH RESOLUTION LABORATORY DETERMINATIONS OF LINE BROADENING AND INTENSITY PARAMETERS: PH_3, CH_3D AND CO_2

C. B. SUAREZ*, C. CHACKERIAN, JR.*, F.P.J. VALERO* AND G. TARRAGO**
*NASA-Ames Research Center, Moffett Field, CA 94035-1000
**Laboratoire d'Infrarouge, Universite de Paris-sud, Bat. 350
91405 Orsay, France

ABSTRACT

We review our recent unpublished laboratory work on rovibrational line strengths and broadening coefficients which is of interest in the study of planetary atmospheres. The molecules discussed are PH_3, CH_3D and CO_2.

Introduction

High spectral resolution infrared rovibrational observational astronomy is a powerful tool for understanding the compositional and dynamical structures of planetary atmospheres. At NASA Ames we are engaged in the measurement of line intensity and broadening coefficients (and their temperature dependence) which are required for the proper interpretation of such astronomical observations.

Line broadening coefficients are dependent on the dynamics of molecular collisions and therefore are temperature dependent. Accordingly we have made some of our measurements down to temperatures as low as 80K with specially constructed absorption cells. On the other hand line intensities, aside from the Boltzmann factor, are independent of temperature. Nevertheless we have measured line intensities at low temperatures because in some cases the very complex structure of the spectra of overlapping lines at room temperature is greatly simplified at the lower temperatures and becomes, therefore, more amenable to analysis. To date we have made broadening measurements with self-, He-, and N_2- collision partners.

The spectra we analyze are recorded with a BOMEM Model DA3.002 Fourier transform spectrometer, and the absorption cell we used was internally coated with evaporated gold and cooled with an Air Products Cryotip. The spectral intensity and broadening parameters were obtained via non-linear least-squares fits (of the spectra) wherein small corrections were applied to the theoretical instrumental resolution.

PH_3

In the 5 μm spectral region PH_3 and CH_3D spectra overlap and accurate line intensities and broadening coefficients are needed to obtain column densities for either species. PH_3 spectra have been obtained between 137 and 294 K in the 2000-2500 cm^{-1} spectral region. Fig. 1 shows a portion of a strongly absorbing region of PH_3's spectrum under self-broadening conditions with a path length of 0.21 cm. So far self- and He-broadening coefficients have been measured. Fig. 2. shows a typical result where the line broadening parameter for a particular phospine line at 2250.107 cm^{-1} is plotted versus pressure. To date, 212 line intensities recorded at room temperature have been analyzed with programs (G. Tarrago, paper in preparation) worked out for the frequency and intensity treatment of the pentad, $2\nu_2$, $\nu_2 + \nu_4$, $2\nu_4$, ν_1, ν_3. The two dipole moment derivatives relative to the normal co-ordinates, Q_1 and Q_3, plus three Herman-Wallis type elements of the dipole moment matrix contribute significantly to the fit, and allow the measured intensities to be reproduced to about 5%. Preliminary values, derived for the band strengths S_1 and S_3, confirm the ratio of 0.28 previously determined[1] for S_1/S_3, but lead to an overall strength $S_1 + S_3$ about 10 per-cent higher than the value measured by van Straten.[2] The transition moments for the ν_1 and ν_3 bands are respectively, $\langle\mu_1\rangle$ = 0.0712(23) D and $\langle\mu_3\rangle$ = 0.1351(14) D.

CH_3D

The ν_2 rovibrational band of CH_3D, which is observed in the outer planets is important for understanding the formation of the solar system as well as determining the D to H ratio important in cosmological theories.

At room temperature the Q branch of this band is complicated enough so that even Doppler limited resolution is not sufficient to provide a definitive analysis of the intensities. To circumvent this problem we have made intensity measurements at temperatures down to 80 K with an unapodized instrumental resolution of about 0.0045 cm^{-1}. Figs. 3. and 4. show the evolution of the Q branch with temperature. The resulting rotationless transition moment obtained from the Q branch is compared to that obtained from the P and R branches and work is in progress to understand a global interaction with the ν_6 band. In addition we have determined the low

temperature broadening parameters with N_2 for this band as well as He- and self-broadening coefficients at room temperature.

CO_2

A careful study has been made of the temperature dependence of the self-broadening coefficient,[3] γ, of CO_2 in the parallel band centered at 4978 cm^{-1}. In the temperature range 165 to 300 K the average value of the temperature exponent (for J in the range 6 to 32) is n = 0.745 +- 7%. Here n is defined via the equation $\gamma(T) = \gamma(To)(To/T)^n$, where To is some reference temperature.

References

1. A. Baldacci, V. M. Devi, K. Narahari Rao and G. Tarrago, J. Mol Spectrosc. **81**, 179 (1980).
2. A. J. van Straten, J. Mol. Spectrosc. **65**, 202 (1977).
3. C. B. Suarez and F. P. J. Valero, J. Quant. Spectrosc. Radiat. Transfer (accepted).

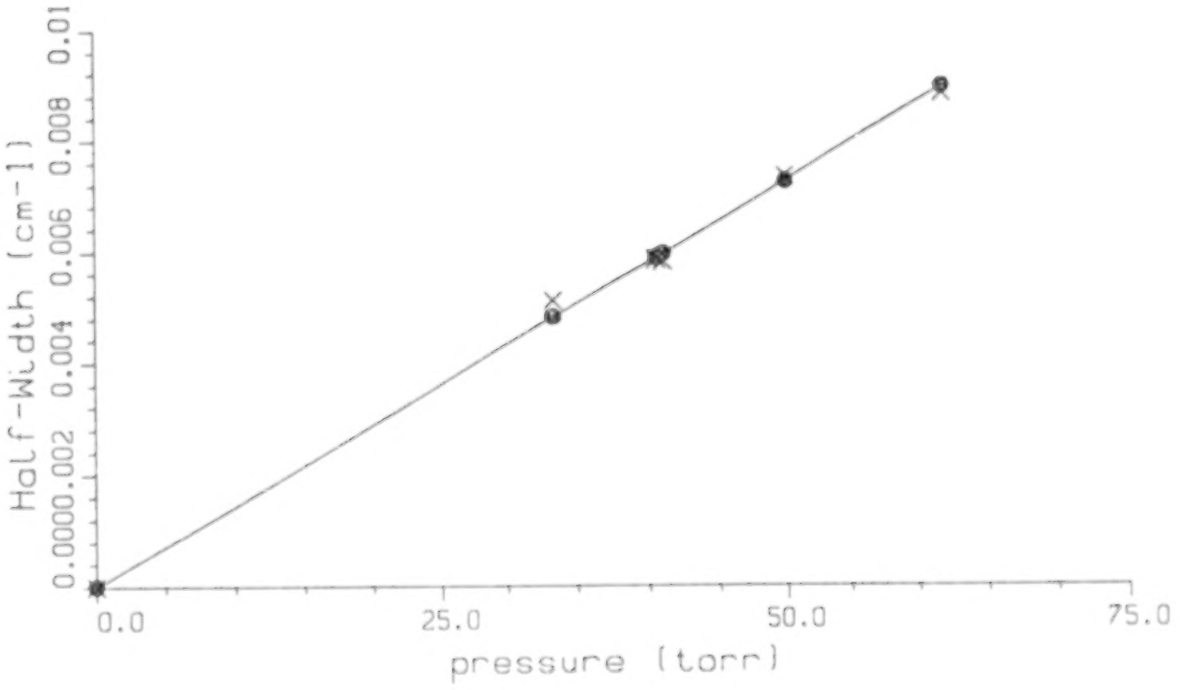

Fig. 1. Retrieved half width (X's) for a PH_3 self-broadened line at T = 293.5 K. •'s represent fitted values. Broadening coefficient determined from slope of the line thru the data.

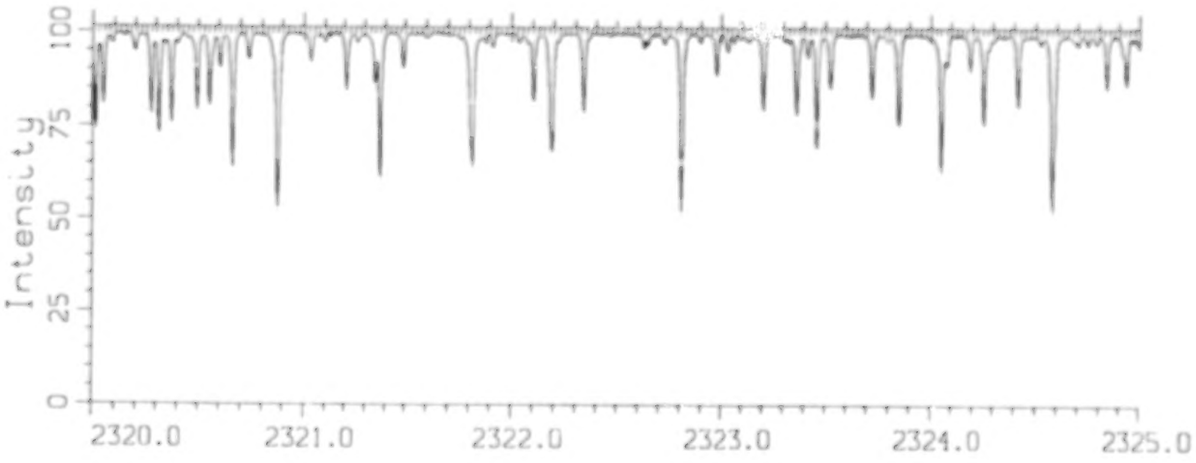

Fig. 2. Portion of the PH_3 rovibrational spectrum between 2320 and 2325 cm^{-1}. T=293.5;L=0.21 cm; P=14.9 torr.

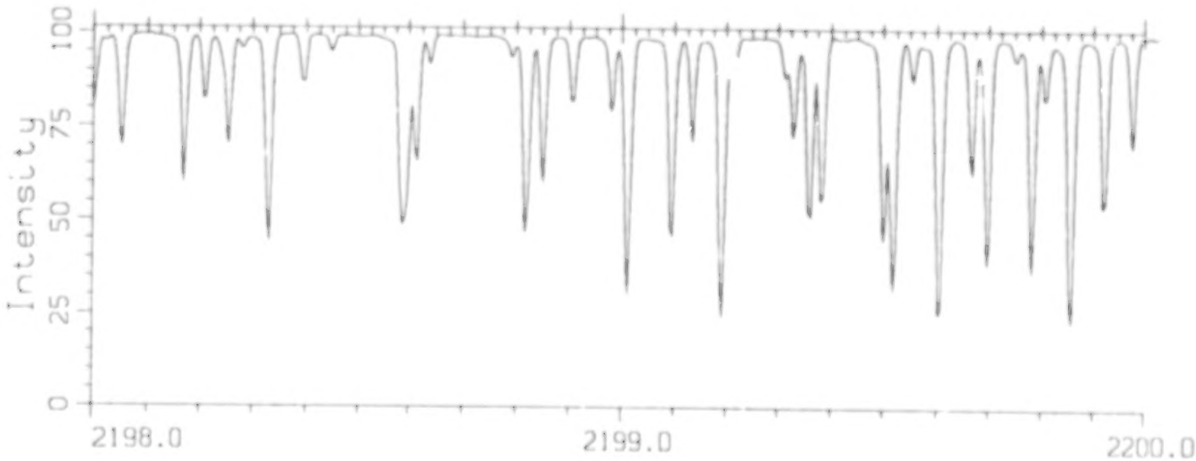

Fig. 3. Q branch of CH_3D ν_2 band. T=296.3 K; L=5.74 cm; P=9.35 torr.

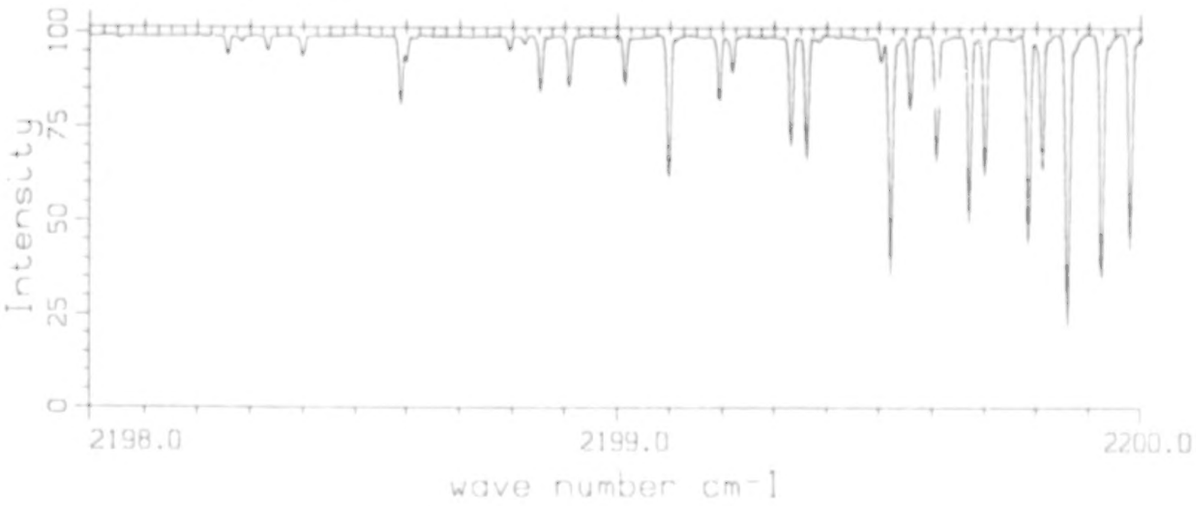

Fig. 4. Q branch of CH_3D ν_2 band. T=81 K; L=5.74 cm; P=0.79 torr.

N90-26752

MICROWAVE SPECTRA OF VAN DER WAALS COMPLEXES OF IMPORTANCE IN PLANETARY ATMOSPHERES

R. D. SUENRAM AND F. J. LOVAS

Molecular Spectroscopy Division, National Institute of Standards and Technology, Gaithersburg, MD 20899

ABSTRACT

The Fourier-transform Fabry-Perot pulsed-molecular-beam microwave spectrometer at NIST has been used to study the microwave spectra of a number of molecular dimers and trimers that may be present in planetary atmospheres. The weak van der Waals bonds associated with these species usually give rise to rotational-tunneling splittings in the microwave spectra. We have used the microwave spectrum of the water dimer species to illustrate the complications that can arise in the study of the rotational spectra of these loosely bound species. In addition to the water dimer species, the microwave spectra of the following hydrogen-bonded and van der Waals complexes have been studied: $(CO_2)_2 \cdot H_2O$, $CO_2 \cdot (H_2O)_2$, $CO_2 \cdot H_2S$, $N_2 \cdot H_2O$, $CO \cdot H_2O$, $SO_2 \cdot H_2O$, and $O_3 \cdot H_2O$.

INTRODUCTION

In a recent paper Jennings[1] summarizes the major and minor molecular species present in planetary and lunar atmospheres. The most abundant species are CO_2, N_2, H_2, and CH_4, with more than 50 other molecular species being present in smaller amounts. Fox and Kim[2] have recently attributed some previously unassigned infrared features in the atmosphere of Titan to arising from the $H_2 \cdot N_2$ van der Waals complex.

Due to the complexity of the spectra caused by internal motions found in most van der Waals and hydrogen bonded complexes and our inability to predict

the structures of these species *a priori*. a thorough understanding of the rotational spectra of such complexes is usually a prerequisite to the understanding of their far-infrared and near infrared spectra. Over the past five years at NIST we have developed a broad program aimed at the study of numerous van der Waals and hydrogen bonded molecular species. Many of the species we have analyzed could be important contributors to the infrared spectra of planetary atmospheres. The analysis of the rotational spectra of these species provides firm ground work for attempts at understanding their far-infrared and near infrared spectral features.

EXPERIMENTAL

a. Instrumentation. A pulsed-molecular-beam Fabry-Perot cavity Fourier-transform microwave spectrometer has been used to study the species described in this paper. A molecular beam of the species of interest is formed by pulsing a 1% mixture of the species in an inert carrier gas (Ne or Ar) through a pulsed solenoid valve. When the molecular beam pulse reaches the center of the Fabry-Perot microwave cavity, a $\pi/2$ microwave pulse of several microseconds duration is applied to the microwave cavity. This produces Fourier components of the microwave radiation over a bandwidth of ~1 MHz around the center frequency. If any of the molecular species in the beam have a rotational transition within this 1 MHz window, they are coherently excited by the microwave radiation. The resulting free-induction decay signal emanating from the microwave cavity is detected using a super heterodyne receiver. This detected signal is digitized at 0.5 μsec intervals for 512 points. Generally the digitized signals are averaged over hundreds or even thousands of microwave pulses. Once this average is obtained, it is Fourier transformed to give the

power spectrum. The linewidths attainable with this instrument are typically <20 kHz and frequency measurements are considered accurate to 4 kHz which is the resolution element corresponding to the digitization channel width. Further details of the construction and operation of the spectrometer are provided in Ref. 3-5. Details pertaining to the chemistry and spectral features of the species studied can be found in the papers referenced in Table I.

b. Water Dimer Spectrum. Over the past decade there has been substantial interest in the microwave and infrared spectroscopy of $(H_2O)_2$. The early work of Dyke and co-workers[6] provided the first preliminary analysis of the rotational spectrum in 1980 Since then much additional work has been carried out in the microwave, far-infrared, and infrared spectral regions. The history of the spectroscopy of $(H_2O)_2$ has been recently reviewed by Fraser, Suenram and Coudert[7]. The group theory necessary to describe the rotational spectrum of $(H_2O)_2$ has been given by Coudert and Hougen[8]. Briefly, the rotational energy levels are first split by a tunneling motion involving a C_2 rotation of the acceptor H_2O molecule in the complex. This splitting is quite large (230 GHz for the $K_{-1}=0$ levels) and as yet not well determined. These two levels are then further split (22.55437 GHz for the A_1/B_1 $K_{-1}=0$ levels) by an exchange motion of the two H_2O subunits in the complex as they interchange their proton donor-acceptor roles within the complex. The energy level diagram is shown schematically in Figure 1. The rotational analysis provided by Fraser, Suenram and Coudert[7] has greatly aided the far-infrared and near infrared analysis of the $(H_2O)_2$ spectrum[9,10].

c. Other Molecular Species. In general, the rotational spectra of the additional species mentioned in the abstract are not as complicated as the

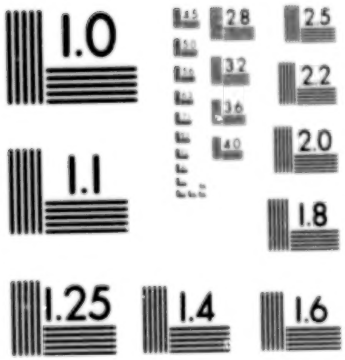

MICROCOPY RESOLUTION TEST CHART
NATIONAL BUREAU OF STANDARDS
STANDARD REFERENCE MATERIAL 1010a
(ANSI and ISO TEST CHART No. 2)

Table I. Structural Summaries and Electric Dipole Moments for Weakly Bound Molecular Complexes of Interest in Planetary Atmospheres.

Species	Ref.	Dipole	Summary
$N_2 \cdot H_2O$	11	μ_a=0.833	Four tunneling states observed due to tunneling of both the H_2O and N_2 subunits The spectral splitting caused by the H_2O is ~ten times greater than that caused by the N_2. Linear heavy atom geometry.
$CO \cdot H_2O$	12	μ_a=1.055	Two tunneling states observed due to internal motion of the H_2O subunit. Linear heavy atom structure with C atom hydrogen bonded to H atom.
$SO_2 \cdot H_2O$	13	μ_a=1.984 μ_c=0.488	Two tunneling states observed due to internal rotation of the H_2O subunit. Sandwich-shaped structure with the S-O distance shorter than the O-H distance.
$O_3 \cdot H_2O$	14	μ_a=1.014 μ_c=0.522	Two tunneling states observed due to the internal motion of the H_2O subunit. Upper state does not conform to rigid rotor theory. Cross shaped complex with water atoms in the plane of the center O atom of ozone. No hydrogen bonding is evident.
$CO_2 \cdot H_2S$	15	μ_a=0.410 μ_c=0.822	Multidimensional tunneling similar to the water dimer spectrum. Large tunneling splittings (12.5 GHz) are observed for the c-type transitions. T-shaped complex with the H_2S plane ~90° to the linear CO_2 axis.
$(CO_2)_2 \cdot H_2O$	16	μ_b=1.982	Two symmetry states observed with 3:1 intensity ratio. Structure has C_2 symmetry axis with the water oxygen located symmetrically below the plane of the slipped parallel CO_2 units.
$CO_2 \cdot (H_2O)_2$	17	μ_a=1.571 μ_b=0.761	Two states observed with small spectral splittings. Structure is a triple hydrogen bonded system in which all heavy atoms are planar and the two water oxygens and the carbon atom of CO_2 are located at the apices of a triangle.

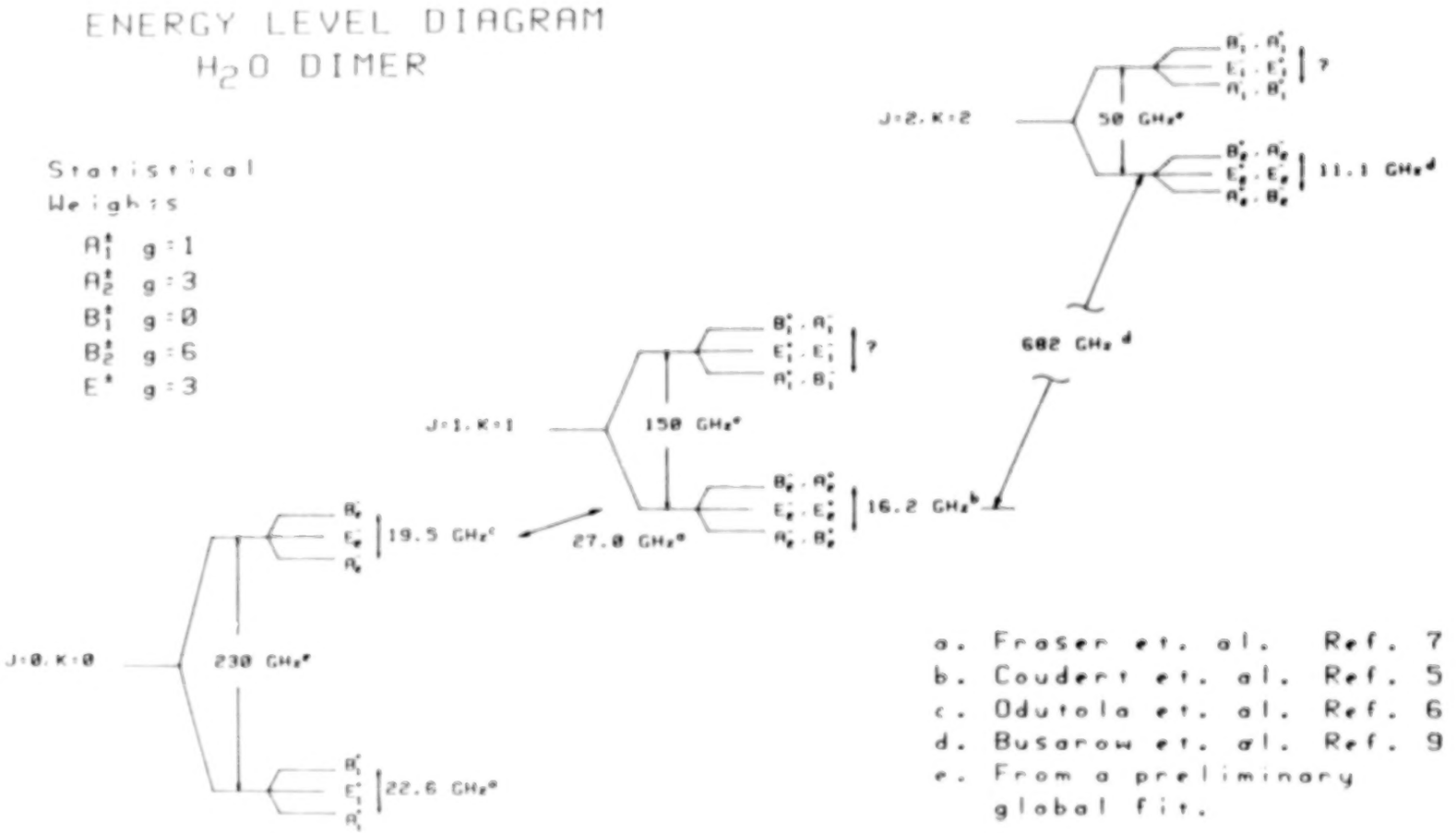

Figure 1. Energy level diagram for $(H_2O)_2$ showing the positions of the K_a and tunneling states as determined from previous studies (Ref. 6 and references cited therein). For the J=1, K_a=1 and J=2, K_a=2 states, two symmetry species are shown for each level to indicate the asymmetry doubling. Frequencies marked with a superscript e are not directly measured but are estimated from a global fit (Ref. 7) of the reported microwave and far-infrared results to a rotational-tunneling Hamiltonian for $(H_2O)_2$.

water dimer spectrum but spectral splittings still occur. There are almost always two states observable due to an internal motion in complexes which contain H_2O. In most cases this is caused by the rather facile motion of water about its C_2 axis within the complex. Structural summaries and electric dipole moments for the complexes which have been studied that are of planetary atmospheric interest are listed in Table I.

CONCLUSION

In this paper, we have summarized the spectral results that have been obtained from the rotational analysis of a number of weakly bound complexes containing CO_2 and/or H_2O. The data presented on the rotational spectra of these species should be useful to experimentalists attempting to analyze the far-infrared and near infrared spectral features of these complexes and also to those investigators involved in the modeling of their spectra in planetary and lunar atmospheres.

REFERENCES

1. D. E. Jennings, J. Quant. Spectrosc. Radiat. Transfer, 40, 221 (1988).

2. K. Fox and S. J. Kim, J. Quant. Spectrosc. Radiat. Transfer, 40, 177 (1988).

3. F. J. Lovas and R. D. Suenram, J. Chem. Phys., 87, 2010 (1987).

4. R. D. Suenram, F. J. Lovas, G. T. Fraser, J. Z. Gillies, C. W. Gillies, and M. Onda., J. Molec. Spectrosc., 137, 127 (1989).

5. L. H. Coudert, F. J. Lovas, R. D. Suenram, and J. T. Hougen, J. Chem. Phys., 87, 6290 (1987).

6. J. A. Odutola and T. R. Dyke, J. Chem. Phys., 72, 5062 (1980).

7. G. T. Fraser, R. D. Suenram, and L. H. Coudert, J. Chem. Phys., 90, 6077 (1989).

8. L. H. Coudert and J. T. Hougen, J. Molec. Spectrosc., in press.

9. Z. S. Huang and R. E. MIller, J. Chem. Phys., 88, 8008 (1988).

10. K. L. Busarow, R. C. Cohen, G. A. Blake, K. B. Laughlin, Y. T. Lee, and R. J. Saykally, J. Chem. Phys., 90, 3937 (1989).

11. H. O. Leung, M. D. Marshall, R. D. Suenram and F. J. Lovas, J. Chem. Phys., 90, 700 (1989).

12. D. Yaron, K. I. Peterson, D. Zolandz, W. Klemperer, F. J. Lovas, and R. D. Suenram, J. Chem. Phys., in press (1989).

13. K. Matsumura, F. J. Lovas, and R. D. Suenram, J. Chem. Phys., in press (1989).

14. J. Z. Gillies, C. W. Gillies, R. D. Suenram, F. J. Lovas, T. Schmidt and D. Cremer, in preparation.

15. J. K. Rice, L. H. Coudert, K. Matsumura, R. D. Suenram, F. J. Lovas, and W. Stahl., in preparation.

16. K. I. Peterson, R. D. Suenram, and F. J. Lovas, J. Chem. Phys., 90, 5964 (1989).

17. K. I. Peterson, R. D. Suenram, and F. J. Lovas, in preparation.

N90-26753

INFRARED LINE PARAMETERS AT LOW TEMPERATURES RELEVANT TO PLANETARY ATMOSPHERES

PRASAD VARANASI
Institute for Atmospheric Sciences, State University of New York at Stony Brook, NY 11794-2300

ABSTRACT

Employing the techniques that we have described in several of our publications for measuring infrared lineshifts, linewidths and line intensities with a tunable diode laser, we have measured these parameters for lines in the important infrared bands of several molecules of interest to the planetary astronomer at low temperatures that are relevant to planetary atmospheres using He, Ne, Ar, H_2, N_2, O_2, and air as the perturbers. In addition to obtaining the many original data on the temperature dependence of the intensities and linewidths, we were also the first to measure the same for the collision-induced lineshift of an infrared line and to show that it was markedly different from that of the corresponding collision-broadened linewidth.

INTRODUCTION AND BRIEF PRESENTATION OF DATA

The parameters describing absorption due to infrared lines of planetary atmospheric molecules are the position, intensity, half-width, lower level energy and the collision-induced lineshift. In the modelling of planetary atmospheres based upon comparison of the observed and calculated planetary spectra, data on the above mentioned infrared line parameters at the relevant atmospheric temperatures would be needed. (Even though the position and the energy level are independent of the temperature of the gas, often in spectra involving hot bands measurements performed at several low temperatures are useful in assigning these two parameters to a line unambiguously.) This need is the primary reason for performing the measurements that have been reported by our laboratory for nearly two decades. To the best of our knowledge, most of the measurements reported in Refs. 1–12 are the first ever

published on the accurate magnitudes as well as the temperature dependence of these parameters. We are the first ever to have measured the temperature dependence of collision-induced lineshifts of any molecule in the infrared at low temperatures. We have used He, Ne, Ar, H_2, N_2, O_2 and air as the gases perturbing the radiative process. Lines formed in the atmospheres of the major planets are broadened predominantly by H_2 and, to a lesser degree, by He. In the atmosphere of Titan, a satellite of Saturn with an atmosphere composed mostly of N_2 and exhibiting CH_4 spectra, N_2-broadening is important. There have been some suggestions, if not indications, recently that Ar might be present in Titan's atmosphere in amounts sufficient to make Ar-broadening also relevant. N_2, O_2 and air were chosen with the terrestrial atmospheric application in mind. Ne was used only in lineshift measurements in an attempt to examine the relationship between the observed lineshifts in the case of the noble gases and of their polarizabilities.

Our tunable diode laser spectrometer, the other necessary equipment, the experimental procedure, and the low temperature absorption cell used in the present studies have been described by us previously.[1-4] The techniques employed for measuring lineshifts, linewidths and intensities have been described in considerable detail by us in Refs. 5, 6, and 7 respectively. We also discussed in detail in Refs. 5–12 the errors to be assigned to the data that we obtained.

This space is too short for a meaningful presentation and discussion of the many data of interest to the planetary astronomer that we have obtained in our laboratory in recent years. The References that we provide at the end of this paper should serve the reader just as well in learning about these data. However, the data that we have measured most recently on the 13.7 μm lines of C_2H_2 have not yet been published and are presented in an abbrieviated form in Tables 1 and 2. The parameter n in Table 1 defines the power law dependence of the collision-broadened linewidth upon temperature.[4]

ACKNOWLEDGEMENTS

This work was supported by the Planetary Atmospheres Program of the Solar System Exploration Division of NASA under Grant-in-Aid No. NGR 33-015-139.

Table 1. Collision-broadened line widths in the 13.7 μ Band of $^{12}C_2H_2$.

Broadener	Line	ν (cm^{-1})	γ_L^0 (cm^{-1} atm^{-1})			n
			295 K	206 K	174 K	
H_2	P(11)	703.2556	0.0926 ±.0020			
	P(8)	710.3198	0.0942 ±.0015	0.1169 ±.0036		
	R(7)	747.9624	0.0928 ±.0017	0.1228 ±.0028	0.1370 ±.0042	0.75
	R(18)	773.7435	0.0851 ±.0016			
	R(19)	776.0810	0.0851 ±.0033	0.1247 ±.0006	0.1055 ±.0025	
	R(21)	780.7532	0.0852 ±.0007		(250 K)	
Broadener	Line	ν (cm^{-1})	γ_L^0 (cm^{-1} atm^{-1})			n
			295 K	206 K	145 K	
N_2	P(11)	703.2556	0.0871 ±.0020			
	P(8)	710.3198	0.0937 ±.0006	0.1246 ±.0031		
	R(7)	747.9624	0.0937 ±.0009	0.1200 ±.0014	0.1617 ±.0013	0.77
	R(18)	773.7435	0.0772 ±.0015			
	R(19)	776.0810	0.0756 ±.0007	0.1018 ±.0032		
	R(21)	780.7532	0.0704 ±.0008			

Table 2. Absolute Intensities, S_J (cm^{-2} atm^{-1}), and Collision-Broadened Line Widths, γ_L^0 (cm^{-1} atm^{-1}), in the 13.7 μm Band of $^{12}C_2H_2$ at 294 K.

Line	ν (cm^{-1})	S_J (cm^{-2} atm^{-1})	γ_L^0 (cm^{-1} atm^{-1})		
			He	Ar	air
P(11)	703.2556		0.0479 ±.0018	0.0597 ±.0011	
P(8)	710.3198	3.76 ±0.06	0.0553 ±.0020	0.0708 ±.0026	0.0980 ±.0034
R(7)	747.9624	16.64 ±0.25	0.0463 ±.0007		0.0897 ±.0006
R(18)	773.7435	2.54 ±0.08	0.0465 ±.0013	0.0473 ±.0002	
R(19)	776.0810		0.0455 ±.0007		
R(21)	780.7532	4.49 ±0.05	0.0442 ±.0006	0.0462 ±.0009	

The absolute intensities reported by Varanasi et al., [*JQSRT* **30**, 497 (1983)] and later adapted into the GEISA and AFGL's HITRAN Data Bases are 3.72, 16.68, 2.50 and 4.58 for the P(8), R(7), R(18) and R(21) lines, respectively.

REFERENCES

1. P. Varanasi, S. Chudamani, and S. Kapur, *JQSRT* **38**, 167 (1987).
2. S. Chudamani and P. Varanasi, *JQSRT* **38**, 179 (1987).
3. P. Varanasi and S. Chudamani, *JQSRT* **38**, 173 (1987).
4. P. Varanasi, *JQSRT* **39**, 13 (1988)
5. P. Varanasi and S. Chudamani, *JQSRT* **41**, 345 (1989).
6. P. Varanasi and S. Chudamani, *JQSRT* **41**, 173 (1989).
7. P. Varanasi and S. Chudamani, *JQSRT* **41**, 335 (1989).
8. P. Varanasi and S. Chudamani, *J. Mol. Spectrosc.*, **134**, 440 (1989).
9. P. Varanasi and S. Chudamani, *Appl. Optics*, **28**, 2119 (1989).
10. P. Varanasi and S. Chudamani, *J.Geophys. Res.* **94**, 13,073 (1989).
11. P. Varanasi and S. Chudamani, *J.Geophys. Res.* **94**, 11,175 (1989).
12. P. Varanasi and S. Chudamani, *JQSRT* **42** (in press).
13. S. Chudamani, *Infrared Spectroscopic Measurements on Planetary Atmospheric Gases.* Ph. D Dissertation, State University of New York at Stony Brook, May 1989.

SPECTROSCOPY AND MOLECULAR DYNAMICS

INVITED

AND

CONTRIBUTED

PAPERS

N90-26754

ABSOLUTE VACUUM ULTRAVIOLET PHOTOABSORPTION CROSS SECTION STUDIES OF ATOMIC AND MOLECULAR SPECIES: TECHNIQUES AND OBSERVATIONAL DATA

D.L. JUDGE and C.Y.R. WU
Space Sciences Center and Department of Physics
University of Southern California
Los Angeles, California 90089-1341

ABSTRACT

Absorption of a high energy photon (> 6eV) by an isolated molecule results in the formation of highly excited quasi-discrete or continuum states which evolve through a wide range of direct and indirect photochemical processes. These are: photoionization and autoionization, photodissociation and predissociation, and fluorescence. The ultimate goal of the study of these processes is to understand the dynamics of the excitation and decay processes and to quantitatively measure the absolute partial cross sections for all processes which occur in photoabsorption. In this paper, typical experimental techniques and the status of observational results of particular interest to solar system observations will be presented.

INTRODUCTION

The spectral region from 2 - 2000Å is called the vacuum ultraviolet radiation (VUV) because, even on a laboratory scale, electromagnetic radiation in this region is absorbed by air, and vacuum techniques are required. As is well known by planetary atmosphere scientists, this is also the wavelength range which is absorbed by all planetary atmospheres and, hence, is of major importance in determining atmospheric heating, photochemistry, and atmospheric structure.

To understand atmospheric structure and dynamics it is thus essential to accurately know the absolute total cross sections for all atoms and molecules which may play a significant role in determining the physical state of an atmosphere. It is also necessary to know the absolute and specific partial cross sections for the fragmentation products as well as their kinetic energy. Tabulations of much of the available data on such processes may be found in publications by Gallagher et al.,[1] Koch and Sonntag,[2] Hudson and Kiefer,[3] Hudson,[4] and Watanabe.[5] Unfortunately, much of the early work on specific cross sections suffered due to a number of experimental difficulties. Early work on photodissociative ionization, for example, was carried out using magnetic sector

PRECEDING PAGE BLANK NOT FILMED

mass spectrometers which severely discriminated against short lived and/or energetic species. Thus, even the relative amounts of ions formed were not well established. Furthermore, such a technique provides no information about the state of excitation, except as can be inferred from energy conservation considerations.

During the past twenty years, however, much has been accomplished with respect to determining both total and partial absolute cross sections throughout the VUV. Such progress has been possible in large measure because of newly developed experimental techniques and technological advances. While an exhaustive in-depth review of the experimental techniques generally employed will not be given here, representative techniques used to obtain the data required for understanding atmospheric processes will be presented in later sections.

A schematic summary of the absorption and decay processes which can occur in the VUV is presented in Fig.1. As can be seen from the figure, ionization,

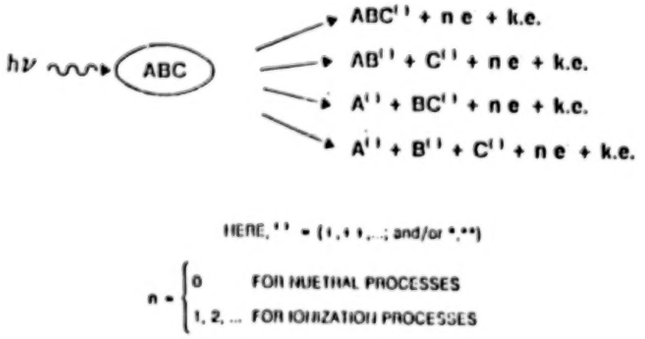

Fig.1. Molecular absorption and decay processes.

dissociation, excitation, or a combination of all three processes may occur. The products all appear in the atmospheric soup driven by the solar VUV radiation and can lead to complex atmospheric chemistry and dynamics. Fortunately, it is now technologically possible to determine the absolute cross sections for all of the reactions shown in Fig.1. In fact, absolute measurements of such processes are being obtained in various laboratories. Recent technological advances of particular importance to such comprehensive measurements are discussed in the next section.

INSTRUMENTATION ADVANCES

There have been several cleverly applied technical advances in the last two decades which have permitted a detailed understanding of many atomic and molecular processes. These advances fall into two categories: 1) Light source development and 2) Detector development. In both of these areas tremendous

progress has been realized.

Light Source Development

Pure continuum light sources for the VUV, particularly the extreme ultraviolet, were not available until the advent of dedicated synchrotron radiation sources. It is now possible for scientists around the world to have access to such sources and to thereby study absorption processes as a continuous function of photon energy. There are about twenty such facilities currently in operation, many of them providing continuum radiation down to wavelengths of a few Angstroms. Representative synchrotron source spectra are shown in Fig.2.

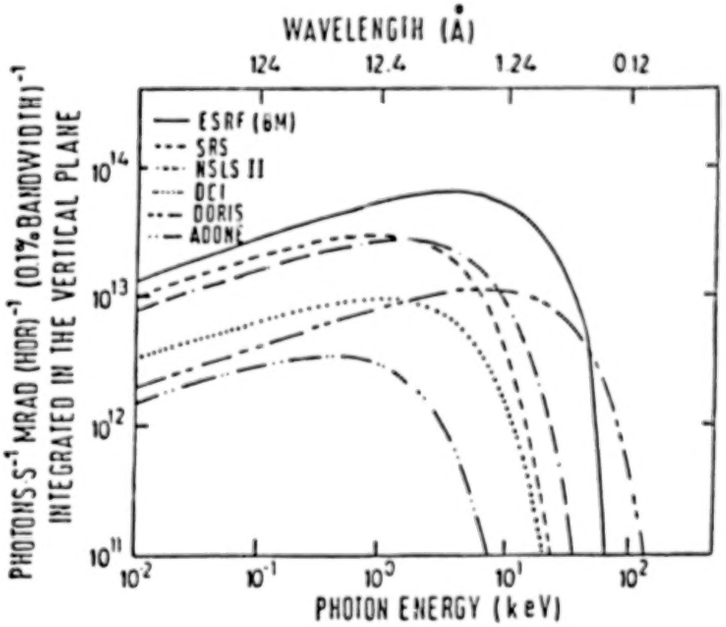

Fig.2. Intensity spectra for several storage rings used as synchrotron radiation sources.

Such sources provide a pure continuum of radiation, with intensities comparable to the average intensities available in conventional laboratory sources which, at best, cover limited wavelength regions and typically have both line and continuum features mixed. Using such mixed sources makes it difficult to measure true absorption cross sections except in regions of continuum absorption with no superposed structure. This is so because the bandwidth for which a monochromator is set generally corresponds not to the bandwidth of the incident source line but to the bandwidth for continuum radiation.

In addition to the synchrotron source another significant advance in light source capability has come from advances in laser technology. It is now possible to purchase lasers which are tunable over a significant wavelength region in the VUV. Nd:YAG tunable dye lasers with appropriate non-linear elements provide

useful radiation down to about 760Å. The linewidth of such sources can be $<0.3 cm^{-1}$ so that features as narrow as several mÅ can be resolved in the VUV. Such sources[6,7] have been shown to have a VUV linewidth comparable to that previously available from a 6.5-m spectrograph. Thus, the prospect of carrying out high resolution spectroscopy in a conventional laboratory is now both possible and affordable in the window region of the VUV. This is also a particularly important region since it includes the spectral range where absorption by hydrocarbons, and other molecules present in the lower atmospheres of several planets, show significant diagnostic absorption features.

Detectors

To complement the improved light sources, photoelectric detectors have been highly developed and are now used almost exclusively in lieu of photographic recording. This has permitted a number of experimental advances which are now widely employed in both particle and electromagnetic detection. Fast photoelectric detectors (and short pulse light sources) permit direct measurement of lifetimes as short as ~ 1 ns. Synchronous detection of events has made it possible to identify correlated events, again on a time scale of several nanoseconds.

The development of photoelectric array detectors has been particularly important as a replacement for photographic plates in the focal plane of spectrometers. Such detectors have made it possible to greatly improve the speed with which a spectrum can be obtained. In addition, they also make it possible to follow the temporal and spatial evolution of dynamical processes in unimolecular systems, as well as in high density, collision dominated systems. Such detectors are commercially available as charge coupled detectors (CCD's), intensified CCD's (ICCD's), and resistive anode arrays.

The time scales for electric dipole and other transitions, in the absence of collisions, are given in Table I, and have been included as a reminder of the tremendous range of times of interest in the investigation of molecular processes. The temporal requirements imposed on laboratory instrumentation, both on the light sources and the detectors, are of course determined by such time scales.

An overview of the data obtained in photon-molecule interaction studies in the VUV is briefly described in the next section.

Table I Time Scale for Electric Dipole, Magnetic Dipole and Quadrapole Transitions for Photon-monomolecular Processes

Process	Type of Transition	Time (sec)
Excitation	Electronic - Electric Dipole	$\sim 10^{-15}$-10^{-16}
	Vibration - Electric Dipole	$\sim 10^{-13}$
	Rotation - Electric Dipole	$\sim 10^{-12}$
	Metastable - Magnetic Dipole	$\sim 10^{-12}$
	Metastable - Quadrupole	$\sim 10^{-9}$
Ionization	(Direct or Indirect)	$\sim 10^{-15}$-10^{-12}
Dissociation	(Direct or Indirect)	$>10^{-13}$
Radiative Decay	Electronic - Electric Dipole	$>10^{-9}$
	Vibrational - Electric Dipole	$>10^{-4}$
	Rotational - Electric Dipole	$>10^{-3}$
	Metastable - Magnetic Dipole	$>10^{-3}$
	Metastable - Quadrupole	>1

Absorption and Ionization Cross Section Measurements

The total absorption cross section at a given incident photon energy is a measure of the sum of the partial cross sections shown in Fig.1. At wavelengths shortward of the ionization limit of the gas of interest, electrons and ions are produced. The photoionization yield can be determined through measurement of the ions produced and/or photoelectron spectroscopy. A recent review of such measurements, primarily in the XUV ($\lambda \leq 1000$Å), and a compilation of the absolute cross sections for a number of gases of planetary interest for molecular photoabsorption, and partial photoionization, is given by Gallagher et al.[1]

The measurements discussed above have been concerned with the primary photoabsorption process and the initially formed products. The "final" products which evolve through predissociation, preionization, etc. are also of great interest. It is the final products, in fact, which in general are of the most importance in atmospheric chemistry. Most redistribution of energy within a molecular system occurs on a time scale which is short compared with the mean time between collisions, except for metastable states (see Table I).

To probe these final states, fluorescence spectroscopy provides a powerful tool. To identify excited final state fragments one can simply disperse the fluorescence and thereby determine the species formed, their states of excitation, and (from the brightness) the cross sections for the production of specific states down to the rotational level. To detect species which have been formed either in the ground state, or in a metastable state, the observation of scattered radiation from tunable laser sources provides an effective technique. The fluorescence technique has been pioneered by our group at USC and has proven quite useful for the determination of absolute cross sections for the production of final state products. Examples of final state identification for molecular fragments of particular planetary interest will be given in the next section as specific results of interest in planetary and cometary physics.

Another final state determination of particular interest to planetary atmosphere physics is the kinetic energy carried by the fragments produced. Such experiments have also been recently initiated in our laboratory. It has been found that quite a large kinetic energy is produced in both N and H fragments through photodissociation of N_2 and H_2. Implications for the optical thickness of a planetary atmosphere as well as non-thermal escape may be seen in the observational data. Results of this recent work will be reviewed in the following section.

SELECTED LABORATORY RESULTS AND DISCUSSION

In the present section we show selected results of interest in planetary and cometery investigations. These are of four types: 1) Modest resolution absorption spectra showing the dependance of measured cross sections on temperature and spectral resolution, 2) Photofragment identification (through radiative decay observations), 3) Kinetic energy distribution of photofragments, 4) Photon sputtering of ice. These few observational areas have been selected for discussion because they are representative of the laboratory data base which is required to support solar system atmospheric studies. The chemistry, convection, radiative transfer, and general characteristics of planetary atmospheres are all coupled to the primary photoabsorption processes which are discussed.

Cross Section Data

With regard to the cross section data, item 1) in the above list, it is

a fact that the supporting laboratory spectroscopic data are almost always less complete and of lower quality than the flight observational data. This deficiency will become much worse as observational capability in other areas increases, for example with the launch of Space Telescope. As may be seen in Fig.3, data obtained at room temperature and low pressures are still incomplete,

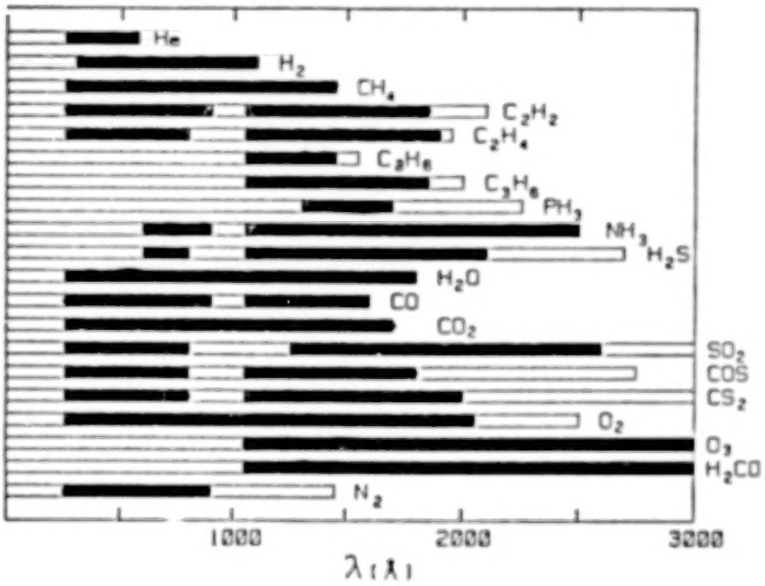

Fig.3. This figure summarizes the absorption region of the molecules of primary interest. The solid area indicates that gaseous photoabsorption cross sections have been measured as a continuous function of the incident photon wavelength.

and are virtually absent for other conditions of temperature, pressure, and relative abundance. Virtually all of the presently available absorption cross section data were taken at pressures, temperatures, and relative abundances very different from atmospheric conditions and are, therefore, of limited utility. It is known, for example, that when more than two kinds of molecules in a gas mixture absorb light in the same wavelength region, the total absorption cross section may become more complicated than merely the sum of the individual absorption cross sections, obtained at the usual laboratory conditions, i.e., 300°K and low pressure. The reasons are as follows: (i) at elevated temperature the population of higher vibrational levels (overtones and combination bands) may become significantly increased. This can result in a significant change in the amount of absorption at a given wavelength, and shift the effective ionization and dissociation thresholds. This in turn affects the penetration of solar ultraviolet radiation and ion production rates at high altitude,[8] and the molecular lifetimes.[9] The cross sections of molecules at low temperatures thus cannot be accurately obtained from the extrapolation of room temperature data, since at room temperature the absorption from vibrational and rotational levels other than the vibrationless ground state contribute to the observed cross

section. (ii) High pressure, up to several atmospheres, in an absorbing system can cause line broadening, line shifts, and pressure-induced transitions. The line shift may be to the blue or to the red of the spectral line, showing asymmetric broadening, while dipole-forbidden transitions become allowed transitions.[10,11] (iii) Real atmospheres consist of a mixture of various molecules. As we know from (ii) the pressure effects may vary in nature depending on the characteristics of the collision constituents.[12] It is thus desirable to measure the cross sections of molecules under the conditions of the planetary atmosphere of interest. For example, to model the albedos of Jupiter, Saturn, and other planets, obtained from IUE data, Caldwell and Owen[13] have pointed out the need for the absorption cross sections of PH_3, H_2S, C_2H_2, NH_3 and C_2H_6 in the 1600 - 2100Å spectral region, at temperatures varying from 300 to 150°K and absorber abundances varying from 0.2 - 5cm-atm. Unfortunately, very little progress has been made since this need was pointed out.

Continuing research using IUE data further indicates that cross sections for a number of complex hydrocarbons will soon be required. As an example, we review the IUE data of Jupiter[14] in the 1400 - 1900Å region, shown in Fig.4. Since Jovian C_2H_2 dominates in the 1750 - 1900Å absorption region, a mixing ratio of $3x10^{-8}$ (Fig.4a) is required in order to obtain a good fit between observational data and model calculations.[14,15] With this mixing ratio it is obvious that there must be additional absorbers present in the wavelength region shortward of 1750Å. If small amounts of allene (C_3H_4, Fig.4b) and also cyclopropane (C_3H_6, Fig.4c) are included in the model calculations[14] an improved fit to the general variation of albedo with wavelength is obtained, although information on the positions and bandwidths of many features in the spectrum

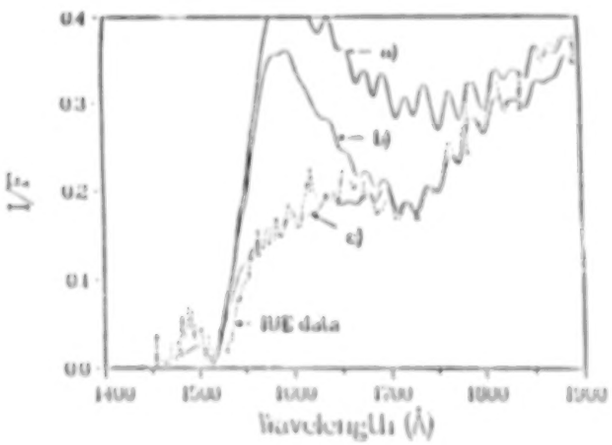

Fig.4. Dashed line: IUE data. (a) Model spectrum with C_2H_2 (mixing ration $3x10^{-8}$, C_2H_6 ($2x10^{-6}$) and CH_4($1.7x10^{-3}$) in Jovian stratosphere (0 to 100mbar) and the model of Goldstone and Yung (1983) for 100 to 60mbar. (b) Model spectrum as in (a)but including allene ($7x10^{-10}$). (c) Model spectrum as in (b)but including cyclopropane ($8x10^{-9}$)

clearly needs to be improved. The fit is not good enough to prove conclusively that the identification of trace gases other than C_2H_2 is unique.

One strong possibility for the discrepancy in fine detail may be the fact that the molecular cross section data used in the calculations were measured at room temperature (≈300°K), which is very different from that in the Jovian atmosphere (~150°K) at the absorbing level. The temperature effect may well explain why the IUE data show a spectral bandwidth narrower than model calculations predict. Further, inclusion of the temperature effect on the molecular cross sections will accordingly change the required mixing ratios of various absorbers. It is therefore clear that such measurements are required and will contribute to our current understanding of planetary atmospheres.

Absorption Cross Section for Acetylene

In the absorption cross section discussion presented below we will only discuss the temperature dependence of the absorption cross section of C_2H_2 (Acetylene) in a wavelength region of significant absorption in the outer planets. Figures 5 and 6, respectively, show our recently obtained absolute cross sections of C_2H_2 in the 1530 - 1930Å region measured at room temperature (295°K) and at 115°K.

As can be seen from Fig.5, the complex absorption features are clearly superimposed on a broad "continuum" (or "continua"), with the most intense features being the 3_o^6 and 3_o^7 peaks. Under room temperature conditions, the largest cross section value of the B - X transition is 1.7Mb (1Mb = $10^{-18}cm^2$) for

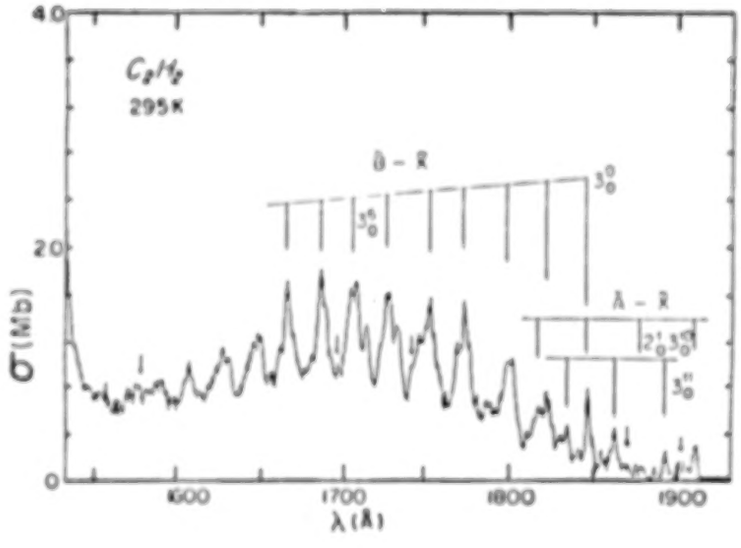

Fig.5. The absolute photoabsorption cross section of C_2H_2 in the 1520 - 1900Å region. The data are obtained with a spectral bandwidth (FWHM) of 0.8Å and at a temperature of 295°K.

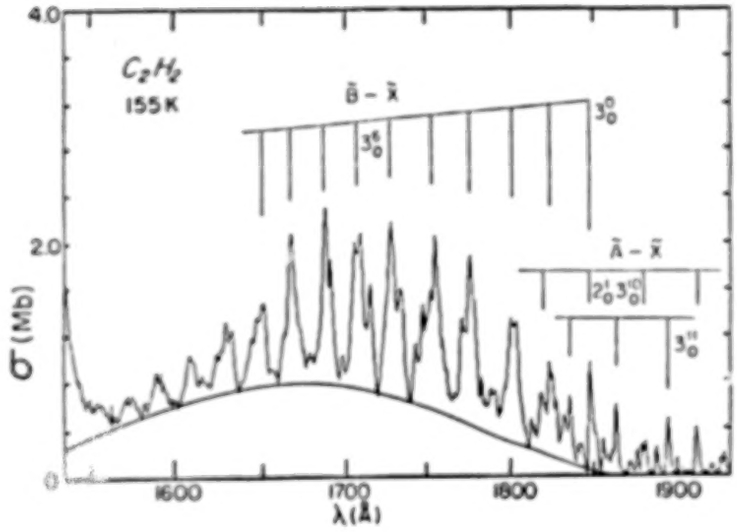

Fig.6. Same as Fig.5 except the cross section data are obtained at a temperature of 155°K.

the 3_o^6 peak. The smallest is less than $10^{-19}cm^2$ for the $\tilde{A}$ - $\tilde{X}$ transition on the long wavelength side.

Clearly the low temperature cross sections obtained at 155°K are quite different from those measured at room temperature. As one can see from Fig.6, the peak cross sections of the 3_o^5, 3_o^6 and 3_o^7 bands are about equal in magnitude (i.e., 2.2 Mb) with 3_o^7 being the largest peak. The drop in peak cross sections from the 3_o^7 peak to the 3_o^n with n≥8 becomes quite pronounced. Such a sudden drop can be due to vibrational predissociation through perturbations.

The resolution of the low temperature spectrum is "apparently" (but only apparently) better than that obtained under room temperature conditions. Many broad features become resolved into several peaks. The most striking effect on the absorption profiles occurs in the 1580Å region and in the wavelength region longward of 1800Å. Several unmeasurable band heads of the $\tilde{A}$ - $\tilde{X}$ transition under room temperature conditions clearly become identifiable peaks at low temperature. These peaks are the $2_o^1 3_o^n$ progression with n=8 and 7 and the 3_o^n progression with n=8 and 9. Further, the sharpness of the peaks allows a better wavelength measurement and, hence, a better determination of the vibrational constants which are applicable to high quantum numbers. Those peaks marked by an arrow as shown in Fig.7 appear to be hot bands. Considering a polyatomic molecule as large as C_2H_2, it is suprising that hot band absorption is apparently quite sparse in this spectral region, particularly in the region of the $\tilde{B}$ - $\tilde{X}$ transition.

To summarize the temperature dependent studies, it is found that the low temperature cross section values at absorption peaks increase by 10% - 40% while

those at absorption valleys decrease by as much as 30%, when compared to the room temperature measurement. The cross section values of the "continuum" absorption are also correspondingly reduced somewhat. The application of the new low temperature data to the interpretation of Saturn's albedo has been discussed in the Conference Proceedings by Caldwell et al.

An example of how the low resolution also affects such cross section data may be found in the review by Hudson.[4] Figure 7 shows $n\sigma\ell$ vs. $\ln(A_0/A)$ for various ratios of α ($\alpha=\Delta\lambda/\Delta L$). Here n is the gas density in an absorption cell of length ℓ, the cross section is σ, A_0 and A are the incident and transmitted intensities, respectively, $\Delta\lambda$ is the monochromator bandwidth for a continuum background, and ΔL is the Lorentz full width at half maximum (FWHM) for an absorption feature. If the resolution of the instrument is significantly less than the true width of the structure (spectral features) being observed then the true cross sections, σ_T, will be measured. If $\sigma_T=\bar{\sigma}_T$, the average cross section, a straight line of slope one would be obtained in the above plot. If $\alpha \leq 0.3$

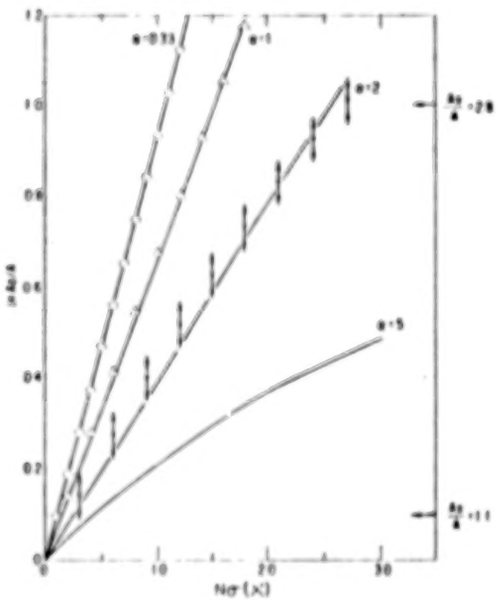

Fig.7. Calcculated values of $\ln(A_0/A)$ vs. $N\sigma(\lambda')$ for four values of α ($\alpha=\Delta\lambda/\Delta L$) assuming a Lorentz line shape.

measurements of σ_T to an accuracy of $\lesssim 1\%$ are obtained. For $\alpha=1$, the measured cross sections, i.e. $\bar{\sigma}_T$, will be only ~70% of σ_T. As might be expected, particularly in the early literature, it is often not clear what the effective resolution of the instrument and light source combination actually was. All cross sections should thus be carefully considered before they are used in modelling calculations. Remeasurement of many of the cross sections in the literature will unfortunately need to be carried out. In any case, most of them should be remeasured for planetary atmosphere applications since room temperature

data are only applicable to a very limited range of planetary atmosphere conditions.

Photofragment Identification

Photofragments, as discussed earlier, can be identified by a variety of techniques. Photoelectron spectroscopy provides data on the initial fragments formed in ionization processes. As internal rearrangements occur, the final products may be different from the initial state products. In addition, neutral fragments are not detected by such techniques.

A dispersed fluorescence spectroscopy technique which detects and identifies the final state products was developed at USC in the early 1960s. In such work both the photons incident on the gas of interest and the emitted photons are dispersed. In this way excited fragments ultimately produced in photoabsorption processes are observed and the absolute partial cross sections for their production are determined. As an example of the results which can be obtained from such work, let us consider the photoabsorption and photofragmentation spectrum of H_2O (see Fig.8).

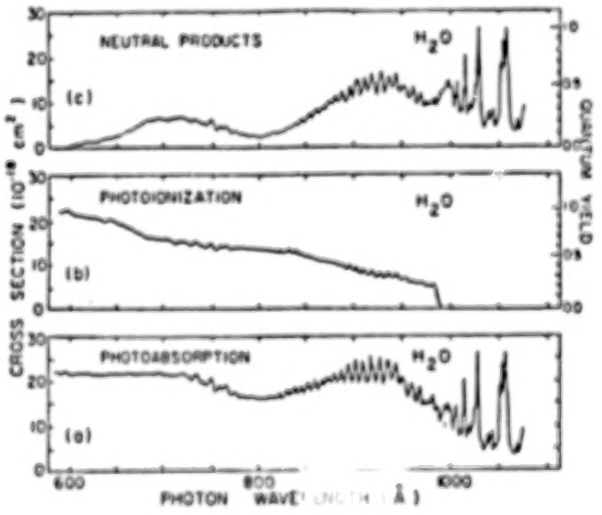

Fig.8. The absolute cross sections of (a) photoabsorption, (b) photoionization, and (c) neutral products in the 600Å (20.66 eV) - 1200Å (10.33 eV) region.

H_2O Fragmentation

The photoabsorption and photoionization cross sections of H_2O in the 600 - 1100Å region are shown in Figs.8a and 8b, respectively. In this region significant dissociation into neutral fragments is clearly evident since the total absorption and ionization cross sections are not equal to each other. For wavelengths shorter than ~600Å, the photoionization cross section is equal to the total photoabsorption cross section; i.e., the photoionization efficiency

of H_2O is unity. By subtracting the ionization cross section from the total absorption cross section, we obtain the cross section for neutral products which is shown in Fig.8c. The neutral products include ground, metastable, and excited state neutral photofragments. The quantum yield, which is defined as the ratio of the partial cross section of interest to the total photoabsorption cross section, for the respective neutral products and ionization is indicated on the right-hand side of Figs.8b and 8c. As can be seen, the maximum quantum yield for producing the neutral products is 1.0, ~0.6, and ~0.3 for the wavelength range > 984, 800 - 984, and 600 - 800Å, respectively.

It is well known that fluorescence from the excited states of the neutral H_2O molecule and parent H_2O^+ ion have rarely been observed.[16] The fluorescence quantum yield of the first excited state of the $H_2O^+(\tilde{A}\ ^2A_1)$ ion is extremely small. The second excited ion state $\tilde{B}\ ^2B_2$ is not known to fluoresce, while the third excited ion state $\tilde{C}\ ^2A_1$ is completely predissociated.[16] In contrast with this, the fluorescence from excited photofragments, especially the H Balmer series and OH(A→X), is intense and has high quantum yields. Since the OH fragment is of particular interest a brief description of the OH observations follows.

The partial cross section for producing the OH(A→X) emission has been measured at several discrete primary photon wavelengths longer than 760Å using an atomic line emission source. The band contours of the (0,0) band are shown in Fig.9. A fraction of the photon excitation energy is converted into internal energy. It is quite evident from Fig.9 that higher rotational energy levels are excited as the incident photon energy is increased.

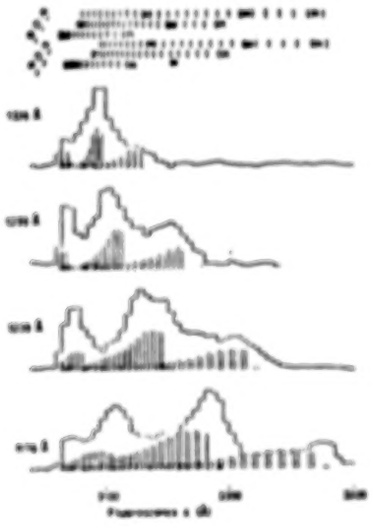

Fig.9. The OH($A\ ^2\Sigma^+ \rightarrow X^2$) fluorescence spectra in the λλ 3060 - 3300Å region produced at various primary photon wavelengths, compared with the theoretical synthetic rotational spectra of the OH($A\ ^2\Sigma^+$, $\nu'=0,J' \rightarrow X^2$, $\nu''=0,J''$) band, for which the radiation rates are indicated as vertical lines. The positions of the rotational lines for the six intense branches of the OH band are also indicated at the top of the figure.

ORIGINAL PAGE IS
OF POOR QUALITY

The OH(A→X) fluorescence excitation functions in the 180 - 760Å and 1050 - 1350Å regions have also been obtained using a synchrotron radiation source. In the former spectral region, the maximum partial cross section occurs at about 703Å and is $3.4 \times 10^{-20} cm^2$, giving a quantum yield of 2×10^{-3}. Shortward of 700Å the partial cross section decreases sharply to a magnitude of $\sim 5 \times 10^{-21} cm^2$.

Atomic hydrogen fragments associated with the dissociation of H_2O have also been observed as well as upper limits to the production of atomic oxygen and molecular hydrogen, but a discussion of these results is beyond the purpose of the present work.

Kinetic energy measurements of molecular fragments

The kinetic energy distribution of atomic fragments is particularly important since these fragments may have considerable kinetic energy, thus modifying atmospheric reaction rates and escape rates. In the example given below, the processes which correlate with the photo-production of an excited neutral hydrogen atom and a hydrogen ion are discussed.

Specifically, we have utilized a fluorescence photon-photoion coincidence technique to study the processes:

$$H_2 + h\nu\ (\lambda 304Å) \rightarrow H(n\ell,\ n \geq 2) + H^+ + e^- \qquad (1)$$

$$H(2p) \rightarrow H(1s) + h\nu'(\lambda = 1216Å)$$

We have carried out the experiment by measuring the coincidence time delay between the detection of the emission of a H Lyα photon and a H^+ ion produced through photon excitation of H_2 at a photon wavelength of 304Å. It should be noted that from energy and momentum conservation the excess excitation energy, defined as the difference between the incident photon energy and the threshold energy for the process of interest, minus the kinetic energy of the photoelectron will be equally divided between the excited $H(n\ell)$ atom and the H^+ ion. Thus, the kinetic energy distribution measured for the H^+ ions is equivalent to that for the excited $H(n\ell)$ atoms.

The experimental data are obtained by means of a coincidence detection system.[17] A true coincidence count results when the output of the TAC is turned-on by a photon pulse, e.g., λ = 1216Å, and turned-off by the H^+ pulse. Both the 1216Å photon and the H^+ ion have to be produced from the same H_2 molecule. Only under these conditions would the process indicated in Eq.(1) show up preferentially in a specific range of time delay, Δt, resulting in the observed

peak. False coincidences result from everything else and would show up as background since they are random events.

From Fig.10 we see a clear increase in the coincidence counts at a time delay of 5.6 μs. After reaching a maximum at Δt ~ 6.5 μs the coincidence counts start to slowly decrease, followed by a much weaker peak in the 7.7 -8.5 μs region. The asymmetry obvious in the shape of the major peak suggests that it may arise from more than one dissociative excitation process. The kinetic energy distribution obtained is shown in Fig.11. As one can see, the H^+ ions (and excited H atoms) produced through photoexcitation of H_2 at 40.8 eV possess kinetic energies ranging from 1.2 to 7.5 eV.

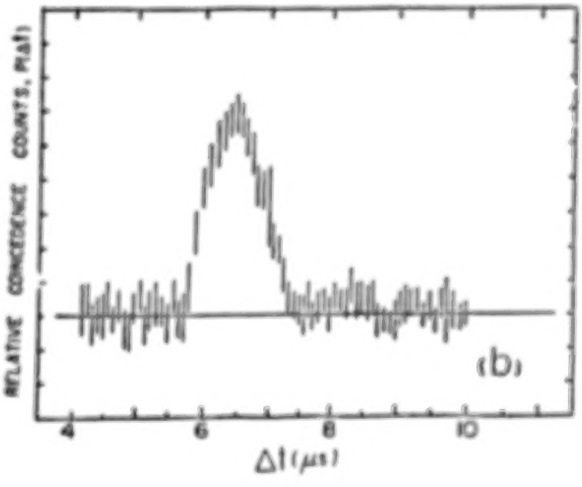

Fig.10. Relative coincidence counts vs. time delay.

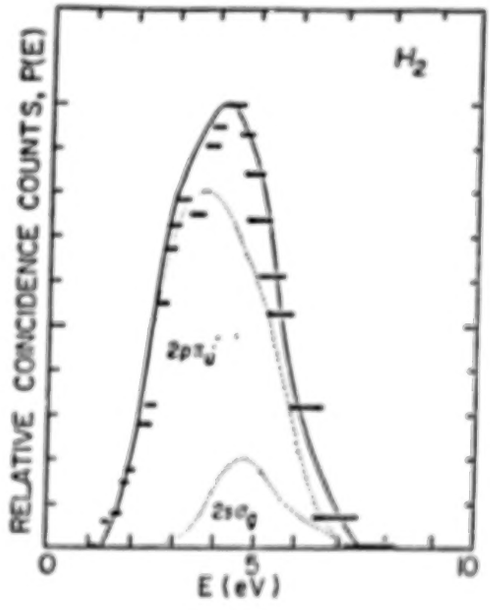

Fig.11. Relative coincidence counts vs. energy.

Using He II 304Å (40.8 eV) photons, Gardner and Samson[18] found that the direct dissociative ionization of H_2 involving the $2p\sigma_u$ state accounts for 44.4% of the total signal while dissociative ionization involving states of higher energy than the $2p\sigma_u$ accounts for the remaining 55.6%. Combined with the present results, we now find the relative partial cross section for dissociative photoionization of H_2 to be the following:

$$2p\sigma_u : 2p\pi_u : 2s\sigma_g \sim 1.0:1.0:0.25 \qquad (2)$$

The partial cross section for producing H Lyα emission through photoexcitation of H_2 has recently been reported by Glass-Maujean.[19] As

indicated in Eq.(1), the present experiment measures cross sections related to those of Glass-Maujean. After subtracting the contribution from the two-electron excited states, $Q_1\ ^1\Pi_u(1)$ and $Q_2\ ^1\Pi_u(1)$, the partial cross section for producing H Lyα from H_2 at 40.8 eV is $4.5 \times 10^{-20}cm^2$ (see, Fig.3 of Ref.19). If we assume, as Glass-Maujean implicitly did, that the partial cross section in the energy region higher than 40 eV is solely due to the $^2\Pi_u$ state, i.e., the $2p\pi_u$, then we can deduce the partial cross section for the dissociative photoionization of the $2p\sigma_u$, $2p\pi_u$, and $2s\sigma_g$ states to be 3.6×10^{-20}, 3.6×10^{-20}, and $9.0\times10^{-21}cm^2$, respectively.

From the above results it is thus clear we have demonstrated that the present technique is a powerful tool for studying dissociative photoionization excitation processes. It allows us to study states correlating only with excited neutral and ion photofragments. The kinetic energy distributions obtained from the present work show that the H^+ ions as well as the H atoms produced possess high kinetic energies. For an H atom, the escape velocity on Earth is 11.179 km/s which is equivalent to a kinetic energy of 0.65 eV. Since solar extreme ultraviolet photons at 304Å, and shortward, are absorbed in the Earth's upper atmosphere, it is clear that the presently observed photodissociative ionization of H_2 contributes to the non-thermal escape of atomic hydrogen from the Earth's atmosphere.

Photon sputtering of ices

Investigations of the efficiency of photon sputtering of ices have been extremely limited, and the available data are quite incomplete and inconclusive (Haff et al.[20]). The only measurements of adsorbed gases which exist are those by L. Greenberg[21] using a broadband UV (~ 2000 - 2750Å) photon source. The molecular ices which he studied have virtually no absorption in the case of H_2O, CH_4, and CO_2, and little absorption in the case of CS_2, O_2 and NH_3. Not surprisingly, he found a desorption quantum yield of ~ 10^{-6}, see Table II.

Given the complete lack of data in the strongly absorbing region of these molecular gases it is clear that such data are sorely needed. We have accordingly initated experiments to measure the required sputtering rates. The first data have just been obtained on water ice at 584Å and the preliminary results are included in the Conference Proceeding in a paper by Wu and Judge. This report, it should be noted, only addressed the charged particles which were ejected. It should also be noted that the yield of positive ions above, at

Table II Photodesorption Yield for Physically Adsorbed on Quartz

Yield	Molecule	Temp(K)	k(P)	Comment	Ref.
$\sim 1\times10^{-5}$ a)	CS_2	77	Broadband 2000-2750Å from a Hg-Xe lamp	abs. <2200P $\sigma\geq8\times10^{-22}cm^2$ b)	Greenberg [1973]
$\sim 1\times10^{-6}$ a)	CO_2	"	"	no abs.	"
"	O_2	"	"	Herzbergband $\sigma\geq10^{-23}cm^2$	"
"	CO	"	"	no abs.	"
$10^{-7}\sim10^{-8}$ a)	H_2O	"	"	"	"
"	NH_3	"	"	abs <2150Å $\sigma\geq1.5\times10^{-17}cm^2$ c)	"
"	CH_4	"	"	no abs.	"
1.3×10^{-2}	I_2	"	5900Å dye laser	Spin-forbidden Transition (B-X); $\sigma\sim1.2\times10^{-18}cm^2$ c)	Bourdon et al. [1982]
4.8×10^{-4}	"	"	4880Å Ar^+ laser	" ; $4.0\times10^{-18}cm^2$ c)	"
1.8×10^{-1}	Br_2	60	5500Å dye laser	" ; $3.8\times10^{-20}cm^2$ c)	"
$<9.2\times10^{-5}$	"	20	"	"	"
2.9×10^{-2}	Cl_2	60	4880Å Ar^+ laser	" ; $3.8\times10^{-21}cm^2$ c)	"
$<1.5\times10^{-5}$	"	20	"	"	"

a) According to Bourdon et al. [1982], those yields measured by Greenberg should be $\lesssim 10^{-10}$. b) Gas phase data taken from Wu and Judge [1981b].
c) Solution data taken from Mellor [1963].

584Å, was a factor of 100 higher than the total yield reported by Greenberg.[21]

In order to appreciate the spectral range where photon sputtering should be important, it should be noted that the molecular ices listed above are like electrical insulators with electronic band gaps of ≥ 10 eV. Because of the lack of conduction electrons both the electrical conductivity and the thermal conductivity in these ices are poor. This lack of free electrons in the ices enhances the probability that energy deposited in electronic excitations will be converted partly to translational energy of the excited icy molecules and thereby contribute to the sputtering efficiency.

The desorption rate strongly correlates with the excitation of electronic

states of the adsorbed molecule which is physisorbed and/or chemisorbed on the substrate. Thus, it is clear that the low desorption yields measured in Greenberg's experiment[21] are not surprising, as neither the electronic states of the adsorbed molecular ices, nor the substrate, significantly absorb the incident long wavelength UV photons. Further, it is highly probable that the ~ 10^{-1} yields in the halogen photon desorption experiments reported by Bourdon et al.[22] may show a significant increase if electric-dipole allowed transitions were to be excited rather than the spin-forbidden processes which they observed. As can be seen from Table II, a wide range of desorption yields are possible, depending on the molecule and the photon energy.

In the work just begun at USC, strong transitions involving Rydberg states of H_2O ices will be excited using VUV/EUV photons. The substrates which will be used are LiF and sapphire, and are transparent for $\lambda > 1050$Å, and > 1410Å, respectively. Additional contributions to the desorption rate may be observable if the substrate absorbs the incident photons.

Since the sputtered products include both neutral particles and ions a variety of experimental techniques are required for their detection. Namely, (a) excited particles will be detected by a fluorescence photon counting technique, (b) ions will be detected by a mass spectrometer, (c) neutral particles will be detected by a selective photoionization mass spectrometer, and (d) certain special radicals and ground state species will be detected by a laser-induced fluorescence technique.

CONCLUDING COMMENTS

It is clear that experimentalists working in support of the planetary atmospheres program must endeavor to fill the data voids in the research areas discussed in this report. There is almost no absorption cross section data available which is truly representative of the temperature, pressure, and mix of gases actually encountered in planetary and cometary environments. For those processes which occur in the lower strata of planetary atmospheres, it is crucial that cross section data at temperatures at least as low as 50°K be obtained. It is, of course, only the long ($\lambda \gtrsim 1000$Å) and short ($\lambda \lesssim 100$Å) wavelength VUV radiation which reaches the lower altitudes where such temperatures typically occur.

The upper atmospheres of planets are normally hot (Mars being a rather notable exception, as well as Venus on the night side) with thermospheric

temperatures of ~ 1000°K. The absorption spectrum of gases at such high temperatures is, of course, quite different from room temperature and/or low temperature spectra. A rather dramatic example of this may be seen in the molecular oxygen absorption spectrum of Hudson and Carter[23] as shown in Fig.12 where the temperature values are 300, 600, and 900°K.

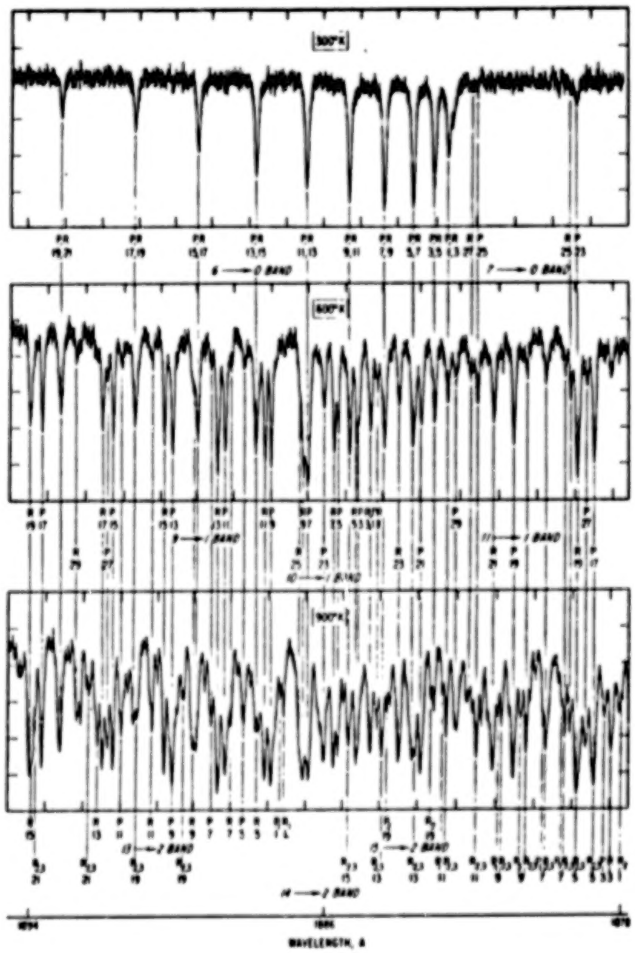

Fig.12. Absorption by molecular oxygen between 1878 and 1894Å at 300, 600, and 900°K.

All of these data, i.e., low and high temperature data, with and without buffer gases, must be obtained at high resolution in the structured regions. Spectral resolution of the order of ~ mÅ is required to approach the linewidth of the absorbing atoms and molecules in planetary atmospheres in the regions of significant structure in the absorption spectra.

Product identification of the species formed in photoabsorption is another data set which is required in order to correctly interpret atmospheric processes. Since the chemistry which occurs in planetary atmospheres is crucially dependent on the state of excitation of the reacting species, the absolute cross sections for the formation of all product species must be determined. In such work, significant progress has been realized. However, the identification of, and

ORIGINAL PAGE IS
OF POOR QUALITY

absolute cross sections for, the production of important metastable and ground state species remains in a very early state of development. Here, laser induced fluorescence techniques can be quite useful in resonance scattering identification or, in the case of metastable species, by exciting them to higher states from which they can fluoresce, and thereby be detected.

The measurement of photofragment kinetic energies is also an area where much remains to be done. Since non-thermal escape may be an important loss process for exospheric gases, it is essential that the kinetic energies for exospheric species be accurately measured as a function of wavelength, at least for the major solar emission lines in the VUV. The optical thickness of an atmosphere also depends on the kinetic energy of the atmospheric species and so radiation transfer calculations require data on the production rate of hot atoms.

Another area which was not discussed in this review is the lack of absolute absorption and fragmentation cross section data for radicals. This area is particularly devoid of data because the experimental techniques required are particularly demanding. Such research, however, is also quite important and should be vigorously pursued since radicals are highly reactive species.

Finally, photon sputtering of ices has been briefly discussed here because it may produce gases which are important constituents of planetary environments. As indicated earlier, this type of research has been almost completely ignored and must be investigated down into the soft X-ray region of the solar output. Non-thermal escape (sputtering) processes may well be far more significant than thermal processes alone.

While the above review was by no means exhaustive it has discussed the major deficiencies in the experimental data base relevant to the primary interactions of VUV photons with planetary gases (and solids).

Acknowledgments - This work was supported by NASA Grant #NGR-05-018-180. We are also grateful to the staff of the Synchrotron Radiation Center of the University of Wisconsin where much of the work presented here was obtained. The Synchrotron Radiation Center is supported by the National Science Foundation.

References

1. Gallagher, J.W., C.E. Brion, J.A.R. Samson, and P.W. Langhoff, "Absolute Cross Sections for Molecular Photoabsorption Partial Photoionization, and Ionic Photofragmentation Processes", J. of Phys. and Chem. Ref. Data, 17, 9 (1988).

2. Koch, E.E., and B.F. Sonntag, "Synchrotron Radiation", Topics in Current

Physics, 10, ed. C. Kunc, (Springer-Verlag, Berlin: 1979).

3. Hudson, R.D., and L.J. Kieffer, "The Nature of Stratosphere of 1974", CIAP Monograph 1. Department of Transportation Climatic Impact Assessment Program, Chap. 5 - 156, (1975).

4. Hudson, R.D., "Critical Review of Ultraviolet Photoabsorption Cross Sections for Molecules of Astrophysical and Aeronomic Interest", Nat. Stand. Ref. Data. Ser., NBS-38 (U.S. Government Printing Office, Washington, D.C.: 1971).

5. Watanabe, K., Adv. Geophys., 5, 153 (1958).

6. La Roque, P.E., R.H. Lipson, P.R. Hermann, and B.P. Stoicheff, J. Chem. Phys., 84, 6627 (1986).

7. Marinero, E.E., L.T. Rettner, R.N. Zare, and A.H. Kung, Chem. Phys. Lett., 95, 486 (1983).

8. Hunten, D.M., and M.B. McElroy, J. Geophys. Research, 73, 2421 (1968).

9. Stief, L.J. Mulecules in the Galactic Environment, eds. M.A. Gordon and L.E. Snyder, 313, (John Wiley and Sons, N.Y.: 1973).

10. Welsh, H.L., M.F. Crawford, and J.L. Locke, Phys. Rev., 76, 580 (1969).

11. Lutz, B.L., J. Chem. Phys. 51, 706 (1969).

12. Wu, C.Y.R., and W.C. Stwalley, Phys. Rev., A18, 1066 (1978).

13. Caldwell, J., and T. Owen, Newsletter of Laboratory Spectroscopy for Planetary Sciences, 11, NASA Ames Research Center, (1981).

14. Wagner, R., J. Caldwell, T. Owen, S.J. Kim, T. Encrenza, and M. Combes, ICARUS, 66, 222 (1985).

15. Gladstone, G.R., and Y.L. Yung, Astrophys. J. 266, 415 (1983).

16. Wu, C.Y.R., and D.L. Judge, J. Chem. Phys. 89, 6275 (1988).

17. Wu, C.Y.R., T.S. Chien, and D.L. Judge, J. Chem. Phys. (in press, 1989).

18. Gardner, J.L., and J.A.R. Samson, Phys. Rev. A12, 1404 (1975).

19. Glass-Maujean, M., J. Chem. Phys. 85, 4830 (1986).

20. Haff, P.K., A. Eviatar, and G.L. Siscos, ICARUS, 56, 426 (1983).

21. Greenberg, L.T., in IAU Symposium 52, Interstellar Dust and Related Topics, eds, J.M. Greenberg and H.C. Van der Hulst (Dordracht: Reidel; 1973).

22. Bourdson, E.B., R.H. Prince, and W.W. Dulay, Astrophys. J. 260, 909 (1982).

23. Hudson, R.D., and V.L. Carter, J. Opt. Soc. Amer., 58, 1621 (1968).

N90-26755

DETERMINATION OF MOLECULAR SPECTROSCOPIC PARAMETERS AND ENERGY-TRANSFER RATES BY DOUBLE-RESONANCE SPECTROSCOPY

J.I. STEINFELD, B. FOY*, J. HETZLER*, C. FLANNERY, J. KLAASSEN, Y. MIZUGAI#, AND S. COY

Department of Chemistry and G.R. Harrison Spectroscopy Laboratory, Massachusetts Institute of Technology, Cambridge, Mass. 02139

ABSTRACT

The spectroscopy of small to medium-size polyatomic molecules can be extremely complex, especially in higher-lying overtone and combination vibrational levels. The high density of levels also complicates the understanding of inelastic collision processes, which is required to model energy transfer and collision broadening of spectral lines. Both of these problems can be addressed by double-resonance spectroscopy, *i.e.*, time-resolved pump-probe measurements using microwave, infrared, near-infrared, and visible-wavelength sources. Information on excited-state spectroscopy, transition moments, inelastic energy transfer rates and propensity rules, and pressure-broadening parameters may be obtained from such experiments. Examples are given for several species of importance in planetary atmospheres, including ozone, silane, methane, and ammonia.

INTRODUCTION

Research on the properties and dynamics of planetary atmospheres of the outer planets makes extensive use of spectroscopic probes of local atmospheric conditions obtained either from ground-based platforms or remote probes such as the Voyager or Galileo missions. Planetary observations of the spectra of dominant and trace atmospheric constituents in the form of absorption, emission, or reflectance spectra make it possible to

PRECEDING PAGE BLANK NOT FILMED

estimate local temperatures, to measure local partial pressures of the species observed, and to estimate the local pressures of other species, but only when supporting data such as spectroscopic assignments, absolute intensities (transition strengths), and sufficiently complete measurements of self- and foreign-gas pressure-broadening energy-transfer processes are available. With the ambitious program of planetary probes planned for the coming decade, there is an urgent need for such data to be provided.

Double-resonance (transient pump-probe) spectroscopy is a powerful technique for providing data of this kind, especially for higher-lying molecular vibrational levels. In this survey, we shall describe the principles of the double-resonance technique (with emphasis on infrared double-resonance [IRDR] spectroscopy), and present some applications to several species of importance in planetary atmosphere research.

PRINCIPLES OF DOUBLE RESONANCE SPECTROSCOPY

Double-resonance spectroscopy may be defined[1] as the use of two resonant one-photon interactions in a single molecule to probe molecular energy levels and relaxation properties. One of the radiation fields, denoted the pump, is a monochromatic, high-intensity field which saturates a pair of energy levels in the system, *i.e.*, transfers a substantial amount of population from the lower level to the (normally unpopulated) upper level. The pump source is typically a high-power infrared or optical-frequency laser. The probe field, which is tuned to another transition in the system, monitors intensity changes correlated with the presence of the pump radiation.

A *three-level* double-resonance scheme is one in which fields at two different frequencies couple a given molecular energy level to two other levels. The common level may be either lower in energy than the other two, as in Fig. 1(a), or may be higher than the other two, as in Fig. 1(b). Three-level configurations of this

type are often used for *spectrum simplification;* since the number of transitions which are correlated in pairs as shown in Figs. 1(a) and 1(b) is substantially less than the total number of absorption lines, a congested molecular spectrum may be reduced to a much smaller number of lines, and combination differences may be readily identified. The common level may also be intermediate between the lower and upper levels, as shown in Fig. 1(c). In this case, the transition at frequency ν_2 is termed an *excited-state absorption*, and provides information on the fine-structure levels of vibrationally or electronically excited states which are frequently not accessible to ordinary one-photon absorption or emission spectroscopy. If both pump and probe levels are at visible wavelengths, the upper state *a* can often be detected by u.v. fluorescence; this technique is referred to as "optical-optical double resonance"[2].

In a *four-level* double-resonance scheme, the two radiation fields connect pairs of levels not possessing a level in common, as shown in Figs. 1(d) - 1(f). In order for a double-resonance effect to occur, at least one level in each of the two pairs must be coupled to one of the directly pumped levels by collisional relaxation processes. Four-level double-resonance experiments thus yield information on both the kinetic rates and state-to-state propensity rules for inelastic molecular collisions.

Double-resonance signals may be described by steady-state solutions of the Optical Bloch Equations[3,4,5]. Indeed, the basic theory for the three-level double-resonance experiment was first developed by Javan[6] in 1957 for describing the three-level maser. Since the transition moment for the pumped level is a fun-damental parameter in the theory, it is often possible to extract information about such moments from quantitative modeling of double-resonance signal shapes and intensities.

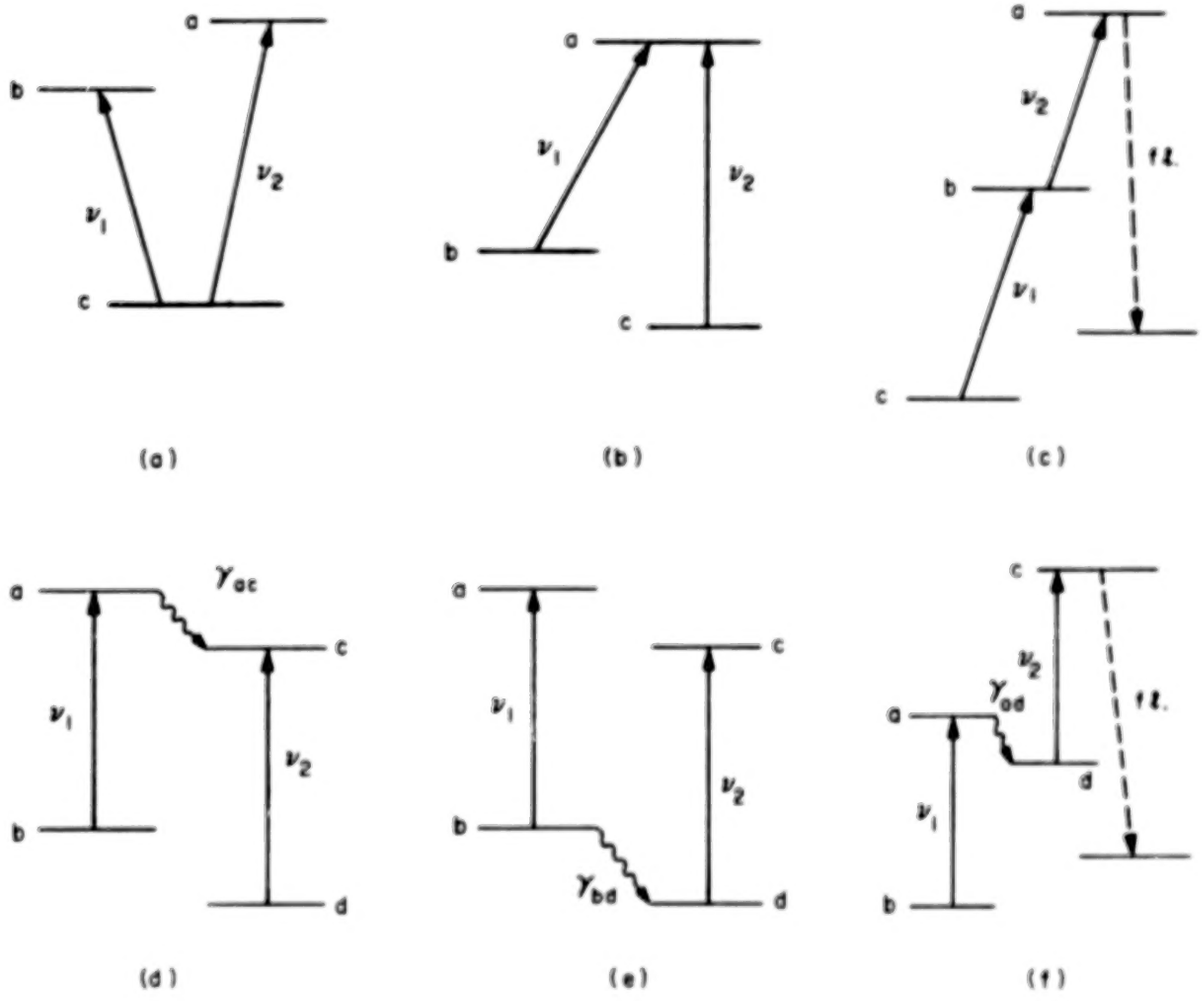

Figure 1. Diagrammatic representations of (a)-(c) three-level double-resonance spectroscopy and (d)-(f) four-level double-resonance spectroscopy [from Ref. 1].

EXPERIMENTAL TECHNIQUES

As noted above, the pump field in a double-resonance scheme must be capable of saturating the transition with which it is in resonance. This implies two requirements on the experiment: first, the population of the upper pumped level should be substantially less than that of the lower level, so that transfer of population from the lower to the upper level will be reflected in changes in transmitted probe radiation intensity. Second, the pump source must have sufficient intensity to at least partially saturate its transition. The first criterion would suggest a limitation to pumping vibrationally or electronically excited levels; however, because of the sensitivity of phase-sensitive microwave detection,

microwave-microwave double-resonance has been applied with great success to the study of collisional relaxation among rotational levels[1,7].

The development of tunable, high-power infrared and visible-wavelength lasers has made it possible to extend the double-resonance technique to vibrationally and electronically excited states. In particular, the pulsed CO_2 laser, which is line-tunable in the 9 - 11 micron region, has been used in many experimental investigations, including those in our laboratory. At high IR laser fluences (> 1 J cm^{-2}), these lasers can induce molecular dissociation or isomerization via infrared multiple-photon excitation processes[8,9,10]; double-resonance pump-probe experiments have been a valuable technique for characterizing the level distributions produced in IRMPE processes.

The essential requirements on the probe radiation in a double-resonance experiment are those of frequency and amplitude stability. Microwave klystrons, c.w. dye lasers, and tunable semiconductor diode lasers have all been used as double-resonance absorption probes[1]; when fluorescence excitation/emission spectroscopy can be used, its high sensitivity, energy resolution, and time resolution make it an excellent probe choice. A large proportion of the experiments in our laboratory are based on diode-infrared laser-double resonance spectroscopy (IRDR)[11], and the results to be discussed in the following section have been obtained primarily using this technique.

To avoid some of the limitations of absorption or fluorescence excitation spectroscopy, several other spectroscopic techniques have been applied to double-resonance experiments. Raman spectroscopy, for example, is applicable to all molecules, is state-specific, and affords good time resolution when a pulsed laser is used as the Raman probe source. Its major and obvious disadvantage is the extremely small magnitude of the spontaneous Raman scattering cross section, which severely limits the sensitivity. This problem can be alleviated by using resonance-

enhanced or coherent Raman scattering, such as Coherent Anti-Stokes Raman (CARS); the nonlinearity inherent in such techniques, however, make interpretation of the data quite difficult. Resonant multiphoton ionization (REMPI) is another promising probe technique; a CO_2-laser-pump/REMPI-probe experi-ment on ammonia has recently been carried out by Shultz and co-workers[12], in which the formation and decay of $v_2 = 1^-$ levels could be monitored.

APPLICATIONS TO ATMOSPHERIC SPECIES

The primary objective of our IRDR investigations of small polyatomic molecules has been the determination of energy transfer rates and pathways in these systems, and subsequent comparison with collision models. The experiments also provide information on spectroscopic parameters for vibrationally excited states, transition moments, and pressure-broadening coefficients. In this section, we briefly summarize some key results of these investigations, and suggest directions for future work.

Methane

Methane is both a trace constituent of the terrestrial atmosphere, where it may contribute to global temperature change via the "greenhouse effect"[13], and a major constituent of the atmospheres of the outer planets and their satellites. While the vibration-rotation spectroscopy of methane and other spherical tops has been analyzed in great detail by several research groups, there was a paucity of data, both qualitative and quantitative, on state-to-state energy transfer in such molecules. Microwave double-resonance spectroscopy[7] is not generally applicable to such molecules, due to the absence of a permanent dipole moment. Laser-excited infrared fluorescence, which is very useful for elucidating vibrational relaxation pathways in polyatomic molecules, does not have sufficient resolution to probe the rotational fine structure. Other techniques for studying relaxation

processes, such as ultrasonic dispersion, thermal lensing, and photoacoustic spectroscopy, are essentially bulk rather than state-resolved measurements.

Our IRDR studies on methane[14] represented the first measurement of state-to-state rotational energy transfer in a spherical top molecule. To obtain a good coincidence between a methane absorption line and a CO_2 laser pump line, we had to use the doubly labeled isotope $^{13}CD_4$; however, the results obtained are applicable to the normal CH_4 isotope and to other spherical tops such as silane (following section). The overall relaxation rates are approximately equal to the Lennard-Jones collision rate and are nearly independent of collision partner, as might be expected for collisions taking place via a short-range intermolecular potential. By applying a kinetic Master-Equation analysis, we were able to represent the rotationally inelastic collision rates by an exponential energy-gap law:

$$k_{fi} = (2J_f + 1)\ k_o \exp(-C(E_i - E_f)/k_B T) \qquad (1)$$

with the scaling parameter $C = 0.8$; this permits rotationally inelastic collisions with J changes of up to ± 5, which is also consistent with the action of short-range, impulsive forces.

The surprises were found in the final-state specificity of the rotationally inelastic collisions, which reveal a dramatic selectivity of rotational energy transfer pathways with respect to rotational fine-structure states. The first point noted was that molecules tend to remain within the initially pumped Coriolis sublevel of the $v_4 = 1$ state; this can be expressed as a propensity rule for conserving the vibrational angular momentum $\mathbf{R} - \mathbf{J}$ in the collision. In addition, rotational relaxation appears to proceed via "principal pathways", which constitute a small subset of the energetically accessible levels. The nature of these pathways was clarified by subsequent experiments on silane, which we now consider.

Silane

Although silane has not been identified as a major component of planetary atmospheres, experiments on this system provide considerable insight into rotational energy transfer mechanisms discerned in the earlier experiments on methane, and suggest important connections between these measurements and pressure-broadening phenomena. In addition, silane is widely used for preparation of electronic materials by thermal and laser-assisted chemical vapor deposition[15], so the study of laser-pumping mechanisms and collisional relaxation in this system has considerable practical importance.

The SiH_4 infrared absorption lines which lie nearest to the 10P(20) CO_2 laser line are the A_2, F_2, and E components of the J = 13 <-- J = 12, v_4 = 1 <-- 0 band. These are detuned from the laser frequency by 1015, 600, and 378 MHz, respectively. As a result of these detunings, IRMPE of silane can occur only under pressure-broadened[16] or laser-induced breakdown conditions[17]. The v_4 = 1 <-- 0 transition moment is sufficiently large, however[18], that the pulsed TEA CO_2 laser can pump a considerable fraction of the population of each of these symmetry levels into the excited ro-vibrational state[19], which can then be followed by diode absorption at appropriate hot-band transitions.

Both rotational[20] and vibrational[21] relaxation have been measured in silane using IRDR. V-V energy transfer between v_4 = 1 and v_2 = 1 levels is nearly as efficient as pure rotational energy transfer, as a result of the strong Coriolis mixing between these two states. The scaling coefficient C in Eq. (1) for rotationally inelastic collisions is 0.05 - 0.08 for the three symmetry species; when the larger rotational level spacing of silane in J = 13, as compared with $^{13}CD_4$ in J = 11, is taken into account, this corresponds to a somewhat slower fall-off of inelastic collision probability with increasing ΔJ. The **R - J** conserving propensity rule found in methane is validated for all three symmetry species

in silane; in addition, the pattern of "preferred pathways" for rotational state changing collisions now shows an interesting regularity[22]. Rotational states of spherical tops, such as methane and silane, are split into numerous fine-structure components by centrifugal and anharmonic interactions; these components arrange themselves in level clusters according to whether the rotation is quantized along the 6-fold or the 8-fold symmetry axis of the molecule. The preferred pathways for all three symmetry species of a given rotational state always lie as close to each other as possible in the cluster structure, and these generally correspond to the same quantization as that for the initially pumped level. One way to summarize the selectivity found for rotationally inelastic collisions is that a "conservation of coupling" propensity rule is at work.

The ability to interrogate all three nuclear-spin symmetry species of silane has led to an observation with important implications for understanding pressure-broadening coefficients, which are essential for atmospheric remote sensing methods. The total rotational relaxation rates for these symmetry species show significant differences at the 95% confidence level[20], with the ordering $k(F_2) > k(A_2) > k(E)$. This is the same ordering as has been found for the infrared absorption pressure-broadening coefficients for methane[23,24], as well as in recent measurements by the Dijon group[25] of pressure broadening in the Q branch of the ν_1 Raman band of $^{13}CD_4$. Furthermore, the ratio of the symmetry-averaged Raman-broadening coefficients for silane[25] to that of $^{13}CD_4$ (R = 1.24) is very close to the correspondingly averaged IRDR relaxation times (R' = 1.28). The direct measurements thus provide details of the inelastic collision rates which are averaged out in the usual experimental and theoretical treatments of pressure broadening, and can serve as stringent tests of the theories. In the following section, we describe the application of this approach to ozone, for which a major effort in determining accurate pressure broadening parameters is now under way.

Ozone

The role of ozone in stratospheric photochemistry and in the radiative properties of the upper atmosphere is too well known to elaborate upon here. Although a large data base exists with respect to the spectroscopic and kinetic properties of this molecule, a recent survey[26] identified a nearly total lack of data for rotational energy transfer in ozone collisions. Without such data, current theories for pressure broadening can receive only limited testing.

The IRDR technique is admirably suited for the measurement of these data. In earlier u.v. absorption - infrared laser double resonance experiments, we had identified coincidences of ozone absorption features with CO_2 laser lines, and made use of the u.v. spectral changes following vibrational excitation to determine Hartley band absorption in the vibrational excited state[27] and to map out part of the vibrational relaxation pathways for this molecule[28]. Using the IRDR technique, we are able to follow these processes at the rotational state-to-state level.

The IRDR scheme for the CO_2 9P(12) laser line is shown in Fig. 2. This line pumps the $^{17}_{4,13}$ <-- $^{16}_{4,12}$, $v_3 = 1$ <-- $v_3 = 0$ transition. Relaxation into the depleted J = 16 level can be monitored by the three-level IRDR transition at 1026.51 cm^{-1}, and relaxation out of the J = 17, $v_3 = 1$ level by the hot-band transition at 1028.58 cm^{-1}. By monitoring four-level IRDR signals at other frequencies, some of which are shown in Fig. 2, the propensity rules governing rotationally inelastic collisions can be determined. Additional measurements of hot-band transitions originating in the $v_1 = 1$ level will permit us to measure the V-V rate between the $v_3 = 1$ and $v_1 = 1$ levels, which could not be resolved in the earlier u.v./IR double resonance experiments[28].

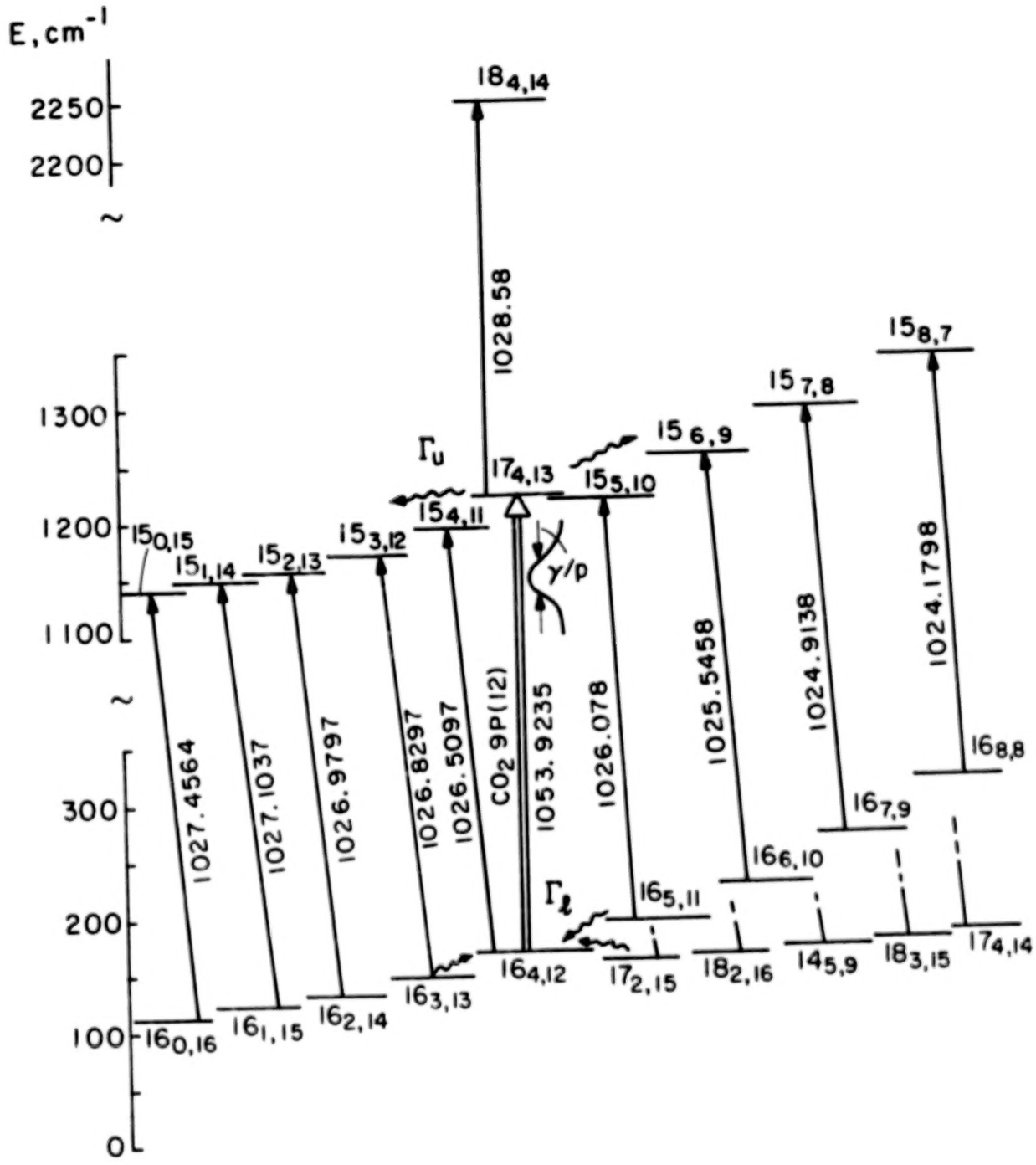

Figure 2. Infrared double-resonance level scheme for CO_2 laser 9P(12) pumping of ozone, showing probe frequencies for three- and four-level IRDR configurations.

CONCLUSIONS AND FUTURE PROSPECTS

The examples described in this report illustrate the power of the double-resonance technique in determining energy transfer

rates and pathways, in both the ground and vibrationally excited states of polyatomic molecules. The resulting data base can then be employed to test inelastic scattering theories and assess intermolecular potential models, both of which are necessary for the systematization and prediction of infrared pressure-broadening coefficients, which are in turn required by infrared remote sensing techniques for both terrestrial and planetary atmospheres. In addition, accurate measurements on excited-state absorption transitions permits us to improve the determination of rotational and vibrational spectroscopic parameters for excited vibrational levels, and to derive band strengths for hot-band transitions involving such levels.

Further development of this technique will make use of pulsed visible and near-infrared laser sources to pump vibrational overtone levels, which can then be interrogated by tunable infrared diode laser absorption. As an example, consider the overtone spectrum of normal methane, CH_4. The spectrum is particularly difficult to rotationally assign because the spectral congestion caused by Fermi resonance interactions increases dramatically with the number of H atoms. While CHD_3 has a resolved and assignable room temperature spectrum in the 5 C--H quanta region, the CH_4 spectrum is essentially unresolved at this temperature. When cooled to temperatures characteristic of planetary atmospheres (40 - 200 K), however, the spectrum resolves into Doppler-limited features[29]. The identification of these features will be greatly facilitated by the spectrum simplification afforded by double-resonance spectroscopy. Further information on relaxation out of these highly excited vibrational levels will be enormously interesting for comparison with current theories of molecular dynamics[30], as well as for developing models for pressure broadening in overtone absorption spectra.

ACKNOWLEDGMENTS

The development and previous applications of the double-resonance technique in our laboratory have been supported by the National Science Foundation and the Air Force Office of Scientific Research. The current research on inelastic collision processes in ozone is supported by NASA Upper Atmosphere Research Program Grant NAGW-1667.

References and Notes

* Present address: Center for Atomic, Molecular, and Optical Physics, National Institute of Standards and Technology, Gaithersburg, Md. 20899.

Permanent address: Department of Physics, Sophia University, Tokyo, Japan.

1. J.I. Steinfeld and P.L. Houston, "Double-Resonance Spectroscopy", in *Laser and Coherence Spectroscopy*, J.I. Steinfeld, ed., Plenum Press, New York (1978), pp. 1 - 123.

2. R.W. Field, Disc. Faraday Soc. **71**, 111 (1981).

3. K. Shimoda and T. Shimizu, "Nonlinear Spectroscopy of Molecules", *Prog. Quantum Electronics* **2**(2), 45 (1972).

4. J.I. Steinfeld, *Molecules and Radiation*, 2nd ed., M.I.T. Press, Cambridge, Mass. (1985), pp. 394 - 402.

5. H.W, Galbraith, M. Dubs, and J.I. Steinfeld, Phys. Rev. **A26**, 1528 (1982).

6. A. Javan, Phys. Rev. **107**, 1579 (1957).

7. T. Oka, Adv. Atom. Mol. Phys. **9**, 127 (1973).

8. J.I. Steinfeld, ed. *Laser-Induced Chemical Processes*, Plenum Press, New York (1981).

9. J.S. Francisco and J.I. Steinfeld, in *Multiphoton Processes and Spectroscopy, Vol. 2*, (S.H. Lin, ed.), World Publishing Co. Pty. Ltd., Singapore (1986), pp. 79 - 173.

10. M. Quack, Infrared Physics **29**, 441 (1989).

11. L. Laux, D. Harradine, B.R. Foy, J.I. Steinfeld, and M. Dubs, Proc. 3rd International Conf. on Infrared Physics (Zurich, 1984), W. Ruegsegger and F. Kneubuhl, eds., pp. 572 - 575.

12. M.J. Shultz and J. Wei (unpublished results).

13. S.H. Schneider, Science **243**, 771 (1989).

14. L. Laux, B. Foy, D. Harradine, and J.I. Steinfeld, J. Chem. Phys. **80**, 3499 (1984);
B. Foy, J. Hetzler, G. Millot, and J.I. Steinfeld, J. Chem. Phys. **88**, 6838 (1988).

15. J.M. Jasinski, B.S. Meyerson, and B.A. Scott, Ann. Rev. Phys. Chem. **38**, 109 (1987);
J.I. Steinfeld, Spectrochim. Acta **46A**, in press (1990).

16. T.F. Deutsch, J. Chem. Phys. **70**, 1187 (1979).

17. Dong Lifang, Fu Guangsheng, Li Xiaowei, Han Li, Zhang Lianshui, Lu Furun, and Xue Chunyin, Chinese J. Semiconductors **10**(3), 1 (1989).

18. K. Fox and W.B. Person, J. Chem. Phys. **64**, 5218 (1976) report $\langle M_4 \rangle = (0.232 \pm 0.016) \times 10^{-18}$ esu-cm.

19. G. Millot, J. Hetzler, G. Pierre, and J.I. Steinfeld, Spectrochim. Acta **45A**, 5 (1989).

20. G. Millot, J. Hetzler, B. Foy, and J.I. Steinfeld, J. Chem. Phys. **88**, 6742 (1988).

21. J. Hetzler, G. Millot, and J.I. Steinfeld, J. Chem. Phys. **90**, 5434 (1989).

22. J. Hetzler (to be published).

23. K. Fox, J. Chem. Phys. **80**, 1367 (1984).

24. J. Ballard and W.B. Johnston, J. Quant. Spectrosc. Rad. Transfer **36**, 365 (1986).

25. G. Millot, B. Lavorel, A. Boutahar, C. Wenger, and H. Berger (to be published).

26. J.I. Steinfeld, S.M. Adler-Golden, and J.W. Gallagher, J. Phys. Chem. Ref. Data **16**, 911 (1987).

27. S.M. Adler-Golden, E.L. Schweitzer, and J.I. Steinfeld, J. Chem. Phys. **76**, 2201 (1982).

28. S.M. Adler-Golden and J.I. Steinfeld, Chem. Phys. Letts. **76**, 479 (1980).

29. G.J. Scherer, Ph.D. Thesis, Harvard University (1983).

30. K.K. Lehmann and S.L. Coy, J. Chem. Soc. Faraday Trans. 2, **84**, 1389 (1988).

N90-26756

NOVEL LASER GAIN AND TIME-RESOLVED FTIR STUDIES OF PHOTOCHEMISTRY

STEPHEN R. LEONE†

Joint Institute for Laboratory Astrophysics, National Institute of Standards and Technology and University of Colorado, and Department of Chemistry and Biochemistry, University of Colorado, Boulder, Colorado 80309-0440

ABSTRACT

Several novel techniques are discussed which can be used to explore laboratory photochemical processes and kinetics relevant to planetary atmospheres; these include time-resolved laser gain-versus-absorption spectroscopy and time-resolved Fourier transform infrared (FTIR) emission studies. The laser gain-versus-absorption method employs tunable diode and F-center lasers to determine the yields of excited photofragments and their kinetics. The time-resolved FTIR technique synchronizes the sweep of a commercial FTIR with a pulsed source of light to obtain emission spectra of novel transient species in the infrared. These methods are presently being employed to investigate molecular photodissociation, the yields of excited states of fragments, their subsequent reaction kinetics, Doppler velocity distributions, and velocity-changing collisions of translationally fast atoms. Such techniques may be employed in future investigations of planetary atmospheres, for example to study polycyclic aromatic hydrocarbons related to cometary emissions, to analyze acetylene decomposition products and reactions, and to determine spectral features in the near infrared and infrared wavelength regions for planetary molecules and clusters.

INTRODUCTION

The atmospheres of many planets other than the Earth can involve extreme temperatures and pressures, and they contain many highly chemically reactive constituents as well. For example, several planets exist in a strongly reducing atmosphere, composed largely of methane and other hydrocarbon species at high pressures near the surface and low outer temperatures.[1] Thus the typical mixtures of gases are not only unfamiliar, but their spectral signatures as we might

know them are strongly perturbed by the unusual conditions of temperature and pressure. The molecular species are also undoubtedly in a state of flux, undergoing dramatic transformations because of photochemistry and solar heating. As a result, there is a definite need to develop techniques to study the kinds of planetary atmosphere species which may only be formed under such unusual conditions. Recording their molecular spectra and studying their distinctive photochemistry will be of great importance.

A wide variety of powerful spectroscopic probes have been developed in the past several years, which have provided a means for detection of novel transient species and for probing their kinetics. These include methods such as laser-induced fluorescence in the visible and ultraviolet,[2] laser multiphoton ionization,[3] intracavity laser absorption,[4] and transient absorption/gain probing with lasers.[5]

Of special interest in this article are two methods applicable to the spectral features of molecular species in the infrared and near infrared. These are time-resolved Fourier transform infrared (FTIR) emission spectroscopy[6] and tunable infrared laser gain-versus-absorption spectroscopy.[5,7,8] These methods rely heavily on lasers, both for the initial preparation of transient species, and in the case of the laser gain/absorption method, also for the transient detection. Lasers are extremely useful for the preparation of large number densities of transient and reactive species. With the time-resolved FTIR method, it is possible to form a variety of excited molecular species and to study the infrared spectral details of the emitting states. With the laser gain-versus-absorption technique, we can study quantum yields for the formation of excited states and the kinetics of radical reactions.

Work is ongoing in our laboratory to develop a variety of these infrared and near infrared techniques and to achieve advanced capabilities in their application to important problems. The methods are applicable to a number of challenges related to planetary atmospheres, including infrared cometary emissions which may be due to large molecules, such as polycyclic aromatic hydrocarbons,[9] and acetylene chemistry and photochemistry.[10] In the remainder of this paper, the general experimental setups for these two types of methods will be described, and a few examples will be given, for each method, of the kinds of problems that have already been addressed in our laboratory. We close with a brief introduction to several subjects related to planetary atmospheres that might be studied by these techniques.

TIME-RESOLVED FTIR EMISSION METHOD

Commercial Fourier transform infrared (FTIR) instruments provide a powerful means to detect and study a wide range of molecular species in the infrared and near infrared. A novel

adaptation[6] takes advantage of the sensitive emission capabilities in the infrared by using a laser to prepare photofragments or other excited species and then imaging their infrared emission through the FTIR. By synchronization of the timing of a pulsed laser with the sweep of the mirror in the FTIR, complete time histories of the spectral information can be obtained of transient radical species, chemically reacting systems, and energy transfer processes. Such a method may be well suited to studies of unusual species and conditions typical of planetary atmospheres. In some cases, direct laboratory spectral information may be compared to emissions observed by planetary and cometary probes.

Figure 1 shows a schematic of a time-resolved FTIR system in use in our laboratory.[11,12] A pulsed high repetition rate excimer laser (200-400 Hz) is paired with a commercial high resolution FTIR (0.02 cm^{-1}), which is operated in the emission mode. The laser produces photofragments in either a low pressure chamber or in a high pressure flow cell reactor, and emission is collected into the interferometer from the infrared emitting species. The timing of the pulsed laser is synchronized to the sweep of the mirror in the FTIR through the reference fringes of the He:Ne laser. Data may be collected at either a single time or multiple times after the laser pulse (Fig. 2). If signals are acquired at multiple times, then on the next sweep of the mirror, the timing

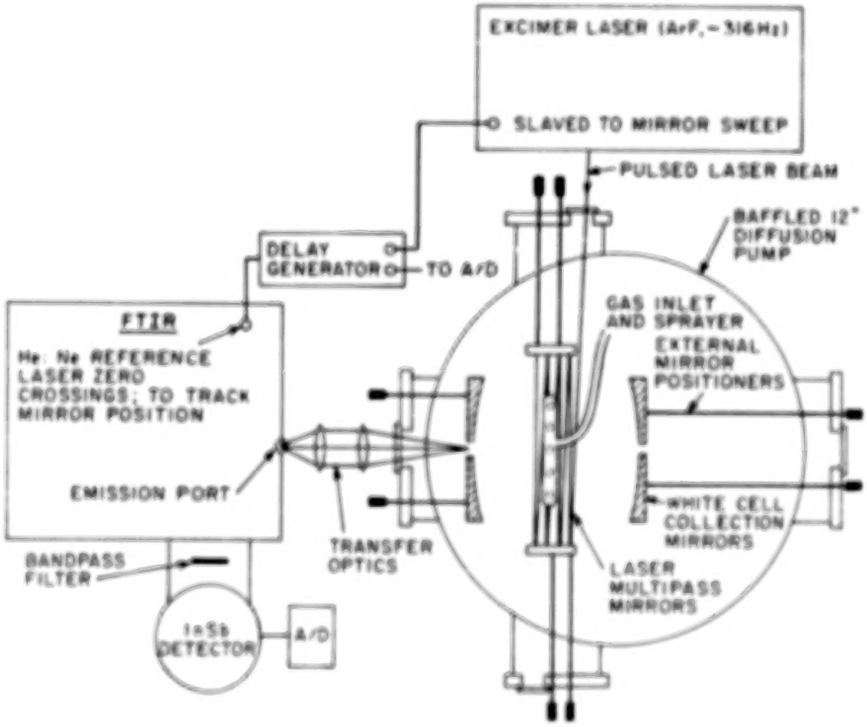

Fig. 1. Experimental apparatus for time-resolved FTIR emission experiments initiated by laser photodissociation.

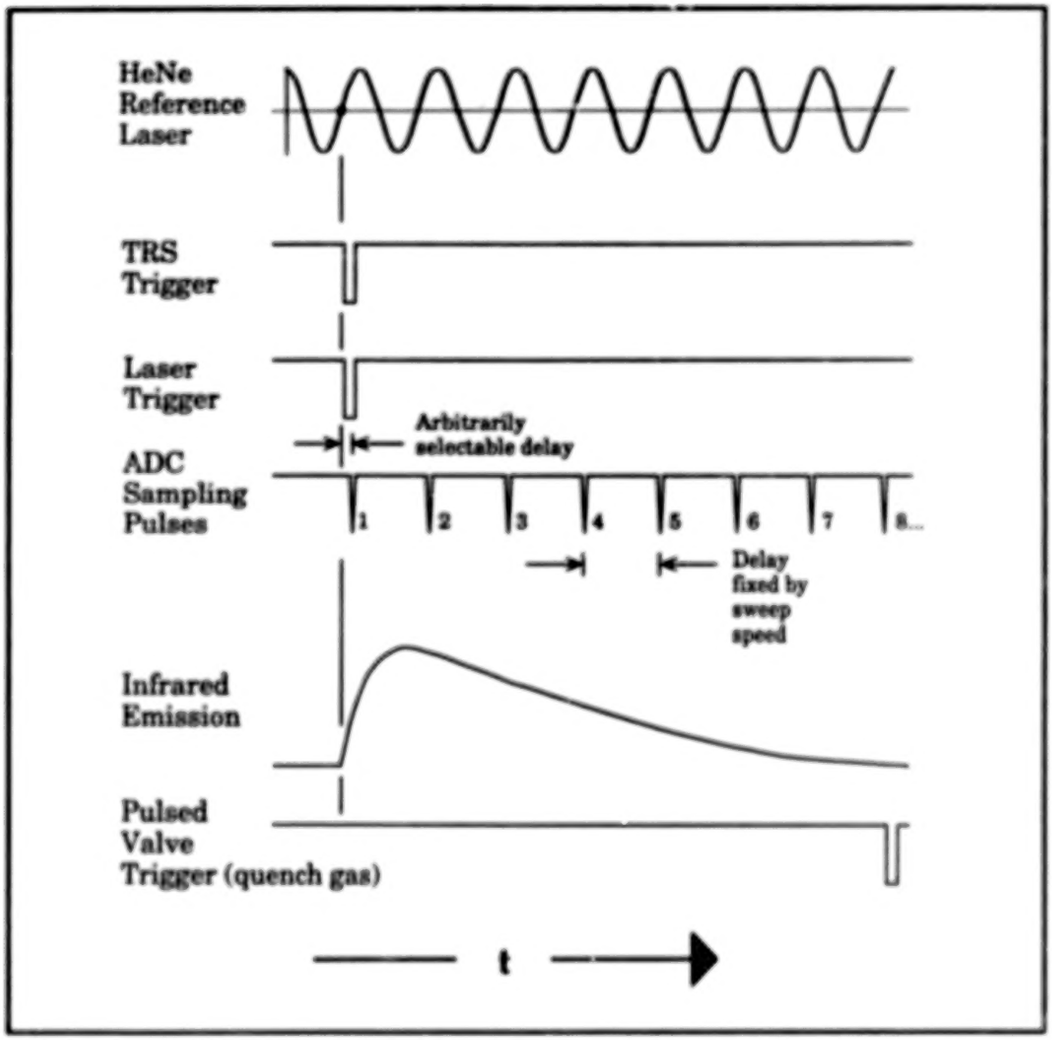

Fig. 2. Timing diagram for time resolved IR emission experiment, showing 8 time samples after each laser pulse.

of the acquisition is adjusted such that the next laser pulse is incremented in order to obtain data at each time delay for every mirror displacement.

Infrared emission has the advantage that relatively low numbers of excited species are readily detectable (10^9-10^{11}), in contrast to absorption, where long pathlengths and large volumes are often necessary. Thus, small numbers of highly exotic species may be prepared and observed under desired conditions through their emission. The pulsed laser may also be replaced by a cw laser, flashlamp, or other excitation source, in order to obtain high average emissions, and the cells may be heated or cooled or operated under high pressures to simulate planetary atmosphere conditions.

Acetylene Photochemistry

The photodissociation of acetylene (HCCH) at 193 nm in the ultraviolet has an important radical-forming channel, CCH+H; the CCH radical, which may be excited both vibrationally and in a low-lying electronically excited state ($\tilde{A}\ ^2\Pi$) has been observed in infrared emission following the photodissociation of acetylene with the time-resolved FTIR method.[13] Figure 3 shows a survey spectrum of the CCH radical emission, which required only about 1 hour to acquire with the FTIR. While the CCH radical has been studied in line-by-line detail with transient laser absorption probing,[14] the power of the FTIR method to obtain rapid information about the broad spectral content of unusual species is readily apparent. Not only are infrared bands of vibrationally excited states of CCH expected, but the strongest infrared and near infrared emission features of this radical are composed of bands involving the ($\tilde{A}\ ^2\Pi$) electronically excited state, which occur at unanticipated wavelengths. In terms of planetary photochemistry and spectral signatures, the potential capability of the broad spectral coverage of the FTIR method may be advantageous for laboratory studies.

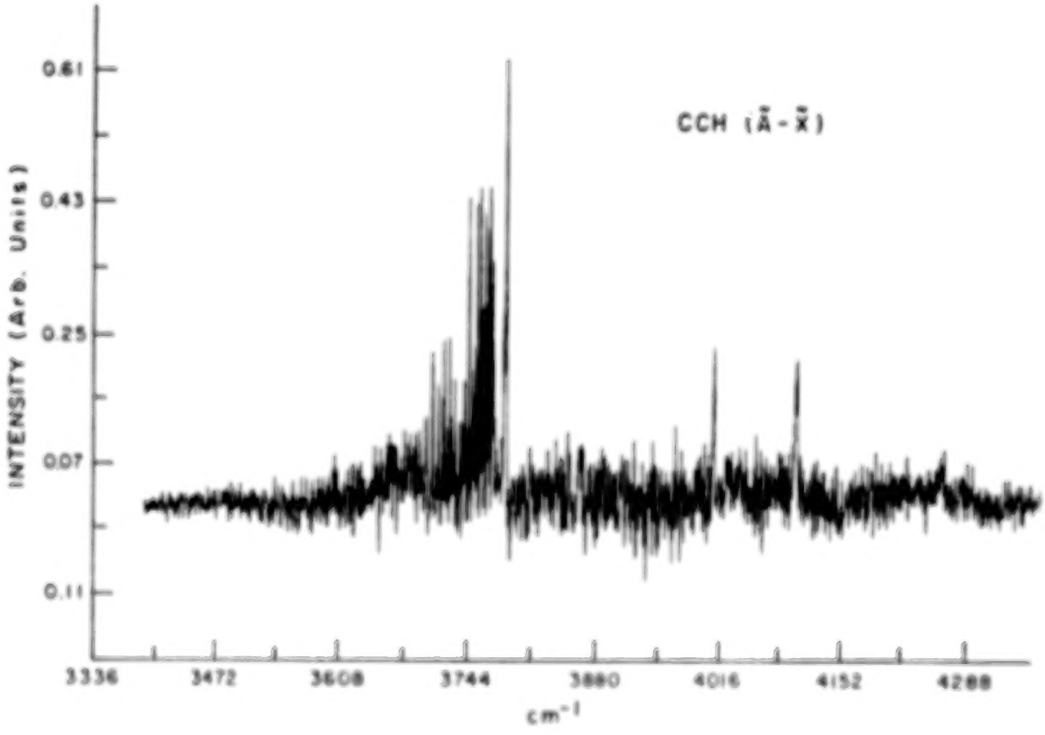

Fig. 3. Infrared emission spectrum of CCH taken with the FTIR at 0.6 cm^{-1} resolution at a time of 7 μs after the photolysis of acetylene.

In work carried out in our laboratory, the vibrational band intensities produced by the UV photolysis of acetylene were obtained. In addition, an intriguing problem arises in the primary photochemistry of acetylene concerning the rotational excitation of the CCH radical that is caused by the momentum transfer of the departing H atom.[13] The rotational excitation of the CCH radical is found, surprisingly, to be colder than the initial excitation in the parent acetylene. This is an unanticipated result, because the momentum transfer from the departing H atom might typically be expected to produce additional rotational excitation in the radical. The rotational dynamics are modeled in terms of both a trans-bent and linear transition state. It is found that in the trans-bent configuration the constraint of the available energy in the photodissociation may cause a constraint on the allowed angular momentum states, resulting in a "cooling" of the radical product.[13]

Acetone Photodissociation

The photochemistry of acetone also offers several intriguing aspects of study.[12] The 193 nm photodissociation produces a three-body dissociation pathway to form two methyl radicals (CH_3) and carbon monoxide (CO). The broad spectral features of the emission from this dissociation were obtained initially with low resolution infrared circular variable filters (CVF).[15] Emission is observed from CH stretching regions and from the vibration-rotation excitation of the CO fragment. While such low resolution spectra are useful to gain a coarse perspective on the infrared emitting species, the much higher resolution of the FTIR method allows detailed state-resolved information to be obtained (Fig. 4). From the high resolution spectra taken at low pressures, it is found that the CO is born with very high excitation in both rotation and vibration. The high rotational excitation can only be explained if the three body dissociation occurs by a nonsymmetric break-up.[12]

Figure 5 shows a portion of the FTIR spectrum of the methyl radical antisymmetric stretching region, observed in the photolysis of acetone.[16] All of the lines are assignable to methyl radical features, based on the known spectroscopy. An intriguing problem which is yet to be resolved concerns the origin of this methyl radical infrared emission. Laser multiphoton ionization detection of the methyl radical following the photodissociation of acetone has not observed the antisymmetric stretch excitation.[17] Either the radical is born with excitation in other modes, which is then transferred to the antisymmetric stretch vibration and emits in the infrared, or the multiphoton ionization detection is insensitive to the antisymmetric stretch because of unusual Franck-Condon factors or some other spectroscopic subtlety.

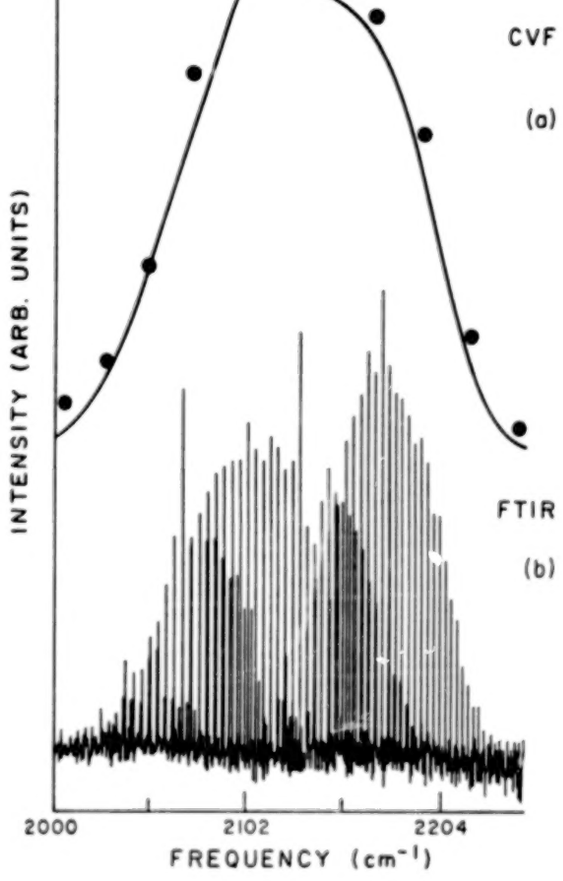

Fig. 4. Comparison of CO emission spectra following acetone photodissociation taken with (a) a low resolution circular variable filter (CVF) and (b) the high resolution FTIR.

Radical-Radical Reactions

The FTIR method is proving to be a powerful tool not only to investigate primary photochemical events, but to study potentially novel, subsequent reaction chemistry. In a new series of experiments, a high density of Cl atoms is produced by excimer laser photolysis of Cl_2 in the presence of a low density of ethane. A reaction between Cl and C_2H_6 occurs, producing a quantitative yield of ethyl radicals, C_2H_5. Since the Cl atoms are initially in excess compared to the ethane, then a rapid reaction can occur between the remaining Cl atoms and the ethyl radicals, C_2H_5, to form HCl and ethylene, C_2H_4. The signature of the radical-radical reaction is the formation of highly vibrationally excited HCl, which cannot occur for the reactions of the atoms with stable molecules, as ascertained from the known thermochemistry. Highly vibrationally excited HCl has now been observed in an initial series of experiments,[16] suggesting that intriguing new investigations will be possible to study systems in a state of high energization, such as radical-radical chemistry. Such reactions are likely to be much more rapid and more exothermic than

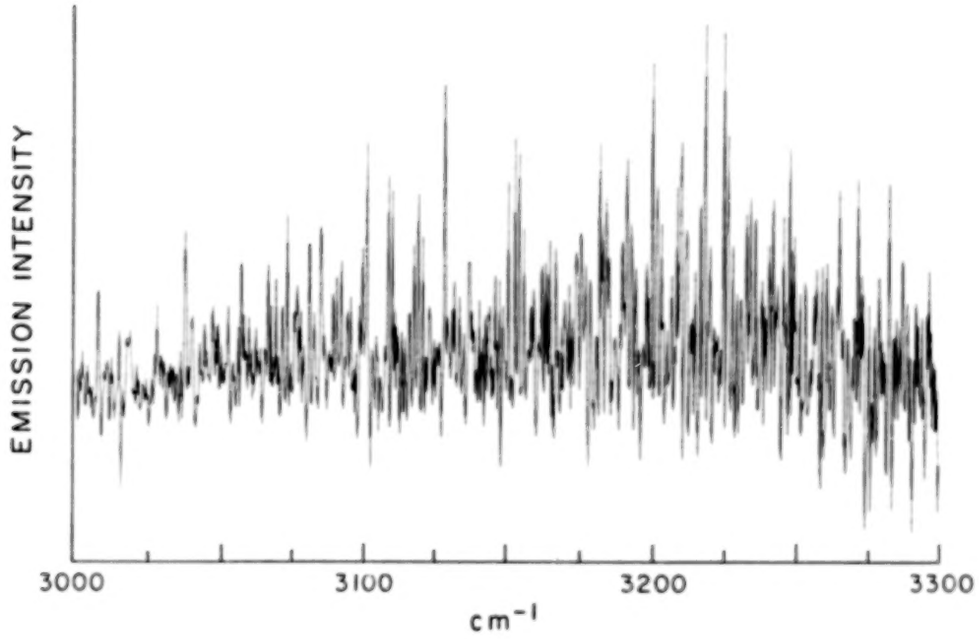

Fig. 5. Methyl radical antisymmetric stretch emission spectrum following the photolysis of acetone.

traditional abstraction reactions with stable molecules, and may be sources of strong infrared emission and highly excited products.

TRANSIENT GAIN-VERSUS-ABSORPTION LASER KINETICS METHOD

While the FTIR method is an excellent tool for surveys of emitting systems and detailed investigations of state distributions in photochemistry, other methods provide accurate complementary information on such questions as kinetics or quantum yields of formation for excited or ground state species. One such method is the time-resolved laser gain-versus-absorption technique, which has also been used extensively for laser spectroscopic measurements. In our laboratory, the laser gain-versus-absorption method was initially developed to obtain some of the most accurate values for quantum yields of formation. The method was applied to the excited $Br^*(^2P_{1/2})$ and $I^*(^2P_{1/2})$ states of the halogen atoms using a tunable infrared F-center laser and a tunable room temperature diode laser as the probes, respectively.

Figure 6 illustrates the typical setup for the transient gain-versus-absorption kinetics determinations.[5,18,19] A pulsed photolysis laser forms a population of ground and excited halogen atoms, in this case I and I*. A tunable diode laser, which is set to probe the transition between the

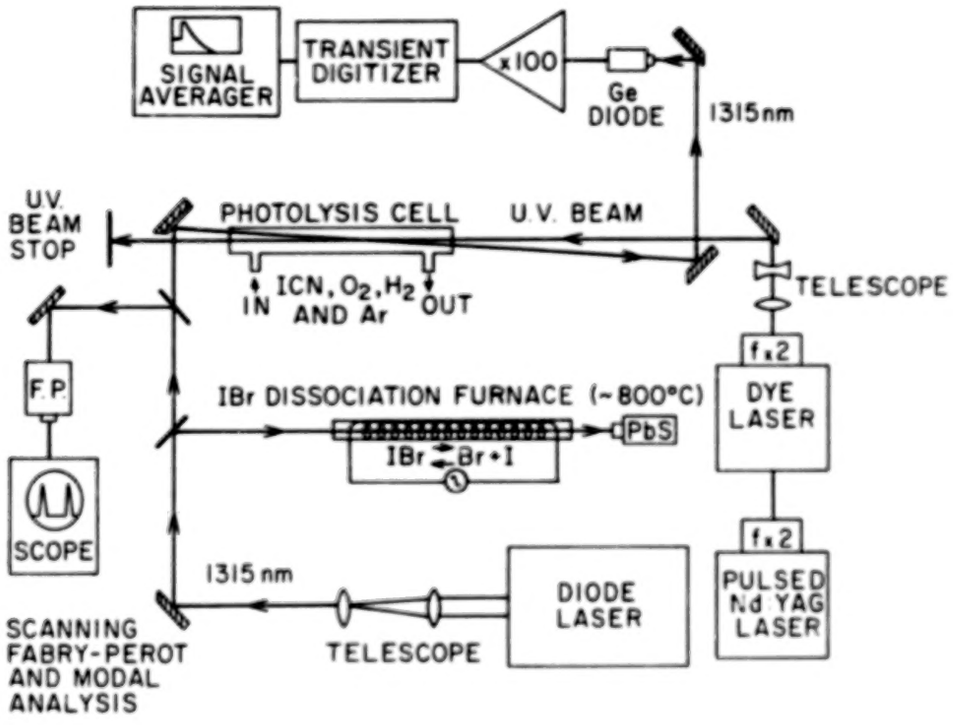

Fig. 6 . Laser gain-versus-absorption apparatus using a diode laser to study I* quantum yields. The heated IBr cell is for tuning the diode laser to the I atom transition.

two states at 1315 nm, is propagated collinearly in order to measure the transient gain or absorption of the atomic population. If the population of atoms contains more excited states than ground states, when the factor of the differing degeneracies is taken into account, then laser gain will be observed initially (shown in Fig. 7 for ICN photolysis). If the ground state population dominates, then an initial absorption is observed. At a later time, when all the excited states are relaxed by a suitable quenching species, the relative population of the total number of atoms formed in both states is determined. From the initial and final measurements, a highly accurate relative quantum yield is determined. If, in addition, it is known that the molecules fragment to the desired atom with a certain yield, then absolute quantum yields are obtained.

Quantum Yield Determinations

For the case of I*, the degeneracy of the upper state is 2 and for the ground state, 4. Thus, a very simple expression may be derived under the conditions of the experiment, namely that the quantum yield of formation of the I* state is given by:[5,18,19]

$$\Phi_{I^*} = (1/3)\,(S_i/S_f + 1). \qquad (1)$$

Thus, if the initial and final amplitudes of the laser gain-versus-absorption signal are measured, the quantum yield is immediately obtained. By making determinations as a function of wavelength, the quantum yield is immediately obtained over various spectral bands, as shown in Fig. 8 for the case of the ultraviolet photodissociation of ICN. In our work on the halogen atom quantum yields, typical accuracies of ±2% are achieved. This improves on the accuracy of previous determinations by one order of magnitude. The method may be extended to obtain quantum yields of other excited states of atoms.

The laser gain-versus-absorption method also allows accurate quenching rate constants and kinetic parameters to be determined from the time behavior of the signals. Tunable diode lasers operating throughout the entire infrared spectral region have now been employed in this method, used in various laboratories.

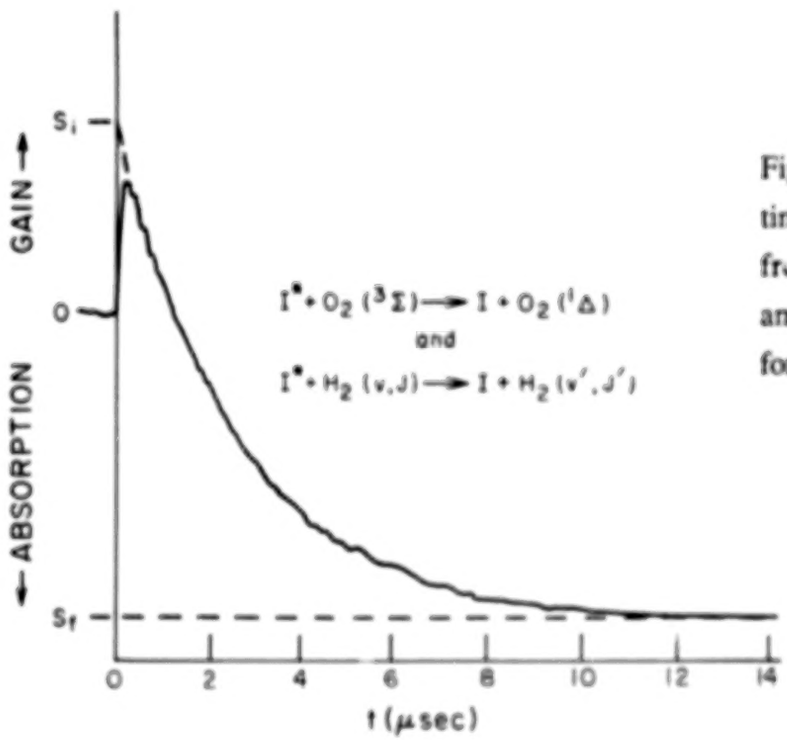

Fig. 7. Laser gain-versus-absorption time transient from ICN dissociation; from the initial and final signal amplitudes, a quantum yield for I* formation is obtained.

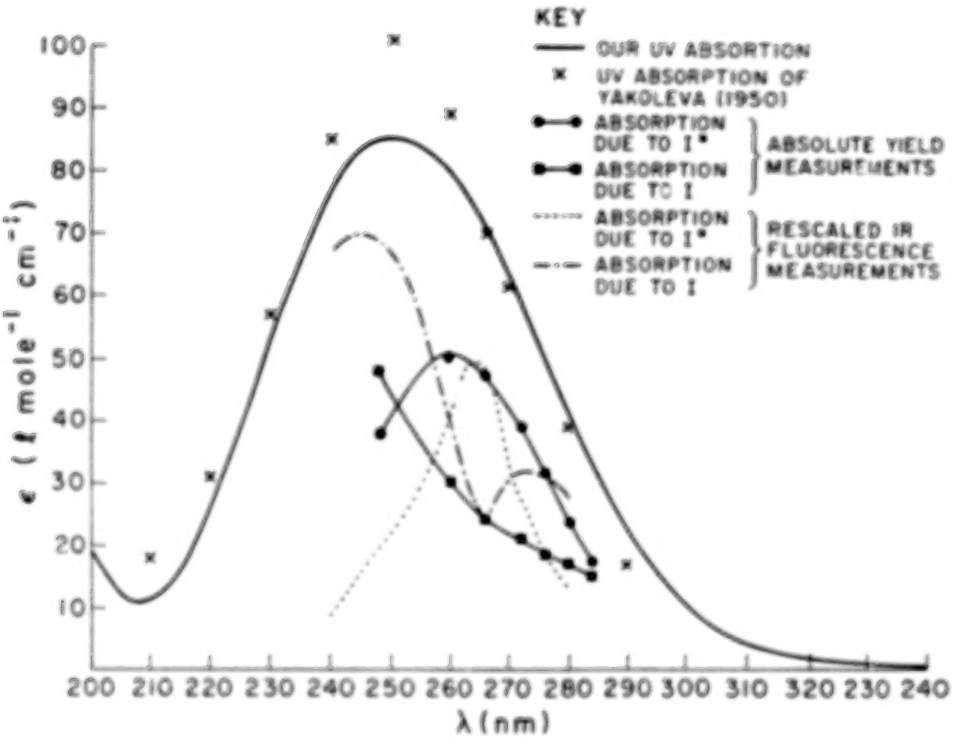

Fig. 8. Spectrally-resolved I* quantum yields as a function of dissociating wavelength. For the details of the legend, see Ref. 19.

POTENTIAL APPLICATIONS TO PLANETARY ATMOSPHERES

The time-resolved FTIR emission technique and laser gain-versus-absorption method provide an excellent basis for further studies of exotic species related to laboratory investigations of planetary atmospheres.[20] Future work may utilize the FTIR to study the infrared emission spectra of polycyclic aromatic hydrocarbons (PAH's) excited by ultraviolet light, in order to determine their role in cometary emissions. Additional species related to the PAH's are the classes of hydrogenated amorphous carbon and vitrinite coal particles, which are characterized by higher oxygen contents.[9,21] Acetylene photochemistry and reactions may also be investigated in a broad way by these methods, as well as individual atom-radical reactions which may play an important role in the planetary atmospheres. One example is the reaction of N atoms with CH_3 radicals, which may play a role in the atmosphere of Titan.[22] The FTIR method would allow the identification of product species and emitting states, in order to determine the role of this reaction in the possible formation of HCN in the atmosphere of this moon. Use of the laser gain/absorption technique will provide refined kinetic determinations and quantum yields of novel species.

ACKNOWLEDGMENTS

The author gratefully acknowledges the Department of Energy for support of the FTIR research, the National Science Foundation for FTIR instrumentation, and the National Science Foundation and the Air Force Weapons Laboratory for support of the laser gain-versus-absorption research. The author has enjoyed the enthusiastic collaboration of many excellent students and post-doctorals who participated in these projects, including, D. J. Donaldson, T. R. Fletcher, E. L. Woodbridge, H. K. Haugen, and W. P. Hess.

REFERENCES

†Staff Member, Quantum Physics Division, National Institute of Standards and Technology.

[1]J. I. Lunine, Science **245**, 141 (1989).

[2]U. Hefter and K. Bergmann, in Atomic and Molecular Beam Methods, edited by G. Scoles (Oxford Univ. Press, New York, 1988), Vol. 1, p. 193.

[3]D. Bassi, in Atomic and Molecular Beam Methods, edited by G. Scoles (Oxford Univ. Press, New York, 1988), Vol. 1, p. 180.

[4]P. V. Cvijin, J. J. O'Brien, G. H. Atkinson, W. K. Wells, J. I. Lunine, and D. M. Hunten, Chem. Phys. Lett. **159**, 331 (1989).

[5]H. K. Haugen, E. Weitz, and S. R. Leone, J. Chem. Phys. **83**, 3402 (1985).

[6]S. R. Leone, Acc. Chem. Res. **22**, 139 (1989).

[7]J. A. O'Neill, C. X. Wang, J. Y. Cai, G. W. Flynn, and R. E. Weston, J. Chem. Phys. **88**, 6240 (1988).

[8]H. Kanamori and E. Hirota, J. Chem. Phys. **88**, 6699 (1988).

[9]L. J. Allamandola, A. G. G. M. Tielens, and J. R. Barker, in Physical Processes in Interstellar Clouds, edited by G. E. Morfill and M. Scholer (Reidel , Dordrecht, 1987), p. 305.

[10]S. K. Atreya, J. Bergstrahl, J. J. Caldwell, K. Fox, J. F. Kasting, J. G. Luhmann, J. Lunine, D. J. McCleese, J. Rahe, and R. E. Young, "Laboratory Research for Planetary Atmospheres," Report of the Subgroup on Strategies for Planetary Atmospheres Exploration, NASA.

[11]T. R. Fletcher and S. R. Leone, J. Chem. Phys. **88**, 4720 (1988).

[12]E. L. Woodbridge, T. R. Fletcher, and S. R. Leone, J. Phys. Chem. **92**, 5387 (1988).

[13]T. R. Fletcher, and S. R. Leone, J. Chem. Phys. **90**, 871 (1989).

[14]R. F. Curl, Jr., P. G. Carrick, and A. J. Merer J. Chem. Phys. **82**, 3479 (1985); **83**, 4278 (1985).

[15]D. J. Donaldson and S. R. Leone, J. Chem. Phys. **85**, 817 (1986).

[16]E. L. Woodbridge, T. R. Fletcher, and S. R. Leone (unpublished results).

[17]K. A. Trentelman, S. H. Kable, D. B. Moss, and P. L. Houston, J. Chem. Phys. (in press).

[18]W. P. Hess, S. J. Kohler, H. K. Haugen, and S. R. Leone, J. Chem. Phys. **84**, 2143 (1986).

[19]W. P. Hess and S. R. Leone, J. Chem. Phys. **86**, 3773 (1987).

[20]S. K. Atreya, J. B. Pollack, and M. S. Matthews, eds., Origin and Evolution of Planetary and Satellite Atmospheres (Univ. of Arizona Press, Tucson (1989).

[21]R. Papoular, J. Conard, M. Guiliano, J. Kister, and G. Mille, Astr. Astrophys. Lett. (in press).

[22]G. Marston, F. L. Nesbitt, D. F. Nava, W. A. Payne, and L. J. Stief, J. Phys. Chem. **93**, 5769 (1989).

N90-26757

HIGH RESOLUTION, LOW TEMPERATURE PHOTOABSORPTION CROSS-SECTION OF C_2H_2, WITH APPLICATION TO SATURN'S ATMOSPHERE

JOHN CALDWELL*, C.Y.R. WU**, T.J. XIA**, D.L. JUDGE** AND R. WAGENER*

* Space Astrophysics Laboratory, Institute for Space and Terrestrial Science, 2700 Steeles Ave. West, Concord, Ontario L4K 3C8, Canada
** Space Science Center and Dept. of Physics, University of Southern California, Los Angeles, California 90089-1341

ABSTRACT

New laboratory observations of the VUV absorption cross-section of C_2H_2, obtained under physical conditions approximating stratospheres of the giant planets, have been combined with IUE observations of the albedo of Saturn, for which improved data reduction techniques have been used, to produce new models for that atmosphere. When the effects of C_2H_2 absorption are accounted for, additonal absorption by other molecules is required. The best-fitting model also includes absorption by PH_3, H_2O, C_2H_6 and CH_4. A small residual disagreement near 1600 Å suggests that an additional trace species may be required to complete the model.

INTRODUCTION

Extensive solar system observations of absorption and emission spectra have been obtained from a diverse collection of Earth-orbital satellites, interplanetary probes and ground-based telescopes. The pressures and temperatures of the various planetary environments being observed are generally very different from the usual laboratory conditions. There has been little incentive for the laboratory workers to go to the extra trouble of emulating the planetary conditions, and this has led to a situation where much of the laboratory spectral data which are required to interpret the planetary observations are obtained under conditions that are inappropriate for direct application to planetary modelling.

In the ultraviolet, planetary observations have been obtained for more than a decade by the NASA/ESA International Ultraviolet Explorer satellite. In the near future, it is expected that data from the Hubble Space Telescope will be available. The IUE data have provided significant new insights to the composition and auroral processes in planetary atmospheres. However, it is universally recognized that the advent of the HST will produce spectra that are greatly superior to the IUE data with respect to spatial resolution, spectral resolution, dynamic range and signal-to-noise. Whereas existing laboratory data are marginally acceptable for interpreting data of the quality produced by the IUE, it is clear that they are absolutely inadequate for modelling HST data.

Motivated by this mismatch between laboratory and observatory capabilities, we have implemented an experimental program to investigate systematically the temperature- and pressure-dependent absorption cross-sections of gases of interest for studying planetary atmospheres. Our first species is C_2H_2, chosen because it is one of the most important UV absorbers in the stratospheres of the giant planets. We have applied the new data to previous

IUE observations of Saturn, where C_2H_2 is clearly the dominant absorber. The reduction of the IUE spectra has been improved over previously published versions, as discussed below. After the effects of C_2H_2 absorption have been accounted for, other gases have been added to the model to optimize agreement with the planetary spectra.

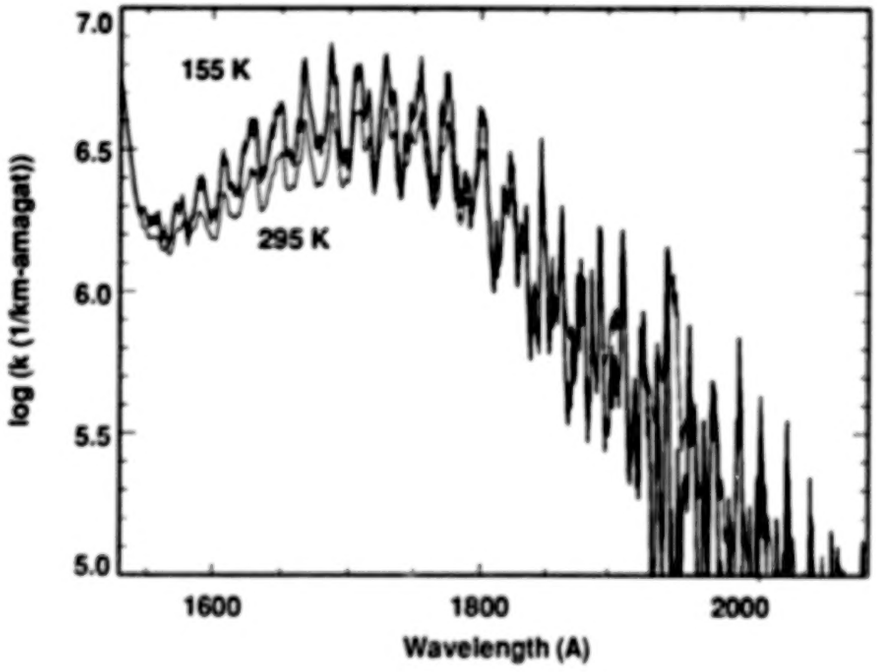

Fig. 1: New absorption coefficients, obtained by Wu *et al.*[1] at two temperatures.

LABORATORY RESULTS

The VUV photoabsorption cross-section measurements of C_2H_2 were performed at the Synchrotron Radiation Center at the University of Wisconsin-Madison. The data were obtained at a spectral resolution of 0.07 Å FWHM. The absorption coefficient spectra shown in Fig. 1 were smoothed by a 5 point gaussian filter to reduce high frequency noise. In the region between 1530 and 1800 Å the absorptions at low temperature (155K) compared to the room temperature data show stronger peaks (10 to 50%) and some enhancement in the valleys (up to 20%). In the region between 1900 and 2100 Å hot bands due to the $\tilde{A}\,^1A_u - \tilde{X}\,^1\Sigma_g^+$ transition are observed in the room temperature data. Further details are given in Ref. 1. The lower temperature absorption coefficients are more applicable to outer planet stratospheres and are used for the first time in the following reanalysis of the UV spectrum of Saturn.

IMPROVEMENTS IN IUE DATA ANALYSIS

Since the study of Saturn's UV spectrum by Winkelstein *et al.*[2] a number of improvements have been made in the IUE data reduction. All of the data taken between 1978 and 1980 was reprocessed by the IUE Standard Image Processing System at Goddard Space Flight Center using the latest software and the new Intensity Transfer Functions (ITF), in particular correcting for a known error in the ITF of the short wavelength prime camera (SWP, 1100 to 1980 Å) at low exposure levels.

Because of the very limited dynamic range of the IUE cameras and because of the rapidly decreasing planetary flux from long to short wavelengths, it is necessary to combine a large number of individual spectra, having a wide range in exposure times, from seconds to hours, to cover the useful range of the IUE. The individual spectra are normalized in the overlapping region and averaged together.

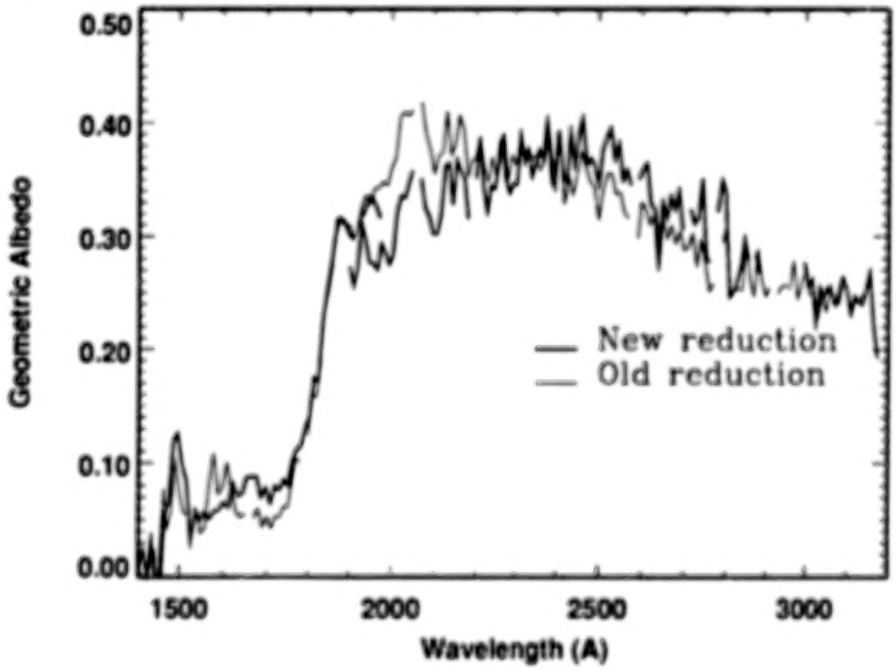

Fig. 2: The composite Saturn spectrum obtained by the IUE. The older extraction process is shown by the lighter line, the newer, improved one by the darker line.

Since the SWP camera is sensitive to longer wavelength photons, some contribution due to long wavelength light scattered within the spectrograph has to be corrected for in solar type spectra. An improved algorithm was used in this analysis that explicitly included the contribution of H_2 emission. The newly derived albedo spectrum is shown in Fig. 2 together with the previous version of Winkelstein *et al.*.

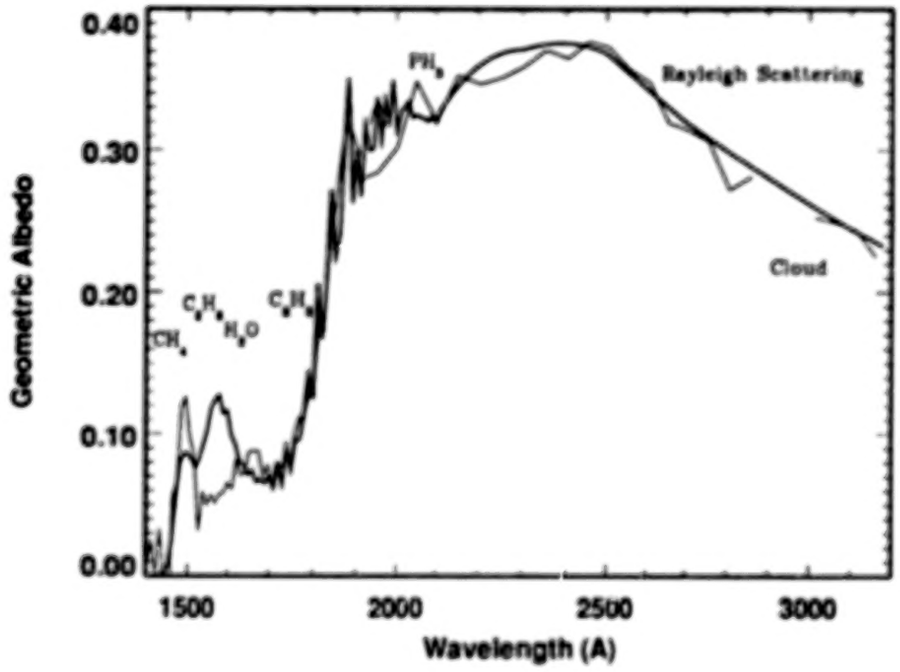

Fig. 3: The Saturn albedo spectrum (thin line) with the best-fitting model obtained to date (thick line), showing the regions where various absorbers are thought to be important.

MODELS OF THE ULTRAVIOLET ALBEDO OF SATURN

The new extraction process has introduced a relative albedo maximum near 2500 Å, in good agreement with OAO albedos obtained in the early 1970s[3]. The low albedo at 3000 Å must be due to some absorbing cloud at a pressure level of about 170 mbar in the Saturnian atmosphere (Fig. 3). The rise in reflectivity at shorter wavelengths is due to Rayleigh scattering from overlying H_2. The decreasing albedo below 2500 Å can be explained by PH_3 absorption. The best fitting model in Fig. 3 had no PH_3 at pressure levels $p < 60$ mbar, a mixing ratio of 5×10^{-7} between 60 and 120 mbar and 1.5×10^{-6} for $p > 120$ mbar, consistent with the distribution of Tokunaga *et al.*[4], but incompatible with the distribution of Courtin *et al.*[5].

Below 2000 Å, the spectrum (Fig. 4) is dominated by C_2H_2 absorption. Our best fitting model has C_2H_2 distributed between 2 and 20 mbar at a mixing ratio of 1.2×10^{-7}. A model with C_2H_2 alone is unsatisfactory, an additional continuum absorber in the top 2 mbar is required. We have examined the following candidate species C_2H_4, C_3H_4, C_4H_2, and H_2O and find that H_2O at a mixing ratio of 1.5×10^{-7} provides the best fit, although still unsatisfactory between 1550 and 1600 Å. The same conclusion was reached by Winkelstein *et al.*, but the abundance of H_2O is reduced by a factor of 2 as a direct consequence of the new low temperature absorption coefficients of C_2H_2.

Since we restricted the C_2H_6 distribution to follow the C_2H_2, i.e. uniform between 2 and 20 mbar, the influence of C_2H_6 is felt only weakly near 1500 Å. CH_4 causes the drop to essentially zero albedo near 1450 Å.

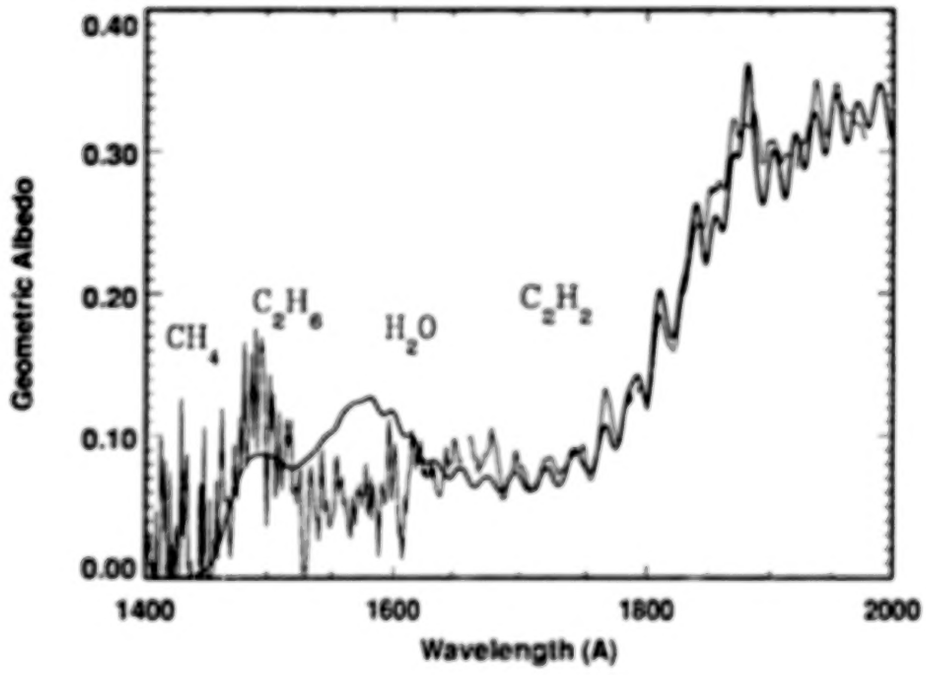

Fig. 4: Details of the best-fitting model below 2000 Å, with the regions where several absorbers may be important.

To conclude, we speculate on the possible cause of the remaining discrepancy between the model and the observations, near 1600 Å, and indicate where future laboratory effort may be required. The discrepancy suggests that another gas may be present on Saturn but not yet recognized in the modelling. One possibility for the missing gas is arsine, recently detected in Saturn's mid-infrared spectrum by Bézard *et al.*[6]. The observed mole fraction is of order several parts per billion, with the clear indication that the abundance is decreasing with increasing altitude, "a possible consequence of UV photolysis". If that is indeed the explanation for the vertical distribution of AsH_3 on Saturn, then it is reasonable to expect that some effect of that absorption may be visible in the UV spectrum. Unfortunately, no relevant laboratory observations of AsH_3 have been made, and it will be a prime candidate for future work in our program.

1. C.Y.R. Wu, T.S. Chien, G.S. Liu, D.L. Judge and J.J. Caldwell, *J. Chem. Phys.* **91**, 272 (1989).

2. P. Winkelstein, J. Caldwell, T. Owen, M. Combes, Th. Encrenaz, G. Hunt and V. Moore, *Icarus* **54**, 309 (1983).

3. L. Wallace, J. Caldwell and B.D. Savage, *Astrophys. J.* **172**, 755 (1972).

4. A.T. Tokunaga, H.L. Dinerstein, D.F. Lester and D.M. Rank, *Icarus* **42**, 79 (1980); *Icarus* **48**, 540 (1981).

5. R. Courtin, J.P. Baluteau, D. Gautier, A. Marten and W. Maguire, *Saturn Conference*, Tucson, AZ, May 1982.

6. B. Bézard, P. Drossart, E. Lellouch, G. Tarrago and J.-P. Maillard, *Astrophys. J.* **346**, 509 (1989).

N90-26758

GAUSSIAN QUADRATURE EXPONENTIAL SUM MODELING OF NEAR INFRARED METHANE LABORATORY SPECTRA OBTAINED AT TEMPERATURES FROM 106 TO 297 K.

LAWRENCE P. GIVER*, D. C. BENNER**, M. G. TOMASKO***, U. FINK***, and D. KEROLA***

*NASA-Ames Research Center, N245-4, Moffett Field, CA 94035-1000.

**College of William and Mary, Physics Dept., Williamsburg, VA 23185.

***University of Arizona, Lunar and Planetary Lab., Tucson, AZ 85721.

ABSTRACT

Transmission measurements made on near-infrared laboratory methane spectra have previously been fit using a Malkmus band model. The laboratory spectra were obtained in three groups at temperatures averaging 112, 188, and 295 K; band model fitting was done separately for each temperature group. These band model parameters cannot be used directly in scattering atmosphere model computations, so an exponential sum model is being developed which includes pressure and temperature fitting parameters. The goal is to obtain model parameters by least square fits at 10 cm^{-1} intervals from 3800 to 9100 cm^{-1}. These results will be useful in the interpretation of current planetary spectra and also NIMS spectra of Jupiter anticipated from the Galileo mission.

INTRODUCTION

Three sets of about 30 near-infrared spectra of methane have previously been fit using a Malkmus band model.[1] These spectra were obtained at NASA-Ames using a refrigerated White cell with path lengths from 3 to 61 meters, pressures of pure methane from several torr to several atmospheres, and temperatures clustered at 112, 188, and 295 K; at the lowest temperatures the maximum pressure used was limited to 0.5 atmosphere. An Eocom interferometer was used at 1 cm^{-1} resolution; the quartz

beam-splitter together with the InSb detector produced a useful range for these spectra from 3760 to 9200 cm^{-1}. The laboratory conditions of the spectra used in the Malkmus band model analyses are listed in Tables 1-3. The transmissions measured at the 10 cm^{-1} interval centered at 4650 cm^{-1} are also listed, along with the calculated transmissions from the Malkmus band model fit and the exponential sum fit, which are described below.

At pressures sufficiently high that line profiles can be described by the Lorentz formulation, the Malkmus band model can be written in the form

$$\bar{T} = \exp\left\{-2\pi\gamma_\nu P\left[\left(\frac{k_\nu u}{\pi\gamma_\nu P}+1\right)^{1/2}-1\right]\right\}, \qquad (1)$$

where $\bar{T}$ is the mean transmission of the spectral interval centered at wavenumber ν, u is the gas abundance, and P is the pressure. Only two parameters are determined from least square fits to the laboratory spectra: the absorption coefficient k_ν, and the pressure coefficient y_ν. Our notation is similar to that used by Fink, *et al.*[2] for the Mayer-Goody band model. Some of our spectra were obtained at low pressures, making it necessary to include an approximation to the Voigt line profile in our computations of the Malkmus band model parameters. But since we adopted mean pressure broadening coefficients for methane lines at our three temperatures, there were still only two parameters, k_ν and y_ν, determined from least square fits to the spectra in each temperature group.

Methane bands are major features in the spectra of all the outer planets and the satellites Titan and Triton. Having obtained these laboratory spectra, determining parameters describing the methane spectrum that can be used in modeling the moderate resolution near-infrared spectra of these planets and satellites becomes a major goal. The Malkmus band model parameters have been extrapolated to conditions applicable for modeling Triton's spectrum, assuming a clear atmosphere.[3] But scattering processes are important in the other atmospheres, and although spectral band models have been an accepted approach for nearly 50 years,[4] the radiative transfer equation in multi-layer scattering model atmospheres cannot be solved with band model formulations of gaseous

absorption. Additionally, the Malkmus band model parameters were determined only at three specific temperatures; a representation of the temperature dependence at each interval is also needed for atmospheric modeling computations.

For applications in scattering atmospheres, it is preferred that the gaseous absorption be expressed as a weighted sum of exponentials. For example, McKay, *et al.*[5] used the following expression to transform the room temperature Mayer-Goody band model parameters of Benner and Fink[6] into exponential sum parameters at intervals of about 500 cm^{-1} for use in Titan greenhouse model computations:

$$\bar{T} = \sum_{i=1}^{4} w_i \exp\left(-k_i u P^n\right) . \qquad (2)$$

Here w_i are weights, and k_i are the absorption coefficients, scaled by a pressure factor P^n, where the exponent n is a fitting parameter; this exponential sum model thus has 8 parameters to be determined from least square fits.

EXPONENTIAL SUM MODELS

In a similar fashion, Tomasko, *et al.*[7] made some preliminary transformations of the Malkmus band model parameterization of the Ames spectra for use in modeling certain intervals of the Titan spectrum of Fink and Larson.[8] For computational efficiency in the scattering model atmosphere, Tomasko preferred an 8 term exponential sum using fixed Gaussian quadrature weights. Despite the higher number of terms, this model has about the same number of parameters to determine as the 4 terms used by McKay, et al., since the weights are fixed: $w_1 = w_8 = 0.0506$, $w_2 = w_7 = 0.1112$, $w_3 = w_6 = 0.1569$, and $w_4 = w_5 = 0.1813$. In this model the absorption coefficients are required to increase in order with the term number, i.

Instead of determining exponential sum parameters from transmission values computed from band model fits, a more direct approach should be to determine the exponential sum parameters directly from the measured transmission values of the laboratory

spectra. Pressure and temperature parameters should be included; with the large number of parameters, better fits should be obtained than from 2 parameter band models. The exponential sum model should have the following form:

$$\bar{T} = \sum_{i=1}^{l} w_i \exp\left[-k_i u\, f_1(P)\, f_2(T)\right], \qquad (3)$$

where u is the methane abundance, $f_1(P)$ is a function of pressure, and $f_2(T)$ is a function of temperature.

This expression requires that a number of decisions be made before final results can be determined by least square fits. Since a P^n dependence is not realistic at very low pressures, we introduced a second pressure parameter, P':

$$f_1(P) = \left(P + P'\right)^n. \qquad (4)$$

Since the spectra were obtained in three temperature groups, we initially selected a 2 parameter temperature dependence:

$$f_2(T) = \exp\left[a\left(\ln T/T_0\right)^2 + b \ln T/T_0\right], \qquad (5)$$

where $T_0 = 273$ K, and a and b are fitting parameters. An additional term-dependent temperature parameter, c, was introduced when it was realized this would permit better fits in the lower temperature groups:

$$\bar{T} = \sum_{i=1}^{l} w_i \exp\left(-k_i \left\{1 + \left[(1+c)^{i-4} - 1\right] \ln \frac{T}{T_0}\right\} u\, f_1(P)\, f_2(T)\right). \qquad (6)$$

PRELIMINARY RESULTS

The exponential sum model in equation (6) above has 13 fitting parameters; the Ames transmission measurements of the 10 cm^{-1} spectral interval centered at 4650 cm^{-1}

was fit quite well by this model. Comparisons of the observed transmissions, the exponential sum model computations, and the Malkmus band model computations are presented in Tables 1-3. This spectral interval has both a substantial pressure dependence and temperature dependence; being high in the R branch of the $\nu_2 + \nu_3$ band, the absorption decreases dramatically at low temperatures.

The fitting parameters for equation (6) determined at 4650 cm^{-1} are: k_1=0.0227, k_2=0.0319, k_3=0.0415, k_4=0.0501, k_5=0.1173, k_6=0.4775, k_7=1.159, k_8=17.0, a=-0.845, b=0.472, c=0.085, P'=0.0383 atm., and n=0.615.

DISCUSSION

Several problems must be overcome before determining exponential sum model parameters at all the spectral intervals where Malkmus band modeling was done. The forms of the pressure and temperature functions must be chosen which can adequately represent the transmission data at all spectral intervals. Spectra were obtained at pressures from several Torr to several atmospheres; the 2 pressure parameters P' and n of equation (4) may be insufficient to fit the data well at all intervals. Similarly, a temperature dependence may be found to improve equation (5). We have made a few tests to see if fits could be improved by allowing the pressure exponent, n, to vary with the term index, i, in equation (6). Fits were significantly improved, but more fitting parameters increase the risk of coupling between parameters, raising concerns about the uniqueness of the fits, and significantly increasing computation time.

Even to get unique values for all 8 absorption coefficients, transmission values must range from over 0.95 to less than 0.05. This requirement was readily met by the Ames spectra at 4650 cm^{-1}, as shown in Tables 1-3, but certainly not at all spectral intervals. In regions of strong absorption, it will be useful to combine the Ames room temperature spectra with some of the room temperature spectra obtained by Benner and Fink[6] at the Lunar and Planetary Laboratory. The conditions of some of these spectra are listed in Table 4. Since the abundance and pressure conditions of some of

Table 1.

Ames Room Temperature Spectra

Spectrum Number	Methane Abund. m-amgts.	Pressure atm.	Temp. Kelvin	Transmission at 4650 cm^{-1} measured	Malkmus model	Exp. Sum model
A002	0.2825	0.0971	296	0.946	0.952	0.939
A003	0.7274	0.2500	296	0.875	0.888	0.871
A004	1.66	0.5697	296	0.747	0.767	0.738
A005	4.048	1.3878	296	0.520	0.527	0.513
A006	8.806	3.0070	296	0.260	0.249	0.262
A007	19.53	6.6260	295	0.043	0.046	0.043
A012	1.145	0.1003	295	0.867	0.879	0.871
A013	2.854	0.2500	295	0.725	0.741	0.727
A014	6.498	0.5684	295	0.497	0.513	0.522
A015	16.04	1.4010	295	0.228	0.195	0.232
A016	34.55	3.0070	295	0.039	0.030	0.035
A017	76.87	6.6460	295	0.000	0.000	0.000
A026	0.295	0.0052	295	0.960	0.962	0.961
A027	0.817	0.0144	295	0.930	0.929	0.920
A028	2.243	0.0395	295	0.849	0.862	0.847
A029	5.672	0.1000	295	0.704	0.724	0.693
A030	14.19	0.2500	295	0.462	0.466	0.464
A034	32.35	0.5697	295	0.202	0.179	0.196
A036	170.9	2.9930	295	-0.003	0.000	0.000
A041	2.558	0.1000	295	0.795	0.812	0.799
A042	6.399	0.2501	296	0.609	0.614	0.602
A043	14.59	0.5699	296	0.369	0.336	0.366
A044	35.76	1.3950	295	0.092	0.070	0.084
A054	0.5775	0.1004	295	0.911	0.921	0.909
A055	1.438	0.2499	295	0.801	0.825	0.812
A056	3.276	0.5696	295	0.637	0.652	0.637
A057	8.081	1.4010	295	0.378	0.351	0.379
A058	17.33	2.9930	295	0.124	0.107	0.126
A059	44.7	7.6600	295	0.001	0.003	0.002

Table 2.

Ames Methane Spectra near T=188 K.

Spectrum Number	Methane Abund. m-amgts.	Pressure atm.	Temp. Kelvin	Transmission at 4650 cm^{-1} measured	Malkmus model	Exp. Sum model
A063	0.293	0.0637	187	0.965	0.968	0.966
A064	0.767	0.1725	194	0.920	0.923	0.910
A065	1.705	0.3771	191	0.822	0.839	0.827
A066	4.257	0.9296	189	0.634	0.647	0.630
A067	9.518	2.0610	189	0.387	0.379	0.389
A068	61.47	12.2450	187	0.000	0.002	0.001
A069	24.44	5.1770	189	0.073	0.084	0.081
A072	0.59	0.0646	186	0.938	0.950	0.943
A073	1.479	0.1620	186	0.869	0.884	0.879
A074	3.467	0.3791	186	0.732	0.750	0.747
A078	19.22	2.0880	187	0.222	0.206	0.235
A081	1.147	0.0647	190	0.908	0.925	0.913
A082	2.87	0.1609	189	0.808	0.828	0.822
A083	6.803	0.3788	188	0.623	0.642	0.640
A084	16.81	0.9276	187	0.368	0.337	0.373
A087	38.93	2.1429	188	0.084	0.080	0.093
A090	2.666	0.0650	184	0.863	0.879	0.868
A091	6.605	0.1636	187	0.708	0.732	0.717
A092	15.24	0.3828	190	0.489	0.486	0.492
A093	37.07	0.9378	192	0.200	0.172	0.189
A096	84.92	2.0880	188	0.019	0.019	0.015
A099	0.302	0.0642	183	0.962	0.968	0.966
A100	0.765	0.1633	184	0.916	0.924	0.916
A101	1.782	0.3818	185	0.822	0.834	0.828
A102	4.346	0.9330	186	0.640	0.643	0.631
A105	9.619	2.0820	189	0.396	0.376	0.385
A108	0.311	0.0036	191	0.965	0.979	0.976
A109	0.842	0.0096	191	0.952	0.961	0.945
A110	2.306	0.0263	191	0.912	0.917	0.892
A111	5.674	0.0647	191	0.806	0.822	0.790
A112	14.38	0.1622	189	0.591	0.616	0.587
A115	26.47	0.3726	189	0.405	0.376	0.385
A116	66.58	0.9342	189	0.081	0.086	0.086
A120	192.8	2.6780	190	0.000	0.001	0.000

Table 3.

Ames Methane Spectra near T=112 K.

Spectrum Number	Methane Abund. m-amgts.	Pressure atm.	Temp. Kelvin	Transmission at 4650 cm^{-1} measured	Malkmus model	Exp. Sum model
A123	0.1295	0.0020	115	0.993	0.996	0.997
A124	0.3652	0.0054	112	0.989	0.990	0.993
A125	1.009	0.0146	109	0.978	0.977	0.982
A126	2.575	0.0382	112	0.945	0.946	0.947
A127	6.27	0.0931	112	0.875	0.878	0.881
A128	14.21	0.2109	112	0.728	0.745	0.754
A129	35.08	0.5208	112	0.477	0.486	0.496
A132	0.0608	0.0020	113	0.999	0.998	0.999
A133	0.1626	0.0053	I09	0.997	0.994	0.997
A134	0.464	0.0147	107	0.989	0.986	0.992
A135	1.179	0.0371	106	0.979	0.968	0.977
A136	3.612	0.1147	107	0.924	0.909	0.919
A137	7.36	0.2338	107	0.846	0.825	0.843
A138	15.34	0.5237	115	0.663	0.666	0.646
A141	0.295	0.0020	112	0.984	0.992	0.995
A142	0.799	0.0054	113	0.980	0.983	0.985
A143	2.183	0.0150	115	0.954	0.962	0.958
A144	5.41	0.0369	114	0.906	0.916	0.908
A145	13.73	0.0929	113	0.793	0.806	0.807
A146	31.27	0.2112	113	0.618	0.615	0.615
A147	77.68	0.5250	113	0.317	0.300	0.313
A150	0.0294	0.0020	114	0.993	0.999	0.999
A151	0.0823	0.0055	114	0.992	0.997	0.998
A152	0.2194	0.0147	114	0.989	0.992	0.995
A153	0.552	0.0371	114	0.978	0.982	0.985
A154	1.709	0.1158	115	0.944	0.948	0.942
A155	3.472	0.2333	114	0.895	0.897	0.887
A156	7.815	0.5204	113	0.784	0.785	0.765
A159	0.0149	0.0019	110	0.995	0.999	1.000
A160	0.0426	0.0054	109	0.998	0.998	0.999
A161	0.1164	0.0147	109	0.995	0.996	0.998
A162	0.2911	0.0368	109	0.987	0.990	0.993
A163	0.747	0.0937	108	0.972	0.974	0.978
A164	1.673	0.2117	109	0.948	0.944	0.939
A165	4.015	0.5314	114	0.870	0.869	0.839

Table 4.

L.P.L. Methane Spectra

Spectrum Number	Methane Abund. m-amgts.	Pressure atm.	Temp. Kelvin
170A	0.856	0.905	294
170C	0.851	0.901	294
140A	0.477	0.505	294
120A	0.260	0.275	294
120C	0.260	0.275	294
110A	0.129	0.137	294
105A	0.0653	0.0691	294
102A	0.0255	0.0270	294
H70A	0.439	0.911	294
H40A	0.254	0.528	294
H40C	0.254	0.528	294
H20A	0.125	0.259	294
H10A	0.0609	0.126	294
H05A	0.0322	0.0668	294
Q70A	0.224	0.922	294
Q40A	0.129	0.528	294
Q20A	0.0641	0.263	294
Q10A	0.0317	0.130	294
Q05A	0.0163	0.0671	294
M11A	0.590	0.0083	297
M12A	1.06	0.0150	297
M13A	1.99	0.0280	297
M15A	9.57	0.1347	297
M21A	1.18	0.0083	297
M22A	2.13	0.0150	297
M23A	3.98	0.0280	297
M31A	2.35	0.0083	297
M32A	4.26	0.0150	297
M33A	7.96	0.0280	297
M41A	4.71	0.0083	297
M42A	8.52	0.0150	297
M51A	9.42	0.0083	297

these spectra are quite different from the spectra listed in Table 1, combining these 2 sets in exponential sum modeling will increase the number of regions where good fits can be determined directly from the transmission data.

In the weak absorption regions between the main bands, the number of parameters that can be determined directly from the transmission measurements on the spectra will be greatly reduced. Nevertheless, some of these weak absorption regions are of primary interest in the spectra of the outer planets and Titan, and exponential sum model parameters are needed. Our original expectation was that exponential sum parameters could best be determined from the measured transmissions, as compared to computed transmissions based on band model parameters.[7] In regions of strong absorption with sufficient lab data, this approach should give the best results. But in the weak absorption regions it will be necessary to augment the measured transmissions with computed transmissions based on the Malkmus model parameters in order to determine complete sets of exponential sum parameters. Such a procedure could become quite arbitrary unless it is closely coupled to intended applications. At this time methane exponential sum parameters are needed for modeling Titan's spectrum, and thus improving knowledge of Titan's haze, cloud elevations, and methane abundance. In six years Galileo will be in orbit around Jupiter, and the NIMS instrument should be producing many interesting spectra, requiring intensive modeling of various regions of the Jovian atmosphere.

REFERENCES

1. L. P. Giver, D. C. Benner, and R. W. Boese,
Bull. Amer. Astron. Soc. 16, 711 (1984).
2. U. Fink, D. C. Benner, and K. A. Dick,
J.Q.S.R.T. 18, 447 (1977).
3. D. P. Cruikshank, R. H. Brown, L. P. Giver, and A. T. Tokunaga,
Science 245, 283 (1989).
4. R. Goody, R. West, L. Chen, and D. Crisp,
J.Q.S.R.T. in press (1989).
5. C. P. McKay, J. B. Pollack, and R. Courtin,
Icarus 80, 23 (1989).
6. D. C. Benner and U. Fink,
Bull. Amer. Astron. Soc. 12, 697 (1980).
7. M. G. Tomasko, S. K. Pope, D. Kerola, P. H. Smith, and L. P. Giver,
Bull. Amer. Astron. Soc. 21, 961 (1989).
8. U. Fink and H. P. Larson,
Astrophys. J. 223, 1021 (1979).

N90-26759

MEASUREMENTS OF THE METHANE RELAXATION TIMES FOR APPLICATION TO THE INFRARED EMISSION MODELS OF THE UPPER ATMOSPHERES OF OUTER PLANETS AND TITAN

RANGASAYI N. HALTHORE[1,3], JOHN J. CALDWELL[2,4], JOHN E. ALLEN, JR.[3], JIM A. BURT[4], KUANGHUA YANG[4] AND PAUL DELANEY[4]

1. Applied Research Corporation, Landover, MD 20785.
2. Space Astrophysics Laboratory, Institute for Space and Terrestrial Science, Concord, Ontario, L4K3C8.
3. Laboratory for Extraterrestrial Physics, NASA Goddard Space Flight Center, Greenbelt, MD 20771.
4. Department of Physics and Astronomy, York University, Downsview, Ontario, M3J1P3, Canada.

ABSTRACT

The 7.8 μm emission from the ν_4 band of methane (CH_4) is a regularly observed feature in the stratosphere of all the giant planets and Titan. On Jupiter, enhancements in this emission are associated with the infrared hot spots in the auroral zone. Attempts to model this phenomenon in particular, and to understand the role of methane in general, have been hampered in part by a lack of adequate laboratory measurerments of the collisional relaxation times for the ν_3 and ν_4 levels over the appropriate temperature range. To provide this needed data, we have initiated a series of laboratory experiments.

In our experimental arrangement the ν_3 band of methane is pumped at 3.3 μm using a pulsed infrared source (Nd:YAG/dye laser system equipped with a wavelength extender). The radiative lifetime of the ν_3 level (~ 37 ms) is much shorter than the ν_4 lifetime (~390 ms); however, a rapid V-V energy transfer rate ensures that the ν_4 level is substantially populated. The photoacoustic technique is used to acquire relaxation rate information. The experiments are performed using a low-temperature, low-pressure cell.

In this paper we describe our experimental apparatus and technique. In addition we discuss some of the experimental difficulties associated with making these measurements and present some preliminary results.

INTRODUCTION

After hydrogen and helium, methane is the third most abundant molecule in the atmospheres of the giant planets - Jupiter, Saturn, Uranus and Neptune - and is an important constituent in the atmosphere of Titan. Of the four fundamental vibrations the molecule possesses, two - ν_3 at 3.3 μm and ν_4 at 7.8 μm - are strongly infrared active. Furthermore, the molecule possesses several combination and overtone bands spread throughout the visible and near IR spectrum. In the atmospheres of outer planets, methane primarily absorbs solar radiation at 3.3 μm and emits in the 7.8 μm. Jupiter, for example, exhibits limb brightening in the 7.8 μm band due to methane emission from the stratosphere[1,2]. In the same band, Jupiter also exhibits an extremely varied and complicated disc, ranging from hot spots in the polar regions to wave like disturbances in the equatorial regions. Since methane does not condense on Jupiter and since alteration in its abundance due to photochemical destruction is negligible, the brightness variations in the 7.8 μm emission is inferred as due changes in the stratospheric temperature. Other hydrocarbons such as ethane and acetylene, which are formed by the solar UV dissociation of methane, also have emissions in the mid-IR range of 8 to 13 μm and along with methane form an important group of molecules taking part in the energy transfer of the uppter atmospheres.

Based on the scant laboratory data available up to the present, it has been customary to assume that the emission in the ν_4 band is Planckian in deriving the temperatures and the minor hydrocarbon species abundances[3]. This assumption of local thermodynamic equilibrium (LTE) may or may not be valid depending on the parameters η_C and η_r, which are the collisional relaxation time and the spontaneous emission time respectively for the transition in question. The collisional relaxation time (η_C) is strongly dependent on temperature and is inversely proportional to pressure. It is also dependent on the type of collision partners. If η_C is smaller than η_r at a given height in the atmosphere, the emission from that height is likely to be Planckian, since a sufficient number of collisions would have occured to maintain the Boltzman distribution among the energy levels before a photon is spontaneously emitted. The emission in this case is thermal, since brightness can be related to the kinetic temperature. However if η_C is greater than η_r, such as at high altitudes where the collisions are infrequent, spontaneous emission occurs before energy is equilibrated, and the brightness of this emission will have less to do with the kinetic temperature and is more indicative of the vibrational temperature of the molecule. In the limiting case, as η_C approaches a large value (as in the interstellar medium), the population of the molecules in the stationary states is radiatively controlled and therefore represents a case of scattering.

Since η_c is a strong function of temperature, pressure and composition, it is important that measurements be made under simulated planetary environment. In the past, methods using shocks, ultra-sound and light (both ordinary and laser light) have been used to measure the relaxation time in methane and mixtures containing methane at different pressures but room temperature[4-10]. For pure methane, it was found using the opto-acoustic method that the relaxation times for both ν_3 and ν_4 excitation were the same[4] - 1.6 μs at 1atm. Further studies[5] with ν_3 excitation indicated that the measured ν_3 relaxation time in the earlier study was actually for ν_4 as well since in methane the V-V transfer between ν_3 and ν_4 occurs at a rapid rate in preference to direct ν_3 relaxation. The lifetime of the ν_3 state (0.03 s) is an order of magnitude faster than that for the ν_4 state (0.39 s) and will, for example, end up as a competing mechanism for ν_3 de-excitation above the 40 μbar pressure level on Jupiter. In this study we have adopted two methods to determine the vibrational relaxation: opto-acoustic method and laser induced fluorescence. We use compositions and pressures which are of interest to the planetary science studies and temperatures as low as liquid nitrogen temperature (77 K).

EXPERIMENTAL

Figure 1 shows a schematic of the experimental arrangement. A portion of the pulsed Nd:YAG laser output at 1.064 μm (750 mJ @ 10 per second) is doubled in frequency using a second harmonic generator (SHG). The 532 nm beam is converted to approximately 813 nm beam (30 mJ) by a pulsed dye laser (PDL). Residual 1.06 μm beam and the PDL output beam are combined in a $LiNbO_3$ crystal in the wavelength extender (WEX) to produce a beam with a difference wavelength of approximately 3.3 μm. The wavelength of this beam is continuously tunable, since the output of the dye is tunable. About 1 mJ per pulse was obtained at 3.3 μm using this commercial (Spectra Physics) setup. Pulse to pulse power fluctuations are monitored by an InSb detector D, which measures the diffuse reflection off of one of the beam steering mirrors. A helium neon laser is used for alignment purposes.

The opto-acoustic cell is about 2.5 cm diameter and 2.4 m long with ZnSe windows positioned at Brewsters angle at the ends to admit the 3.3 μm beam with minimum loss at the interfaces. The microphone (B&K 4134) is mounted flush with the inner wall at the center of the cell. The cell is cooled using liquid nitrogen in the annular space surrounding the long arms. The long arms were thought to be necessary to minimize interference from the acoustic noise arising due to energy absorption by the window material as observed in [11]. Tests have shown that the window interference is minimal in our setup and efforts are underway to use the cell without the long arms, since aligning the 3.3 μm beam will be appreciably simplified. The cell is enclosed in an evacuated QVF glass envelop to prevent condensation on the cell

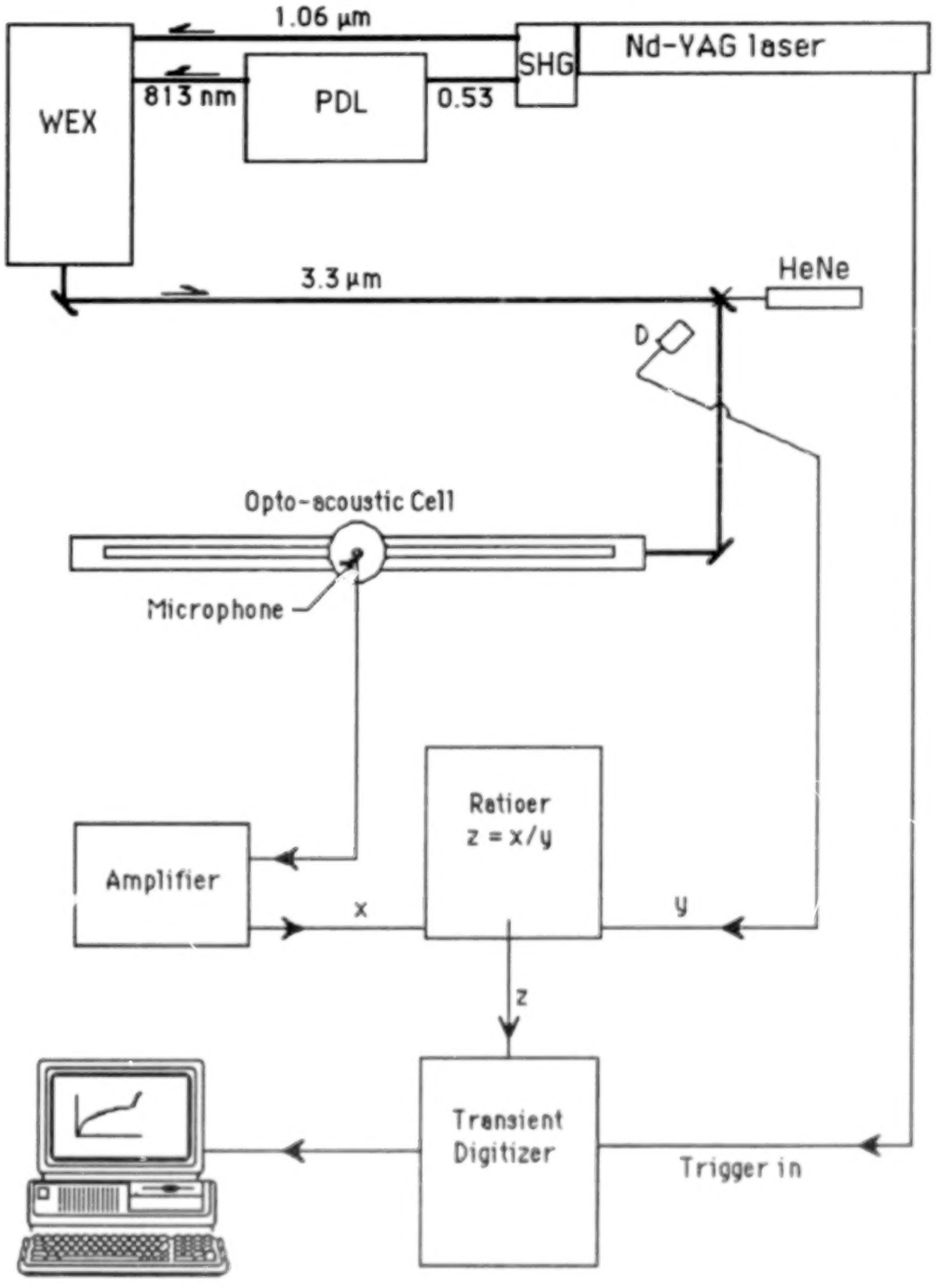

Fig. 1: SCHEMATIC OF THE EXPERIMENTAL ARRANGEMENT

SHG Second Harmonic Generator (Converts 1060 nm output to 532 nm).
PDL Pulsed Dye Laser.
D A detector to sense the laser energy per shot.
WEX Wavelength Extender. Produces the difference of 1060 nm and 813 nm

windows. A 4" diffusion pump is used to evacuate the QVF and the inner manifold. Pressures down to 1 mtorr have been achieved using this setup.

After amplification, the microphone signal is normalized for laser power fluctuations by dividing the output of the detector D in the ratioer. The output is then fed to a transient digitizer which is triggered by the synchronous Q-switched output of the Nd:YAG laser. The data is stored on floppy disks using a personal computer.

PRELIMINARY RESULTS

When the laser is tuned to the Q-branch, methane absorbs along the beam path. Rapid V-V transfer ensures that all the vibrational modes are excited quickly. Subsequent collisional deactivation of v_4 level results in the V-T transfer or an increase in kinetic temperature along the beam path. The pressure therefore increases as well. The resultant pressure wave travels radially outwards at sonic speed and is picked up by the microphone. The trace of microphone output versus time will then give the relaxation rate. If the thermal diffusion coefficient α is very high as at low pressures, the energy due to absorption will be conducted to the wall complicating the process thus requiring modelling to unravel the pressure trace.

Three traces are shown in figure 2 - on-line, off-line and the difference. The on-line trace is obtained when the laser beam is tuned in wavelength to the Q-branch and thus represents signal plus noise. The off-line trace is obtained with the laser tuned off-line to get an estimate of the noise. The difference gives the relaxation rate. The figure here pertains to a mixture containing 10% methane in argon at room temperature and 1.2 torr pressure, and the relaxation time is seen to be approximately 0.6 ms. Analysis is not yet complete, for instance, the origin of the peak at about 3 ms is unknown.

ACKNOWLEDGEMENTS

The experiments are being performed at the Ontario Laser and Lightwave Research Center, Toronto, Ontario, Canada. This research is supported by the Institute for Space and Terrestrial Science, Concord, Ontario, Canada and by the NASA Planetary Atmospheres Program through the Goddard Space Flight Center.

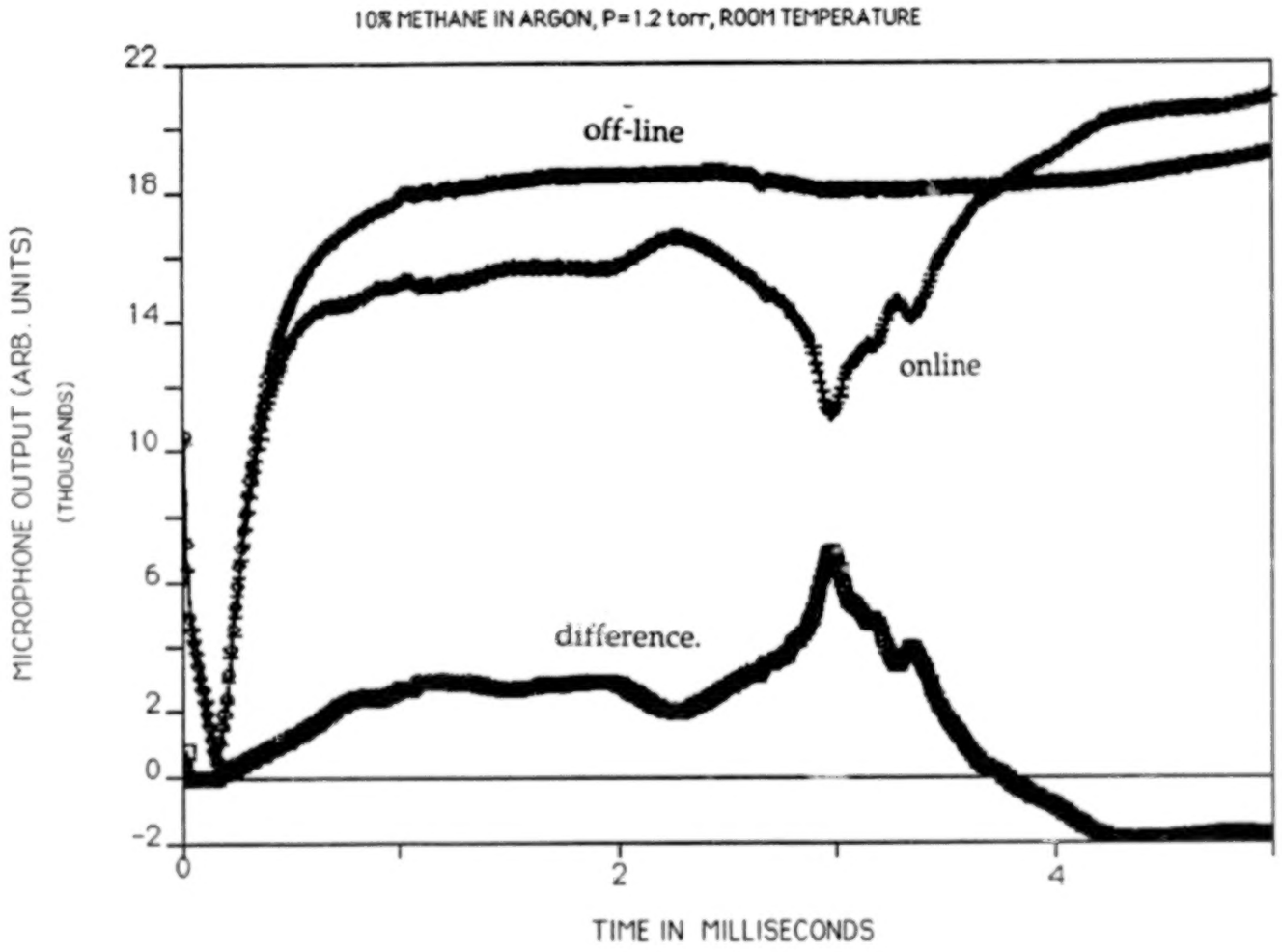

Figure 2. Opto-Acoustic Signal.

REFERENCES

[1]F.C.Gillet and J.A.Westphal,*The Ap.J*, 179:L153-L154, (1973).

[2]G.Orton, *Icarus*, 32, 41-57 (1977).

[3]R.N.Halthore, A.Burrows and J.J.Caldwell, *Icarus*,74, 340-350 (1988).

[4]T.L.Cottrell, I.M.MacFarlane,A.W.REad and A.H.Young, *Trans.Faraday Soc.* 62,2655 (1966).

[5]E.Avramides and T.F.Hunter, *Chem. Phys.* 57, 441-451 (1981).

[6]J.T.Yardley and C.B.Moore, *J.Chem. Phys.* 45, 1066 (1966).

[7]J.T.Yardley and C.B.Moore, *J.Chem.Phys.* 49, 1111 (1968).

[8]J.T.Yardley, M.N.Fertig and C.B.Moore, *J.Chem. Phys.* 52, 1450 (1970).

[9]M.Huetz-Aubert, R.Lenormond and H.Manceau, *Adv. Mol. Relax. Processes* 6, 153 (1974).

[10]R.Klein and P.Hess, *Acustica* 33, 198 (1975).

[11]E.A.Rohlfing, J.Gelfand and R.B.Miles, *J.Appl. Phys.*, 53, 8, 5420-5426 (1982).

N90-26760

NEW ELECTRONIC STATES OF NH AND ND OBSERVED BY RESONANCE ENHANCED MULTIPHOTON IONIZATION SPECTROSCOPY

Russell D. Johnson III and Jeffrey W. Hudgens
Chemical Kinetics Division, National Institute of Standards and Technology
Gaithersburg, MD 20899

ABSTRACT

We report Resonance Enhanced MultiPhoton Ionization (REMPI) spectra of NH and ND, which reveal four new electronic states. Transitions from NH $a\ ^1\Delta$ to 3s and 3p Rydberg states in both NH and ND have been observed and rotationally analyzed. The transitions were observed in the wavelength range of 258 to 288 nm. The state assignments are : $e\ ^1\Pi\ (3s\sigma)$ at 82857 cm^{-1}, $f\ ^1\Pi\ (3p\sigma)$ at 86378 cm^{-1}, $g\ ^1\Delta\ (3p\pi)$ at 88141 cm^{-1}, and $h\ ^1\Sigma\ (3p\pi)$ at 89151 cm^{-1}.

INTRODUCTION

REMPI (Resonance Enhanced MultiPhoton Ionization) spectroscopy has proven to be a useful laboratory tool in obtaining new electronic spectra of many transient species.[1] NH in the metastable $a\ ^1\Delta$ state was the first transient to be observed by REMPI.[2] During a search for the REMPI spectra of N_3 we observed spectra of NH produced from the photolysis of HN_3. Six bands which are produced by excitations from the $a\ ^1\Delta$ state to vibrational levels of four new electronic states have been analyzed.

APPARATUS AND METHODS

The apparatus has been described in detail elsewhere.[3] Briefly the NH $a\ ^1\Delta$ was produced by the photolysis of HN_3 (10% in helium) in a vacuum chamber at 10^{-4} Torr. The NH $a\ ^1\Delta$ then absorbed two photons to prepare a Rydberg state, which subsequently absorbed one more photon to ionize. The ions are extracted into a time-of-flight mass spectrometer and detected. A

spectrum consists of the ion current of the mass of interest versus the laser wavelength. The rotational constants ν_0', B', D', B", D" were obtained by using a least-squares procedure to fit the observed lines. ν_0'' was set to the value for the $a\ ^1\Delta$ state, after the lower state was determined to be the $a\ ^1\Delta$ state by minimum J values and rotational constants. The formula used for the rotational fitting was:

$$F(J) = \nu_0 + B[J(J+1)-\Lambda^2] - D[J(J+1)-\Lambda^2]^2 \qquad (1)$$

The values of ν_0 for the $a\ ^1\Delta$ state were obtained from Herzberg[4].

RESULTS

Spectra were observed from 258 to 288 nm. A typical band is shown in Figure 1. Six bands were observed and assigned. The assignments and least-squares fits to the data of the rotational constants are shown in Table I.

Table I. Rotational Assignments of NH and ND bands observed from 258 to 288 nm. All transitions are from the $a\ ^1\Delta$ state.

Species and Transition	Band Origin, (cm^{-1})	B (cm^{-1})	D ($10^3\ cm^{-1}$)	quantum defect
NH e $^1\Pi(3s\sigma)$ (0-0)	82 856.76(15)	14.0831(66)	1.680(30)	0.94
ND e $^1\Pi(3s\sigma)$ (0-0)	82 927.60(12)	7.5704(42)	0.479(10)	
NH e $^1\Pi(3s\sigma)$ (1-0)	85 343.38(16)	13.4451(73)	1.597(33)	
ND e $^1\Pi(3s\sigma)$ (1-0)	84 805.43(19)	7.3099(75)	0.413(19)	
NH f $^1\Pi(3p\sigma)$ (0-0)	86 378.13(13)	14.2281(65)	1.629(33)	0.79
ND f $^1\Pi(3p\sigma)$ (0-0)	86 456.89(13)	7.7268(45)	0.494(13)	
NH g $^1\Delta(3p\pi)$ (1-1)	87 419.75(15)	13.7490(240)	4.188(486)	
ND g $^1\Delta(3p\pi)$ (1-1)	87 746.75(17)	7.6469(61)	0.852(40)	
NH g $^1\Delta(3p\pi)$ (0-0)	88 140.54(25)	14.9496(146)	2.236(109)	0.70
ND g $^1\Delta(3p\pi)$ (0-0)	88 228.76(32)	7.8096(249)	1.403(134)	
NH h $^1\Sigma(3p\pi)$ (0-0)	89 531.25(23)	15.2584(210)	2.077(212)	0.61
ND h $^1\Sigma(3p\pi)$ (0-0)	89 568.70(22)	8.1510(116)	0.343(77)	

The symmetry assignments come from tracing the branches to their minimum J values.[4] In most cases this uniquely determines the electronic symmetry of the upper and lower states involved in the transition. The Rydberg

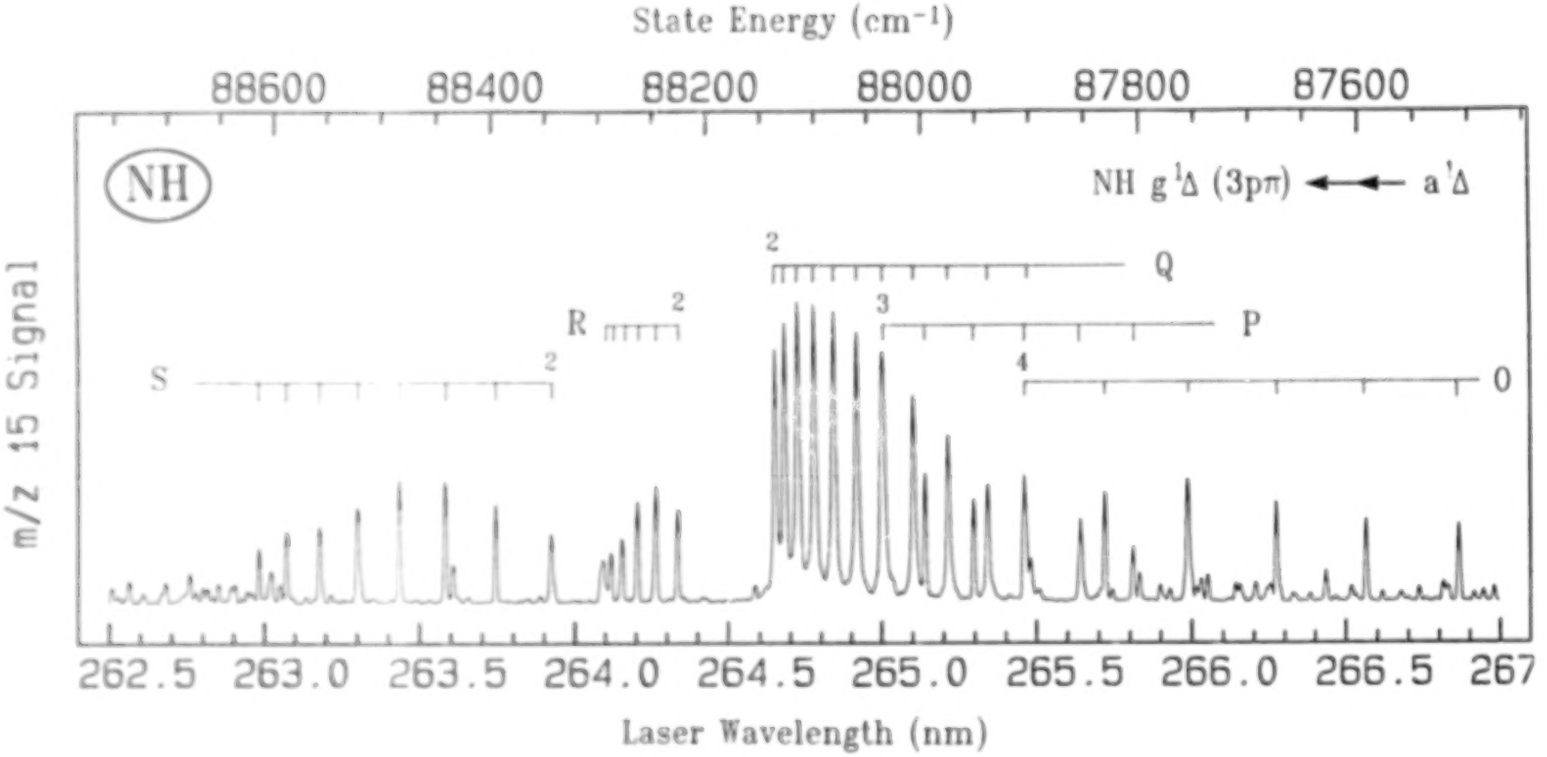

Figure 1. REMPI spectrum of NH from 262.5 to 267 nm. The transition is g $^1\Delta(3p\pi) \leftrightarrow a\ ^1\Delta$. Five rotational branches are observed, with a strong Q branch as expected for a two-photon transition with $\Delta\Lambda = 0$. The branches and minimum J values are indicated with festoons.

assignments come from calculating the quantum defect, δ, using the Rydberg formula:

$$\nu_{00} = IP - R/(n-\delta)^2 \qquad (2)$$

where ν_{00} is the state origin, IP is the ionization potential (108800 cm^{-1} for NH)[5], R is the Rydberg constant (109737 cm^{-1}), and n is the principal quantum number (3 in this case). For Rydberg states built on nitrogen appropriate quantum defects are: ns 0.95 to 1.1, np 0.6 to 0.8, nd -0.05 to 0.15.[6]

The symmetry assignments are consistent with the possible electronic states given the Rydberg configurations: For an electron in the 3sσ Rydberg orbital the electronic configuration is $\sigma\pi$, which gives rise to $^1\Pi$ and $^3\Pi$ states, of which only the $^1\Pi$ state is accessible through allowed transitions from the a $^1\Delta$ state. Similarly a $^1\Pi$ state is formed from the 3pσ orbital configuration. For the 3pπ orbital the configuration is $\pi\pi$, which gives rise to $^1\Sigma^+$, $^1\Sigma^-$, and $^1\Delta$ states, as well as triplet states. All of the possible states which are accessible through allowed transitions have been observed except one of the Σ states. The data do not allow differentiation between the $^1\Sigma^+$ and $^1\Sigma^-$ states. The other Σ state may reside at an energy above the region surveyed.

REFERENCES

1 J. W. Hudgens, in *Advances in Multi-photon Processes and Spectroscopy*, Vol. 4, edited by S. H. Lin (World Scientific, Singapore, 1988).

2 G. C. Nieman and S. D. Colson, J. Chem. Phys. **68**, 5656 (1978).

3 R. D. Johnson III, B. P. Tsai, J. W. Hudgens, J. Chem. Phys. **89**, 4558 (1988).

4 G. Herzberg, *Spectra of Diatomic Molecules, p. 117*, (Van Nostrand Reinhold, New York, 1950)

5 S. G. Lias, J. E. Bartmess, J. L. Holmes, R. D. Levin, and J. F. Liebman, J. Chem. Phys. Ref. Data 17, Suppl. 1 (1988)

6 S. T. Manson, Phys. Rev. **182**, 97 (1969) and C. Moore, *Atomic Energy Levels*, Vol. 1, NBS Circular 467, (National Bureau of Standards, Washington, DC, 1949).

N90-26761

INTRACAVITY DYE-LASER ABSORPTION SPECTROSCOPY (IDLAS) FOR APPLICATION TO PLANETARY MOLECULES

TODD M. LANG* AND JOHN E. ALLEN, JR.**

*NASA Graduate Student Researcher, University of Maryland, Dept. of Physics, College Park, MD 20740

**NASA Goddard Space Flight Center, Astrochemistry Branch, Code 691, Greenbelt, MD. 20771

ABSTRACT

Time-resolved, quasi-cw, intracavity dye-laser absorption spectroscopy is applied to the investigation of absolute absorption coefficients for vibrational-rotational overtone bands of water at visible wavelengths. Emphasis is placed on critical factors affecting detection sensitivity and data analysis. Typical generation-time dependent absorption spectra are given.

Experimental Apparatus

The basic experimental apparatus is shown in Figure 1. Quasi-cw pumping of a Rhodamine 6G dye-laser is achieved by passing a 514.5 nm beam from an argon ion laser through a 25 ns rise/fall time electro-optic modulator. An output coupler taken from a synchronously pumped dye-laser is used to extend the cavity to a length of 1.8 meters to accomodate an absorption cell and other intracavity elements. A 5 micron intracavity pellicle functions as a tuning element over the broadband Rhodamine 6G dye gain curve. The intracavity aperture provides significant loss to higher order spatial modes while allowing the TEM_{00} mode. Prior to analysis, the dye-laser output is fed through a neutral density filter to reduce the signal to a level compatible with the photomultiplier tube. The beam then passes through a pseudodepolarizer to eliminate any polarization-dependent grating response The beam then enters a microprocessor controlled scanning monochromator with a

FIGURE 1

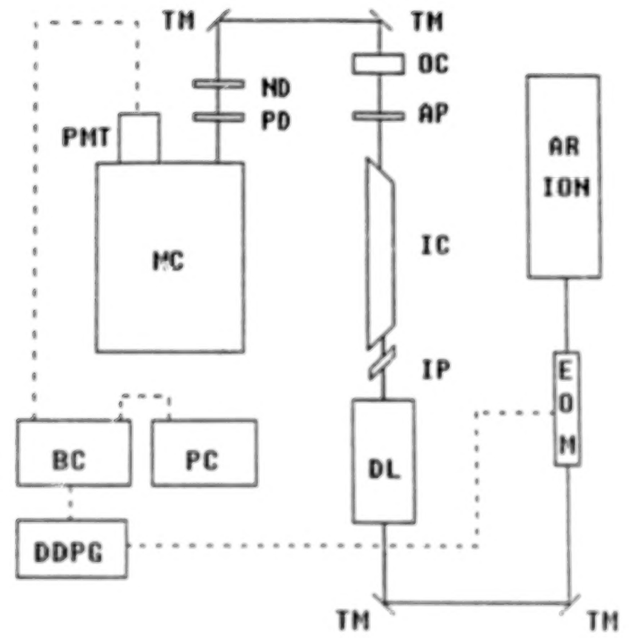

AR ION	Argon Ion Laser
EOM	Electro-optic Modulator
TM	Tuning Mirror
DL	Dye Laser
IP	Intracavity Pellicle
IC	Intracavity Cell
AP	Aperture
OC	Output Coupler
ND	Neutral Density Filter
PD	Pseudo-depolarizer
MC	Monochromator
PMT	Photomultiplier Tube
BC	Boxcar Averager
PC	Microprocessor/Terminal
DDPG	Digital Delay Pulse Generator

Experimental Setup

resolution of 0.006 nm in first order at 579.1 nm. The dispersed energy is detected by a photomultiplier tube close coupled to the monochromator. The signal from the photomultiplier is sent to a boxcar averager which is connected to the laboratory data acquisition unit that controls the monochromator. A spectral profile of the dye-laser output intensity and the attendant absorption dips appears on the video display and can be manipulated and/or plotted on a digital plotter. The boxcar and the electro-optic modulator are both driven by the same digital delay generator which provides picosecond accuracy. The delay allows the time position of the boxcar gate to be adjusted prior to data acquisition. In this way, it is possible to study the spectral intensity distribution of the dye-laser as a function of the generation time.

Theory

Intracavity dye-laser absorption has been shown to follow a modified Beer-Lambert type relationship and has demonstrated enhancements as great as a factor of 100,000 over conventional (extra-cavity) techniques. This is due to three main effects: the multipass effect, mode competition, and the threshold effect. Since the output coupler is highly reflective, photons make many passes through the cavity before being transmitted; this increases the likelihood of absorption by an intracavity sample. Mode competition is fostered by the homogeneous broadening of the dye gain; an added frequency selective loss due to an absorber allows all of the unaffected modes to steal energy away from the affected modes. And finally, when the dye-laser is operated near threshold, any slight increase in loss can destroy the lasing ability of the affected modes.

Results and Future Work

Typical absorption spectra of weak vibrational-rotational overtones of laboratory-air water vapor are shown in Figure 2. Quantitative determination of absolute absorption coefficients for specific lines will be determined in the near future.

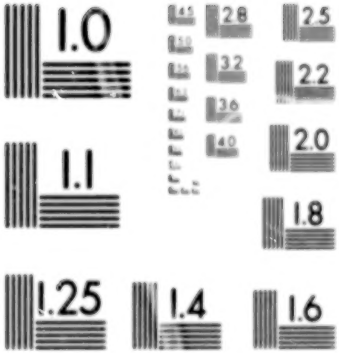

MICROCOPY RESOLUTION TEST CHART
NATIONAL BUREAU OF STANDARDS
STANDARD REFERENCE MATERIAL 1010a
(ANSI and ISO TEST CHART No. 2)

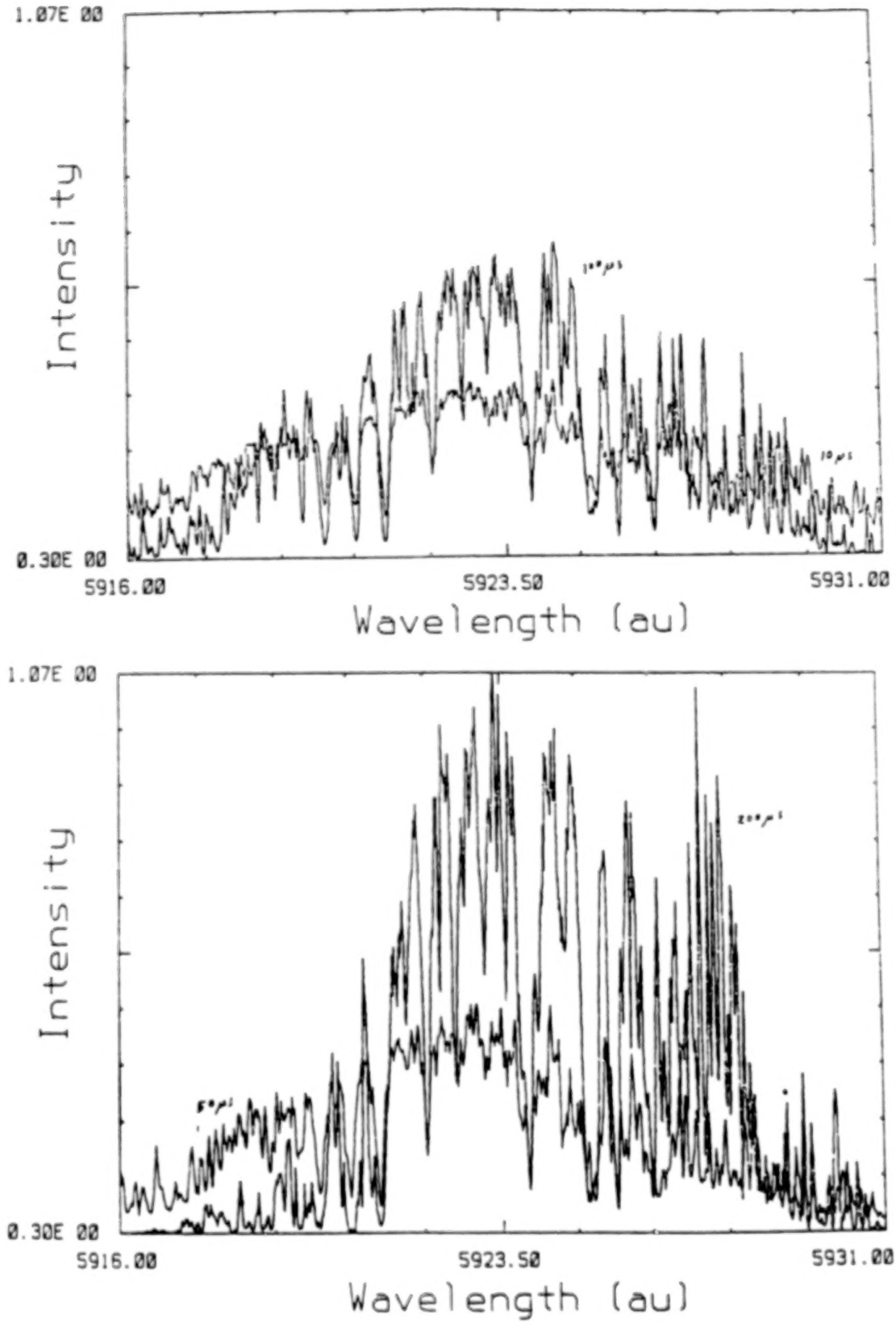

FIGURE 2 Typical Absorption Spectra

C-3

The design and construction of a low temperature intracavity cell is currently underway and will be used in the study of certain weak, visible rotational-vibrational transition coefficients of methane at temperatures simulating those of the outer planets. Specifically, the band at 619 nm will be studied. Laboratory measurements of this nature are of critical importance to those modelling planetary atmospheres.

Numerical simulations to determine critical factors affecting the sensitivity and data analysis of the technique of intracavity absorption spectroscopy are also underway.

N90-26762

METHANE OVERTONE ABSORPTION BY INTRACAVITY LASER SPECTROSCOPY

JAMES J. O'BRIEN
Department of Chemistry, University of Missouri-St. Louis, St. Louis, MO 63121-4499

ABSTRACT

Interpretation of planetary methane (CH_4) visible-near IR spectra, used to develop models of planetary atmospheres, has been hampered by a lack of suitable laboratory spectroscopic data. The particular CH_4 spectral bands are due to intrinsically weak, high overtone-combination transitions too complex for classical spectroscopic analysis. The traditional multipass cell approach to measuring spectra of weakly absorbing species is insufficiently sensitive to yield reliable results for some of the weakest CH_4 absorption features and is difficult to apply at the temperatures of the planetary environments.[1] A time modulated form of intracavity laser spectroscopy (ILS), has been shown to provide effective absorption pathlengths of 100 - 200 km with sample cells less than 1 m long. The optical physics governing this technique and the experimental parameters important for obtaining reliable, quantitative results are now well understood.[2] Quantitative data for CH_4 absorption obtained by ILS have been reported recently.[3] Illustrative ILS data for CH_4 absorption in the 619.7 nm and 681.9 nm bands are presented. New ILS facilities at UM-St. Louis will be used to measure CH_4 absorption in the 700 - 1000 nm region under conditions appropriate to the planetary atmospheres.

INTRODUCTION

CH_4 absorption features in the visible-near IR spectra of the outer planets and their major planets provide some of the most important diagnostic data for the atmospheres of those bodies. With the possible exception of the 614-624 nm region, however, laboratory data appropriate for properly interpreting the planetary observational data are unavailable.[4] Data from measurements made with long, multipass White cells are usually used. These have provided only room temperature absorption coefficients at pressures largely dictated by detection sensitivities since it is experimentally difficult to employ this approach under conditions applicable to the outer planets.[1] Smith and coworkers[5] have used photoacoustic absorption spectroscopy (PAS) to obtain temperature dependent (77-300 K) pressure broadening coefficients for prominent vibration-rotation lines in the CH_4 619 nm and 682.5 nm absorption bands and relative absorption coefficients for

the 604-627 nm region. Absolute line intensity measurements can be obtained by PAS only indirectly, however, and with the assumption that nonradiative quantum yields are constant over a given wavelength region.[6] Computation of the temperature dependence of the CH_4 visible-near-IR absorption spectrum has not been possible to date and does not seem likely in the foreseeable future.[7] Consequently, in models of the albedo spectra of the planetary bodies, it has been necessary to adopt mostly room-temperature laboratory data for the CH_4 absorption coefficients. This has impaired the precision to which the structure and dynamics of the planetary atmospheres can be constrained.

A time-modulated form of intracavity laser spectroscopy (ILS) has been adopted recently to measure CH_4 absorption coefficients at the range of cryogenic temperatures of the planetary environments. When properly implemented, ILS has been shown to provide true, quantitatively accurate absorption line strengths and profiles. For example, ILS data for weak, visible H_2O and O_2 absorption bands[8] are in excellent agreement with data obtained by other methods such as with the FT spectrometer associated with the McMath Solar Telescope at Kitt Peak, Arizona.

EXPERIMENTAL

Sensitivity enhancement factors > 10^6 corresponding to absorption pathlengths of 100's km have been achieved with ILS lasers.[2] In ILS, enhanced sensitivity for measuring absorption spectra is obtained by placing the absorbing species inside the cavity of a longitudinally multimode laser. The ILS laser is operated just above threshold in a time resolved, quasi-CW fashion. Absorptions by intracavity species constitute losses within the laser resonator and alter the competition that occurs as the modes of the laser resonator cavity compete for gain. The absorption spectrum of the intracavity absorber becomes superimposed on the output of the ILS laser and can be measured by dispersing the output of the laser and observing its spectral profile at a well-defined time, the generation time t_g (~10^{-4} seconds), after the onset of ILS laser operation. The enhanced detection sensitivity obtained by ILS has been accounted for by the effect of intracavity mode competition.[8-10] It has been shown that when the ILS laser is operating close to threshold[2,11] and within certain boundary conditions of absorption strength and t_g values, the absorbance data obtained by ILS obey a Beer-Lambert relationship.[8,9,12] The averaged, time-resolved spectrum observed by ILS is given by

$$\ln[I_0(\nu)/I(\nu)] = k(\nu)\ \phi(\nu)\ N(l/L)\ c\ t_g \qquad (1)$$

where $I_0(\nu)$ is the intensity of the laser at spectral frequency ν in the absence of intracavity absorption, $I(\nu)$ is the intensity of the laser at ν when there is intracavity absorption at ν, $k(\nu)$ is the intensity of the absorption line, $\phi(\nu)$ is the normalized absorption line profile, N is the number density of the intracavity absorber, l/L is the fraction of the laser resonator cavity occupied by the absorber, c is the velocity of light, and $(l/L)ct_s$ is the effective absorption pathlength. The sensitivity and dynamic range of ILS measurements can be controlled, therefore, by adjustment of t_s. In practice, it is found for ILS systems based on dye lasers that equation (1) applies for t_s values up to 300 - 500 μs.[2,10-13] Mechanical instabilities in the resonator cavity impose an upper limit on the value of t_s that can be used.[10] There also exist limits to absorptivity beyond which equation (1) is not a good representation of the absorption. Detailed descriptions of the instrumentation have been provided elsewhere.[14]

RESULTS AND FUTURE WORK

Illustrative temperature dependent ILS data for the weakest CH_4 band distinguishable in the long pathlength absorption spectra obtained by Giver,[1] are presented in Fig. 1 where they are compared with pressure dependent ILS data for the CH_4 619 nm band recorded at room temperature. The data are presented in the form of spectral profiles of the ILS laser's broadband output, which consists of a Gaussian spectral distribution on which is superimposed the spectral features due to an intracavity absorber. Control and precise specification of sample conditions were not possible in some of the measurements because the gas cell was improvised and sample pressures varied dramatically when temperatures were near the CH_4 phase transition temperatures. The series of profiles shown in Fig. 1 reveal pronounced variations in the intensity distribution within the 681.89 nm feature with changes in temperature and pressure. These data are in complete accord with corresponding PAS results recently submitted for publication.[5b] In contrast to this, the most prominent line in the 619 nm CH_4 band (i.e., 619.68 nm) shows nothing like this degree of variation as pressure and temperature conditions are altered. Line strength and self-broadening coefficients obtained by ILS for the 619.68 nm line of CH_4 at room temperature have been reported recently.[3] Since the instrumental resolution employed in these studies (0.18 cm^{-1}) is significantly broader than the absorption line-width (Doppler half-width = 0.025 cm^{-1}), line intensity and line-width information were obtained using the curve of growth method.[15] An illustrative curve of growth, obtained for the 619.68 nm line of CH_4, is presented in Fig. 4 of Ref. 3. The validity and accuracy of the approach were first verified by establishing that line strength

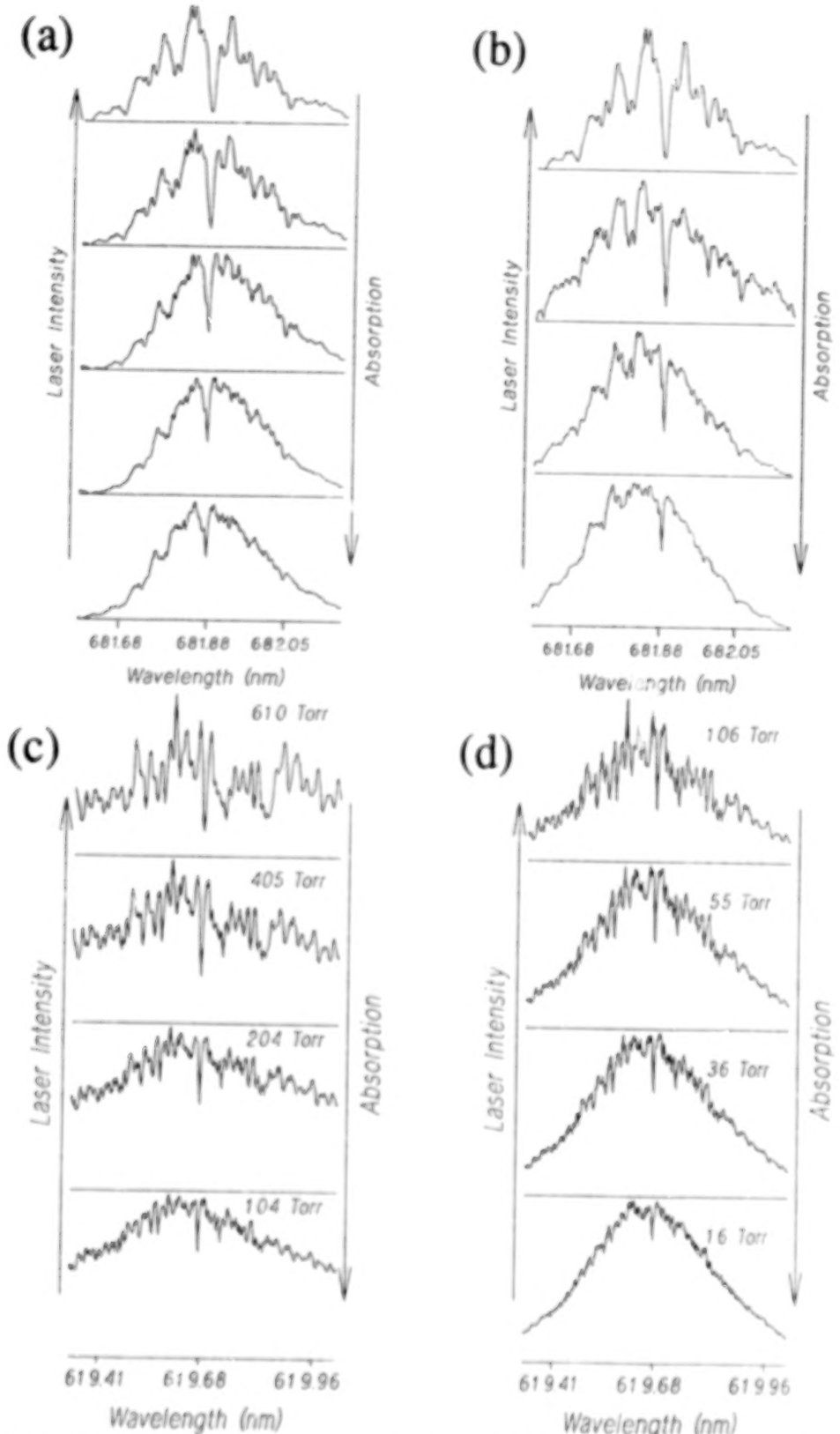

Figure 1. ILS spectral profiles for CH_4 absorption in the 681.86 nm (top panels) and 619.68 nm (bottom panels) bands under various conditions: (a) ~180 K, CH_4 pressures from top to bottom profile: 364, 184, 95, 45, 22 Torr, t_s=170 μs, effective absorption pathlength (L_{eff})=36 km; (b) L_{eff}=36 km, conditions from top to bottom profile: 364 Torr & 175K, 70 Torr & 110-160 K, 20 Torr & ~110 K, 10 Torr & <110 K; (c) 295 K, t_s=10 μs; (d) 295 K, t_s=100 μs.

and line shape parameters for well studied lines of the O_2 γ band replicated results obtained by other workers using ILS and other methods. Stoeckel and coworkers,[8] using much higher spectral resolution (0.18 cm^{-1}), have determined absorption line strength and width parameters by fitting ILS data directly to Voigt profiles.

Plans are that new, recently installed ILS equipment at UM-St. Louis be used in obtaining quantitative absorption data for methane absorption bands in the 700-1000 nm region for the range of of conditions applicable to the atmospheres of outer planetary bodies. Special attention will be given to determining the absorption parameters for the relatively weaker bands and for the inter-band regions of pseudo-continuum absorption. Models of planetary atmospheres based on conventional laboratory measurement show the most severe discrepancies in these regions. It is hoped that the current dye-laser based ILS system can be enhanced by the addition of a Ti:sapphire laser which in addition to providing superior performance and convenience of operation over dye lasers in the near-IR, have intrinsic advantages over dye lasers when utilized in ILS applications.

ACKNOWLEDGEMENT: The illustrative ILS spectral data reported here were obtained at the University of Arizona while the author was a post-doctoral research associate of Prof. G.H. Atkinson. The first of the data was recorded in August of 1986.

1. L.P. Giver, *J. Quant. Spectrosc. Radiat. Transfer* **19**, 311 (1978).
2. P.E. Toschek and V.M. Baev, *Lasers, Spectroscopy and New Ideas*, edited by W.M. Yen and M.D. Levenson (Springer Verlag, Berlin, 1987), pp 89-111.
3. P.V. Cvijin, J.J. O'Brien, G.H. Atkinson, W.K. Wells, J.I. Lunine and D.M. Hunten, Chem. Phys. Letters **159**, 331 (1989).
4. For example, (a) R.A. West, P.N. Kupferman and H. Hart, *Icarus* **61**, 311 (1985); (b) K.H. Baines and J.T. Bergstralh, *Icarus* **65**, 406 (1986); (c) K.H. Baines and W.H. Smith, *Icarus* (in press).
5. (a) C.E. Keffer, C.P. Conner and W.H. Smith, *J. Quant. Spectrosc. Radiat. Transfer* **35**, 495 (1986); (b) W.H. Smith, C.P. Conner and K.H. Baines, *Icarus* (submitted).
6. A.C. Tam, *Rev. Modern Phys.* **58**, 381 (1986).
7. M.W. Crofton, C.G. Stevens, D. Klenerman, J.H. Gutow and R.N. Zare, *J. Chem. Phys.* **89**, 7100 (1988).
8. (a) F. Stoeckel, M.A. Melieres and M. Chenevier, *J. Chem. Phys.* **76**, 2191 (1982); (b) M.A. Melieres, M. Chenevier and F. Stoeckel, *J. Quant. Spectrosc. Radiat. Transfer* **33**, 337 (1985).
9. E.N. Antonov, A.A. Kachanov, V.R. Mironenio and T.V. Plakhotnik, *Opt. Commun.* **46**, 126 (1983).
10. F. Stoeckel and G.H. Atkinson, *Appl. Opt.* **24**, 3591 (1985).
11. Yu. M. Ajvasjan, V.M. Baev, V.V. Ivanov and S.A. Kovalenko, *Sov. J. Quantum Electron.* **17**, 168 (1987).
12. N. Goldstein, T.L. Brack and G.H. Atkinson, *Chem. Phys. Lett.* **116**, 223 (1985).
13. H. Atmanspacher, H. Scheingraber and M.V. Baev, *Phys. Rev. A* **35**, 142 (1987).
14. J.J. O'Brien and G.H. Atkinson, *J. Phys. Chem.* **92**, 5782 (1988).
15. P.A. Jansson and C.K. Korb, *J. Quant. Spectrosc. Radiat. Transfer* **8**, 1399 (1968).

CHEMICAL KINETICS

INVITED

AND

CONTRIBUTED

PAPERS

N90-26763

CHEMICAL KINETICS AND MODELING OF PLANETARY ATMOSPHERES

YUK L. YUNG
Division of Geological and Planetary Sciences, California Institute of Technology, Pasadena, California 91125

ABSTRACT

A unified overview is presented for chemical kinetics and chemical modeling in planetary atmospheres. The recent major advances in our understanding of the chemistry of the terrestrial atmosphere make the study of planets more interesting and relevant. A deeper understanding suggests that the important chemical cycles have a universal character that connects the different planets and ultimately link us together to the origin and evolution of the solar system.

The completeness (or incompleteness) of the data base for chemical kinetics in planetary atmospheres will always be judged by comparison with that for the terrestrial atmosphere. In the latter case, the chemistry of H, O, N, and Cl species is well understood. S chemistry is poorly understood. In the atmospheres of Jovian planets and Titan, the C–H chemistry of simple species (containing 2 or less C atoms) is fairly well understood. The chemistry of higher hydrocarbons and the C–N, P–N chemistry is much less understood. In the atmosphere of Venus, the dominant chemistry is that of chlorine and sulfur, and very little is known about Cl–S coupled chemistry.

A new frontier for chemical kinetics both in the Earth and planetary atmospheres is the study of heterogeneous reactions. The formation of the ozone hole on Earth, the ubiquitous photochemical haze on Venus and in the Jovian planets and Titan all testify to the importance of heterogeneous reactions. It remains a challenge to connect the gas phase chemistry to the production of aerosols.

PRECEDING PAGE BLANK NOT FILMED

INTRODUCTION

In this review I will give a highly personal overview of chemical modeling in planetary atmospheres. I will show why it is interesting, important, and exciting. I will also suggest how laboratory kinetics studies can make this enterprise more interesting, important, and exciting. No attempt is made to survey the field. The interested reader may pursue a particular subject more deeply by reading the references.

In the beginning, Nature in her infinite kindness gave us matter. This is designated by the box "origin" in Figure 1. The distribution of various elements is not arbitrary, but is determined by a cosmic yardstick called the cosmic abundance, as shown in Table 1. This table is the result of synthesizing recent observations of the sun and C1 chondrites, but the results are believed to be representative of the cosmos at large.

Nature manifested her kindness again in giving us chemical kinetics, the time rate of chemical reactions. Once determined in the laboratory (or computed accurately enough), a kinetic rate coefficient sets the absolute yardstick governing the rate of transformation of one species into another. Why is this so important? I will illustrate my view by a quote from Robert Emden:

> As a student, I read with advantage a small book by F. Wald entitled 'The Mistress of the World and her Shadow'. These meant energy and entropy. In the course of advancing knowledge the two seem to me to have exchanged places. In the huge manufactory of natural processes, the principle of entropy occupies the position of manager, for it dictates the manner and methods of the whole business, whilst the principle of energy merely does the bookkeeping, balancing credits and debits.

Now read the sentences again after substituting the words "energy" and "entropy" by "chemical species" and "chemical kinetics", respectively.

As an illustration of the above ideas, consider the relative abundance of C and O in Table 1. As given in this table the ratio C/O is 0.42 making C slightly less abundant than O in the solar nebula. This implies that CO would be the dominant form of carbon in the solar nebula. Its subsequent reduction to CH_4 would depend on the kinetic rate of the reduction reactions, the rate of mixing in the nebula, and the lifetime of the nebula. Now there is sufficient uncertainty in the C/O ratio that the possibility C/O > 1 cannot be ruled out. In this case CO might not be the dominant form of carbon. Additional reservoirs of carbon (such as graphite) could exist. In this case the reduction of carbon to CH_4 could happen more readily. We can start to appreciate the importance of just a little difference in the relative abundance of chemical species at the time of the origin of the solar system, and the rate of interconversion of these species.

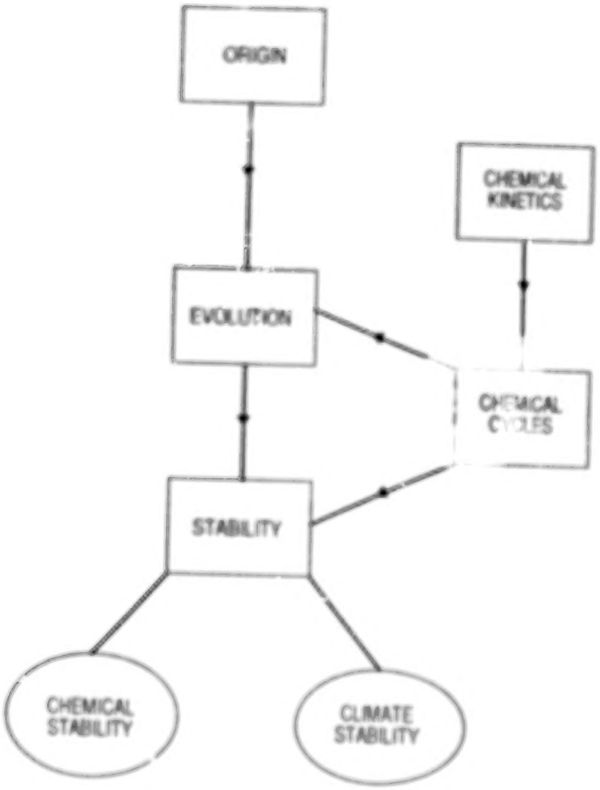

Fig. 1

Schematic diagram showing the relation of chemical kinetics and chemical modeling to origin, evolution, and stability of planetary atmospheres.

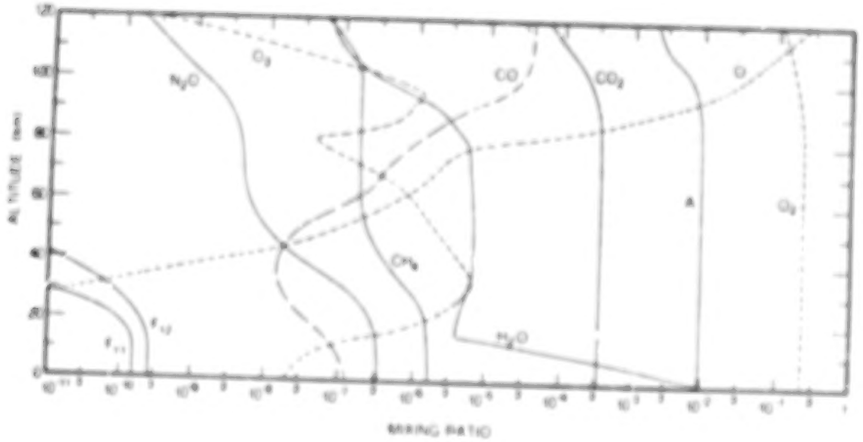

Fig. 2

Vertical profiles of mixing ratios of selected species in the terrestrial atmosphere at mid-latitude at high sunlit

TABLE 1

Solar-System Abundances of the First 35 Elements, Based on Meteorites (Atoms/10^6 Si)

Element	Abundance
1 H	2.79×10^{10}
2 He	2.72×10^{9}
3 Li	57.1
4 Be	0.73
5 B	21.2
6 C	1.01×10^{7}
7 N	3.13×10^{6}
8 O	2.38×10^{7}
9 F	843
10 Ne	3.44×10^{6}
11 Na	5.74×10^{4}
12 Mg	1.074×10^{6}
13 Al	8.49×10^{4}
14 Si	1.00×10^{6}
15 P	1.04×10^{4}
16 S	5.15×10^{5}
17 Cl	5240
18 Ar	1.01×10^{5}
19 K	3770
20 Ca	6.1×10^{4}
21 Sc	34.2
22 Ti	2400
23 V	293
24 Cr	1.35×10^{4}
25 Mn	9550
26 Fe	9.00×10^{5}
27 Co	2250
28 Ni	4.93×10^{4}
29 Cu	522
30 Zn	1260
31 Ga	37.8
32 Ge	119
33 As	6.56
34 Se	62.1
35 Br	11.8

Figure 1 gives the intellectual framework in which our field of study is imbedded. The unifying theme that ties the planets in the solar system is "origin" — we all share a common origin, about 5 billion years ago. The subsequent divergence in the solar system is attributed to evolution. Now the time rate of change becomes crucial and this is where the chemical cycles and their kinetic rates play a pivotal role. The fact that a certain reaction proceeds in a microsecond rather than in a billion years has the most profound consequences for the speciation observed in planetary atmospheres. However, the purpose of science is not just to reconstruct the past or to explain the present. It has a more aggressive motive. That is, to predict the future. Thus, we are deeply interested in studying the response of atmospheres to perturbations, i.e., the stability (chemical and climatic) of atmospheres. The exercise is more than academic, because we now live on a planet whose composition we seriously perturbing in an irreversible fashion. The answer to the questions we ask will have immediate impact on our welfare and style of living.

In the following sections, I will highlight the current chemical modeling efforts in planetary atmospheres from the perspective described in Figure 1, with emphasis on problems that present new challenges and opportunities to chemical kinetics.

EARTH

Earth is a planet and comparative studies between the terrestrial atmosphere and planetary atmospheres are interesting for at least two reasons. First, although the chemical species and their interactions in planetary atmospheres exhibit bewildering richness and variety, we note with satisfaction that underneath this apparent diversity is a pattern of simplicity, order, and unity. The chemical cycles that are important in one planetary atmosphere may also be important in other planetary atmospheres (as will be seen in subsequent sections). Second, current modeling of the terrestrial atmosphere is strongly motivated by the need to answer two very important questions: How stable is the ozone layer to anthropogenic perturbations (chemical stability, see Fig. 1)? How stable is the global climate in response to a doubling of CO_2 concentration in the atmosphere (climatic stability, see Fig. 1)? These questions have analogs in planetary atmospheres, where the physical and chemical parameters are extended over a much wider range.

The principal constituents of the Earths atmosphere are listed in Table 2. The vertical profiles of these species are presented in Figure 2. A primary focus of photochemical modeling in the terrestrial atmosphere is stratospheric O_3, formed by the photolysis of O_2,

$$O_2 + h\nu \rightarrow O + O \qquad (R1)$$

TABLE 2

The composition of dry air

Molecule	Fraction by volume in the troposphere	Comments
N_2	7.8084×10^{-1}	Photochemical dissociation high in the ionosphere; mixed at lower levels
O_2	2.0946×10^{-1}	Photochemical dissociation above 95 km; mixed at lower levels
A	9.34×10^{-3}	Mixed up to 110 km; diffusive separation above
CO_2	3.45×10^{-4}	Slightly variable; mixed up to 100 km, dissociated above
CH_4	1.6×10^{-6}	Mixed in troposphere; dissociated in mesosphere
N_2O	3.5×10^{-7}	Slightly variable at surface; dissociated in stratosphere and mesosphere
CO	7×10^{-8}	Variable photochemical and combustion product
O_3	$\sim 10^{-8}$	Highly variable; photochemical origin
$CFCl_3$ and CF_2Cl_2	$1\text{–}2 \times 10^{-10}$	Industrial origin; mixed in troposphere, dissociated in stratosphere

$$O + O_2 + M \rightarrow O_3 + M \qquad \text{(R2)}$$

In a pure oxygen atmosphere, O_3 is removed by reacting with O,

$$O_3 + O \rightarrow 2O_2 \ , \qquad \text{(R3)}$$

with kinetic rate coefficient $k_3 = 8.0 \times 10^{-12}\ e^{-2060/T}\ cm^3\ s^{-1}$. At stratospheric temperatures (~250 K) $k_3 = 2.1 \times 10^{-15}\ cm^3\ s^{-1}$. This is a very slow reaction indeed. It should be noted that if k_3 were as high as $1 \times 10^{-11}\ cm^3\ s^{-1}$, we would have an ozone layer about 1% of the current layer, and all the anthropogenic perturbations would be utterly trivial. However, because the pure oxygen reactions are so inefficient for destroying O_3, this gives rise to a number of catalytic mechanisms for removing O_3,

$$O_3 + X \rightarrow XO + O_2 \qquad \text{(R4)}$$

$$XO + O \rightarrow O_2 + X \qquad \text{(R5)}$$

$$\text{net} \quad O_3 + O \rightarrow 2O_2 \ , \qquad \text{(I)}$$

where X = OH, NO, ClO, or BrO. The reactive species "X" are supplied by source molecules in the troposphere such as H_2O, CH_4, N_2O, $CFCl_3$, CF_2Cl_2, CH_3Cl, CH_3Br. Since the tropospheric concentrations of CH_4, N_2O, $CFCl_3$, CF_2Cl_2, and CH_3Br are increasing due to industrial and agricultural activities, this would result in a depletion of the O_3 layer. The consequences can be quantitatively predicted using measured rate coefficients for the appropriate reactions. This predictive capability of current models lead M.B. McElroy to announce "Give us the perfect rate constants, and we will compute the perfect answer." It is a triumph of chemical kinetics and photochemical models that there is satisfactory agreement between the observations and models.

I will not say more about CO_2 and climatic change mainly because CO_2 is regulated by ocean chemistry and biochemistry. This is still chemical kinetics in a generalized sense, but it is remote from this community. I will, however, say something about photochemical aerosols and their impact on climate. Volcanoes inject large quantities of SO_2 into the stratosphere, where it is oxidized by

$$SO_2 + OH \rightarrow SO_3 + H \qquad \text{(R6)}$$

$$H + O_2 + M \rightarrow HO_2 + M \qquad \text{(R7)}$$

$$HO_2 + O_3 \rightarrow 2O_2 + OH \qquad \text{(R8)}$$

$$SO_3 + H_2O + M \rightarrow H_2SO_4 + M \qquad \text{(R9)}$$

$$SO_2 + O_3 + H_2O \rightarrow H_2SO_4 + O_2 \qquad (II)$$

(Note that HO_x is used as catalyst and not consumed. The amount of H_2O consumed is negligible.) The presence of this photochemical aerosol can affect the UV radiation field in the stratosphere and troposphere, and the thermal radiation budget of the atmosphere. The current kinetics suggests that the oxidation of SO_2 to sulfate is fairly rapid, and aerosol formation is completed in less than three months. There are indications that these aerosols may provide sites for heterogeneous reactions in the stratosphere, such as denitrification, and decomposition of $ClONO_2$ into more reactive species such as

$$ClONO_2 + H_2O \xrightarrow[\text{aerosol}]{} HOCl + HNO_3 \text{ (sequestered)} \qquad (R10)$$

analogous to what is believed to be taking place in the Antarctic O_3 hole in springtime. I would like to point out that the study of heterogeneous reactions is the frontier of chemical kinetics, and these reactions now appear to be important in planetary atmospheres and the solar nebula.

MARS

The composition of the atmosphere of Mars is given in Table 3. CO_2 is the principal constituent, followed by N_2, Ar, H_2O, O_2, CO, and O_3. In the upper atmosphere (~100 km), H, O, as well as ionic species have been detected. The atmosphere is thin, with surface pressure equal to 5.5 mb (4.2 Torr). The mean surface temperature is 220 K, close to the equilibrium temperature of 216 K. (This means that there is no "greenhouse effect" to make the surface warmer.)

The central theme of the photochemistry of the Martian atmosphere is CO_2 stability. The problem can be stated very simply as follows. CO_2 photolyzes readily with absorption of UV radiation $\lambda < 2300$ Å,

$$CO_2 + h\nu \rightarrow CO + O(^1D) \qquad (R11a)$$

$$\rightarrow CO + O \qquad (R11b)$$

$$O(^1D) + M \rightarrow O + M \qquad (R12)$$

Regardless of the initial state of O in R11, the ultimate product is always CO and O in the ground state (^3P). The recombination of CO and O is spin forbidden

$$CO + O + M \rightarrow CO_2 + M \qquad (R13)$$

TABLE 3

Principal Constituents in the Martian Atmosphere

Species	Volume mixing ratio
CO_2	0.9532
N_2	2.7×10^{-2}
A	1.6×10^{-2}
H_2O	3.3×10^{-3}
O_2	1.3×10^{-3}
CO	7×10^{-4}
O_3	5×10^{-8}

Table 4

Comparison of some important features of the stratospheres of Earth and Venus.

Feature	Earth	Venus
Altitude (km)	20–40	60–80
Pressure (mbar)	100–5	300–5
Temperature (K)	200–250	270–200
Mixing ratios of major constituents		
N_2	78.1 percent	3–4 percent
O_2	21.0 percent	$< 1 \times 10^{-6}$
Ar	0.93 percent	0.01 percent
CO_2	0.03 percent	96 percent
Mixing ratios of minor constituents		
Total chlorine	2.3×10^{-9}	4×10^{-7}
Total sulfur	$\sim 1 \times 10^{-9}$	$\sim 2 \times 10^{-6}$
Total NO_x	2×10^{-8}	$\leq 3 \times 10^{-8}$
Water	$\sim 5 \times 10^{-6}$	$1\text{–}30 \times 10^{-6}$
Methane	$\sim 1 \times 10^{-6}$	~ 0
Hydrogen	0.5×10^{-6}	Unknown*
N_2O	0.25×10^{-6}	~ 0

with rate coefficient $k_{13} = 6.5 \times 10^{-33}\ e^{-2184/T}\ cm^6\ s^{-1}$. At 220 K, $k_{13} = 3.2 \times 10^{-37}\ cm^6\ s^{-1}$, a very slow rate constant indeed. The challenge then is to explain the low abundances of CO and O_2 in Table 3, since they could all be generated in less than 10^3 years. The resolution of the problem lies in the trace amount of H_2O in the atmosphere as listed in Table 3. Photolysis of H_2O produces OH and H radicals (HO_x), which catalyze the recombination of CO and O,

$$CO + OH \rightarrow CO_2 + H \qquad \text{(R14)}$$

$$H + O_2 + M \rightarrow HO_2 + M \qquad \text{(R15)}$$

$$O + HO_2 \rightarrow OH + O_2 \qquad \text{(R16)}$$

$$\text{net} \quad CO + O \rightarrow CO_2 \qquad \text{(III)}$$

The results of a photochemical modeling incorporating the chemical cycle (III) are shown in Figure 3. Three things are noteworthy: (a) The stability problem was solely "created" by the fact that k_{13} is so small. If k_{13} were as large as $1 \times 10^{-31}\ cm^6\ s^{-1}$, the direct recombination of CO and O could account for the low concentrations of CO and O_2 on Mars, and there is no need to invent cycle III. (b) This cycle, first identified for the Martian atmosphere, is important in the terrestrial mesosphere and thermosphere. The crucial reaction CO + OH is known to be important also in the terrestrial troposphere and the atmosphere of Titan. (c) The abundance of the reactive radical OH in the atmosphere is of the order of 10^5 molecules cm^{-3}, and yet it exerts a major control over the composition of this atmosphere via catalytic cycle (III). This is an illustration of the beauty, subtlety, and extraordinary power of photochemistry.

The field of Martian photochemistry reaches its apex through the early work of Hunten and the later classic studies of McElroy and Donahue, with kinetics data on HO_x chemistry being supplied by DeMore and Kaufman. Since HO_x chemistry is a very well defined subject nowadays, it is hard to envision any breakthrough, except perhaps for one loose end. The reaction

$$H + HO_2 \rightarrow 2OH \qquad \text{(R17a)}$$

$$\rightarrow H_2O + O \qquad \text{(R17b)}$$

$$\rightarrow H_2 + O_2 \qquad \text{(R17c)}$$

has been well studied. The rate constant $k_{17} = k_{17a} + k_{17b} + k_{17c} = 8.1 \times 10^{-11}$ is known to within 30% with no temperature dependence. However, the branch R17c is poorly known:

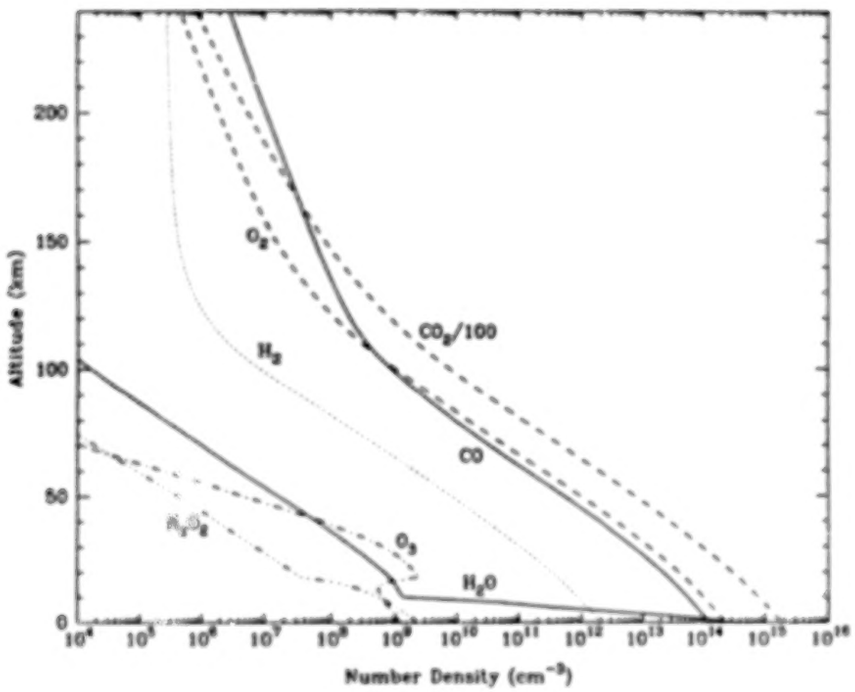

Fig 3
Vertical profiles of concentrations of selected major species in the Martian atmosphere

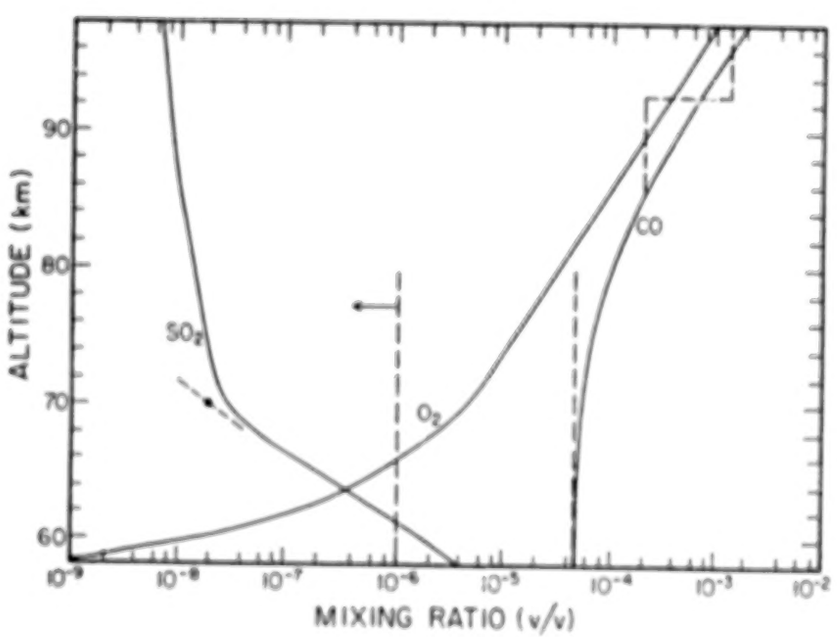

Fig 4
Same as Figure 1 for Venus

$k_{17c}/k_{17} = 0.08 \pm 0.04$. This branch is important for the evolution of the Martian atmosphere because it is the primary source of H_2, and H_2 is the major carrier of hydrogen from the surface to the exosphere to fuel the escape of hydrogen from Mars (H_2O does not reach the top of the atmosphere due to condensation at high altitudes). A better determination of this branch of R17 would constrain the escape rate of hydrogen from Mars. Incidentally, this branch also has an impact on the HO_x chemistry in the terrestrial mesosphere and the escape of hydrogen.

Recent revival in our interest for Martian photochemistry (after the field was perfected and closed by the brilliant pioneers) was motivated by progress in heterogeneous chemistry associated with the Antarctic ozone hole. It was recognized that ice particles (H_2O) could denitrify the Martian atmosphere, and that on average, the molecules in the Martian atmosphere collide with a dust grain (mainly silicate) every 10^3 sec. Therefore, heterogeneous chemistry may play a hitherto unsuspected role in the Martian atmosphere. Is it possible that

$$N_2O_5, NO_3 + \text{ice} \rightarrow HNO_3 \qquad \text{(R18)}$$

$$\text{or} \qquad CO + O \xrightarrow[\text{dust}]{} CO_2 \quad ? \qquad \text{(R19)}$$

Is it possible to sequester large amounts of NO_x on the surface of Mars via R18? This is a unique atmosphere in the sense that the "surface" extends into the atmosphere (up to 60 km) via the ubiquitous Martian dust. These questions can only be answered by a series of well designed laboratory experiments on the kinetics of the above reactions on ice and dust grains.

VENUS

Although the surface of Venus is 95 bars and at 750 K, it is of little interest to photochemistry due to the lack of UV photons. The part of the atmosphere of Venus that is most interesting to us is the stratosphere region, where the physical conditions are comparable to the terrestrial stratosphere. As shown in Table 4, the chemical composition also has striking similarity to the Earth's due to the presence of chlorine and sulfur on both planets.

Since the atmosphere is primarily composed of CO_2, the stability problem first discussed on Mars is more serious here. The mixing ratios of CO and O_2 are even lower than those on Mars. Catalysis by chlorine was finally recognized as the key to the resolution of the stability problem. The atmosphere contains 4×10^{-7} HCl, which readily photolyzes in the UV,

$$HCl + h\nu \rightarrow H + Cl \qquad \text{(R20)}$$

releasing the reactive Cl radical. Subsequent reactions may be summarized by the cycle

$$Cl + CO + M \rightarrow ClCO + M \quad (R21)$$

$$ClCO + O_2 + M \rightarrow ClCO_3 + M \quad (R22)$$

$$ClCO_3 + O \rightarrow Cl + CO_2 + O_2 \quad (R23)$$

$$\text{net} \quad CO + O \rightarrow CO_2 \quad (IV)$$

The stratosphere of Venus also contains huge amounts (by terrestrial standards, see Table 4) of SO_2. Oxidation of SO_2 to sulfate is again readily catalyzed by Cl

$$Cl + SO_2 + M \rightarrow ClSO_2 + M \quad (R24)$$

$$ClSO_2 + O_2 + M \rightarrow ClSO_4 + M \quad (R25)$$

$$ClSO_4 + Cl \rightarrow ClO + ClSO_3^* \quad (R26)$$

$$ClSO_3^* \rightarrow Cl + SO_3 \quad (R27)$$

$$SO_3 + H_2O + M \rightarrow H_2SO_4 + M \quad (R9)$$

$$Cl + SO_2 + O_2 + H_2O \rightarrow H_2SO_4 + ClO \quad (V)$$

Note that the oxidation of SO_2 provides an effective sink for O_2 on Venus. The photochemical aerosols generated by (V) have profound consequences for the planet. First, they completely envelope the planet with a white scattering cloud, increasing the planetary albedo and filtering out most UV radiation. Second, they dry the upper atmosphere (since H_2SO_4 is hydroscopic).

Figure 4 shows the vertical profiles of the most important minor species in the stratosphere. The photochemical model is based on the chemistry summarized by Scheme IV. Needless to say, much of the kinetics associated with cycles IV and V remains to be studied in detail. In general, the photochemistry of sulfur species is poorly known, due in part to the difficulty of handling sulfur compounds in the laboratory. A major uncertainty exists, for example, on the quantum yield of predissociation for SO

$$SO + h\nu \rightarrow SO^* \rightarrow S + O \quad (R28)$$

This molecule has recently been detected on Venus. It is produced from SO_2 photolysis. The analogous reaction (R1) predissociates 100% in the Schumann-Runge bands. However, the lifetime of SO^* is nanoseconds, whereas that for O_2^* is picoseconds. Therefore, it appears that the quantum yield for photolysis may be considerably less than unity. A careful laboratory experiment monitoring the fluorescence of SO^* would be able to determine the quantum yield. Why is this reaction important? It can drive a cycle for breaking the O–O bond,

$$SO + h\nu \rightarrow S + O \qquad \text{(R28)}$$

$$S + O_2 \rightarrow SO + O \qquad \text{(R29)}$$

$$\text{net } O_2 \rightarrow 2O \qquad \text{(VI)}$$

In addition, R28 is a source of S atoms, and ultimately of polysulfur (S_x), which is a leading candidate for the unidentified UV absorber on Venus. (A similar mechanism using S_x has been suggested for shielding the primitive Earth from UV radiation — sort of a primordial UV shield without O_3.) I will leave it as a challenge to the laboratory chemical kineticist to settle this issue.

JOVIAN PLANETS

The chemistry of the giant planets, Jupiter, Saturn, Uranus, and Neptune, has a distinct character of their own. Tables 5a,b summarize the composition of the atmospheres of Jupiter and Saturn, respectively. Very little is known about the atmospheres of Uranus and Neptune and this knowledge is summarized in a comparative study with the other planets in Table 5c. The chemistry is completely dominated by the huge amount of H_2 present in these atmospheres. The abundance of other elements roughly follows that of cosmic abundance (see Table 1).

The questions of chemical stability and evolution, which are the compelling themes in the atmospheres of the inner planets, do not concern us here. The giant planets have undergone little or no evolution since formation, and whatever disequilibrium in speciation produced in the upper atmosphere is ultimately restored to thermodynamic equilibrium in the planetary interiors, where the pressures and temperatures exceed 1 kilobar and 10^3 K, respectively. Therefore, the observed chemical composition of these atmospheres represents a "tug-of-war" between photochemistry (driven by the sun) and thermodynamics (drive by interior heat left over from the time of formation of the planets). A schematic diagram showing the recycling of hydrocarbons between the upper atmosphere and the planetary interior is shown in Figure 5a for Saturn, but this figure applies to all the other giant planets.

TABLE 5a

Composition of Jupiter's Atmosphere

Constituent	Volume mixing ratio
H_2	0.89
He	0.11
CH_4	1.75×10^{-3}
C_2H_2	2×10^{-6}
C_2H_4	7×10^{-9}
C_2H_6	5×10^{-6}
CH_3C_2H	2.5×10^{-9}
C_4H_2	2×10^{-9}
CH_3D	3.5×10^{-7}
NH_3	1.8×10^{-4}
PH_3	6×10^{-7}
H_2O	$1–30 \times 10^{-6}$
GeH_4	7×10^{-10}
CO	$1–10 \times 10^{-9}$

TABLE 5b

Composition of Saturn's Atmosphere

Constituent	Volume mixing ratio
H_2	0.94
He	0.06
CH_4	1.75×10^{-3}
C_2H_2	1.1×10^{-7}
C_2H_6	4.8×10^{-6}
CH_3D	2.3×10^{-7}
PH_3	2×10^{-7}
CO	2×10^{-9}
H_2O	1×10^{-7}

Table 5c

OBSERVED ABUNDANCES OF SIMPLE HYDROCARBONS

	CH_4	C_2H_6	C_2H_2
Jupiter	1.75×10^{-3}	5×10^{-6}	2×10^{-6}
Saturn	1.76×10^{-3}	4.8×10^{-6}	1.1×10^{-7}
Titan	$1-3 \times 10^{-2}$	2×10^{-5}	2×10^{-6}
Uranus	$< 3 \times 10^{-4}$	$< 1 \times 10^{-6}$	8×10^{-9}
Neptune	$1-10 \times 10^{-3}$	2×10^{-6}	1×10^{-6}

Table 5d

GEOMETRIC ALBEDO AT 3075 Å

Jupiter	0.25
Saturn	0.3
Titan	0.054
Uranus	0.5
Neptune	0.5
Mars	0.15
Venus	0.3
Conservative Isotropic	0.69
Conservative Rayleigh Scattering	0.80

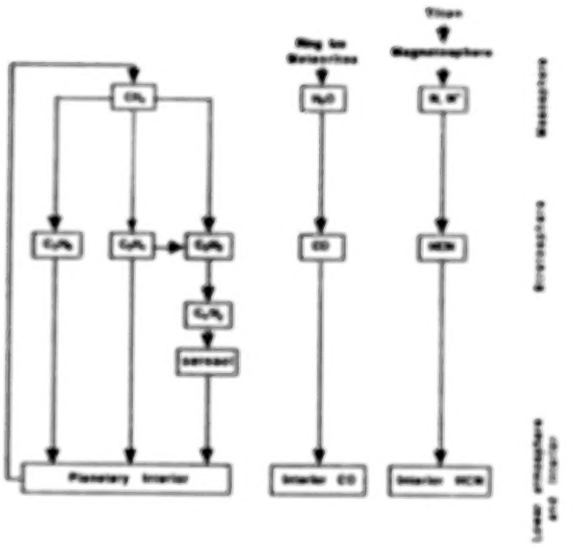

Fig 9a

Schematic diagram showing the major chemical cycles in the atmosphere of Saturn

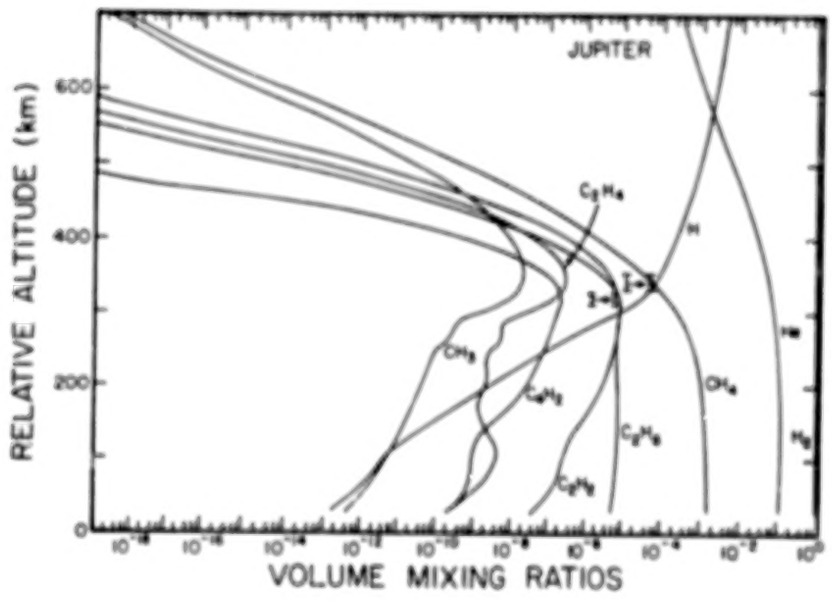

Fig 9b

Same as Figure 1 for Jupiter

The dominant theme of the chemistry of the outer solar system is organic synthesis. Since CH_4 is an abundant source molecule, its breakdown leads to a large number of simple organic compounds, such as C_2H_6, C_2H_4, and C_2H_2. Since the pioneering work of Strobel, the chemistry of CH_4 conversion to C_2 (containing two carbon atoms) compounds is fairly well understood. Figure 5b shows the results of a photochemical model for the simple hydrocarbons on Jupiter. But there remains the challenge to quantitatively account for the difference in C_2H_6 to C_2H_2 ratio in the outer solar system (see Table 5c). This ratio is predicted by current models is about unity, and should be compared with the observed values ~100 for Jupiter and Saturn.

The most important chemical input in the photochemical model is the rate coefficient for chemical reactions, k(T, P). In general, this quantity is a function of temperature (T) and pressure (P). To be useful for application to planetary atmospheres, we must know k(T, P) for the ambient atmospheric environments. Typical values for P varies from 1 to 10^{-9} bars, and T ranges from 300 K in the inner solar system to less than 100 K in the outer solar system. Since the bulk of chemical kinetics data is related to work on combustion (at higher temperature and pressure), it remains a challenge to extract useful information from the combustion literature and apply them to the planetary atmospheres. In addition to T and P dependence is the important evaluation of k(T, P) for the different product channels. We have reasons to believe that the hydrocarbon chemistry may still be incomplete or improperly extrapolated to low temperatures. As most reactions involve transfer of an H atom, extrapolation of a rate constant based on activation energies measured at high temperatures may be disastrous due to the possibility of H atom tunneling (because it is so small) at low temperatures.

But looking at Table 5d, we may perceive that Nature is hinting at a more imaginative solution to the C_2H_6/C_2H_2 ratio problem. We note that at 3075 Å, Jupiter and Saturn are quite dark whereas Uranus and Neptune are much brighter, and Titan is extremely dark (I also show Mars, Venus, and theoretical models for comparison). Something other than Rayleigh scattering is going on in these atmospheres. The UV absorption is believed to be caused by photochemical aerosols made from hydrocarbons (the Axel-Danielson dust). It is most likely that the hydrocarbon haze is made from C_2H_2 and not from C_2H_6 since we know that C_2H_2 but not C_2H_6 can polymerize in the laboratory experiments. Suppose there is a photopolymerization reaction that turn C_2H_2 into more complex hydrocarbons,

$$C_2H_2 + h\nu \rightarrow C_2H_2^* \qquad \text{(R30a)}$$

$$C_2H_2^* + C_2H_2 \rightarrow C_4H_4 \qquad \text{(R30b)}$$

$$C_2H_2^* + C_2H_4 \rightarrow C_6H_6 \qquad \text{(R30c)}$$

As the carbon number increases, the saturated vapor decreases, and the excess gas molecules would form aerosols. This would kill two birds with one stone. It provides a sink for C_2H_2, thus raising the value of the ratio C_2H_6/C_2H_2 in the model to agree with the observations, and at the same time create more UV opacity to explain the lower albedo of Jupiter and Saturn relative to Uranus and Neptune. The detailed chemical kinetics of C_2H_2 polymerization remains a challenge to the laboratory chemist. I would not be surprised if it turns out to be related to soot formation in combustion of hydrocarbons.

The presence of the ubiquitous Axel-Danielson dust in the outer solar system has a profound consequence on the climatology of these planets. A large amount of solar energy is absorbed by these aerosols, creating a thermal inversion. (A similar process takes place in the terrestrial stratosphere where UV radiation is absorbed by O_3.) The thermal inversion inhibits transport between the stratosphere and the troposphere. This means that the aerosols have an even longer lifetime in the stratosphere, absorbing more solar energy. Hence, the feedback is positive. One can imagine a clear and turbulent stratosphere with little aerosol content, and that would be allowed by the laws of chemistry and physics. Why Nature does not choose this particular solution for any planet in the outer solar system remains a mystery to me. I hope some brilliant kineticist or climatologist can take this challenge one day.

A planet like Saturn is surrounded by objects with large volatile content (such as H_2O in the rings and N_2 from Titan). The planet serves as the ultimate "garbage can" for the entire Saturnian system. The fate of these extraplanetary material in the upper atmosphere of Saturn is to be converted to the most stable molecules. As shown in Figure 5a, I believe that all oxygen and nitrogen species would wind up as CO and HCN, respectively. The chemistry is fairly well understood, thanks to the extensive research in combustion.

Now according to thermodynamics, the planetary interior is also a source of CO and HCN (produced as products of CH_4 and H_2O equilibrium, and NH_3 and CH_4 equilibrium, respectively). A sensitive issue arises as to the lifetimes of CO and HCN as they emerge from the region of thermodynamic equilibrium. It was conjectured that the lifetime of CO is determined by the following reactions,

$$4(H + CO + M \rightarrow HCO + M) \qquad \text{(R31)}$$

$$HCO + HCO \rightarrow H_2CO + CO \qquad \text{(R32)}$$

$$H + H_2CO + M \rightarrow CH_3O + M \qquad \text{(R33b)}$$

$$CH_3O + HCO \rightarrow CH_3OH + CO \qquad \text{(R34)}$$

$$CH_3OH + H \rightarrow CH_3 + H_2O \qquad \text{(R35)}$$

$$CH_3 + HCO \rightarrow CH_4 + CO \qquad \text{(R36)}$$

$$CO + 6H \rightarrow H_2O + CH_4 \qquad \text{(VII)}$$

The crucial part of Scheme VII is the reaction R33b forming the methoxy radical. Actually the dominant path of R33 is

$$H + H_2CO \rightarrow H_2 + HCO \qquad \text{(R33a)}$$

which does not lead to the conversion of the carbonyl bond to a single bond (as in CH_3O). However, if k_{33b}/k_{33a} were as high as 1%, it would be significant. Note that it is always exceedingly hard to convert CO to CH_4 (because C–O is one of the strongest bonds in chemical kinetics). If this scheme works on the giant planets, it may also be important in the solar nebula, where a similar problem exists for converting CO to CH_4. Again, the challenge is to the laboratory kineticist.

In the lower atmosphere of Jupiter and Saturn there is interesting photochemistry involving NH_3, PH_3, GeH_4, and AsH_3. Very little is known about the chemistry of these compounds. We do not know, for example, whether P_2H_4 (produced from PH_3 photolysis) and N_2H_4 (produced from NH_3 photolysis) are stable to UV irradiation in the form of ices. There may be "mixed" compounds involving C–P and P–N bonds that we currently know little about. I will only conclude that whoever leads a laboratory investigation in studying these species will be pioneering the field for planetary atmospheres.

TITAN

Titan occupies a unique position in the photochemistry of the solar system. It is a moon of Saturn with a massive atmosphere. The important physical parameters and compositional data are summarized in Table 6 (see also Figs. 6b-d). Note that the surface pressure is 1.5 bar. (This is a lot more N_2 than at the Earth's surface because T is so low.) In many ways Titan resembles a small planet in the inner solar system rather than a kin of the giant planets family. In terms of chemical composition, Titan's atmosphere is intermediate between the highly oxidized atmospheres in the inner solar system and the Jovian planets with massive amounts of H_2. Both reducing species H_2, CH_4, and oxidized species CO_2 are present. Why is Titan so interesting?

Simplicity underlying complexity. The large number of chemical species listed in Table 6 can all be derived from three parent molecules, N_2, H_2O, and CH_4 using known chemical kinetics. The chemical network connecting these species is presented in Figure 6a. Due to the

Table 6

Titan

Physical or Chemical Data

At the Surface (altitude $z = 0$):
- r_0 = distance to center = 2575 km
- g_0 = gravity = 135 cm s^{-2}
- P_0 = total pressure = 1.50 bar
- T_0 = temperature = 94 K
- n_0 = number density = 1.2×10^{20} cm^{-3}

Composition of the Troposphere (volume mixing ratio):
- $N_2 > 0.97$
- $CH_4 < 0.03$
- $H_2 = 0.002$

At the Tropopause ($z = 45$ km):
- $P = 130$ mbar
- $T = 71.4$ K
- $n = 1.1 \times 10^{19}$ cm^{-3}

Composition of the Stratosphere (volume mixing ratio):
- $CH_4 = 1\text{-}3 \times 10^{-2}$
- $H_2 = 2.0 \times 10^{-3}$
- $C_2H_6 = 2 \times 10^{-5}$
- $C_2H_2 = 2 \times 10^{-6}$
- $C_2H_4 = 4 \times 10^{-7}$
- $C_3H_8 = 2\text{-}4 \times 10^{-6}$
- $CH_3C_2H = 3 \times 10^{-8}$
- $C_4H_2 = 10^{-8}\text{-}10^{-7}$
- $HCN = 2 \times 10^{-7}$
- $HC_3N = 10^{-8}\text{-}10^{-7}$
- $C_2N_2 = 10^{-8}\text{-}10^{-7}$
- $CO = 6 \times 10^{-5}$

- $CO_2 = 1.5 \times 10^{-9}$
- $H_2O < 1 \times 10^{-9}$
- CH_3D detected, abundance not available

Composition of Mesosphere and Thermosphere:
- $N_2 = 2.7 \times 10^{8}$ cm^{-3} at $z = 1280$ km
- $CH_4 = 1.2 \times 10^{8}$ cm^{-3} at $z = 1140$ km
  (mixing ratio = 0.08)
- C_2H_2 mixing ratio 1%–2% at $z = 840$ km
- H atoms: disk-averaged Lyα airglow ~ 500 R^a

Haze Layers:
- optical haze $z = 300$ km
- UV haze $z = 400$ km

Table 7a

Observed isotopic ratio of deuterium to hydrogen, normalized with respect to the Jovian standard (1.6×10^{-5}).

Planetary body (species used)	D/H
Jupiter (CH_3D)	1
Saturn (CH_3D)	1
Uranus (CH_3D)	6
Titan (CH_3D)	30 10
Comet Halley (HDO)	4-30
Earth (HDO) Venus (HD, HDO)	10 1000
Mars (HDO)	60
Meteorite (organic)	5-100

Table 7b

Fractional abundances by volume of the major carbon species in planetary atmospheres.

Planet	CO_2	CO	CH_4
Earth	3.2×10^{-4}	1.7×10^{-7}	1.5×10^{-6}
Mars	0.95	7×10^{-4}	—
Venus	0.96	5×10^{-5}	—
Jupiter	—	2×10^{-9}	1.8×10^{-3}
Saturn	—	2×10^{-9}	4.5×10^{-3}
Titan	1.5×10^{-9}	6×10^{-5}	2×10^{-2}
Comet	4×10^{-2}	0.2	2×10^{-2}

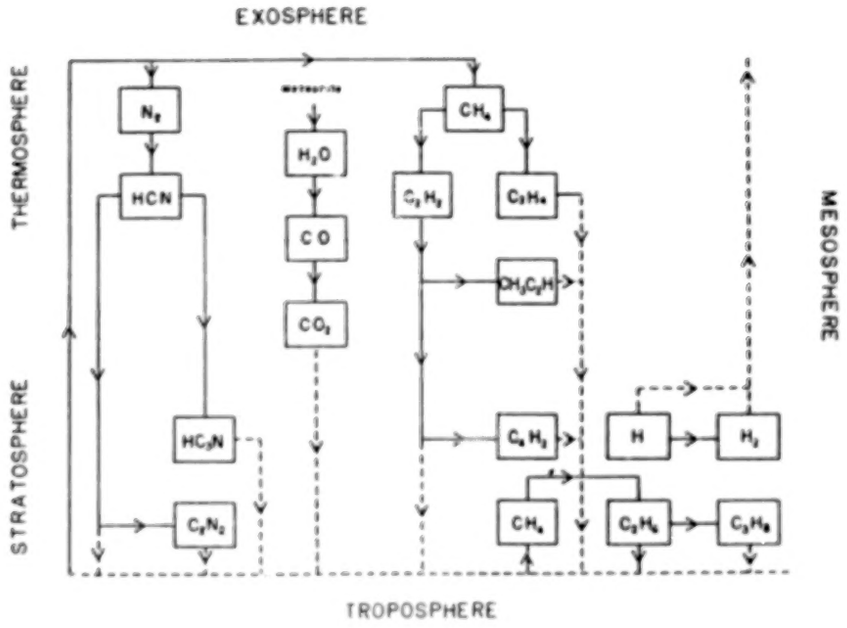

Fig 6a

Schematic diagram showing the relation between the parent molecules, N_2, CH_4, and H_2O and the photochemical products derived in a photochemical model

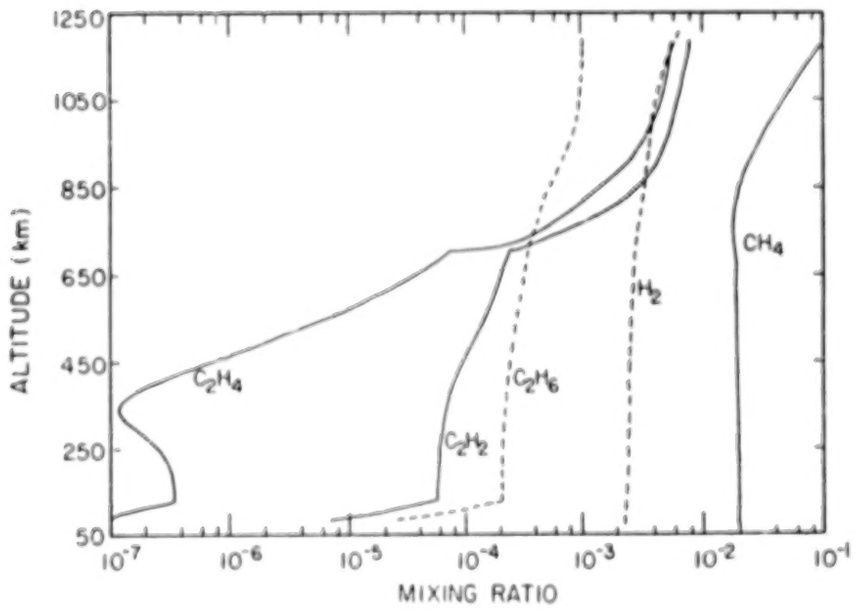

Fig 6b

Vertical profiles of the mixing ratios of the principal hydrocarbon species in the atmosphere of Titan

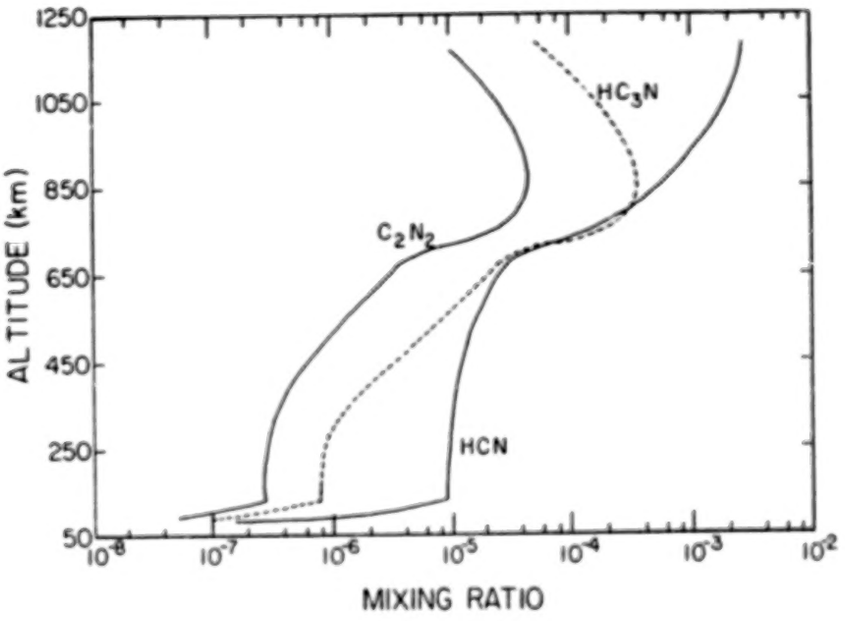

Fig 6c

Same as Figure 6b, for nitrogen bearing species.

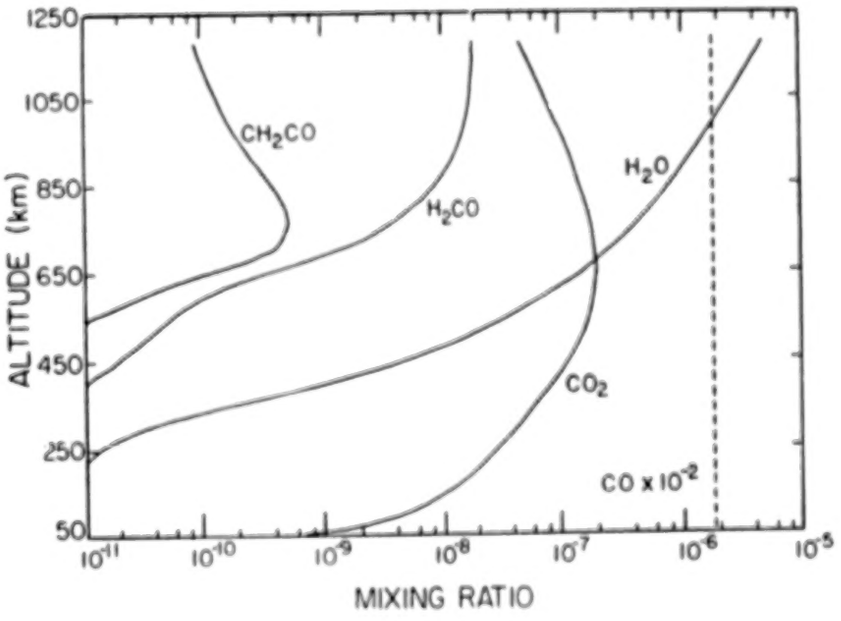

Fig 6d

Same as Figure 6b, for oxygen bearing species

unique ability of carbon to form complex compounds, we can generate more complex compounds from the simpler ones. For example:

$$CH_2 + C_2H_2 + M \rightarrow CH_3C_2H + M \qquad \text{(R37)}$$

Early work on this reaction suggests that R37 is a fast reaction. Recent work indicates that R37 is much slower (it is spin forbidden). Why is it so easy to synthesize higher hydrocarbons on Titan? There is a beautifully simple kinetic reason. UV sunlight provide a source of radicals. The recombination of organic radicals to form complex organic compounds is extremely rapid in a place like Titan. For example, the reaction

$$C_2H_5 + CH_3 + M \rightarrow C_3H_8 + M \qquad \text{(R38)}$$

is believed to have a three body rate constant $k_{38} = 5.6 \times 10^{-22}$ cm^6 s^{-1} in Titan's atmosphere (the two-body limit is "normal", $k = 4.2 \times 10^{-11}\, e^{-200/T}$ cm^3 s^{-1}). Now this is a fantastically large rate constant compared with that for

$$O + O_2 + M \rightarrow O_3 + M \qquad \text{(R2)}$$

$k_2 = 6 \times 10^{-34}$ cm^6 s^{-1} at 300 K. The reason for the enormous discrepancy between k_{41} and k_2 is contained in the framework of RRKM theory. A molecule like C_3H_8 has so many degrees of freedom that the energy of formation can be distributed over the tens of vibrational modes. Thus the intermediate complex can be stabilized, leading to the formation of C_3H_8. However, I should point out that the kinetic rates of very low pressures (10^{-3}–1 Torr) for associative reactions have not been well studied experimentally.

A great deal remains to be investigated in the chemical kinetics of Titan's atmosphere. The important reactions,

$$C_2H + H_2 \rightarrow C_2H_2 + H \qquad \text{(R39)}$$

$$C_2H + CH_4 \rightarrow C_2H_2 + CH_3 \qquad \text{(R40)}$$

$$C_2H + C_2H_2 \rightarrow C_4H_2 + H \qquad \text{(R41)}$$

respectively, lead to photosensitized dissociation of H_2, CH_4, and polyacetylene chain propagation. There are major discrepancies (factors of 10) for the rate constants of the above reactions at room temperatures reported in the literature. At lower temperatures, appropriate for

the outer solar system, there is practically no information. This is an extremely unsatisfactory situation.

The quantum yield and fragmentation patterns of the hydrocarbons and the nitrile compounds are poorly known. For example, we do not accurately know the following yields as a function of wavelengths

$$C_2H_2 + h\nu \rightarrow C_2H + H \quad \text{(R42a)}$$

$$\rightarrow C_2 + H_2 \quad \text{(R42b)}$$

$$C_4H_2 + h\nu \rightarrow C_4H + H \quad \text{(R43a)}$$

$$\rightarrow 2C_2H \quad \text{(R43b)}$$

$$C_2N_2 + h\nu \rightarrow 2CN \quad \text{(R44)}$$

Other compounds whose photofragmentation patterns remain to be determined include C_3H_8, C_4H_{10}, HC_3N, and C_4N_2.

Since Titan is a tiny planetary body carrying a massive atmosphere, the atmosphere is not stable both physically and chemically. Physically, hydrogen species and N atoms produced in exothermic reactions can escape from the satellite. Chemically there is an inexorable drive towards the synthesis of complex organic compounds, which are removed from the atmosphere by condensation at the tropopause, and ultimately on the surface. With the irreversible loss of hydrogen due to escape from the top of the atmosphere, recycling back to CH_4 is impossible. Therefore, the chemistry represents a one-way evolution towards species with heavier molecular weight and their permanent sequestering on the surface. For comparison, we note that H escapes from all the inner planets. Since H_2O is the obvious reservoir of hydrogen, this irreversible loss of hydrogen results in the accumulation of oxygen on these planets. This may be one reason why their atmospheres are so oxidizing. On Titan the physical and chemical environment is such that a molecule like CH_4 with H/C ratio of 4 is intrinsically unstable. Evolution would inevitably lead to the production of more sooty or tarry materials (of low H/C ratio).

The continuing chemical evolution of the atmosphere produces large amounts of dark photochemical aerosols. As can be seen in Table 5d, Titan is one of the darkest objects in the solar system in the UV, with geometric albedo less than 5% (geometric albedo (p) = brightness of planet at zero solar phase relative to a white disk of the same diameter. p = 2/3 for a white ping pong ball). A thick photochemical haze completely envelopes the satellite. The impact on the climatology of the stratosphere is similar to that of the O_3 layer on Earth, the dust on Mars, and the unidentified UV absorber (most probably polysulfur) on Venus. However, on Titan,

there is an even deeper chemical implication. The sequence of events leading to the current state of the atmosphere is as follows:

1. Photolysis of CH_4 in the mesosphere leads to a production of C_2H_2 and C_2H_4.
2. C_2H_2 abundance builds up in the stratosphere.
3. Photosensitized dissociation of CH_4 becomes important, producing C_2H_6, polymers, and aerosols.
4. Sunlight absorption by aerosols leads to thermal inversion, dynamic stability.
5. Stratosphere becomes more stable, resulting in a further increase of the abundances of higher hydrocarbons and leading back to step 3.

Therefore, in addition to a dynamical positive feedback discussed in the section "Jovian Planets", there is a strong chemical positive feedback in the generation of the hydrocarbon aerosols. And that is how we end up with such a dark body. Magic without magic results when chemical kinetics is coupled to all other processes in the atmosphere: radiation and dynamics. However, it is still mysterious to me why this particular planetary state is chosen, given Nature has many alternatives.

An intriguing observation reported by the Voyager UVS instrument is the detection of a high altitude (400 km) UV haze. It is probably created by the condensation of a complex hydrocarbon (such as a polyacetylene), but no one has sufficient kinetic information to predict such a haze layer in a photochemical model.

DEUTERONOMY

Again Nature has been kind in giving us deuterium as well as hydrogen. This is like Moses giving us the laws of God once in Exodus and once again in Deuteronomy (from Greek Deuteronomion, a second law, literally meaning "a copy of the law." Although I am not a scholar in ancient classics, I have no doubt that all these words: deuterium, deuteron, duo, deuce, duel, and duologue are derived from the same source with meaning associated with two, number two, second, and a copy of). Deuterium is, of course, "a copy of" hydrogen with nearly the same chemical properties. There is a difference due to mass, which allows us to trace and check the origin and evolution of planetary systems. Table 7a gives a compilation of D/H ratio in the solar system. An inspection of this Table enables us to assess how closely the various parts of the solar system are related to a common origin. It is convenient to divide the deuterium inventory in the solar system into three types: the primordial nebula gas (HD), the organics, and the ices (HDO and CH_3D). It is known that the water in hydrated silicates have D/H ratios close

to the terrestrial value. Suppose we consider a uniformitarian hypothesis that all ices in the solar nebula were enriched by the same factor (about 10) relative to the molecular hydrogen reservoir. (The kinetics of this fractionation has not been worked out.) This will have little effect on the observed D/H ratio on Jupiter and Saturn because of dilution by the massive H_2 atmospheres in these planets. However, on planetary bodies with large rocky cores, the isotopic signature will be preserved, and in some cases, may be further enhanced by subsequent planetary evolution. Such an enhancement has obviously occurred on Mars and Venus due to the preferential escape of H over D.

On Titan, preferential escape of H will apparently not work, because the gravity is so low that H and D will both escape. Therefore, in order to explain the large observed enrichment of D/H (relative to Saturn), we have to explore the possibility of a chemical enrichment such as a difference in the following reactions,

$$C_2H + CH_4 \rightarrow C_2H_2 + CH_3 \qquad \text{(R45)}$$

$$C_2H + CH_3D \rightarrow C_2H_2 + CH_2D \qquad \text{(R46)}$$

Since these are the primary sinks for CH_4 and CH_3D (more important than direct photolysis) a faster rate for R45 will result in an enrichment of CH_3D over CH_4 over geological time. However, reaction R46 has never been studied in the laboratory and this whole idea of chemical enrichment remains speculative. I would like to point out a similar idea is being pursued in the terrestrial atmosphere in trying to track down the sources of CH_4 (which is increasing) using $^{13}CH_4$. The analogous reactions in this case are

$$OH + CH_4 \rightarrow H_2O + CH_3 \qquad \text{(R47)}$$

$$OH + {}^{13}CH_4 \rightarrow H_2O + {}^{13}CH_3 \qquad \text{(R48)}$$

(These experiments are much harder to do because the difference between k_{47} and k_{48} is only 0.5–1.0%! Please try to study R45 and R46 first. The difference here is about 25%.)

I will conclude by pointing out what is behind this unity of chemical kinetics for the solar system. The reason, I think, lies in the fact that there is a common set of molecules that occur throughout the solar system. God gave us multiple copies of the same laws (multironomy). As an illustration of this idea, consider all the observed carbon species in planetary atmospheres summarized in Table 7b. Given one species, the laws demand that it be connected to the other species via chemical reactions. Indeed, as discussed in previous sections, some of the most interesting chemistry in the solar system involves changes in the oxidation state of the simple carbon species. The chemical pathways for the conversion of CH_4 to CO and CO_2 in an

oxidizing atmosphere are for the most part known. The reverse process, the reduction of CO to CH_4 in an H_2 atmosphere is, however, poorly understood. This is, of course, the key to organic synthesis in a mildly reducing atmosphere. One such scheme (VII) has been proposed and it is up to the kineticist to face the challenge of proving or disproving it. The reward is a deep satisfaction that this scheme works in all the Jovian planets, solar nebula, and even the primitive Earth's atmosphere.

ACKNOWLEDGEMENT

I thank M. Allen for many valuable discussions in writing this article and a critical review of the manuscript. Contribution number 4825 from the Division of Geological and Planetary Sciences, California Institute of Technology. The work is supported by NASA Planetary Atmosphere Program grant NAGW 1509to the California Institute of Technology.

ANNOTATED REFERENCES

INTRODUCTION:

The quotation on energy and entropy is from R. Emden, Why do we have winter heating? *Nature* **141**. 908, 1938.

The table of abundances of the elements is from E. Anders and N. Grevesse, Abundances of the elements: Meteoritic and solar, *Geochim. Coschim. Acta* **53**, 197, 1989.

An excellent text on the composition of planetary atmospheres has been written by a laboratory kineticist R.P. Wayne, *Chemistry of Atmospheres*, Clarenton Press, Oxford, 1985.

Discussion of atmospheric radiation in Earth's atmosphere is based on R.M. Goody and Y.L. Yung, *Atmospheric Radiation*, Oxford University Press, 1989.

EARTH

A comprehensive document summarizing O_3 and the state of current knowledge of the upper atmosphere is R.T. Watson et al., ed. *Atmospheric Ozone*, World Meteorological Organization, 1986.

The critical compilation of chemical kinetics and photochemical data for the terrestrial atmosphere is W.B. DeMore et al., Chemical kinetics and photochemical data for use in stratospheric modeling, JPL publication 87–41, 1987.

Quantitative modeling of the terrestrial troposphere, stratosphere, mesosphere, and thermosphere is described in J.A. Logan, M.J. Prather, S.C. Wofsy, and M.B. McElroy, Tropospheric chemistry: A global perspective, *J. Geophys. Res.* **86**, 7210, 1981; J.A. Logan, M.J. Prather, S.C. Wofsy, and M.B. McElroy, Atmospheric chemistry: Response to human influence, *Phil. Trans. Roy. Soc. London Ser A* **290**, 187, 1978; and M. Allen, J.I. Lunine, and Y.L. Yung, The vertical distribution of ozone in the mesosphere and lower thermosphere, *J. Geophys. Res.* **89**, 4841, 1984.

MARS AND VENUS

Definitive models of Martial photochemistry are by M.B. McElroy, Mars: An evolving atmosphere, *Science* **175**, 443, 1972; M.B. McElroy, and T.M. Donahue, Stability of the Martian atmosphere, *Science* **177**, 986, 1972; and T.Y. Kong, and M.B. McElroy, Photochemistry of the Martian atmosphere, *Icarus* **32**, 168, 1977. Update of this model has been carried out by Y.L. Yung et al., HDO in the Martian atmosphere: Implications for the abundance of crustal water, *Icarus* **76**, 146, 1988. There is an excellent review by

C.A. Barth, Photochemistry of the atmosphere of Mars, in *The Photochemistry of Atmosphere* (J.S. Levine, ed.), pp. 337–392, Academic Press, New York, 1985.

Heterogeneous reactions in the Martian atmosphere were discussed by J. Blamont (private communication) and by Y.L. Yung, Is the Martian atmosphere denitrified by ice clouds? *Bulletin American Astronomical Society* **21**(3), 979, 1989.

A comprehensive modeling paper on Venus is by Y.L. Yung and W.B. DeMore, Photochemistry of the stratosphere of Venus: Implications for atmospheric evolution, *Icarus* **51**, 197, 1982.

There is a conference publication (exceeding 1000 pages) summarizing existing knowledge of Venus including Pioneer Venus by D.M. Hunten ed., *Venus*, University of Arizona Press, 1983.

OUTER SOLAR SYSTEM AND DEUTERONOMY

There is an excellent review article by D.F. Strobel, Photochemistry of the reducing atmospheres of Jupiter, Saturn, and Titan, *Intern. Rev. Phys. Chem.* **3**, 145, 1983.

The chemical kinetics for modeling the outer solar system is reviewed by Y.L. Yung, M. Allen, and J.P. Pinto, Photochemistry of the atmosphere of Titan: Comparison between model and observations, *Astrophys. J.* **55**, 465, 1984.

A recent book summarizing Voyager observations is by S. Atreya, *Atmospheres and Ionospheres of the Outer Planets and their Satellites*, Springer-Verlag, 1986.

The origin and evolution questions are discussed extensively by J.P. Pollack and Y.L. Yung, The origin and evolution of planetary atmospheres, *Ann. Rev. Earth Planet. Sci.* **8**, 425, 1980 and by D.M. Hunten and T.M. Donahue, Hydrogen loss from the terrestrial planets, *Ann. Rev. Earth Planet. Sci.* **4**, 265–292, 1976.

Isotopic chemistry is recently reviewed by J.A. Kaye, Mechanisms and observations for isotopic fractionation of molecular species in planetary atmospheres, *Rev. Geophys.* **25**, 1609, 1987.

N90-26764

KINETICS AND THERMOCHEMISTRY OF POLYATOMIC FREE RADICALS: NEW RESULTS AND NEW UNDERSTANDINGS

DAVID GUTMAN AND IRENE R. SLAGLE
Department of Chemistry, Catholic University of America
Washington D. C. 20064

ABSTRACT

An experimental facility for the study of the chemical kinetics of polyatomic free radicals is described which consists of a heatable tubular reactor coupled to a photoionization mass spectrometer. Its use in different kinds of chemical kinetic studies is also discussed. Examples presented include studies of the $C_2H_3 + O_2$, $C_2H_3 + HCl$, $CH_3 + O$, and $CH_3 + CH_3$ reactions. The Heat of Formation of C_2H_3 was obtained from the results of the study of the $C_2H_3 + HCl$ reaction.

INTRODUCTION

Hydrocarbon photochemistry and kinetics are an integral part of the chemical processes occurring in the atmospheres of the outer planets (Jupiter and Saturn) and their larger satellites (e.g., Titan). Significant concentrations of CH_4 have been detected in these atmospheres as have lesser concentrations of higher hydrocarbons (e.g., C_2H_6, C_2H_4, C_2H_2, and CHCCCH), compounds that are produced by free-radical processes initiated by the photodecomposition of CH_4 by solar radiation.

The complex chemical processes that are responsible for producing the spectrum of hydrocarbons observed in these atmospheres involve reactions of many free-radical intermediates, some simple (such as H atoms and CH_2 radicals) and some more complex (e.g., CH_3, C_2H_5, and C_2H_3). To obtain a quantitative understanding of the chemical processes occurring in these atmospheres requires, among other things, knowledge of the chemical kinetics of these labile species. While there is considerable knowledge available today on the chemical kinetics of the simpler intermediates (i.e., radicals containing from 1-3 atoms), far less is known about the chemistry of the larger reaction intermediates. This dearth of knowledge for the larger species is due principally to the greater difficulty in detecting them and monitoring their behavior under controlled laboratory conditions that are suitable for obtaining quantitative information on their chemical kinetics. The powerful techniques that are available to detect atoms and small free radicals (such as laser-induced fluorescence, laser magnetic resonance, and atomic and molecular absorption) are either less sensitive, less selective, or simply not applicable for monitoring larger free radicals under the desired laboratory conditions.

Over the past several years, we have focused our attention on developing a versatile experimental facility specifically designed

for investigating the gas-phase chemical kinetics of polyatomic free radicals. It includes a heatable tubular reactor coupled to an ultrasensitive photoionization mass spectrometer.[1] Pulsed UV laser photolysis is used to produce the polyatomic free radicals of interest in the reactor. Reactants and products (stable as well labile) are monitored in time-resolved experiments. In this paper, we describe the facility and give examples of kinetic studies of free-radical reactions which have been conducted with this facility. Some of the examples presented are elementary reactions known to be involved in the chemical transformations occurring in the atmospheres of the outer planets and their satellites.

While these examples involve exclusively hydrocarbon free radicals, it should be recognized that the versatility of this experimental facility makes it well suited for studying the kinetics of other reactions that are important in planetary atmospheres including those of radicals containing sulfur, oxygen, phosphorus, and nitrogen. Reactions involving some of these additional classes of radicals have already been conducted with earlier versions of this apparatus.[2-4]

THE EXPERIMENTAL FACILITY

The apparatus consists of a one-cm.-diam. quartz or Pyrex heatable tubular reactor coupled to a photoionization mass spectrometer (See Fig. 1). Gas flowing through the tube at 5 m/sec contains the free-radical precursor (e.g., acetone to produce CH_3 radicals), the molecular reactant (if a second species is also involved in the reaction under study) and the carrier gas (which is in large excess, typically 98+% He).

Pulsed homogeneous photolysis of the free-radical precursor is done with unfocused 193 or 248 nm radiation from an excimer laser (Lambda Physik 201 MSC). The laser is operated at 5 Hz to permit the gases in the reactor to be completely replaced between repetitions of the experiment.

Gas is continuously sampled through a small conical orifice (0.044-cm-diameter at the apex) located in the wall of the reactor. The emerging flow is formed into a beam by a conical skimmer before entering the vacuum chamber containing the photoionization mass spectrometer. As the gas beam traverses the ion source, a portion is photoionized and mass selected. Photoionization is accomplished using simple yet intense atomic resonance lamps.[5,6] The gas flowing through the lamp can be changed quickly as can the window of the lamp. The window acts as a short-wave cutoff filter to eliminate radiation from the lamp that is more energetic than the resonance radiation used for photoionization. Ionizing energies from 8.6-11.6 eV are available in about 0.5 eV steps depending on the gas flowing through the lamp. The combinations of resonance energies available for photoionization and window materials used with each lamp are shown in Figure 2. In each experiment, a photoionization energy is used, from among those available, that is as close to the ionizing energy of the free radical as possible. For example to detect CH_3 (I.P. = 9.8 eV), the hydrogen lamp is used which has a resonance energy of 10.2 eV.

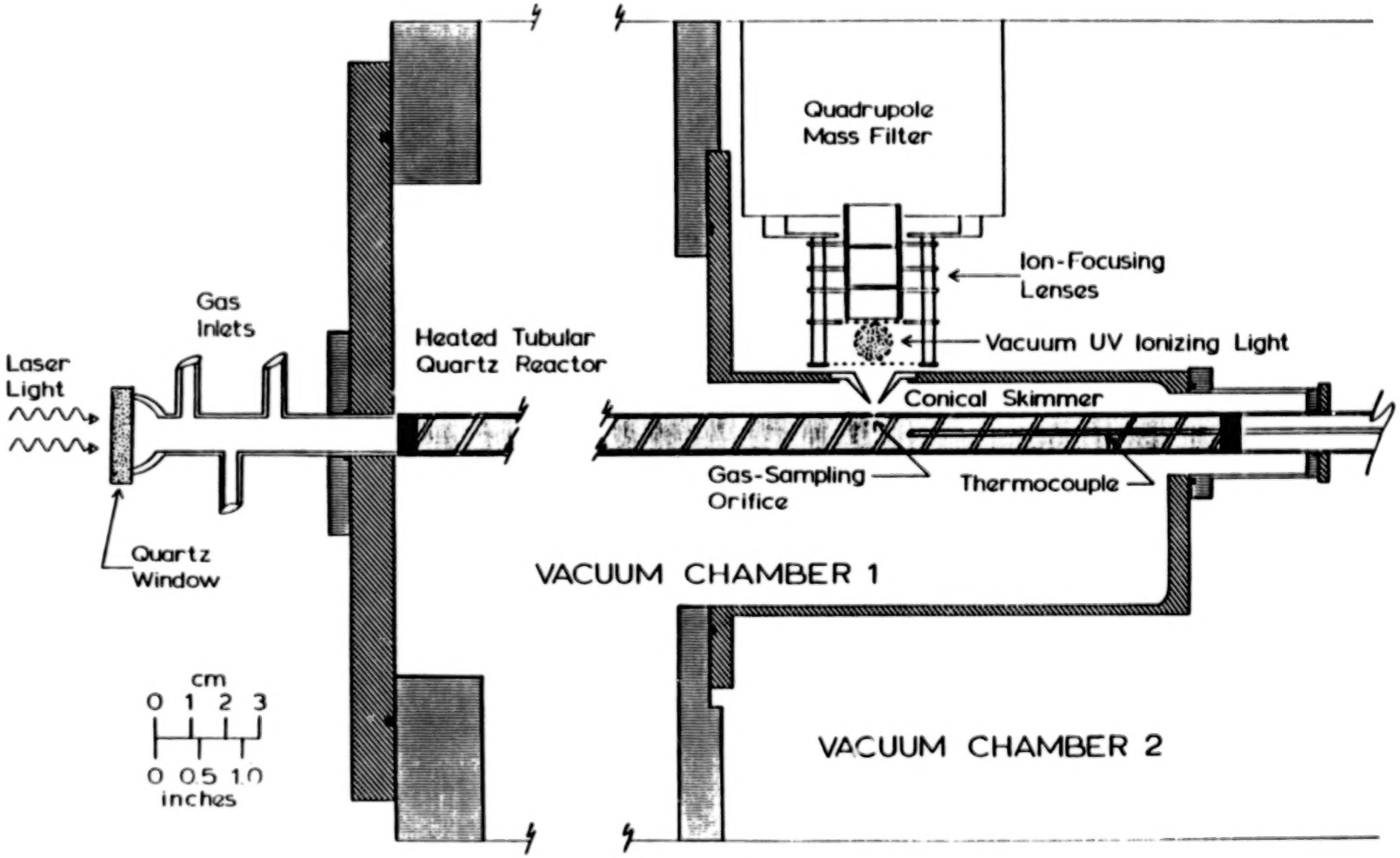

Figure 1. Drawing of Experimental Apparatus

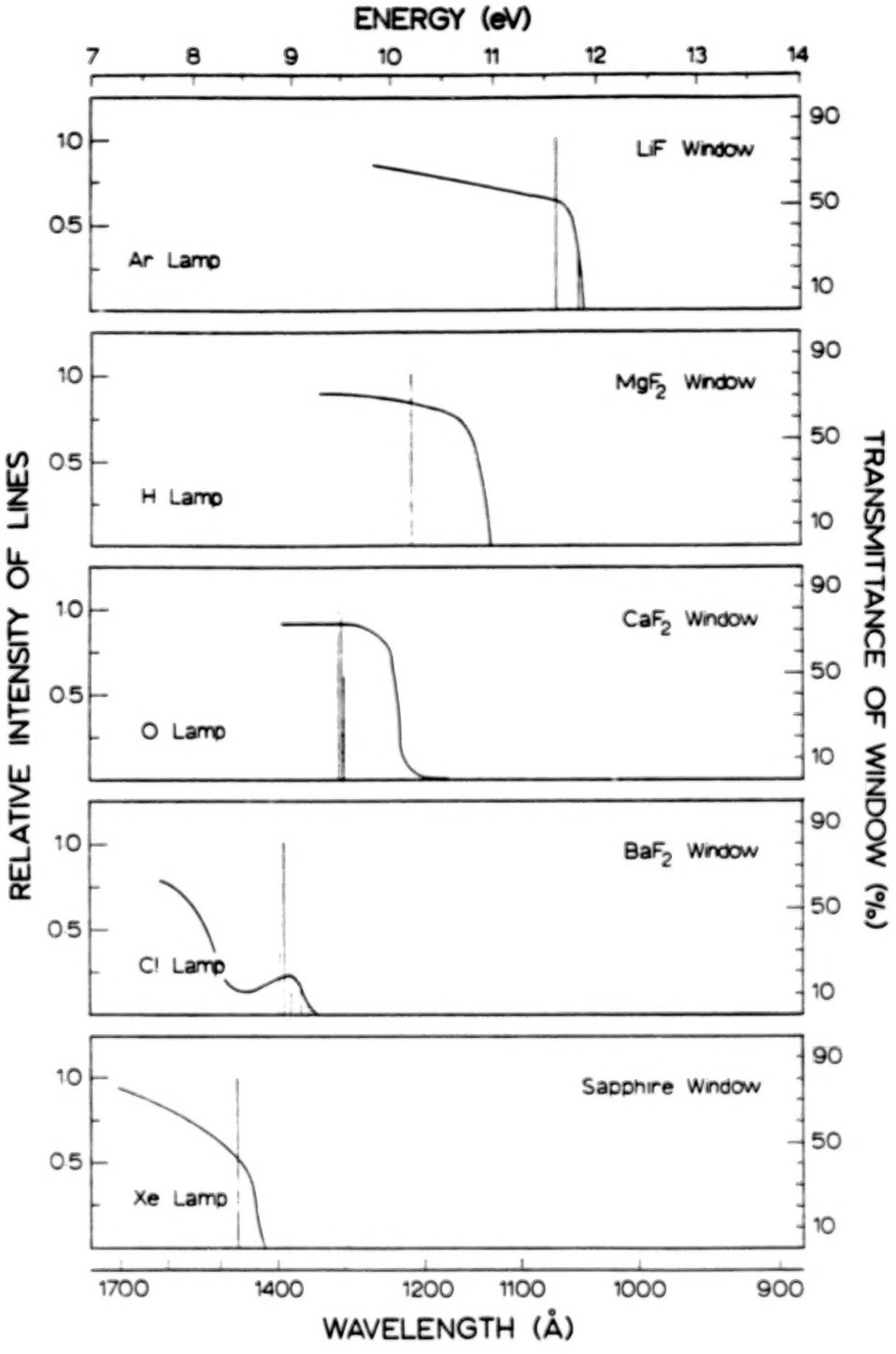

Figure 2. Characteristics of Atomic Resonance Lamps used for Photoionization. Shown are lamp gases, resonance energies, and transmission characteristics of lamp windows used with each lamp gas.

Several factors combine to give this facility unparalleled sensitivity for the detection of polyatomic free radicals. First there is the use of intense radiation from atomic resonance lamps for photoionization.[5,6] Second, there is the high ionization selectivity that results from using essentially monoenergetic ionizing energy just above the radical's ionization potential. This practice essentially eliminates detection interference from fragmentation processes involving the free-radical precursor or the background gases in the mass spectrometer vacuum system. Third, extra sensitivity is obtained from the extreme close coupling of the reactor to the photoionization mass spectrometer in the differentially pumped vacuum system (The distance from the gas sampling point to the center of the ionizing region of the photoionization mass spectrometer is under 2 cm.). Finally, sensitivity is enhanced by using ion counting of the mass spectrometer signal and multichannel scaling, the latter to obtain time resolution and to accumulate the ion-signal profiles from repetitions of the experiment (typically 1,000-10,000).

The sensitivities of this facility for detecting polyatomic free radicals that are given below are "operational", i.e., the lowest <u>initial</u> free-radical concentrations that can be used in a typical experiment designed to measure free-radical decay constants. In such experiments, data acquisition is continued until the radical decay constant determinations have an uncertainty under ±5%. Determinations of this sort that require over 30 minutes are considered impractical. Therefore, the detection sensitivities given here refer to experiments conducted for this duration.

Several factors influence the overall free-radical detection sensitivity, including photoionization cross section, degree of background interference, and the importance of heterogeneous loss of the the free radical. Because photoionization cross sections scale with the size of the free radical, detection sensitivity varies significantly, from $\approx 10^{8}$ radicals cm^{-3} (for larger radicals such as $(CH_3)_3C$ and SiH_3) to $\approx 10^{10}$ radicals cm^{-3} (for small radicals such as CH_3).

While the use of low-energy, nearly monochromatic, photoionization reduces fragmentation processes (sometimes totally), fragmentation occasionally is a problem and in those instances reduces effective detection sensitivity (by providing a large constant background signal). Suppression of fragmentation is excellent for most hydrocarbon radicals (where there is usually ≈1 eV difference between the radical ionization potential and the hydrocarbon fragmentation threshold for producing the same radical ion). Interference is significant for many nitrogen-containing compounds. This latter fact has made the technique less applicable for studies of nitrogen-centered radicals than for hydrocarbon free radicals.

First-order heterogeneous loss of the free radicals does occur at the walls of the reaction vessel. It is fully characterized through measurements of the first-order decay constant (k_w) for the radical when the second reactant is absent. However, its presence influences detection sensitivity, because reaction conditions must be used (with the second reactant present) that channel most of the

radicals through the reaction under study. In a typical set of experiments designed to determine a reaction rate constant, varying amounts of the second reactant are added to increase the radical decay constant at least a factor of 5 above k_w. It is the need to determine a set of higher decay constants under these circumstances that affects detection senstitivity. The highest wall-loss rate constant that can be tolerated is $\approx 100\ s^{-1}$ because radical decay constants can be measured accurately only up to $\approx 500\ s^{-1}$.

Reduction in detection sensitivity due to heterogeneous radical loss is inversely proportional to the wall-loss rate constant. If k_w is $100\ s^{-1}$, then the effective detection sensitivity is a factor of 4 lower than if $k_w = 25\ s^{-1}$. To reduce wall loss, reactor coatings are used which include boric acid, Halocarbon Wax, fluorinated Halocarbon Wax, and polytetrafluoroethylene. Recently we have begun to use a larger diameter reactor (2-cm-diameter) to lower the k_w a factor of two.

KINETIC STUDIES UNDER PSEUDO-FIRST-ORDER CONDITIONS

Radical + Molecule Reactions

The ability to use extremely low initial concentrations of polyatomic free radicals makes it possible to study their reactions with molecular species under pseudo first-order conditions, ones in which the reaction of the radical R with the molecule (M) and the heterogeneous loss of the radical are the only reactions that need be considered in the data analysis:

$$R + M \longrightarrow \text{Products} \qquad (A)$$

$$R \longrightarrow \text{Heterogeneous Loss} \qquad (B)$$

In these experiments, $[R]_o \ll [M]$. The potentially important R + R recombination reactions are suppressed by using initial radical concentrations below 10^{10}-10^{11} radicals cm^{-3}. Free-radical decays are exponential under these conditions as can be seen in Figure 3 where a C_2H_3 radical decay profile is shown that was recorded during the study of the $C_2H_3 + O_2$ reaction.[7] The rate constant for the reaction under study is obtained simply from the slope of the line through the data on a plot of decay constants vs. [M].

$C_2H_3 + O_2$ Reaction - In addition to rate constant determinations, the experimental facility is used to detect reaction products and hence to identify reaction channels. For example, in the case of the $C_2H_3 + O_2$ reaction, two mechanisms had been proposed prior to our investigation, one producing $C_2H_4 + HO_2$ and the other $HCO + H_2CO$. Only the latter were observed as initial products indicating that the overall reaction is

$$C_2H_3 + O_2 \text{ -----> } HCO + H_2CO \qquad (1)$$

The product concentration profiles of Reaction 1 are also displayed in Figure 3. Primary processes are clearly separated from secondary ones under the conditions of these experiments. This is evident in the HCO profile in which the growth of HCO produced by reaction 1 is clearly separated from the subsequent decay of HCO due to secondary reaction of this radical with O_2. H_2CO, being a stable product, simply accumulates until the rection is complete.

C_2H_3 + HCl Reaction - Accurate thermochemistry of polyatomic free radicals can be derived from the results of kinetic studies. When the rate constant of an elementary reaction can be measured as a function of temperature both in the forward and reverse directions, the enthalpy change of the reaction can be obtained directly from the difference in activation energies of the forward and reverse reactions.[8]

We have recently determined the heat of formation of the vinyl radical from a study of the kinetics of the equilibrium,[9]

$$C_2H_3 + HCl \text{ <=====> } C_2H_4 + Cl \qquad (2)$$

Measurements in our laboratory of the rate constant of the forward reaction as a function of temperature yielded the Arrhenius parameters for the forward reaction. This information was combined with Arrhenius parameters for the reverse reaction obtained by Parmer and Benson[10] to obtain the C_2H_3 Heat of Formation. Both Second Law calculations (using the difference in activation energies) and Third Law calculations (using values of k_2 and k_{-2} at a single temperature as well as calculated entropies of reactant and products) yielded virtually identical values for the C_2H_3 Heat of Formation, 67.1±0.6 kcal mol^{-1} for the former and 66.9±0.3 kcal mol^{-1} for the latter analysis. The closeness of the values using two quite different data analyses is an indication of the high accuracy of determinations of free radical Heats of Formation from the results of experiments of this kind.

Radical + Atom Reactions

Recently we have developed a procedure to study the kinetics of reactions of polyatomic radicals with atomic oxygen, R + O.[11,12]
It involves the simultaneous production of both reactants by 193 nm photolysis. SO_2 is the source of O:

$$SO_2 \text{ -----> } SO + O \qquad (2)$$

We have investigated several R + O reactions including CH_3 + O and C_2H_5 + O,[11,12] the former considered to have been important in the early chemistry of the Earth's atmosphere. Acetone was used as the source of CH_3,

$$(CH_3)_2CO \text{ -----> } 2\ CH_3 + CO \qquad (3)$$

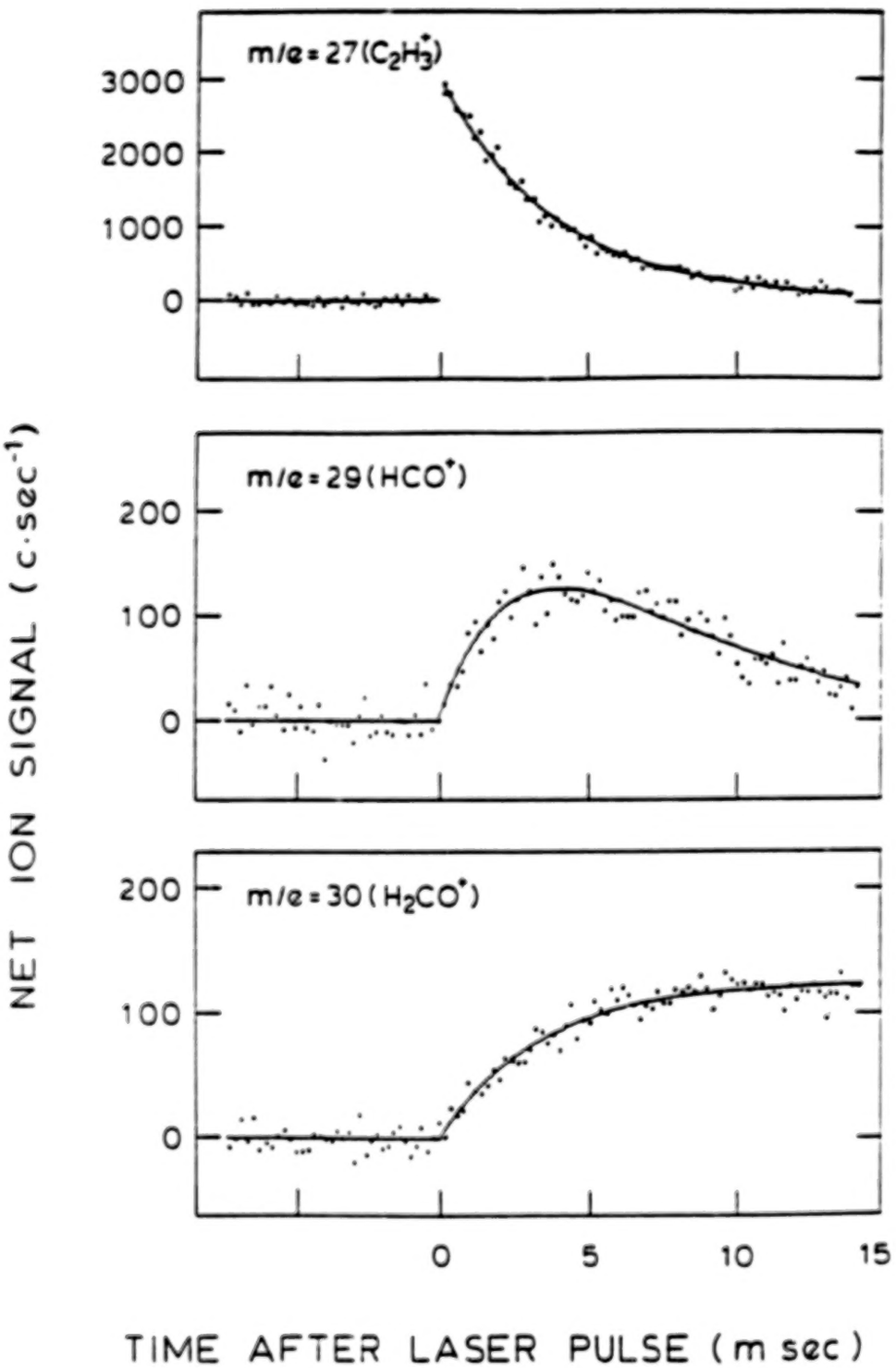

Figure 3 Plot of reactant and product ion-signal profiles recorded during $C_2H_3 + O_2$ ---> $HCO + H_2CO$ reaction.[7] T=599 K; $[O_2]=1.42\times10^{13}$ molecule cm^{-3}

The oxygen atoms are produced in excess and are not depleted to a significant degree during the course of the reaction. The O-atom concentration is determined by measuring the depletion of SO_2 by photolysis.

Radical + Radical Reactions

By using higher initial free radical concentrations (e.g., 10^{13} radicals cm^{-3}) recombination processes can be investigated. We have studied the recombination of CH_3 radicals,[13] a process believed to be responsible for producing C_2H_6 in the atmospheres of the outer planets and on Titan:

$$CH_3 + CH_3 + M \longrightarrow C_2H_6 + M \qquad (4)$$

In such studies, the initial concentration of the radical must be determined, and there must not be competing R + R' reactions also consuming CH_3. Again, 193 nm photolysis of acetone was used to produce CH_3. Its concentration was determined from direct observation of the depletion of acetone by the pulsed 193 nm light. Pictures of the acetone depletion and CH_3 decay profiles recorded during a set of experiments conducted to measure k_4 are shown in Figure 4.

CONCLUDING REMARKS

The apparatus described here is a versatile tool for the study of the chemical kinetics of polyatomic free radicals. It is well suited for the study of many classes of free-radical reactions. It is hoped that this introduction to the facility and its capabilities will draw attention to its potential usefulness for gaining new knowledge of the chemical processess occurring in the planetary atmospheres.

ACKNOWLEDGEMENTS

Financial assistance for the construction and development of the experimental facility and for conducting the kinetic studies described here was obtained from grants from the Chemistry Division of the National Science Foundation and the Office of Basic Energy Sciences of the Department of Energy.

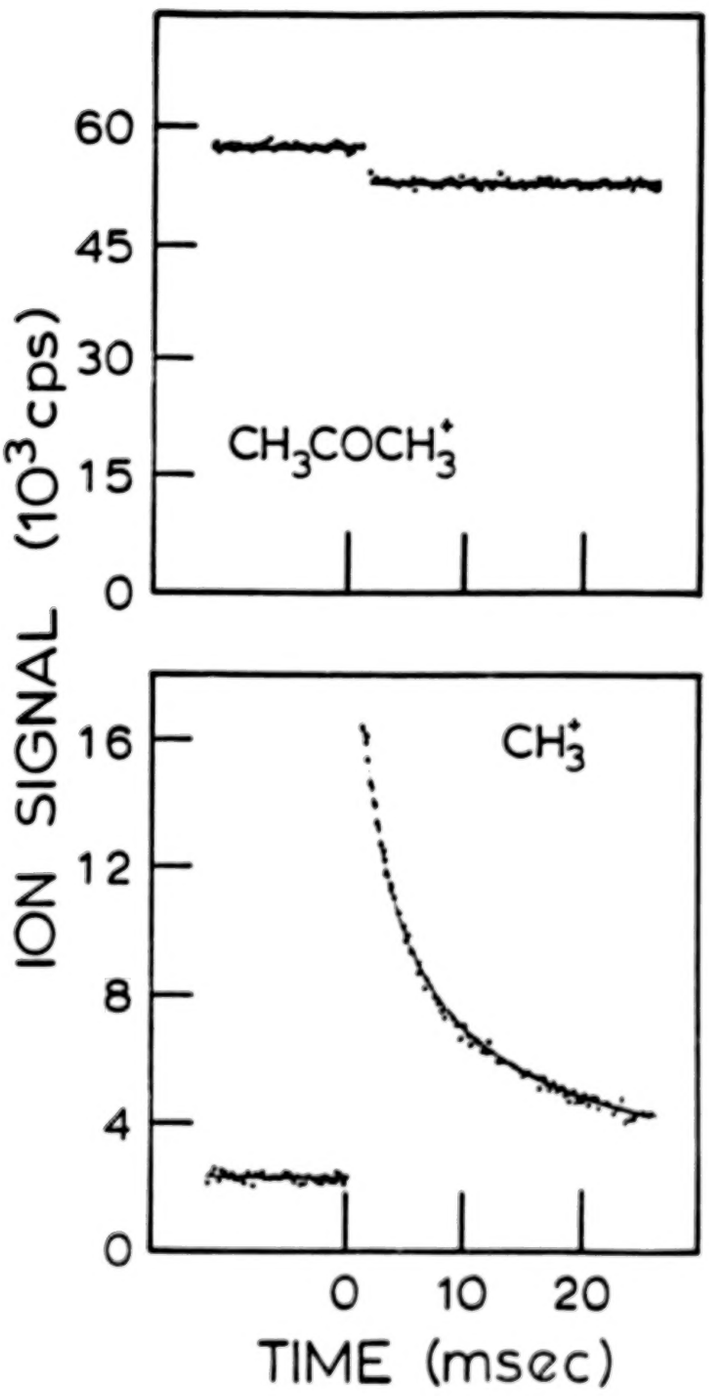

Figure 4 Plot of CH_3^+ decay recorded during $CH_3^+ + CH_3$ ---> C_2H_6 reaction.[13] T=810 K; $[CH_3]_o=1.04\times10^{13}$ radicals cm^{-3}; [He]=2.1×10^{17} atoms cm^{-3}.

REFERENCES

1. I. R. Slagle and D. Gutman, J. Am. Chem. Soc. **107**, 5342 (1985).
2. I. R. Slagle, J. R. Gilbert, and D. Gutman, J. Chem. Phys. **61**, 704 (1974).
3. I. R. Slagle and D. Gutman, Int. J. Chem. Kinet. **11**, 453 (1979).
4. I. R. Slagle, J. F. Dudich, and D. Gutman, J. Phys. Chem. **83**, 3065 (1979).
5. R. Gordon Jr., R. E. Rebbert, and P. Ausloos, "Rare Gas Resonance Lamps, N.B.S. Technical Note 496.
6. J. R. Kanofsky and D. Gutman, Chem. Phys. Lett. **15**, 236 (1972).
7. I. R. Slagle, J.-Y. Park, M. C. Heaven, and D. Gutman, J. Am. Chem. Soc. **106**, 4356 (1984).
8. H. E. O'Neal and S. W. Benson, "Free Radicals", J. K. Kochi, Ed., Wiley, New York, 1973, Vol. 2, Chapt. 17.
9. J. J. Russell, S. M. Senkan, J. A. Seetula, and D. Gutman, J Phys. Chem. **93**, 5184 (1989).
10. S. S. Parmer and S. W. Benson, J. Phys. Chem. **92**, 1608 (1988).
11. I. R. Slagle, D. Sarzynski, and D. Gutman, J. Phys. Chem. **91**, 4375 (1987)
12. I. R. Slagle, D. Sarzynski, D. Gutman, J. A. Miller, and C. F. Melius, J. Chem. Soc. Faraday Trans. 2, **84**, 491 (1988).
13. I. R. Slagle, D. Gutman, J. W. Davies, and M. J. Pilling, J. Phys. Chem. **92**, 2455 (1988).

N90-26765

THE HEAT OF FORMATION OF CN RADICALS AND RADIATIVE LIFETIMES OF THE $A^1\Sigma^-$ STATE OF C_2N_2

SAMUEL A. BARTS, KAREN V. PINNEX AND JOSHUA B. HALPERN
Howard University, Dept. of Chemistry, Washington, DC 20059, USA

ABSTRACT

Radiative lifetimes have been measured for the stable vibrational levels of the $A^1\Sigma^-$ electronic state of C_2N_2. They range from 1.3 μs for the 4_0^1 level to 0.66 μs for the $1_0^1 4_0^1$ level and in general decrease with increasing vibrational excitation. Self-quenching rate constants range from gas kinetic to ten times that. Foreign gas quenching rates are slower. Observation of emission from the $1_0^1 4_0^1$ level sets a lower limit for the heat of formation of CN of 439.11 kJ mol^{-1}.

INTRODUCTION

Simple nitriles play important roles in the photochemistry of nitrogen-methane planetary atmospheres. Cyanogen is a photochemically important molecule found in the atmosphere of Titan, and in other astronomical systems[1]. Cyanogen is also an extremely simple tetra-atomic system in which predissociation can be studied. Potential energy surfaces have been calculated for all of the excited states which means that models of dissociation dynamics can be tested in detail[2].

We have recently discovered that this molecule has a strong and distinctive emission spectrum. The lowest lying vibrational bands of $A^1\Sigma^-$ state of cyanogen (C_2N_2) fluoresce. The absorption, emission and photodissociation yield spectra of C_2N_2 have been measured between 220 and 210 nm, spanning the region between the 4_0^1 and $1_0^1 4_0^1$ bands of the $A^1\Sigma^- \leftarrow X^1\Sigma^+$ system[3]. A recent paper deals with the emission and fluorescence spectra of the 4_0^1 state and its radiative lifetime[4]. In this paper we report emission lifetimes of all the stable vibrational bands.

EXPERIMENTAL

The apparatus was similar to that described in Reference 5. C_2N_2 from Matheson was purified by freeze-thaw cycling. The cyanogen gas flow from a 3 liter reservoir was controlled by a flowmeter. The pressure was monitored by a capacitance manometer.

The excitation source was a Spectra Physics PDL-2 dye laser pumped by a DCR-11 Nd-YAG system. Dye laser light was frequency doubled in a KDP crystal and Raman shifted in about 10 atmospheres of hydrogen. For this experiment the third anti-Stokes shifted beam was used.

Emission from C_2N_2 was detected directly through an unfiltered 11 stage EMR VUV photomultiplier. Emission decay lifetimes were measured by fixing the exciting laser on the absorption line and scanning the boxcar gate delay or by using a DSP 2100 100 MHz transient digitizer. The

experiments were controlled by an IBM PC\XT microcomputer based data acquisition system constructed in our laboratory. The firing of the lasers and the dye laser scanning was controlled by the microcomputer. Absorption spectra were measured directly on a Cary 2390 UV-VIS-NIR spectrophotometer.

RESULTS

Figure 1 shows an absorption spectra measured on the Cary 2390 spectrophotometer between 200 and 230 nm. The lower half of the diagram shows the difference between spectra measured at 20 and 70 ^{o}C when the cell was heated by water from a thermostated bath. This identifies lines that originate in excited vibrational states and makes the assignment of the vibrational bands quite easy. Extra bands at wavelengths below 210 nm belong to the $B^1{}_u \leftarrow X^1\Sigma^+$ transition. We are in the process of setting up a VUV monochromator with better (0.02 nm) resolution to be able to analyze this second electronic transition. Figure 2 shows the emission spectrum from the $1_0{}^1 4_0{}^1$ band and the yield of CN fragments as a function of wavelength. Figure 3 shows the yield of CN fragments as a function of wavelength in the region of the $1_0{}^1 4_0{}^1$ band.

Table I lists the measured radiative lifetimes and quenching rate constants.

TABLE I
LIFETIMES AND QUENCHING RATES OF CYANOGEN $A^1\Sigma^-$

BAND	WAVELENGTH nm	VIBRATIONAL ENERGY cm^{-1}	LIFETIME μs	QUENCHING GAS	QUENCHING RATE cm^3-s/molecule
$4_0{}^1$	218.9	276	1.34	C_2N_2	4.3
$4_0{}^1$				He	1.7
$4_0{}^1$				Ar	1.9
$4_0{}^1$				N_2	2.5
$4_0{}^1$				CH_4	3.4
$4_1{}^2$	220.1	519	0.72	C_2N_2	8.4
$4_0{}^3$	216.6	770	0.67	C_2N_2	10.4
$4_0{}^3$				Ar	6.7
$2_1{}^1 4_1{}^0$	218.3	632	1.25	C_2N_2	9.9
$2_1{}^1 4_0{}^1$	218.6	908	0.94	C_2N_2	12.5
$2_0{}^1 4_0{}^1$	214.7		0.68	Ar	3.1
$1_0{}^1 4_0{}^1$	208.3	2606	0.66	C_2N_2	13.0

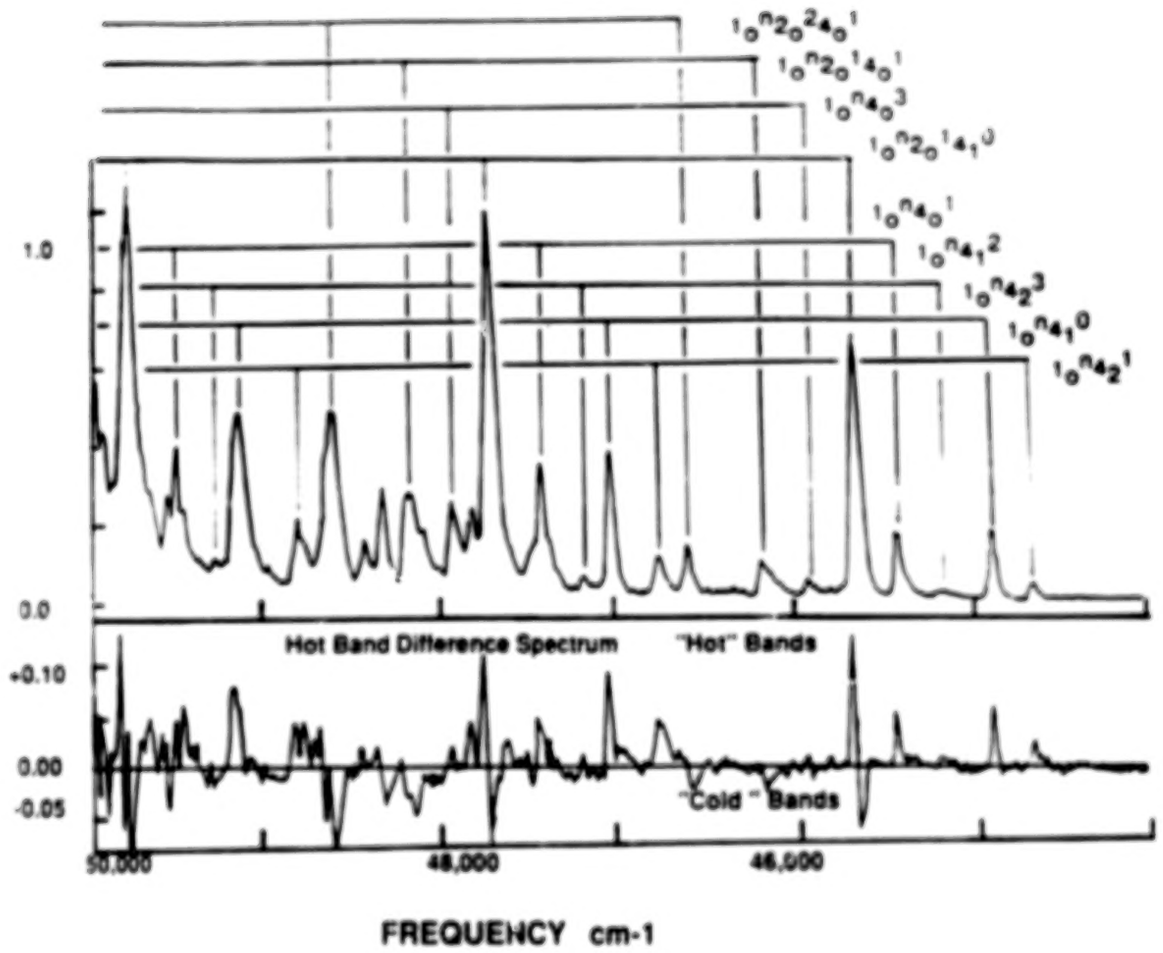

FIGURE 1. Absorption spectrum of C_2N_2

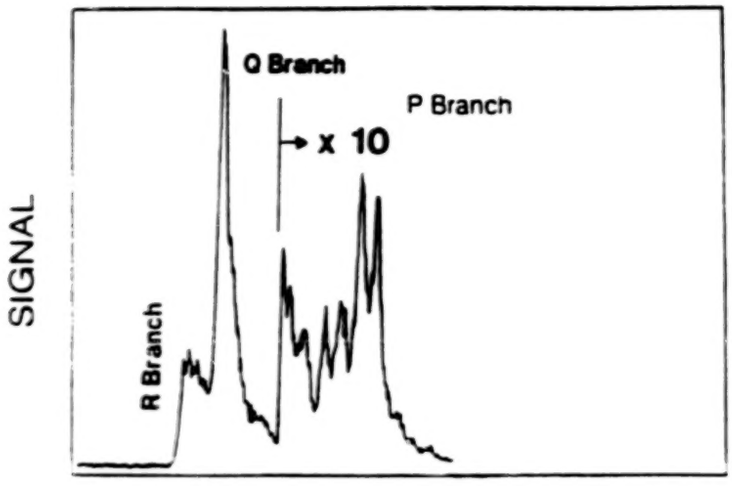

Figure 2. CYANOGEN EMISSION SPECTRUM

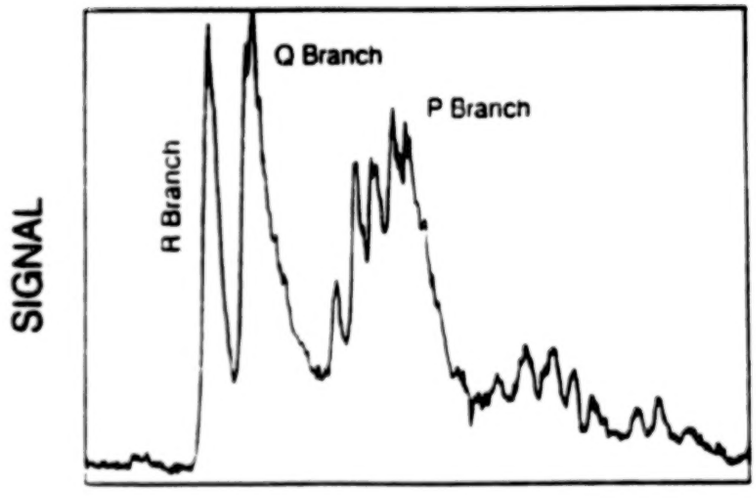

Figure 3. CN FRAGMENT QUANTUM YIELD

DISCUSSION

Using photodissociative excitation Davis and Okabe measured a dissociation energy of 5.58 $\pm$ 0.05 eV and a threshold wavelength of 222.2 nm[6]. Eres, Gurnick and McDonald observed the rotational distribution of CN ($X^2\Sigma^+$) fragments in the 193 nm photolysis of C_2N_2[7]. Based on the highest observed fragment rotational state they calculate a bond strength of 5.83 $\pm$ 0.04 eV and a photodissociation limit of 212.7 $\pm$ 1.5 nm. Most of the uncertainty is related to the 1 nm bandwidth of the excimer laser. Recently Lin, Johnston and Jackson have used a narrower bandwidth doubled dye laser to photodissociate cyanogen at 206 nm[8]. Their fragment LIF spectra implies an upper limit to the bond energy of 5.70 eV and a dissociation limit of 217.5 nm, assuming that there were no hot band contributions to the photolysis. The observation of rotational structure in bands above 218 nm[9] show that the actual dissociation limit must lie below this point.

The observation of strong fluorescence from the $1_0^1 4_0^1$ band at 209.5 nm is strong evidence that at least some rotational states of this level are bound. As can be seen in Figures 2 and 3 the Q branch of the emission spectrum is narrower than the Q branch in the fragment yield spectrum. The P and R branches in the emission spectrum are much weaker than those in the fragment yield spectrum. This also shows that low rotational states of the $1_0^1 4_0^1$ band are bound and high rotational states are dissociative. Thus, we assign a lower limit of the NC-CN bond strength of 5.92 eV. Using the standard value of the heat of formation for C_2N_2 of 307.223 $\pm$ 1.80 kJ mol^{-1},[10] this yield a lower limit of 439.11 $\pm$ 2.00 kJ mol^{-1} for the heat of formation of CN radicals, as compared to Davis and Okabe's value of 423 $\pm$ 4 kJ mol^{-1}.[6]

The radiative lifetimes range from 1.4 μs in the 4_0^1 band to 0.6 μs for the $1_0^1 4_0^1$ band. Self quenching rates range from gas kinetic (4.3×10^{-10} cm^3/molecule-s) for the 4_0^1 band to 13.0×10^{-10} cm^3/molecule-s for the $1_0^1 4_0^1$ band. Foreign gas quenching rates for the 4_0^1 band have been measured against He, Ar, N_2 and CH_4. As expected the quenching rate constants increase as the molecular weight and the complexity of the quenching gas, with the rate for quenching against He being the slowest and that against CH_4 being the fastest.

CONCLUSIONS

Earlier work done in our laboratory has demonstrated that dicyanoacetylene (C_4N_2) will also have several bound vibrational states in the $A^1\Sigma^+$ electronic state. We are currently synthesizing a sample of this compound in order to look for the fluorescence. Cyanoacetylene is known to have no bound levels in its first excited singlet state, and cannot be monitored by fluorescence. The UV emission of simple nitriles offers a method of remote detection, and will also be useful in the laboratory for study of such reactions as $CN + HCN \rightarrow C_2N_2 + H$.

ACKNOWLEDGEMENTS

Parts of this work were supported by NASA under Grant NAG-785, and grants from the Department of Energy and the Howard University Research Development Program. S. A. Barts was supported by a Danforth Foundation Fellowship. K. V. Pinnix was supported by a grant from the Department of Education.

REFERENCES

1. Y. L. Yung, M. Allen and J. P. Pinto, Astophys. J. Supp., **55**, 465 (1984).
2. C. E. Dateo, Thesis, University of California, Berkeley, I987.
3. S. A. Barts and J. B. Halpern, to appear in *Proceedings of the 1989 NASA/HBCU Colloquium*.
4. S. A. Barts and J. B. Halpern, Chem. Phys. Letts., **161**, 207 (1989).
5. J. A. Russell, I. A. McLaren, W. M. Jackson and J. B. Halpern, J. Phys. Chem., **91**, 3248 (1987).
6. D. D. Davis and H. Okabe, J. Chem. Phys., **49**, 5526 (1968).
7. D. Eres, M. Gurnick and J. D. McDonald, J. Chem. Phys., **81**, 5552 (1984).
8. H. Lin, E. A. Johnson and W. M. Jackson, Chem. Phys. Letts., **152**, 477 (1988)
9. G. B. Fish, G. J. Cartwright, A. D. Walsh and P. A. Warsop, J. Mol. Spec., **41**, 20 (1972).
10. D. R. Stull, E. F. Westrum, Jr. and G. C. Sinke, "JANAF Thermochemical Tables", 2nd Edition, *Natl. Stand. Ref. Data Ser.*, Natl. Bur. Stand. (US) **37** (1971).

N90-26766

A LABORATORY INVESTIGATION OF THE PRODUCTION AND PROPERTIES OF MOLECULAR AND RADICAL SPECIES PERTINENT TO PLANETARY ATMOSPHERES

ASKAR FAHR, JOHN HERRON* and ALLAN H. LAUFER**
* Askar Fahr and John Herron: Chemical Kinetics Division National Institute of Standards and Technology, Gaithersburg, Maryland 20899
** Allan H. Laufer: Office of Basic Energy Sciences U. S. Department of Energy, Washington, D. C. 20545

ABSTRACT

Vinylidene($H_2C=C$) is shown to be the largest photodecomposition channel in the direct photolysis of both C_2H_2 and C_2H_4. The chemistry of $H_2C=C$ as it relates to planetary atmospheres is discussed. The vinyl radical (C_2H_3), important in the acetylene chemistry cycle, has been directly observed spectroscopically and the kinetics of several key reactions of this species measured.

INTRODUCTION

An understanding of the chemistry of planetary atmospheres is critically dependent upon knowledge of the kinetic parameters of a suite of elementary chemical reactions. In the outer planets and several of their satellites, where carbon-hydrogen chemistry is paramount, the important vacuum ultraviolet photochemically induced processes and reactions involve small hydrocarbon molecules and radicals. Photochemical processes of the major planetary hydrocarbon, CH_4, have been known quantitatively for several decades. The carbon containing free radicals formed in the CH_4 photolysis, CH_2 and CH_3 corresponding to H_2 and H formation respectively, lead, through self-reactions, to C_2H_2 and C_2H_4[1].

$$CH_2 + CH_2 = C_2H_2 + H_2 \text{ (or } 2H) \quad (1)$$

$$CH_2 + CH_3 = C_2H_4 + H \quad (2)$$

In this paper, we review the quantum yield of formation and identity of the free radicals produced in the vacuum ultraviolet photolysis of the two unsaturated hydrocarbons, C_2H_2 and C_2H_4, and kinetic processes of several previously non-investigated species.

EXPERIMENTAL

The experimental apparatus used in the work to be described has been discussed in several papers from this laboratory[2], so will be described only briefly here. A photolysis flash of about 5us, full width at half-maximum intensity, has an output maximized in the vacuum ultraviolet region, the spectral region where the energy of the incident solar flux is sufficient to dissociate small hydrocarbon molecules and where the molecules of interest have their maximum optical absorption. Following the initial flash, a Garton-type analysis lamp of 1 us pulse width probed the photolysis mixture. The photolysis cells, constructed of either LiF or Suprasil, permitted photolysis to 105 nm or 155 nm, respectively. The output of the analysis flash, essentially continuous from 120 through 185nm, was focused through LiF optics onto the entrance slit of a 2 m Eagle vacuum spectrograph whose dispersion was 2.77A/mm. The temporal profile of all species was monitored directly through well-characterized absorptions.

RESULTS

Vinylidene Formation

Vinylidene ($H_2C{=}C$) was initially observed, in its electronically excited triplet state at 137 and 151 nm, following the photolysis of C_2H_2 in the vacuum ultraviolet[3]. The species has a long lifetime toward isomerization to acetylene and, therefore, may be of importance as an intermediate in planetary hydrocarbon systems if its quantum yield of formation from reasonable precursors is large. Acetylene is known to form both C_2H and C_2 from photolysis in the vacuum ultraviolet with estimated primary quantum yields of 0.3 and 0.1 at 147 nm, respectively[4]. We find that $H_2C{=}C$ is formed with a quantum yield of 0.4 making it the single largest dissociative channel in the acetylene photodecomposition.

Previously, the formation of unmixed H_2 or D_2 from the low intensity photolysis of C_2H_4 and its deuterated isotopes provided evidence for production of vinylidene radicals, i.e.,

$$CH_2CD_2 = CH_2C + D_2 \text{ and } CD_2C + H_2 \qquad (3)$$

In our direct determination, we find a quantum yield equal to 0.75 +/- 0.2 for triplet vinylidene formation from ethylene. Though not directly observed, there

is evidence that the remainder proceeds through vinyl (C_2H_3) radical formation. The work has been described in greater detail earlier[5].

Vinylidene Chemistry

The long-lived vinylidene moiety we observe is the electronically excited triplet that is calculated to be about 40-50 kcal/mol above the ground singlet state. The singlet, by comparison, has an ephemeral existence with a lifetime of the order of 10^{-12} seconds with respect to isomerization to acetylene. We have looked specifically for a chemical reaction, i.e., hydrogen abstraction, by triplet vinylidene with H_2, CH_4 and C_2H_4. Under conditions of our experiments, that is room temperature, we found no evidence for direct chemical reaction although the results with ethylene were less clear. Removal of the $H_2C{=}C$ in the absence of chemical reaction, presumably by quenching to the ground electronic state by added Ar, H_2, CO and N_2, occurred with reasonable rate constants. The slow rate observed for reaction agrees with predicted calculated values based upon a simple BEBO model[6].

Vinyl Radical Absorption Spectrum

The vinyl (C_2H_3) radical has been implicated in the acetylene chemical cycle. Although several studies have utilized mass spectrometric detection for analysis, there has not been an observable, intense ultraviolet or visible spectral signature for this species, an omission that has probably limited kinetic studies of this species.

Using flash photolysis of selected precursors in conjunction with vacuum ultraviolet absorption spectroscopy we have observed two relatively intense transient absorption features that we attribute to the vinyl radical (Figure 1). The features at 164.71 and 168.33 nm are assigned on the basis of precursor, kinetic data, and the spacing between the bands. The optimum precursors were $Sn(C_2H_3)_4$ and $Hg(C_2H_3)_2$. The photolysis of either resulted in 1) the observed spectrum, 2) produced the expected dimerization product, 1,3-butadiene, that was observed by gas chromatographic analysis and 3) a spacing between the transitions of 1306 cm^{-1} in agreement with both calculations and measurements of the vinyl ion spectrum. The spectrum was sufficiently intense, with extinction coefficients in excess of 1100 $atm^{-1}cm^{-1}$ that it could serve as a probe for kinetic studies. The work has been described in greater detail elsewhere[7].

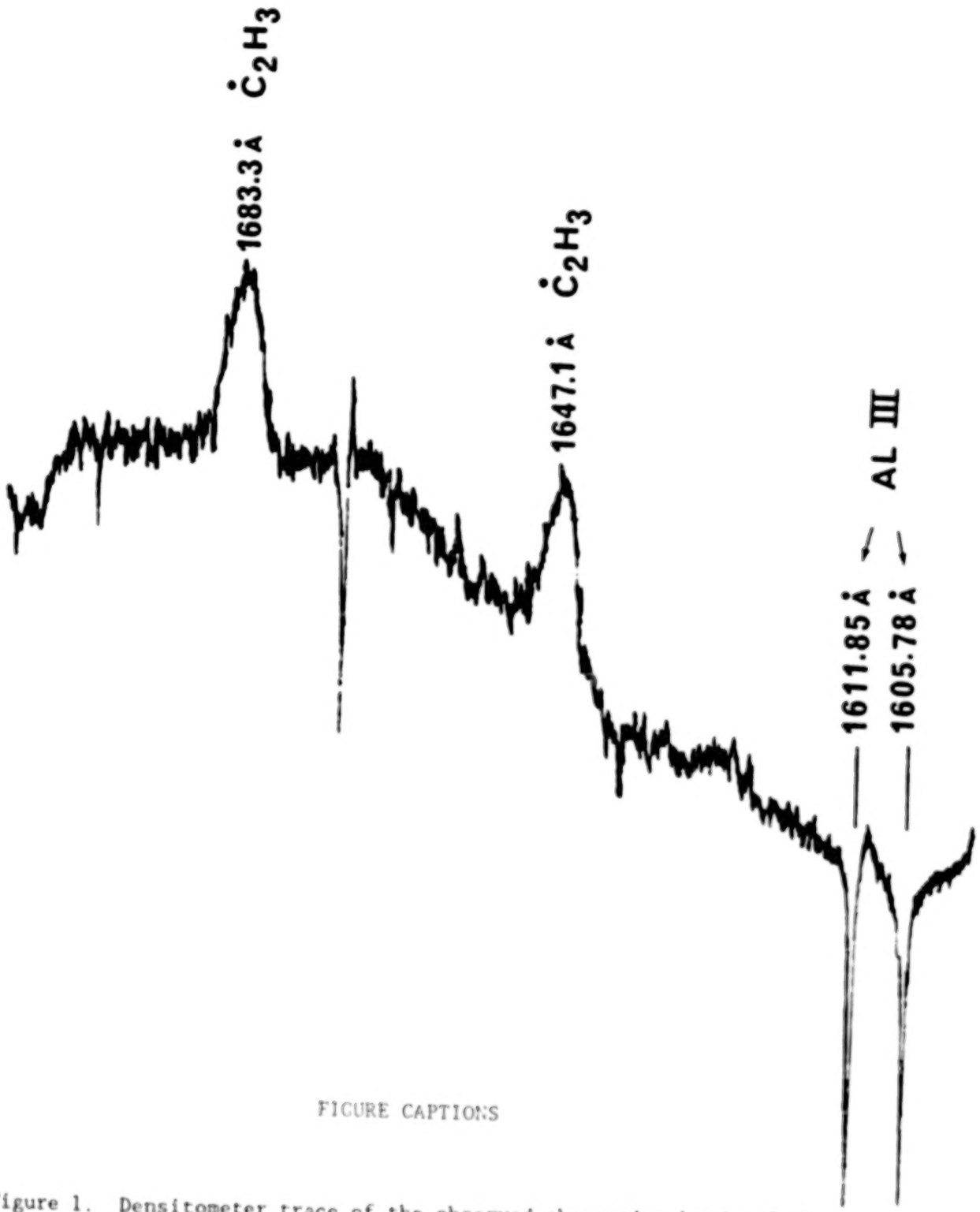

FIGURE CAPTIONS

Figure 1. Densitometer trace of the observed absorption bands of the C_2H_3 radical. The identified emission lines of Al III are from the source.

Vinyl Radical Chemistry

The initial reaction of vinyl radicals studied using its optical absorption was its reaction with molecular O_2. This reaction had been examined earlier with alternate techniques[8] and confirmation of the kinetic parameters using the C_2H_3 vacuum ultraviolet absorption served, in part, to confirm the assignment of the carrier to the vinyl radical. A major loss mechanism in any system containing free radicals is the self-reaction of the two radicals; in this case to disproportionate forming C_2H_2 and C_2H_4 or to combine yielding 1,3-butadiene. The optical measurement of the radical concentration with time following its production by flash photolysis resulted in a rate constant of $1.0 \times 10^{-10} cm^3 molec^{-1} s^{-1}$. A ratio of 4.7 was found for the combination/disproportionation ratio as ascertained through gas chromatographic analysis of the products.

Future efforts in our studies of vinyl radical chemistry will be to examine other rapid radical-radical reactions that are conceptually of importance in planetary atmospheres; e.g., its reaction with CH_3 radicals. The reactions will also be investigated over a wide range of temperature to permit the direct use of the kinetic information in atmospheric models and to permit improved mechanistic understanding, on a molecular level, of this important class of reactions.

REFERENCES

1. A. H. Laufer, Rev. Chem. Intermediates, 4, 225 (1981)
2. A. Fahr and A. H. Laufer, J. Phys. Chem., 92,7229 (1989) and references therein
3. A. H. Laufer, J. Chem. Phys., 73, 49 (1980)
4. H. Okabe, J. Chem. Phys., 78, 1312 (1983)
5. A. Fahr and A. H. Laufer, J. Photochem., 34, 261 (1986)
6. A. H. Laufer and Y. L . Yung, J. Phys. Chem. 87, 181 (1983)
7. A. Fahr and A. H. Laufer, J. Phys. Chem., 92, 7229 (1989)
8. I. R. Slagle, J.Y. Park, M.C. Heaven, D. Gutman, J. Am. Chem. Soc., 106,4356(1984); H. Krueger and E. Weitz, J. Chem. Phys., 88, 1608(1988)

N90-26767

DISSOCIATIVE RECOMBINATION OF MOLECULAR IONS WITH ELECTRONS

Rainer Johnsen, Dept. of Physics and Astronomy,
University of Pittsburgh, Pittsburgh, PA 15260

Abstract

I will present an overview of the present state of the art of laboratory measurements of the dissociative recombination of molecular ions with electrons. Most work has focussed on obtaining rates and their temperature dependence, as these are of primary interest for model calculations of ionospheres. A comparison of data obtained using the microwave afterglow method, the flowing afterglow technique, and the merged beam technique shows that generally the agreement is quite good, but there are some serious discrepancies, especially in the case of H_3^+ recombination, that need to be resolved. Results of some earlier experimental work need to be reexamined in the light of more recent developments. I intend to point out such cases and will present a compilation of rate coefficients that have withstood scrutiny.

Recent advances in experimental methods, such as the use of laser-induced fluorescence, make it possible to identify some neutral products of dissociative recombination. I will briefly review what has been done so far and what results one might expect from future work.

Recombination rates and their dependence on temperature.

Traditionally, much of the experimental work on dissociative electron-ion recombination, i.e. a process of the type $AB^+ + e \longrightarrow A + B$, has focussed on measurements of recombination rates and their dependence on electron temperature. Experimental techniques are either of the "swarm" type (microwave afterglow plasmas[1], flowing afterglow plasmas,[2] or shock tubes[3]) or they make use of single collision techniques (merged beams[4] and ion traps[5]). In most cases, the agreement of results obtained by different methods is fairly good, as may be seen in Table I which contains a substantial subset of known recombination coefficients. The, historically oldest, microwave-afterglow technique, developed by Biondi[1], has contributed possibly the largest data base, but it has been discovered recently that the heating of electrons by application of microwave fields can be complicated in presence of molecular additives in the plasma afterglow[6]. The remarks entered in Table I point out cases where some revisions may be required. In several instances, the complications have been taken into account adequately (e.g. NO^+, O_2^+) and the agreement among different methods is very good. A problem is likely to exist in the measurements of water and ammonia cluster ions. While no detailed calculations have been carried out, there is a strong suspicion that the observed lack of a variation of the recombination

coefficient with electron temperature was due to a strong reduction of the electron temperature resulting form inelastic collisions of electrons with water or ammonia molecules. The large 300 K values of α should be correct, however.

The history of the measurements of the H_3^+ recombination coefficient is rather complicated. A short time ago, it appeared to this author that the issue had been settled [7] and that the very small recombination rates found by the FALP technique [8] should be accepted, but new experimental data by Amano[9] seem to suggest that the recombination rates are not as small as the FALP data. Theoretical calculations [10] clearly support the small values. In view of the importance of the H_3^+ ion, more experimental work is needed to resolve the problem.

Table I. Experimental data on electron-ion recombination coefficients α (T). Temperature exponent x defined by $\alpha(T) = \alpha(300\ K)\ (T/300)^{-x}$. Abbreviations of experimental methods: mwa-ms - microwave afterglow-mass spectrometer. mwa- microwave afterglow. MB-merged beam. FALP- flowing-afterglow-Langmuir-probe. Trap-ion trap. Remarks. (A): no revisions required. (B): x is more likely to be about 0.5. (C): finding of x=0 may have been caused by lack of electron heating in the experiment. (D): Absolute value of a may be too high as a result of impurity ions in the afterglow. (E): α should be reduced by factor of two (Mitchell, private comm.). (F): Ions were vibrationally excited. (G): believed to refer to ions in v=o vibr. state.

Ion	α (300 K) [cm^3/s]	x	Temp. K	Method	Remarks	Ref.
NO^+	4.3 [-7]	0.38	300-4,600	mwa-ms		11
	4.2 [-7]	0.9	200-600	FALP		12
	2.3 [-7]	0.5	> 10,000	MB		13
	4.3 [-7]	0.85	300-5,000	trap		14
	4.4 [-7]	0.75	300-4,500	mwa-ms	(A)	15
N_2^+	1.8 [-7]	0.39	300-5,000	mwa-ms	(A)	16
	3.5 [-7]	0.5	300-10,000	MB	(E)	13
	2.2 [-7]	--	300	mwa-ms	(F)	17
	1.78 [-7]	0.37	700-200	shock tube		3

Table I continued

Ion	α (300 K) [cm³/s]	x	Temp. K	Method	Remarks	Ref.
O_2^+	1.95 [-7]	0.7	300-1200	mwa-ms	(A)	16
		0.56	1200-5,000	mwa-ms		
	1.95 [-7]	0.7	200-600	FALP		12
	1.95 [-7]	0.66	200-5,000	trap		14
	2.3 [-7]	0.5	300-10,000	MB		13
H_3^+	2.3 [-7]		300	mwa-ms	(D)	18
	1.7 [-7]	1.0	500-3000	mwa-ms	(D)	19
	~3.5 [-7]	0.5	0.01-0.7 eV	MB	(F)	20
	<2 [-8]	--	95 , 300	FALP	(G)	12
	1.8 [-7]	--		afterglow		
HCO^+	2.0 [-7]	1	300, 205	mwa-ms	(A)	21
	1.1 [-7]	~0.8	300, 95	FALP		8
	2.4 [-7]	0.69	293- 5500	mwa-ms	(A)	22
$H_3O^+\cdot(H_2O)$	2.5 [-6]	0.08	300-8000	mwa-ms	(C)	23
$H_3O^+\cdot(H_2O)_2$	3.0 [-6]	0.08	300-8000	mwa-ms	(C)	"
$H_3O^+\cdot(H_2O)_3$	3.6 [-6]	0	300-8000	mwa-ms	(C)	"
$H_3O^+\cdot(H_2O)_4$	~5 [-6]	0	300-8000	mwa-ms	(C)	"
$H_3O^+\cdot(H_2O)_5$	~5 [-6]	0	300-8000	mwa-ms	(C)	"
$NH_4^+\cdot(NH_3)$	2.82 [-6]	0.174	300-3000	mwa-ms	(C)	24
$NH_4^+\cdot(NH_3)_2$	2.68 [-6]	0 05	300-3000	mwa-ms	(C)	"
$NH_4^+\cdot(NH_3)_3$	~3 [-6]	0	200	mwa-ms	(C)	"
$NH_4^+\cdot(NH_3)_4$	~3 [-6]	0	200	mwa-ms	(C)	"
$N_2^+N_2$	1.4 [-6]	0.41	300-6000	mwa-ms	(B)	25
CO^+CO	1.3 [-6]	0.34	300-4000	mwa-ms	(B)	"
$CO.(CO)_2^+$	1.9 [-6]	~0	300-1000	mwa-ms	(B)	"
		0.33	1000-2000	mwa-ms	(B)	
$O_2^+O_2$	4.2 [-6]	0.48	143-5500	mwa-ms	(A)	26

Products of dissociative recombination

While the question of the rates of dissociative recombination can be regarded as reasonably well settled except for some important ions, the state of the art of determining the neutral products of dissociative recombination of polyatomic ions is far less well developed. Important progress has been made, especially by the Birmingham group who have developed laser-induced fluorscence techniques to quantitatively determine neutral products of dissociative recombination[27]. The technique has been successfully applied to the ion HCO_2^+. A similar experimental method, which also uses a flow tube, is presently being developed at the University of Pittsburgh. A related problem is that of determining the excited states of the neutral products of recombination of diatomic ions. Using vacuum uv absorption techniques, Rowe [28] has successfully detected metastable products of the recombination of N_2^+ and O_2^+.

It appears likely that we will see considerable further progress in the area of measuring neutral products of recombination, but such work is far more difficult than measuring rate coefficients. In order to take advantage of these developments for planetary atmosphere modelling, it will be important to identify ions that are relevant to planetary atmospheres, and to establish cooperations between experimentalists and modelers.

Acknowledgements: Work supported, in part by the NASA Planetary Atmospheres Program under Grants NGL 39-0110137 and NAGW-1764.

References

1 M.A. Biondi, in Applied Atomic Collision Physics, Vol. 3, Academic Press, New York 1982

2 D. Smith and N. G. Adams, in Physics of Ion-Ion and Electron-Ion Collision, F.Brouillard and J.W. McGowan eds., Plenum 1983

3 A.J. Cunningham and R.M. Hobson, J. Phys. B **5**, 2320 and 2328.(1972)

4 J.B.A. Mitchell, C.T. Ng, L. Forand, R. Janssen, and J.W. McGowan, J. Phys. B **17**, L909 (1984)

5 F.L. Walls and G.H. Dunn, J. Geophys. Res. **79**, 1911 (1974)

6 J.L. Dulaney, M.A. Biondi, and R. Johnsen, Phys. Rev. ,**A 34**. 3252 1986)

7 See discussion by R. Johnsen, Int. J. of Mass Spectrometry and Ion Physics **81**, 67 (1987)

8 N.G. Adams, D. Smith, and E. Alge, J. Chem. Phys., **81**, 1778 (1984)

9 T. Amano, Ap. J. **329**, L121, (1988)

10 H.H. Michels and R.J. Hobbs, Ap. J. Lett. **27** , L286(1984)
11 C. Huang, M.A. Biondi, and R. Johnsen, Phys. Rev, A **11**, 901 (1977)
12 E. Alge, N.G. Adams, and D. Smith, J. Phys. B **16**, 1433 (1983)
13 P.M. Mul, and J.W. McGowan, J. Phys. B, **12** 1591 (1972)
14 F.L. Walls and G.H. Dunn, J. Geophys. Res., **79**, 1911 (1974)
15 J.L. Dulaney, M.A. Biondi, and R. Johnsen, Phys. Rev. A, **36**, 1342 (1987)
16 F.J. Mehr and M.A. Biondi, Phys. Rev. **181**, 264 (1969)
17 E.C. Zipf, Geophys. Res. Lett. 4, 661 (1980)
18 M.T. Leu, M.A. Biondi, and R. Johnsen, Phys. Rev. A, **8**, 413 (1973)
19 J.A. Macdonald, M.A. Biondi, and R. Johnsen, Planet, Space Sci. **32**, 651 (1984)
20 J.B.A. Mitchell, C.T. Ng, L. Forand, R. Jannsen, and J.W. McGowan, J. Phys. B, **17** (1984)
21 M.T. Leu, M.A. Biondi, and R. Johnsen, Phys. Rev. A**8**, 420 (1973)
22 B. Ganguli, M.A. Biondi, R. Johnsen, and J.L. Dulaney, Phys. Rev. A **37**, 2543 (1988)
23 C.M. Huang, M. Whitaker, M.A. Biondi, and R. Johnsen, Phys. Rev. A **18**, 64 (1978)
24 C.M. Huang, , M.A. Biondi, and R. Johnsen, Phys. Rev. A **14**, 984 (1976)
25 M. Whitaker, M.A. Biondi, and R. Johnsen, Phys. Rev. A **24**, 743 (1981)
26 J.L. Dulaney, M.A. Biondi, and R. Johnsen, Phys. Rev. A, **37**, 2539 (1988)
27 N.G. Adams, C.R. Herd, and D. Smith, J. Chem. Phys. **91**, 963 (1989)
28 B.R. Rowe, in "Dissociative Recombination, Theory, Experiment and Applications", J.B. A. Mitchell and S.G. Guberman editors, World Scientific 1989

N90-26768

RATE CONSTANT FOR REACTION OF ATOMIC HYDROGEN WITH GERMANE

DAVID F. NAVA, WALTER A. PAYNE, GEORGE MARSTON AND LOUIS J. STIEF

Astrochemistry Branch, Laboratory for Extraterrestrial Physics
NASA/Goddard Space Flight Center, Greenbelt, Maryland 20771, U.S.A.

ABSTRACT

Due to the interest in the chemistry of germane in the atmospheres of Jupiter and Saturn, and because previously reported kinetic reaction rate studies at 298 K gave results differing by a factor of 200, we performed laboratory measurements to determine the reaction rate constant for $H + GeH_4$. Results of our study at 298 K, obtained via the direct technique of flash photolysis-resonance fluorescence, yield the reaction rate constant, $k = (4.08 \pm 0.22) \times 10^{-12}$ cm^3 s^{-1}.

INTRODUCTION

The possibility of detecting germane (GeH_4) in the reducing atmosphere of Jupiter by means of high resolution infra-red absorption spectroscopy was suggested by Corice and Fox[1] in 1972. Germane was subsequently identified as present in Jupiter's atmosphere by Fink et al.[2] It has also been recently reported by Noll et al.[3] as observed in the atmosphere of Saturn. Of particular note is the conclusion that GeH_4 is not the major reservoir of the total expected germanium in either planet. Thus studies of germanium-containing molecules to determine their photochemistry and reactions which may either produce or remove GeH_4 are of interest. One of these reactions to consider is that of $H + GeH_4$. Based on a correlation of activation energy vs. bond length for a series of H-atom abstraction reactions, a 298 K value of 1.3×10^{-11} cm^3 s^{-1} is predicted for the rate constant of this reaction. Previously reported studies[4,5] yielded results at 298 K of 2×10^{-12} cm^3 s^{-1} and 4×10^{-10} cm^3 s^{-1}, values differing by a factor of 200. Due to the interest in germanium chemistry in the atmospheres of the giant planets, and because of this discrepancy in the kinetic data, we have initiated a study to measure the reaction rate constant for $H + GeH_4$.

EXPERIMENTAL

The present kinetic experiments were performed by the direct technique of flash photolysis production of hydrogen atoms coupled with time-resolved resonance fluorescence detection and measurement of H-atom decay signal due to reaction with GeH_4. A schematic diagram of the apparatus is shown in Figure 1. Previous publications from this laboratory have described in detail the apparatus and experimental procedures employed as well as applications to atmospheric hydrogen atom reaction studies.[6-8]

Briefly, in the present study, flash photolysis of germane and methane highly diluted in argon was the source for production of atomic hydrogen. Methane was chosen as an additional H-atom source in most experiments to obtain sufficient initial signal intensity beyond that produced from the relatively low germane concentrations. In this study, the $[CH_4]$ ranged from 0 to 8.91×10^{15} cm^{-3}. The $[GeH_4]$ was $\sim 10^{13}$ cm^{-3} which is $\gg$ [H] $\ll$ 10^{11} atoms cm^{-3}. Thus, pseudo first-order conditions were achieved and the decay of H-atoms is represented by the equation:

$$\ln[H] = -k_{observed}t + \ln[H]_o.$$

The observed pseudo first-order decay constant is given by:

$$k_{observed} = k_1[GeH_4] + k_d$$

where k_1 is the effective bimolecular rate constant and k_d (measured under identical conditions as for the reaction experiments, except in the absence of GeH_4) is the first-order rate constant for diffusional loss of H-atoms from the reaction zone viewed by the photon detector.

RESULTS

Since [H] is proportional to fluorescent counts, $k_{observed}$ and k_d were determined from linear least-squares analysis of plots of the logarithm of accumulated fluorescent counts vs. time. The linearity of such plots, as illustrated in Figure 2, demonstrates that the measurements are representative of a first-order process. Experiments to determine the

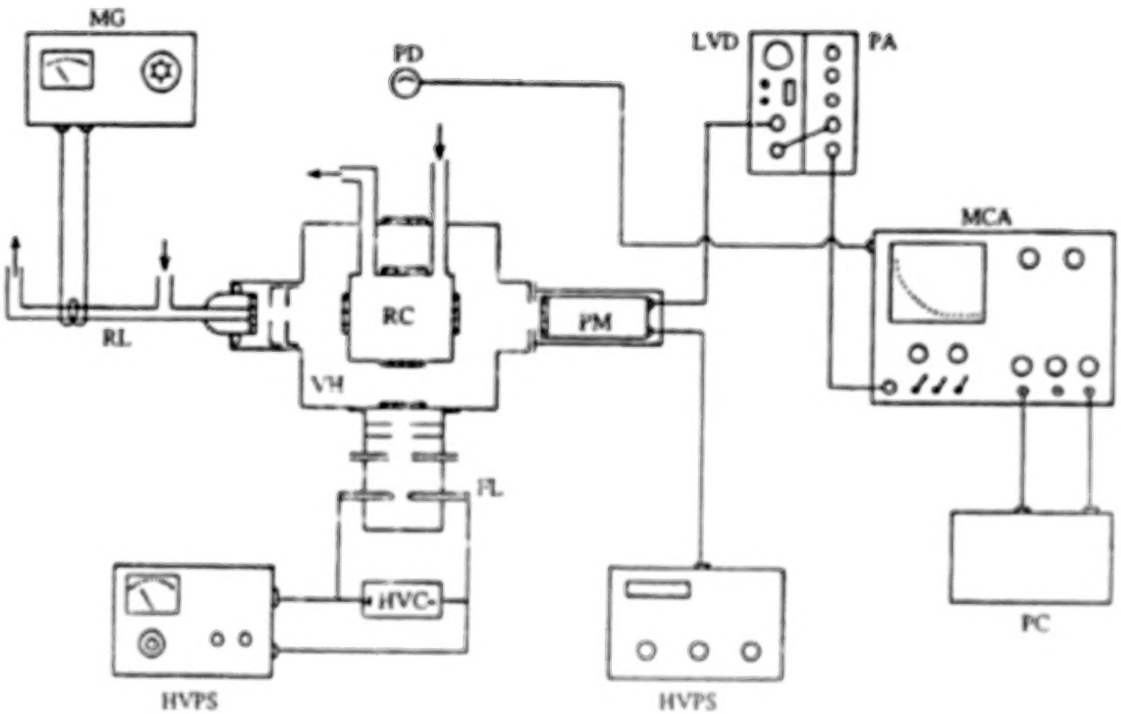

FLASH PHOTOLYSIS-RESONANCE FLUORESCENCE SYSTEM.
MG = MICROWAVE GENERATOR RL = RESONANCE LAMP RC = REACTION CELL
VH = EVACUATED OUTER CHAMBER FL = FLASH LAMP PM = PHOTOMULTIPLIER
PC = PERSONAL COMPUTER HVPS = HIGH VOLTAGE POWER SUPPLY PD = PHOTODIODE
HVC = HIGH VOLTAGE CAPACITOR LVD = LOW VOLTAGE DISCRIMINATOR
MCA = MULTICHANNEL ANALYZER PA = POWER AMPLIFIER
(RL, FL, AND PM are at right angles to each other)

Figure 1. SCHEMATIC OF THE FLASH PHOTOLYSIS-RESONANCE FLUORESCENCE APPARATUS

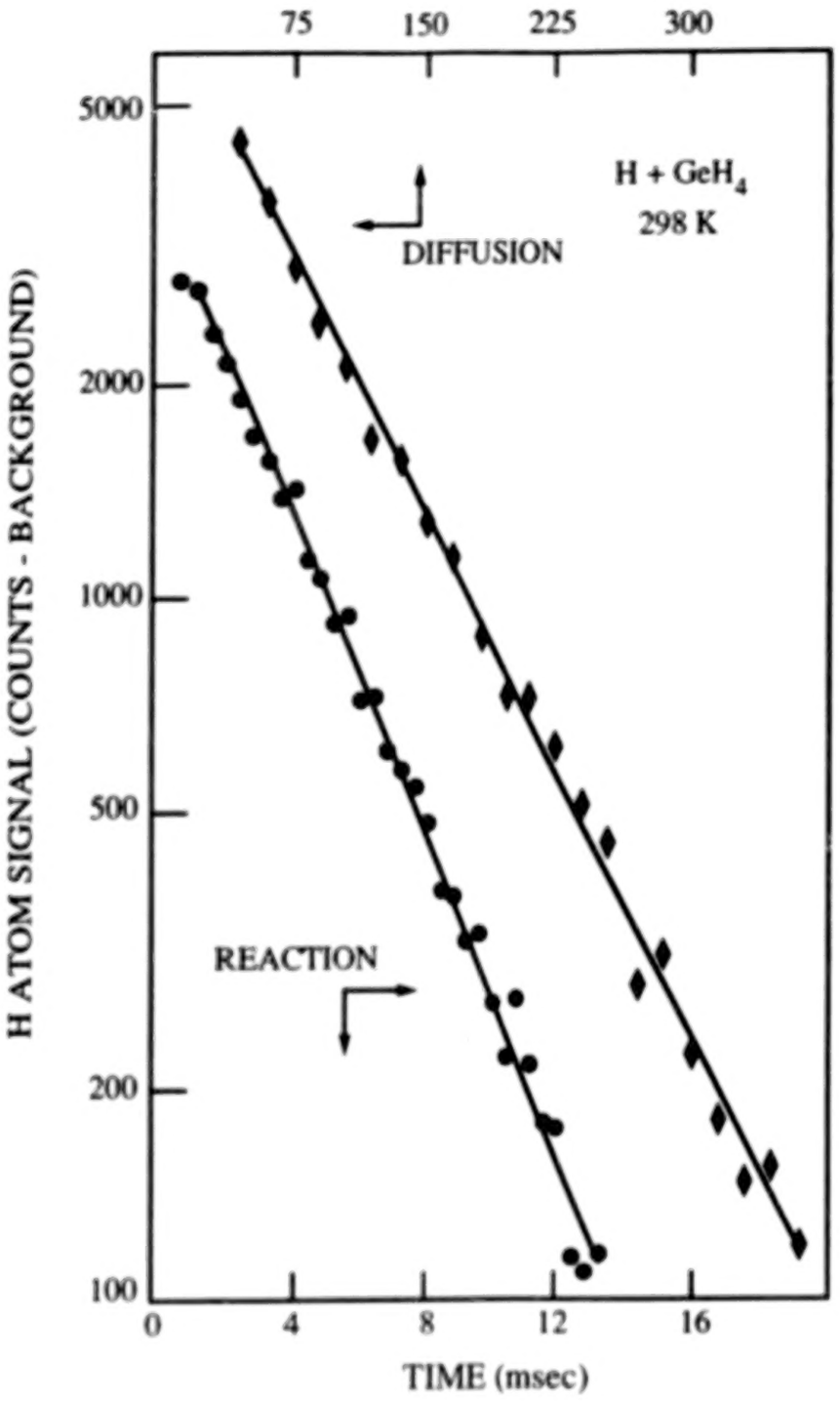

Figure 2. Examples of first-order decay plots of H atom diffusion and reaction at 298 K. The lines are determined from linear least-squares analysis of the data points.

reaction rate constant for H + GeH_4 were more difficult to perform than usual because, in most cases, the measured $k_{observed}$ values exhibit a positive dependence upon flash intensity. A modified experimental procedure was therefore necessary. Sets of experiments were performed as a function of flash intensity; each set at a fixed total pressure of reaction mixture (i.e., constant concentration of GeH_4). The intercept from the linear least-squares analysis of each pressure set plot of ($k_{observed} - k_d$) vs. flash energy yielded the resultant ($k_{observed} - k_d$) for the respective total pressure set of experiments. The minimum measured ($k_{observed} - k_d$) value (i.e., at the lowest flash energy) generally was not significantly different from the zero flash energy intercept. Results from the experiments are summarized in Table 1. The bimolecular reaction rate constant for H + GeH_4 was then obtained from the slope of the linear least-squares fit of this ($k_{observed} - k_d$) data plotted in Figure 3 vs. [GeH_4].

DISCUSSION

Results of our study of H + GeH_4 at 298 K yield the reaction rate constant, $k = (4.08 \pm 0.22) \times 10^{-12}$ cm^3 s^{-1}. The difficult nature of interpreting the kinetic behavior of this reaction may have led to the higher rate constant value previously reported by Choo et al.[5] The moderate reaction rate constant, which we obtained by our direct technique, is in reasonable agreement with the relative value reported by Austin and Lampe[4] and is within a factor of ~3 of that predicted from a correlation of activation energy vs. H-atom bond length. This moderate reaction rate constant warrants additional laboratory interest for its potential relevance regarding the atmospheres of Jupiter and Saturn. We are initiating a temperature dependence study in order to provide kinetic data more appropriate to the atmospheric temperatures of the giant planets.

Acknowledgment

This work was supported by the NASA Planetary Atmospheres Program.

Table 1: REACTION RATE DATA FOR H + GeH_4 AT 298 K

P_{TOTAL} (Torr)	[GeH_4] (10^{13} cm^{-3})	FLASH ENERGY (J)	# of DECAYS	$k_{obs} - k_d$ (s^{-1})
25	0.837	20 - 352	7	52.0
25	0.837	81 - 352	4	55.0
55	1.59	36 - 225	6	77.5
25	1.72	36 - 225	3	131
50	2.48	36 - 324	4	154
25	2.65	20 - 182	4	148
110	3.18	36 - 225	6	138
100	3.35	20 - 352	7	144
100	3.35	36 - 352	6	171
50	3.43	56, 81	2	149
50	4.19	20 - 182	4	202
75	5.15	56, 81	2	242
75	6.28	20 - 182	4	277
100	6.86	56, 81	2	325
150	7.44	36 - 81	3	323

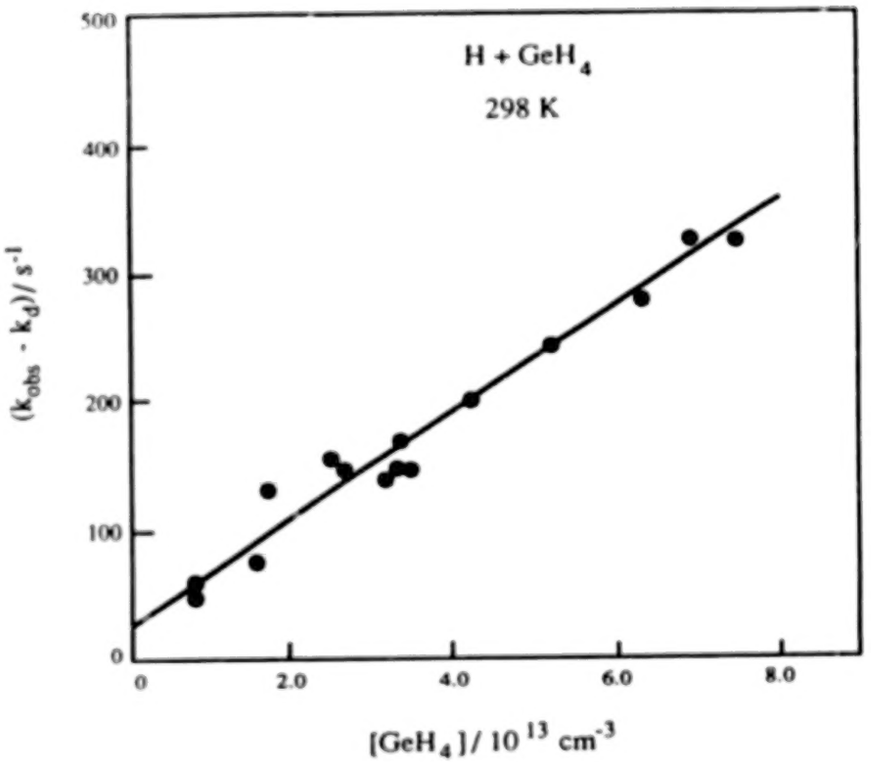

Figure 3. First-order decay constants vs. germane concentrations. The line is the linear least-squares fit of these data. The slope of this line is the reaction rate constant, k, for H + GeH_4 at 298 K.

References

[1] R. J. Corice, Jr., and K. Fox, Icarus 16, 388 (1972).
[2] U. Fink, H. P. Larson, and R. R. Treffers, Icarus 34, 344 (1978).
[3] K. S. Noll, R. F. Knacke, T. R. Geballe, and A. T. Tokunaga, Icarus 75, 409 (1988).
[4] E. R. Austin and F. W. Lampe, J. Phys. Chem. 81, 1134 (1977).
[5] K. Y. Choo, P. P. Gaspar, and A. P. Wolf, J. Phys. Chem. 79, 1752 (1975).
[6] J. H. Lee, J. V. Michael, W. A. Payne, D. A. Whytock, and L. J. Stief, J. Chem. Phys. 65, 3280 (1976).
[7] L. J. Stief, D. F. Nava, W. A. Payne, and J. V. Michael, J. Chem. Phys. 73, 2254 (1980).
[8] D. F. Nava, M. B. Mitchell, and L. J. Stief, J. Geophys. Res. 91, 4585 (1986).

N90-26769

ROLE OF THE METHYLENE AMIDOGEN (H_2CN) RADICAL IN THE ATMOSPHERES OF TITAN AND JUPITER

F. L. Nesbitt, G. Marston and L. J. Stief
Astrochemistry Branch, Laboratory for Extraterrestrial Physics
NASA/Goddard Space Flight Center
Greenbelt, Maryland 20771, U.S.A.

ABSTRACT

The methylene amidogen (H_2CN) radical can be shown to be an important intermediate in models for the formation of HCN (via $N + CH_3$) and the recombination of H to H_2 (via H + HCN) on Titan as well as in models for the formation of HCN (via $NH_2 + C_2H_3$) in the atmosphere of Jupiter. Experiments in our laboratory in a discharge flow system with mass spectrometric detection of both reactants and products have established that the major product channel (90%) for the reaction $N + CH_3$ is that leading to $H_2CN + H$. The same result was obtained for $N + CD_3 \rightarrow D_2CN + D$. We have also measured for the first time the rate constant for the reaction $D + D_2CN \rightarrow DCN + D_2$ and find $k(298\ K) > 7 \times 10^{-11}\ cm^3 s^{-1}$. The same result was obtained for the H atom reaction. This is the final step in the reaction sequence leading to HCN on both Titan and Jupiter and to formation of H_2 from H on Titan. We have also made the first measurement of the ionization potentials for H_2CN and D_2CN. From electron impact studies we obtain I.P. = (9.6+/-1.0) ev for both radicals. An upper limit of I.P. < 11.6 ev came from observations of the H_2CN radical by photoionization mass spectrometry using an Ar resonance lamp (106.7 nm). Further photoionization experiments are planned using synchrotron radiation plus monochromator as a tunable vacuum UV light source.

INTRODUCTION

The methylene amidogen (H_2CN) radical can be shown to be an important intermediate in models for the formation of HCN in the atmospheres of Titan and Jupiter and H atom recombination on Titan. Experiments in our laboratory have demonstrated that H_2CN is formed very efficiently by reaction (1)[1a].

$$N + CH_3 \rightarrow H_2CN + H \quad (90\%) \qquad (1a)$$
$$\rightarrow HCN + 2H \qquad (1b)$$
$$\rightarrow HCN + H_2 \qquad (1c)$$

Measurements were made of k_1 as a function of temperature from 200K to 423K[1b]. Reaction (1) was found to be very rapid and thus a good but limited laboratory source of H_2CN.

Very limited kinetic information is available for this radical. Only the reactions $H_2CN + H_2CN$ and $H_2CN + NO$ have been studied[2]. Therefore using reaction (1) as a source of H_2CN, we studied the reactions $N + H_2CN$ (D_2CN) (2) and (H/D) + D_2CN (3). The technique employed was discharge flow mass spectrometry at 1 Torr total pressure. Reaction (2) was studied over the temperature range 200K to 363K, whereas reaction (3) was studied at room temperature. Measurements were also made of the ionization potential for H_2CN and D_2CN.

EXPERIMENTAL

All experiments were performed in a pyrex flow tube 60 cm long and 28 mm in diameter. The flow tube was coupled via a two stage stainless steel collision-free sampling system to a quadrupole mass spectrometer (Extranuclear Laboratory Inc.). For reaction (2), N atoms and F atoms were admitted at the back of the flow tube and CH_4 or CD_4 was added through the sliding injector. For reaction (3), D_2CN was generated at the back of the flow tube by admitting N, F, and CD_4 through the sidearms, while H or D were added through the sliding injector.

RESULTS

Rate constants for reactions (2) and (3) were measured and these reactions were found to be efficient processes for the formation of HCN and DCN[3].

$$N + H_2CN \rightarrow NH + HCN \qquad (2)$$
$$N + D_2CN \rightarrow ND + DCN$$

Reaction (2) was studied at three temperatures and the following values (in units of $10^{-11} cm^3 s^{-1}$) were obtained: (3.9+/-2.2), 200K; (4.4+/-1.4), 298K; (6.7+/-2.0), 363K. Reaction (3)

$$H + D_2CN \rightarrow HD + DCN \qquad (3)$$
$$D + D_2CN \rightarrow D_2 + DCN$$

was studied at 298K and $k_3 > 7 \times 10^{-11}$ $cm^3 s^{-1}$. No isotope effect was observed for either reaction.

Ionization potentials were measured for H_2CN and D_2CN. The mass spectrometer was calibrated for NO and HCN. From the calibration runs it was found that I.P.(ev) = I.P.(measured) - 2.6. Figure 1 shows the uncorrected results for H_2CN and D_2CN. Applying the above correction, an ionization potential of (9.6+/-1.0) ev was obtained for H_2CN and D_2CN. Photoionization experiments were performed with an Argon lamp. H_2CN was readily detected thus suggesting I.P. < 11.6 ev. A theoretical calculation of the ionization potential of H_2CN yields the value 10.8 ev[4].

DISCUSSION AND CONCLUSION

Our results show that an important source of HCN in Titan's atmosphere is the sequence of reactions

$$N + CH_3 \rightarrow H_2CN + H \qquad (1)$$
$$H + H_2CN \rightarrow H_2 + HCN \qquad (3)$$

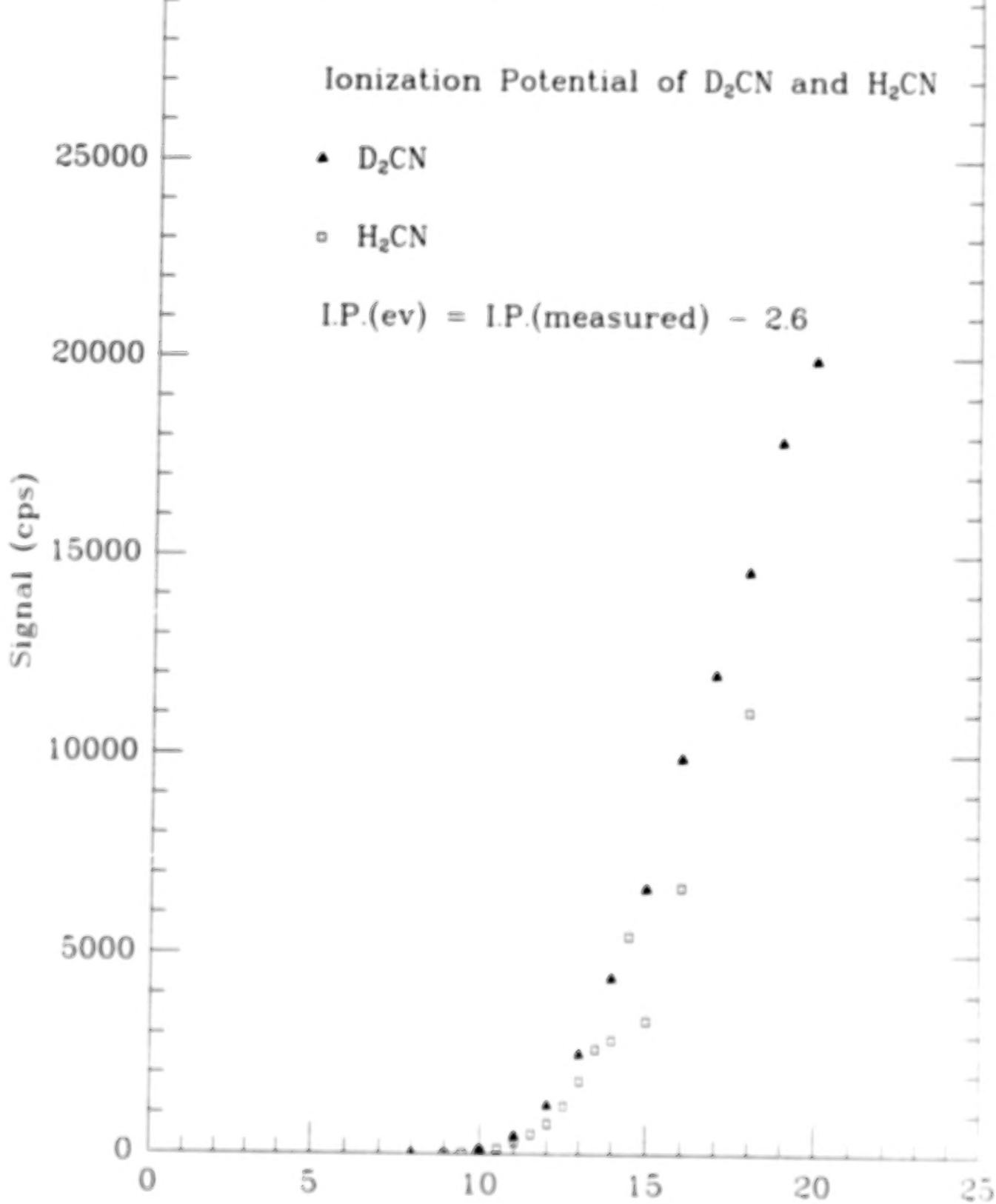

Figure 1: Electron volts (ev) uncorrected

Yung et al [5] have proposed that HCN can participate in the recombination of H on Titan by the reactions

$$H + HCN + M \rightarrow H_2CN + M \quad (4)$$

$$H + H_2CN \rightarrow HCN + H_2 \quad (3)$$

On Jupiter the coupled photochemistry of ammonia and acetylene has been proposed by Kaye and Strobel [6] to lead to the reaction

$$NH_2 + C_2H_3 \rightarrow C_2H_5N \quad (5)$$

The photolysis of the various isomers of C_2H_5N can lead to the following reactions

$$C_2H_5N \rightarrow HCN + CH_3 + H \quad (6)$$

$$\rightarrow H_2CN + CH_3 \quad (7)$$

Subsequent reaction of H_2CN with H yields HCN.

Our results provide the quantitative information needed for modelers to determine altitude profiles for H_2CN, HCN and subsequent nitrile compounds in Titan's atmosphere. These results may have important implications for modelers and instrument designers in selecting experiments to study the chemical composition of Titan's atmosphere in the upcoming Cassini mission.

References

1a. Marston, G., Nesbitt, F.L. and Stief, L.J., J. Chem. Phys. 1989, 91,3481.

1b. Marston, G., Nesbitt, F.L., Nava, D.F., Payne, W.A. and Stief, L.J., J. Phys. Chem. 1989, 93, 5769.

2. Horne, D. G., Norrish, R.G.W., Proc. Roy. Soc. (Lond.) 1970.A315,301.

3. Nesbitt, F. L., Marston, G. and Stief, L.J., J. Phys. Chem., Submitted for publication.

4. Zahradnik, R., Carsky, P., Theoret. Chim. Acta (Berlin), 1972, 27, 121.

5. Yung, Y. L., Allen, M.A. and Pinto, J.P., Astrophys. J. Suppl. Ser. 1984, 55, 465.

6. Kaye, J. A., Strobel, D. F., Icarus, 1983, 54, 4176.

N90-26770

LABORATORY MEASUREMENTS AND METHANE PHOTOCHEMISTRY MODELING

P. N. Romani†

Science Systems and Applications Inc., 7375 Executive Place, Suite 300, Seabrook, MD 20706

†Author's mailing address:

Mail Code 693.2, NASA/Goddard Space Flight Center, Greenbelt, MD 20771

ABSTRACT

Methane is photolyzed by the solar UV in the stratosphere of Saturn. Subsequent photochemistry leads to the production of acetylene (C_2H_2) and diacetylene (C_4H_2). These species are produced where it is relatively warm (T ≥ 140K), but the tropopause temperature of Saturn (≈80K) is low enough that these two species may freeze out to their respective ices. Numerical models which include both photochemistry and condensation loss make predictions about the mixing ratios of these species and haze production rates. These models are dependent upon knowing reaction pathways and their associated kinetic reaction rate constants and vapor pressures. How uncertainties in the chemistry and improvements in the vapor pressures affect model predictions for Saturn are discussed.

PHOTOCHEMISTRY

Acetylene (C_2H_2) is produced from the photolysis of methane (CH_4) in the stratosphere of Saturn by the solar UV and subsequent photochemistry. The sink for C_2H_2 is either transport downward, condensation in the lower stratosphere (to its ice), or photolysis;

$$C_2H_2 + h\nu \longrightarrow C_2H + H \quad (1)$$

$$\longrightarrow C_2 + H_2 \quad (2)$$

C_2H either recycles C_2H_2;

$$C_2H + CH_4 \longrightarrow C_2H_2 + CH_3 \quad (3)$$

$$C_2H + H_2 \longrightarrow C_2H_2 + C_2H_3 \quad (4)$$

$$C_2H + C_2H_6 \longrightarrow C_2H_2 + C_2H_5 \quad (5)$$

or makes diacetylene (C_4H_2);

$$C_2H + C_2H_2 \longrightarrow C_4H_2 + H \quad (6)$$

which condenses out in the lower stratosphere (also to its ice).

Reaction rates for (3) - (6) have been measured only at room temperature, while the temperature range in the region of interest in the stratosphere of Saturn is $80 < T < 150K$. The extrapolation of the reaction rates to lower temperatures can be done using the Arrhenius equation;

$$A \cdot \exp[- \Delta E / (R \cdot T)] \quad (7)$$

where A is the frequency factor and ΔE is the activation energy. Either A or ΔE can be calculated from theory. Then from the measured room temperature reaction rate, the other term can be deduced. Calculating ΔE from BSBL theory and then deriving A produces rate constants of (cm^3 $molecules^{-1}$ sec^{-1});[1]

$$C_2H - H_2 \quad k = 5.7 \times 10^{-11} \exp(-1762 / T) \quad (8)$$

$$C_2H - CH_4 \quad k = 6.5 \times 10^{-12} \exp(-503 / T) \quad (9)$$

$$C_2H - C_2H_6 \quad k = 1.8 \times 10^{-11} \exp(-302 / T) \quad (10)$$

(Set 1). Calculating A from BEBO theory and then deriving ΔE yields the following different rate constants;[1]

$$C_2H - H_2 \quad k = 1.9 \times 10^{-11} \exp(-1460 / T) \quad (11)$$

$$C_2H - CH_4 \quad k = 3.1 \times 10^{-12} \exp(-252 / T) \quad (12)$$

$$C_2H - C_2H_6 \quad k = 6.9 \times 10^{-12} \quad (13)$$

(Set 2). This is the same as used by Allen and Pinto in modeling Titan photochemistry.[2] Using Set 2 leads to less C_4H_2 production and more C_2H_2 recycling than using Set 1. Recently, Stephans et al. measured the reaction rates of $C_2H - H_2$ and $C_2H - C_2H_2$.[3] Their rates are 3 and 5 times the rates

reported by Laufer and Bass.[4] Note, however, that Laufer and Bass measured the appearance of products (C_2H_2 and C_4H_2) while Stephans measured the disappearance of C_2H (a reactant).

The fate of the C_2 produced in (2) is uncertain;

$$C_2 + H_2 \longrightarrow C_2H + H \qquad (14)$$

$$C_2 + CH_4 \longrightarrow C_2H + CH_3 \quad a \qquad (15a)$$

$$\longrightarrow C_2H_2 + {}^1CH_2 \quad b \qquad (15b)$$

Even though $[CH_4] \ll [H_2]$ in the stratosphere of Saturn, the reaction rate with CH_4 is fast enough to overcome the relative abundance difference. These two reactions have been measured only at room temperature and above.[5,6]

VAPOR PRESSURES

Previously, the lowest temperatures at which the vapor pressures of C_4H_2 and C_2H_2 had been measured were 190K and 98K respectively. The new vapor pressure measurements by Masterson et al., have extended this to 127K and 80K for diacetylene and acetylene respectively.[7] This has removed the need for extrapolating the C_2H_2 vapor pressure, and reduced the temperature range of extrapolation for C_4H_2 from 110K to 47K. The analysis of the this new vapor pressure data is not yet complete, however.

DISCUSSION

The C_2H_2 mixing ratio from the photochemical model is compared to its saturation mixing ratio (from the data of Masterson et al.[7]) in Figure 1. The lower boundary condition is downward transport with the maximum possible velocity. Lowering the downward transport velocity increases the C_2H_2 mixing ratio at the tropopause and thus increases the supersaturation and the likelihood of condensation. Extrapolation of the previous vapor pressure data resulted in higher vapor pressures and the model would have predicted no possible condensation. The chemical production rate of acetylene in the model is on the order of 6.5×10^8 molecules cm^{-2} sec^{-1}, or 3×10^{-14} grams cm^{-2} sec^{-1}, capable of dominating the haze production rate (Table 1.). However, the

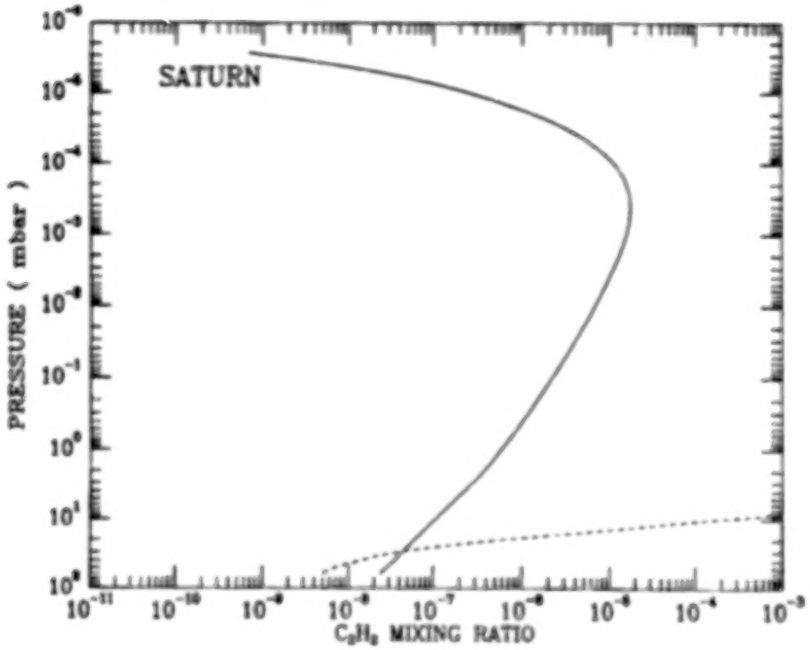

Figure 1 - Acetylene mixing ratio vs. pressure in the stratosphere of Saturn. Solid line is from the photochemical model, dashed line is maximum mixing ratio from saturation vapor pressure data of Masterson et al.[7]

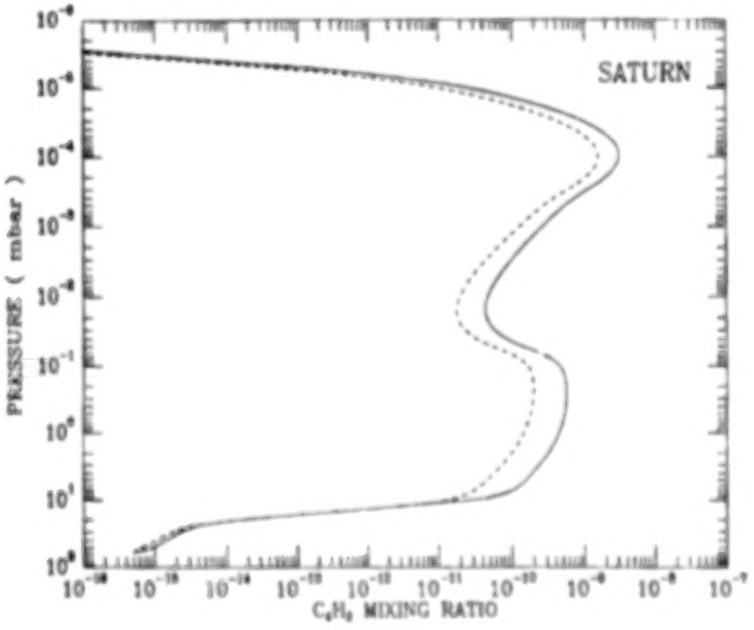

Figure 2 - Diacetylene mixing ratio vs. pressure in the stratosphere of Saturn. Solid line is for Set 1 C_2H reaction rates, dashed line Set 2 reaction rates, both assume (a) pathway for $C_2 + CH_4$. Rapid decrease in mixing ratio for pressures greater than 10 mbar is due to condensation.

TABLE I

DIACETYLENE HAZE LOCATION AND PRODUCTION RATES

CHEMISTRY	T	P	#	grams
a pathway for $C_2 + CH_4$ Set 1 C_2H reaction rates	103.0	11.0	1.3×10^{7}	1.9×10^{-15}
b pathway for $C_2 + CH_4$ Set 1 C_2H reaction rates	103.0	11.0	4.8×10^{6}	4.0×10^{-16}
a pathway for $C_2 + CH_4$ Set 2 C_2H reaction rates	100.0	12.0	1.8×10^{6}	1.5×10^{-16}
b pathway for $C_2 + CH_4$ Set 2 C_2H reaction rates	100.0	12.0	6.7×10^{5}	5.5×10^{-17}

T - Temperature in degrees Kelvin at which C_4H_2 begins to condense

P - Pressure in mbar at which C_4H_2 begins to condense

- Column production rate of C_4H_2 haze in molecules cm^{-2} sec^{-1}

grams - Column production rate of C_4H_2 haze in grams cm^{-2} sec^{-1}

supersaturation with the maximum downward velocity case is ≈ 4 and may not be enough to initiate condensation.

Changes in the C_4H_2 mixing ratio due to changes in the C_2H reaction rates are shown in Figure 2. Similar effects are seen with changes in the C_2 + CH_4 pathway with the (a) pathway producing the larger C_4H_2 mixing ratios. As can be seen in Table I, uncertainties in the chemistry cause more than an order of magnitude variation in the predicted C_4H_2 haze production rate.

Measurements of the C_2H and C_2 reaction rates at lower temperatures are needed to improve model predictions. Secondarily the products of the C_2 + CH_4 reaction should be identified. Improved C_2H_2 vapor pressures have shown that C_2H_2 is now a possible source of the observed stratospheric haze on Saturn. C_4H_2 is a probable source, whose importance could be better constrained with better knowledge of the chemistry and vapor pressure measurements at lower temperatures (the C_4H_2 vapor pressure is still being extrapolated over 50K).

REFERENCES

[1]R. L. Brown and A. H. Laufer, J. Phys. Chem. **85**, 3826 (1981).

[2]Y. Yung, M. Allen, and J. Pinto, Ap. J. Supp. **55**, 564 (1984).

[3]J. W. Stephans, J. L. Hall, H. Solka, W.-B. Yan, R. F. Curl, and G. P. Glass, J. Phys. Chem. **91,** 5740 (1987).

[4]A. H. Laufer and A. M. Bass, J. Phys. Chem. **83**, 310 (1979).

[5]L. Pasternack and J. R. McDonald, Chem. Physics **43**, 173 (1979).

[6]W. M. Pitts, L. Pasternack, and J. R. McDonald, Chem. Physics **68**, 417 (1982).

[7]C. Masterson, J. Allen, G. Kraus, R. Khanna, in prep. (1989).

ACKNOWLEDGEMENTS

I am deeply indebted to L. Stief, J. E. Allen, C. Masterson, and R. Khanna for assistance in understanding laboratory data. I am supported at NASA Goddard Space Flight Center, Greenbelt, Maryland, by NASA contract NAS5-30134.

N90-26771

UV AND VUV SPECTROSCOPY AND PHOTOCHEMISTRY OF SMALL MOLECULES IN A SUPERSONIC JET

E. RÜHL* AND V. VAIDA

Department of Chemistry and Biochemistry, University of Colorado, Boulder, CO 80309
*permanent address: Institut für Physikalische und Theoretische Chemie, Freie Universität Berlin, Takustr. 3, D-1000 Berlin 33, Federal Republic of Germany.

ABSTRACT

UV and VUV absorption and emission spectroscopy is used to probe jet cooled molecules, free radicals, and clusters in the gas phase. Due to efficient cooling inhomogeneous effects on spectral line widths are eliminated. Therefore from these spectra, both structural and dynamical information is obtained. The photoproducts of these reactions are probed by resonance enhanced multiphoton ionization.

INTRODUCTION

In the last years an experimental research program has been developed in our laboratory which allows study of reactive small molecules, radicals, and their molecular aggregates. This program employs a combination of supersonic molecular beams for sample preparation with spectroscopic and photofragment techniques, used to characterize these reactive species.

RESULTS AND DISCUSSION

Jet cooled molecules such as NH_3, CS_2, OCS, and CH_3I have been studied during the last years by vacuum UV spectroscopy. [1-3] These improved spectra provided structural and dynamical models for the excited states of these small reactive molecules. Besides absorption features known for the isolated molecules, new absorption bands have been observed at high stagnation pressure. These bands have been assigned as dimer absorption bands. The experimental scope has been extended recently to high resolution UV spectroscopy in order to understand monomolecular reaction dynamics of photoreactive systems. This is accomplished

by using a Fourier transform spectrometer (FTS) with a free jet expansion. Compared to the best conventional free jet absorption technique,[1] the FTS offers a 15 times greater sensitivity and two orders of magnitude better spectral resolution. This technique has been applied to study reactive electronic states of chlorine dioxide (OClO).[4] Upon electronic excitation ($\tilde{A}(^2A_2) \leftarrow \tilde{X}(^2B_1)$, 260-480 nm) OClO predissociates into the fragments ClO + O. With rotational cooling in a supersonic expansion spectral congestion due to inhomogeneous effects can be reduced substantially. From the rotational envelopes of the vibrational bands a rapid increase in the line widths is observed as the energy of the transition is increased. Figure 1 shows a portion of the jet cooled ($\tilde{A}(^2A_2) \leftarrow \tilde{X}(^2B_1)$ absorption band of chlorine dioxide. The splittings in each band are caused by the ^{35}Cl and ^{37}Cl isotopes.

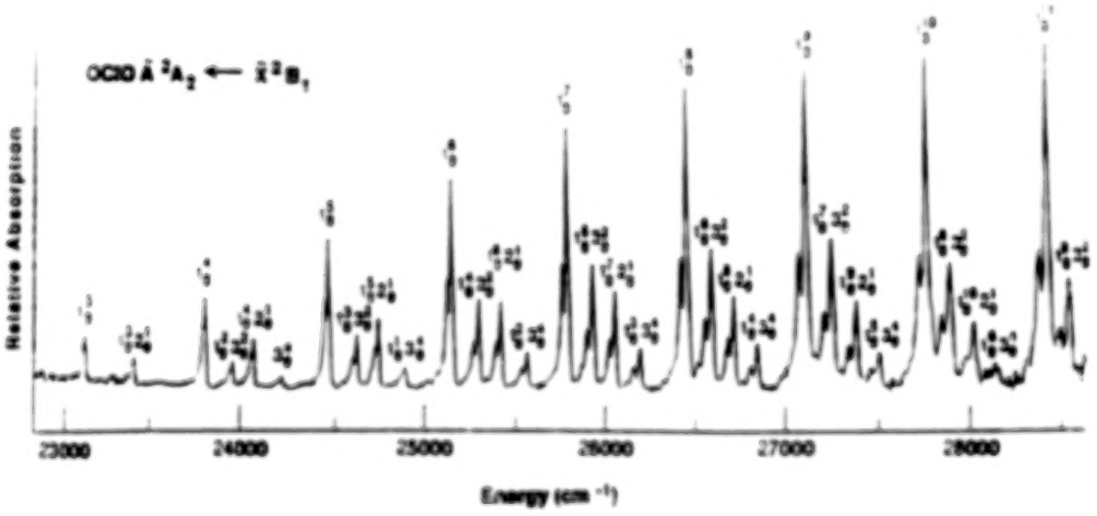

Figure 1: Portion of the jet cooled absorption spectrum of chlorine dioxide. Recorded at $5cm^{-1}$ resolution and 2 atm total stagnation pressure (3% OClO in He).

The Fourier transform technique can be also used for emission spectroscopy. This has been demonstrated for emission of jet cooled CN($B\ ^2\Sigma$) radicals.[5] The spectroscopic sample is formed in a continuous corona discharge. The B→X emission spectrum of CN is shown in Figure 2. The advantage of the corona discharge radical source is that high vibrationally excited levels can be studied in a relatively uncongested rotationally cold spectrum.[6] From the spectrum a vibrational temperature of 2200 K and a rotational temperature of 75 K has been deduced. New and more accurate rotational constants for the CN B-state have been obtained by the use of K values up to 62.

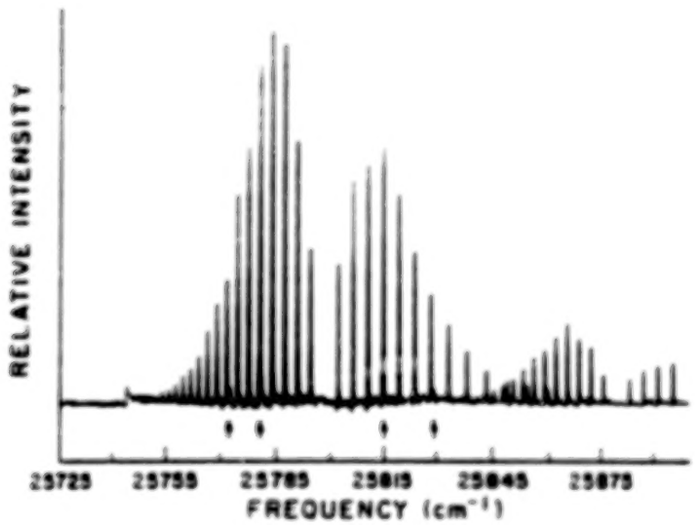

Figure 2: CN (B→X) emission spectrum recorded at 0.25 cm^{-1} spectral resolution under stagnation conditions of 0.13 atm CH_3CN in 1 atm He. The spectrum includes both the 0-0 and 1-1 transitions. Arrows indicate perturbations from A-state rotational levels.

Besides spectroscopic probes we have employed mass spectrometry to analyze the products of reactive electronic states of jet cooled molecules. The technique used is resonance enhanced multiphoton ionization (REMPI). Chlorine dioxide has been studied in the spectral regime of ($\tilde{A}(^2A_2)$←$\tilde{X}(^2B_1)$ transition.[7] The main products of the above mentioned predissociation is ClO + O. Chlorine oxide is probed in a (2+2) REMPI process, in which the $C(^2\Sigma)$←$(^2\Pi)$ is accessed (see Figure 3a). All REMPI bands observed are due to vibrationally excited ClO ($X(^2\Pi)$(v=3-6)). The rotational profiles of the REMPI bands corresponds to a thermal Boltzmann population with T=100 K. At higher photon energy (around 340 nm) additional rotational fine structure of vibrationally excited ClO ($A(^2\Pi)$←$X(^2\Pi)$) occurs in the REMPI spectrum of ClO^+. Besides predissociation of OClO we find evidence for photoisomerization of OClO ($\tilde{A}(^2A_2)$). A single resonance in the Cl^+ REMPI signal occurs at 362 nm (see Figure 3b). This agrees with matrix work on chlorine dioxide, where around 365 nm photoisomerization into ClOO was observed.[8]

Due to its low binding energy ClOO decays into Cl + O_2. Because of the low multiphoton ionization cross section of molecular oxygen we observe only a Cl^+ REMPI signal which suggests photoisomerization. We have recently discussed the potential importance of OClO photoisomerization with respect to polar ozone depletion.[9]

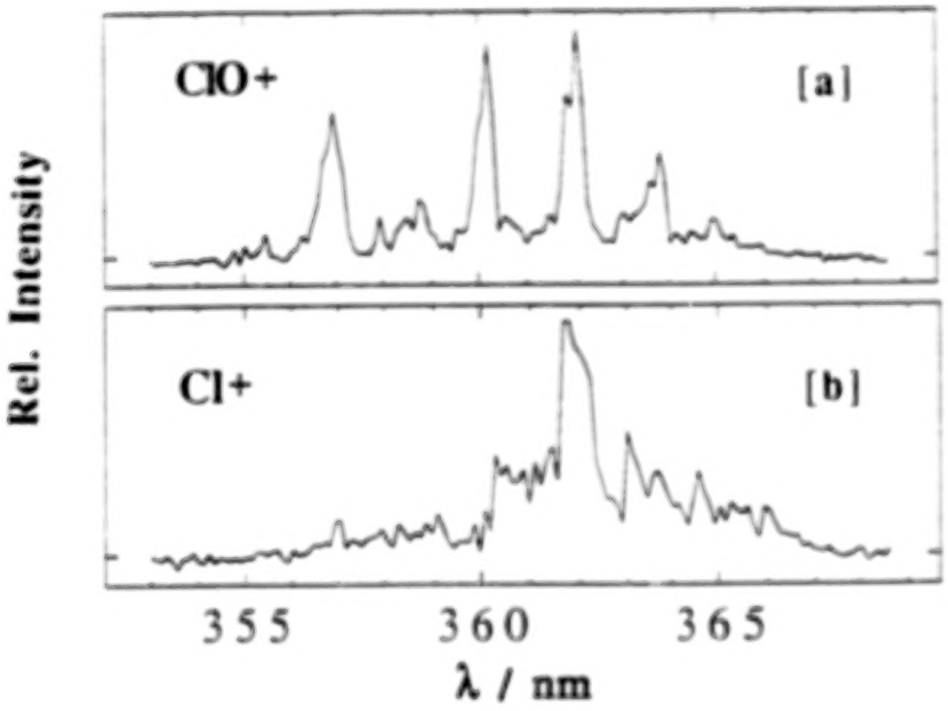

Figure 3: Resonance enhanced multiphoton ionization (REMPI) spectrum of ClO^+ [a], and Cl^+ [b] between 353 and 369 nm.

Currently we are extending our research program to small predissociating molecules which are of interest for planetary atmospheres, such as HCN, H_2S, and H_2O. We are also interested in the spectroscopy and photoreactivity of homogeneous and heterogeneous clusters of these species. Because cluster formation is enhanced at low temperatures, their photoreactivity might be important to understanding the chemistry of the atmospheres of outer planets.

ACKNOWLEDGEMENTS

This work is supported the National Science Foundation and Petroleum Research Fund. E.R. acknowledges financial support by Deutsche Forschungsgemeinschaft.

REFERENCES

1 V. Vaida, Acc. Chem. Res. **19**, 114 (1986)

2 V. Vaida, M.I. McCarthy, P.C. Engelking, P. Rosmus, H.J. Werner, and P. Botschwina, J. Chem. Phys. **86**, 6669 (1987); P. Rosmus, P. Botschwina, H.J. Werner, V. Vaida, and P.C. Engelking, J. Chem. Phys. **86**, 6677 (1987); M.I. McCarthy, P. Rosmus, H.J. Werner, P. Botschwina, and V. Vaida, J. Chem. Phys. **86**, 6693 (1987).

3 V. Vaida, D.J. Donaldson, S.P. Sapers, R. Naaman, and M.S. Child, J. Phys. Chem. **93**, 513 (1989).

4 E.C. Richard, C.T. Wickham-Jones, and V. Vaida, J. Phys. Chem. **93**, 6346 (1989).

5 E.C. Richard, D.J. Donaldson, and V. Vaida, Chem. Phys. Lett., **157**, 295 (1989).

6 P.C. Engelking, Rev. Sci. Instr. **57**, 2274 (1986).

7 E. Rühl, A. Jefferson, and V. Vaida, J. Phys. Chem., submitted (1989).

8 A. Arkell and I. Schwager, J. Am. Chem. Soc. **89**, 5999 (1967).

9 V. Vaida, S. Solomon, E.C. Richard, E. Rühl, and A. Jefferson, Nature, in press (1989).

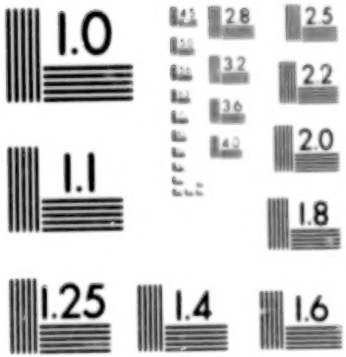

MICROCOPY RESOLUTION TEST CHART
NATIONAL BUREAU OF STANDARDS
STANDARD REFERENCE MATERIAL 1010a
(ANSI and ISO TEST CHART No 2)

N90-26772

LABORATORY STUDIES OF PHOTODISSOCIATION PROCESSES RELEVANT TO THE FORMATION OF COMETARY RADICALS

R.S. URDAHL, Y. BAO, AND W.M. JACKSON
Department of Chemistry, University of California, Davis, CA 95616

The strength of the $C_2(d^3\Pi_g \rightarrow a^3\Pi_u)$ Swan band emission in the spectra of cometary comae identifies this species as a prominent constituent of the coma gas, although its photochemical origin remains yet uncertain. It was previously suggested[1] that the formation of cometary C_2 proceeds via the secondary photolysis of the C_2H radical, which is itself generated by dissociation of the stable acetylene molecule. The detection of C_2H in the interstellar medium[2] and the recent analysis of the radial variation in $C_2(\Delta V=0)$ surface brightness of Comet Halley[3] support the postulate that C_2 is a third-generation molecule. Although these astrophysical observations provide evidence for the proposed two-step dissociation process, laboratory verification of the mechanism is currently incomplete.

Measurement of the C_2 and C_2H translational energy distributions produced from the multiphoton dissociation (MPD) of acetylene at 193nm[4] identifies the primary processes to be:

$$C_2H_2(X^1\Sigma_g^+) + h\nu_{193nm} \text{ ----> } C_2H(X^2\Sigma^+, A^2\Pi) + H(^2S) \quad (1)$$

$$C_2H(X^2\Sigma^+, A^2\Pi) + h\nu_{193nm} \text{ ----> } C_2(X^1\Sigma_g^+, a^3\Pi_u, A^1\Pi_u) + H(^2S) \quad (2)$$

Time-resolved FTIR emission studies of the nascent C_2H radical formed in reaction (1)[5] verify that this species is produced both vibrationally and electronically excited. A survey of the internal energy distributions of the C_2 fragments produced from the MPD of acetylene using a high intensity ArF laser is currently in progress in this laboratory. Previous results using the techniques of laser-induced fluorescence (LIF) and time-resolved emission[6] allowed estimation of nascent radical concentrations, with $[C_2(A^1\Pi_u)] >> [C_2(C^1\Pi_g)]$, $[C_2(a^3\Pi_u)] > [C_2(d^3\Pi_g)]$, and $[C_2(a^3\Pi_u)] \simeq [C_2(A^1\Pi_u)]$.

Recent experiments have focused on the measurement of rotational energy distributions for the $C_2(A^1\Pi_u, a^3\Pi_u)$ fragments. Figure 1 illustrates the distribution of rotational energies for the nascent $C_2(A^1\Pi_u)$ fragment produced during the MPD of various C_2H precursors. The distributions can each be fit using low and high temperature components, which implies the dissociation of C_2H occurs through a statistical process such as predissociation or internal conversion to the ground state continuum. The rotational energy distribution of nascent $C_2(a^3\Pi_u)$ from the MPD of acetylene is shown in Figure 2. Although the fit to a single temperature is fair, there is some indication of a low temperature component in the region of low rotational energies. Since the measurement of this distribution requires the use of low gas

PRECEDING PAGE BLANK NOT FILMED

C-4

pressures and short pump/probe delay times, interference from $C_2(d^3\Pi_g \rightarrow a^3\Pi_u)$ emission limits the achievable signal to noise ratio. We are currently trying to improve our $C_2(a^3\Pi_u)$ detection capability by performing this experiment in a molecular beam, thus allowing for discrimination between initial emission and LIF.

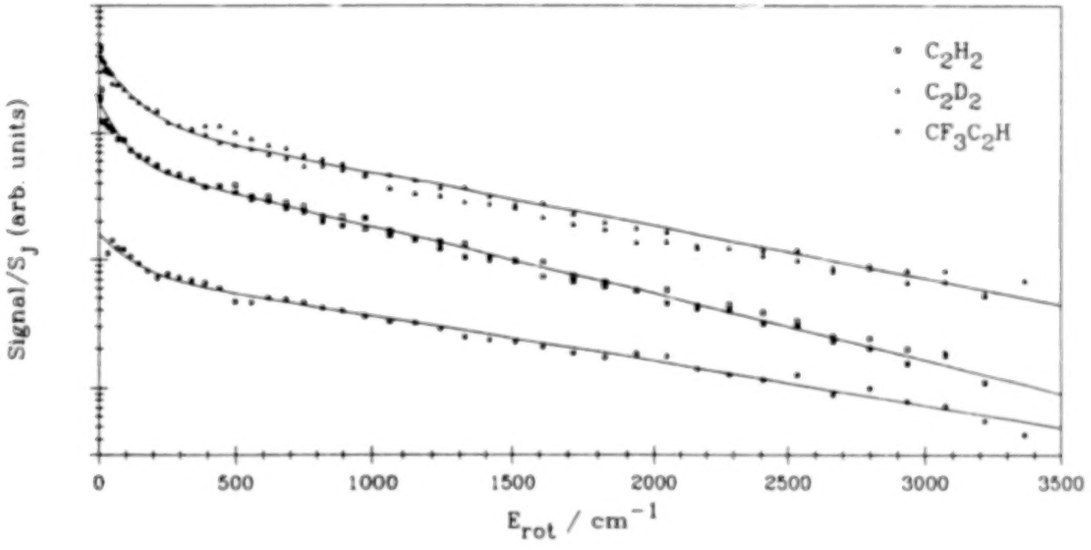

Figure 1. Rotational energy distributions for nascent $C_2(A^1\Pi_u, v''=0)$ formed in the photolysis of various C_2H precursors. The solid curves are fit to the temperature pairs of 100K+1200K, 150K+1500K, and 150K+1800K for C_2H_2, C_2D_2, and CF_3C_2H, respectively.

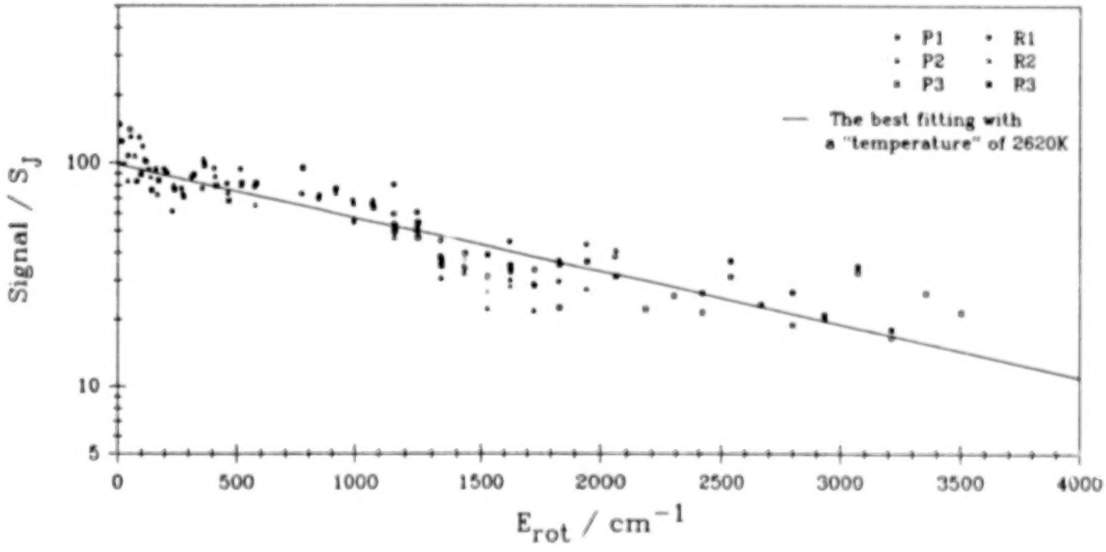

Figure 2. Rotational energy distribution for nascent $C_2(a^3\Pi_u, v''=0)$ formed in the photolysis of C_2H_2.

A portion of the two-photon laser excitation spectrum of $C_2(X^1\Sigma_g^+)$ is shown in Figure 3. Since the signal was only observable after the inclusion of a buffer gas, it appears that $C_2(X^1\Sigma_g^+)$ is not formed appreciably during the initial dissociation process but rather as a result of radiative and collisional quenching of the $A^1\Pi_u$ and $a^3\Pi_u$ primary fragments.

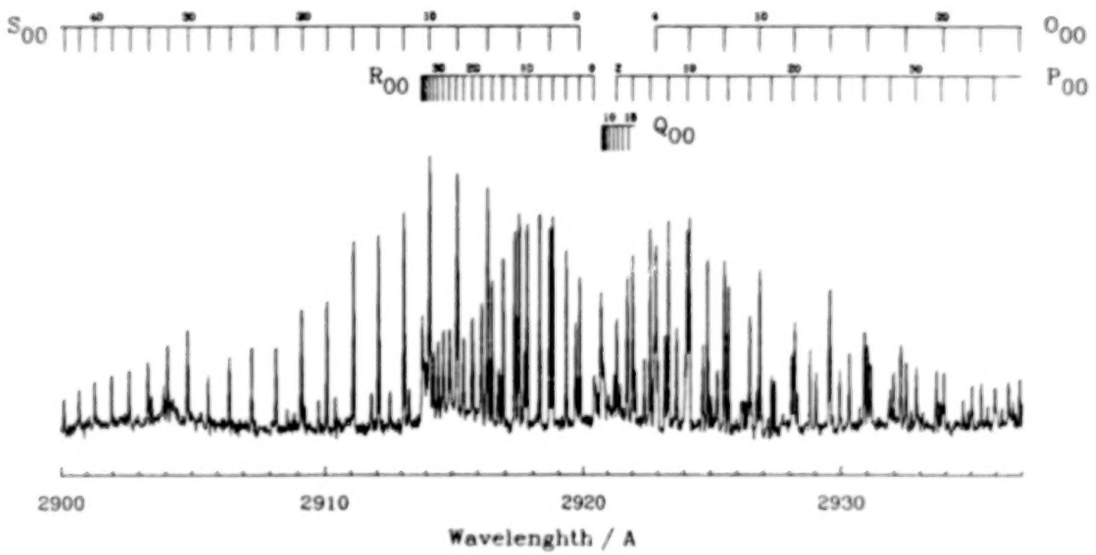

Figure 3. Two-photon laser excitation spectrum of $C_2(X^1\Sigma_g^+)$ produced in the MPD of C_2H_2 at 193nm, observed at a delay of 2μs (100mtorr C_2H_2, 10torr Ar).

Another class of experiments being performed considers the mechanism and dynamics of CH and C_3 formation during the photodissociation of allene with a focused ArF laser. The laser excitation spectra of $CH(X^2\Pi)$ and $C_3(X^1\Sigma_g^+)$ given in Figures 4 and 5 verify the production of these cometary radicals, but give little insight into whether they are formed by primary or secondary dissociation processes. Again, the extraction of this information may be possible through the use of a molecular beam, since the possibility of forming a product by collisional processes is minimized.

Although the experiments performed to date provide considerable evidence in support of reaction (2), there is an important distinction to be made when comparing the laboratory conditions to those typically found in comets. Since the C_2H radicals generated in the laboratory experiments are formed vibrationally and/or electronically excited, the theoretical calculations of Shih et al.[7] predict 193nm vertical excitation of the bent(115°) $C_2H(1^2A' \rightarrow 2^2A'')$ transition. Alternatively, any rotationally/vibrationally excited C_2H present in cometary comae will quickly undergo radiative relaxation in the infrared to their lowest rotational and vibrational state. The vertical excitation energy for the linear(180°) $C_2H(X^2\Sigma^+ \rightarrow {}^2\Pi)$ transition then increases to $\simeq$8.1eV[7], well into the vacuum UV region. Experiments are currently under

way in our laboratory to confirm the cometary formation of C_2 via the VUV dissociation of cold C_2H.

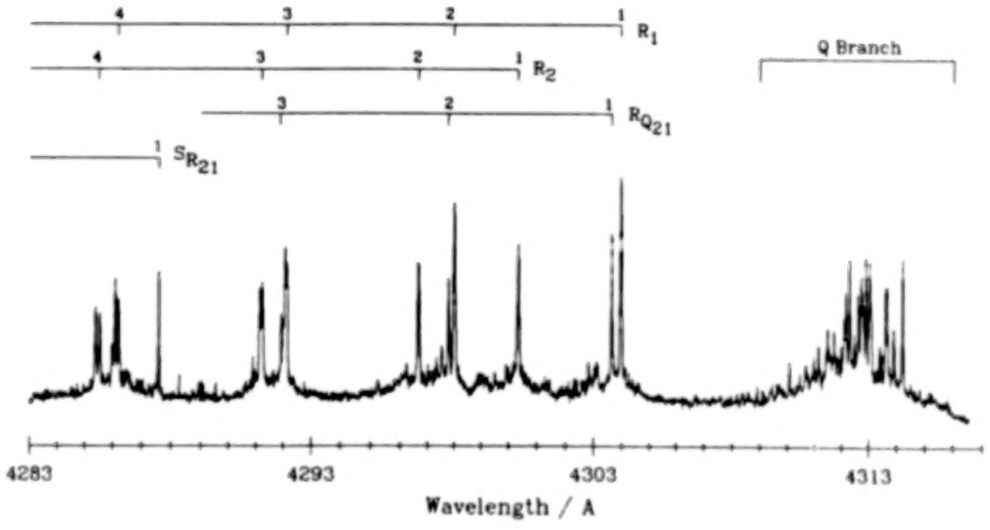

Figure 4. Laser excitation spectrum of CH($X^2\Pi$, v"=0) formed in the photolysis of allene, observed at a delay of 5μs (50mtorr C_3H_4, 10torr Ar).

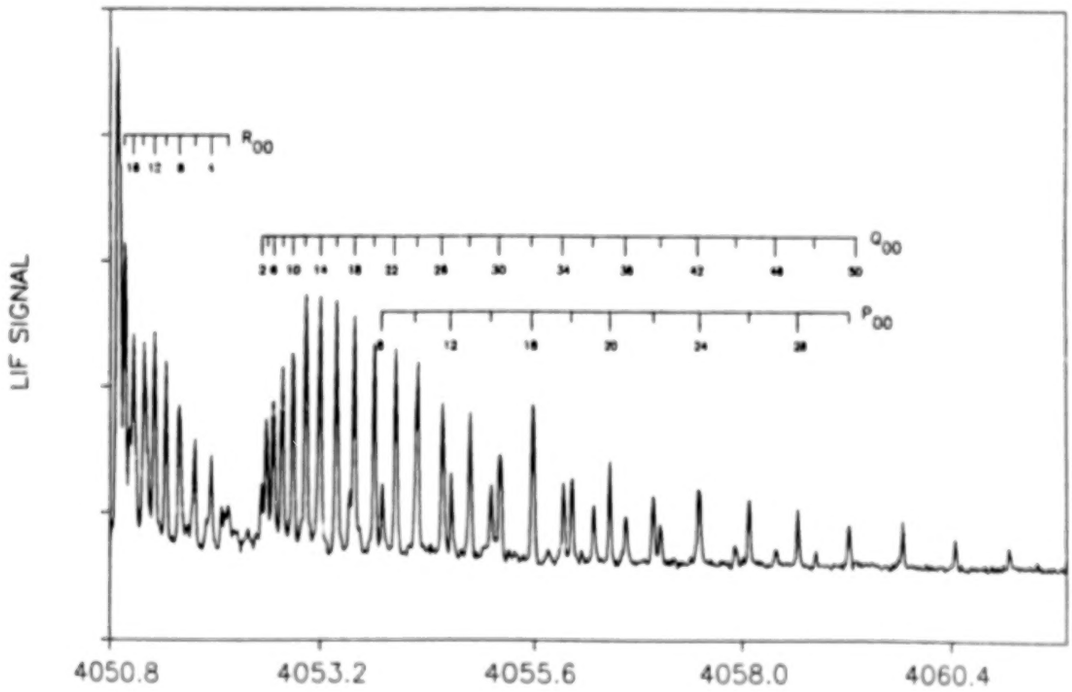

Figure 5. Laser excitation spectrum of $C_3(X^1\Sigma_g^+, 000)$ formed in the photolysis of allene, observed at a delay of 5μs (100mtorr C_3H_4, 10torr Ar).

ACKNOWLEDGEMENTS

The allene dissociation experiments were performed in cooperation with Dr. D. Winkoun. The authors gratefully acknowledge support by the Planetary Atmospheres Program of NASA under grant NAGW-903.

REFERENCES

1. W.M. Jackson, J. Photochem. **5**, 107 (1976).
2. K.D. Tucker, M.L. Kutner, and P. Thaddeus, Astrophys. J. **193**, L115 (1974).
3. C.R. O'Dell, R.R. Robinson, K.S.K. Swamy, P.J. McCarthy, and H. Spinrad, Astrophys. J. **334**, 476 (1988).
4. A.M. Wodtke and Y.T. Lee, J. Phys. Chem. **89**, 4744 (1985).
5. T.R. Fletcher and S.R. Leone, J. Chem. Phys. **90**, 871 (1989).
6. R.S. Urdahl, Y. Bao, and W.M. Jackson, Chem. Phys. Lett. **152**, 485 (1988).
7. S. Shih, S.D. Peyerimhoff, and R.J. Buenker, J. Mol. Spectrosc. **64**, 167 (1977); **74**, 124 (1979).

CHEMICAL THERMODYNAMICS

INVITED

AND

CONTRIBUTED

PAPERS

N90-26773

THE APPLICATIONS OF CHEMICAL THERMODYNAMICS AND CHEMICAL KINETICS TO PLANETARY ATMOSPHERES RESEARCH

BRUCE FEGLEY, JR.
Abteilung Kosmochemie, Max-Planck-Institut für Chemie (Otto-Hahn Institut),
Saarstrasse 23, D6500 Mainz, Federal Republic of Germany

ABSTRACT

A review of the applications of chemical thermodynamics and chemical kinetics to planetary atmospheres research during the past four decades is presented with an emphasis on chemical equilibrium models and thermochemical kinetics. Several current problems in planetary atmospheres research such as the origin of the atmospheres of the terrestrial planets, atmosphere-surface interactions on Venus and Mars, deep mixing in the atmospheres of the gas giant planets, and the origin of the atmospheres of outer planet satellites all require laboratory data on the kinetics of thermochemical reactions for their solution.

INTRODUCTION

The disciplines of chemical thermodynamics and chemical kinetics have been applied to planetary atmospheres research for over four decades. A large number of investigators (including observers and theoreticians) have used thermodynamics and kinetics to model the chemistry of planetary atmospheres and of atmosphere-surface interactions in order to interpret existing Earth-based, Earth-orbital, and spacecraft spectroscopic data, to guide future observations, and to plan experiments on future spacecraft missions.

In this paper I give a selective review of the history of these applications that leads up to the present day and illustrates the background of several current problems in planetary atmospheres research that require new thermodynamic and kinetic data for their solution. I start with a brief discussion of the retention of chemically reactive volatiles in solid grains in the solar nebula and then proceed to discuss one or more topics of interest for the atmospheres of Venus, Mars, the giant planets, and the outer planet satellites Titan and Triton. My emphasis is on atmosphere-surface interactions for the terrestrial planets, deep atmospheric chemistry for the outer planets, and the origin of the atmospheres of the outer planet

PRECEDING PAGE BLANK NOT FILMED

satellites. The companion paper by Yung in this volume focuses on upper atmospheric chemistry and photochemistry for Venus, Mars, Earth, the giant planets, and Titan while the companion paper by Thompson focuses on phase equilibria of cryogenic systems believed to be important for atmosphere-surface interactions on outer planet satellites such as Titan and Triton. The reader is therefore referred to these papers for discussion of these topics.

SOLAR NEBULA CHEMISTRY AND THE ORIGIN OF THE ATMOSPHERES OF THE TERRESTRIAL PLANETS

During the period 1920 - 1950, several authors pointed out that the rare gases (Ne, Ar, Kr, Xe) are much less abundant than chemically reactive volatiles (H, O, C, N, etc.) on the surface of the Earth[1-3]. These large depletions, which are displayed in Table 1, are generally interpreted as showing that the terrestrial atmosphere is almost entirely secondary and originated as a result of chemical processes connected with the formation of the Earth. These processes would retain the chemically reactive volatiles as chemical compounds in solid grains while the rare gases could only be retained by physical processes such as adsorption and absorption. Similar depletions of non-radiogenic rare gases relative to chemically reactive volatiles, which are observed on Venus and Mars, also imply a secondary origin for these atmospheres as well[4]. Thus, in order to understand the origin of the atmospheres of Venus, Earth, and Mars we must first understand the chemical processes responsible for retention of chemically reactive volatiles (e.g., H_2O, C, N, F, Cl, S, etc.) by the solid grains that accreted to form the planets.

During the early 1950's both Latimer[9] and Urey[10] became interested in this problem and in two seminal contributions set the stage for much of the subsequent work during the next 3 decades on chemical models of volatile element chemistry in the solar nebula. For example Latimer and Urey both suggested that hydrated silicate formation in the solar nebula was responsible for the retention of the water that eventually formed the Earth's oceans, that carbon and nitrogen could have been retained in solid grains as carbides and nitrides, that sulfur could have been retained as sulfides (primarily as troilite FeS), and that the halogens could have been retained as halide salts such as NH_4Cl, NaCl, CaF_2, etc. Urey also pioneered the application of chemical thermodynamics to models of solar nebula chemistry and showed how for a given set of assumptions about elemental abundances, pressure,

and temperature, the stability fields of volatile-bearing compounds could be calculated. By comparing the calculated stability fields to the pressure, temperature conditions believed to be appropriate for the formation of the different planets Urey could then make predictions about the reactions responsible for volatile retention by the terrestrial planets.

Table 1. Depletions of important volatiles in the Earth relative to solar abundances [(g/gSi)/(g/gSi)]*

Volatile	Earth[b]
CO_2	3×10^{-5}
H_2O	2×10^{-4}
F	2×10^{-2}
$^{20,22}Ne$	4×10^{-11}
N_2	4×10^{-5}
S	7×10^{-5}
Cl	7×10^{-3}
$^{36,38}Ar$	2×10^{-9}
^{84}Kr	1×10^{-7}
^{132}Xe	9×10^{-8}

*Solar abundances from Cameron [5]. The atmospheric plus oceanic plus crustal inventories for the Earth were obtained from Ronov and Yaroshevsky[6], Turekian[7] and Ozima and Podosek[8].

[b]Bulk composition model E5 from the Basaltic Volcanism Study Project was used to determine the terrestrial silicon inventory.

During the next 3 decades, the availability of a large body of thermodynamic data coupled with advances in our knowledge of the solar abundances of the elements led to increasingly sophisticated chemical equilibrium calculations of volatile element chemistry in the solar nebula[11-22].

The principal results of these calculations can be summarized as follows. The important hydrated silicates serpentine [$Mg_3Si_2O_5(OH)_4$] and talc [$Mg_3Si_4O_{10}(OH)_2$], which exemplify the hydrated silicates observed in carbonaceous chondrites[23], do not become thermodynamically stable until low temperatures below 400 K are reached in

the solar nebula[24]. (This conclusion is true over a wide range of pressures extending up to 10 bars--a pressure much higher than suggested in any currently accepted models of the solar nebula.) Formation of these silicates is calculated to occur by the hydration of either single or composite mineral grains via reactions exemplified by

$$\underset{\text{forsterite}}{Mg_2SiO_4(s)} + \underset{\text{enstatite}}{MgSiO_3(s)} + 2H_2O(g) = \underset{\text{serpentine}}{Mg_3Si_2O_5(OH)_4(s)} \quad (1)$$

$$2\underset{\text{forsterite}}{Mg_2SiO_4(s)} + 2H_2O(g) = \underset{\text{serpentine}}{Mg_3Si_2O_5(OH)_4(s)} + \underset{\text{brucite}}{Mg(OH)_2(s)} \quad (2)$$

$$4\underset{\text{enstatite}}{MgSiO_3(s)} + 2H_2O(g) = \underset{\text{talc}}{Mg_3Si_4O_{10}(OH)_2(s)} + \underset{\text{brucite}}{Mg(OH)_2(s)} \quad (3)$$

Secondly, retention of sulfur is calculated to occur via sulfurization of Fe metal grains to form troilite via the reaction

$$Fe(\text{metal}) + H_2S(g) = \underset{\text{troilite}}{FeS} + H_2(g) \quad (4)$$

which becomes thermodynamically favorable at the pressure independent temperature of 687 K. Fe metal is also calculated to react with enstatite and nebular water vapor via the net thermochemical reaction

$$2MgSiO_3(s) + 2Fe(\text{metal}) + 2H_2O(g) = Fe_2SiO_4(s) + Mg_2SiO_4(s) + 2H_2(g) \quad (5)$$

which is predicted to control the oxidation state of the solid grains incorporated into the terrestrial planets[11,13]. Any unreacted Fe metal grains that remain in contact with the nebular gas may then be "rusted" by reaction with water vapor to form magnetite via the net thermochemical reaction

$$3Fe(\text{metal}) + 4H_2O(g) = \underset{\text{magnetite}}{Fe_3O_4} + 4H_2(g) \quad (6)$$

which first becomes thermodynamically favorable at the pressure independent temperature of 400 K.

Finally, depending on the oxidation state of the nebular gas, carbon and nitrogen are predicted to be retained in solid grains either in solution in Fe metal (for nebular gas having the solar C/O atomic ratio of about 0.4) or as carbides

and nitrides (for nebular gas having a C/O atomic ratio greater than or equal to about 0.8). The former retention mechanism is exemplified by the reactions

$$Fe(metal) + H_2(g) + CO(g) = C(in\ Fe) + H_2O(g) \quad (7)$$

$$Fe(metal) + CH_4(g) = C(in\ Fe) + 2H_2(g) \quad (8)$$

$$2Fe(metal) + N_2(g) = 2N(in\ Fe) \quad (9)$$

$$2Fe(metal) + 2NH_3(g) = 2N(in\ Fe) + 3H_2(g) \quad (10)$$

while the latter process is exemplified by the reactions

$$Si(g) + CO(g) + H_2(g) = SiC(s) + H_2O(g) \quad (11)$$

$$3Fe(metal) + H_2(g) + CO(g) = Fe_3C(cohenite) + H_2O(g) \quad (12)$$

$$2Ti(g) + N_2(g) = 2TiN(osbornite) \quad (13)$$

These results coupled with models for the variation of temperature and pressure with radial distance in the solar nebula then lead to specific predictions about the volatile endowments of the terrestrial planets. For example, Lewis[13] has explained the fact that Venus has about 100,000 times less observable water than the Earth by the failure of Venus to have accreted hydrated silicates which did not become thermodynamically stable until further out in the cooler regions of the solar nebula.

However chemical equilibrium models of solar nebula chemistry neglect the fact that chemical interactions between gases and grains in the solar nebula took place in a dynamic environment. Therefore the rate of chemical reactions is as important (if not even more important) than the final equilibrium configuration. It is interesting to note that the importance of chemical kinetics for solar nebula chemistry was probably first recognized by Urey[25]. While discussing the applications of chemical thermodynamics to solar nebula chemistry he stated that "Our data in this field give much information relative to possible reactions, and at higher temperatures they certainly give us practically assured knowledge of the chemical situations due to the high velocities of the reactions, at least in homogeneous systems, provided the data are adequate, which is unfortunately not

always the case. At lower temperatures thermodynamic equilibrium may not be reached even in periods of time that are long compared to the age of the universe, and at these temperatures the kinetics of thermal reactions or of photochemical reactions become important."

In recent years it has become recognized that kinetic data for volatile retention reactions such as silicate hydration, iron sulfurization, FeO-bearing silicate formation, and iron oxidation are necessary to compare the rates of these reactions to the rates of nebular mixing and/or nebular cooling to determine quantitatively the extent to which each reaction proceeded in the solar nebula. Unfortunately, this cannot be done at present because the relevant kinetic data are unavailable.

Despite the unavailability of experimental data, reaction rate estimates, which are based on the kinetic theory of gases and on the few available measurements of activation energies, show that some reactions are impossible slow, while others are fairly rapid, and still others are on the borderline. Figure 1 illustrates this point. This estimated chemical time constants t_{chem} for three exemplary volatile retention reactions--troilite formation via reaction (4), magnetite formation via reaction (6), and hydrated silicate formation via reaction (2)--are calculated by considering the initial rate of the gas-grain reaction. This depends on the collision rate of the reactant gas with the grain surfaces, which is given by

$$\sigma_i = 2.635 \times 10^{25} [P_i/(M_i T)^{1/2}] \qquad (14)$$

where σ_i has units of $cm^{-2}sec^{-1}$, P_i is the partial pressure of reactant gas i, M_i is the molecular weight of gas i, and T is the absolute temperature in Kelvins. The total number of collisions with all grains in each cubic centimeter of the nebula is given by

$$\nu_i = \sigma_i A \qquad (15)$$

where ν_i has units of cm^{-3} sec^{-1} and A is the total surface area of all reactant grains per each cm^3 of the nebula. The grains are assumed to be monodisperse, spherical particles that are crystalline (i.e., fully dense) and are uniformly distributed at solar abundance in the gas. The results shown in Figure 1 also assume a grain radius of 0.1 micrometers. This grain size is comparable to the very fine-grained matrix found in chondritic meteorites and to the silicate grains observed in

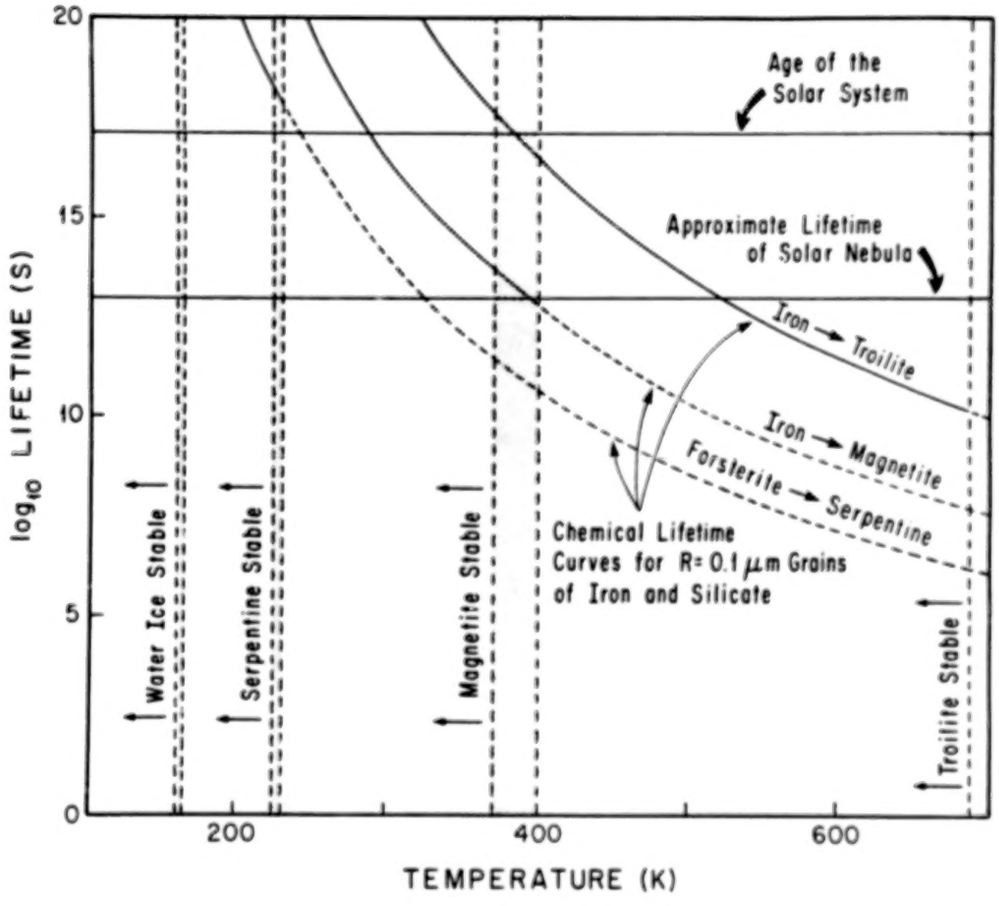

Figure 1. Estimated chemical time constants for three exemplary volatile retention reactions. The thermodynamic stability fields for troilite FeS, magnetite Fe_3O_4, serpentine $Mg_3Si_2O_5(OH)_4$, and water ice are displayed along the horizontal axis. The shaded regions indicate the ranges of formation temperatures appropriate for all carbon being present as CO or CH_4. The chemical lifetime curves for these three reactions are compared to the solar nebula lifetime (approximately 10^{13} seconds) and the age of the solar system (approximately 10^{17} seconds). All chemical lifetime curves are extended to temperatures above the formation temperatures of the different reaction products to illustrate their trends with temperature. This figure is from Fegley[29].

interplanetary dust particles[26-28], but is significantly smaller than the majority of silicate grains observed in chondrites.

The collision time constant t_{coll} for all reactant gas molecules to collide with all grains in each cm^3 of the nebula is then

$$t_{coll} = (\nu_i[i])^{-1} \tag{16}$$

where [i] is the molecular number density of gas i. If every collision led to chemical reaction, equation (16) would also be the expression for the chemical time constant t_{chem}. However, only a small fraction of collisions that possess the necessary activation energy lead to chemical reaction. This fraction is given by

$$f_i = \nu_i \exp(-E_a/RT) \tag{17}$$

where E_a is the activation energy and R is the ideal gas constant. The chemical time constant t_{chem} is then given by the expression

$$t_{chem} = (f_i/[i])^{-1} = t_{coll}/\exp(-E_a/RT) \tag{18}$$

where the activation energies used in the calculations are taken from the literature reviewed by Fegley[29].

Figure 1 compares the calculated chemical time constants with the lifetime of the solar nebula, which is approximately 10^{13} seconds in currently accepted solar nebula models[30-32], and with the age of the solar system. It is clear that hydrated silicate formation is one of the impossibly slow reactions which probably requires a time greater than the age of the solar system to go to completion. On the other hand, FeS formation is one of the relatively rapid reactions and takes place in a fraction of the solar nebula lifetime. Apparently, magnetite formation is on the borderline and may or may not be possible over the lifetime of the solar nebula.

However, the estimated chemical lifetimes shown in Figure 1 are based on activation energies which are taken from experiments done by materials scientists under conditions of pressure, temperature, and composition which are generally far removed from the conditions hypothesized as appropriate for the solar nebula. Clearly what is needed to confirm or refute the theoretical estimates and to establish the actual rate laws and mechanisms for the volatile retention reactions of

interest are properly designed experimental measurements under the appropriate conditions. For example, a systematic study of how the rate of magnetite formation varies as a function of temperature, H_2 pressure and H_2/H_2O ratio is necessary to determine if this reaction either was or was not important in the solar nebula.

To summarize this section, the principles of chemical thermodynamics have been applied to studies of solar nebula chemistry over the past four decades in an attempt to determine how the volatiles seen in the present day atmospheres of Venus, Earth, and Mars and in the oceans of the Earth were originally retained by these planets. While sophisticated and apparently comprehensive models have been generated as a result of this effort, the neglect of chemical kinetics has left us without a clear understanding of the relative importance of the various reactions hypothesized to have been important for volatile retention in the solar nebula. The kinetic data required to remedy this distressing situation can be obtained only by properly designed experimental measurements under the appropriate conditions.

ATMOSPHERE-SURFACE INTERACTIONS ON VENUS AND MARS

Venus and Mars provide two different natural laboratories for studying the relative contributions of thermochemical and photochemical processes to chemical weathering at the atmosphere-surface interface. The global mean Venus surface temperature is about 740 K and the global mean surface pressure is about 92 bars. Only a few percent of the solar flux incident on Venus manages to penetrate to the lower atmosphere below the clouds and the short wavelength solar UV radiation capable of photolyzing CO_2 does not manage to reach the surface. In contrast, the Martian global mean surface temperature is 214 K and the global mean surface pressure is about 6 millibars[83]. In other words the Martian surface is about 530 degrees colder than the surface of Venus and the surface pressure is about 15,000 times lower than at the surface of Venus. Furthermore photodissociation of CO_2, the major atmospheric gas, occurs all the way down to the surface of Mars. Venus would therefore appear to be a good natural laboratory for studying thermochemically dominated chemical weathering processes while Mars would appear to be a good natural laboratory for studying photochemically dominated chemical weathering processes.

(a) Venus

The concept of chemical equilibrium between the surface of Venus and the reactive gases in its atmosphere was first suggested by Urey[10,33] and was later developed by Mueller[34-39] who presented a chemical interaction model to reconcile the known chemical composition of the Venus atmosphere with the high surface temperature of Venus. Lewis and coworkers developed the concept of chemical equilibrium between the atmosphere and surface of Venus in some detail[40-46], and used the concept of complete chemical equilibrium plus observational data on the composition of the atmosphere of Venus to place limits on the surface composition, abundance of trace gases in the atmosphere, the oxidation state of the crust, and on chemical weathering of the surface. Several related studies by Soviet investigators[47-62] used the assumption of chemical equilibrium, in some cases coupled with Venera and Vega atmospheric and surface chemical analyses, to investigate a variety of topics such as trace gas abundances in the Venus atmosphere, cloud particle compositions, mineral stabilities on the Venus surface, and predicted rock types on the Venus surface.

These chemical equilibrium studies were important pioneering efforts. However, aside from some cursory acknowledgements that the achievement of chemical equilibrium was conditional upon thermochemical reactions proceeding sufficiently rapidly with respect to photolysis of reactants/products or with respect to atmospheric mixing times, none of these studies established the reality of chemical equilibrium at the Venus surface.

In fact a number of recent observations strongly suggest that chemical equilibrium is not achieved at the atmosphere-surface interface on Venus. Lewis and Kreimendahl[44] showed that at chemical equilibrium the reduced sulfur gases H_2S and COS will be present in much larger concentrations than the most stable oxidized sulfur gas SO_2, and in fact will be the dominant sulfur-bearing gas at and near the surface of Venus. This prediction disagrees with the SO_2 and H_2S absolute abundance data reviewed by von Zahn et al[63] which showed that SO_2 dominated H_2S and COS above 22 km altitude and had a mixing ratio of about 150 ppm between 22 km and 50 km (the cloud base). Also, preliminary Pioneer Venus (PV) mass spectrometer data suggested that the H_2S mixing ratio was 3 ± 2 ppm below 20 km while the PV gas chromatograph data showed an upper limit of 2 ppm at 22 km[63].

Further evidence against equilibrium is provided by other observations which suggest temporal variations in the abundances of oxidized sulfur gases in the Venus

atmosphere. Esposito[64] and Esposito et al[65] analyzed PV Orbiter UV spectrometer data over the 1978-86 time period and concluded that the SO_2 mixing ratio in the clouds decreased by an order of magnitude over this period. In this connection it is interesting to note that in 1978 three groups[66-68] discovered SO_2 on Venus at mixing ratios in the range 0.02 to 0.8 ppm, levels which are 2 to 80 times higher than the SO_2 upper limit of 0.01 ppm given by Owen and Sagan[69] seven years earlier. Also spectroscopic measurements (at 200 to 400 nm) by the Vega spacecraft indicated a SO_2 mixing ratio of 50 ppm between 26 and 53 km[70]. This is a factor of 3 less than the value obtained by the PV and Venera 12 gas chromatographs 6.5 years before. Moroz[71] also reported that the Venera 13 and 14 gas chromatographs showed H_2S and COS levels more than ten times higher than the upper limits for these gases obtained by PV and Venera 11 and 12 four years before.

At the same time, observations of the surface of Venus also suggest chemical disequilibrium. Pettengill et al[72,73] suggested that high altitude regions of high radar reflectivity may contain substantial abundances of sulfide minerals (e.g., pyrite FeS_2 or troilite FeS). Subsequently Jurgens et al[74,75] also reported evidence for high radar reflectivity materials on the surface of Venus. However, with the observed H_2S and COS concentrations[63], Fe-bearing sulfides are thermodynamically unstable on the surface of Venus and must be spontaneously weathered to form sulfur-bearing gases. Also, Surkov et al[76,77] reported that the X-ray fluorescence experiments on the Venera 13,14, and Vega 2 landers showed larger amounts of CaO than SO_3 thus implying an excess of Ca-bearing minerals for spontaneous incorporation of SO_2 from atmosphere into sulfate-bearing minerals in the crust.

Taken together, these observations of Venus atmospheric chemistry and surface composition suggest that chemical disequilibrium prevails (at least with respect to sulfur chemistry) at the atmosphere-surface interface on Venus. However, the thermodynamic models of Venus atmosphere-surface chemical interactions do not tell us anything about the rates of gas-solid reactions responsible for incorporating SO_2 into sulfate minerals on Venus. Therefore, these models alone are insufficient to correctly describe the disequilibrium chemistry which is observed on Venus. It is also necessary to have information on the actual reaction rates. Fortunately, in this case a recent study[78] provides the required reaction rate data.

In this study, the rate of the net reaction

$$CaCO_3(calcite) + SO_2(g) \text{ ----> } CaSO_4(anhydrite) + CO(g), \quad (19)$$

was studied by heating calcite crystals in SO_2-bearing gas mixtures for varying time periods. The reaction of calcite with SO_2 is predicted to be a net sink for SO_2 on Venus because as Figure 2 illustrates, the observed SO_2 abundance is about 100 times larger than the amount in equilibrium with calcite at Venus surface conditions[79]. Furthermore, calcite is one of the essential phases involved in the Urey equilibrium

$$CaCO_3(calcite) + SiO_2(quartz) = CaSiO_3(wollastonite) + CO_2(g) \quad (20)$$

which is believed to buffer the CO_2 pressure in the Venus atmosphere[33,36,42,55,80] because the equilibrium CO_2 pressure of 102 bars at the mean Venus surface temperature of 740 K is identical within the thermodynamic uncertainties to the observed CO_2 partial pressure of 92 bars at the Venus surface.

The experimentally determined reaction rate data are plotted in Figure 3 and a micrograph of a representative reaction product is shown in Figure 4. The rate data shown in Figure 3 can be applied to the problem of atmosphere-surface disequilibrium on Venus by extrapolating the experimental results downward to Venus surface temperatures (which range from 660 to 750 K) using the rate equation[78] [$R = 10^{(19.64 \pm 0.28)} \exp(-15{,}248(\pm 2{,}970)/T)$ molecules cm^{-2} sec^{-1}], the PV radar altimetry data[81], and the atmospheric P, T-profile[82] to take into account the altitude dependence of the rate. The resulting extrapolation is illustrated in Figure 5 and the derived global-mean SO_2 reaction rate is 4.6×10^{10} molecules cm^{-2} sec^{-1}. This is equivalent to about 1 micrometer of anhydrite being deposited each year. Aeolian weathering will presumably remove the anhydrite layers on a timescale shorter than the 15-25 years required for a layer to build up to the maximum thickness produced in the laboratory experiments, so the laboratory rate data are applicable to Venus.

Assuming that the derived global-mean rate is representative of the rate at which SO_2 is depleted by reaction with Ca-bearing minerals on the Venus surface, the observed SO_2 column density of 2.2×10^{23} molecules cm^{-2} would be removed from the Venus atmosphere in about 1.9×10^6 years in the absence of a comparable sulfur source.

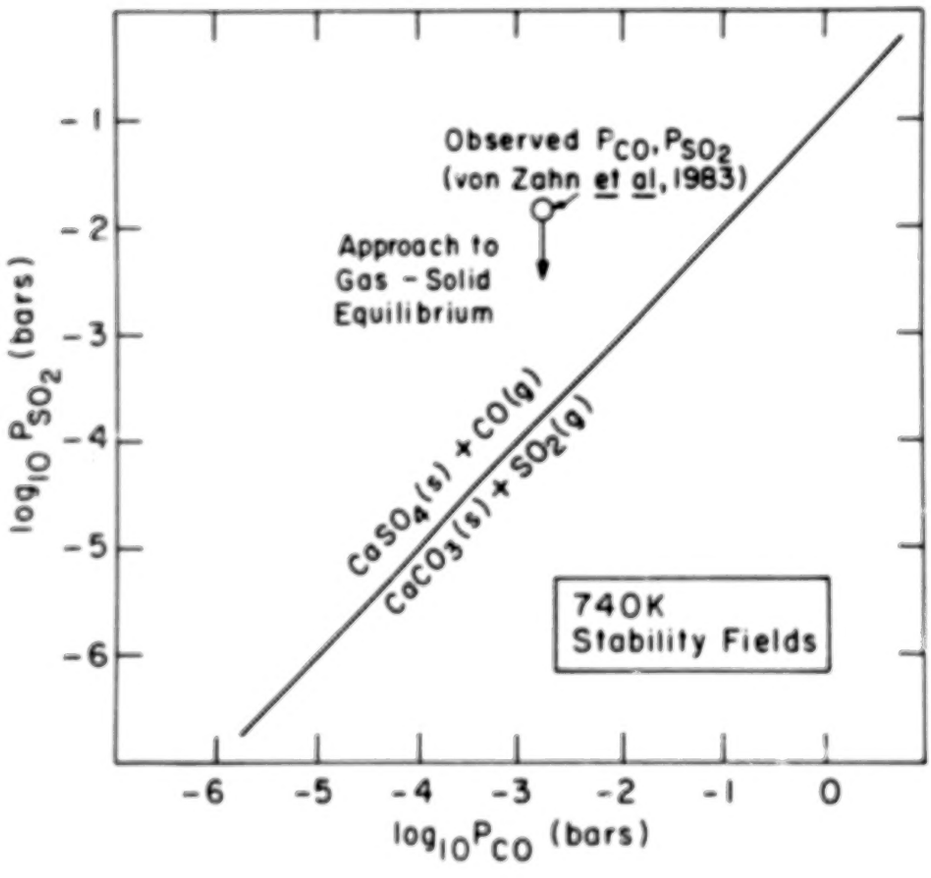

Figure 2. A comparison of the observed sulfur dioxide abundance on Venus with the predicted chemical equilibrium value. The observed value, which is taken from the critical review by von Zahn et al[63] of Pioneer Venus and Venera 11 and 12 measurements, is about 100 times higher than the SO_2 abundance in equilibrium at the mean Venus surface temperature of 740 K with the known CO abundance and the calcite-anhydrite mineral assemblage. This figure is from Fegley[79].

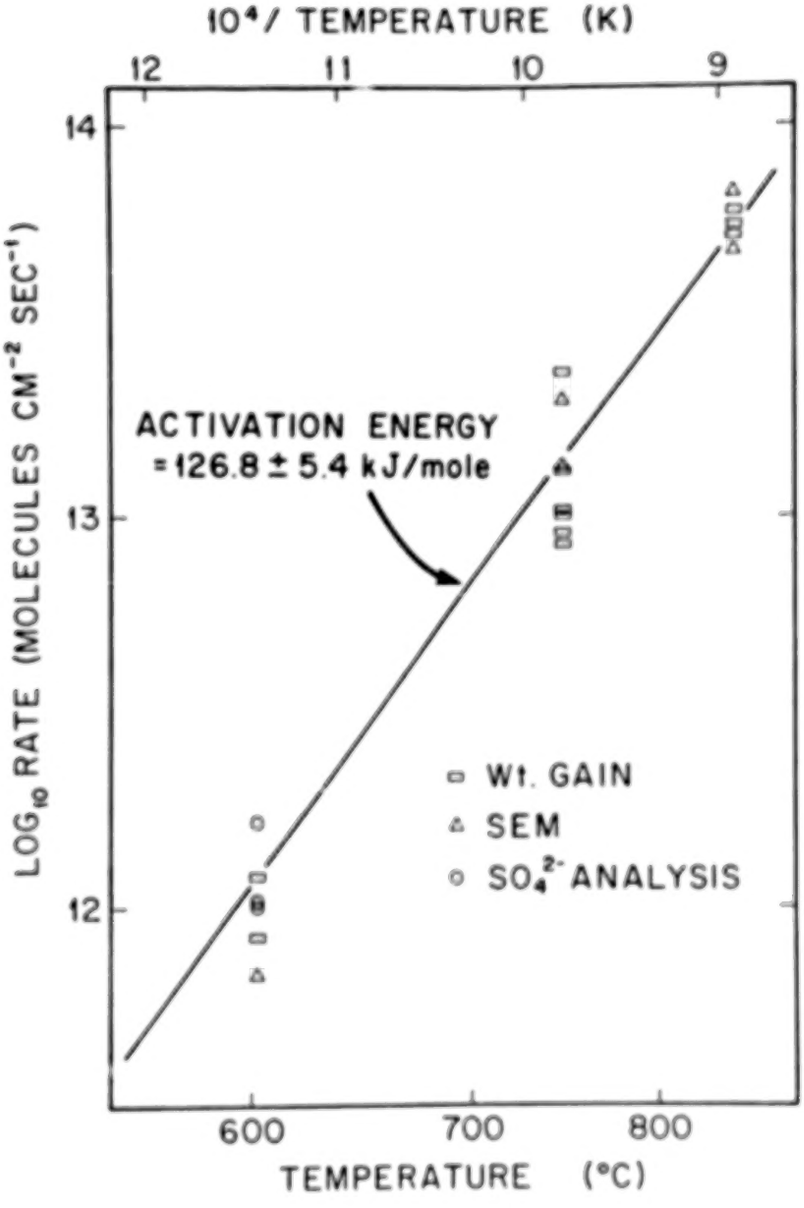

Figure 3. An Arrhenius plot of rate data for the reaction of SO_2 with calcite versus 1/T. The line is a weighted linear least squares fit. Rates determined from two or more independent methods for the same sample agree within the one sigma experimental uncertainties. The experimentally determined rate law is R(molecules cm^{-2} sec^{-1}) = $10^{(19.64 \pm 0.28)}$ exp(-15,248 (±2,970)/T),and the activation energy E_a = 126.8 ± 5.4 KJ/mole.

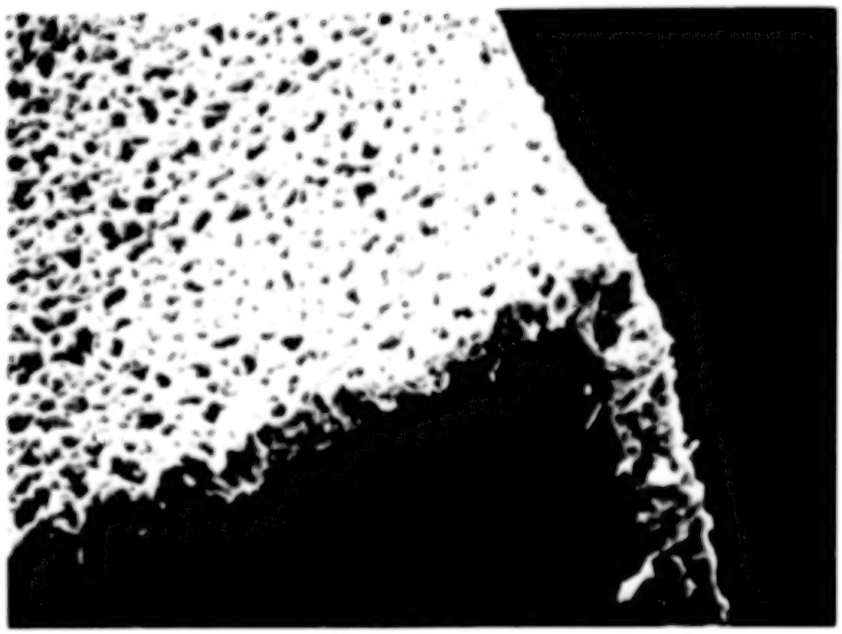

Figure 4. A scanning electron microscope photograph of the fracture surface of a reacted calcite crystal. The scale bar is 100 micrometers long. All external surfaces of the crystal are covered with a layer of anhydrite ($CaSO_4$) grains. The layer gradually becomes thicker and more dense as the gas-solid reaction continues. This figure is from Fegley[129].

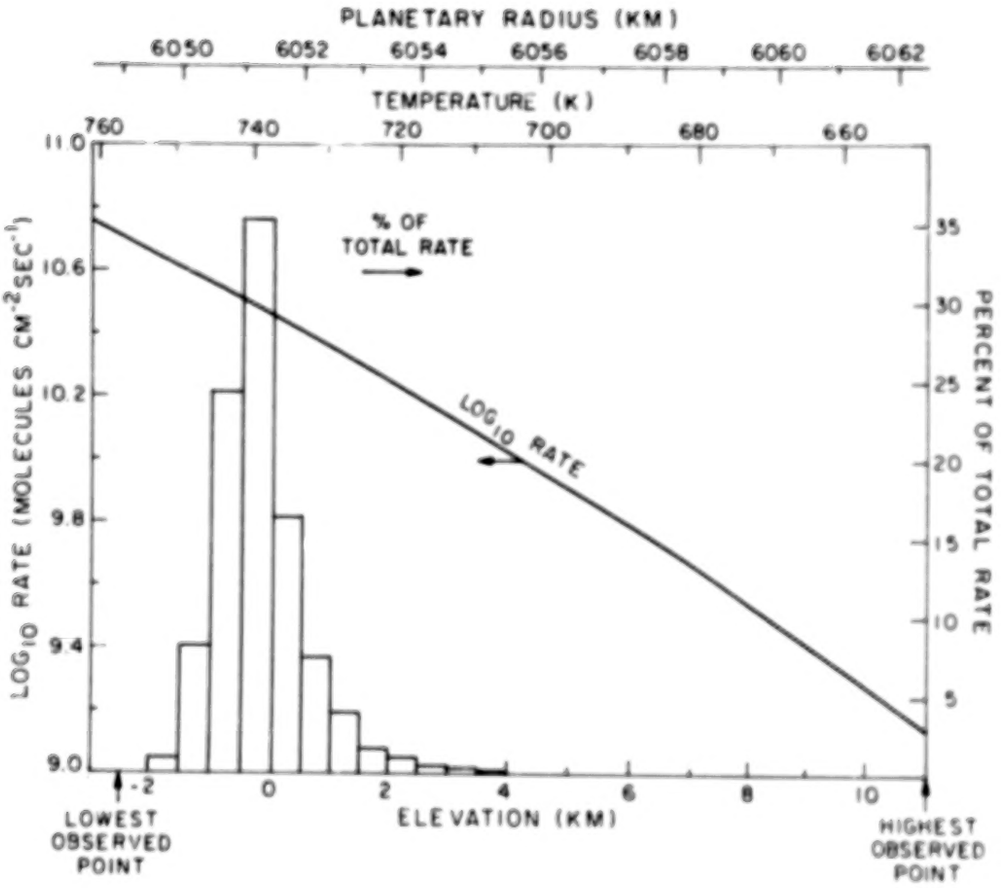

Figure 5. The rate of the SO_2 + calcite reaction as a function of temperature and elevation on Venus. The bar graph shows the % of the total rate in each elevation increment. The solid line shows how the rate decreases with decreasing temperature and is an extrapolation of the line in Figure 3. The global mean rate is about 4.6×10^{18} molecules cm^{-2} sec^{-1} and corresponds to a 1 micrometer thick layer of anhydrite being deposited each year.

(This calculation also assumes that because of similar rock and oxide densities, the areal percentage of CaO on the Venus surface is equal to 7.90%, the weighted mean of the Venera 13,14 and Vega 2 analyses[76,77]). This geologically short lifetime for SO_2 in the atmosphere of Venus has been used to argue that maintenance of the global sulfuric acid clouds requires volcanism to replenish the SO_2 [78], which is the precursor of the clouds.

However, there are a large number of other atmosphere-surface reactions, exemplified by those listed in Table 2, which have been proposed to be important on Venus. These reactions include the formation/decomposition of carbonates, the formation/decomposition of hydrated minerals, the formation/decomposition of halogen-bearing phases, and oxidation/reduction reactions. Although some of these proposed reactions, such as those involving the chemically reactive hydrogen halides HCl and HF, may approach equilibrium on a very short timescale, other proposed reactions such as those involving water vapor and oxidation/reduction reactions involving CO/CO_2 equilibria may be very sluggish, even under the high temperatures and pressures at the Venus surface. Unfortunately, no rate data are available for any of these reactions and therefore the critical questions that remain to be answered, such as the history of water and CO_2 on Venus, trace gas atmospheric lifetimes, and chemical weathering rates will remain the subject of speculation until the appropriate laboratory measurements are made. To summarize this section, chemical equilibrium models of atmosphere-surface interactions on Venus have been used to predict the abundances of trace gases in the atmosphere, the oxidation state of the crust, mineral stabilities on the Venus surface, the abundances of possible cloud forming condensates, and so on. However, these models cannot explain the observed disequilibrium chemistry for sulfur, which is indicated by in situ spacecraft analyses of the lower atmosphere and crust, by Earth-based radar observations, and by the PV Ultraviolet Spectrometer orbital analyses of the upper atmosphere of Venus. Instead, reaction rate data for an important SO_2 sink on Venus have been used to estimate the lifetime of SO_2 (and thus the sulfuric acid clouds) in the atmosphere of Venus and to infer the existence of extant volcanism on Venus. Laboratory measurements of the kinetics of other gas-solid reactions postulated to occur on Venus are also needed to determine the importance of these reactions for the chemical cycles of other trace gases (e.g., H_2O, CO_2, HCl, HF, etc.) in the Venus surface-atmosphere system.

Table 2. Exemplary Atmosphere-Surface Reactions on Venus*

Formation/Decomposition of Carbonates

$CaCO_3$(calcite) + SiO_2(quartz) = $CaSiO_3$(wollastonite) + CO_2(g) (1)

Mg_2SiO_4(forsterite) + $2CO_2$(g) = $2MgCO_3$(magnesite) + SiO_2(quartz) (2)

Mg_2SiO_4(forsterite) + CO_2(g) = $MgCO_3$(magnesite) + $MgSiO_3$(enstatite) (3)

Formation/Decomposition of Hydrated Minerals

$Ca_2Mg_5Si_8O_{22}(OH)_2$(tremolite) = $2CaMgSi_2O_6$(diopside) + $3MgSiO_3$(enstatite) + SiO_2(quartz) + H_2O(g) (4)

$4NaAlSi_3O_8$(albite) + $6CaAl_2Si_2O_8$(anorthite) + $6CaMgSi_2O_6$(diopside) + $2Fe_3O_4$(magnetite) + $5H_2O$(g) + CO_2(g) = $6Ca_2FeAl_2Si_3O_{12}(OH)$(epidote) + $2Na_2Mg_3Al_2Si_8O_{22}(OH)_2$(glaucophane) + $6SiO_2$(quartz) + CO(g) (5)

Formation/Decomposition of Halogen-Bearing Phases

$2NaCl$(halite) + $CaAl_2Si_2O_8$(anorthite) + SiO_2(quartz) + H_2O(g) = $2NaAlSiO_4$(nepheline) + $CaSiO_3$(wollastonite) + 2HCl(g) (6)

$2CaF_2$(fluorite) + SiO_2(quartz) + $MgSiO_3$(enstatite) = $Ca_2MgSi_2O_7$(akermanite) + 4HF(g) (7)

$KAlSi_3O_8$(orthoclase) + $3MgSiO_3$(enstatite) + 2HF(g) = $KMg_3AlSi_3O_{10}F_2$(fluorphlogopite) + $3SiO_2$(quartz) + H_2O(g) (8)

Oxidation/Reduction Reactions

FeS_2(pyrite) + $2CaCO_3$(calcite) + $5CO_2$(g) = $2CaSO_4$(anhydrite) + FeO(in silicates) + 7CO(g) (9)

$3FeMgSiO_4$(olivine) + CO_2(g) = $3MgSiO_3$(enstatite) + Fe_3O_4(magnetite) + CO(g) (10)

*Reactions taken from several papers by Lewis[42,44,46] and Khodakovsky[52].

(b) Mars

Historically, thermochemically controlled weathering reactions were the first ones to be examined on Mars. Beginning in the early 1960's several authors became interested in the thermodynamic stabilities of Fe-bearing minerals on the Martian surface (e.g. hematite Fe_2O_3, goethite FeO(OH), siderite $FeCO_3$), the possibility that "fossil" weathering products could survive to the present day on the Martian surface, the thermodynamic stabilities of various clay minerals, and the major gas-solid decomposition reaction involving the major mineral constituents of mafic igneous rocks[83-89]. Although a substantial body of information now exists about the preferred thermodynamically driven weathering reactions and the stable weathering products on the Martian surface, virtually nothing is known about the kinetics of these reaction. In fact, aside from some general considerations about gas-solid reaction rates given by Gooding[88,90] the topic of reaction rates has been virtually ignored in the literature, in large part due to lack of relevent experimental data.

More recently, photochemically driven weathering reactions have been studied experimentally. This work began in the early 1970's with experiments by Huguenin on the photostimulated oxidation of magnetite[91,92] and later was extended to the formation of goethite and hydrated clay minerals on Mars[93] and to the unusual chemical activity observed in the Viking biology experiments[94,95]. Although Huguenin reported the photostimulated oxidation of magnetite, and derived rate laws and proposed a reaction mechanism, attempts to repeat his work by other investigators, for example by Morris and his colleagues[96,97], have been unsuccessful. Furthermore a study of carbonate formation under Martian surface conditions by Booth and Kieffer[98] found that direct UV illumination of the reactants did not significantly alter carbonate formation.

Despite the apparently contradictory experimental results published in the literature, theoretical considerations imply that photochemically driven chemical weathering may be an important process at the Martian surface. The penetration of UV radiation with wavelengths as short as 195 nm to the Martian surface[99] and the predicted production of significant amount of reactive species such as hydrogen peroxide H_2O_2 at the Martian surface[99,100] indicate a chemically reactive environment. Further laboratory experiments, perhaps with surface sensitive analytical techniques, appear to be in order to resolve the question of photochemically driven chemical weathering on Mars.

Thus, to summarize this section extensive theoretical studies of thermochemical weathering reactions have led to predictions of the preferred weathering reactions and stable reaction products. However, no data are available on the kinetics of the relevant reactions and their rates under present day Martian surface conditions cannot be evaluated. On the other hand, theoretical considerations and some published laboratory experiments indicate that photochemical weathering reactions may proceed rapidly under present day Martian surface conditions. But other published laboratory experiments find negative results and the contradictory situation has not yet been satisfactorily resolved.

DEEP MIXING IN THE ATMOSPHERES OF JUPITER, SATURN, URANUS, AND NEPTUNE

The atmospheres of the four gas giant planets (Jupiter, Saturn, Uranus, and Neptune) are qualitatively different from those of the terrestrial planets. Whereas the atmospheres of the terrestrial planets make up about 100 ppm of the total planetary mass, are relatively oxidizing, and are terminated by sharp atmosphere-surface boundaries; the atmospheres of the gas giant planets are the dominant fraction of the masses of Jupiter and Saturn and a significant fraction of the masses of Uranus and Neptune, are dominated by H_2, and do not have distinct lower boundaries. Furthermore, three of the gas giant planets (Jupiter, Saturn, and Neptune) emit more heat than they absorb from the Sun and thus have internal heat sources. Convection is required to transport the observed heat out of these planets and also provides a mass transport mechanism between the cooler, observable regions of their atmospheres, and the hotter unobservable regions thousands of kilometers below the visible cloud decks. Although an internal heat source has not been observed on Uranus, interior structure models and the need to replenish the CH_4 lost by photodecomposition in the upper atmosphere also imply the existence of vertical transport on this planet.

Historically, it was thought that the deep, hot atmospheres of the gas giant planets, which are believed to reach temperatures of 1000 - 2000 K and pressures of hundreds to thousands of bars, are the perfect environments for chemical reactions to come to equilibrium. Indeed, the first comprehensive chemical model of Jupiter which attempted to predict the abundances of a large number of spectroscopically active species explicitly assumed complete chemical equilibrium[101]. However, the observation of PH_3 in the atmosphere of Jupiter[102] at an abundance about 30

orders of magnitude greater than its predicted equilibrium value[101] demonstrated the existence of a powerful disequilibrating mechanism in the Jovian atmosphere. The subsequent observations[103-107] of other gases (CO, GeH_4, HCN) on Jupiter at abundances which are also many orders of magnitude greater than their predicted chemical equilibrium values[101] and of PH_3, CO, GeH_4, and AsH_3 on Saturn[108-111] reinforced the existence of a potent disequilibrating mechanism in the atmospheres of these two gas giant planets. Table 3 summarizes the observed abundances of these species on Jupiter and Saturn.

Table 3. Observed Abundances of Disequilibrium Trace Gases on Jupiter and Saturn.

	Volume Mixing Ratio	
Gas	Jupiter	Saturn
PH_3	7×10^{-7}	4×10^{-6}
AsH_3	$<3\times10^{-10}$	2×10^{-9}
GeH_4	7×10^{-10}	5×10^{-10}
CO	1×10^{-9}	1.6×10^{-8}
HCN	2×10^{-9}	$<7\times10^{-9}$

Very shortly after the discovery of PH_3 on Jupiter, it was recognized that the disequilibrating mechanism responsible for the observed PH_3 is rapid vertical mixing from the deep atmosphere of Jupiter[112]. As Figure 6 illustrates, PH_3 is the dominant phosphorus-bearing gas in the deep atmosphere of Jupiter. As the temperature decreases with increasing altitude however, PH_3 becomes thermodynamically unstable with respect to oxidation by water vapor and if chemical equilibrium is attained PH_3 will eventually be totally converted to P_4O_6 gas. At even cooler temperatures (and even higher levels in the atmosphere) the P_4O_6 gas will itself become thermodynamically unstable and will react with the atmospheric NH_3 to form a condensate cloud of $NH_4H_2PO_4$ solid.

A comparison of Table 3 and Figure 6 shows that the observed PH_3 mixing ratio of about 0.7 ppm is the same as the PH_3 mixing ratio in the deep atmosphere of Jupiter at temperatures greater than about 1100 K.

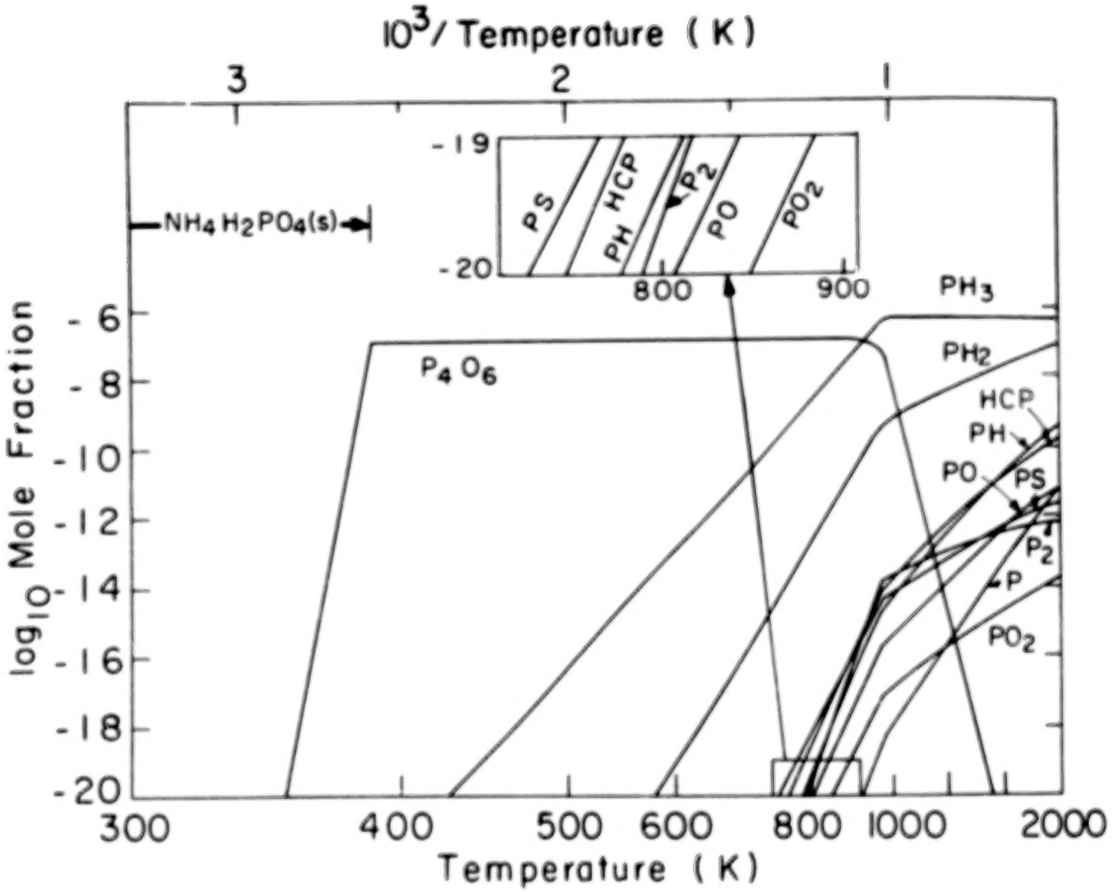

Figure 6. The predicted equilibrium chemistry of phoshorus in the deep atmosphere of Jupiter. At high temperatures PH_3 is 100% of the total phosphorus abundance, but as temperature decreases it becomes thermodynamically unstable and is converted to P_4O_6 gas via oxidation by water vapor. The P_4O_6 in turn becomes thermodynamically unstable at lower temperatures and reacts with atmospheric NH_3 to condense out as $NH_4H_2PO_4$ solid. The observed PH_3 abundance near the Jovian cloud tops is the same as the PH_3 abundance at and below the 1100 K level in Jupiter's deep atmosphere. Rapid vertical mixing at a rate consistent with that required to transport the observed internal heat flux on Jupiter is able to supply the observed PH_3. This figure is from Barshay and Lewis[138].

Rapid vertical mixing from these deep atmospheric regions could thus provide the observed PH_3 abundance in the much cooler observable regions of Jupiter's upper atmosphere if the mixing were sufficiently rapid to transport the PH_3 upward at a rate faster than the rate at which it is destroyed by oxidation to P_4O_6 gas. (Once the PH_3 reaches the observable regions the temperature is sufficiently low (e.g., 200 K) to prevent any thermochemical destruction from occurring even on a geologically long time period.) Similarly, the observed abundances of CO,HCN, and GeH_4 on Jupiter are the same as the abundances of these gases at temperatures of about 900 to 1500 K in the deep atmosphere of Jupiter and the observed abundances of AsH_3, GeH_4, PH_3, and CO on Saturn also match the predicted abundances at much deeper atmospheric levels.

Because nonequilibrium gases such as PH_3, GeH_4, AsH_3, CO and HCN are being transported upward from much deeper atmospheric levels on Jupiter and Saturn they have been called chemical probes of the deep atmospheres of these two planets. Given a quantitative framework for relating the vertical transport rates on Jupiter and Saturn to the thermochemical destruction rates for these gases it should then be possible to use the observed chemical probes to deduce the strength of vertical mixing in the 1000 to 2000 K region of the atmospheres of these two planets. Conversely, given an independent constraint on the strength of vertical mixing in the deep atmospheres of Jupiter and Saturn the same quantitative framework should permit deductions about the chemistry in these atmospheric regions. Mathematically, the situation can be described as follows. Vertical mixing is parameterized using the one dimensional vertical eddy diffusion coefficient K_{eddy}. Then, the characteristic convective mixing time t_{conv} over a pressure scale height H, which is just the time required for the convection driven by the internal heat flux to lift a gas parcel over a pressure scale height, is given by

$$t_{conv} = H^2/K_{eddy}. \qquad (21)$$

In order to determine how rapid vertical mixing must be in order to transport a nonequilibrium gas such as PH_3 upward without any destruction, the convective mixing time t_{conv} must be compared to the characteristic thermochemical destruction time t_{chem}, which depends on the rates of the reactions responsible for destroying the nonequilibrium gas. Now the convective mixing time is fairly insensitive to temperature because the pressure scale height H (equal to $RT/\mu g$ where R is the gas constant, μ is the molecular weight of atmospheric gas, and g is

the gravitational acceleration) is proportional to the temperature. However the thermochemical destruction time is very sensitive to temperature because it depends on reaction rates which themselves are exponential functions of temperature. At some constant vertical mixing rate, there is a level in the atmosphere at which $t_{conv} = t_{chem}$; this is defined as the quench level because for reactions with sufficiently large activation energies, vertical mixing over a very small distance compared to the pressure scale height H results in the thermochemical reactions being quenched at the equilibrium concentrations prevailing at the quench level. At lower levels below the quench level, there is a region where t_{chem} is less than t_{conv}, or in other words, chemistry is proceeding more rapidly than dynamics. Conversely at higher levels above the quench level, there is a region where t_{chem} is greater than t_{conv}, or in other words a region where chemistry is proceeding more slowly than dynamics. It is clear from equation (21) that as K_{eddy} increases, t_{conv} decreases and thus the quench level will be at higher temperatures (i.e., lower in the atmosphere) where t_{chem} is also smaller. Conversely, as K_{eddy} decreases, t_{conv} increases and thus the quench level will be at lower temperatures (i.e., higher in the atmosphere) where t_{chem} is also larger. Because the nonequilibrium trace gas abundances are generally also decreasing with decreasing temperature, larger K_{eddy} values (meaning faster vertical mixing) generally results in larger abundances of the nonequilibrium gases (and vice versa).

So given an atmospheric model (e.g., pressure, temperature, and composition) and the relevant mechanisms and kinetic data for the thermochemical destruction of nonequilibrium trace gases such as PH_3, GeH_4, AsH_3 CO and HCN it should then be possible to use the observed abundances of these gases to make deductions about the deep atmospheres of Jupiter and Saturn. In fact, this is what has been done in a recent series of papers[113-120], which have established the deep mixing origin of the observed nonequilibrium trace gases, predicted many other potential chemical probes of the deep atmospheres of Jupiter and Saturn, and extended the deep mixing theory to Uranus and Neptune.

However, despite this progress, further advances in our knowledge of the chemistry of the deep atmospheres of the gas giant planets require advances in our knowledge of the reaction mechanisms and rate constants for the thermochemical reactions responsible for the destruction of several nonequilibrium trace gases. For example, in some cases absolutely no kinetic data are available and the reaction mechanisms and rate constants have been proposed by analogy with other species and on the basis of qualitative studies. In other cases, rate constants have been

calculated from the equilibrium constants and the rate constants of the reverse reactions. While better knowledge of the reaction mechanisms and rate constants is unlikely to qualitatively change our present understanding (e.g., metal hydrides such as PH_3, AsH_3, and GeH_4 must be provided by deep mixing because there is no extraplanetary source that would provide these species and at the same time not provide enormously larger quantities of SiH_4--which is not observed--on Jupiter and Saturn), this improved knowledge may help to resolve some of the minor discrepancies between theory and observation that currently exist. More importantly, these laboratory data will provide a firm quantitative footing for using species such as PH_3, GeH_4, AsH_3, etc. to probe dynamics at different levels in the atmospheres of Jupiter and Saturn and for using spatially resolved observations (e.g., as may be possible from the CASSINI orbiter) to probe the depth of various storm features in these atmospheres.

To summarize this section, the first chemical models of the atmosphere of Jupiter assumed that chemical equilibrium governed the abundances of gases at all levels in the atmosphere. However, the detections of nonequilibrium trace gases such as PH_3, GeH_4, CO, HCN, and AsH_3 at abundances orders of magnitude greater than their chemical equilibrium values in the cool, observable regions of the Jovian and Saturnian atmospheres demonstrated the existence of a powerful disequilibrating mechanism in the atmospheres of these two planets. The similarity of the observed abundances with the predicted abundances of these nonequilibrium gases in the much hotter, deep unobservable regions of the atmospheres of Jupiter and Saturn suggests that rapid vertical mixing driven by the internal heat sources on these planets is the source of these species. Quantitative calculations of the amounts of nonequilibrium gases transported upward as a function of the assumed vertical mixing rate and atmospheric bulk composition have established the validity of the deep mixing model. However advances in our knowledge of reaction mechanisms and rate constants for several nonequilibrium gases will allow us to use spatially and temporally resolved observations of gaseous abundances to probe atmospheric dynamics at different levels and at different times in the atmospheres of the gas giant planets.

ORIGIN OF THE ATMOSPHERES OF OUTER PLANET SATELLITES

The two large icy satellites Titan, which is a satellite of Saturn, and Triton, which is a satellite of Neptune, possess atmospheres composed of N_2 and CH_4. The atmosphere of Titan was discovered in 1944 by Kuiper[121] and the atmosphere of Triton was first positively identified by observations from the Voyager 2 spacecraft[122,123]. Both atmospheres are most plausibly derived from the outgassing of carbon and nitrogen-bearing volatiles in Titan and Triton, and an understanding of their origin therefore depends on an understanding of the solid materials that were accreted to form these two satellites.

Extensive theoretical studies of low temperature condensation chemistry in the solar nebula[24,124-127] have provided a framework for discussing the composition of the solid grains that were accreted to form the icy satellites of the gas giant planets. In the outer regions of the solar nebula, the first major volatile-bearing condensate to form is water ice. As the temperature continues to decrease, CO and N_2, which are the dominant gaseous forms of carbon and nitrogen in the solar nebula are predicted to equilibrate with the water ice and form clathrate compounds having the ideal formula $G \cdot 6H_2O$ (G = gas). The actual clathrate formed will probably be a solid solution containing both CO and N_2 with the equilibrium composition depending on the thermodynamic properties of the two endmember clathrates and the mixing properties of the solid solution (i.e., the extent of nonideality). Further decreases in temperature are predicted to lead to the condensation of pure CO and N_2 ices.

In the higher pressure environments of the subnebulae, which are believed to have existed around Jupiter, Saturn, and possibly also around Uranus and Neptune during their formation, the initial volatile-bearing condensate is still predicted to be water ice but the subsequent condensates are different. As discussed in detail elsewhere[24], the dominant gaseous forms of carbon and nitrogen in the hypothesized outer planet subnebulae are predicted to be CH_4 and NH_3, respectively. As the temperature decreases below the water ice condensation point, NH_3 is predicted to react with the ice to form ammonia hydrate $NH_3 \cdot H_2O$. Subsequent decreases in temperature lead to formation of methane clathrate $CH_4 \cdot 6H_2O$ and eventually to the condensation of pure CH_4 ice.

As Figures 7 and 8 illustrate, the composition of low temperature condensates formed in the solar nebula and in the hypothesized outer planet subnebulae are quite different and are manifested not only in terms of the volatile-bearing phases themselves, but also in the composition of the outgassed volatiles and in the ice to rock ratios in the two cases. These points and their implications for the origin of the atmosphere of Titan have been discussed at length in the literature[24,128]. However, despite the importance of the low temperature condensation models for questions such as the origin of the atmosphere of Titan, some of the fundamental thermodynamic and kinetic data which are inputs to the models are poorly known, A few examples will serve to illustrate this point.

The models of low temperature chemistry predict that clathrate compounds (e.g., CH_4, CO, and N_2 clathrates) will form at temperatures below 100 K in the outer nebula or in the outer planet subnebulae. (This is true over a wide range of pressures believed to be appropriate in these environments.) However, virtually no laboratory measurements exist for clathrate stabilities under these conditions. In the case of methane clathrate, most of the available laboratory studies are at much higher temperatures, are directed toward understanding the formation of clathrates in natural gas pipelines, and are up to 50 years old. In the case of N_2 and CO clathrates, virtually no laboratory data on clathrate stabilities are available at all. Furthermore, very little experimental data is available on the solid solution properties of CH_4-CO-N_2 clathrates. Again, the laboratory data that are available have mainly been obtained under conditions of significantly higher temperature and pressure than believed to be appropriate for the natural environments of interest to the cosmochemist.

However, to some extent, theoretical models of clathrate thermodynamics and solid solution properties can be used in place of the missing experimental data. What is much more difficult to remedy by theory is the lack of data on the kinetics of clathrate formation under pressure and temperature conditions believed to have existed in the outer solar nebula and in the outer planet subnebuiae. Furthermore, theoretical reaction rate estimates based on the kinetic theory of gases, indicate that clathrate formation is probably kinetically inhibited in the solar nebula but not in the outer planet subnebulae[24,29]. Thus, laboratory measurements of the rate of clathrate formation are highly desirable.

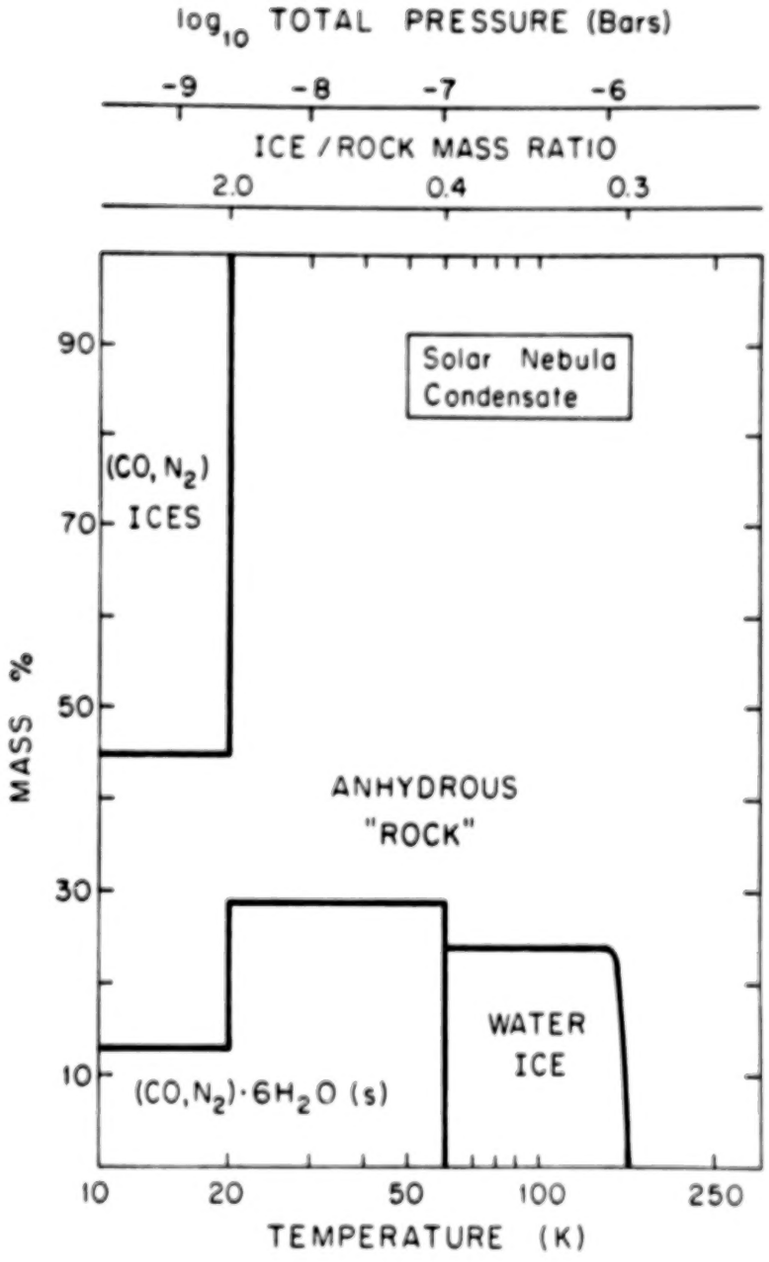

Figure 7. The predicted compositions of low temperature condensates formed in the solar nebula. Theoretical estimates of reaction rates[24,29] predict that the formation of CH_4, NH_3, and of hydrous "rock" will be kinetically inhibited under the prevailing pressure/temperature conditions in the solar nebula. Furthermore CO and N_2 clathrate formation may also be kinetically inhibited[24,29] and experimental measurements of clathrate formation rates are needed to assess this prediction. From Fegley and Prinn[24].

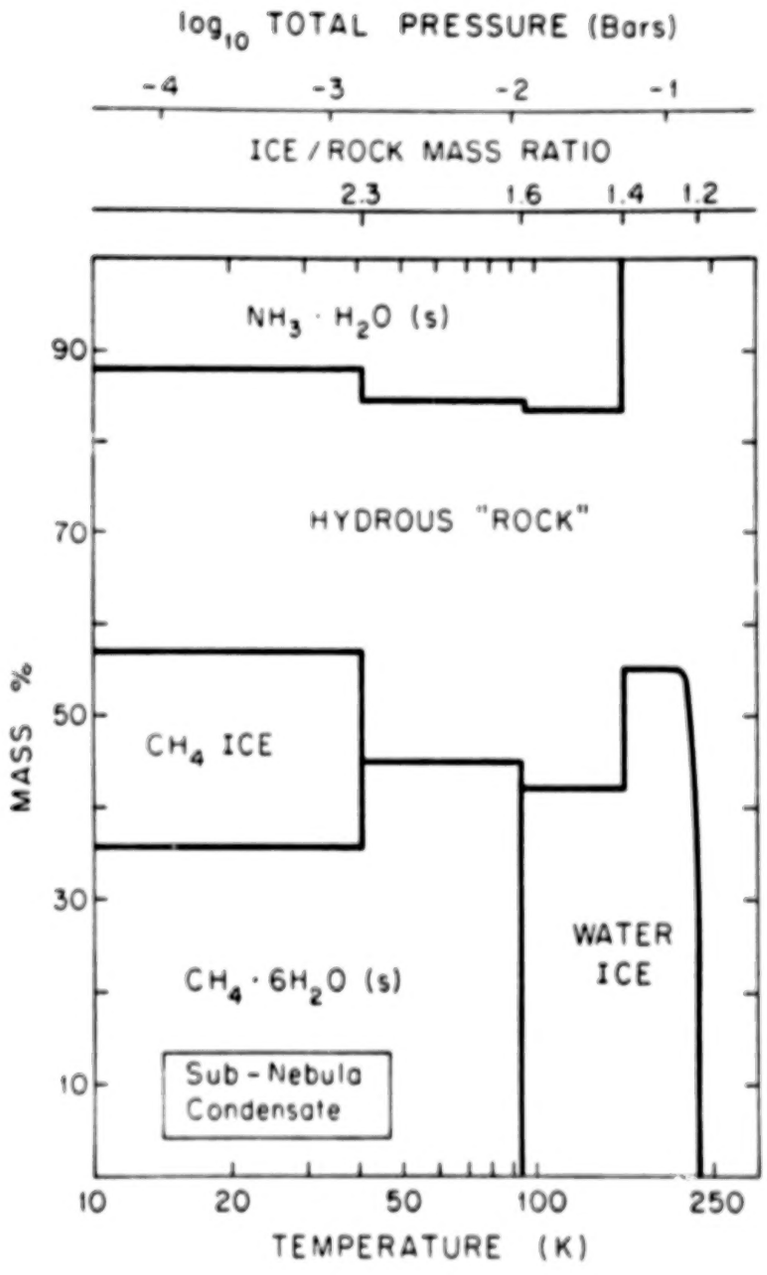

Figure 8. The predicted composition of low temperature condensates formed in an outer planet subnebula. Theoretical estimates of reaction rates[24,29] predict that the formation of CH_4, NH_3, and of hydrous "rock" will be kinetically favorable under the prevailing pressure/temperature conditions in the subnebulae. Furthermore, CH_4 clathrate formation is also predicted to be kinetically favorable[29] and experimental measurements of clathrate formation rates are needed to assess this prediction. From Fegley and Prinn[24].

A related topic which also requires laboratory measurements of reaction rates to remedy our lack of knowledge is the action of solar UV light and charged particles on clathrates. Even if it is kinetically feasible to form a clathrate in a particular environment, long term exposure to solar UV photons or to cosmic rays or to charged particles in a magnetosphere may adversely affect the clathrate (e.g., by releasing the trapped CO, CH_4, or N_2; by chemically reprocessing the trapped volatiles into different and perhaps less volatile species; etc.). Our knowledge of these effects is very limited and potentially is a stumbling block to our understanding of the origin and long term evolution of the atmospheres of icy bodies in the outer solar system.

SUMMARY AND RECOMMENDATIONS

The application of chemical thermodynamics and chemical kinetics to planetary atmospheres research during the past four decades has produced an impressive array of accomplishments which have widely expanded our knowledge of the origin, evolution, and chemistry of planetary atmospheres. Nevertheless despite these advances, our knowledge of many fundamental questions is still in its infancy. For example, we still do not know why Venus has 100,000 times less observable water than the Earth, the rates of atmosphere-surface chemical interactions on Venus and Mars, the relative importance of photochemical versus thermochemical weathering at the atmosphere-surface interface on Mars, the nature of the deep atmospheres of the gas giant planets, and so on.

Although it is likely that a combination of experimental, observational, and theoretical studies will be essential to improve our understanding of these (and other) unresolved issues tied to the origin, evolution, and chemistry of planetary atmospheres, I believe that the following experimental studies are worth emphasizing:

1. Quantitative laboratory studies of the kinetics and mechanisms of important volatile retention reactions in the solar nebula. These reactions include the vapor phase hydration of anhydrous silicates, the formation of magnetite Fe_3O_4 and FeO-bearing silicate formation (both reactions are important for controlling the oxidation state of solid grains that formed the terrestrial planets), and clathrate formation (especially for CO, CH_4, and N_2-bearing clathrates).

2. Quantitative laboratory studies of the kinetics and mechanisms of important thermochemical weathering reactions at the atmosphere-surface interface on Venus. These reactions include the formation/decomposition of hydrated silicates, the release/retention of hydrogen halides, the weathering of sulfide minerals, and the incorporation of SO_2 into crustal minerals.
3. Quantitative laboratory studies to determine if photochemically stimulated chemical weathering reactions such as the oxidation of ferrous to ferric iron are taking place under present day conditions at the atmosphere-surface interface on Mars.
4. Quantitative laboratory measurements of the kinetics and mechanisms of thermochemical reactions postulated to destroy chemical probes of atmospheric dynamics on the gas giant planets. The species of interest include CO, PH_3, GeH_4, AsH_3, and HCN. Unlike the other studies listed above, these studies are homogeneous gas phase chemical kinetic studies.
5. Quantitative laboratory measurements of the effects of UV photons and charged particles on the stability of clathrate compounds of CH_4, CO, and N_2. It is especially important to examine mixed clathrates containing both carbon and nitrogen species.

ACKNOWLEDGMENTS

My planetary atmospheres research is currently supported by the Max-Planck-Institut für Chemie. During the Nov. 1986 - Nov. 1989 period my work on the chemistry of the outer planets was supported by NASA Grant NAGW-997 from the NASA Planetary Atmospheres Program. During the Nov. 1985 - Nov. 1989 period my work on Venus chemical weathering was supported first by NASA Grant NAGW-821 from the NASA Innovative Research Program and second by NASA Grant NAGW-1816 from the NASA Planetary Atmospheres Program. I want to thank Ken Fox for his patience during the writing of this paper and Diana Quillen for volunteering to do word processing. Finally I also want to thank Heidi Hansen, Chris Sobon, and the Staff and Students of the MPI for the help and support.

REFERENCES

1. F.W. Aston. Nature 114 786 (1924).
2. H.N. Russell and D.H. Menzel. Proc. Natl. Acad. Sci USA 19 997 (1933).
3. H. Brown. In The Atmospheres of the Earth and Planets, edited by G.P. Kuiper, p.260. Univ. of Chicago Press, Chicago (1949).
4. R.G. Prinn and B. Fegley, Jr. Ann. Rev. Earth Planet. Sci.15 171 (1987).
5. A.G.W. Cameron. In Essays in Nuclear Astrophysics, edited by C.A. Barnes, D.D. Clayton, and D.N. Schramm, p.23. Cambridge University Press, Cambridge, England(1982).
6 A.B. Ronov and A.A. Yaroshevsky. Geochem. Intl. 12 89 (1976).
7. K.K. Turekian. In Handbook of Geochemistry, edited by K.H. Wedepohl, vol. 1, p.297, Springer-Verlag, Berlin, FRG (1969).
8. M. Ozima and F.A. Podosek. Noble Gas Geochemistry, Cambridge University Press, Cambridge, England (1983).
9. W.M. Latimer. Science 112 101 (1950).
10. H.C. Urey. The Planets, Their Origin and Development. Yale University Press, New Haven, CT (1952).
11. J.W. Larimer. Geochim. Cosmochim. Acta 31 1215 (1967).
12. J.W. Larimer and E. Anders. Geochim. Cosmochim. Acta 31 1239 (1967).
13. J.S. Lewis. Earth Planet. Sci. Lett. 15 286 (1972).
14. J.S. Lewis Science 186 440 (1974).
15. J.W. Larimer. Geochim. Cosmochim. Acta 39 389 (1975).
16. J.W. Larimer and M. Bartholomay. Geochim. Cosmochim. Acta 43 1455 (1979)
17. S.S Barshay and J.S. Lewis. Ann. Rev. Astron. Astrophys. 14 81 (1976).
18. J.S. Lewis, S.S Barshay, and B. Noyes. Icarus 37 190 (1979)
19. B. Fegley, Jr. and J.S. Lewis. Icarus 41 439 (1980)
20. S.S Barshay. Ph.D. Thesis, MIT (1981).
21. B. Fegley, Jr. Proc. Lunar Planet. Sci Conf. 13 J. Geophys. Res. 88 p. 853 (1983)
22. A. Hashimoto and L. Grossman. Geochim. Cosmochim. Acta 51 1685 (1987).
23. D.J. Barber. Clay Min. 20 415 (1985).
24. B. Fegley, Jr. and R.G. Prinn. In the Formation and Evolution of Planetary Systems, edited by H.A. Weaver and L. Danly, p. 171, Cambridge University Press, Cambridge, England (1989).
25. H.C. Urey. in XIIIth International Congress Pure and Applied Chemistry and Plenary Lectures, p.188, Almquist and Wiksells, Stockholm, Sweden (1953).
26. J.A. Peck. Lunar Planet. Sci XIV, p. 598 (1983).
27. J.A. Peck. Lunar Planet. Sci XV, p. 635 (1984).
28. I.D.R. MacKinnon and F.J.M. Rietmeijer. Rev Geophys. 25 1527 (1987).

29. B. Fegley, Jr. In Workshop on The Origins of Solar Systems edit by J.A. Nuth and P. Sylvester, LPI Tech. Report 88-04, p. 31 (1988).
30. A.G.W. Cameron. In Protostars and Planets II, edited by D.C. Black and M.S Matthews, p. 1073, University of Arizona Press, Tucson, Arizona (1985).
31. D.N.C. Lin and J. Papaloizou. In Protostars and Planets II, edited by D.C. Black and M.S. Matthews, p. 981, University of Arizona Press, Tucson, Arizona (1985).
32. G.E. Morfill, W. Tscharnuter, and H.J. Volk. In Protostars and Planets II, edited by D.C. Black and M.S. Matthews, P. 493, University of Arizona Press, Tucson, Arizona (1985).
33. H.C. Urey. In Handbuch der Physik, vol. 52, p. 363, Springer-Verlag, Berlin, Federal Republic of Germany (1959).
34. R.F. Mueller. Science 141 1046 (1963).
35. R.F. Mueller. Nature 203 625 (1964).
36. R.F. Mueller. Icarus 3 285 (1964).
37. R.F. Mueller. Icarus 4 506 (1965).
38. R.F. Mueller. Nature 220 55 (1968).
39. R.F. Mueller. Science 163 1322 (1969).
40. J.S. Lewis. Icarus 8 434 (1968).
41. J.S. Lewis. Icarus 11 367 (1969).
42. J.S. Lewis. Earth Planet. Sci. Lett. 10 73 (1970).
43. J.S. Lewis. J. Atmos. Sci. 28 1084 (1971).
44. J.S. Lewis. and F.A. Kreimendahl. Icarus 42 330 (1980).
45. K.A. Goettel and J.S. Lewis. J. Atmos. Sci 31 828 (1974).
46. S.L. Nozette and J.S. Lewis. Science 216 181 (1982).
47. V.L. Barsukov, V.P. Volkov, and I.L. Khodakovsky. Proc. 11th Lunar Planet. Sci. Conf. p. 765 (1980).
48. V.L. Barsukov, V.P. Volkov, and I.L. Khodakovsky. Proc. 13th Lunar Planet. Sci. Conf., J. Geophys. Res. 87 A3 (1982).
49. V.L. Barsukov, Yu. A. Surkov, L.V. Dmitriyev, and I.L. Khodakovsky, Geochem. Intl. 23 53 (1986).
50. C.P. Florensky, V.P. Volkov, and O.V. Nikolaeva. Icarus 33 537 (1978).
51. I.L. Khodakovsky Planet. Space Sci. 30 803 (1982).
52. I.L. Khodakovsky, V.P. Volkov, Yu. I. Sidorov, and M.V Borisov. Icarus 39 352 (1979).
53. V.A. Khodakovsky. Planet. Space Sci. 33 109 (1985).
54. V.A. Khodakovsky. Icarus 80 202 (1989).
55. A.S. Vinogradov and V.P. Volkov. Geochem. Intl. 8 463 (1971).
56. V.P. Volkov. Lunar Planet Sci. XVII, p. 915 (1986).
57. V.P. Volkov, M.Yu, Zolotov, and I.L. Khodakovsky. In Chemistry and Physics of the Terrestrial Planets, ed. S.K. Saxena, p. 136, Springer-Verlag, New York (1986).
58. M. Yu. Zolotov. Lunar Planet. Sci. XVI, p. 942 (1985).
59. M. Yu. Zolotov. Lunar Planet. Sci. XVII, p. 971 (1986).
60. M. Yu. Zolotov. Lunar Planet. Sci. XVIII, p. 1134 (1987).
61. M. Yu. Zolotov and I.L. Khodakovsky. Lunar Planet. Sci. XVI, p. 944 (1985).
62. M. Yu. Zolotov, I.L. Khodakovsky, and E.F. Westrum, Jr. Lunar Planet Sci. XVIII, p. 1136 (1987).
63. U. von Zahn, S. Kumar, H. Niemann, and R.G. Prinn. In Venus, edited by D.M. Hunten, L. Colin, T.M. Donahue, and

V.I. Moroz, p. 299, University of Arizona Press, Tucson, Arizona (1983).
64. L.W. Esposito. Science 223 1072 (1984).
65. L.W. Esposito, M. Copley, R. Eckert, L. Gates, A.I.F. Stewart, and H. Worden. J. Geophys. Res. 93 5267 (1988).
66. E.S. Barker. Geophys. Res. Lett. 6 117 (1979).
67. R.R. Conway, R.P. McCoy, C.A. Barth, and A.L. Lane. Geophys. Res. Lett. 6 629 (1979).
68. A.I. Stewart, D.E. Anderson, Jr. L.W. Esposito, and C.A. Barth. Science 203 777 (1979).
69. T. Owen and C. Sagan. Icarus 16 557 (1972).
70. J.L. Bertaux, A.P. Ekonomov, B. Mege, V.I. Moroz, A. Abergel, V.I. Gnedykh, A.V. Grigoryev, B.E. Moshkin, A. Houchecorne, J.P. Pomereau, and S.B. Sergeeva. Cosmic Res. 25 691 (1987).
71. V.I. Moroz. In Venus, edited by D.M. Hunten, L. Colin, T.M. Donahue, and V.I. Moroz, p. 45, University of Arizona Press, Tucson, Arizona(1983).
72. G.H. Pettengill, P.G. Ford, and S. Nozette. Science 217 640 (1982).
73. G.H. Pettengill, P.G. Ford, and S. Nozette. Lunar Planet. Sci. XIV, p.602 (1983).
74. R.F. Jurgens, M.A. Slade, and R.S. Saunders. Science 240 1021 (1988).
75. R.F. Jurgens, M.A. Slade, L. Robinett, S. Brokl, G.S. Downs, C. Franck, G.A. Morris, K.H. Farazian, and F.P. Chan. Geophys. Res. Lett. 15 577 (1988).
76. Yu. A. Surkov, V.L. Barsukov, L.P. Moskalyova, V.P. Kharyukova, and A.L. Kemurdzhian. Proc. 14th Lunar Planet. Sci Conf. J. Geophys. Res. 89 B393 (1984).
77. Yu. A. Surkov, L.P. Moskalyova, V.P. Kharyukova, A.D. Dudins, G.G. Smirnov, and S. Ye. Zaitseva. Proc. 17th Lunar Planet. Sci. Conf. J. Geophys. Res. 91 E215 (1986).
78. B. Fegley, Jr. and R.G. Prinn. Nature 337 55 (1989).
79. B. Fegley, Jr. Lunar Planet. Sci. XIX, p. 315 (1988).
80. J.A. Adamcik and A.L. Draper. Planet. Space Sci. 11 1303(1963).
81. H. Masursky, E. Eliason, P.G. Ford, G.E. McGill, G.H. Pettengill, G.G. Schaber, and G. Schubert. J. Geophys. Res. 85 8232 (1980).
82. A. Seiff. In Venus, edited by D.M. Hunten, L. Colin, T.M. Donahue, and V.I. Moroz, p. 1045, University of Arizona Press, Tucson, Arizona (1983).
83. C.A. Barth. In the Photochemistry of Atmospheres, ed. J.S. Levine, p. 337, Academic Press, New York (1985).
84. J.A. Adamcik. Planet. Space Sci. 11 355 (1963).
85. F.F Fish, Jr. J. Geophys. Res. 71 3063 (1966).
86. J.T. O'Connor. J. Geophys. Res. 73 5301 (1968).
87. J.T. O'Connor. Icarus 8 513 (1968).
88. J.L. Gooding. Icarus 33 483 (1978).
89. Yu. I. Sidorov and M. Yu. Zolotov. In Chemistry and Physics of the Terrestrial Planets, ed. S.K. Saxena, p. 191 Springer-Verlag, New York (1986).

90. J.L. Gooding, R.E. Arvidson, and M. Yu. Zolotov. In Mars, edited by H. Kieffer and M.S. Matthews, In Press, University of Arizona Press, Tucson, Arizona (1990).
91. R.L. Huguenin. J. Geophys. Res. 78 8481 (1973).
92. R.L. Huguenin. J. Geophys. Res. 78 8495 (1973).
93. R.L. Huguenin. J. Geophys. Res. 79 3895 (1974).
94. R.L. Huguenin. J. Geophys. Res. 87 10069 (1982).
95. R.L. Huguenin, K.J. Miller, and W.S. Harwood. J. Mol. Evol. 14 103 (1979).
96. R.V. Morris and H.V. Lauer, Jr. Geophys. Res Lett. 7 605 (1980).
97. R.V. Morris and H.V. Lauer, Jr. Geophys. Res. 86 10893 (1981).
98. M.C. Booth and H.H. Kieffer. J. Geophys. Res. 83 1809 (1978).
99. T.D. Parkinson and D.M. Hunten. J. Atmos. Sci. 29 1380 (1972).
100. T.Y. Kong and M.B. McElroy, Icarus 32 168 (1977).
101. J.S. Lewis. Icarus 10 393 (1969).
102. S.T. Ridgway. Bull. Amer. Astron. Soc. 6 376 (1974).
103. R. Beer and F.W. Taylor. Astrophys. J. 221 1100 (1978).
104. U. Fink, H.P. Larson, and R.R Treffers. Icarus 34 344 (1978).
105. H.P. Larson, R.R. Treffers, and U. Fink, Astrophys. J. 211 972 (1977).
106. H.P. Larson, U. Fink, and R.R Treffers. Astrophys. J. 219 1084 (1978).
107. A.T. Tokunaga, S.C. Beck, T.R. Geballe, J.H. Lacy, and E. Serabyn. Icarus 48 283 (1981).
108. H.P. Larson, U. Fink, H.A. Smith, and D.S. Davis. Astrophys. J. 240 327 (1980).
109. B. Bezard, P. Drossart, E. Lellouch, G. Tarrago, and J.P. Maillard. Astrophys. J. 346 509 (1989).
110. K.S. Noll, R.F. Knacke, T.R. Geballe, and A.T. Tokunaga. Astrophys. J. 309 L91 (1986).
111. K.S. Noll, R.F. Knacke, T.R. Geballe, and A.T. Tokunaga. Icarus 75 409 (1988).
112. R.G. Prinn and J.S. Lewis. Science 190 294 (1975).\
113. B. Fegley, Jr. and R.G. Prinn. Astrophys. J. 299 1067 (1985).
114. B. Fegley, Jr. and R.G Prinn. Astrophys. J. 324 621 (1988).
115. B. Fegleg, Jr. and R.G. Prinn. Astrophys. J. 326 490 (1988).
116. B. Fegley, Jr. Bull. Amer. Astron. Soc. 20 879 (1988).
117. R.G. Prinn and S.S Barshay. Science 198 1021 (1977).
118. B. Fegley, Jr. and R.G. Prinn. Nature 318 48 (1985).
119. B. Fegley, Jr. and R.G. Prinn. Astrophys. J. 307 852 (1986).
120. B. Fegley, Jr. In Preparation (1990).
121. G.P. Kuiper Astrophys J. 100 378 (1944).
122. A.L. Broadfoot et al. Science 246 1459 (1989).
123. B. Conrath et al. Science 246 1454 (1989).
124. S.L. Miller. Proc. Natl. Acad. Sci. USA 47 1798 (1961).
125. J.S. Lewis. Icarus 16 241 (1972).
126. J.S. Lewis and R.G. Prinn. Astrophys. J. 238 357 (1980).
127. J.I. Lunine and D.J. Stevenson. Astrophys. J. Suppl. 58 493 (1985).
128. J.I. Lunine, S.K. Atreya, and J.B. Pollack. In Origin and Evolution of Planetary and Satellite Atmospheres, edited by

S.K. Atreya, J.B. Pollack, and M.S. Matthews, p. 605, University of Arizona Press, Tucson, Arizona (1989).
129. B. Fegley, Jr. In Planetary Geosciences-1988, edited by M. Zuber, O. James, G. MacPherson, and J. Plescia, p. 13, NASA SP-498 (1989).
130. S.S. Barshay and J.S. Lewis. Icarus 33 593 (1978).

N90-26774

LIQUID-VAPOR EQUILIBRIUM OF MULTICOMPONENT CRYOGENIC SYSTEMS

W. REID THOMPSON,* JORGE C. G. CALADO** AND JOHN A. ZOLLWEG†

*Laboratory for Planetary Studies, Space Sciences Bldg., Cornell Univ., Ithaca, NY 14853

**Complexo I, Instituto Superior Técnico, 1096 Lisboa, Portugal

†School of Chemical Engineering, Olin Hall, Cornell Univ., Ithaca, NY 14853

ABSTRACT

Liquid-vapor and solid-vapor equilibria at low to moderate pressures and low temperatures are important in many solar system environments, including the surface and clouds of Titan, the clouds of Uranus and Neptune, and the surfaces of Mars and Triton. The familiar cases of ideal behavior ($p_i = X_i p_i^\circ$, where p_i is the vapor pressure of a species present at mol fraction X_i in a condensate, and p_i° is its vapor pressure in the pure state), and Henry's law [$X_i = p_i/K_H$, where K_H is the Henry's law constant for a given solute (gas) and solvent (liquid)] are limiting cases of a general thermodynamic representation for the vapor pressure of each component in a homogeneous multicomponent system: $p_i = \gamma_i X_i p_i^\circ$, where γ_i is the activity coefficient. The fundamental connections of laboratory measurements to thermodynamic models are through the Gibbs-Duhem relation $G_i^E = [\partial(n_T G^E)/\partial n_i]_{T,p,n_j}$ and the Gibbs-Helmholtz relation $[\partial(G^E/T)/\partial T]_{p,X} = -H^E/T^2$. G^E is the excess free energy of mixing — that is, in excess of the ideal term $G_{mix}^I = RT\sum_i X_i \ln X_i$ — and H^E is the excess enthalpy. G_i^E is generally represented in terms of a physical model containing dependencies on all $X_j (j \neq i)$ and T, and adjustable parameters which characterize the interaction of a single species with all others in solution. Using laboratory measurements of the total pressure, temperature, and compositions of the liquid and vapor phases at equilibrium, the values of these parameters can be determined. The resulting model for vapor-liquid equilibrium can then conveniently and accurately be used to calculate pressures, compositions, condensation altitudes, and their dependencies on changing climatic conditions. A specific system being investigated in our work is CH_4-C_2H_6-N_2, at conditions relevant to Titan's surface and atmosphere. We discuss: the modeling of existing data on CH_4-N_2, with applications to the composition of Titan's condensate clouds; some new measurements on the CH_4-C_2H_6 binary, using a high-precision static/volumetric system, and on the C_2H_6-N_2 binary, using the volumetric system and a sensitive cryogenic flow calorimeter; and describe a new cryogenic phase-equilibrium vessel with which we are beginning a detailed, systematic study of the three constituent binaries and the ternary CH_4-C_2H_6-N_2 system at temperatures ranging from 80 to 105°K and pressures from 0.1 to 7 bar.

VOLATILES IN CRYOGENIC PLANETARY ENVIRONMENTS

From the Earth's orbit sunward, ambient temperatures are sufficiently high that only refractory (ionic, metallic, or polymeric) materials and compounds with strong intermolecular forces (for example, hydrogen bonds in sulfuric acid and water) condense to solid and liquid form. However, at many locations farther from the sun, the surface or atmospheric temperatures are sufficiently cold that more weakly associating polar and nonpolar molecules (dominated by van der Waals forces) constitute most of the volatiles, where by volatiles we mean compounds which have sufficient vapor pressure to be present in the gas, as well as the liquid and/or solid, states. These systems fall within the temperature regime referred to as cryogenic in laboratory research.

The solid-vapor equilibrium of CO_2 in the atmosphere and surface of Mars, of NH_3 in the atmospheres of Jupiter and Saturn, and of SO_2 on the surface of Io involve molecules of moderate bond polarities and temperatures ranging down to about 100°K. These examples form a transition to the truly nonpolar volatiles mostly participating in equilibria near and below 100°K: CH_4, Ar, and perhaps N_2, as components of cloud condensates on Uranus and Neptune; CH_4, N_2, and perhaps Ar, as components of both clouds and, with C_2H_6 and C_3H_8, of surface liquid on Titan; and finally N_2, CH_4, and perhaps Ar, CO, or other species in solid-vapor equilibrium on the surfaces of Triton and Pluto.

The first goal of laboratory research on these species is to obtain a complete description of the vapor pressures, gas equations of state, and volumetric and thermodynamic characteristics of the compounds in their pure liquid and gaseous states, at temperatures and pressures relevant to planetary environments. Generally, published work at the low pressures p and temperatures T appropriate to these cryogenic planetary conditions tends to be sparse compared to that available at higher p and T. This problem is least serious for the pure components, for which good data is generally available.[1,2] However, most (if not all) of the condensate-vapor equilibrium systems mentioned above involve more than one species, so that one needs to study in the laboratory, and accurately represent by empirical or theoretical models, the equilibria in binary and multicomponent systems as well.

This need is especially realized at Titan, where N_2 can form a substantial part of CH_4 condensate in the clouds, and a large inventory (about 700 m) of C_2H_6 and C_3H_8 expected from photochemistry virtually guarantees a liquid CH_4-C_2H_6-N_2-C_3H_8-... system at the surface, in equilibrium with the atmosphere. Present as minor solutes in the cloud and ocean will be other hydrocarbons and nitriles: the nine detected by Voyager and, on the basis of plasma chemistry studies,[3] several others. These arrive from above in the

form of precipitating stratospheric condensates. Measuring and/or modeling the solubilities of these minor solutes is another relevant topic, but one which we do not address further here.

The major condensates and thermodynamic regimes relevant at Titan are summarized in Figure 1. We use the interesting examples of Titan's CH_4-N_2 clouds and N_2-hydrocarbon multicomponent surface to illustrate the thermodynamic principles involved. We describe some of the techniques which can be applied to study experimentally, and accurately model, such systems. The focus of this paper reflects experimental work and modeling by W. Reid Thompson of Space Sciences at Cornell, Jorge Calado of the Technical University of Lisbon, Portugal, and John Zollweg of Chemical Engineering at Cornell, who, along with Chris McKay of NASA/Ames, are coinvestigators in a laboratory research project funded by the NASA Planetary Atmospheres Program.

LABORATORY DATA ON N_2-(Ar)-HYDROCARBON SYSTEMS

Due in part to their engineering importance, N_2, CH_4, C_2H_6, and C_3H_8 are well-characterized in the pure state. But for mixtures, the increased degrees of freedom which must be explored in the laboratory makes the availability of data covering all relevant p-T-X space less likely. (X is the mol fraction of a component in the liquid.) Data at the relevant low temperatures and pressures are particularly sparse.

We summarize the available data for vapor-liquid equilibrium in binary and higher combinations of N_2, CH_4, C_2H_6, C_3H_8, and Ar in Table I. In order to accurately model the Titan clouds, one needs good data on the N_2-CH_4 system. This system is the best studied of the binaries, but available data does not guarantee consistent data.[4] Most of the other binaries have few if any measurements at $T \leq 110$°K, relevant to Titan's surface. In order to understand the vapor-liquid equilibrium (VLE) at Titan's surface, and form a working model of, for example, the thermal opacity—temperature—VLE feedback processes which are active on Titan, we must form a good working knowledge of the constituent binaries of the N_2-CH_4-C_2H_6 system, and preferably perform direct experiments on the N_2-CH_4-C_2H_6 ternary relevant to surface-atmosphere equilibrium. After some discussion of the basic thermodynamics and models, we describe two existing types of experimental apparatus with which we are better characterizing the N_2-C_2H_6 and CH_4-C_2H_6 binaries, and a third apparatus with which we can perform direct vapor-liquid composition measurements of multicomponent systems.

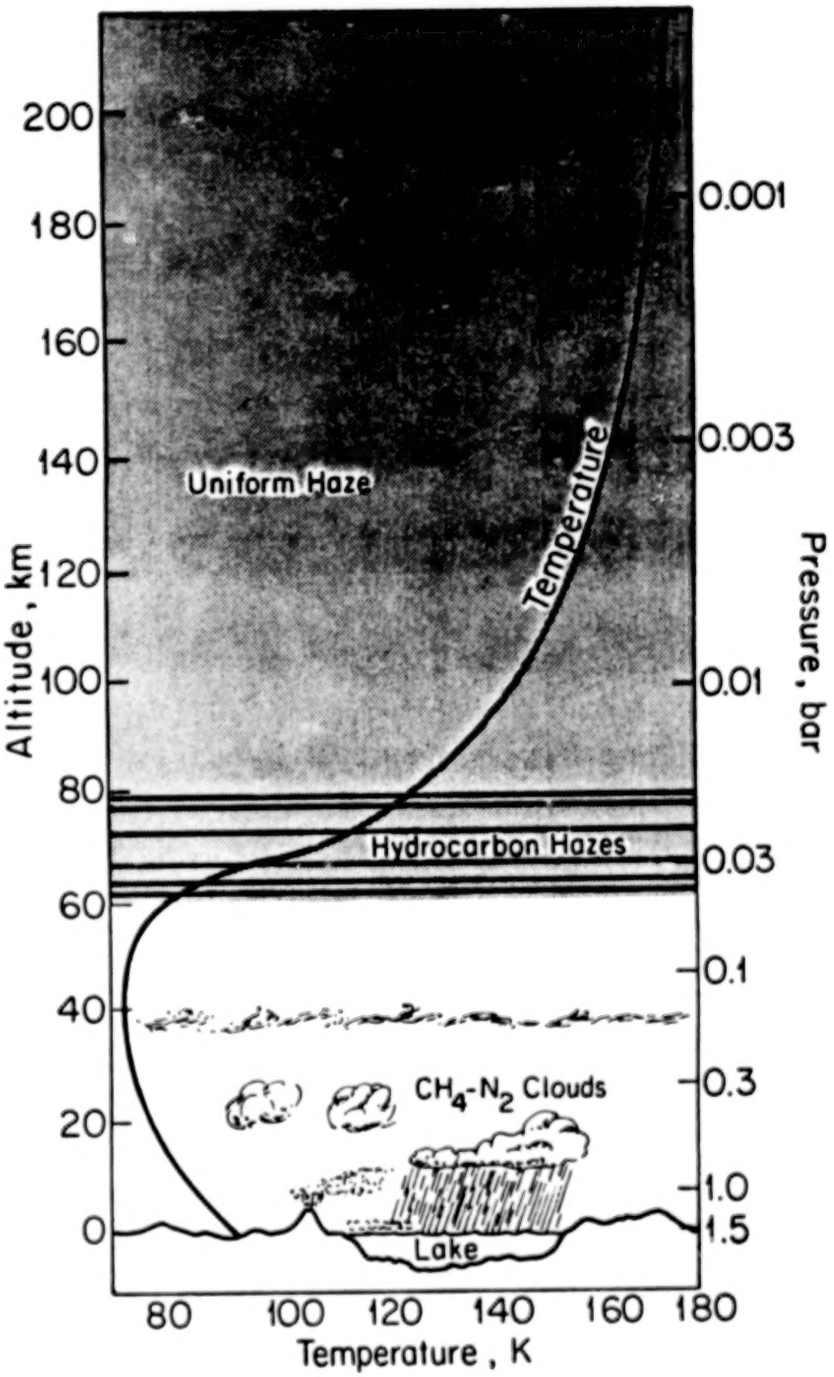

Figure 1. A sketch of Titan's atmosphere, surface, and condensates. A thick haze extends high into the stratosphere, while organic gases condense near the base of the stratosphere. Various types of CH_4-N_2 clouds are shown in the troposphere. There is evidence for precipitating clouds of CH_4-N_2 and surface lakes or oceans of C_2H_6-CH_4-N_2-..., as shown. The suggestion of geologic activity is artistic speculation only.

Table I

Availability of Experimental Data,
N_2–Ar–Hydrocarbon Systems

System	(p,T) Coverage	Assessment and Comments
N_2-CH_4	$T \geq 91°K$ $p \geq 0.2$ bar	Fair coverage of (p,T) relevant to surface-atmosphere equilibrium if several studies are combined (about 20 p,T,X measurements total). Data applicable to atmosphere-cloud equilibrium more limited, with only a few measurements down to 80°K (cf. review of Kidnay *et al.*[4]) *New modeling discussed here.*
Ar-CH_4	$T \geq 92°K$ $p \geq 0.16$ bar; $T \geq 105°K$ $p \geq 1.8$ bar	Six points below 92°K (ref. 5). Adequate coverage above 105°K (refs. 6, 7). Poor below 105°K and for low p relevant to small Ar abundances expected.
N_2-Ar-CH_4	$T = 112°K$ $p \geq 3.0$ bar	Limited to one temperature.[8] At T this high, low pressures correspond to Ar-dominated gas.
CH_4-C_2H_6	$T \geq 111°K$ $p \gtrsim 0.1$ bar	Good coverage above 111°K, cf. review by Hiza, Miller and Kidnay.[9] Needs extension down to 91°K or even lower (eutectic at 72.5°K). *New work and modeling discussed here.*
N_2-C_2H_6	$T = 110.9°K$ $p \gtrsim 0$ bar; $T \geq 101°K$ $p \geq 6.9$ bar	Useful data at 110.9°K (ref. 10); range of T only at high pressures.[11] Need coverage at lower (p,T). *New work and modeling discussed here.*
N_2-CH_4-C_2H_6	$T \geq 144°K$ $p \geq 68.9$ bar; $T \geq 171°K$ $p \geq 1.9$ bar	Available data[12,13] only at (T,p) much different than found on Titan. Three-phase $(\ell - \ell - v)$ data exists for $T \geq 117°K$, $p \geq 14$ bar (ref. 14). This most relevant ternary system needs study in the two-phase $(\ell - v)$ region to 90°K and lower.
CH_4-C_3H_8	$T \geq 90°K$ $p \gtrsim 0.01$ bar	Good coverage above 90°K, cf. review by Miller, Kidnay and Hiza.[15] Study could be extended to lower T, toward eutectic.
N_2-CH_4-C_3H_8	$T \geq 114°K$ $p \geq 2.9$ bar	Fair coverage above 114°K (ref. 16). Also three-phase $(\ell - \ell - v)$ data for $T \geq 117°K$, $p \geq 13.8$ bar (ref. 14).
Ar-CH_4-C_2H_6	$T = 116°K$ $p \geq 4.0$ bar	Limited to one temperature and relatively high pressures.[17]
CH_4-C_2H_6-C_3H_8	$T \geq 115°K$ $p = 1.0$ bar	Some useful data.[18] Needs study at lower (p,T).
N_2-Ar-C_2H_6, etc.	—	Other relevant systems not studied, or at much higher (p,T) than relevant for Titan.

CONDENSATE-VAPOR THERMODYNAMICS OF MIXED SYSTEMS

For the simple case of an ideal solution, the pressure of a component p_i is simply proportional to its mol fraction X_i in the liquid. The statement of Raoult's law, and the free energy of mixing for an ideal solution, are

$$p_i = X_i p_i^\circ$$

$$G^I_{mix} = RT \sum_i X_i \ln X_i \tag{1}$$

where p_i° is the vapor pressure of i in the pure state, G^I_{mix} is the Gibbs free energy of mixing in the ideal case, and R is the universal gas constant.

For molecules with similar polarizabilities and sizes, Raoult's law can provide a reasonable first guess, but real systems always show some deviation from ideality. To characterize the thermodynamic behavior of real systems, the concept of excess quantities is introduced. An excess quantity is simply the *actual* measurement for a mixture minus that which would apply for the hypothetical *ideal* mixture. A pivotal quantity is the excess free energy

$$G^E = \sum_i X_i \mu_i^E \tag{2}$$

where μ_i^E is the chemical potential for species i,

$$\mu_i^E = RT \ln \gamma_i \tag{3}$$

and γ_i is the *activity coefficient*. For calculating equilbria an expression for γ_i is central, since the general expression for the vapor pressure in a mixture is

$$p_i = \gamma_i X_i p_i^\circ \tag{4}.$$

[Here, to facilitate readability, we write pressures p_i, implicitly assuming that the gases are ideal. In the real case, gases near their condensation temperatures are nonideal, and pressures are replaced by fugacities f_i. See Prausnitz *et al.*[19] for a good description of the details.]

Several empirical, semi-empirical, and theoretical approaches can be followed to develop a mathematical or computational model for G^E. The usual approach is to adopt a mathematical representation for G^E, and obtain the expression for activity coefficents via the Gibbs-Duhem relation

$$\mu_i^E = RT \ln \gamma_i = \frac{\partial}{\partial n_i}\left[n_T G^E\right]_{T,P,n_j} \tag{5}$$

where n_i is the mols of component i and $n_T = \sum n_i$.

In developing a model, it is possible to perform a power-series expansion in (for the binary case) $(X_1 - X_2)$, or to formulate a model assuming that nonideality results mostly from enthalpic effects, or one which is dominated by entropic effects. At this time we do not consider the details of these models, but proceed to ask how one can pragmatically extract the needed information, and present examples of some accurate approaches and checks for consistency.

METHODS OF OBTAINING AND EVALUATING VLE DATA

First-order approximations can be obtained from Raoult's law, where for the ideal solution $\gamma_i \equiv 1$, or from Henry's law, a good approximation for gases far above their condensation T's: $X_i = p_i/K_H$, where K_H is the Henry constant, $K_H = \lim_{X_i \to 0} \gamma_i p_i^o$. For rough calculations, this suffices for the CH_4-N_2 system, where CH_4 is approximately ideal and N_2 approximately follows Henry's law. However, for accurate results the system must be modeled in a more general way. This is illustrated in Figure 2, where we show the degree of nonideality of CH_4 and N_2 under Titan conditions.

Another simple approach useful in some cases would be to simply extrapolate experimental data. This can to some degree be done for the CH_4-N_2 system, but the data are seldom sampled in a uniform way, coverage of parameter space is limited, and Table 1 shows that little data is available for the other important systems. Generally, then, we need to formulate a model for the system, fit limited experimental data to that model, then use the model to compute the required quantities. As theoretical work progresses, it is also possible to predict some thermodynamic quantities and use them as a check on certain experimental quantities. Specifically, we may (1) experimentally measure the complete equilibrium by determining X_i and p_i for all components at a number of T's; (2) experimentally measure only X_i and total pressure p_T, which is sufficient if an explicit form for G^E is adopted; (3) determine the form of G^E from thermodynamically related measurements, such as calorimetry; or (4) rely on theoretical calculations, at least in part.

Empirical Modeling of X_i, p_i Measurements

First we discuss the CH_4-N_2 system, and demonstrate that both the compositional and temperature dependence of the nonideality can be well modeled by a form beginning from theory but modified empirically. We use the data of Parrish and Hiza[20] from 95 to 120°K, and of McClure *et al.*[21] for 90.68°K. It will turn out that these data are very consistent within the eventual adopted model.

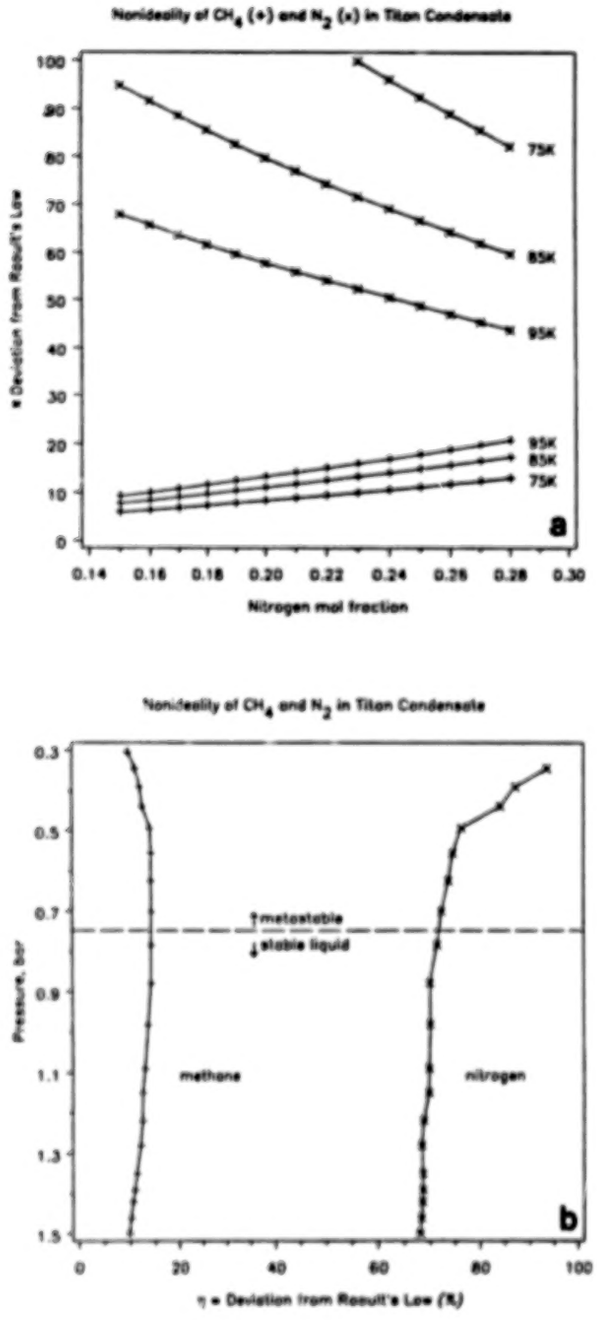

Figure 2. (a) Nonideality $\eta \equiv \gamma - 1$ of CH_4 and N_2 in binary solutions over temperatures and mol fractions spanning ranges appropriate to Titan's troposphere. The deviation from ideality (from Raoult's law) for CH_4 is about 10–15% and shows some concentration and temperature dependence. For N_2 it is much larger; also, the strong, nonlinear compositional dependence indicates that a Henry's law approximation would be inaccurate. (b) Nonideality η of CH_4 and N_2 in Titan tropospheric cloud, for condensate computed to be in thermodynamic equilibrium with the atmosphere. The (p, T) conditions[23] vary from about $p = 1.5$ bar, $T = 94°$K near the surface to $p = 0.30$ bar, $T = 73.5°$K at the highest altitude where condensation is computed to occur. These plots pertain to liquid CH_4-N_2 condensate, which is metastable (with respect to solid solutions) above the indicated level.

The first exercise was to model the data with the same simple regular-solution form previously used by Thompson,[22]

$$RT \ln \gamma_i = \sum_{j \neq i} a_{ij} X_j^2, \text{ or}$$
$$\gamma_i = \exp[(1/T)(\sum_{j \neq i} a_{ij} X_j^2)], \tag{6}$$

where R has been absorbed into the parameter a. This is equivalent to the first term of a Redlich-Kister expansion, which will be presented later. In this modeling, the activity coefficients were computed directly from the VLE data of Parrish and Hiza[20] by $\gamma_i = p_i/(X_i p_i^\circ)$. Letting subscript 1 denote CH_4 and 2 denote N_2, these fits yielded values $a_{1,2} = 156.5 \pm 4.5$ (γ_1 residual 0.0770) and $a_{2,1} = 53.1 \pm 1.6$ (γ_2 residual 0.0024). In Figure 3 we show the residuals, which are largest for CH_4 in N_2-rich mixtures and, although a much better fit overall, also large for N_2 in CH_4-rich mixtures. The arcing of the residuals indicates a need for more complex terms in (X_i, X_j) in the model equation. Even more noticeable are the trends with varying T, which cannot be removed just by adding those terms: a generalization of the T dependence is indicated.

Substantial experimentation with equations leads to a fairly simple form that describes the data very well, and is therefore useful as a model for calculations of vapor-cloud equilibrium on Titan. The form

$$\ln \gamma_i = (b_i + c_i/T)[X_j^2 + q_i(X_i - X_j)X_j] \tag{7}$$

when fit to the 90.68°K data of McClure *et al.*[21] with the 95, 100, and 105°K data of Parrish and Hiza[20] yields the fits shown in Table II.

Table II

Least-Squares Coefficients for N_2 and CH_4
Activity Coefficient Expressions

i	b_i	c_i	q_i	σ
N_2	-0.935 ± 0.041	150.2 ± 4.0	-0.133 ± 0.013	4.3×10^{-5}
CH_4	3.773 ± 0.131	-204.3 ± 12.2	0.307 ± 0.011	1.1×10^{-3}

From Figure 4 we see that any remaining systematic trends are very small. This model can be used to compute the composition of cloud droplets in Titan's atmosphere to high accuracy. (Note that in this case, nonideality of the gases has been absorbed into the model. While this simplifies calculations for the present application, an analysis separating the two effects, and considering other types of models, will be published elsewhere.)

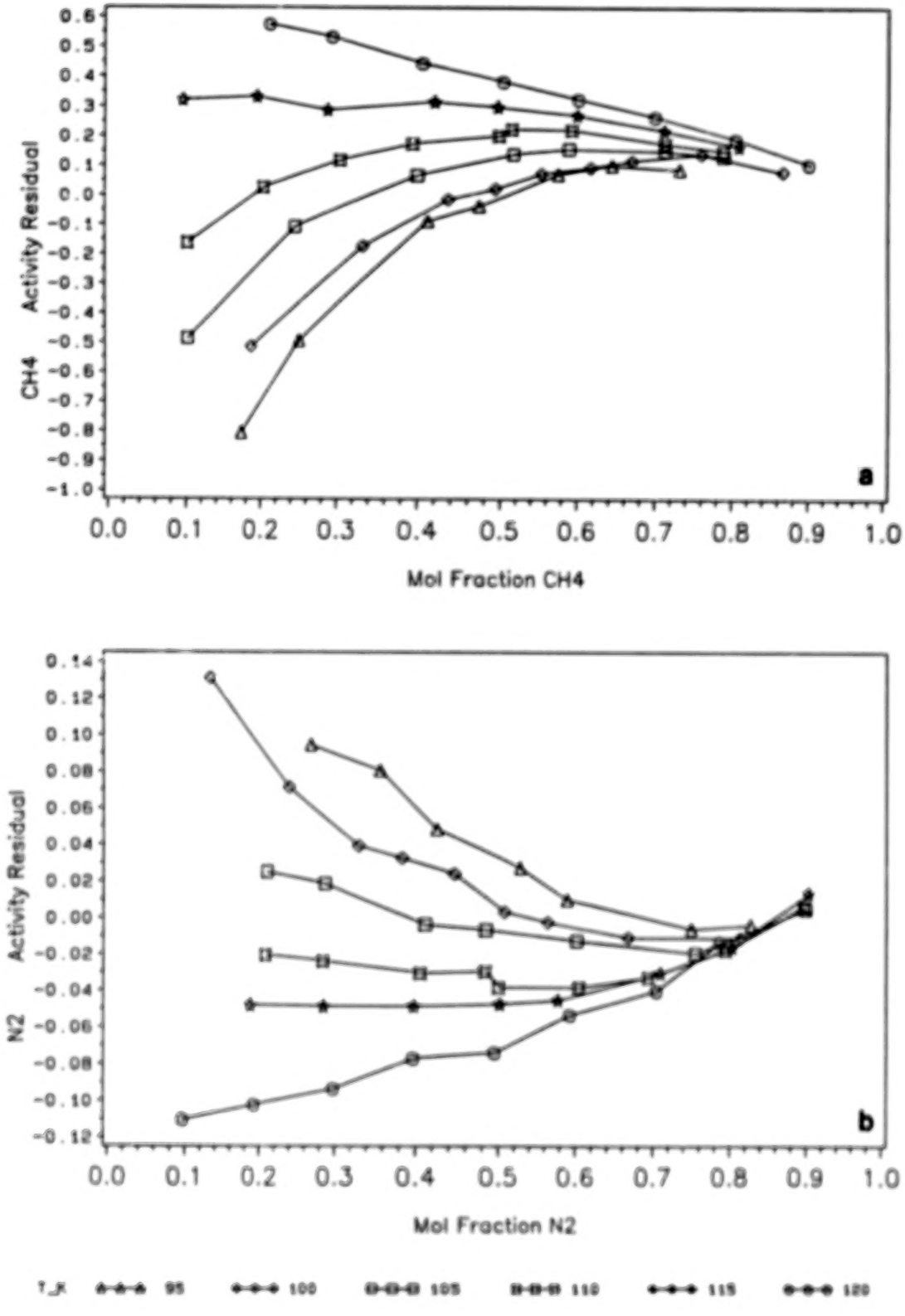

Figure 3. Residuals for fits of the experimental CH_4-N_2 VLE data of Parrish and Hiza[20] to simple activity coefficent expressions $\ln \gamma_i = a_i X_j^2 / T$. Large deviations (especially for CH_4) and regular trends in the residuals indicate that a more complex expression is needed.

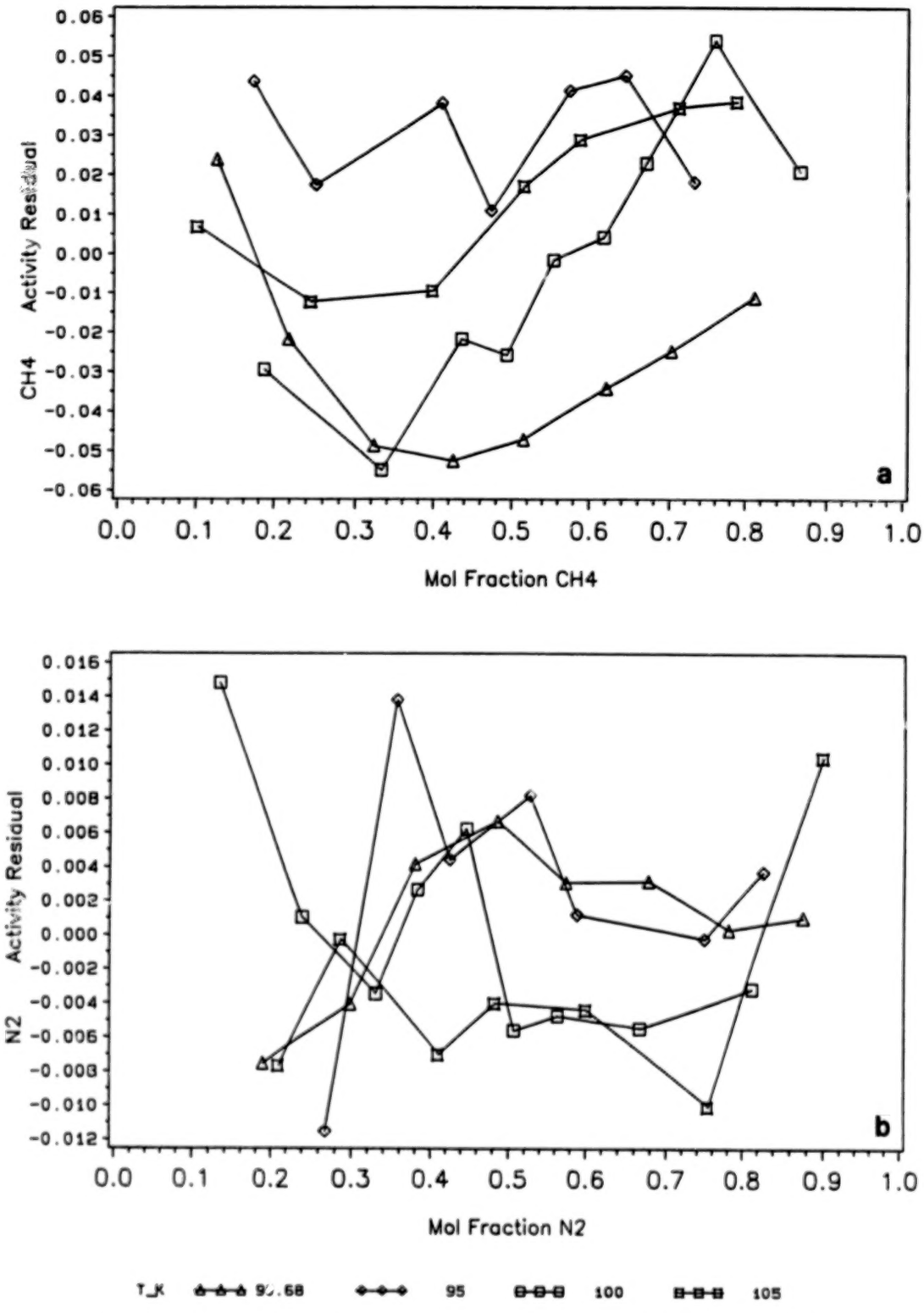

Figure 4. Residuals (a,b) for fits of the experimental CH_4-N_2 VLE data of McClure *et al.*[21] at 90.68°K and Parrish and Hiza[20] at 95, 100, and 105°K to a more complex empirical expression, $\ln \gamma_i = (b_i + c_i/T)(X_j^2 + q_i(X_i - X_j)X_j)$. Residuals are small, and systematic trends in the residuals are nearly eliminated. The derived parameters (Table II) in the above form provide an accurate basis for vapor-liquid equilibrium calculations.

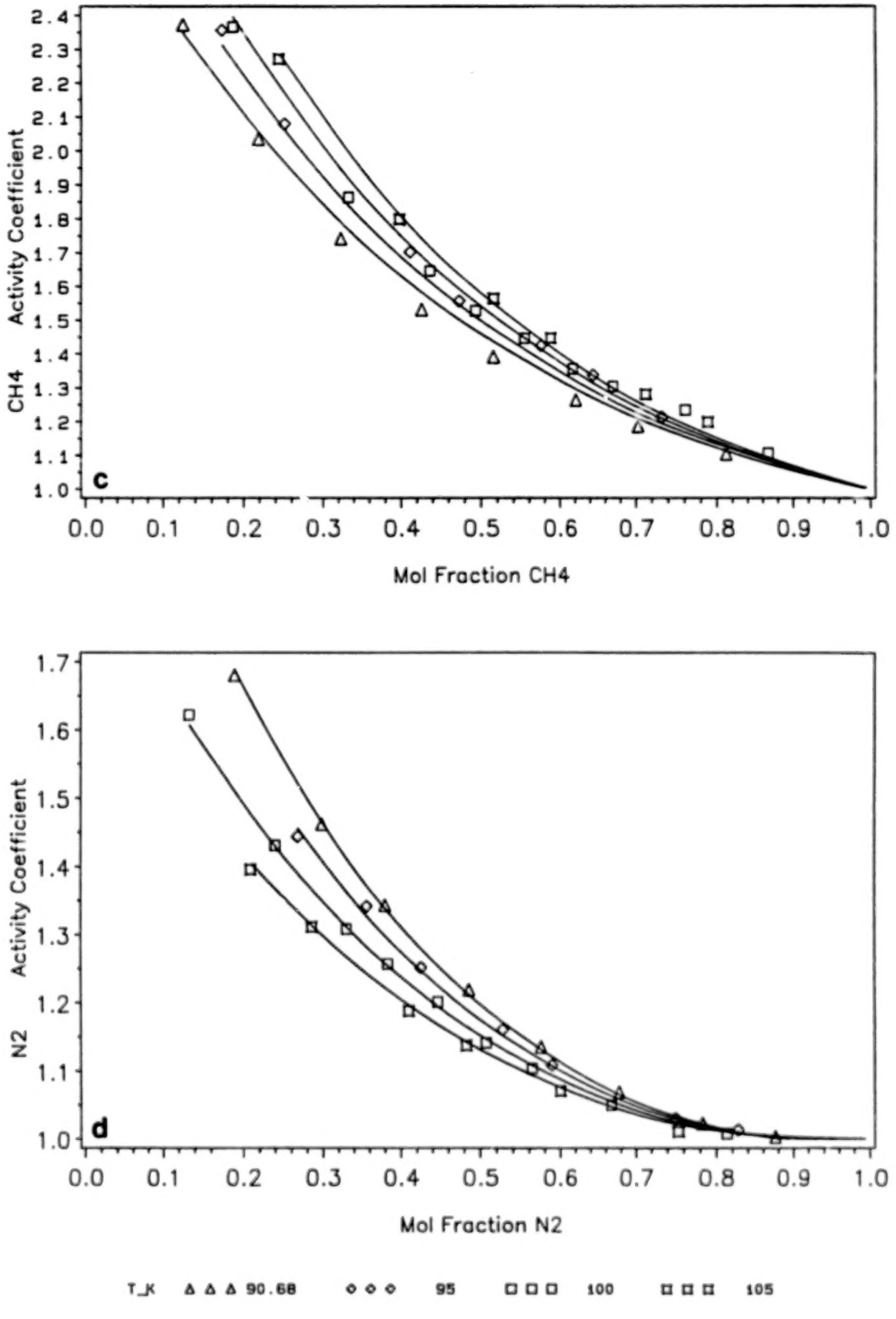

Figure 4 (continued). Experimental points and the fitted function (solid lines) are plotted in (c,d).

We proceed to use the model to compute the composition of cloud droplets as a function of altitude in Titan's atmosphere. The physical process envisioned is the lifting of a parcel of N_2+CH_4 gas from Titan's surface, checking for condensation at each level. CH_4 does not simply condense when its partial pressure exceeds the vapor pressure. Rather, in this binary system, condensation occurs when the chemical potential of the gas is greater than that of the equilibrium liquid. This is equivalent to having the sum of the CH_4 and N_2 mol fractions computed for the liquid (given the gas composition, p_T, and T) exceed unity. Every calculation of liquid composition requires an iterative solution, and if condensation occurs, calculation of the self-consistent liquid and (new) gas compositions (constrained by p_T) requires two coupled iterations. [The author can provide a computer program, or see ref. (19) for the strategies and some general implementations. We use the atmospheric structure of Lindal *et al.*[23] in these calculations.]

The results are shown in Table III and Figure 5. We begin with a large CH_4 gas-phase mol fraction $Y_{CH_4} = 0.14$ at the surface, so that the entire profile of composition can be seen. If the surface liquid is poor in C_2H_6, condensation can begin close to the surface, and droplets of low-altitude fog will contain about 16% N_2. Condensates at higher altitudes will have increasing N_2 abundances, at least through 12 km, where $X_{N_2} = 0.25$. Above that altitude, T falls below 82°K and freezing can begin. While the N_2 fraction in metastable liquid continues to increase, solubility in the solid is not as great, only about 15% at 14 km (81°K) [ref. (22)]. Droplets mixed vertically will partially degas 40% of their N_2 (about 10% of their total volume) upon freezing, no doubt producing distinctly shaped "sleet." At higher altitudes, the N_2 content of the solid condensate again increases as T decreases. Above 28 km, the T gradient becomes so low that no further condensation can take place in the CH_4-depleted gas, which by now has only 2.0% CH_4, whatever the abundance near the surface. Y_{CH_4} will remain at 2.0% to very high alititudes, where diffusive separation eventually causes it to rise again. The gas abundance of CH_4 and the composition and phase of the condensate are shown in Figure 6. There the radius of the outer circle is proportional to Y_{CH_4}, while the fractional area of the inner circle is proportional to X_{N_2}. A solid inner circle indicates solid condensate; in that case X_{N_2} is determined from the phase diagram shown by Thompson.[22]

EXPANSION FORMS FOR G^E AND THERMODYNAMIC CONSISTENCY

Another approach to evaluating and modeling VLE data involves adopting an expansion form for G^E and recognizing that, given this form, liquid compositions and p_T alone (without gas compositions Y_i) can be used to determine the activity coefficients γ_i.

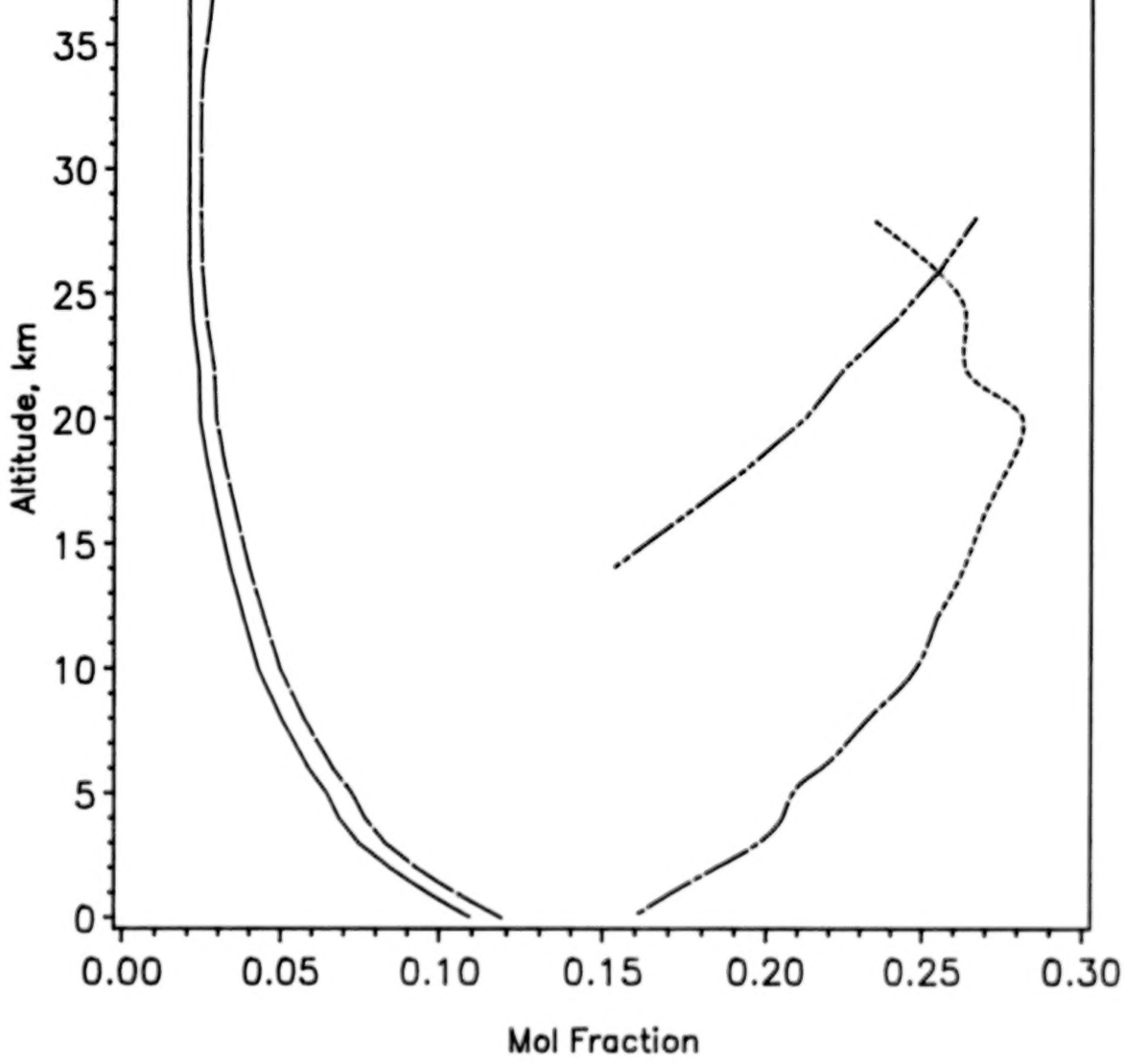

Figure 5. Computed equilibrium CH_4 and N_2 fractions in the gas and in liquid or solid CH_4-N_2 condensate in Titan's troposphere. Here, the equilibrium compositions are computed for all altitudes. The actual lowest altitude where CH_4+N_2 droplets can condense is determined by the CH_4 partial pressure at the surface, which is in turn determined by the C_2H_6 mol fraction in the ocean.[22] The solid line at left shows the actual saturation gas-phase mol fraction $Y^{sat}_{CH_4}$, while the accompanying dashed line shows the value $Y^{sat,pure}_{CH_4}$ which would apply if CH_4 condensed as the pure liquid. For the liquid, N_2 mol fractions are plotted at right. The long-short dashed line beginning at the surface gives X_{N_2} for liquid condensate. Its extension (short-dashed line) to higher altitudes shows X_{N_2} computed for the liquid, which is metastable with respect to solid at these altitudes ($T < 82$°K). The double-dashed line gives the mol fraction of N_2 in *solid* condensate, which is also a CH_4-N_2 solution.[22] Through most of the upper troposphere, the solubility of N_2 is less in the solid, which means that N_2 gas would exsolve upon freezing.

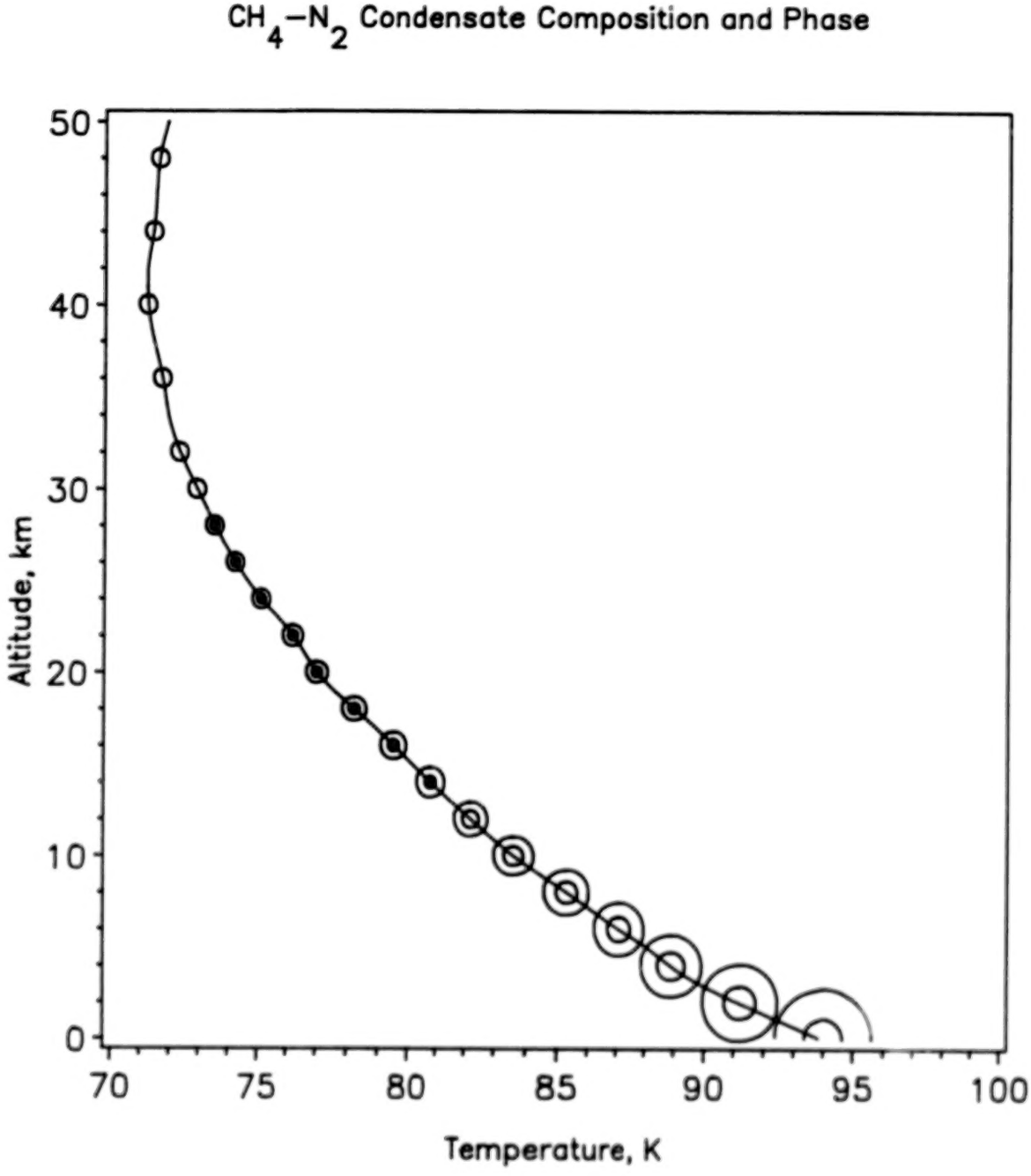

Figure 6. A nominal temperature profile for Titan's troposphere[23] is combined with the results of vapor-liquid equilibrium calculations for CH_4-N_2 (see Table III) to indicate the gas and condensate composition and phase. The *radius* of the outer circle drawn at selected altitudes is proportional to the true gas-saturation mol fraction $Y^{sat}_{CH_4}$, while the *fractional* area occupied by the inner circle equals the N_2 mol fraction in the liquid, X_{N_2}. Above 12 km, T falls below 82°K and the equilibrium phase of the condensate changes from liquid (open inner circles) to solid (solid inner circles). N_2 constitutes at least 15% and as much as 25% of the condensate particles, depending on altitude and condensate phase. Condensation does not occur above 28 km.

Table III

Vertical Profiles of Liquid-Vapor Equilibrium in Titan's Troposphere

z, km	p, bar	T, °K	$p^{\circ}_{N_2}$, bar	$p^{\circ}_{CH_4}$, bar	$Y^{\circ}_{CH_4}$	p_{N_2}, bar	$p^{sat}_{CH_4}$, bar	$Y^{sat}_{CH_4}$	X_{CH_4}	γ_{N_2}	γ_{CH_4}
0.0	1.50	94.0	4.97	1.77E-1	0.1183	1.33	1.63E-1	0.1093	0.841	1.680	1.099
0.5	1.46	93.3	4.71	1.63E-1	0.1116	1.31	1.50E-1	0.1027	0.835	1.683	1.102
1.0	1.42	92.6	4.45	1.49E-1	0.1051	1.28	1.37E-1	0.0963	0.829	1.685	1.105
1.5	1.39	91.9	4.21	1.37E-1	0.0989	1.26	1.25E-1	0.0902	0.822	1.686	1.109
2.0	1.35	91.2	3.98	1.25E-1	0.0929	1.24	1.14E-1	0.0843	0.816	1.686	1.113
3.0	1.28	89.9	3.56	1.06E-1	0.0828	1.19	9.54E-2	0.0744	0.802	1.684	1.120
4.0	1.22	88.9	3.27	9.30E-2	0.0764	1.13	8.30E-2	0.0683	0.795	1.688	1.124
5.0	1.15	88.1	3.05	8.34E-2	0.0723	1.08	7.43E-2	0.0644	0.791	1.698	1.125
6.0	1.09	87.1	2.78	7.26E-2	0.0664	1.03	6.42E-2	0.0587	0.782	1.698	1.129
8.0	0.981	85.3	2.35	5.61E-2	0.0572	0.932	4.89E-2	0.0499	0.767	1.701	1.136
10.	0.879	83.6	1.99	4.35E-2	0.0495	0.841	3.74E-2	0.0425	0.752	1.700	1.142
12.	0.785	82.2	1.73	3.50E-2	0.0445	0.756	2.98E-2	0.0379	0.745	1.714	1.142
14.	0.701	80.8	1.49	2.79E-2	0.0397	0.678	2.35E-2	0.0335	0.737	1.724	1.143
16.	0.625	79.5	1.30	2.24E-2	0.0358	0.606	1.87E-2	0.0299	0.731	1.738	1.142
18.	0.556	78.2	1.12	1.78E-2	0.0321	0.541	1.48E-2	0.0265	0.723	1.746	1.142
20.	0.494	77.0	0.972	1.44E-2	0.0291	0.482	1.18E-2	0.0238	0.719	1.763	1.140
22.	0.438	76.2	0.883	1.24E-2	0.0283	0.428	1.03E-2	0.0234	0.737	1.841	1.125
24.	0.389	75.1	0.771	1.00E-2	0.0258	0.380	8.28E-3	0.0213	0.736	1.871	1.120
26.	0.344	74.2	0.687	8.41E-3	0.0244	0.337	6.97E-3	0.0203	0.747	1.936	1.110
28.	0.304	73.5	0.628	7.30E-3	0.0240	0.298	6.14E-3	0.0202	0.767	2.038	1.096
30.	0.269	72.9	0.579	6.45E-3	0.0240	0.264	5.42E-3	0.0202	—	—	—
32.	0.238	72.3	0.534	5.69E-3	0.0239	0.233	4.79E-3	0.0202	—	—	—
34.	0.210	71.9	0.506	5.22E-3	0.0249	0.206	4.23E-3	0.0202	—	—	—
36.	0.185	71.7	0.492	5.00E-3	0.0270	0.181	3.73E-3	0.0202	—	—	—
38.	0.163	71.4	0.472	4.69E-3	0.0287	0.160	3.30E-3	0.0202	—	—	—
40.	0.144	71.2	0.459	4.49E-3	0.0311	0.141	2.91E-3	0.0202	—	—	—

While there are many other analytic forms that can be developed for G^E, a useful general one is the Redlich-Kister expansion

$$\frac{G^E}{RT} = X_1 X_2 [a + b(X_1 - X_2) + c(X_1 - X_2)^2 + ...] \tag{8}.$$

Applying the Gibbs-Duhem relation and retaining three terms yields

$$\ln \gamma_1 = \frac{X_2^2}{RT}[a - (1 - 4X_1)b + (1 - 8X_1 + 12X_1^2)c]$$
$$\ln \gamma_2 = \frac{X_1^2}{RT}[a + (1 - 4X_2)b + (1 - 8X_2 + 12X_2^2)c] \tag{9}.$$

The parameters a, b, c, ... can be determined either by computing γ_i from X_i and p_i (as illustrated for CH_4-N_2 above), and computing least-squares fits directly, or by using only X_i and p_T to achieve an interative least-squares solution for the parameters.[24] In particular, this approach amounts to a least-squares solution to the equation

$$p_T = \exp\left[\frac{X_2^2}{RT}(a - b(1 - 4X_1) + ...)\right] + \exp\left[\frac{X_1^2}{RT}(a + b(1 - 4X_2) + ...)\right] \tag{10}.$$

This method does not depend on Y_i measurements, which tend to be more uncertain than X_i measurements, and guarantees that p_T and X_i are consistent with the thermodynamic model.

Using this approach, data that seems inconsistent can sometimes be reevaluated. It has been applied to the data of Wilson[10] for the C_2H_6-N_2 system, determining the values $a = 2.472$, $b = 0.479$ at 110.9°K. (Reevaluations and new measurements of C_2H_6-N_2 are due to coinvestigator J. Calado.) These parameters can be used to evaluate a quantity often used to intercompare data, $G^E_{X=0.5}$, which for C_2H_6-N_2 at 110.9°K is 570 J mol^{-1}. We report below some new measurements on this system.

EXPERIMENTAL TECHNIQUES

We describe techniques for obtaining vapor-liquid equilibria and relevant thermodynamic quantities for mixed systems in this section, giving examples corresponding to equipment which is being used in our investigations. The three systems can be described as total-pressure/volumetric, flow/calorimetric, and recirculation/liquid-vapor sampling systems.

Volumetric Total-Pressure System

In the all-glass volumetric VLE system at the Technical University of Lisbon, carefully measured quantities of gases are condensed into a pyknometer, which very accurately measures liquid volumes. Very stable T is achieved by using gases at their triple points as thermostats: CH_4 at 90.69°K and C_2H_4 at 103.99°K are particularly relevant for Titan studies. Measuring the total pressure and knowing the total composition and volumes allows an iterative calculation of the exact liquid and vapor compositions. Both VLE and liquid volumetric data are obtained. The experimental layout is shown in Figure 7; for more details, see ref. (25).

C_2H_6-N_2 experiment and theory.

Recent work with this system has provided new data on the C_2H_6-N_2 system at 90.69°K, which we summarize here. The C_2H_6-N_2 system shows only limited solubility, separating into two liquid phases over much of the compositional range. The miscibility gap extends from a maximum solubility of about 10–20% N_2 on the C_2H_6-rich side to about 3–6% C_2H_6 on the N_2-rich side. [See ref. (22) for a ternary phase diagram showing the miscibility limits for C_2H_6-CH_4-N_2 and (on its lower boundary) for C_2H_6-N_2; also see ref. (26) and below.]

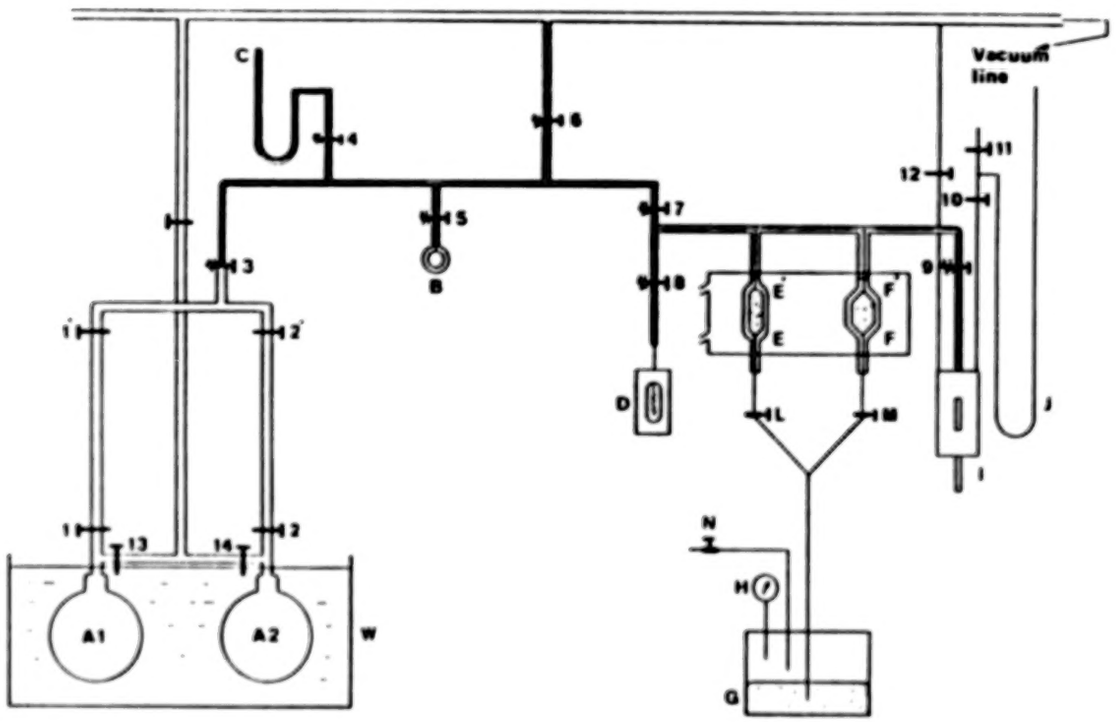

Figure 7. The low-to-moderate pressure, volumetric-manometric VLE system at the Technical University of Lisbon.[25] Thermostatted gas samples in A1-A2 are used to supply known quantities of two gases, which are condensed in the calibrated pyknometer (volumetric assembly) I. Once the gases are transferred, equilibrium is attained by expanding and contracting the vapor space using the volumes E and F, which can be filled either with vapor or with mercury from reservoir G. Knowing the initial composition, liquid volume, and total pressure provides data sufficient to compute G^E at a given temperature.

Details on the C_2H_6-N_2 system integrating data from several sources will be published elsewhere; however, we find the value of $G^E_{X=0.5}$ at 90.69°K is 508.6 J mol^{-1}. Using the Gibbs-Helmholtz relation

$$\left[\frac{\partial(G^E/T)}{\partial T}\right]_{p,X} = -\frac{H^E}{T^2} \tag{11}$$

gives a value for the enthalpy of mixing $H^E_{X=0.5} = 235$ J mol^{-1}. An absolute theoretical approach using the Kohler-Fischer perturbation theory and a WCA division of the intermolecular potential is also being pursued. N_2 and C_2H_6 molecules are modeled as hard spheres (1-center) or hard fused spheres (2-center). Results for calculations with both N_2 and C_2H_6 represented as 2-center fused spheres yield $G^E_{X=0.5} = 526$ J mol^{-1}, $H^E_{X=0.5} = 358$ J mol^{-1}, and $V^E_{X=0.5} = -1.74$ cm^3 mol^{-1}. [V^E is the excess volume, which can be estimated[27] to be -1.89 cm^3 mol^{-1}.] Comparison of these preliminary results with the experimental measurements shows good agreement for G^E and V^E, but indicates that the theory is too high or experiment is too low in estimating H^E.

CH_4-C_2H_6 studies.

Using this apparatus, the Lisbon investigators have also obtained new data on the CH_4-C_2H_6 system[29] at 90.69 and 103.99°K. In Figure 8 we show the variation of p_T (essentially, p_{CH_4}) with composition, and the departures from ideality in this system. In Figure 9 we show the complete thermodynamic profile of the system (G^E, H^E, and the computed excess entropy term TS^E versus composition). Combining the results of Miller and Staveley[28] for H^E at 91.5 and 112.0°K with the G^E relationships obtained from VLE at 90.69 and 103.99°K allows, through assumption of a Redlich-Kister form and integration of the Gibbs-Helmholtz equation, the derivation of T-dependent parameters:[29]

$$a = 80.43/T + 0.4236 \ln T - 2.183$$

$$b = 29.65/T + 0.2405 \ln T - 1.300$$

$$c = 0.0432.$$

These may be used in eq. (9) to accurately describe the CH_4-C_2H_6 system at temperatures relevant to Titan.

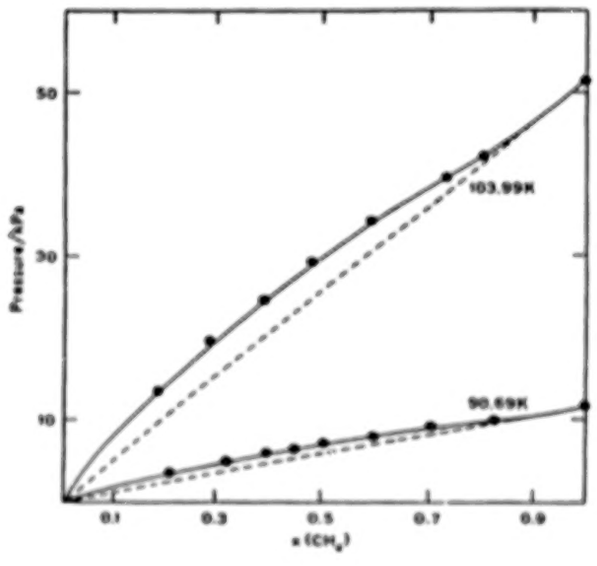

Figure 8. Experimental total vapor pressure versus composition for $CH_4 + C_2H_6$ mixtures at 90.69°K and 103.99°K (ref. 29). Experimental data are solid dots joined by the smooth lines. Dashed lines represent the ideal state (Raoult's law).

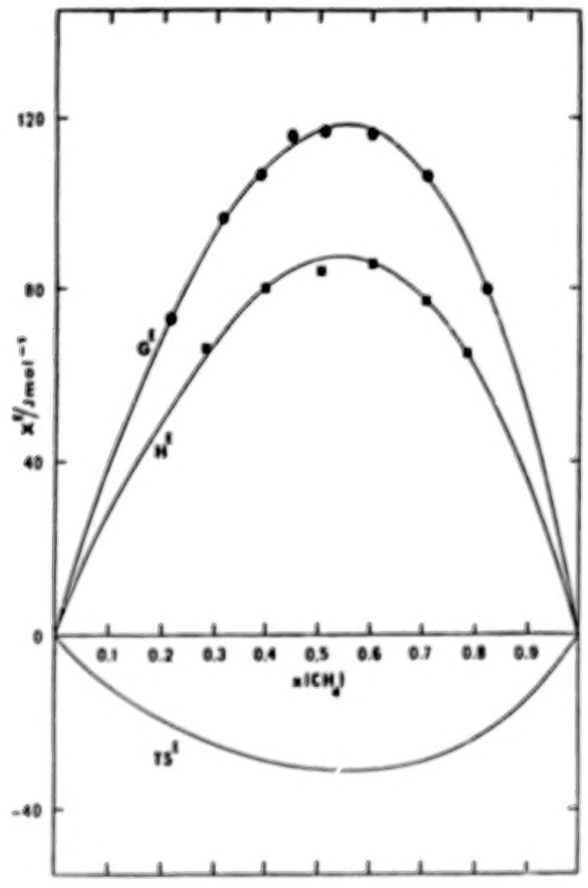

Figure 9. Excess thermodynamic quantities versus composition[29] for CH_4-C_2H_6 mixtures at ~91°K. Excess free energy G^E is derived from fitting volumetric - total pressure results at 90.69°K to a Redlich-Kister equation, while enthalpy of mixing H^E is from calorimetric measurements at 91.5°K (ref. 28). The entropic term $TS^E = H^E - G^E$. Solid curves are computed from least-squares parameters determined for the Redlich-Kister equation.

Flow-Calorimeter System.

A second approach which can yield both direct thermodynamic measurements and, within the context of a model, parameters for VLE calculations is through calorimetric determinations of the heat of mixing H^E. In the School of Chemical Engineering at Cornell, our coinvestigator J. Zollweg and collaborators have developed a cryogenic, continuous-flow calorimeter,[30] a unique device for studying the H^E of liquefied gas binaries from 77 to 300°K and 0–150 bar. In this device (Figure 10), the basic principle is to compensate for the (generally) endothermic heat of mixing by supplying enough power to a heater in order to maintain a constant T in the calorimeter. The unit is computer controlled to monitor inlet, outlet, and calorimeter T's, mass flow rates, and pressure; the computer also processes the data locally.

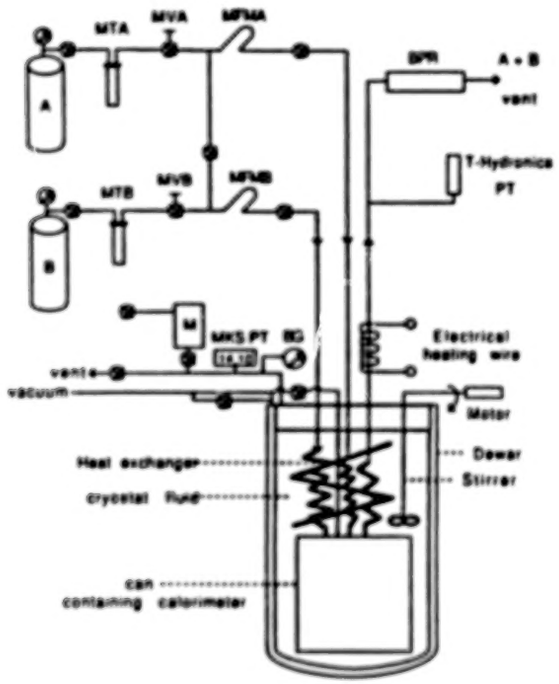

Figure 10. Schematic of the low temperature, high pressure flow calorimeter in the School of Chemical Engineering at Cornell University.[30] Continuous gas streams from A and B are metered, cooled, then mixed in the calorimeter. H^E is determined from the power required to maintain a constant temperature in the calorimeter, with other corrections. Abbreviations: MT: moisture trap; MV: metering valve; MFM: mass flow meter; PT: pressure transducer; BPR: back-pressure regulator; BG: Bourdon gauge; M: manostat.

We have used this unit to measure H^E for the C_2H_6-N_2 system at 92.3°K, both in the single-liquid-phase region and through the region of two liquid phases (the miscibility gap). The unusual ability to measure through the two-liquid region allows the miscibility limits to be defined more precisely. These results[26] have recently been reevaluated, yielding corrected values for the four points within the one-liquid region, shown in Table IV.

Table IV

Recomputed Heat-of-Mixing for C_2H_6-N_2 at 92.3°K

X_{N_2}	H^E, J mol^{-1}
0.1255	104.6
0.2145	150.2
...	...
0.9199	69.4
0.9706	21.5

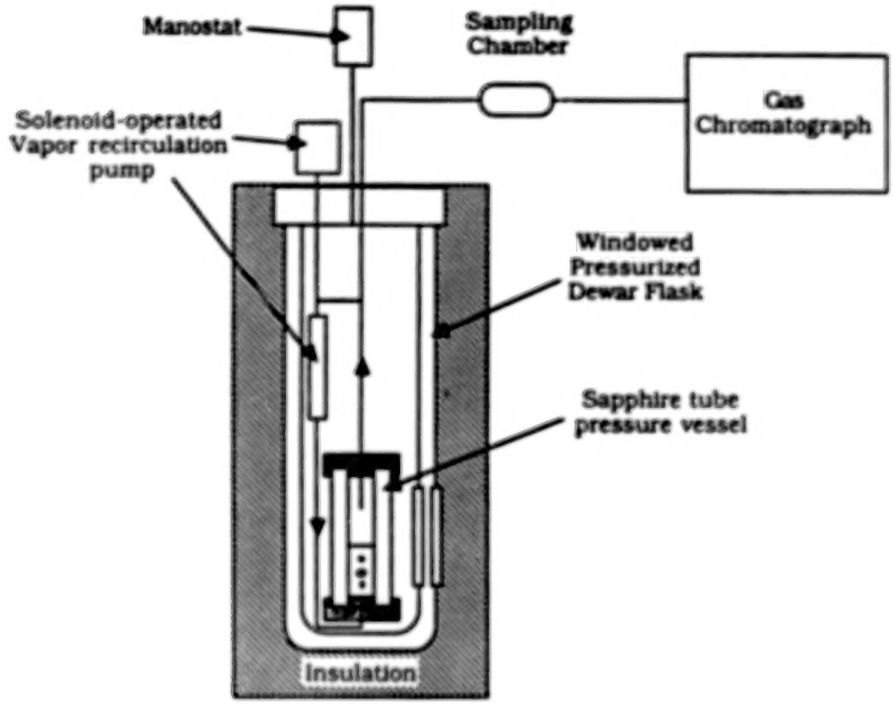

Figure 11. Schematic illustrating the main components of the recirculating vapor, VLE system built recently in Space Sciences at Cornell University. Liquid is condensed into the central pressure vessel from external gas supplies (not shown), then vapor is recirculated using the pump to achieve rapid equilibrium. T is fixed by setting the pressure of the cryogenic fluid in the dewar (surrounding the pressure vessel) using a manostat. Two sample lines (one is shown) allow the withdrawal of both gas and liquid for precise compositional analysis using the gas chromatograph. Both binary and higher-order mixtures, specifically the C_2H_6-CH_4-N_2 system, can be studied with this apparatus.

Fitting this data to a regular solution form $H^E = aX_1X_2$ gives $a = 929$, so this work predicts $H^E_{X=0.5} = 232\,\mathrm{J\,mol^{-1}}$, in good agreement with the value derived above from VLE data ($235\,\mathrm{J\,mol^{-1}}$).

Further work with constituent binaries of the CH_4-C_2H_6-N_2 system at a series of T's is planned for this system. As shown above, adoption of a form for H^E and measurements of its variation with T allow the derivation of G^E through the Gibbs-Helmholtz equation. G^E in turn provides γ_i expressions through the Gibbs-Duhem equation.

Recirculating Vapor-Liquid Equilibrium System.

While the volumetric and calorimetric systems yield very useful data, we wish to obtain both a more thorough coverage of T-dependence for the CH_4-N_2, C_2H_6-N_2, and CH_4-C_2H_6 binaries, and perform direct experiments on the C_2H_6-CH_4-N_2 ternary. For

this purpose, we have designed and built a cyrogenic, recirculating, direct-sampling phase equilibrium vessel. A simplified schematic of this device is shown in Figure 11. It consists of a cylindrical sapphire tube pressure vessel, which has recirculating lines leaving the vapor space and reentering the liquid at the base. Vapor is actively pumped through this loop, so that equilibrium is achieved rapidly. Two sampling lines (one is shown) enter the top of the tube, and can be positioned to sample gas or liquid. Analysis of these samples by gas chromatography (GC) determines the mol fractions accurately and directly, independent of other volumetric or thermodynamic information. The tube is contained in a dewar with windows, so that the sample can be examined to allow tube positioning and to check for phase separation (two liquid layers) or of freezing. Temperature is selected by regulating the pressure of the cryostat fluid in the dewar, usually liquid N_2, with a manostat. Pressure is measured with a quartz-spiral Bourdon tube unit, and temperature with a platinum resistance thermometer. While the interior sample chamber is capable of high pressure, the operating pressure of this unit is intended to be 0–8 bar, 75–120°K, tailored to the many relevant measurements needed for Titan. Lower and higher T, p ranges can be realized with slight modifications. By incremental addition of the more volatile component, complete coverage of compositional ranges can be achieved fairly rapidly.

Our group of investigators has critically assessed and modeled experimental data on the CH_4-N_2, C_2H_6-N_2, and CH_4-C_2H_6 systems while building this unit, which is now undergoing final testing in the Space Sciences Building at Cornell. We will continue other studies while starting to obtain direct VLE measurements with this recirculating equilibrium system early in 1990. We welcome suggestions for experimental work, or technical inquiries about any of the three systems which we are using in this project.

ACKNOWLEDGMENTS.

Thanks to coinvestigator Jorge C. G. Calado for providing unpublished data and other material for the conference presentation. This work is supported by the NASA Planetary Atmospheres Program through grant NAGW-1444.

REFERENCES.

1. G. N. Brown, Jr. and W. T. Ziegler. *Adv. Cryogen. Eng.* **25** 662 (1980).
2. J. H. Dymond and E. B. Smith. *The Virial Coefficients of Pure Gases and Mixtures.* Clarendon, Oxford (1980).
3. W. R. Thompson, T. Henry, J. Schwartz, B. N. Khare and C. Sagan. *Center for Radiophysics and Space Research, Report 941.* CRSR, Cornell Univ., Ithaca NY (1989).

4. A. J. Kidnay, R. C. Miller, E. D. Sloan and M. J. Hiza. *J. Phys. Chem. Ref. Data* **14** 681 (1985).
5. H. Cheung and D. I.-J. Wang. *Indust. Eng. Chem. Fundam.* **3** 355 (1964).
6. D. Gravelle and B. C.-Y. Lu. *Can. J. Chem. Eng.* **49** 114 (1971).
7. A. G. Duncan and M. J. Hiza. *Indust. Eng. Chem. Fundam.* **11** 38 (1972).
8. R. C. Miller, A. J. Kidnay and M. J. Hiza. *J. Phys. Chem. Ref. Data* **9** 721 (1980).
9. M. J. Hiza, R. C. Miller and A. J. Kidnay. *J. Phys. Chem. Ref. Data* **8** 799 (1979).
10. G. M. Wilson. *Adv. Cryogen. Eng.* **20** 164 (1975).
11. A. T. Ellington, B. E. Eakin, J. D. Parent, D. C. Gami and O. T. Bloomer. In *Thermodynamic and Transport Properties of Gases, Liquids, and Solids*, p. 180. McGraw-Hill, New York (1959).
12. H. F. Cosway and D. L. Katz. *Amer. Inst. Chem. Eng. J.* **5** 46 (1959).
13. S.-D. Chang and B. C.-Y. Lu. *Chem. Eng. Progr. Symp. Ser.* **63** 13 (1967).
14. F. M. Llave, K. D. Luks and J. P. Kohn. *J. Chem. Eng. Data* **32** 14 (1987).
15. R. C. Miller, A. J. Kidnay and M. J. Hiza. *J. Phys. Chem. Ref. Data* **9** 721 (1980).
16. D. P. L. Poon and B. C.-Y. Lu. *Adv. Cryogen. Eng.* **19** 292 (1974).
17. I. M. Elshayal and B. C.-Y. Lu. *Cryogenics* **11** 285 (1971).
18. K. Watanabe, M. Kuroki, M. Ogura and I. Saito. *Cryogen. Eng. (Tokyo)* **4** 292 (1969).
19. J. M. Prausnitz, C. A. Eckert, R. V. Orye and J. P. O'Connell. *Computer Calculations for Multicomponent Vapor-Liquid Equilibria*. Prentice-Hall, Englewood Cliffs NJ (1967).
20. W. R. Parrish and M. J. Hiza. *Adv. Cryogen. Eng.* **19** 300 (1974).
21. D. W. McClure, K. L. Lewis, R. C. Miller and L. A. K. Staveley. *J. Chem. Thermodyn.* **8** 785 (1976).
22. W. R. Thompson. In *The Atmospheres of Saturn and Titan*, (ESA SP-241, Edited by E. Rolfe and B. Battrick), p. 109. ESA Public. Div., Noordwijk, Netherlands (1985).
23. G. F. Lindal, G. E. Wood, H. B. Hotz, D. N. Sweetnam, V. R. Eshleman and G. L. Tyler. *Icarus* **53** 348 (1983).
24. J. A. Barker. *Austral. J. Chem.* **6** 207 (1953).
25. J. C. G. Calado, E. J. S. Gomes de Azevedo, and V. A. M. Soares. *Chem. Eng. Commun.* **5** 149 (1980).
26. J. C. G. Calado, P. Gopal, J. A. Zollweg and W. R. Thompson. *Can. J. Chem.* **66** 626 (1988).
27. M. J. Hiza, W. M. Haynes and W. R. Parrish. *J. Chem. Thermodyn.* **9** 873 (1977).
28. R. C. Miller and L. A. K. Staveley. *Adv. Cryogen. Eng.* **21** 493 (1976).
29. E. J. S. Gomes de Azevedo and J. C. G. Calado. *Fluid Phase Equil.* (in press) (1989).
30. P. Gopal, J. A. Zollweg and W. B. Streett. *Rev. Sci. Instrum.* **60** 2720 (1989).

N90-26775

OPTICAL CONSTANTS OF SOLID METHANE

BISHUN N. KHARE,* W.R. THOMPSON,* C. SAGAN,* E.T. ARAKAWA,** C. BRUEL,** J.P. JUDISH,** R.K. KHANNA,*** AND J.B. POLLACK+
*Laboratory for Planetary Studies, Cornell University, Ithaca, New York, 14853
**Oak Ridge National Laboratory, Oak Ridge Tennessee 37831
***Department of Chemistry and Biochemistry, University of Maryland, College Park, Maryland 20742
+NASA Ames Research Center, Moffett Field, California 94035

ABSTRACT

Methane is the most abundant simple organic molecule in the outer solar system bodies. In addition to being a gaseous constituent of the atmospheres of the Jovian planets and Titan, it is present in the solid form as a constituent of icy surfaces such as those of Triton and Pluto, and as cloud condensate in the atmospheres of Titan, Uranus, and Neptune. It is expected in the liquid form as a constituent of the ocean of Titan. Cometary ices also contain solid methane. The optical constants for both solid and liquid phases of CH_4 for a wide temperature range are needed for radiative transfer calculations, for studies of reflection from surfaces, and for modeling of emission in the far infrared and microwave regions. The astronomically important visual to near infrared measurements of solid methane optical constants are conspicuously absent from the literature.

We present preliminary results on the optical constants of solid methane for the 0.4 μm to 2.6 μm region. Deposition onto a substrate at 10°K produces glassy (semi-amorphous) material. Annealing this material at ~33°K for ~1 hour results in a crystalline material as seen by sharper, more structured bands and negligible background extinction due to scattering. We report k for both the amorphous and the crystalline (annealed) states. Typical values (at absorption maxima) are in the 10^{-3} to 10^{-5} range. Below λ = 1.1 μm the bands are too weak to be detected by transmission through the films $\leq$ 215 μm in thickness, employed in our studies to date.

Using our previously measured values of the real part of the refractive index, n, of liquid methane at 110°K [*Bull. Am. Phys. Soc.* **31**, 700 (1986)] we compute n for solid methane using the Lorentz-Lorenz relationship. Values vary monotonically from n = 1.304 at λ = 0.4 μm to n = 1.296 at λ = 2.0 μm. An independent, direct determination using interference fringes at two angles of incidence finds n = 1.31 ± 0.02 for the solid film at λ = 0.4-0.7 μm, a value confirmed by laser interferometry.

Work is in progress to extend the measurements of optical constants n and k for liquid and solid to both shorter and longer wavelengths, eventually providing a complete optical constants database for condensed CH_4.

INTRODUCTION

The absorption, emission, reflection and scattering of radiation by atmospheres and surfaces depends on the vertical and horizontal distribution of material, on particle size and shape, and most fundamentally on the optical characteristics of the materials present. These optical characteristics can be represented by the complex refractive index. The real and imaginary parts are commonly called the optical constants n and k, and can be determined in the laboratory by a variety of techniques.[1] CH_4 optical constants are required in radiative transfer calculations modeling light scattering and the thermal structure of planetary atmospheres, and in studies of reflection from particulate surfaces containing CH_4 ice and frost, such as those of Triton and Pluto; and also in the calculation of the energy deposition profile and penetration depth for charged particles impinging on icy outer solar system surfaces. These quantities can be calculated from the "stopping power":

$$\frac{dE}{dX} \propto \int_0^\infty -Im\left[\frac{1}{\epsilon(\omega)}\right] d\omega,$$

where $\epsilon = \epsilon_1 + \epsilon_2$, $\epsilon_1 = n^2 - k^2$, $\epsilon_2 = 2nk$, n and k are the real and imaginary part of the refractive index, amd ω is the frequency.

We have been engaged for the last several years in the laboratory determination of complex refractive indices of materials of planetary and astronomical interest. The optical constants of Titan tholin[1] produced from ~ 90% N_2 and 10% CH_4 in a plasma discharge similar to that produced by Saturnian magnetospheric charged particles which are intercepted by Titan's upper atmosphere, were utilized in radiation transfer calculations,[2,3,4] producing, for example, reflection spectra[5] and thermal structure[4] of Titan's atmosphere consistent with the ground based spectroscopic observations,[6] with Pioneer 11 polarimetric observations;[7] and with Voyager photometric observations.[8,9] Successful applications were also made with optical constants of H_2/He/CH_4 tholin appropriate to Neptune and the Uranian troposphere.[10] One of our current emphases is the determination of optical properties of condensed hydrocarbons and the effect of irradiation on these properties. Simple hydrocarbons such as methane (CH_4), ethane (C_2H_6), and acetylene (C_2H_2) are prime candidates for such studies because of their importance on several planets and their icy satellites. For example,

(a) Titan's surface probably has lakes or oceans of CH_4 and C_2H_6, with several other minor species.[11,12,13]

(b) C_2H_6, and C_2H_2 form condensate hazes in the stratospheres of Uranus and Neptune.[14]

(c) CH_4 clouds are present on Uranus and Neptune.[15]

(d) Condensed CH_4 is present on both Triton[16] and Pluto[17,18] and

(e) The presence of CH_4 in cometary comae[19] suggests the presence of condensed CH_4 and probably other hydrocarbon ices there.

A critical survey of the literature reveals that the availability of optical constants data for these materials in the visible-near IR region ranges from sparse to totally absent. We present below some preliminary results of the measurements of optical constants of solid CH_4 in the 1.1 μm to 2.6 μm range, and calculations of k and a tabulation of n throughout the visible and near-infrared.

EXPERIMENTAL DETAILS AND RESULTS

Sample Preparation

The solid films of methane were made by pulse deposition of gaseous methane on a substrate attached to the cold finger of a commercial cryocooler[20] as shown in Figure 1. An externally controlled heater wound around the cold finger of the

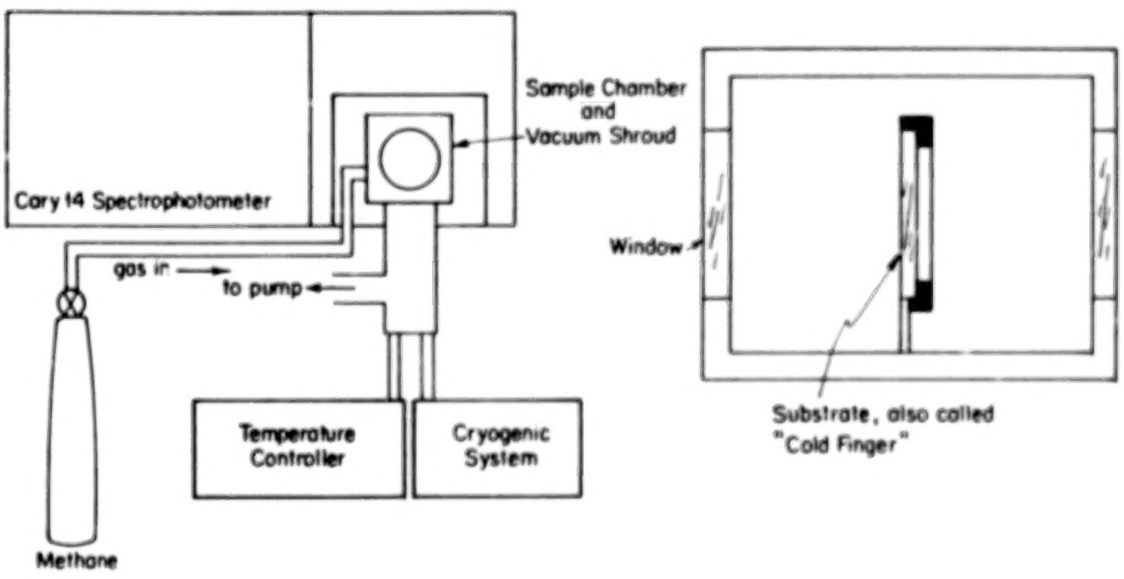

Fig. 1. Experimental set-up to measure transmission through methane film at 10°K

cryocooler enabled us to control the sample temperature to within ± 0.5°K. Both KRS-5 (for transmission) as well as polished silicon (for reflectance) were employed as substrates. Typically, the sample was deposited at 10°K which resulted in amorphous films, as evidenced by broad structureless bands in the infrared region (Figure 2). Annealing the sample at ~33°K for approximately an hour resulted in crystallinity, as evidenced by sharper structured bands and negligible background extinction due to

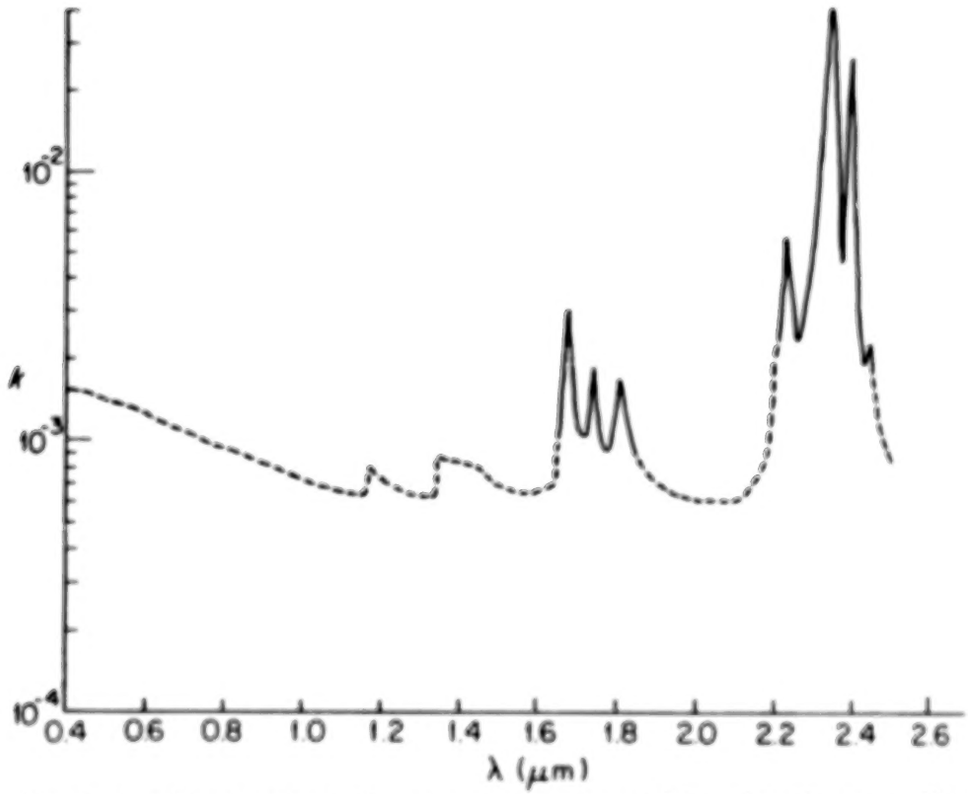

Fig. 2. Freshly deposited glassy (semi-amorphous) film of methane at ~10°K

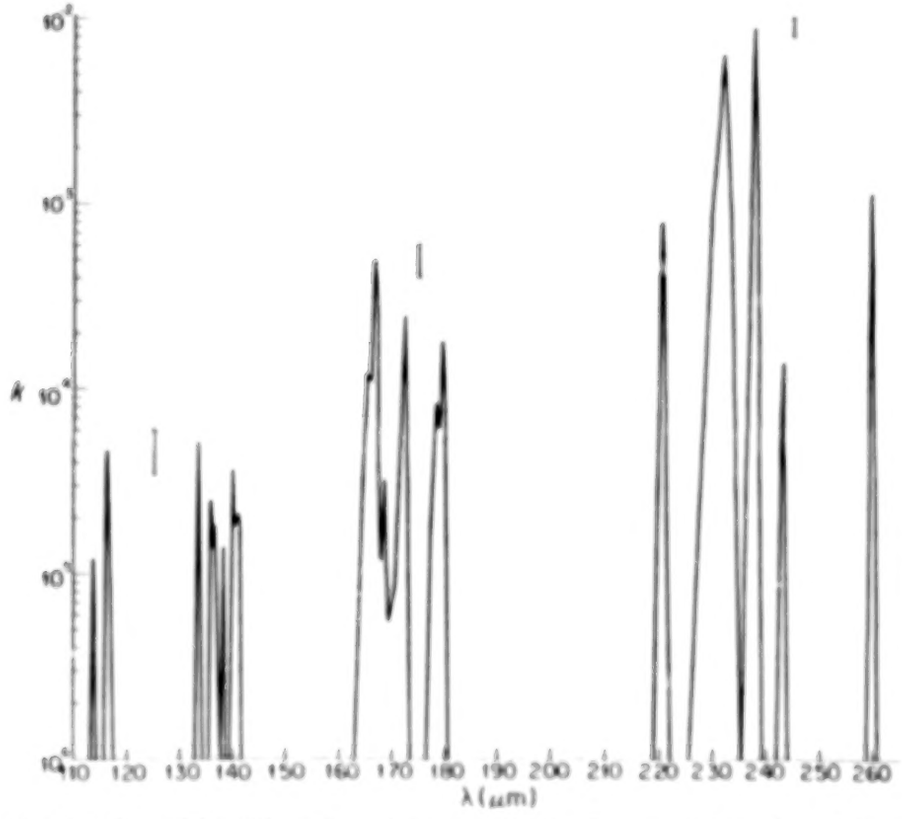

Fig. 3. Crystalline film of methane at ~33°K after annealing for ~1 hour

scattering (Figure 3). Several films from 5 μm to 215 μm thickness were investigated.

Spectral Measurements

The spectra were recorded on a Cary-14 UV-VIS-NIR spectrometer from 0.35 μm to 2.5 μm with a spectral resolution ~6 cm^{-1}. The region 2.0 μm to 2.6 μm was also measured with a Perkin-Elmer 1800 FTIR spectrometer at ~1 cm^{-1} resolution.

Data Analysis

Imaginary part of the refractive index k

The determination of the imaginary part of the refractive index, k, is determined directly by measuring the transmission through a film of thickness t and using the relation,

$$k = \frac{\lambda}{4\pi t} \ln \frac{T_s (1-R)}{T (1-R_0)^2} \qquad (1)$$

where T = transmission, T_s = Transmission of the substrate alone,

$$R_0 = \left(\frac{n_s - 1}{n_s + 1} \right)^2$$

and n_s = the real part of the refractive index of the substrate, known from independent measurements or from the literature.[21] R = the total reflectance of the film and substrate, which can be approximately determined by constructing a baseline through points where the film has no absorption bands. Further details are given by Khare et al.[1]

The only unknown in Equation (1) is the thickness of the film t which we determine from the interference fringes at 0.35 μm to 0.75 μm for two angles of incidence.[22] Since the absorption in this region is very small, the real part of the refractive index does not undergo any appreciable dispersion. Assuming n to be constant, the two equations

$$2t \ (n^2 - \sin^2\theta_1)^{1/2} = \Delta N \left(\frac{\lambda_1 \lambda_2}{\lambda_1 - \lambda_2} \right)$$

and (2)

$$2t \ (n^2 - \sin^2\theta_2)^{1/2} = \Delta N \left(\frac{\lambda_3 \lambda_4}{\lambda_3 - \lambda_4} \right)$$

where ΔN is the number of fringes in the range $(\lambda_1 - \lambda_2)$ and $(\lambda_3 - \lambda_4)$ for the two angles of incidence θ_1 and θ_2 respectively, can be solved for n and t. The thickness of the film can be obtained within about 2-5% accuracy for 5-30 μm thick films. For the

thickest film (215 μm) employed in our work, the fringes are too close to be separated accurately. For this sample, the thickness was estimated from the integrated band intensities of the stronger peaks and from the knowledge of the extinction coefficient of these bands measured for thinner films.

Substituting for t in Eq. (1) yields the k values for crystalline CH_4 tabulated in Table I and plotted in Figure 3.

The k values calculated for the amorphous film of methane are plotted in Figure 2. These results are of much poorer quality than those for crystalline CH_4 because of large background scattering. If the background contribution is subtracted from the observed data, then the k values for amorphous methane are approximately the same magnitude as the corresponding k values for crystalline methane. As we go towards wavelengths shortward of $\lambda = 1.6$ μm (Figure 2) into the visible, the loss of photons due to scattering dominates over the loss due to absorption at the peaks to such an extent that one finds complete loss of absorption features. The k values at peaks for solid glassy amorphous film are higher than those of the corresponding peak values of the crystalline film at ~33°K because of the background scattering by the non-crystalline sample.

For crystalline CH_4 (a 215 μm thick sample), scattering is much less of a problem, allowing determination of values of k as small as 10^{-6} down to a wavelength of 1.1 μm.

Extinction in solid CH_4 in the VIS-NIR region (0.4-1.1 μm) is expected to be extremely small ($k < 10^{-6}$). In Figure 4 we plot k for liquid CH_4[23,24] (solid line) measured by Ramaprasad[23] et al. and Patel[24] et al. and the k values computed[25] from room-temperature gas data obtained by Giver[26] if taken to a liquid density of 0.45 g cm^{-3} (dashed line). At low resolution, both the experimentally measured liquid CH_4 k values and those computed from gas data, are similar (Figure 4), and therefore temperature and density effects for CH_4 are minor in the VIS-NIR ($\lambda < 1.1$ μm). Since CH_4 retains rotational freedom in the solid state, only minor liquid-solid spectral differences are expected.[25] Figure 4 therefore provides a good guide for attempts to measure k in the solid at visual wavelengths. We are attempting to make optical quality solid methane discs varying in thickness from 1 to 10 cm, but Figure 4 would indicate that much thicker samples of the order of a meter or so are required to obtain k data in this region. This work is continuing at present, along with investigations of weak interband absorption and some work on other hydrocarbons.

The measurement accuracy for the crystalline CH_4 results of Figure 3 and Table I is about ± 5%, and is indicated by error bars on the graph. The largest single source of error is uncertainty in the correction of absorbance measurements on the Cary-14 spectrometer, which deviate from linearity at the higher end of the 0-1 absorbance scale. The value of k determined from the data taken on the P.E. 1800 FTIR

Table I

Imaginary Part of the Refractive Index (k) at Various Wavelengths (λ) of a Crystalline Film of CH_4 at ~33°K

λ (μm)	k = a 10^{-b}		λ (μm)	k = a 10^{-b}		λ (μm)	k = a 10^{-b}	
	a	b		a	b		a	b
1.133	1	>6	1.415	1.7	5	1.789	6.2	5
1.138	1.9	5	1.418	1	>6	1.792	7.8	5
1.143	1	>6	1.629	1	>6	1.796	1.8	4
1.156	1	>6	1.646	3.0	5	1.799	8.4	5
1.162	1.9	5	1.652	7.7	5	1.803	1.5	5
1.163	4.6	5	1.655	1.2	4	1.806	1	>6
1.164	4.7	5	1.660	1.1	4	1.830	1	>6
1.169	9.8	6	1.664	1.7	4	2.191	1	>6
1.171	9.8	6	1.669	5.0	4	2.207	7.9	4
1.173	1	>6	1.672	2.8	4	2.220	1	>6
1.330	1	>6	1.675	3.9	5	2.254	1	>6
1.333	2.4	5	1.683	1.2	5	2.299	8.4	4
1.336	5.3	5	1.687	2.8	5	2.323	6.4	3
1.341	1	>6	1.690	1.1	5	2.335	9.5	4
1.355	1	>6	1.694	5.6	6	2.353	1	>6
1.359	2.5	5	1.706	8.6	6	2.374	9.6	4
1.364	1.4	5	1.717	5.1	5	2.380	9.0	3
1.365	1.8	5	1.719	7.4	5	2.383	1.3	3
1.378	1	>6	1.723	2.5	4	2.393	1	>6
1.383	1.4	5	1.728	3.7	5	2.419	1	>6
1.387	1	>6	1.731	5.8	6	2.431	1.4	4
1.394	1	>6	1.735	1	>6	2.439	1	>6
1.402	3.7	5	1.766	1	>6	2.589	1	>6
1.405	1.9	5	1.773	1.8	5	2.600	1.1	3
1.407	1.9	5	1.778	3.8	5	2.608	1	>6
1.410	2.1	5	1.785	8.3	5			

are good to around ± 10%, with most of the error coming from the estimate of the 215 μm-thick sample.

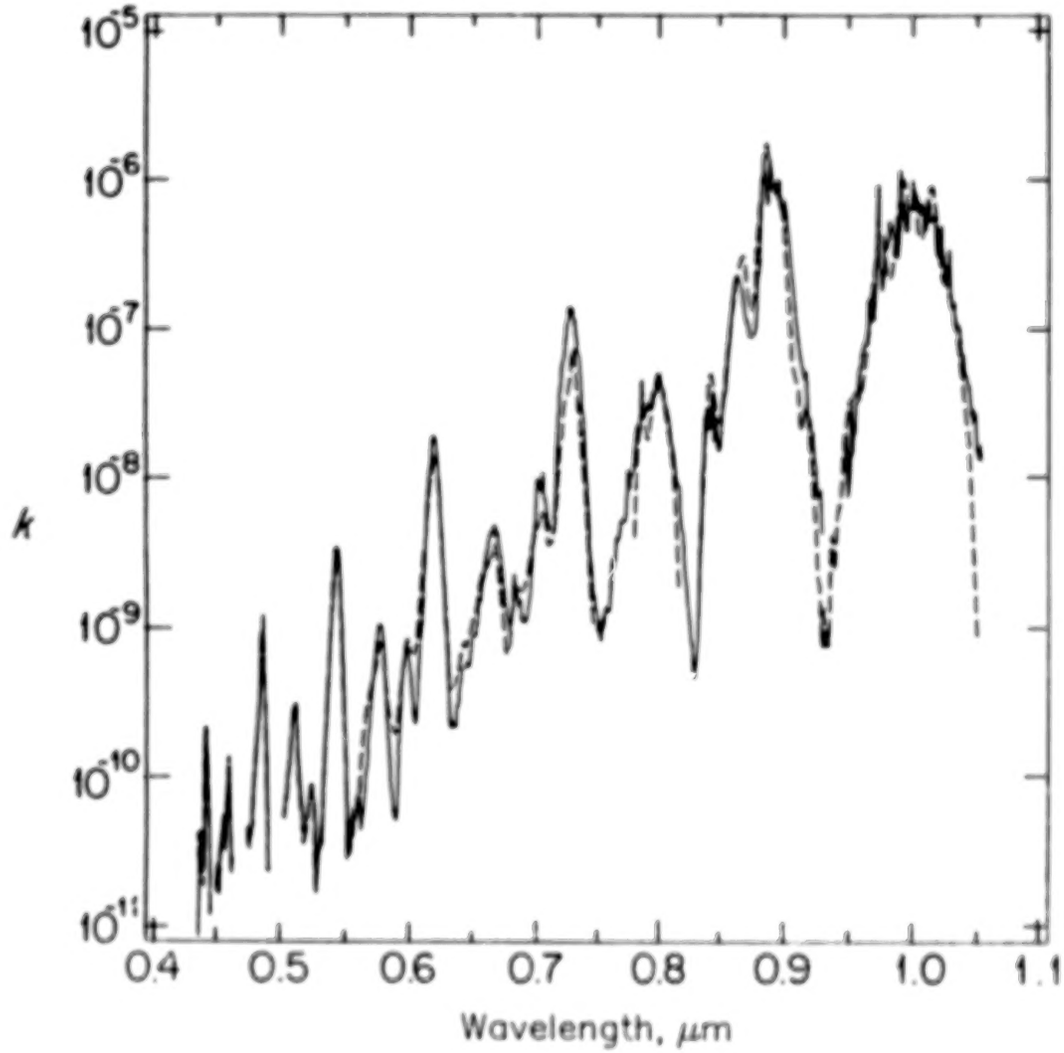

Fig. 4. Comparison[25] of k of liquid CH_4[23,34] (dashed line) with computed k values from room temperature gas data[26] if taken to a liquid density of 0.45 g cm^{-3} (solid line). Values are similar everywhere, and nearly indistinguishable below 0.55 μm.

Real part of the refractive index n

Using the technique of ellipsometric polarmetry, we have measured the refractive indices of liquid methane[27] at ~110°K from $\lambda = 0.4$ to $\lambda = 2.0$ μm. Using the Lorentz-Lorenz relationship

$$\frac{n_s^2 - 1}{n_s^2 + 2} \Big/ \frac{n_l^2 - 1}{n_l^2 + 2} = d_s/d_l \qquad (3)$$

where subscripts *l* and *s* represent the liquid and solid phases of CH_4 respectively, we could estimate the real part of the refractive index knowing the densities of liquid and solid CH_4. The density[28] of liquid CH_4 at 110°K is 0.42441 g cm^{-3}. The density of solid CH_4, d_s = 0.449 g cm^{-3} at the temperature of our solid film, ~20°K. This density is obtained by extrapolating the values of Constantino and Daniels.[29] *n* values calculated by using Lorentz-Lorenz relationship [Eq. (3)] are given in Table II and are in good agreement with the value of n = 1.31 ± 0.02 calculated from interference fringes we obtained during reflection measurements for two angles of incidence (Eq. 2).

Table II

Real Part of the Refractive Index n_s of Solid Methane Calculated from Lorentz-Lorenz Relationship						
λ (μm)	0.4	0.6	0.8	1.0	1.2	2.0
n_l	1.286	1.283	1.281	1.280	1.280	1.278
n_s	1.304	1.301	1.299	1.298	1.298	1.296

n for solid methane at λ = 0.6328 μm was further confirmed independently by a dual angle laser interference technique[30] employed to monitor film thickness and the refractive index. Two He-Ne laser beams were specularly reflected off a polished silicon crystal which was used as a substrate (Fig. 5).

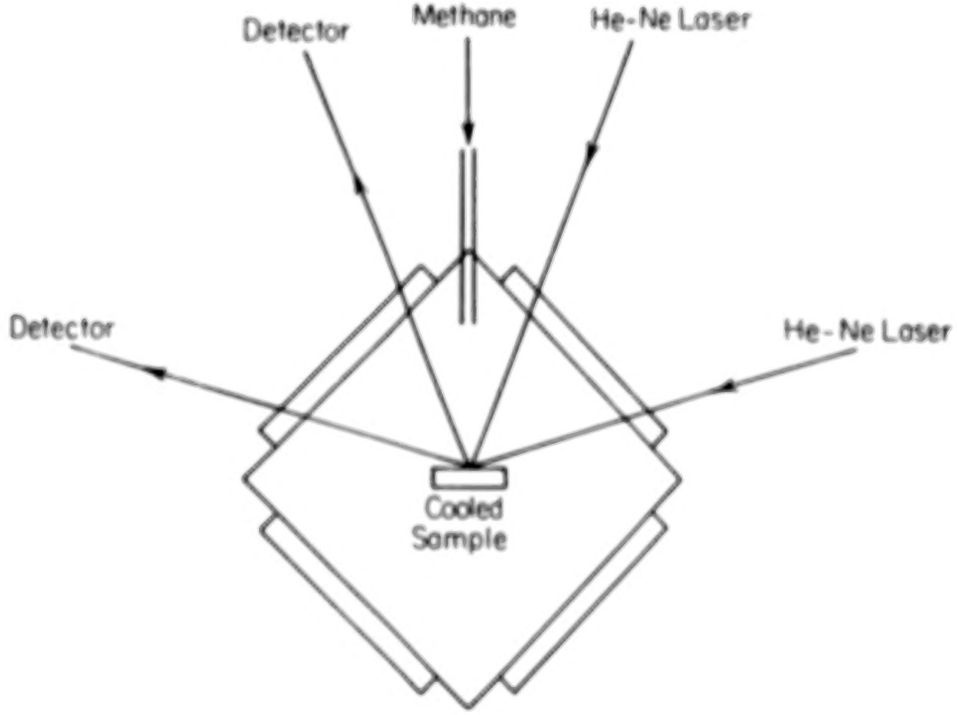

Fig. 5

As the methane gas is condensed at a constant rate, two interference patterns of different periods are recorded in the reflected laser light as a function of film thickness (Fig. 6). If the ratio of separation between adjacent maxima in two

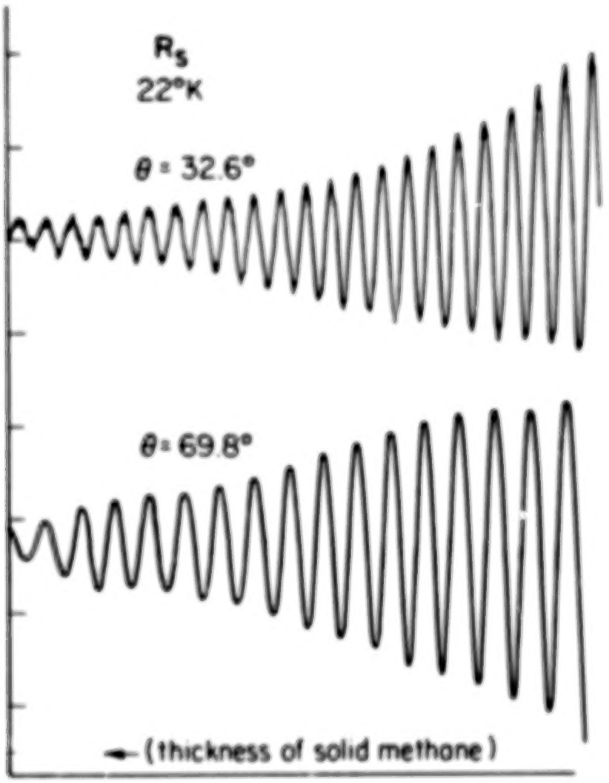

Fig. 6

beams is termed β, then

$$n = \frac{(sin^2\theta_b - \beta^2 sin^2\theta_a)^{1/2}}{(1-\beta^2)^{1/2}} \qquad (4)$$

where θ_a and θ_b are 32.6° and 69.8°, the two laser beam incidence angles. The index of refraction from the data in Fig. 6 gave $n = 1.302 \pm 0.002$ at $\lambda = 0.6328$ μm, confirming again that the value obtained by Lorentz-Lorenz relationship [Eq. (3)] is valid for CH_4.

DISCUSSION AND CONCLUSIONS

Buie et al.[17] have obtained photometric data of Pluto-Charon mutual events at wavelengths 1.53, 1.75, 2.00 and 2.35 μm while Sawyer[31] has obtained data at wave-

lengths from 0.5 to 1.0 μm. This data allows the extraction of spectra of Pluto alone. Our optical constants from 1.1 to 2.63 μm (Table I and Fig. 3) and future determinations down to 0.4 μm are specifically useful in scattering models for Pluto, which are needed to determine how much CH_4 absorption arises from the surface and how much from the atmosphere.[17,18,31] In a similar way, they can be used to model the texture and coverage of CH_4 on Triton.[32]

Fink and Sill[33] have studied the reflection spectra of CH_4 frost at 60°K at a resolution of 11 cm^{-1} from 1.12 μm to 3.85 μm. They also determined transmission spectra through a film 7.1 μm thick, in the mid-IR from 2.63 μm to 20 μm, at 57°K and 72°K. Optical constants of CH_4 for this longer wavelength range could be estimated from that work, but are not computed explicitly here. Our k values are currently determined near band maxima for the near-IR 1.1 μm to 2.6 μm region. Attempts to measure k for CH_4 at shorter wavelengths (0.4-1.1 μm) by direct transmission are difficult due to scattering from surface imperfections. These surface scattering losses dominate the true extinction losses. To overcome this problem, we are investigating the possibility of using a double beam configuration, with a short pathlength through solid CH_4 in the reference beam and a long pathlength through solid CH_4 in the sample beam. This should largely cancel the scattering from the surface and thus allow the extraction of true transmission information.

Since the optical constants of CH_4 have application in a variety of planetary and cometary surface and atmospheric environments, we intend to measure optical constants for a wide variety of temperatures. Some work with C_2H_6 and C_2H_2 has been done, and studies of changes in the optical properties of CH_4 and other hydrocarbon ices after ultraviolet and charged particle irradiation are also planned.

ACKNOWLEDGEMENTS

This research is supported by NASA grants NGR 33-010-220, NGR 33-010-082, and NAGW 637, and by the Office of Health and Environmental Research, U.S. Dept. of Energy under Contract DE-AC05-840R 21400 with Martin Marietta Energy Systems, Inc., ORNL.

References

1. B.N. Khare, C. Sagan, E.T. Arakawa, F. Suits, T. Callcott, and M. Williams, *Icarus* **60**, 127 (1984).

2. C. Sagan, W.R. Thompson, and B.N. Khare, *Proc. IAU Symp. 112*, edited by M.D. Papagiannis, p. 107, D. Reidel, Hingham, Mass. (1985).

3. C. Sagan, W.R. Thompson, S.W. Squyres, and B.N. Khare, *Bull. Amer. Astron. Soc.* **17**, 700 (1985).

4. C.P. McKay, J.B. Pollack, and R. Courtin, *Icarus* **80**, 23 (1989).

5. B.N. Khare, C. Sagan, W.R. Thompson, E.T. Arakawa, F. Suits, T.A. Callcott, M. W. Williams, S. Shrader, H. Ogino, T.O. Willingham, and B. Nagy, *Adv. Space Res.* **4**, 59 (1984).

6. K. Rages and J.B. Pollack, *Icarus* **41**, 119 (1980)

7. M.G. Tomasko and P.H. Smith, *Icarus* **51**, 65 (1982).

8. K. Rages and J.B. Pollack, *Bull. Amer. Astron. Soc.* **13**, 703 (1981).

9. K. Rages and J.B. Pollack, *Icarus* **55**, 50 (1983).

10. B.N. Khare, C. Sagan, W.R. Thompson, E.T. Arakawa, and P. Votaw, *J. Geophys. Res.* **92**, 15067 (1987).

11. C. Sagan and S.F. Dermott, *Nature* **300**, 731 (1982).

12. J.I. Lunine and D.J. Stevenson, in Ice in the Solar System, eds. J. Klinger, D. Benest, A. Dollfus, and R. Smoluchowski (Dordrecht: D. Reidel), pp. 741-757 (1985).

13. J.I. Lunine, D.J. Stevenson, and Y.L. Yung, *Science* **222**, 1229 (1983).

14. S.K. Atreya, *NASA Conference Publication 2330*, p. 55 (1984).

15. G.F. Lindel, J.R. Lyons, D.N. Sweetnam, V.R. Eshleman, D.P. Hinson, and G.L. Tyler, *J. Geophys. Res.* **92**, 14987 (1987).

16. D.P. Cruikshank and J. Apt, *Icarus* **58**, 306 (1984).

17. M.W. Buie, L.A. Lebofsky, E.F. Tedesco, and D.P. Cruikshank, *Bull. Am. Astron. Soc.* **21**, 985 (1989).

18. M.W. Buie and U. Fink, *Icarus* **70**, 483 (1987).

19. H.P. Larson, H.A. Weaver, M.J. Mumma, and S. Drapatz, *Astrophy. J.* **338**, 1106 (1989).

20. Cryocooler was Model LTS-22-Matrix-0.1 Closed Cycle Refrigerator System with Model CSD-3600 Si Diode Temperature Sensor obtained from Cryosystems, Inc., Tucson, AZ.

21. G.W.C. Kaye and T.H. Laby, Tables of Physical and Chemical Constants, pp. 83-86, Wiley, New York (1966).

22. N.J. Harrick, *Applied Optics* **10**, 2344 (1971).

23. K.R. Ramaprasad, J. Caldwell, and D.S. McClure, *Icarus* 35, 400 (1978).

24. C.K.N. Patel, E.T. Nelson, and R.J. Kerl, *Nature* **286**, 368 (1980).

25. W.R. Thompson, *CRSR Report 918*, June 1989, Cornell University, Ithaca, NY.

26. L.P. Giver, *J. Quant. Spectrosc. Radiat. Transfer* **19**, 311 (1978).

27. E.T. Arakawa, P.D. Clapp, T.A. Calcott, B.N. Khare, and C. Sagan, *Bull. Am. Phys. Soc.* **31**, 700 (1986).

28. V.V. Sychev, A.A. Vasserman, V.A. Zagoruchenko, G.A. Spiridonov, and V.A. Tsymarny, *Thermodynamic Properties of Methane*, Hemisphere Publishing Corp., p. 175 (1987).

29. M.S. Constantino and W.B. Daniels, *J. Chem. Phys.* **62**, 3 (1975).

30. K.E. Tempelmeyer and D.W. Mills, *J. App. Phys.* **39**, 2968 (1968).

31. S.R. Sawyer, *Bull. Am. Astron. Soc.* **21**, 986 (1989).

32. W.R. Thompson, *Geophys. Res. Let.* **16**, 969 (1989).

33. U. Fink and G.T. Sill, *Comets*, ed. L.L. Wilkening, The University of Arizona Press, Tucson, Arizona, p. 164 (1982).

N90-26776

OPTICAL CONSTANTS OF KEROGEN FROM 0.15 TO 40 μm: COMPARISON WITH METEORITIC ORGANICS

BISHUN N. KHARE,* W.R. THOMPSON,* C. SAGAN,* E.T. ARAKAWA,** C. MEISSE,** AND I. GILMOUR,†,††
*Laboratory for Planetary Studies, Cornell University, Ithaca, New York, 14853, U.S.A.
**Oak Ridge National Laboratory, Oak Ridge, Tennessee 37831, U.S.A.
†Enrico Fermi Institute and Department of Chemistry, University of Chicago, Chicago, IL 60637, U.S.A.
††Present address: Planetary Sciences Unit, The Open University, Milton Keynes, MK7 6AA, U.K.

ABSTRACT

Kerogens are dark, complex organic materials produced on the Earth primarily by geologic processing of biologic materials, but kerogens have chemical and spectral similarities to some classes of highly processed extraterrestrial organic materials. Kerogen-like solids have been proposed as constituents of the very dark reddish surfaces of some asteroids [Gradie and Veverka, *Nature* **283**, 840 (1980)] and are also spectrally similar to some carbonaceous organic residues and the Iapetus dark material [Cruikshank et al., *Icarus* **53**, 90 (1983)]. Kerogen can thus serve as a useful laboratory analogue to very dark, spectrally red extraterrestrial materials; its optical constants can be used to investigate the effects of particle size, void space and mixing of bright and dark components in models of scattering by dark asteroidal, cometary, and satellite surfaces.

We report measurements of the optical constants of both Type II kerogen and of macromolecular organic residue from the Murchison carbonaceous chondrite via transmission and reflection measurements on thin films. These films, of thickness 0.2-1.3 μm, are produced by vacuum deposition of kerogen powder heated to 550-750°C onto sapphire, CaF_2, and CsI substrates. IR spectra of the thin films show that the spectral features of the kerogen powder are retained. Apparently no substantial change in optical constants occurs upon vacuum deposition, except for the desirable loss of silicate contaminants which can be seen in the spectra of the powder.

The real part of the refractive index, n, is determined by variable incidence-angle reflectance to be 1.60 ± 0.05 from 0.4-2.0 μm wavelength. Work extending the measurement of n to longer wavelengths is in progress. The imaginary part of the refractive index, k, shows substantial structure from 0.15-40 μm. The values are accurate to ± 20% in the UV and IR regions and to ± 30% in the visible. We have also measured k values of organic residues from the Murchison meteorite. Comparison of the kerogen and Murchison data reveals that between 0.15 and 40 μm, Murchison has a similar structure but no bands as sharp as in kerogen, and that the k values for

Murchison are significantly higher than those of kerogen.

INTRODUCTION

Kerogens are dark, complex organic materials produced on earth from biologically derived organic material that has been incorporated into sediments where it has undergone further geological processing.[1,2] Kerogens can be classified as either Type I, II or III depending on their H/C and O/C elemental ratios.[3] These classifications reflect the origins and chemical structures of the kerogens. Type I is derived from predominantly aliphatic algal material, Type II from lipid-rich marine material, and Type III from more aromatic-rich terrestrial organic matter.[4] Within each type, individual samples differ according to the degree of geologic processing but originate from the same type of parent material.[5] While of biotic origin, kerogens have chemical and spectral similarities to some types of highly processed extraterrestrial organic materials. Kerogen-like solids have been proposed as constituents of the very dark reddish surfaces of some asteroids[6] and are also similar to the Iapetus dark material.[7] Kerogens can thus serve as useful laboratory analogues to very dark, spectrally red extraterrestrial materials. Measurements of their optical constants can be used to investigate the effect of particle size, void space, and mixing of bright and dark components in models of scattering by dark asteroids, cometary and satellite surfaces.

Here, using high-vacuum film deposition and transmission spectroscopic techniques, we study and compare the optical constants of a Type II kerogen and of organic residue from the Murchison carbonaceous chondrite. Meteorites were formed in the solar nebula, where organic material is thought to have been produced by catalytic reactions of carbon monoxide, hydrogen, and ammonia,[8] and by ultraviolet and charged particle irradiation.[9] Hayatsu and co-workers[10] have undertaken extensive investigations of the structure of Murchison organic materials using a variety of degradation techniques. They conclude that the material is comprised of condensed aromatic and heterocyclic ring systems cross-linked by short methylene chains, ethers, sulfides, and biphenyl groups.[10,11]. These chemical structures are similar to those of kerogen. Comparison of the spectroscopic properties of the extraterrestrial abiotic Murchison organic residue and the terrestrial metamorphosed biotic material that composes kerogen provides further insight into their structural and chemical similarities and differences.

EXPERIMENTAL

(a) Sample Information

The kerogen sample is a 190 million year old Type II kerogen from the Isle of

Skye, Scotland. The extraction of kerogen from the sedimentary rocks followed the procedure used by Durand and Nicaise.[12] The meteoritic material used is a sample of "macromolecular" organic material isolated by acid-dissolution and solvent extractions from the Murchison carbonaceous chondrite; a similar procedure is used for kerogen.

(b) Film Preparation

Films of kerogen and of Murchison organic material were prepared by thermal evaporation. The experimental set-up is shown in Figure 1.

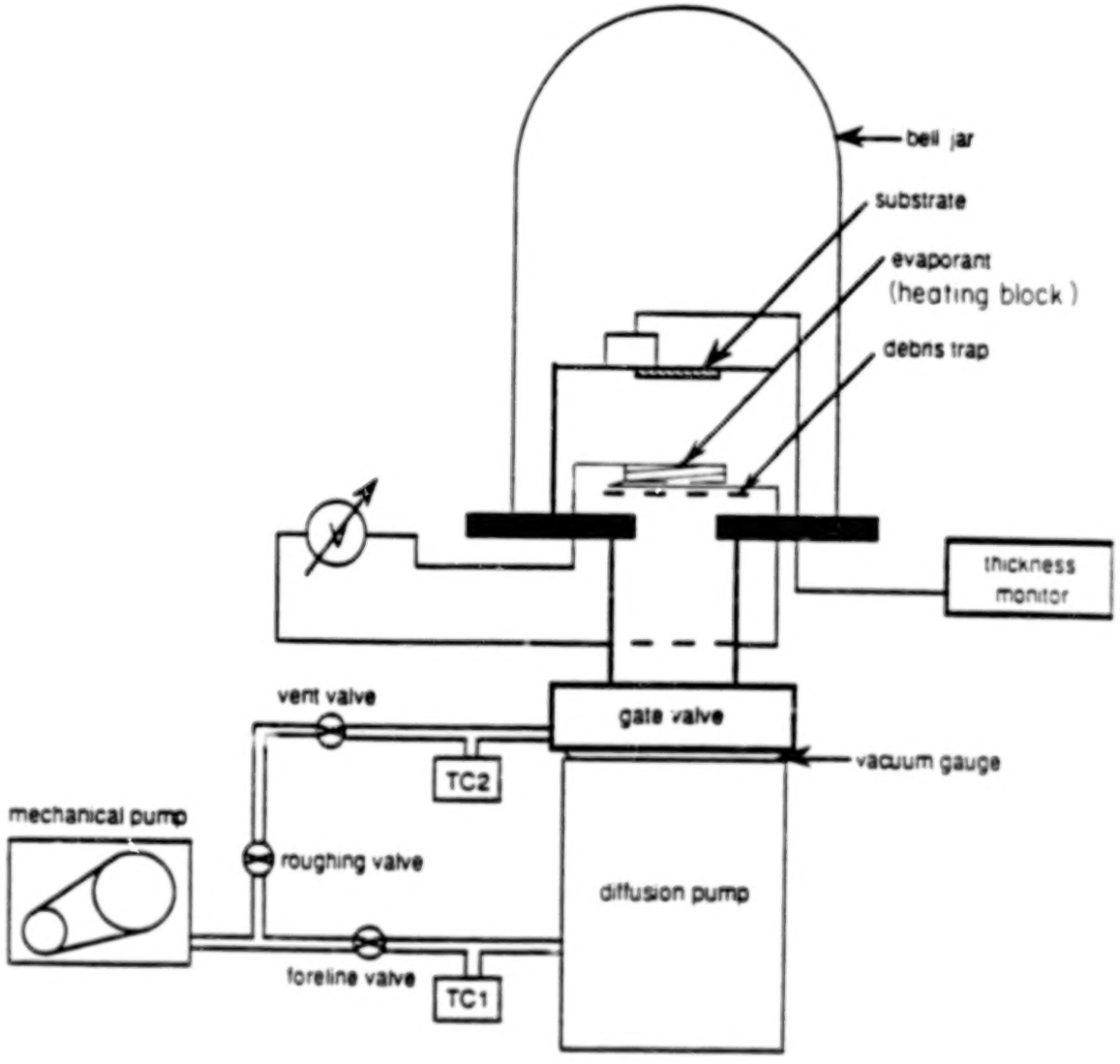

Fig. 1. Apparatus for vacuum-evaporation and film deposition.

It consists of a high vacuum system, a film coating chamber, and a thickness monitor. The temperature was checked by a color scale. The color of the molybdenum heating

wire around the sample heating block determined the temperature at which the sample started to evaporate to within 100°C. The main advantage of preparing the film by vacuum deposition was that the film was protected from contamination, particularly by water. A Veeco/Kronos Model QM311 quartz crystal microbalance was used to monitor the approximate thickness. This allowed us to produce films of optimal thickness for determinations of k in different regions of the spectra. Exact thicknesses were determined after the spectral measurements were completed. The substrates used in this work were sapphire, calcium fluoride, and cesium iodide which are, respectively, transparent over the spectral ranges 0.15-6.5 μm, 0.13-9.0 μm, and 0.30-50 μm. Two substrates and the thickness detector were positioned just above the sample block about 7 cm from the sample, such that the angle of incidence of evaporated sample onto the substrates was close to normal. In all our film depositions, we masked half the area of the substrate with foil in order to measure the transmission through the substrate alone. A thin, even layer of sample around the entire surface of the sample indentation ensured good thermal contact, producing a homogenous beam of evaporated material to be deposited uniformly onto the substrate. Up to 3 depositions were required to produce a sufficiently thick film for optical constants measurements.

The evaporation of kerogen took place in three phases. The rate of deposition was around 10 Å min^{-1} at the beginning, when the temperature was maintained at roughly 550°C. After about 1 hour the rate of deposition drops rapidly. Raising the temperature to roughly 650°C causes a second, faster phase of deposition which lasts about 30 min. After another drop in rate, the temperature was raised to roughly 750°C, and held there for about 2 hrs., after which no further deposition was noted. The fact that new deposition occurs when the temperature is raised may indicate either the evaporation of different fractions or pyrolytic release of large fragments at higher temperatures. Its color is yellow and during the evaporation, a distinctive odor is noticed. A similar odor was produced while evaporating the Murchison organ extract. After the evaporation, some residues remained in both cases. A total of nine kerogen films were deposited. Three sapphire substrates had film thickness of 0.190, 0.733, and 1.213 μm. Five CsI substrates had films that were 1.089, 1.267, 1.213, 2.100, and 3.000 μm thick, and one CaF_2 substrate had a 0.469 μm thick film.

Similar film preparation methods were repeated to produce films of the Murchison organic residue.

(c) Spectroscopic Measurements

Infrared spectra (2.5-25 μm) of the original, pre-evaporation kerogen and Murchison organic residue samples were obtained with a Nicolet FTIR spectrometer by measuring the transmission through a pellet prepared in a potassium bromide matrix.

1 to 2 mg of material is mixed with about 100 mg of spectrograde KBr powder. After grinding well, the mixed powder is made into a pellet about 0.2 mm thick using a standard dual-bolt pellet press. After removing the bolts, the body of the press is inserted into the beam of the FTIR spectrometer to scan the spectrum.

Transmission spectra (2.5-40 μm) of the vacuum-deposited films on a CsI substrate were obtained at 1 cm^{-1} resolution with a Beckman Acculab Model 10 Infrared spectrometer. Spectra were scanned twice for better accuracy.

A Cary Model 14 PM spectrometer was employed for measurements in the 0.4 to 2.5 μm wavelength region. A Shimadzu spectrometer was employed for measurements from 0.19 to 0.7 μm. We will be using a Seya-Namioka monochromator from 0.13 μm to 0.19 μm in the vacuum UV region for transmission as well as reflection measurements. Reflection measurements from 0.01 μm to 0.17 μm will also be made on a MacPherson Model 247 grazing incidence monochromator.

Imaginary Part of the Refractive Index k

The imaginary part of the refractive index k, is given by Khare et al.[13] as

$$k = \frac{\lambda}{4\pi t} \ln \frac{T_s (1-R)}{T (1-R_0)^2} \qquad (1)$$

where T_s = transmission through substrate

$$R_0 = \left(\frac{n_s - 1}{n_s + 1} \right)^2$$

where n_s = the real part of the refractive index of the substrate, and
T = transmission through the substrate plus kerogen.

In our case, T_s and T were directly measured and R, the total normal incidence reflectance from the film-substrate system, was estimated by drawing a baseline through the wavelength regions where the film had no significant absorption. If the refractive index, n_f, of the film is determined by an independent method, the equation for R can be computed by

$$R = \frac{(1 + n_f^2)(n_f^2 + n_s^2) - 4n_f^2 n_s + (1 - n_f^2)(n_f^2 - n_s^2)\cos\delta}{(1 + n_f^2)(n_f^2 + n_s^2) + 4n_f^2 n_s + (1 - n_f^2)(n_f^2 - n_s^2)\cos\delta} \qquad (2)$$

$$\text{where,} \quad \delta = \frac{2\pi n_f}{\lambda} (2t) \qquad (3)$$

Values of n_s are determined from independent measurement or from the literature.[14] At wavelengths where the real part of the refractive index of the film could not be measured independently, an extrapolated value is used to calculate R for use in Eq. (1).

Real Part of the Refractive Index, n

The real part of the refractive index, n, of kerogen was determined by variable-angle reflectance in the 0.4-2.0 μm wavelength region. To obtain n for a wider wavelength range, we ran a program based on the Kramers-Kronig relation between n and k (Inagaki et al.)[15], given by dispersion relation analysis. When the k values are well determined by transmission measurement, an integral over the energies $E = hc/\lambda$,

$$n(E) - 1 = \frac{2}{\pi} \int_0^{\infty} \frac{E'k(E')}{(E')^2 - E^2} \, dE' \qquad (4)$$

was used to obtain n values. This requires a knowledge of k for high energies (short wavelengths). Since we have not yet determined k on our MacPherson grazing spectrometer that goes down to 0.01 μm, we had to estimate k values for the short wavelength region. We know from past experience that all such organics have a strong feature at ~0.12 μm. We introduced this feature numerically and adjusted its magnitude such that the Kramers-Kronig analysis on k produced n values consistent with those actually measured at other wavelengths. We will soon measure the k values for kerogen in the short wavelength region to obtain more accurate values of n. Until then the n values outside the range 0.4-2.0 μm should be considered tentative.

RESULTS AND DISCUSSION

(a) FTIR Spectra of Original Pre-Evaporation Samples

The infrared spectra of complex organic solids such as kerogens generally show a limited number of absorption bands which are due to well-defined chemical groups, and can be assigned on the basis of numerous spectra of simple substances.[5,16,17] The FTIR transmission spectra of the kerogen sample and of the Murchison organic extract are shown in Figure 2. The principle absorption features and their most likely assignments are listed in Table I. The kerogen sample is characterized by strong aromatic absorptions in the 800-1000 cm^{-1} region, and C=O and aliphatic absorptions at 1720 cm^{-1} and 2900 cm^{-1} respectively. It is essentially aromatic in character but has not undergone extensive carbonization as significant amounts of aliphatic and oxygenated material are still present.

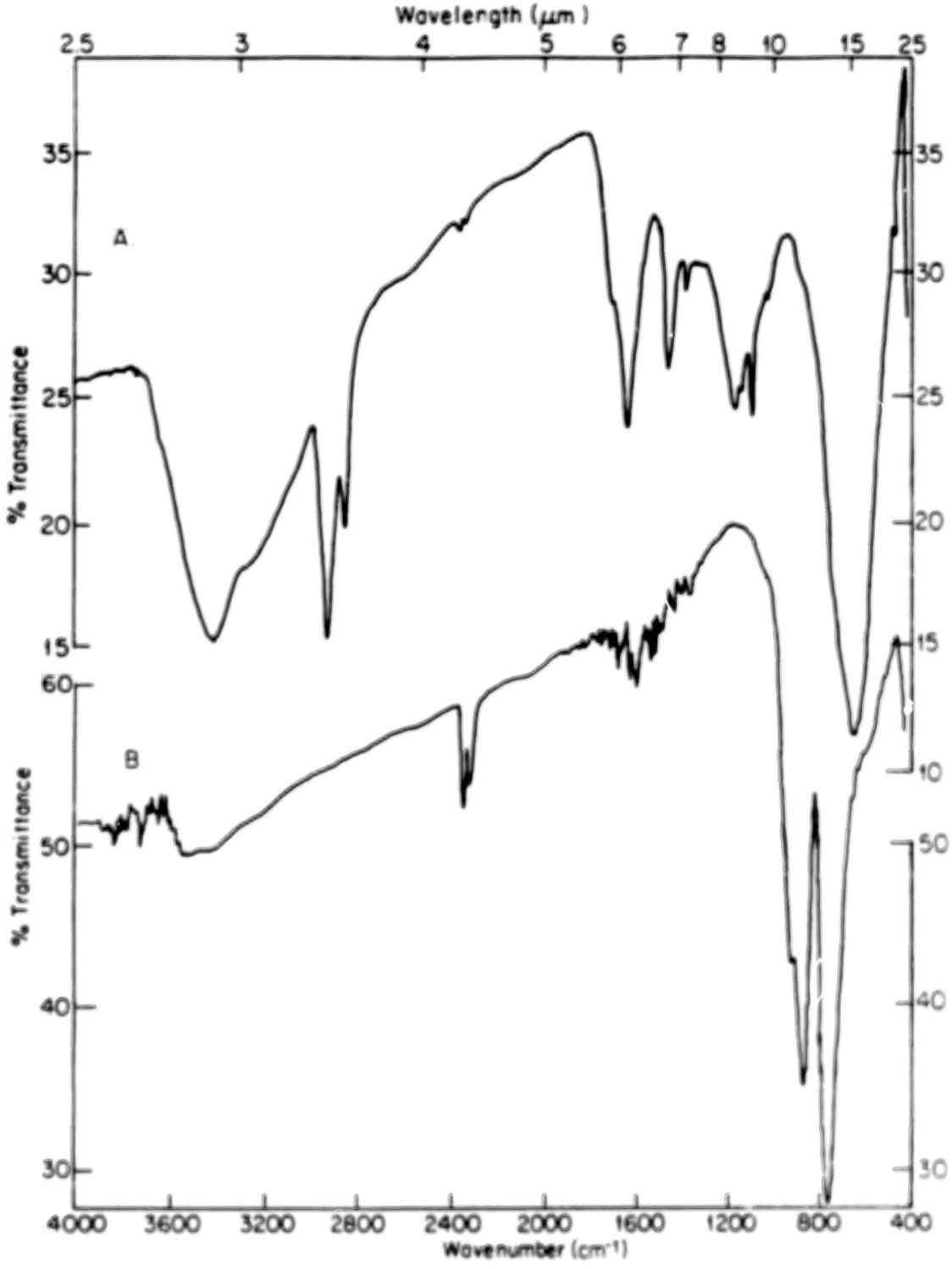

Fig. 2. FTIR transmission spectra in KBr matrix of (A) kerogen Type II (Skye #5) and (B) organic residue from the Murchison meteorite.

Table I

Assignments of absorption features in FTIR spectra of kerogen and organic residue in Murchison meteorite

Wavenumber (cm^{-1})	Structural Assignment
3420	OH stretching (absorbed H_2O and possible contribution from phenolic, alcoholic, carboxylic OH)[4]
2924/2853	Alkyl CH stretching
1710 (shoulder)	C=O stretching (minor)
1630	C=C stretching of aromatic and polyaromatic rings (may contain minor C=O stretching)
1455	Asymmetric bending of CH_2 and CH_3
870/820/750	Aromatic CH deformation absorptions
650	Out of plane deformation of aromatic CH

The band at 2326 cm^{-1} is due to atmospheric CO_2 in the spectrometer.

The Murchison organic residue spectrum is clearly dominated by strong aromatic absorptions in the 800-1000 cm^{-1} region, consistent with existing chemical analysis.[10,11] No aliphatic absorptions are observed as the corresponding functional groups are apparently contained in relatively soluble components removed by the solvent extraction process. The Murchison "macromolecular" organic material was prepared by HF/HCl dissolution (5 cycles) of ~50 g of freeze/thaw disaggregated bulk meteorite followed by solvent extraction with methanol and toluene to leave a black carbonaceous residue. A similar residue was used by Cruikshank et al.[7] for reflectance measurements although they incorrectly denoted it as an extract.

(b) FTIR Spectra of Vacuum-Deposited Kerogen

Figure 3 shows the FTIR spectrum of an evaporated film of kerogen deposited on a CsI substrate and the FTIR spectrum of the original kerogen in a KBr matrix for comparison. The strong similarity of the two spectra demonstrates that while the vacuum evaporation process undoubtedly fractionates the kerogen to some degree, the primary functional units are apparently unchanged, and the essential spectral characteristics are preserved. Indeed, the major difference between the two spectra is the near absence of a silicate absorption at around 1200 cm^{-1} in the evaporated film. The removal of this and other impurities is an incidental benefit of the use of

the thin film vacuum deposition technique for measuring the optical constants of kerogen. The additional detail present in the evaporated film spectrum presumably reflects the higher quality obtainable from optically clear film as opposed to powdered solids.

Figure 4 shows the FTIR spectrum of the residue left after the evaporation. As can be seen, it is essentially featureless, aside from some adsorbed water, some weak

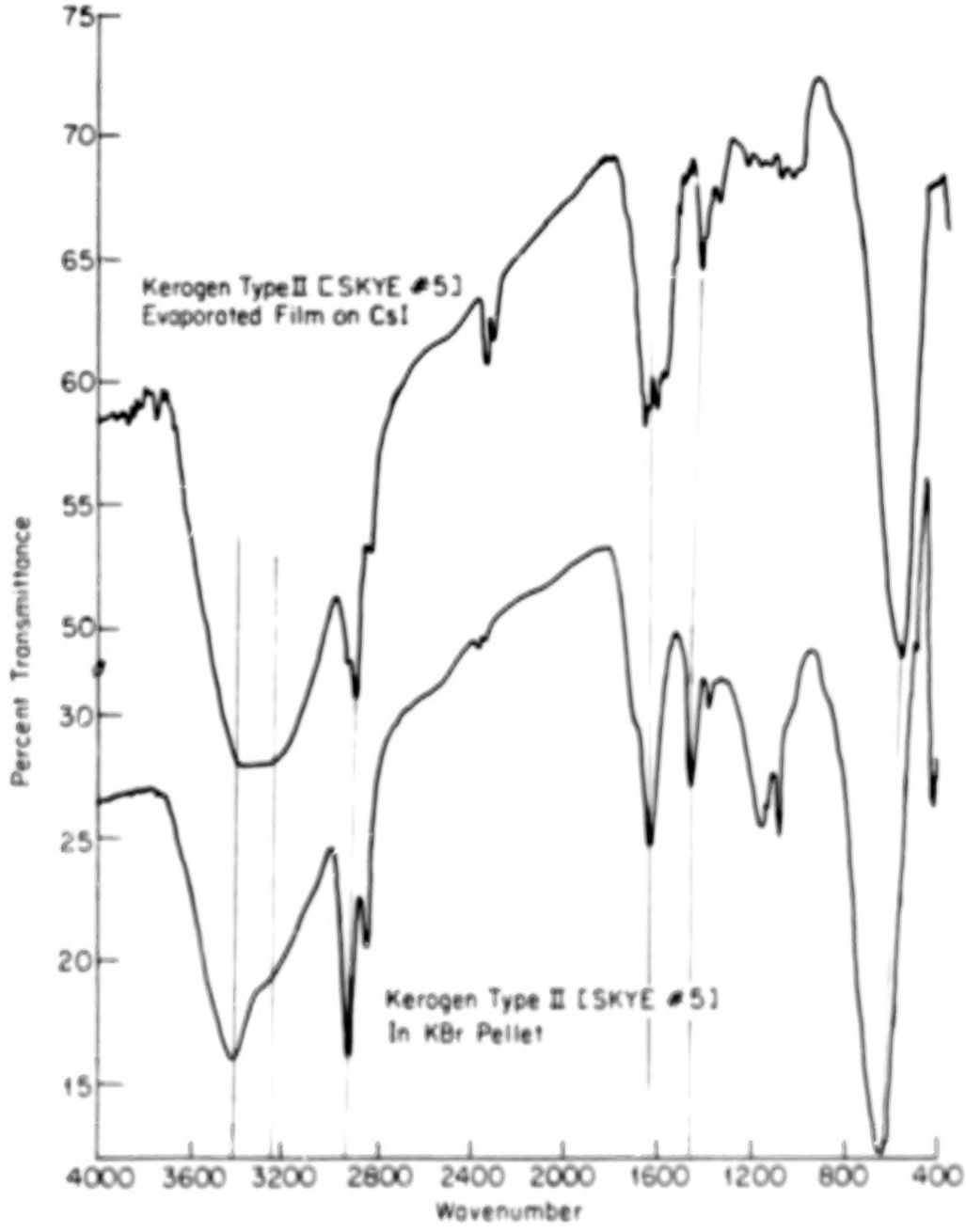

Fig. 3. Vertical lines indicate similarities between the evaporated film of kerogen and the original kerogen in KBr matrix, demonstrating that major spectral features are preserved.

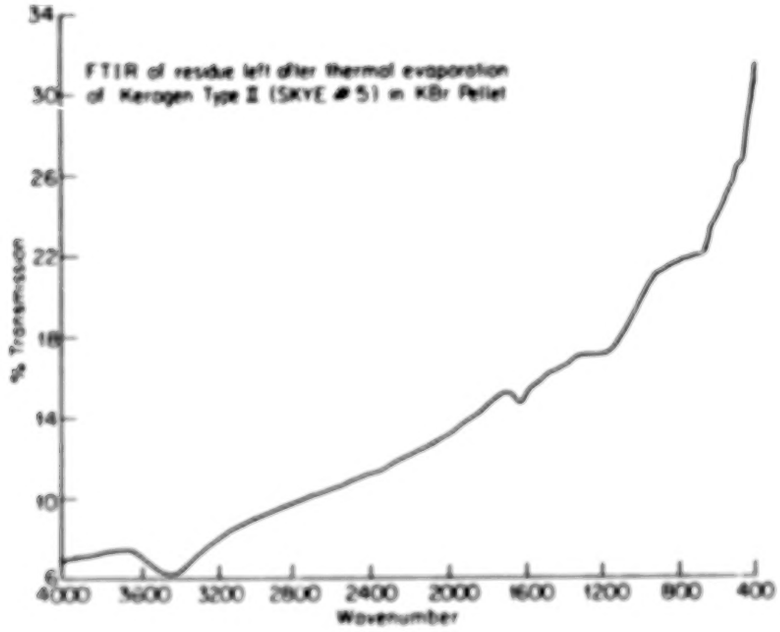

Fig. 4

C-C features, and a slight silicate absorption at 1200 cm^{-1}. Evidently, nearly all of the kerogen is successfully evaporated at 500°C to 750°C.

(c) Infrared Spectra of Films of Murchison Organic Residue and Kerogen

In Figure 5 we show the infrared spectrum of a thermally evaporated film of

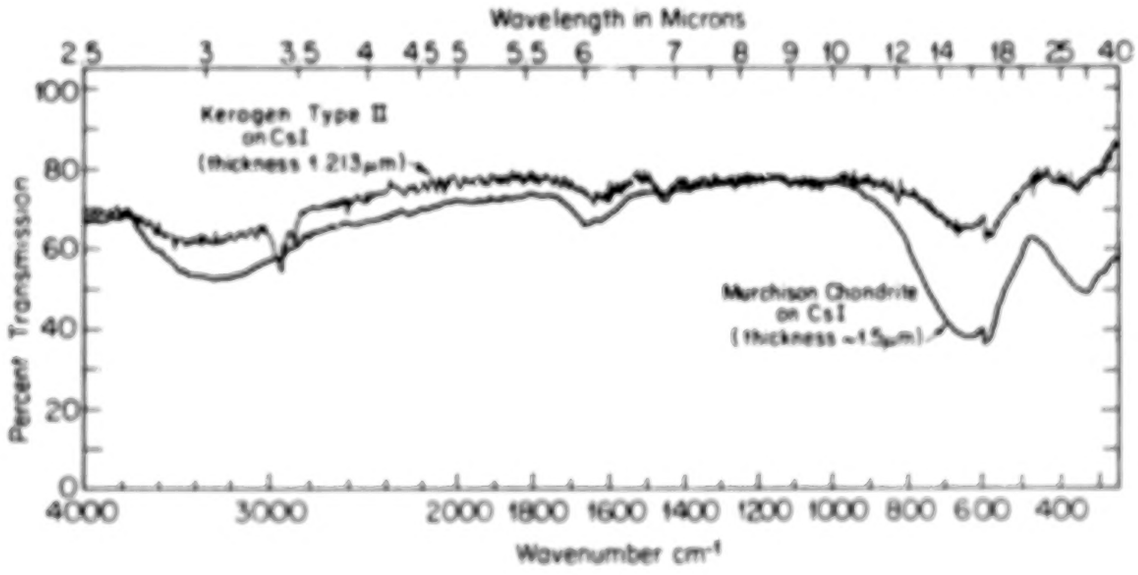

Fig. 5. IR spectra of vacuum-deposited films of Murchison organic residue and Type II kerogen.

Murchison organic residue and compare it with a similarly thermally evaporated film of kerogen. Both of these spectra were obtained with the Beckman Acculab Spectrometer. The films are similar enough in thickness that a direct comparison is possible. The Murchison extract shows spectral features similar to those of the kerogen film, except for the absence of aliphatic CH features near 2900 cm^{-1} and 1450 cm^{-1}. It is significantly more absorbing than the kerogen film we discuss below.

(d) Optical Constants of Kerogen and Meteoritic Organic Material

Using Eq. (1), the spectra, and the measured film thicknesses, the imaginary part of the refractive index, k, was calculated from 0.15-40 μm for both kerogen and the meteoritic samples. Figure 6 shows results for kerogen graphically; the values

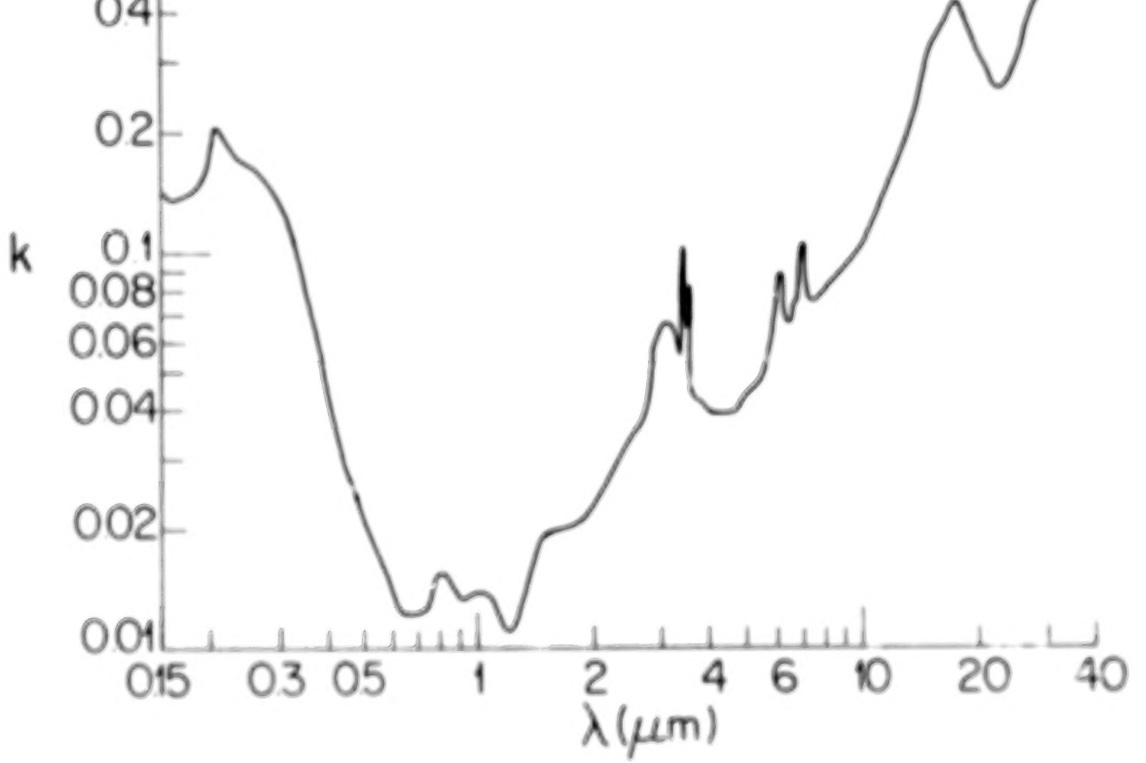

Fig. 6

are also listed in Table II. The values are accurate to ± 20% in the UV and IR regions and to ± 30% in the visible. Fig. 6 shows that k has substantial structure from 0.15-40 μm.

The real part of the refractive index of kerogen, n, was determined by variable incidence-angle reflectance to be 1.60 ± 0.05 from 0.4 to 2.0 μm. Fig. 7 shows the n values computed from k by Kramers-Kronig analysis. The uncertainty is ± 0.05.

Table II.
Imaginary Part of the Refractive Index (k) = $a.10^{-b}$ at Various Wavelengths (λ) of Thermally Evaporated (to 750°C) Film of Kerogen at Room Temperature.

λ (μm)	a	b	λ (μm)	a	b	λ (μm)	a	b	λ (μm)	a	b
0.15	1.40	1	0.9	1.33	2	3.356	7.45	2	6.536	6.67	2
0.155	1.35	1	1.0	1.38	2	3.378	8.58	2	6.623	6.76	2
0.16	1.36	1	1.1	1.30	2	3.401	1.02	1	6.667	7.11	2
0.165	1.38	1	1.2	1.10	2	3.425	7.75	2	6.711	7.46	2
0.17	1.39	1	1.3	1.34	2	3.448	6.45	2	6.757	8.00	2
0.1725	1.39	1	1.4	1.75	2	3.472	6.76	2	6.803	9.09	2
0.175	1.40	1	1.5	1.94	2	3.496	8.07	2	6.849	9.50	2
0.18	1.44	1	1.6	1.98	2	3.521	5.13	2	6.897	1.03	2
0.185	1.48	1	1.7	2.03	2	3.546	4.82	2	6.993	9.09	2
0.19	1.56	1	1.8	2.07	2	3.571	4.52	2	7.042	8.50	2
0.195	1.67	1	1.9	2.11	2	3.623	4.49	2	7.143	8.31	2
0.2	1.92	1	2.0	2.27	2	3.650	4.44	2	7.246	8.20	2
0.205	2.01	1	2.1	2.46	2	3.704	4.20	2	7.299	8.00	2
0.21	1.96	1	2.2	2.62	2	3.846	4.05	2	7.407	7.58	2
0.22	1.80	1	2.3	2.92	2	4.	3.97	2	7.692	7.84	2
0.23	1.72	1	2.4	3.02	2	4.167	3.90	2	8.333	8.39	2
0.24	1.69	1	2.5	3.40	2	4.348	3.89	2	9.091	9.40	2
0.25	1.63	1	2.632	3.71	2	4.545	3.92	2	10.	1.01	1
0.28	1.46	1	2.703	3.86	2	4.762	4.01	2	11.111	1.35	1
0.3	1.29	1	2.740	4.39	2	5.	4.36	2	12.5	1.72	1
0.32	1.06	1	2.778	4.93	2	5.128	4.55	2	13.333	2.01	1
0.35	7.72	2	2.817	5.51	2	5.263	4.51	2	14.289	2.71	1
0.38	5.68	2	2.857	5.83	2	5.556	5.16	2	15.384	3.53	1
0.4	4.31	2	2.899	6.02	2	5.714	5.64	2	15.873	4.08	1
0.45	2.84	2	2.941	6.21	2	5.747	5.93	2	16.667	3.84	1
0.5	2.15	2	2.985	6.41	2	5.882	6.91	2	18.182	3.02	1
0.55	1.77	2	3.030	6.62	2	5.952	7.56	2	20.	2.35	1
0.6	1.23	2	3.125	6.42	2	6.061	8.61	2	22.222	2.09	1
0.65	1.23	2	3.226	6.23	2	6.211	8.57	2	25.	2.68	1
0.7	1.23	2	3.289	5.99	2	6.25	8.34	2	28.571	3.86	1
0.75	1.31	2	3.311	5.67	2	6.329	7.87	2	30.303	4.10	1
0.8	1.53	2	3.322	5.54	2	6.41	7.40	2	33.333	3.78	1
0.85	1.46	2	3.333	5.88	2	6.452	7.16	2	40.	2.74	1

k values for the original kerogen can also be estimated from its transmission spectrum in a KBr matrix as shown in Fig. 3. By knowing the percent of kerogen in the KBr pellet and the thickness of the pellet, it was possible to estimate k from 2.5 to 25 μm. Figure 8 compares k of the original material with that obtained for the thin film. (Values are normalized to unity at 16 μm.)

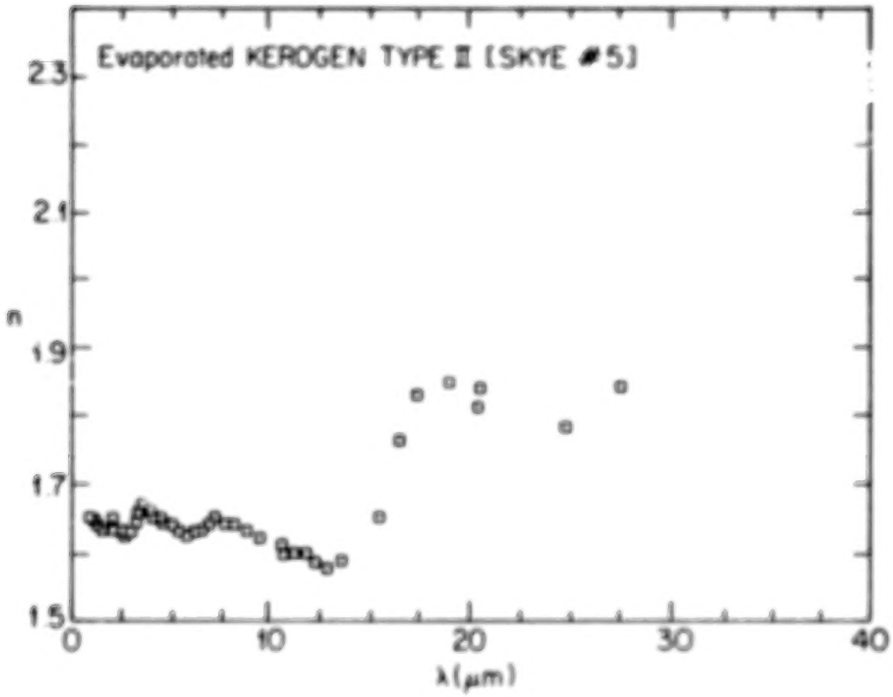

Fig. 7

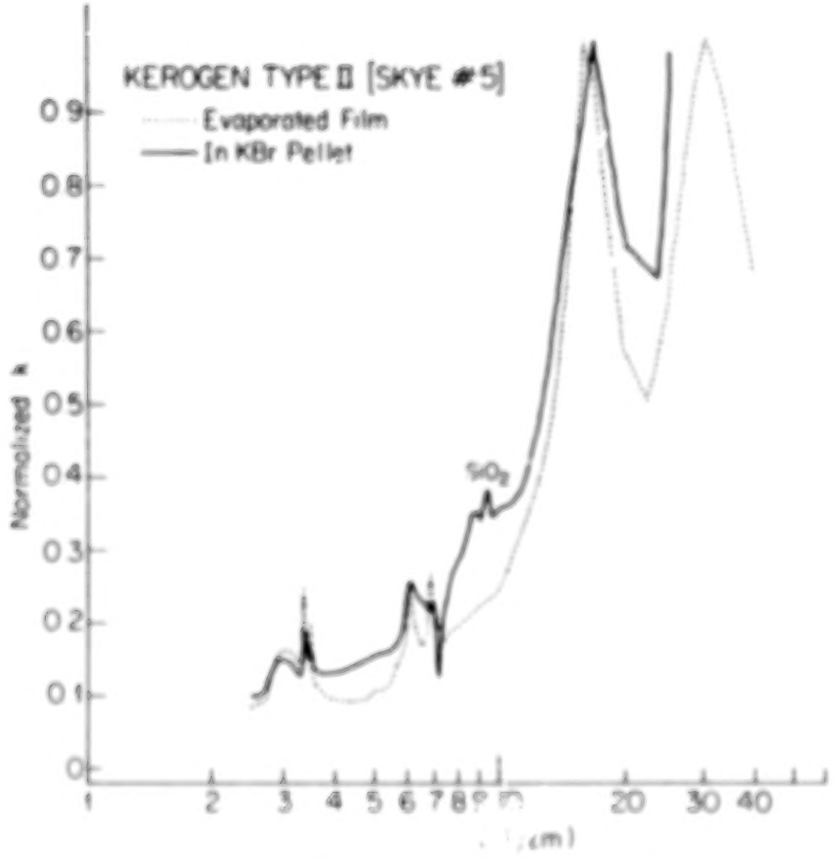

Fig. 8. Comparison of k values for evaporated film of organic matter in Murchison meteorite and evaporated film of kerogen from 2.5 to 40 μm

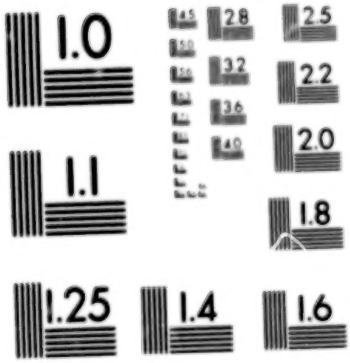

MICROCOPY RESOLUTION TEST CHART
NATIONAL BUREAU OF STANDARDS
STANDARD REFERENCE MATERIAL 1010a
(ANSI and ISO TEST CHART No. 2)

The agreement between the normalized k values before and after evaporation is good, again illustrating the preservation of the spectral characteristics of the kerogen after evaporation. As in the FTIR transmission spectra (Fig. 3), the only major differences are due to the lack of silicate absorption in the evaporated film.

Fig. 9 compares the k values obtained for the evaporated kerogen film with the k values of the evaporated Murchison organic residue. Table III lists the k values for the film produced from the Murchison organic extract. The Murchison sample, like Type II kerogen, also shows substantial structure, although k values obtained for Murchison are significantly higher than those of the kerogen, and as expected, do not show any feature associated with aliphatic functional groups.

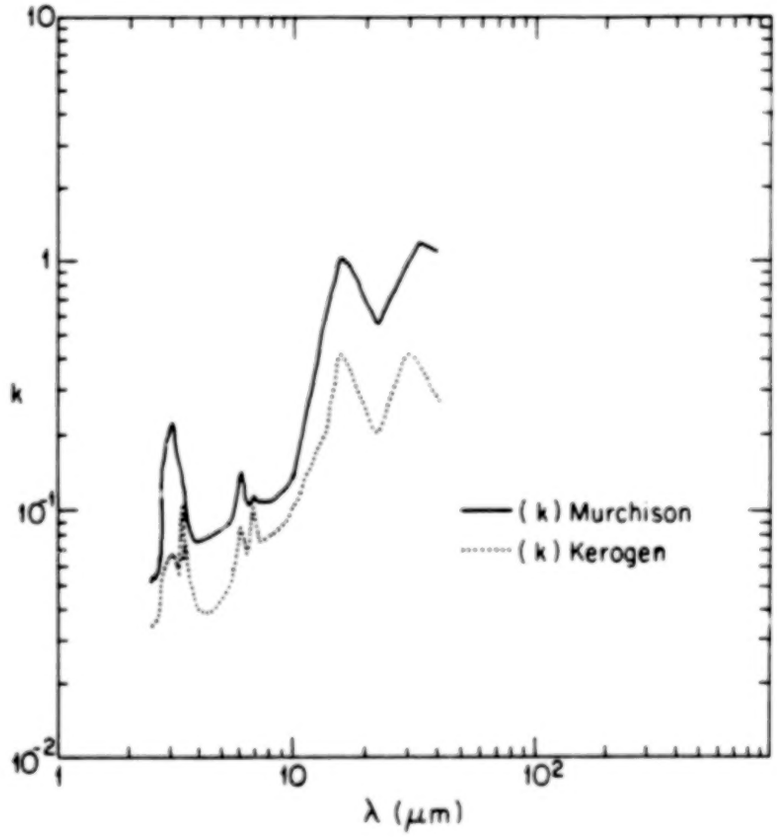

Fig. 9

CONCLUSIONS

(1) The Murchison organic residue has some similarities to Type II kerogen in the infrared, but has a higher k (is more absorbing) and lacks aliphatic spectral features.

Table III.
Imaginary Part of the Refractive Index (k) = $a10^{-b}$ at Various Wavelengths (λ) of Thermally Evaporated (to 750°C) Film of Organics in Murchison Meteorite at Room Temperature.

λ (μm)	a	b	λ (μm)	a	b
2.5	5.28	2	6.25	1.28	1
2.63	5.64	2	6.45	1.09	1
2.70	6.45	2	6.67	1.07	1
2.78	1.09	1	6.89	1.14	1
2.86	1.63	1	7.14	1.09	1
2.94	1.94	1	8.33	1.10	1
3.03	2.16	1	10.00	1.37	1
3.12	1.91	1	11.11	2.25	1
3.23	1.61	1	12.50	3.58	1
3.33	1.40	1	14.29	7.67	1
3.45	1.23	1	15.87	1.02	0
3.57	8.83	2	16.67	9.95	0
3.85	7.55	2	18.18	8.50	0
4.17	7.68	2	20.00	6.96	1
4.55	7.96	2	22.22	5.59	1
5.00	8.35	2	25.00	6.85	1
5.71	9.13	2	28.57	8.90	1
5.88	1.19	1	33.33	1.19	0
6.06	1.41	1	40.00	1.10	0

(2) The thermal evaporation technique is a good method for determining the optical constants of kerogens, organics in meteorites, and probably for other kinds of tholins.[9]

(3) More material is required to produce thick films and pellets to obtain results for the far infrared region to λ = 1 mm. Transmission measurements in the vacuum UV to soft x-ray region are required to obtain the best determination of n through Kramers-Kronig analysis.

(4) Brooke et al.[18] detect strong 3.4 and 2.8 μm emission features in comet P/Brorsen-Metcalf and find that the positions and widths of these features coincide with those observed in comets P/Halley, Wilson (1987 VII), and Bradfield (1987 XXIX). Comets and carbonaceous chondrites probably both accreted from low-temperature condensates in the solar nebula,[10,19] but the organic residues of comets can derive from pre- and post-accretion irradiation of hydrocarbon-containing ices, a somewhat different origin than that generally envisioned for meteoritic organics.[8,9] The 3.4 μm CH and 2.8 μm OH features in the above comets well match spectral features found in organic residues of H_2O-CH_4 and H_2O-C_2H_6 ice irradiation.[20,21,22] Similar spectral features in the kerogen suggest not its presence in comets, but simply some basic spectral similarities due to some commonality of functional groups in these materials.

ACKNOWLEDGEMENTS

This research was supported by the Kenneth T. and Eileen L. Norris Foundation, NASA NGR 33-010-101, NSF (EAR-8609218), and NASA (NAG9-52), and by the Office of Health and Environmental Research, U.S. Dept. of Energy under contract DE-AC05-840R 21400 with Martin Marietta Energy Systems, Inc., ORNL. We appreciate the help of Jonathan Gradie in bringing to our attention some valuable references. We thank Edward Anders for helpful discussions.

REFERENCES

1. B. Durand, Sedimentary organic matter and kerogen. Definition and qualitative importance of kerogen, in Kerogen, Insoluble Organic Matter from Sedimentary Rocks, (ed. B. Durand), Editions Technip, Paris, 1980, pp. 13-34.

2. R.D. McIver, Composition of kerogen, Clue to its role in the origin of petroleum. In Proceedings, 7th World Petroleum Congress, pp. 25-36.

3. B. Tissot, B. Durand, J. Espitalie, and A. Combaz, *Am. Assoc. of Petroleum Geologist Bull.* **58**, 499 (1974).

4. B.P. Tissot and D.H. Welte, Petroleum Formation and Occurrence, Berlin, Springer-Verlag.

5. Robin and Rouxhet, *Geochimica et Cosmochimica Acta* **42**, 1341 (1978).

6. D.P. Cruikshank and R.H. Brown, *Science* **238**, 183 (1987).

7. J.F. Bell, D.P. Cruikshank, and M.H. Goffy, *Icarus* **61**, 192

8. E. Anders, R. Hayatsu, and M.H. Studier, *Science* **182**, 781 (1973).

9. C. Sagan and B.N. Khare, *Nature* **277**, 102 (1979).

10. R. Hayatsu and E. Anders, Topics of Current Chemistry **99**, 1-37 (1981), Berlin and Heidelberg: Springer.

11. R. Hayatsu, S. Matsuoka, R.G. Scott, M.H. Studier, and E. Anders, *Geochimica et Cosmochimica Acta* **41**, 1325 (1979).

12. B. Durand and G. Nicaise, Procedures for kerogen isolation, in Kerogen, Insoluble Organic Matter from Sedimentary Rocks, (ed. B. Durand), Editions Technip, Paris, 1980, pp. 35-54.

13. B.N. Khare, C. Sagan, E.T. Arakawa, F. Suits, T.A. Callcott, and M.W. Williams, *Icarus* **60**, 127 (1984).

14. G.W.C. Kaye and T.H. Laby, Tables of Physical and Chemical Constants, pp. 83-86, Wiley, New York.

15. T. Inagaki, L.C. Emerson, E.T. Arakawa, and M.W. Williams, *Phys. Rev.* **B13**, 2305 (1976).

16. J. Espitalia, B. Durand, J.C. Roussel, and C. Souron, *Rev. de l'Institut Francais de Petrole* **28**, 37 (1973).

17. R.A. Friedel and G.L. Carlson, *Fuel* **51**, 194 (1972).

18. T.Y. Brooke, A.T. Tokunaga, J.S. Carr, K. Sellgren, R.F. Knacke, L.J. Allmandola, S.A. Sandford, and M. Tapia, *Bull. Am. Astron. Soc.* **21**, 993 (1989).

19. A.H. Delsemme, The origin of comets, in Comets Asteroids Meteorites -- Interactions, Evolution and Origins, (ed. A.H. Delsemme), The University of Toledo, 1977, p. 453.

20. C. Chyba and C. Sagan, *Nature* **330**, 350 (1987).

21. C.F. Chyba, C. Sagan, and M.J. Mumma, *Icarus* **79**, 362 (1989).

22. B.N. Khare, W.R. Thompson, B.G.J.P.T. Murray, C.F. Chyba, and C. Sagan, *Icarus* **79**, 351 (1989).

N90-26777

VAPOR PRESSURES OF ACETYLENE AT LOW TEMPERATURES

C. M. Masterson*, J. E. Allen, Jr.**, G. F. Kraus*** and R. K. Khanna*

*University of Maryland, Dept. of Chem. and Biochem., College Park, MD 20742
**Code 691, NASA/Goddard Space Flight Center, Greenbelt, MD 20771
***Charles Co. Comm. Coll., Dept. of Bio. and Phy. Sci., P.O. Box 910 Mitchell Rd., La Plata, MD 20646

The atmospheres of many of the outer planets and their satellites contain a large number of hydrocarbon species. In particular, acetylene (C_2H_2) has been identified at Jupiter, Saturn and its satellite Titan, Uranus and Neptune. In the lower atmospheres of these planets, where colder temperatures prevail, the condensation and/or freezing of acetylene is probable. In order to obtain accurate models of the acetylene in these atmospheres, it is necessary to have a complete understanding of its vapor pressures at low temperatures. The vapor pressures of acetylene above 90K have been measured[1,2], but these measurements were made over 30 years ago and may not be extremely accurate. For temperatures below this, no vapor pressure data exists in the literature. Therefore, to arrive at an estimate for these values, modelers are forced to extrapolate the high temperature data to temperatures more appropriate for planetary atmospheres using the Clausius-Clapeyron equation. This equation employs a linear relationship between lnp and 1/T by assuming that the enthalpy (ΔH) is not temperature dependent. This assumption may not be valid over large temperature ranges and may lead to inaccuracies in the extrapolated values. Therefore, our lab has been engaged in the determination of these vapor pressures at low temperatures for acetylene.

The vapor pressures are measured with two different techniques in order to cover a wide range of temperatures and pressures. In the first, the acetylene is placed in a sample tube which is immersed in a low temperature solvent/liquid nitrogen slush bath whose temperature is measured with a thermocouple. The vapor pressure is then measured directly with a capacitance manometer. Vapor pressures in the 10^{-3} to 10^{2} Torr range are measured with this method.

For lower pressures, a second technique which we call the thin-film infrared method (TFIR) was developed.[3] It involves measuring the disappearance rate of a thin film of acetylene at a particular temperature. A thin film of the material (~1m) is deposited on a substrate (figure 1) that is cooled to 40K, where the acetylene has essentially no vapor pressure. The substrate and film are then heated to the desired temperature for a vapor pressure measurement. At low temperatures where the vapor pressure is less than 1 torr, the rate of evaporation of molecules from a surface in a vacuum is the same as the rate of evaporation of the molecules in the presence of saturated vapor. Therefore, if we have a way to measure this evaporation rate, we can determine the vapor pressure of the molecule at that temperature directly. We accomplish this by taking the spectrum of a characteristic absorption feature for the molecule (1420 cm^{-1} for acetylene) at different time intervals with a Fourier Transform Infrared Spectrophotometer (FTIR). Once the sample film reaches the desired temperature, an initial spectrum is recorded. The spectrum of the absorption feature is then monitored while part of the sample film evaporates. At a certain time, t_1, when a portion of the sample film has evaporated, another absorption spectrum is taken. At a later time, t_2, when more of the sample has evaporated, another spectrum is taken and this process is repeated until the absorption feature is too weak to use for quantitative analysis (see figure2).

The spectra are then analyzed using previously determined extinction coefficient values, to determine the disappearance rate R (where $R=\Delta n/\Delta t$, the number of molecules that disappear per unit time). This can be related to the vapor pressure directly using the formula

$$R = \frac{p}{(2\pi mkT)^{1/2}}$$

where p is the vapor pressure at temperature T, m is the molecular mass of the compound and k is the Boltzmann constant. This technique facilitates measurement of the lower temperatures and pressures (10^{-8} to 10^{-6} Torr). Both techniques have been calibrated using CO_2, and have shown good agreement with the existing literature data. Table I gives values for acetylene using both methods and figure 3 shows a plot of these values as well as the literature values for the higher temperature data.

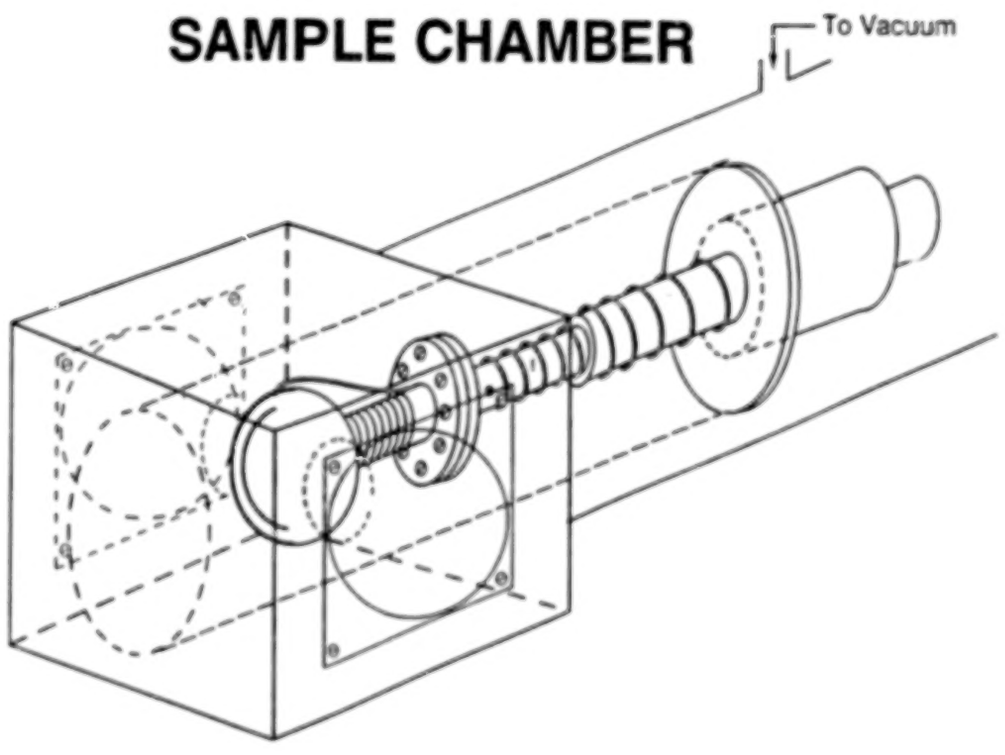

J107.009

Figure 1. Sample chamber for TFIR vapor pressure experiments.

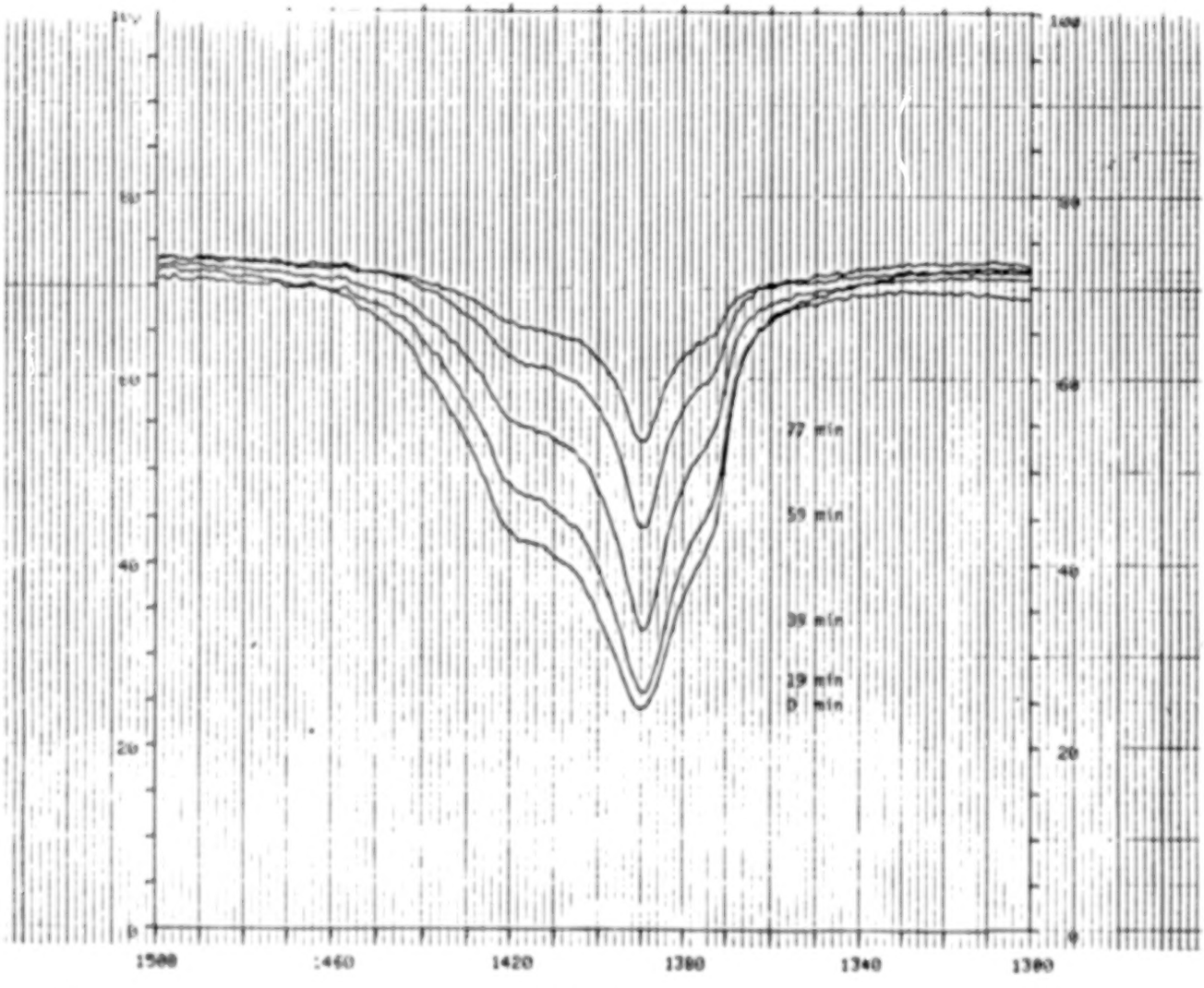

Figure 2. Transmission spectra, at different times of acetylene at 30K.

ORIGINAL PAGE IS
OF POOR QUALITY

Table I - Acetylene Vapor Pressures

Capacitance Manometer		TFIR	
T(K)	P(Torr)	T(K)	P(Torr)
118	5.07×10^{-3}	80.0	1.68×10^{-7}
143	8.12	81.0	3.41×10^{-7}
145	7.69	86.0	1.13×10^{-6}
148	7.82	86.2	1.29×10^{-6}
155	30.3	88.0	1.74×10^{-6}
158	42.8	90.0	5.24×10^{-6}
159	38.0	91.0	4.24×10^{-6}
160	48.5		
171	137		
176	217		
178	361		
180	367		
188	637		

As shown in figure 3, at the lowest recorded temperature, our data differs from the extrapolated value by almost 2 orders of magnitude. This produces a significant difference in the haze production models of Romani[4], for acetylene in the atmospheres of Saturn, Uranus and Neptune. Our laboratory is continuing to make vapor pressure measurements for other molecules such as diacetylene (C_4H_2), hydrogen cyanide (HCN), cyanoacetylene (HC_3N) and dicyanoacetylene (C_4N_2), that are of importance to planetary atmospheres.

References

1. W. T. Ziegler, NBS Tech. Note, **4**, (1959).
2. P. S. Bourbo, J. Phys., **8(6)**, 286 (1943).
3. R. K. Khanna, J. E. Allen, Jr., C. M. Masterson and G. Zhao, J. Phys. Chem., In Press (1989).
4. P. N. Romani, Private Communication, (1989).

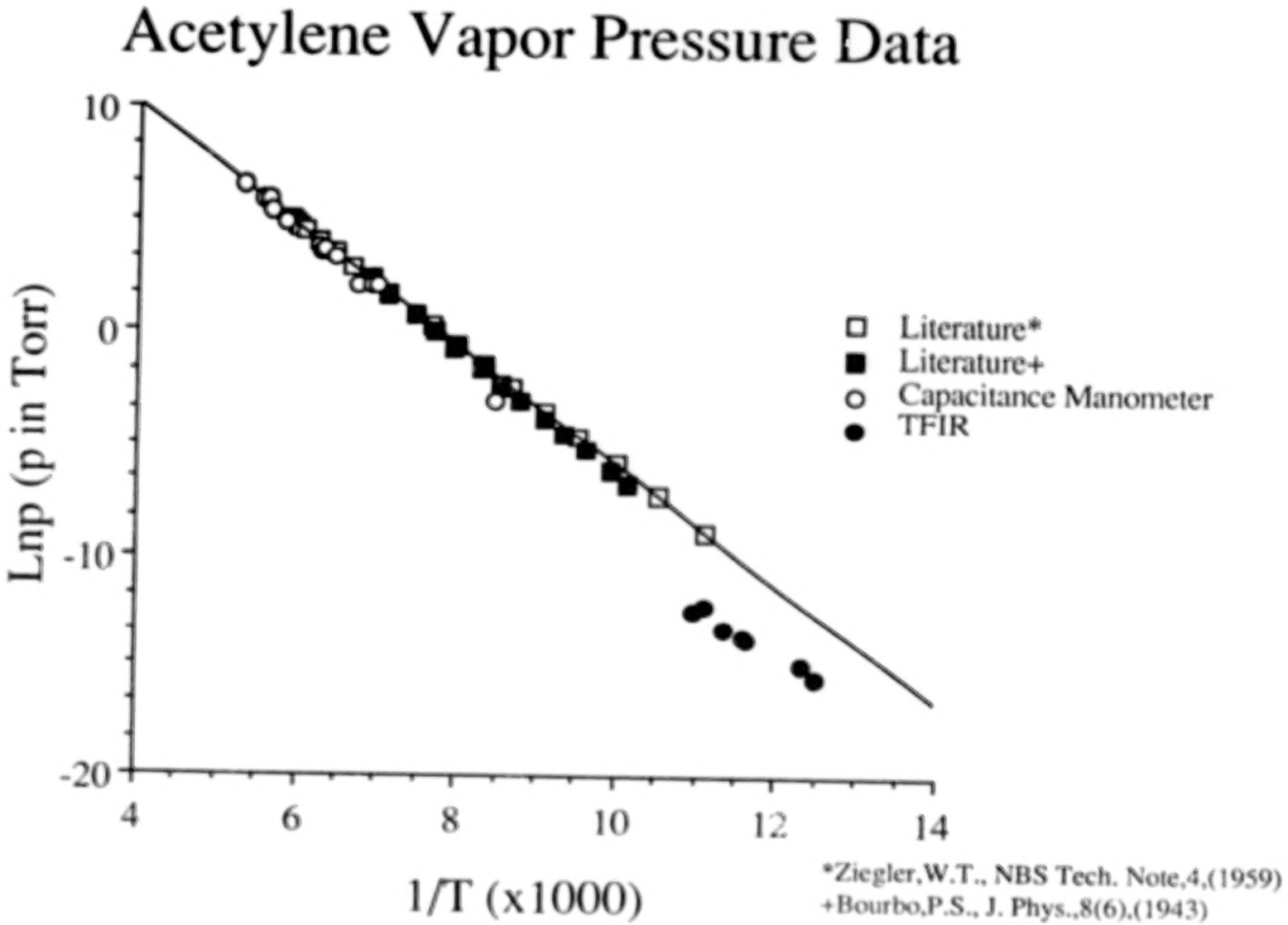

Figure 3. Plot of the literature, capacitance manometer and TFIR vapor pressure data for acetylene.

CHARGED PARTICLE INTERACTIONS

INVITED

AND

CONTRIBUTED

PAPERS

N90-26778

LABORATORY STUDIES OF THE INTERACTION OF IONS WITH CONDENSED GASES: PLANETARY APPLICATIONS

J.W. Boring and R.E. Johnson
Department of Nuclear Engineering and Engineering Physics
University of Virginia
Charlottesville, VA 22901 USA

INTRODUCTION

The work described in this paper is concerned with laboratory studies of the processes that produce the ejection of molecules from the surfaces of condensed gas solids, the change in the chemistry of the surface materials, and the relationship of these results to processes occurring in the solar system. Included is a discussion of the experimental techniques employed in making these laboratory measurements.

In the solar system as one goes away from the sun the temperature of the surfaces of solid bodies decreases, such that many of the surfaces in the outer solar system are composed of substances that are gases at earth temperatures. This means that the binding energy of the molecules that form these solids tends to become smaller as one goes out in the solar system. Since these surfaces are frequently exposed to some form of radiation one has the possibility that these volatile substances can be ejected by the radiation to form an atmosphere in the vicinity of the body. The bodies of principal interest in this context are planetary satellites and rings, as well as comets and asteroids. The relevant radiation that causes ejection from these objects are ions, electrons and photons. In some instances, such as when a comet comes close to the sun, the net radiation flux is large enough to cause the temperature of a large fraction of the surface to become great enough that evaporation of the surface materials occurs. This removal of surface material by increased temperature is reasonably well understood and will not be considered here. Rather, we will concentrate on the ejection of surface molecules as a result of exposure to energetic ions, electrons and photons, where the ejection rate is proportional to the incident radiation flux. This implies that each incident particle produces an effect that is independent of the others. In some situations it is useful to speak of a transient increase in the temperature of the solid in the vicinity of the incident particle. The

PRECEDING PAGE BLANK NOT FILMED

process of the ejection of surface material as a result of incident radiation is called sputtering (or desorption) if the ejection rate is proportional to the incident flux.

Particles (ions, electrons, photons) deposit their energy in a solid in two forms: (1) Kinetic energy of motion of the atoms of the solid (nuclear deposition) and (2) Excitation of the electronic structure of the atoms/molecules of the solid (electronic deposition). Since the ejection of atoms/molecules from the surface of the solid is a result of their having attained a larger than average kinetic energy, it is easy to see how nuclear deposition leads to ejection. In the case of electronic excitation, however, it is necessary that the electronic disturbance lead to repulsion between neighboring particles and subsequent ejection of one or more particles from the surface. In the case of incident electrons and photons there is only an electronic contribution to the ejection, whereas for ions there can be both an electronic and a nuclear contribution, with the latter dominating for heavy ions.

When the solid under consideration has molecules composed of several different kinds of atoms there is the possibility of significant chemical change initiated by the incident radiation, even at the low temperatures of the condensed gas solids. Both the nuclear and electronic energy deposition can result in the breaking of chemical bonds, resulting in various molecular fragments. These fragments can diffuse and combine to form new chemical species, some of which may be volatile enough to leave the solid of their own accord while others may be ejected by subsequent radiation. The net result of all of this activity is that the chemical nature of the solid, along with its physical characteristics, may be permanently altered by the radiation, and various particles are ejected from its surface, both molecules of the original material and the new ones that have been produced by the radiation. Among the characteristics of the surface that are changed are its ability to reflect light and the rate at which it is eroded by subsequent radiation. An example is the bombardment of CH_4 by ions or electrons. The primary ejected species is H_2, resulting in a decreasing H to C ratio (Fig. 1). Eventually the material becomes rather carbon-like, very different from the original clear condensed gas solid. The tendency toward a carbonaceous material is accompanied by an increase in the average binding energy of particles on the surface, with a corresponding decrease in the probability of their ejection.

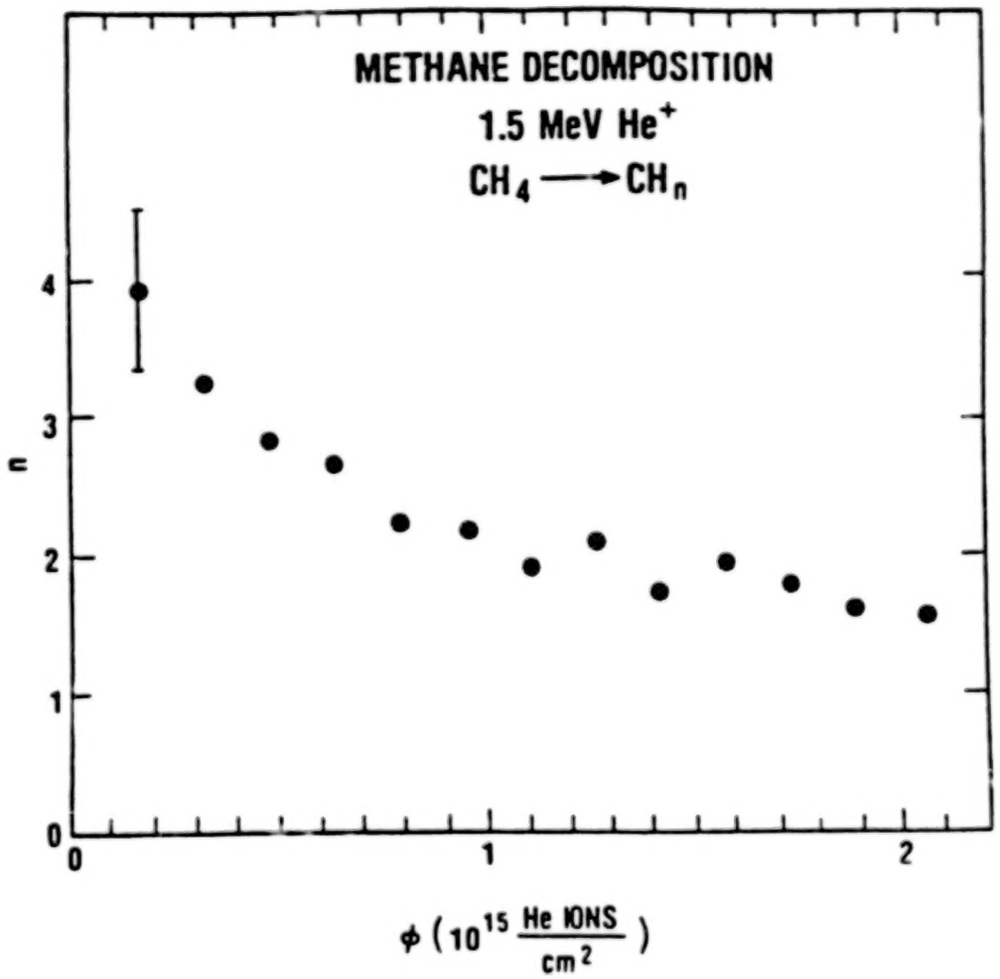

Fig. 1 Hydrogen-carbon ratio vs. fluence for methane bombardment by 1.5 MeV He^+ ions

Processes such as this may well have altered the surfaces of solar system bodies that were originally hydrocarbons but which as a result of radiation bombardment became much like carbon with a corresponding decrease in ability to reflect sunlight.

As implied in the previous discussion the principal factor in determining whether an atom or molecule is ejected from a surface is how strongly it is bound. We have also seen that chemical activity produces new species, some more strongly and some more weakly bound than the molecules of the original material. The ejection rate is, of course, also strongly affected by the density of energy deposited at the surface by the incident particle.

Experimental Techniques

We concentrate here on positive ions and electrons as incident particles and condensed gas solids as targets. The experimental systems described here are at the University of Virginia for keV measurements and Bell Labs for MeV measurements, and the results described later are from these two labs. Electrons with energies in the keV range are produced simply with an electron gun, consisting of a filament, an accelerating voltage and suitable focussing. Ions in the keV range require a little more equipment, including an ion source, an analyzing magnet and suitable pumping to maintain a low pressure at the target. Ions with energies in the MeV range are usually produced by using a van de Graaf accelerator. Condensed gas targets can be produced by deposition of the gas or vapor onto a cold substrate. Temperatures of ~ 15K will allow one to condense any material except He, H_2 and Ne. Temperatures in this range can be obtained using liquid He, but more conveniently with a closed cycle helium refrigerator.

In studying the ejection of atoms and molecules from the surface of the solid one is primarily interested in three quantities: (1) The absolute rate at which the ejection takes place, usually stated as the sputtering yield Y = particles ejected per incident ion. (2) The mass spectrum of ejected particles and (3) The energy spectrum of each of these masses. A typical apparatus for making these measurements is shown in Fig. 2. In this system the ion beam is incident on a condensed gas target. In making measurements of the absolute sputtering yield it is necessary to be able to measure the beam current accurately. This is aided with a flow-through Faraday cup before the target. One also desires to have the pressure at the target as low as

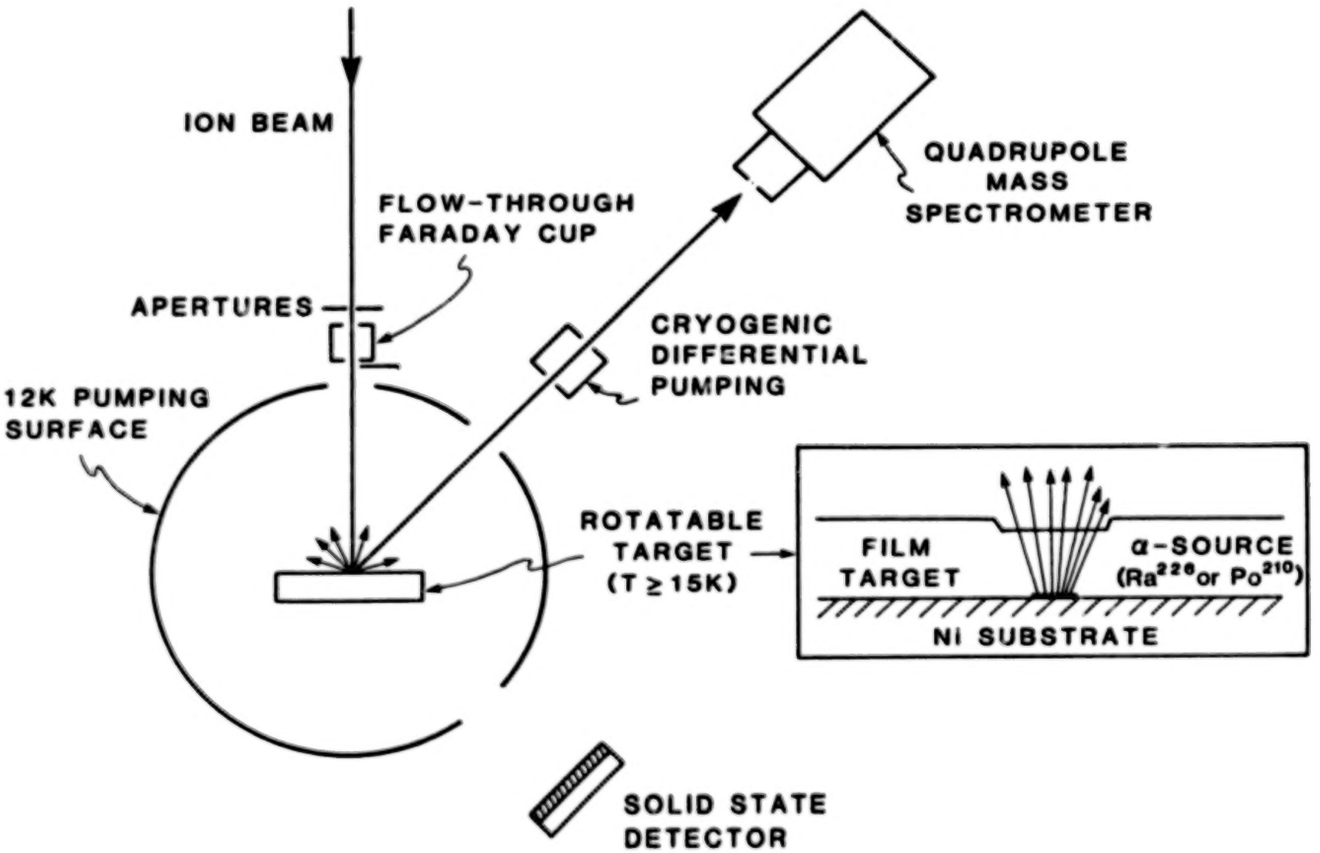

Fig. 2 Experimental system for investigating the sputtering of condensed gas solids

possible. This is accomplished by having the target surrounded by a copper cylinder maintained at a temperature of 12K, which serves to cryopump the target region, maintaining a pressure at the target of $\sim 10^{-10}$ Torr. The mass spectrum of ejected neutral particles is observed with a quadrupole mass spectrometer located in a separate vacuum chamber. Ionization of the neutral particles is by an electron-emitting filament just before the quadrupole. The kinetic energy spectrum of ejected particles is measured by pulsing the ion beam and observing the time spectrum of particles arriving at the quadrupole. Since the distance from target to detector and the mass of the particle are known one can then obtain the energy spectrum of each of the ejected species. In these time-of-flight measurements it is essential that the detected particles come directly from the target. This means that the detector chamber must be well isolated from the target chamber in a vacuum sense so that a pressure rise in the target chamber is not detected in the detector chamber. This is accomplished by having cryogenic differential pumping between the two chambers. In order to determine the total absolute yield of ejected particles one needs a method of determining changes in the thickness of the target as it is eroded by the ion beam. In this system this is accomplished by having an alpha source (R_a^{220} or P_o^{210}) deposited on the substrate that the target film is grown on. After the film is grown the alphas pass through it and their energy is a measure of the film thickness. These alphas are detected and their energy analyzed with a surface barrier solid state detector and a multichannel analyzer.

Since the character of the irradiated condensed gas solid is altered by the radiation it is important to be able to study these changes in the species present in the target. An experimental system capable of monitoring the atomic composition of the target is shown in Fig. 3. In this case the incident beam is composed of incident MeV H^+ or He^+ ions. These ions can be used for sputtering the film, but they can also be used for analyzing the atoms present in the target by Rutherford backscattering of these ions (usually He^+). A small fraction of the incident ions are scattered through an angle near 180°. The energy of these ions is determined only by the mass of the scattering atom and the amount of material through which the ion has passed. One can thus measure the proportion of the various atoms present in the target as a function of the amount of radiation. The incident ions that produce the radiation effect being studied may well be different from those

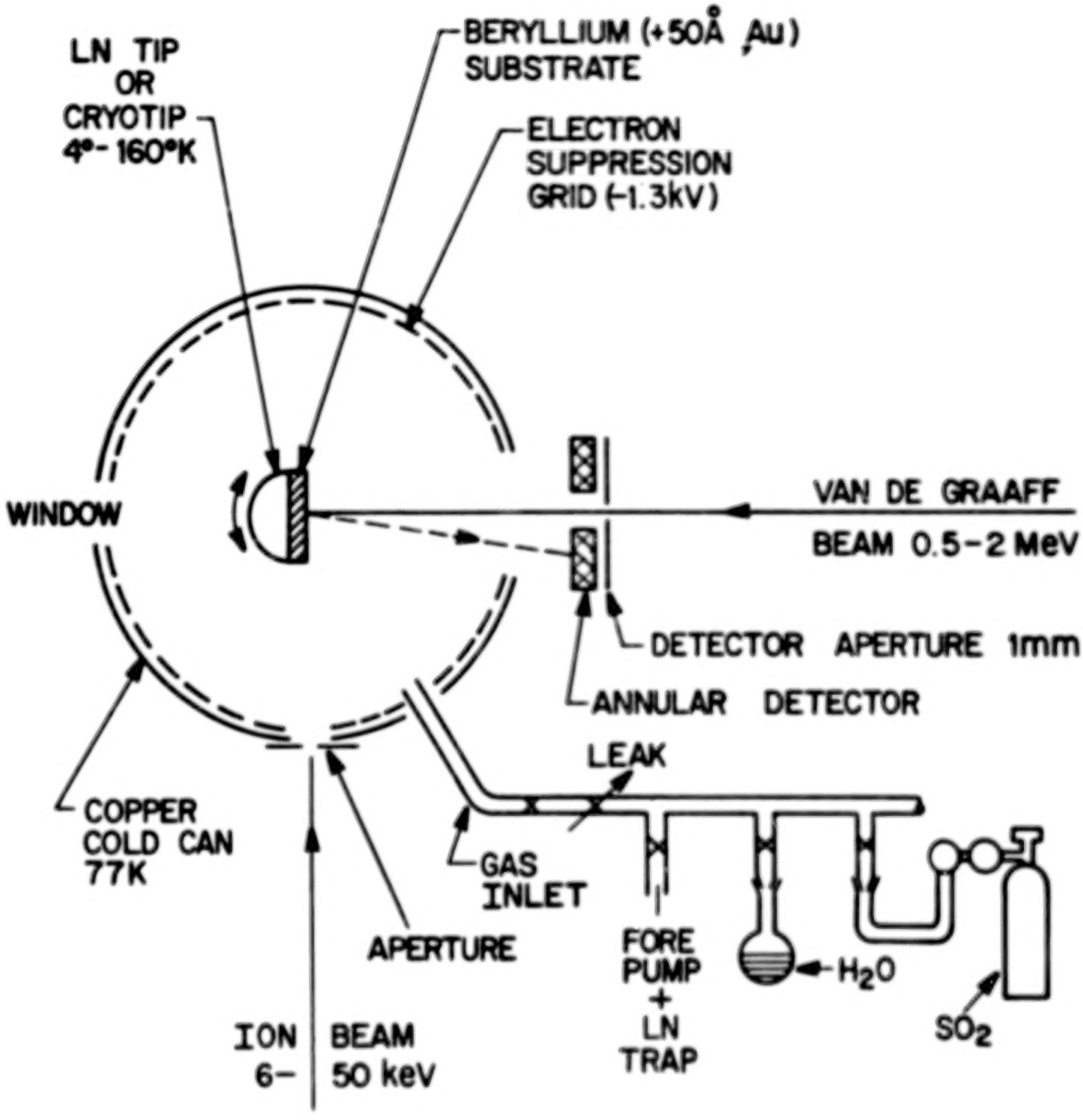

Fig. 3 Experimental configuration for Rutherford backscattering analysis

used in backscattering analysis. The technique gives no information on the molecular character of the target material, but it may also be used to measure the thickness of the target film in much the same manner as the alpha particle method described above.

Information about the molecular character of the solid may be obtained by a number of methods including SIMS, warming the irradiated condensed gas target and looking at the mass spectrum of what comes off, but we concentrate here on information that can be obtained by probing it with photons. The most useful wavelength ranges are in the infrared and ultraviolet. The configuration can utilize either the spectrum of photons transmitted through a thin film or those reflected from its surface region. Shown in Fig. 4 is an experimental system for studying in transmission the absorption of IR photons by a condensed gas target. The target is formed onto a cold KRr substrate with subsequent bombardment by an ion beam. One is principally looking for new absorbing molecular species formed as a result of the bonds broken by the incident particles. An arrangement for studying the reflectance of UV light by solid H_2O is shown in Fig. 5. The light from a high pressure Xe arc is incident on an ice target and the reflected spectrum is observed with a VUV-visible monochrometer. A spectrum is taken before ion bombardment and compared to that after bombardment. In addition to the changes in the molecular structure of the target caused by the breaking of chemical bonds by the ions, one can also expect absorption by new species that are created by the implantation of the ions into the target.

Representative Results

The key statements from the above discussion of the sputtering of condensed gas solids are that: (1) Incident ions and electrons can break chemical bonds, producing fragments. (2) The fragments can diffuse and combine to form new species. and (3) The character of the solid is permanently altered by these processes and particles are ejected from its surface, both the molecules of the original solid and the new species. In this section we present the results of measurements that indicate these features. In Fig. 6 we show the results of the bombardment of D_2O ice (D_2O is chosen over H_2O for reasons of lower background) by 1.5 MeV He^+ ions, where the energy deposition is predominantly electronic. The principal detected species are D_2O, D_2 and O_2, indicating the presence of new species created by the incident ions. In

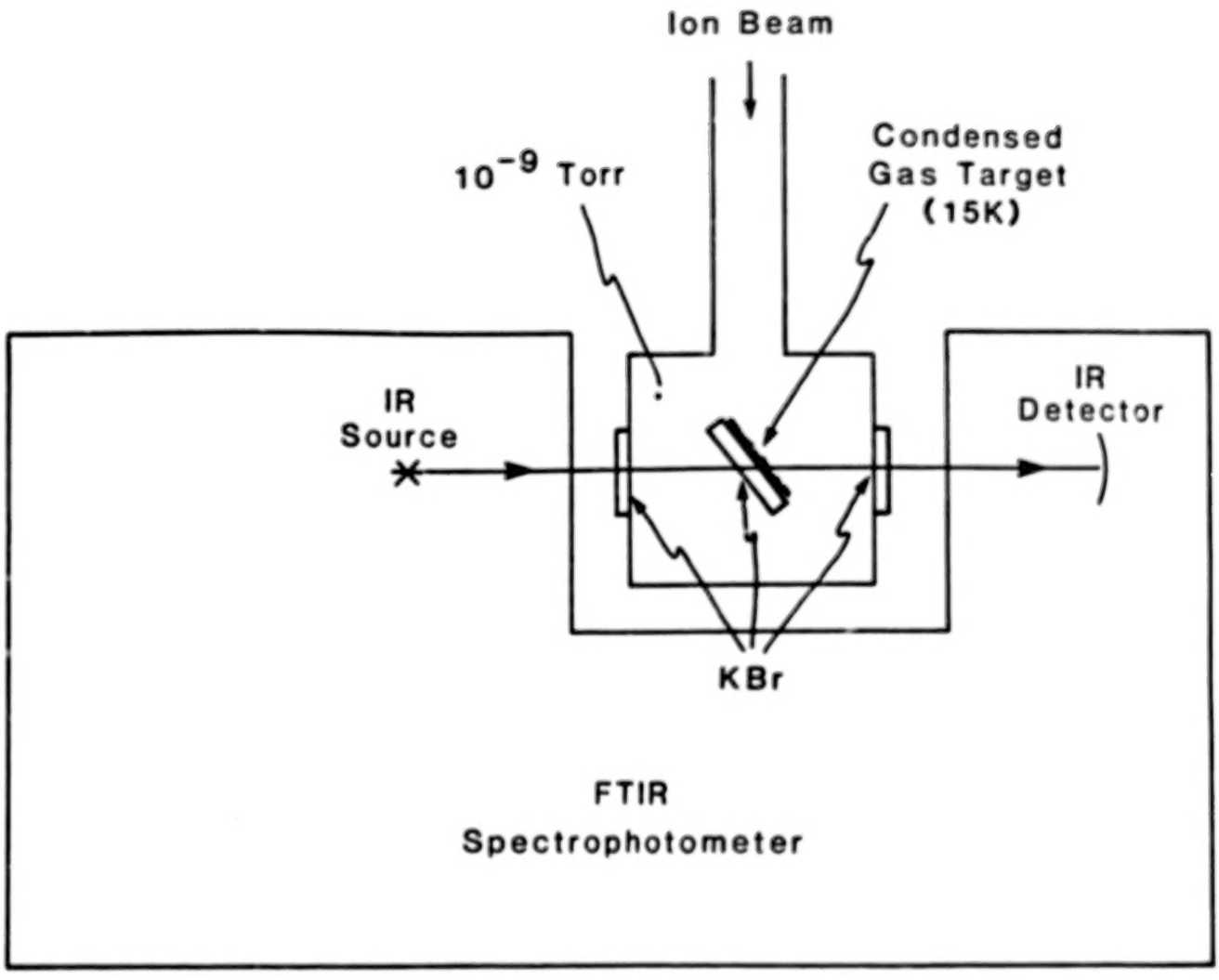

Fig. 4 Apparatus for infrared transmission studies of ion-bombarded condensed gas targets

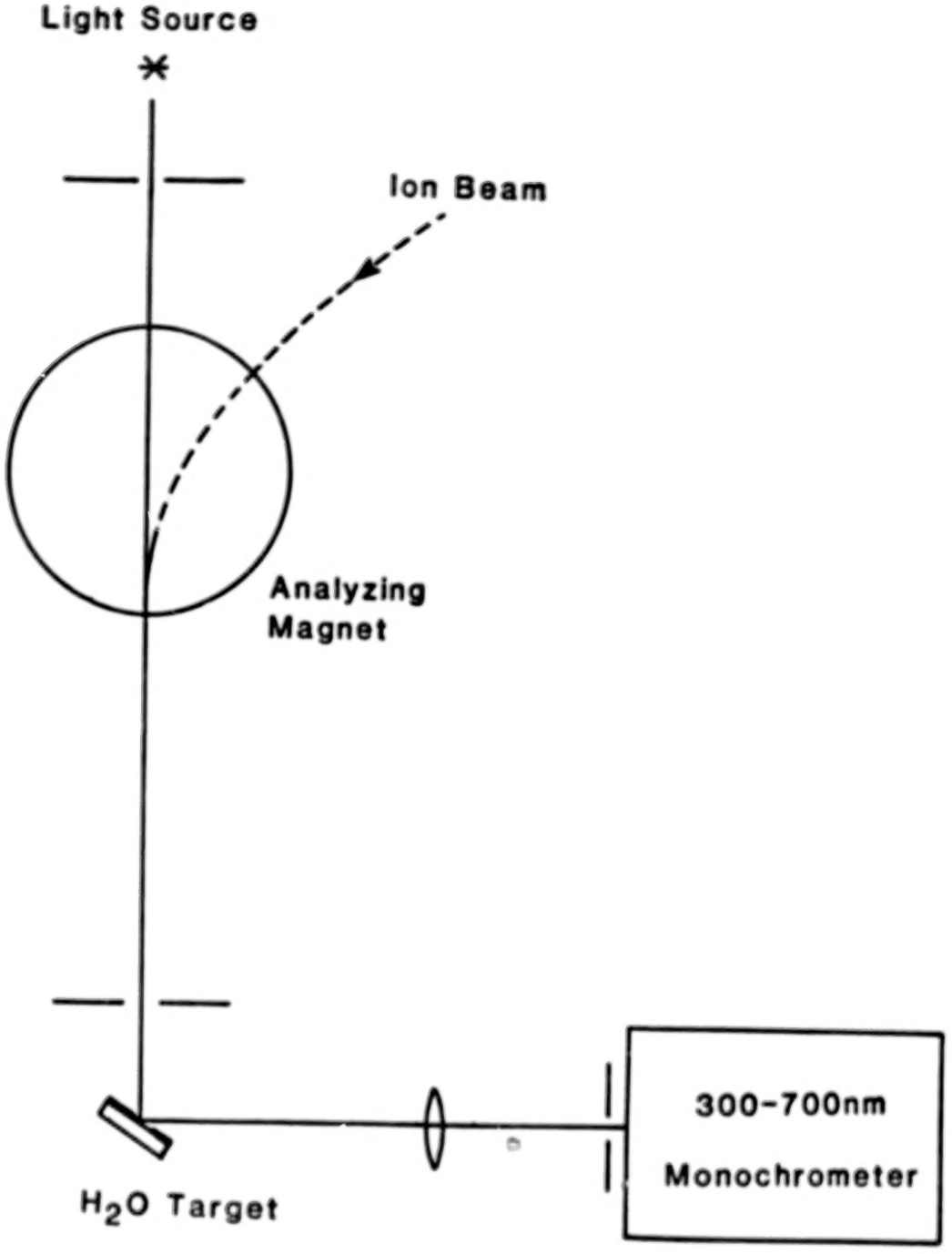

Fig. 5 [illegible]mental system for reflectance studies of ice

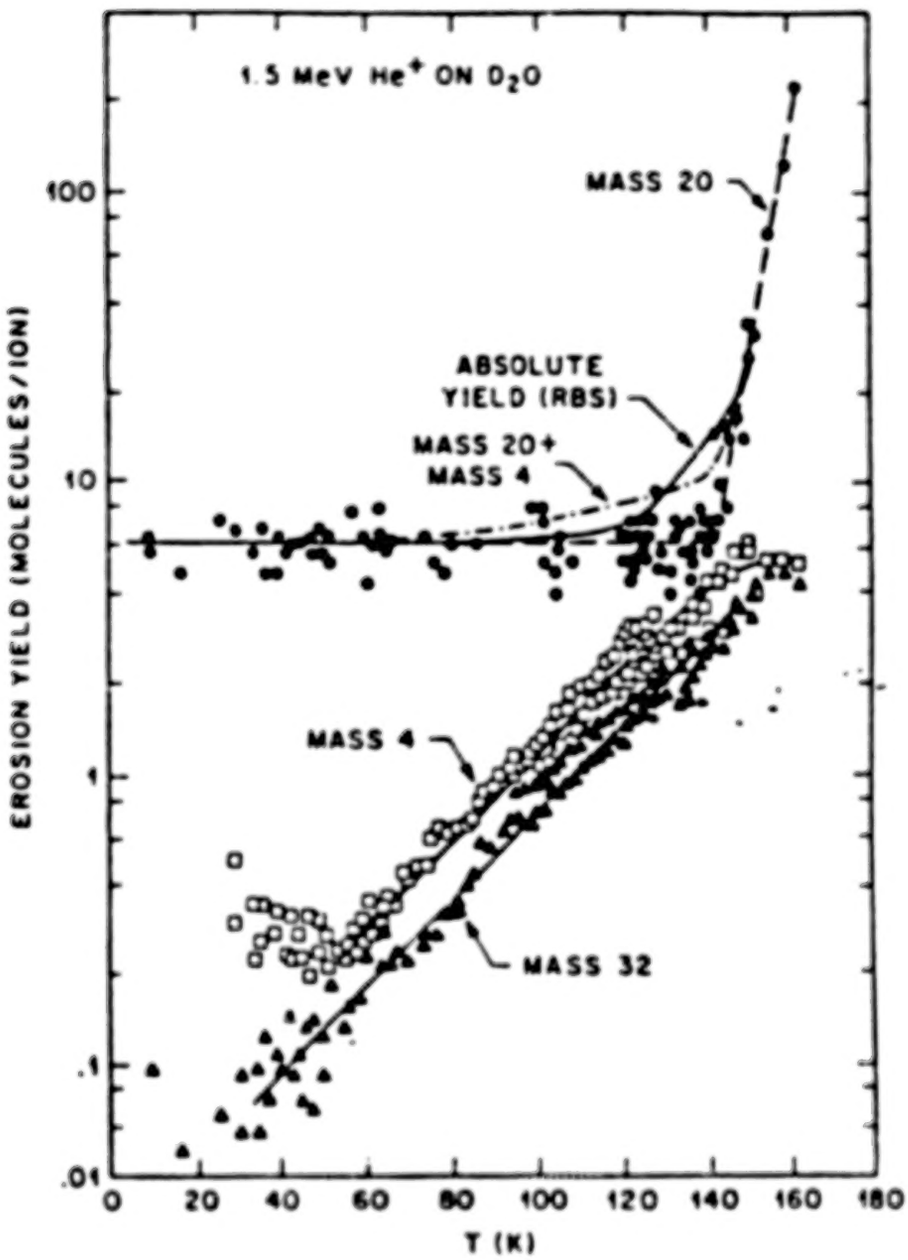

Fig. 6 Temperature dependence of the ejection of D_2O, D and O_2 from solid D_2O.

Fig. 6 we plot the yield of ejected particles as a function of target temperature, as measured by a mass spectrometer. It is seen that in the temperature range 50 - 140K the yield of D_2O is independent of temperature, while the yield of D_2 and O_2 is dependent on temperature over the entire range. This is as expected since D_2 and O_2 are created species which depend on diffusion for their production. Evidence of the production of new species is also shown in Fig. 7 for D_2O where the mass spectrometer signal for D_2O, D_2 and O_2 is displayed as a function of beam fluence (or time after the beam is turned on). One sees that the D_2O signal (mass 20) rises rapidly to a constant value while the O_2 signal (mass 32) rises slowly, indicating the finite time required to produce a significant amount of this new species. The D_2 signal (mass 4) seems to have a more complicated structure with both a rapid and a slow component. The behavior of targets with different possible product species is shown in Fig. 8, where the total sputtering yield is plotted vs. temperature for Ar, CO_2, SO_2 and H_2O. The curve for Ar is the simplest since there are no new chemical species produced. The yield is constant up to a temperature just under where one expects significant sublimation, followed by a rapid rise, probably due to local heating of the target in the vicinity of the track of the incident particle. The H_2O and SO_2 targets show a behavior similar to each other - a region of constant yield followed by a slow rise when the diffusion and ejection of new species becomes comparable to the ejection of the parent species. The CO_2 target exhibits the most complex behavior with two distinct steps, corresponding to the sudden production of new species at the corresponding temperatures.

Satellites of Jupiter and Saturn

The general information discussed above is useful for considering the contributions to atmospheres and plasmas in the environment of planetary bodies. For a specific situation we consider how information of the type presented here applies to two of the Jovian satellites - Io and Europa, and the icy Saturnian satellites.

Io

The surface of Io is composed largely of sulfur-containing compounds, elemental sulfur and SO_2. In the absence of a thick atmosphere (e.g. night side and poles) the surface of Io is continually bombarded by ions of the

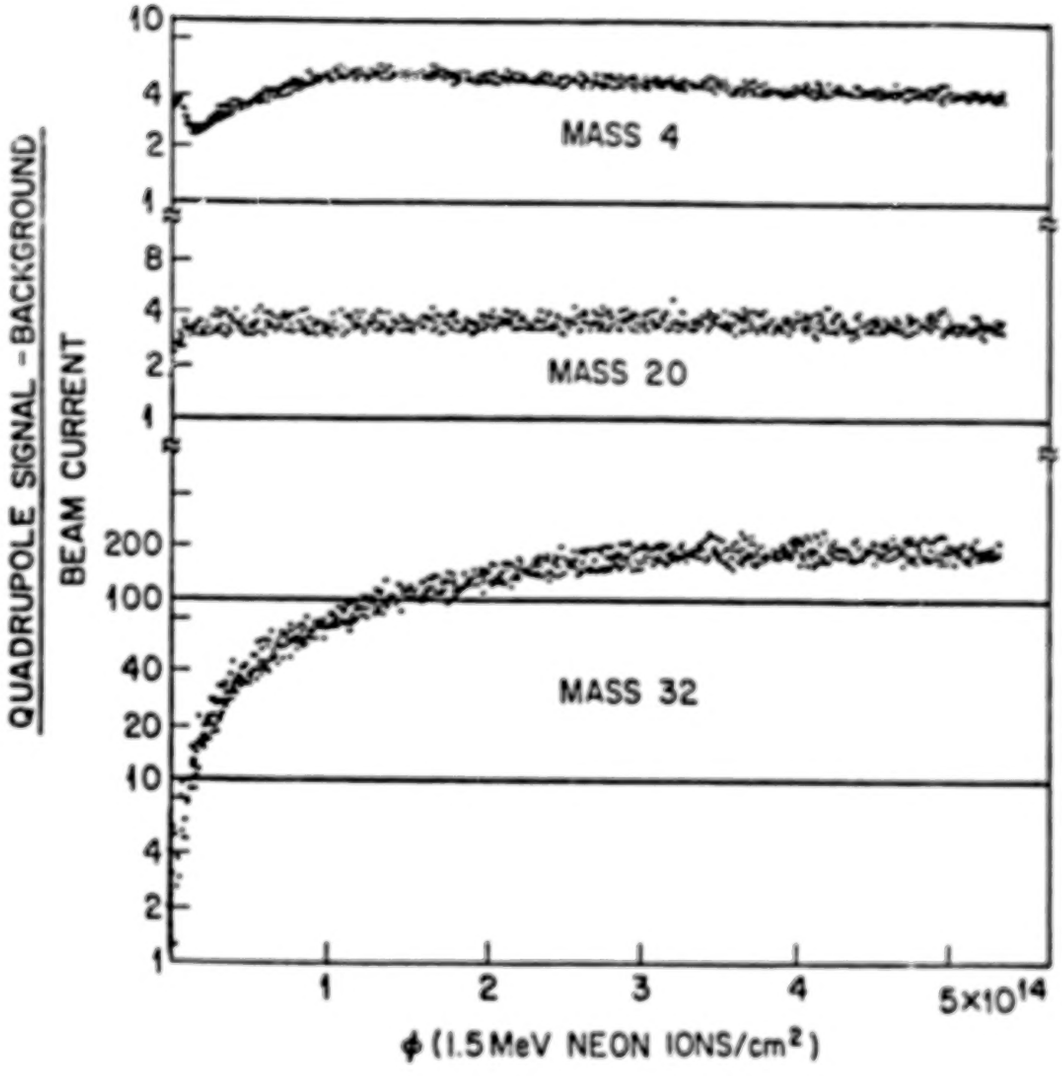

Fig. 7 Transients in the ejection of D_2O, D_2 and O_2O

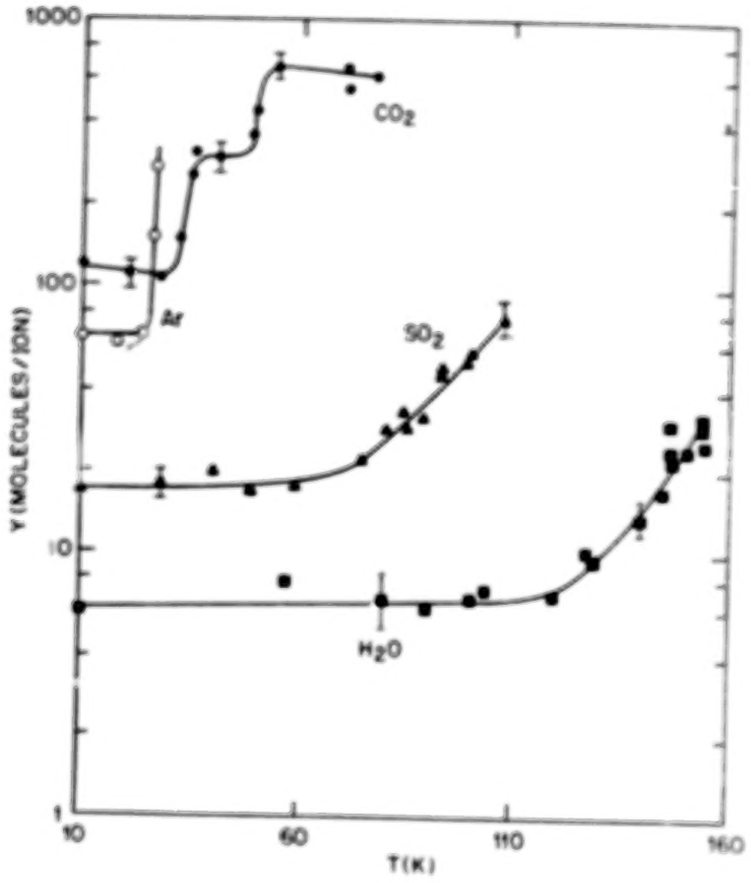

Fig. 8 Temperature dependence of the sputtering of Ar, CO_2, SO_2 and D_2O

plasma torus trapped in Jupiter's magnetosphere. We are thus interested in the rate at which particles are ejected from the surface and their subsequent history. One important factor in the ejection is the energy spectrum of ejected species, since this determines the fraction of ejected particles that escape the gravitational field of the satellite. The ones that do not escape will probably pass in a ballistic trajectory and be redeposited on the surface. The ones that do escape are bound in Jupiter's gravitational field until they are ionized by solar photons or electrons, at which time they become part of the plasma torus around Jupiter, with the likelihood that they will later contribute to the erosion of the surfaces of the satellites embedded in this torus.

For the case of sulfur on the surface of Io we consider first the mass spectrum of ejected particles. Shown in Fig. 9 is a spectrum obtained in the laboratory for the erosion of sulfur by keV ions. Solid sulfur is composed of S_8 rings, but one sees that very few of the ejected species are S_8, with the ejecta being predominantly S_2. This is because it is difficult to have ejecting impulses applied to the whole S_8 ring, whereas S_2 is a particularly stable small fragment of sulfur. Evidence for particles altering the surface and producing fragments may be the dark poles of Io. An example of the energy spectrum of ejected sulfur species is shown in Fig. 10. At the higher ejection energies it is seen that for the small fragments S_1 and S_2 the behavior goes as E^{-2}, which is typical of collision cascade sputtering. For the larger species the curve drops more rapidly, indicating the difficulty of ejecting a large fragment as a result of an energetic impulse in the solid. Similar energy spectra have been obtained for the sputtering of SO_2 by keV ions, allowing one to assess the relative importance of those particles that escape the gravitational field of Io and those that become redeposited on the surface.

A problem of major interest to atmospheric scientists is the source of Na observed in the atmosphere of Io. We have recently measured the ejection of Na from Na_2S and combined that with our sulfur results to help understand Na_2S_x (i.e. any combination of sodium and sulfur on Io). We find that sodium is ejected primarily in the form Na, NaS, and Na_2S. Therefore, both atomic and molecular forms should be observed. Using our measured energy spectra we find we can produce a sodium atom line-of-sight column density with a profile like that observed. Because of the recent observation of H_2S in this system

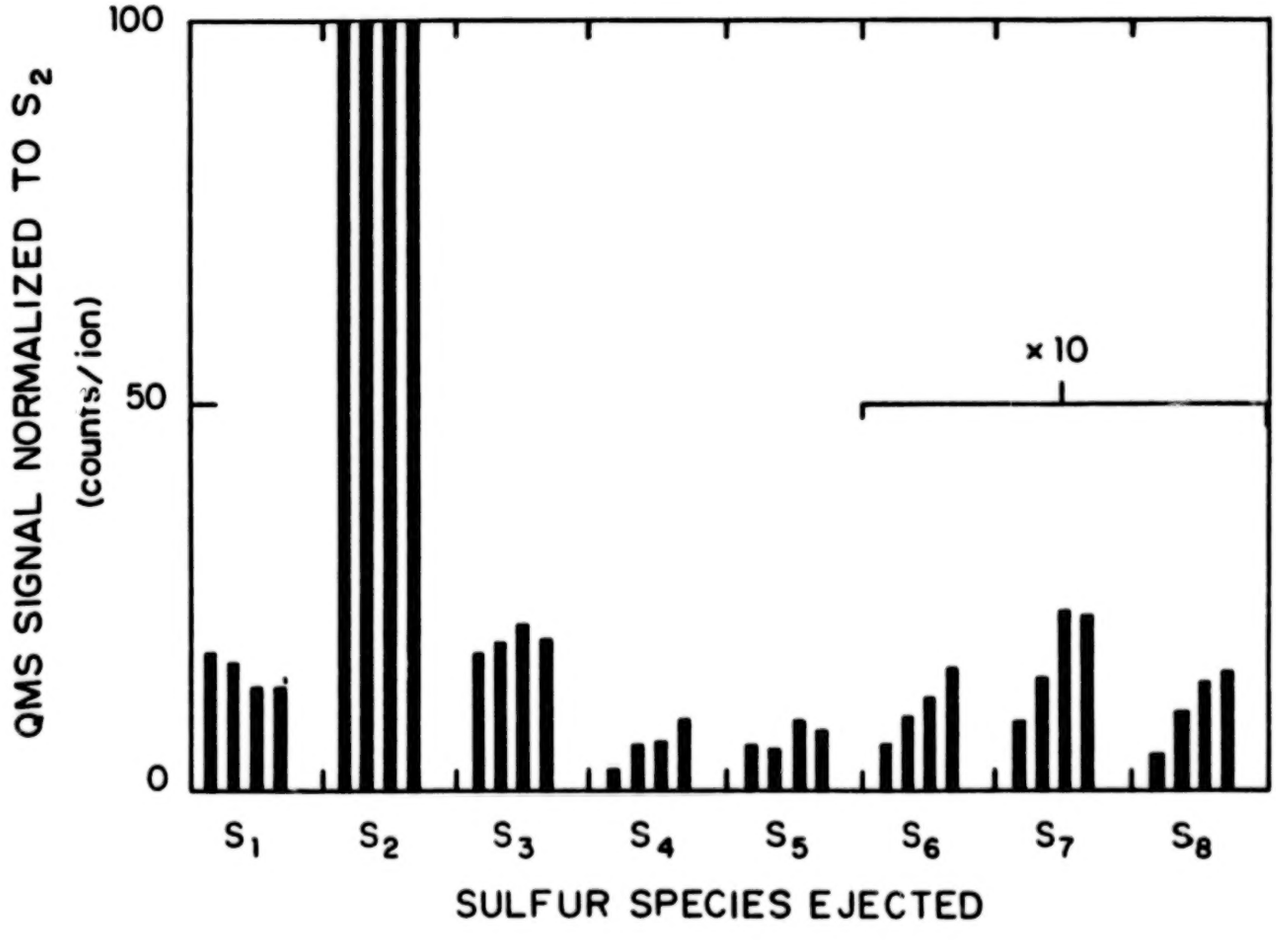

Fig. 9 Mass spectrum of particles ejected from sulfur by keV ions

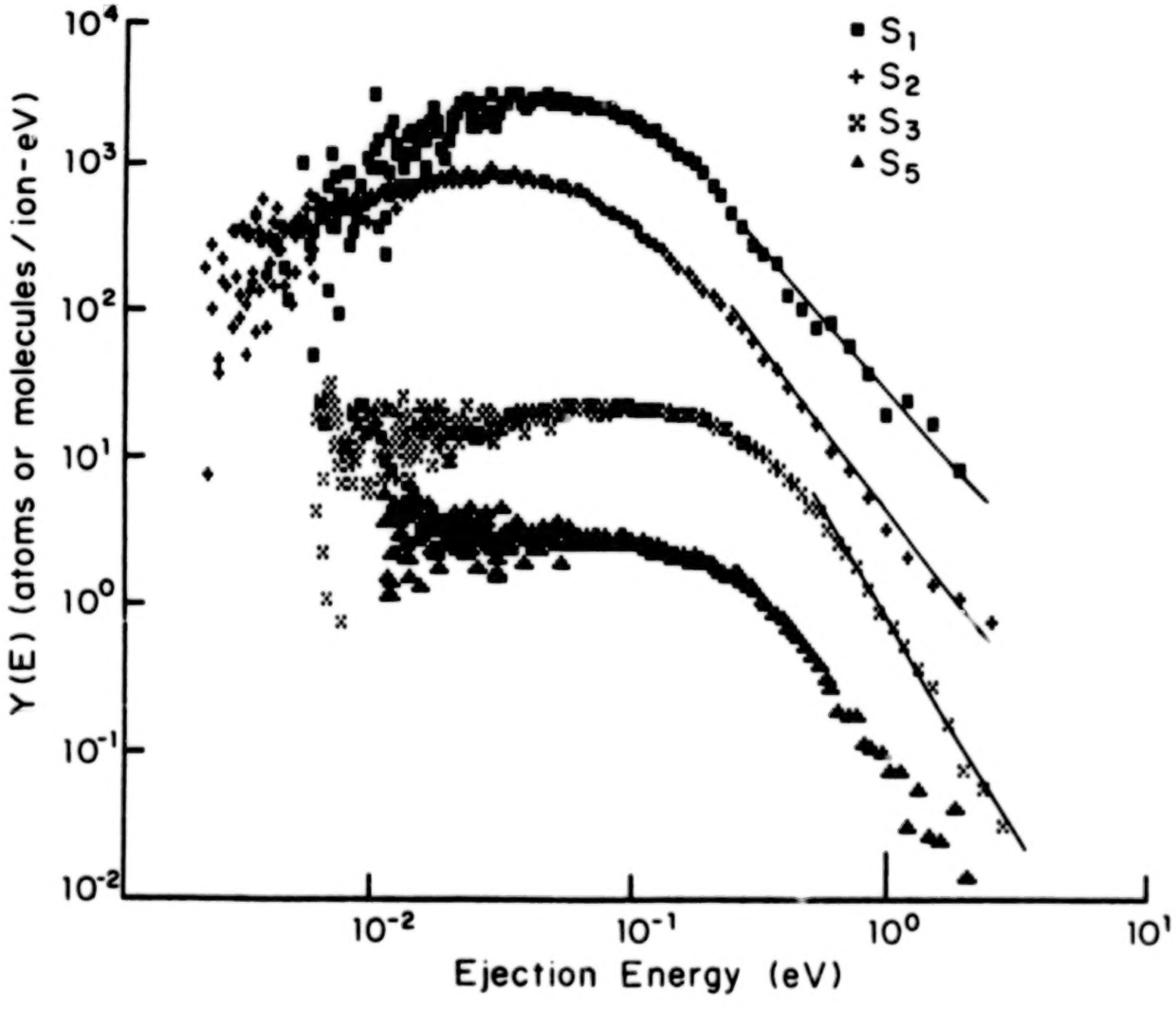

Fig. 10 Energy spectrum for several masses ejected from solid sulfur

we will shortly be studying the yield of H_2S from sulfur bombarded by protons.

Europa

The surface of Europa is largely solid H_2O and much of the information about its composition is obtained by looking at the spectrum of reflected sunlight, particularly in the UV region. Compared to pure ice, one observes in the Europa spectrum a rather strong absorption in the wavelength range 200-500nm. It has been suggested that this may be due to S-O bonds in the solid that result from S^+ implantation into H_2O from the ions in the Jovian magnetosphere. We have explored this hypothesis in the laboratory by observing the reflectance of solid H_2O in the UV, both before ion bombardment and after bombardment by various ions. Shown in Fig. 11 is the ratio of a spectrum taken after bombardment by SO_2^+ ions to that before bombardment for a temperature of 20K. It is seen that there is in fact a strong absorption feature at the lower wavelengths. In order to test whether this was due to S implantation or some more general interaction of the ions with the target we repeated the experiment with Ar^+ ions. The resulting spectrum was substantially the same as for SO_2^+ ions, indicating that the absorbing species was probably a result of bond breaking in the H_2O target rather than being due to an implanted species. When the experiments were repeated at 120K, a temperature more representative of Europa, the absorption feature was absent for all incident ions, indicating that the low temperature was necessary to preserve the absorbing species. This leaves open the question of what does produce the absorption on Europa. One thing that must be kept in mind with regard to the above laboratory results is that the range of the ions in the solid is ~ 20 nm, meaning that only a thin layer contains implanted ions and that these may produce an absorption much too weak to be observed. It is possible that on Europa the implantation of S^+ takes place over a long time, along with simultaneous redeposition of ejected H_2O onto the surface, resulting in a surface region that contains many sulfur atoms to a depth that is large compared to the penetration depth of the light that is reflected.

Icy Saturnian Satellites

From Mimas to Rhea a plasma containing H^+ and O^+ has been identified. Of particular interest here is the heavy species whose source must be the icy satellites. That is, plasma ions bombard the surface and sputter H_2O (H_2 +

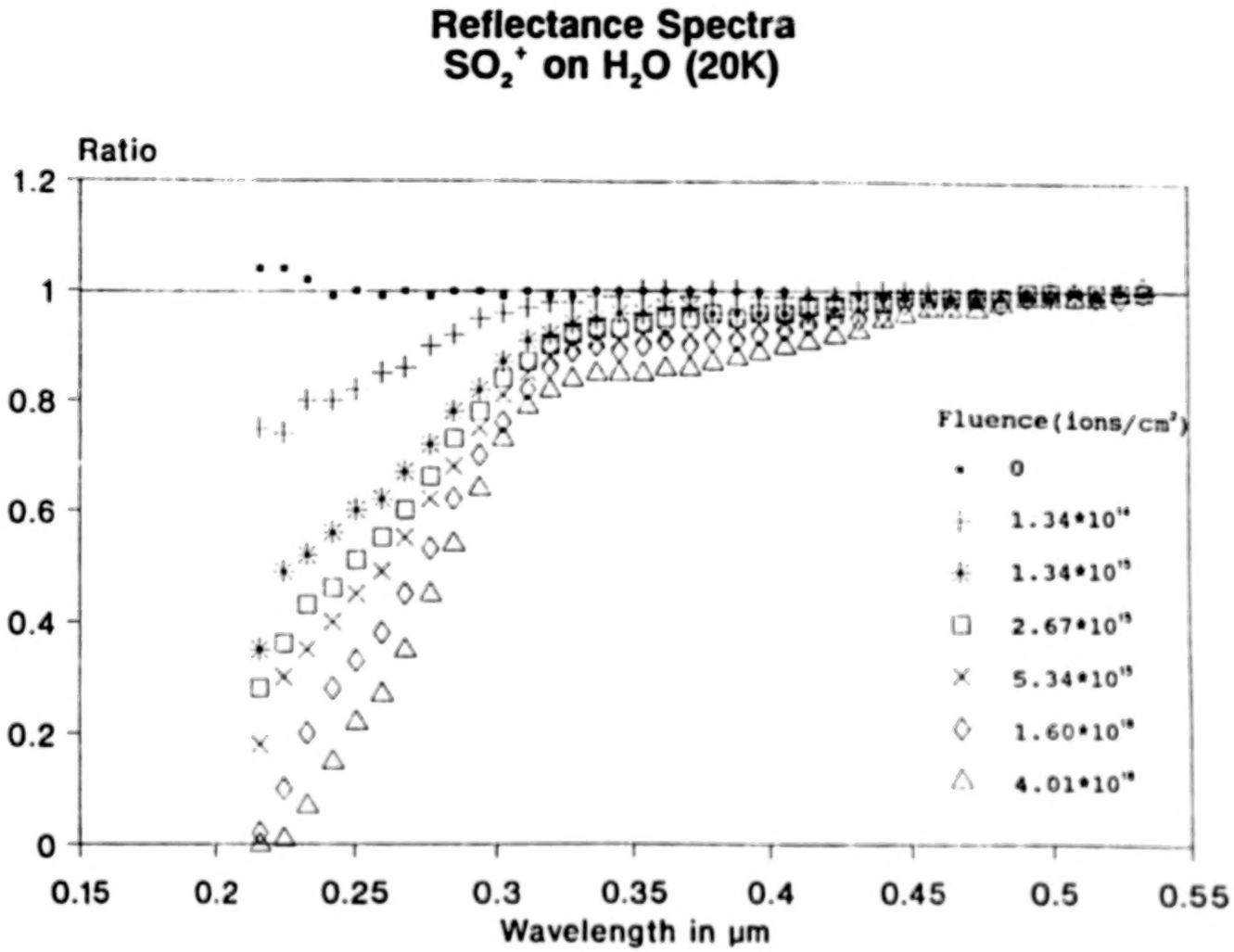

Fig. 11 Reflectance spectrum for SO_2^+ bombardment of H_2O

O_2) which based on our laboratory measurements easily escape the gravitational fields of the small satellites. These molecules reside in the gravitational field of Saturn orbiting at a speed close to that of the parent satellite, as determined by our ejected particle energy spectra. Eventually the molecules are ionized (by electrons or UV photons) producing the observed plasma. We therefore, have been able to take our laboratory measurements and calculate the source rate of ions in the inner magnetosphere. As the electron temperatures inside the orbit of Enceladus are low, the plasma may contain molecular ions, the detection of which by Cassini would be an exciting test of these ideas. These satellites also have reflectance spectra which are not those of pure H_2O and we are at present working on sorting out the role of bombardment vs. that of contaminants in the solid.

As an example of the use of laboratory data to calculate atmospheric densities we show in Fig. 12 the density contours in the vicinity of the Saturnian satellites, as calculated from the ejection rate and energy distribution of particles ejected from these satellites.

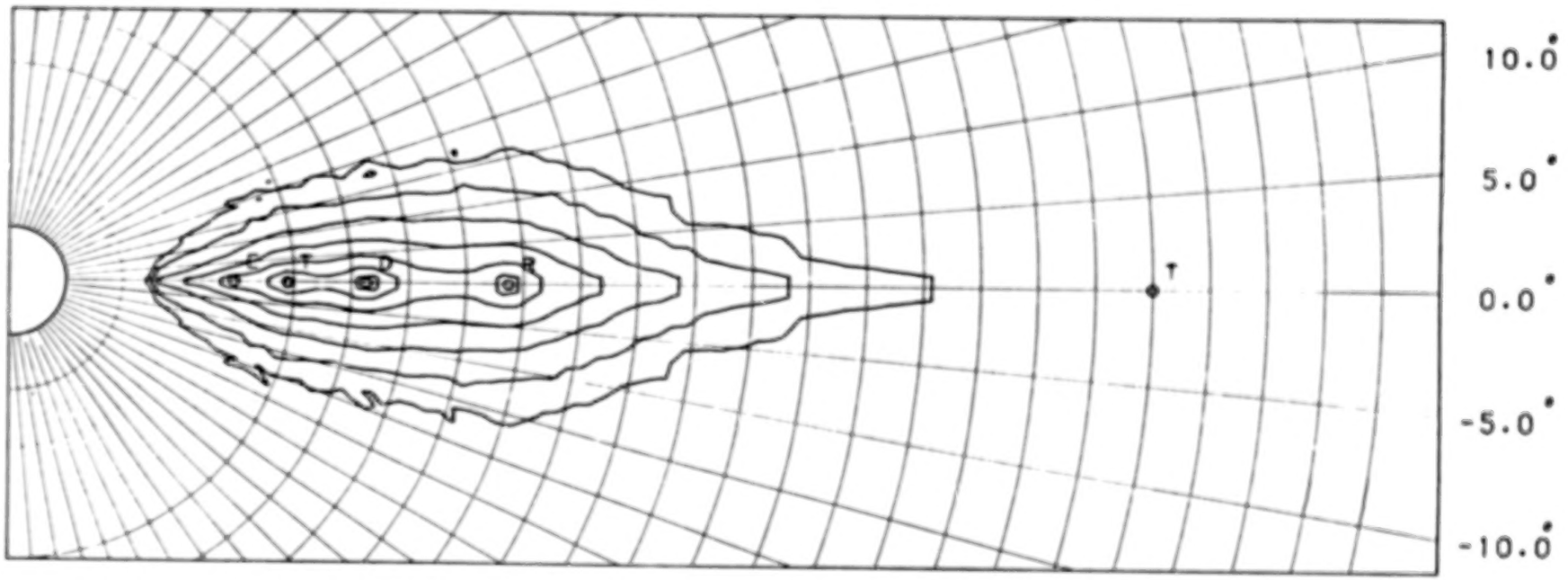

Fig. 12 Density contours near the Saturnian satellites as calculated from ejected energy spectra from the satellite surfaces. The outermost contour is 10^{-1} part/cm^3, the next are $10^{-0.5}$, 10^{0}, etc.

N90-26779

ELECTRON-IMPACT SPECTROSCOPY

S. TRAJMAR, JPL, Caltech, 4800 Oak Grove Dr., Pasadena, CA 91109

ABSTRACT

The methods of electron impact spectroscopy and cross section measurements are discussed and compared to optical spectroscopy. A brief summary of the status of this field and the available data is given.

INTRODUCTION

The first studies of electron collision phenomena in the early 1930's contributed significantly to the understanding of the quantum states of matter by demonstrating that electrons can lose only well defined amounts of energy in collision with atoms. These first activities were followed by a long dormant period up to the 1960's when the field became very active due to need of spectroscopic and cross section data for a large variety of systems (planetary ionospheres, astrophysics, lasers and various plasma devices). The aim of this paper is to briefly describe the status of electron collision field and the methods used to generate spectroscopic and cross section data. A comparison between optical and electron-impact spectroscopy is made and elastic, excitation, dissociation, ionization, momentum transfer and total electron scattering measurements are described. The discussion is limited to electron interactions with neutral molecular (atomic) species.

ELECTRON-IMPACT VERSUS OPTICAL SPECTROSCOPY

In a typical electron scattering experiment (see Fig. 1) an electron beam of well defined energy (E_o) crosses a target gas beam and the scattered electron signal at a direction θ with respect to the incoming beam is measured as a function of energy lost by the electrons under single collision conditions. The resulting curve is an energy-loss spectrum. Fig. 2 shows such spectrum for He. It is very similar to an optical absorption spectrum. The locations of the energy-loss features contain the spectroscopic information (energy level scheme of the target species) and the scattering intensities are related to the corresponding cross sections. Indeed, it can be shown that at high impact energies and small scattering angles (small momentum transfer conditions) the optical absorption and electron-impact energy-loss spectra are equivalent and the same cross sections can be deduced from either of them. In other words, the same (dipole) selection rules apply for both cases and optical absorption

and photoionization cross sections can be obtained by electron scattering techniques. The sharp (in time) electric field experienced by the target in high-energy electron collision, may be Fourier-transformed to represent a wide range of frequencies. The electron, therefore, corresponds to an ideal continuum light source.

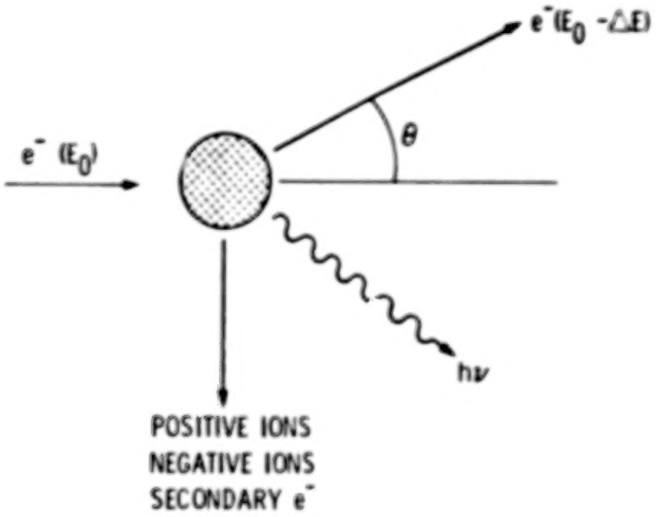

Fig. 1: Schematic representation of electron-beam/molecular-beam scattering experiment. The incoming and scattered electron beam as well as secondary products (electrons, photons, ions, dissociation fragments) are indicated.

At low impact energies and large scattering angles (small momentum transfer conditions) the situation is quite different. Electron collision processes do not obey optical selection rules and all types of symmetry and/or spin forbidden transitions may take place yielding information which is not available from optical spectroscopy. E.g. in Fig. 2 the ($^1S \rightarrow ^3$P) spin forbidden excitation peak is quite prominent, while in optical spectra it is 10^7 times weaker than the optically allowed ($^1S \rightarrow ^1$P) excitation. An additional important difference between the two methods is that in electron-impact spectroscopy the full spectrum ranging from the microwave to the x-ray region can be obtained in a single scan with the same instrument while in optical spectroscopy very different techniques are required for various spectral regions.

Now turning to the quantitative aspects of electron-impact spectroscopy, it should be mentioned that the cross section data can be obtained either from the measurement of the scattered electron signal or from the measurement of the secondary electron, photon, ion or fragment signals associated with the scattering process in question (see Fig. 1). More detailed information concerning the electron molecule interactions (multiply differential cross sections, scattering amplitudes and various coherences among these amplitudes) can be obtained from coincidence measurements of two (or more) particles.

DEFINITION OF CROSS SECTIONS

The parameter which quantitatively characterizes a scattering process is the cross section. It represents the time-independent probability for the occurrence of a particular scattering process. The notion of constant collision cross section, used in gas kinetic collisions, is not appropriate for electron scattering since the interaction is velocity and angle dependent.

Beam-beam scattering measurements yield the differential scattering cross section (DCS) for a given process (n).

$$DCS_n(E_o,\theta) = \overline{\frac{d\sigma_n(E_o,\Omega)}{d\Omega}}, \tag{1}$$

where the averaging over azimuthal angles (ϕ), instrumental energy and angular resolution and experimentally indistinguishable processes is indicated by the horizontal bar. Integration over all solid angles then yields the integral cross section

$$\sigma_n(E_o) = 2\pi \int_o^\pi DCS_n(E_o,\theta)\sin\theta d\theta \tag{2}$$

and in case of elastic scattering, the momentum transfer cross section

$$\sigma^M(E_o) = 2\pi \int_o^\pi DCS_o(E_o,\theta)(1-\cos\theta)\sin\theta d\theta. \tag{3}$$

The total electron scattering cross section represents the sum of all integral cross sections:

$$\sigma_{TOT}(E_o) = \sum_n \sigma_n(E_o) \tag{4}$$

Where the summation includes the elastic, all inelastic and ionization channels.

The most basic quantity, of course, is the complex scattering amplitude and its square modulus represents the differential scattering cross section.

MEASUREMENT OF CROSS SECTIONS

Differential Cross Sections

The experimental techniques used to obtain electron collision cross sections of interest to us here are briefly summarized below. More detailed description of these techniques have been given by Trajmar and Register (1984) and Nickel *et al.* (1989).

Most of the electron collision cross section measurements are carried out with an electron beam-molecular beam configuration (see Fig. 1.) The resulting energy-loss spectra

yield scattering intensities associated with a given process at fixed E_o and θ values. (See Fig. 2).

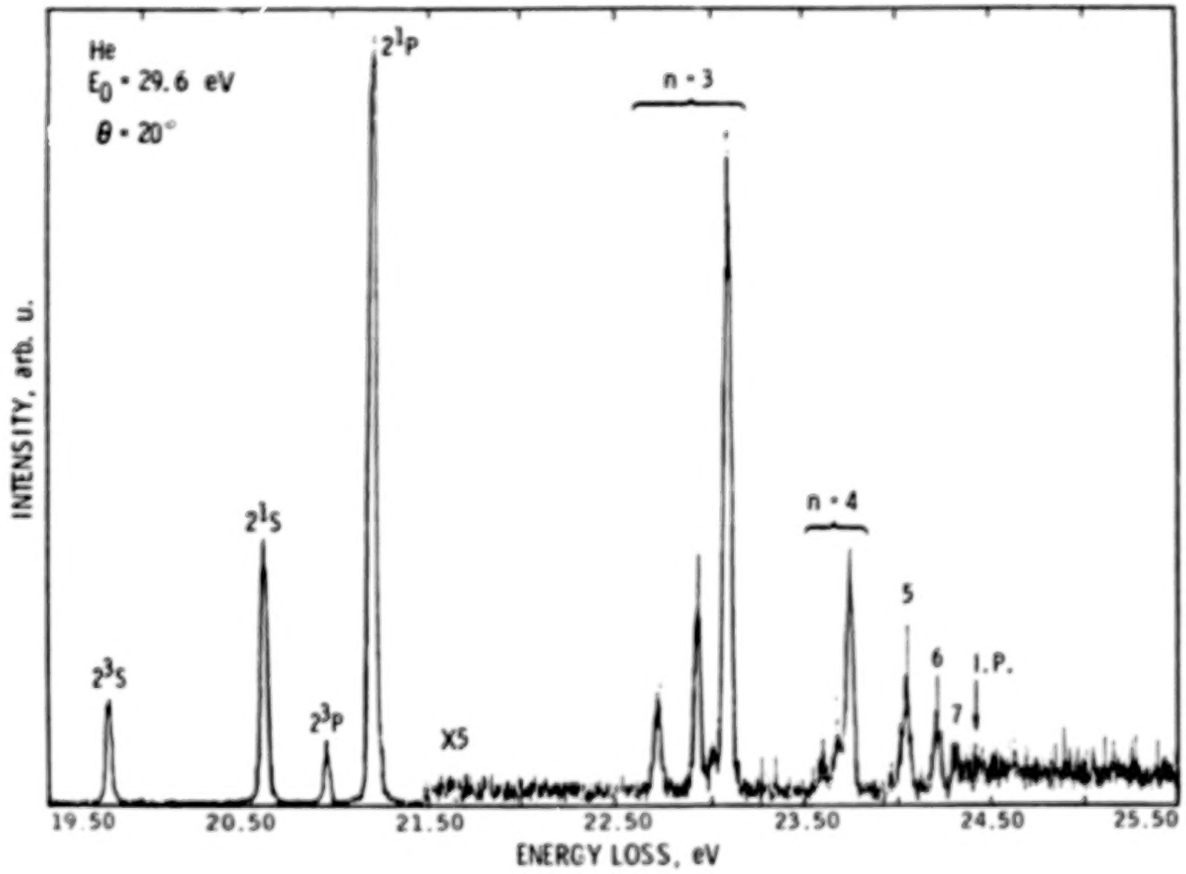

Fig. 2 Energy-loss spectrum of He. The region corresponding to the n = 2, 3... manifold excitations and to the ionization continuum is shown under medium momentum transfer conditions.

The scattering intensity is related to the differential cross section as

$$I_n(E_o,\Omega) = \int_{\vec{r}}\int_{E'_o}\int_{\Omega'(\vec{r})} \rho(\vec{r}) f(E'_o,\vec{r}) F(E'_o,\vec{r}) \times \frac{\partial\sigma_n(E'_o,\Omega')}{d\Omega} d\Omega' dE'_o d\vec{r} \ , \quad (5)$$

where $I_n(E_o,\Omega)$ is the scattering signal (counts sec^{-1}) measured at a nominal impact energy E_o and scattering polar angles $\Omega(\theta,\phi)$, $\rho(\vec{r})$ is the spatial density distribution of the target atoms (molecules cm^{-3}), $f(E'_o,\vec{r})$ is the distribution function (both energy and spatial) of the electron flux (electrons sec^{-1} cm^{-2}), $F(E'_o,\vec{r})$ is the response function of the detector, $d\Omega' = \sin[\theta'(\vec{r})]d\theta'(\vec{r})d\phi(\vec{r})$ and $\vec{r}$ is the position vector for scattering points which contribute to the signal.

The rigorous deconvolution of the cross section from Eq. 5 is complicated but for most practical purposes we can define the differential cross section, which is averaged over the instrumental energy and angular resolution (and azimuthal angles), as defined by Eq. 1

and thus obtain the simple equation

$$I_s(E_o,\theta) = DCS_s(E_o,\theta)V_{eff}. \quad (6)$$

The problem then boils down to the determination, calibration or elimination of V_{eff} (the effective scattering volume) in Eq. 6. It is a lengthy procedure and described in details e. g. by Trajmar and Register (1984) and Nickel *et al.* (1989). Basically, the procedure relies on relative intensity measurements and normalization to He elastic scattering for which accurate cross section values are available.

Integral Cross Sections

In general, the direct measurement of integral cross sections is not feasible for elastic and excitation processes. Integral cross sections then can be obtained from DCS using Eq. 2.

One can, in certain cases, deduce integral excitation cross sections from optical excitation functions which are obtained by measuring the optical radiation intensity caused by electron impact excitation and subsequent decay of the excited level. This procedure requires the knowledge of cascade contributions and branching ratios and is applicable only to optically allowed excitation processes in general. Note that the measurement of the optical excitation functions and electron impact cross sections are complementary to each other. Going the other way around, one can deduce from the measured electron impact excitation cross sections the optical excitation functions. For this purpose the dipole transition probability between the excited and ground levels and knowledge of cascade contributions are needed. The best philosophy is to measure cross sections if cross sections are needed and measure optical excitation functions if photoemission cross sections are needed.

Electron impact excitation to continuum states of molecules results in dissociation. If the dissociation products are ions (dissociative ionization, polar dissociation or dissociative attachment) or if the neutral disociation products are in excited states which consequently decay by radiation, the total dissociation cross sections can be determined by measuring charged particle or photon yields. Similarly direct ionization cross sections of molecules (atoms) can be conveniently determined by measuring the ion signal. One faces, however, a much more difficult task when the concern is dissociation to neutral ground state species. Only recently have these problems successfully been addressed by fast beam coincidence techniques by Helm and Cosby (1987).

At very low electron energies, when only a few inelastic channels are open, integral excitation cross sections can also be deduced from electron swarm measurements. In the swarm method a stream of electrons enter a diffusion chamber containing the target gas and proceed through the gas under the influence of an electric field. The stream proceeds to the anode, on its way colliding with the gas and spreading by diffusion. The behavior of the electrons is governed by the Boltzmann equation. The collisions with the gas

manifest themselves by affecting the Boltzman collision integral and as a consequence the macroscopic transport properties. Treating the applicable cross sections as free parameters, their value can be determined by fitting the measured transport coefficients to those defined by the Boltzmann equation. Obviously when too many parameters are required to characterize the system, the fitting procedure becomes ambiguous.

Momentum Transfer Cross Sections

In the case of elastic scattering Eq. (3) can be utilized to obtain $\sigma^M(E_o)$ from DCS_o (E_o, θ). These cross sections can also be obtained very accurately at low electron energies from swarm measurements. This is a fortunate situation since electron beam techniques become very difficult and uncertain at low electron energies. Therefore, the two methods complement each other in an ideal way and in the energy region of overlap cross checkings are possible.

Total Electron Scattering Cross Sections

Total electron scattering cross sections are measured by various transmission measurements. The attenuation of the electron beam through a gas beam (or static target) or the deflection of the molecular beam crossed by an electron beam (recoil measurements) as a function of electron energy is related to σ_{TOT} (E_o). In some variations, time-of-flight techniques are utilized to build up the full $\sigma_{TOT}(E_o)$ curve by observing the attenuation of electrons distributed over a wide energy.

At very low impact energies again swarm measurements yield reliable total scattering cross sections.

Resonances in Electron Scattering

Low-energy electron scattering processes are frequently dominated by resonances which may cause the cross sections to change drastically with impact energy. The velocity of the incoming electron at these energies is comparable to the velocities of the outer valence electrons of the atom or molecule, and it is appropriate to treat the incident electron as if it were temporarily attached, giving rise to a negative atomic or molecular ion. The negative ion state exists for a time longer than the orbital period, and it has identifiable properties. Although the concept of compound state formation has been widely utilized in nuclear physics, it was discovered in electron scattering only about 15 years ago, and became the subject of extensive studies only recently. (In a quantum mechanical picture, an interference between the direct and resonance scattering amplitudes is responsible for the drastic change of the cross section.)

Resonant electron capture by molecules and subsequent dissociation of the molecules into neutral or ionic species have been the subject of extensive studies in recent years. If the resonance state is repulsive, dissociation may take place in competition with electron detachment. If one atom (or fragment) has a positive electron affinity, a stable negative ion fragment is formed (dissociative attachment), otherwise the products are neutral fragments plus an electron.

Brief Summary of Cross Section Data

Recent reviews and summaries of available cross section data were published by Brandsen and McDowell (1978), Hayashi (1981), Trajmar *et al.* (1983), Mark and Dunn (1984), Christophorou (1984), Shimamura and Takayanagi (1984), Srivastava and Nguyen (1987), McConkey *et al.* (1988), Heddle and Gallagher (1989), Shimamura (1989), Itikawa *et al.* (1986), Itikawa and Ichimura (1989), Itikawa *et al.* (1989), Tawara *et al.* (1989), King *et al.* (1989). The situation can be briefly summarized as follows:

Atomic Species

For H and the rare gas atoms extensive sets of measured differential and integral cross sections are available for elastic scattering and for excitation of the lowest states. Accurate momentum transfer and total electron collision cross sections are also available from a few tenths of an eV to few thousand eV impact energies. Surveys on these subjects have been published by Brandsen and McDowell (1978), Hayashi (1981), Fabricant and Shpenic (1988), Heddle and Gallagher (1989), Shimamura (1989) and King *et al.* (1989). The very recent paper by Shimamura (1989) gives an up-to-date summary of total electron scattering, momentum transfer, integral elastic, total excitation and metastable production cross sections for H and the rare gas atoms.

Extensive measurements have now been reported for atomic oxygen by Shyn and Sharp (1986), Shyn *et al.* (1986), Germany *et al.* (1987), Doering and Gulcicek (1989a and b) and Williams and Allen (1989). The cross section data was reviewed by Itikawa and Ichimura (1989). Measurements on C, N and S have been initiated (Doering and Dagdigian, 1989; Doering, 1989).

Experimental data for the metal atoms are scarce. Most of the information is available in the form of optical excitation functions and this subject was recently reviewed by Heddle and Gallagher (1989). Electron collision measurements are mostly restricted to the alkali atoms.

Ionization cross sections are available for all atomic species to a satisfactory degree for modelling purposes and they are summarized by Mark and Dunn (1984), Bell *et al.* (1983) and Lennon *et al.* (1989a), and Freund *et al.* (1989).

A summary of available experimental cross section data is given in Table I.

Table I. Summary of Experimental Atomic Excitation Cross Section Data

Species	Elastic	Excitation	σ^M	σ_{TOT}	Opt.	σ_{ION}
H	h	h	h	h	h	h
He	h	h	h	h	h	h
Ne, Ar, Kr, Xe	h	m	h	h	m	h
O	m	m	–	–	l	h
C, N, S,	–	–	–	–	–	h
Li, Na, K	m	m	m	h	m	h

h, m and l refer to high, medium and low degree of data availability. Opt. designates optical excitation functions.

Molecular Species

The molecules of principal interest for planetary atmospheres are: H_2, CO, N_2, O_2, H_2O, CO_2, SO_2, CH_4, NH_3.

Elastic Scattering cross sections have been measured for all molecular species of interest to us over a wide range of impact energies. It should be noted, however, that the rotational excitation is not separated from elastic scattering in most of the works and elastic scattering cross sections then represent the sum for these two processes.

Rotational excitation can be resolved with presently available techniques only for H_2. Unfolding of experimentally unresolved rotational structures was carried out for N_2, CO, H_2O and CO_2. At very low impact energies, integral rotational excitation cross sections can be obtained from swarm measurements. For homonuclear diatomic molecules the direct excitation is due to the polarizability or electric quadrupole moment of the molecule and the $\Delta J = \pm 2(\pm 4..)$ selection rule applies. For molecules with permanent dipole the $\Delta J = \pm\ 1$ process dominates over many other processes. At low electron energies resonance processes can greatly increase the rotational excitation cross sections.

Vibrational excitation is effectively achieved by low-energy electronsespecially through resonance processes. Cross sections have been measured for all the diatomic molecules of interest to us but gaps in the energy range persist and the coverage for O_2 is rather limited. In the case of the polatomic molecules, only CO_2 is reasonably well covered and only very fragmentary or no information is available for other species.

Electronic state excitation cross sections for discrete states have been reported for the diatomic molecules but only for a few states and over limited energy ranges. In most

cases the low energy cross sections are scarce. N_2 has been the most extensively studied molecule. Some cross section data exists for SO_2 and CH_4 but practically nothing for H_2O and CO_2. Efforts are now in progress to extend the measurements to low energies but progress is slow because of the difficulties encountered in handling low-energy electrons, the break down of the Franck-Condon principle and the presence of resonance processes. Excitations to continuum states lead to a large variety of dissociation processes (neutral or charged fragments). When the dissociation products are charged or excited they can be conveniently detected and integral cross sections can be directly measured. Most of the experimental data falls in this category. For a review on optical measurements see McConkey (1983). A more recent review on this subject would be timely. Measurements on dissociation to neutral fragments are difficult. Winters (1966) and Winters *et al.* (1964) applied a technique based on measurement of pressure changes (N_2). Recently by Helm and Cosby (1987) devised a fast neutral beam technique which was applied to CO, N_2, O_2 and CO_2 by Cosby (1989).

Momentum transfer cross sections are available for all molecular species with good accuracy over a very wide energy range from combined swarm and beam data and various consistency checks. A comprehensive summary is given by Hayashi (1981).

Total electron scattering cross sections are also available with high accuracy over a wide energy range for all molecular species (see Hayashi, 1981). These are the most reliable cross sections and can serve for consistency checks on integral cross sections.

Total Ionization cross sections are available for all molecular species but the energy range is much more limited and the accuracy of the data is much lower than in the case of atoms. For summary of available data see Mark and Dunn (1984), Ehrhardt and Langer (1987) and Lennon *et al.* (1989b). The situation is complicated by the fact that a large number of ionization channels leading to various charged fragments, besides the parent molecule ionization, are available. Information on partial and multiply differential cross sections are fragmentary.

The status of molecular cross section data is summarized in Table II.

Table II. Summary of Experimental Molecular Excitation Cross Section Data

Species	Elastic	Excitation				σ^M	σ_{TOT}	Opt.	σ_{ION}
		Rot.	Vibr.	El. D.	El. C.				
H_2	h	m	h	m	m	h	h	m	h
CO	h	(m)	h	l	l	h	h	m	h
N_2	h	(m)	h	h	m	h	h	m	h
O_2	h	–	m	h	l	h	h	m	h
H_2O	h	(m)	m	–	l	h	h	m	m
CO_2	h	(m)	h	–	l	h	h	m	m

h, m and l have the same meanings as in Table I. El. D. and El. C. refer to electronic discrete and continuum state excitations, respectively. Opt. refers to optical excitation functions.

For SO_2, CH_4 and NH_3 the cross section information is very fragmentary.

Summary and Future Prospects

The large body of electron collision data which is required for reliable modelling of ionospheric behavior is not available at the present time and can not be expected to be available from laboratory measurements alone in the foreseeable future. This is partly due to experimental difficulties and partly to time and budgetary constraints.

The best approach to generate the necessary information is a joint experimental/theoretical attack. Laboratory measurements should supply benchmark data. Theory checked against experimental data should be able to extend the energy ranges covered by measurements and supply data in cases when measurements are very difficult or impossible with present techniques. This approach should work well for atomic species. For molecules, the situation becomes much more difficult as far as theoretical calculations are concerned and even in the case of simple molecules theoretical methods and approximation will have to be extensively checked against experiment before they can be trusted.

For completeness, it should be mentioned that the introduction of coincidence techniques and the application of lasers (both for preparation of target species and for analyzing collision products) opened up new areas of electron collision physics. Investigation of the fine details of the collision process is now possible, information about the complex scattering amplitudes and their coherences can be obtained, and the measurements can be extended to excited target species.

References

B. H. Brandsen and M. R. C. McDowell, "Electron Scattering by Atoms at Intermediate Energies", *Physics Reports* **46**, 249 (1978).

K. L. Bell, H. B. Gilbody, J. G. Hughes, A. E. Kingston and F. J. Smith, *J. Phys. Chem. Ref. Data* **12**, 891 (1983).

L. G. Christophorou, editor, **Electron-Molecule Interactions and Their Applications**, *Academic Press*, 1984 Volumes 1 and 2.

P. C. Cosby, "Electron Impact Dissociation of Molecules", XVI ICPEAC, New York, July 26-Aug.1, 1989, Book of Abstracts, p. 348.

J. P. Doering, "Electron Scattering Studies of Carbon, Nitrogen, Oxygen and Sulfur Atoms", XVIth Int. Conf. on the Physics of Electronic and Atomic Collisions, New York, July 26-Aug. 1, 1989. Book of Abstracts, p. 203.

J. P. Doering and E. E. Gulcicek, "Absolute Differential and Integral Electron Excitation Cross Sections for Atomic Oxygen VII. The (^{3}P → ^{1}D) and (^{3}P → ^{1}S) Transitions from 4.0 to 30 eV", *J. Geophys. Res.* **94**, 2733 (1989a).

J. P. Doering and E. E. Gulcicek, "Absolute Differential and Integral Electron Excitation Cross Sections for Atomic Oxygen VIII. The ^{3}P → ^{3}S Transition (1356Å) from 13.9 to 30 eV", *J. Geophys. Res.* **34**, 2733 (1989b).

J. P. Doering and P. J. Dagdigian, "Experimental Electron Scattering Spectrum of Atomic Carbon", *Chem. Phys. Lett.* **154** , 234 (1989).

G. Ehrhardt and W. Langer, Princeton Plasma Physics Laboratory Report No. PPL-2477 (1987).

I. I. Fabricant, O. B. Shpenic, A. V. Snegursky and A. N. Zavilopulo, "Electron Impact Formation of Metastable Atoms", *Physics Reports* **159**, 1 (1988).

R. S. Freund, R. C. Wetzel, R. J. Shul and T. R. Hayes, "Cross Section Measurements for Electron-Impact Ionization of Atoms," *Phys. Rev. A.* (to appear, 1989).

G. A. Germany, R. J. Anderson and G. J. Salarno, "Electron Impact Excitation of the 3p (^{5}P) State of Atomic Oxygen", *J. Chem. Phys.* **89**, (1988).

M. Hayashi "Recommended Values of Transport Cross Sections for Elastic Collision and Total Collision Cross Section for Electrons in Atomic and Molecular Gases", Report IPPJ-AM-19, Institute of Plasma Physics, Nagoya University, Japan, November, 1981.

D. W. O. Heddle and J. W. Gallagher, "Measurements of Electron Impact Optical Excitation Functions", *Rev. of Modern Phys.* **61**, 221 (1989).

H. Helm and P. C. Cosby, "Photodissociation Measurement of Rotational Energies and Populations of Molecules in Fast Beams", *J. Chem. Phys.* **86**, 6813 (1987).

Y. Itikawa, M. Hayashi, A. Ichimura, K. Onda, M. Nakamura, H. Nishimura, and T. Takayanayi, "Cross Sections for Collisions of Electrons and Photons with Nitrogen Molecules", *J. Phys. and Chem. Ref. Data* **15**, 985 (1986).

Y. Itikawa, A. Ichimura, K. Onda, K. Sakimoto, K. Takayanagi, Y. Hatano, M. Hayashi, H. Nishimura and S. Tsurubuchi, "Cross Sections for Collisions of Electrons and Photons with Oxygen Molecules" *J. Phys. and Chem. Ref. Data*, **18**, 23 (1989).

Y. Itikawa and A. Ichimura, "Cross Sections for Collisions of Electrons and Photons with Atomic Oxygen", The Institute of Space and Astronautical Science, Japan Report ISAS RN 406, March 1989.

G. King, S. Trajmar and J. W. McConkey, "Electron Impact on Atomic Hydrogen – Recent Results and New Directions", Comments on Atomic and Molecular Physics –, — (1989).

M. A. Lennon, K. L. Bell, H. B. Gilbody, J. G. Hughes, A. E. Kingston, M. J. Murray and F. J. Smith, "Recommended Data on the Electron Impact Ionization of Atoms and Ions: Fluorine to Nickel", *J. Phys. Chem. Ref. Data* **17**, 1285 (1989a).

M. A. Lennon *et al.* Culham Laboratory Report to appear (1989b).

T. D. Mark and G. H. Dunn, eds., **Electron Impact Ionization**, Springer-Verlag (1984).

J. W. McConkey, S. Trajmar and G. C. King, "Electron Impact Excitation of Molecular Hydrogen - What We Do and Do Not Know", Comments on *At. Mol. Phys.* **12**, 17 (1988).

J. W. McConkey, "Optical Excitation Cross Sections for Electron Collisions with Atoms and Molecules" in Proceedings of the Workshop on Electronic and Ionic Collision Cross Sections Needed in Modelling of Radiation Interaction with Matter, Argonne Nat. Lab., Dec. 6-8, 1983 ed. M. Inokuti, Argonne National Laboratory Report ANL-84-28, p.129.

J. C. Nickel, P. Zetner, G. Shen and S. Trajmar, "Principles and Procedures for Determining Absolute Differential Electron-Molecule (Atom) Scattering Cross Sections", *J. Phys. E.* **22**, 730 (1989).

I. Schimamura, "Cross Sections for Collisions of Electrons with Atom and Molecules", Scientific Papers of the Institute of Physical and Chemical Research (Japan) **82**, 1 (1989).

I. Shimamura and K. Takayanagi, **Electron-Molecule Collisions**, *Plenum Press*, 1984.

S. K. Srivastava and H. P. Nguyen, "Parametrization of Electron Impact Ionization Cross Sections for CO, CO_2, CH_4, NH_3 and SO_2", JPL Publication 87-2, April 1, 1987.

T. W. Shyn, S. Y. Cho and W. E. Sharp, "Differential Excitation Cross Sections of Atomic Oxygen Electron Impact: (^{3}P - ^{1}S Transition)", *J. Geophys. Res.* **91**, 1691 (1986).

T. W. Shyn and W. E. Sharp, "Differential Excitation Cross Section of Atomic Oxygen by Electron Impact: (^{3}P - ^{1}D Transition)", *J. Geophys. Res.* **91**, 1691 (1986).

H. Tawara, Y. Itikawa, H. Nishimura and M. Yoshino, "Cross Sections and Related Data for Electron Collisions with Hydrogen Molecules and Their Ions", *J. Phys. and Chem. Ref. Data*, –, — (1989).

S. Trajmar, D. F. Register and A. Chutjian, "Electron Scatterings by Molecules. II. Experimental Methods and Data", *Physics Reports* **97**, 219 (1983).

S. Trajmar and D. F. Register, "Experimental Techniques for Cross- Section Measurements", in **Electron Molecule Collisions**, eds. I. Shimamura and K. Takayanagi, Plenum Press, 1984, pp. 427-493.

J. F. Williams and L. J. Allen "Low Energy Elastic Scattering of Electrons from Atomic Oxygen", XVIth ICPEAC, New York, July 26-Aug. 1, 1989, Book of Abstracts, p. 127.

H. F. Winters, D. E. Horne and E. E. Donaldson, "Adsorption of Gases Activated by Electron Impact", *J. Chem. Phys.* **41**, 2766 (1964).

H. F. Winters, "Ionic Adsorption and Dissociation Cross Section for Nitrogen",*J. Chem. Phys.* **44**, 1472 (1966).

N90-26780

OPTICAL SIGNATURES OF MOLECULAR PARTICLES VIA MASS-SELECTED CLUSTER SPECTROSCOPY

MICHAEL A. DUNCAN
University of Georgia, Dept. of Chemistry, Athens, GA 30602

ABSTRACT

A new molecular beam apparatus has been developed to study optical absorption in cold (< 100K) atomic clusters and complexes produced by their condensation with simple molecular gases. In this instrument, ionized clusters produced in a laser vaporization nozzle source are mass selected and studied with photodissociation spectroscopy at visible and ultraviolet wavelengths. This new approach can be applied to synthesize and characterize numerous particulates and weakly bound complexes expected in planetary atmospheres and in comets.

INTRODUCTION

The extreme conditions present in the atmospheres of the inner and outer planets produce an abundance of unusual chemical species, including small molecular radicals and ions, in the presence of more common molecules formed from the lighter elements. At the characteristic low temperatures (< 100K), condensation phenomena produce small elemental molecules (atomic clusters) as well as neutral or ion-molecule complexes. Condensation produces a distribution of particles ranging in size from molecules to dust grains. In a dynamic interaction with condensation there are photon-induced ionization and dissociation processes. The details of these chemical and physical processes are critical to an understanding of the formation and ongoing evolution of the solar system.

Optical spectroscopy is a time honored method to study planetary atmospheres, which can be accomplished from earth-based observatories or from more direct probes such as the Voyagers or Galileo. However, laboratory measurements are essential to aid in the assignment and interpretation of atmospheric spectra. Unless these laboratory measurements reproduce the extreme temperature and pressure conditions in planetary atmospheres, it is impossible to generate the desired molecules in the appropriate quantum levels to replicate observed spectra. Until recently, the required conditons could not be generated in the laboratory. However, new molecular beam experiments, particularly those in the interdisciplinary area of "cluster science," have made it possible to produce a variety of atomic and molecular aggregates at ultracold temperatures. When combined with new laser spectroscopy methods, the optical absorption and photodissociation processes of these complexes can be characterized. We describe here the applications and potential of this new cluster beam technology for the study of molecular aggregates important in planetary atmospheres. For ionized particles, these experiments provide size selected optical spectra.

EXPERIMENTAL

The molecular beam apparatus for these experiments has been described in the literature.[1,2] It employs laser vaporization of solid samples in a pulsed supersonic expansion to produce a variety of atomic and/or molecular clusters at temperatures of 50-100K. This source produces neutral and/or ionic atomic clusters of virtually any metal, semiconductor, or non-metal material (M_X, where X = 2-50). A modified version of the source produces metal/molecular mixed complexes of the form $M R_y$ where M is a metal or semiconductor atom and R is a rare gas atom or small molecule (e.g. $Al^+(CO_2)_7$). In principle, it is now possible to synthesize virtually any atomic or molecular aggregate in this source. These conditions are the closest laboratory approximation to those in outer planetary atmospheres.

Clusters or complexes produced in this source may condense directly as ions or they may be ionized downstream with ultraviolet lasers. For mass selected spectroscopy we use ions produced in the source which have been supersonically expanded and are therefore internally cold. Mass selection occurs in a reflectron time-of-flight spectrometer system developed in our laboratory[2] and shown in Figure 1. Cold ions are extracted from the molecular beam by pulsed acceleration voltages. They are mass selected by their time-of-flight through an initial drift tube section. Undesired ions are rejected, and the selected size transmitted, with pulsed deflection plates located just before a reflection grid assembly. The reflection assembly decelerates the selected ions with an electric field. At the turning point in the ion trajectory a tunable laser irradiates the ions. Photodissociation may occur if the incident light is resonantly absorbed and if the one-or multiphoton energy exceeds the threshold for dissociation. When dissociation occurs, parent and fragment ions are mass analyzed in a second drift tube section. This process identifies photodissociation products, while the depletion in the parent ion channel provides a measure of the photodissociation cross section. Dissociation spectra are recorded by monitoring the appearance of a selected parent ion as a function of the dissociation laser energy.

Figure 2 shows an example of a new photodissociation spectrum for the diatomic cation Te_2^+ obtained with this instrument.[3] The features shown are assigned to the vibrationally resolved $A^2\Pi \leftarrow X^2\Pi_{g,\frac{1}{2}}$ electronic transition, observed near 670 nm. Analysis of this spectrum yields the ground and excited state vibrational frequencies (279 and 199 cm^{-1}) and the excited state anharmonicity (0.5 cm^{-1}) and dissociation energy (D_e = 2.27 eV). The cross section for photodissociation is approximately 1×10^{-18} cm^2. In principle, rotationally resolved spectra could be obtained with this method using narrower bandwidth lasers and lighter molecules. In addition to Te_2^+, we have recently observed similar spectra, which are not yet completely assigned, for Bi_2^+, Al_2^+ and S_2^+. Other experiments in our laboratory have used fixed energy lasers to probe product channels and dissociation cross sections for atomic clusters of carbon, sulfur, silicon, aluminum and silver, and for metal/molecular complexes of aluminum/benzene and aluminum/acetone.

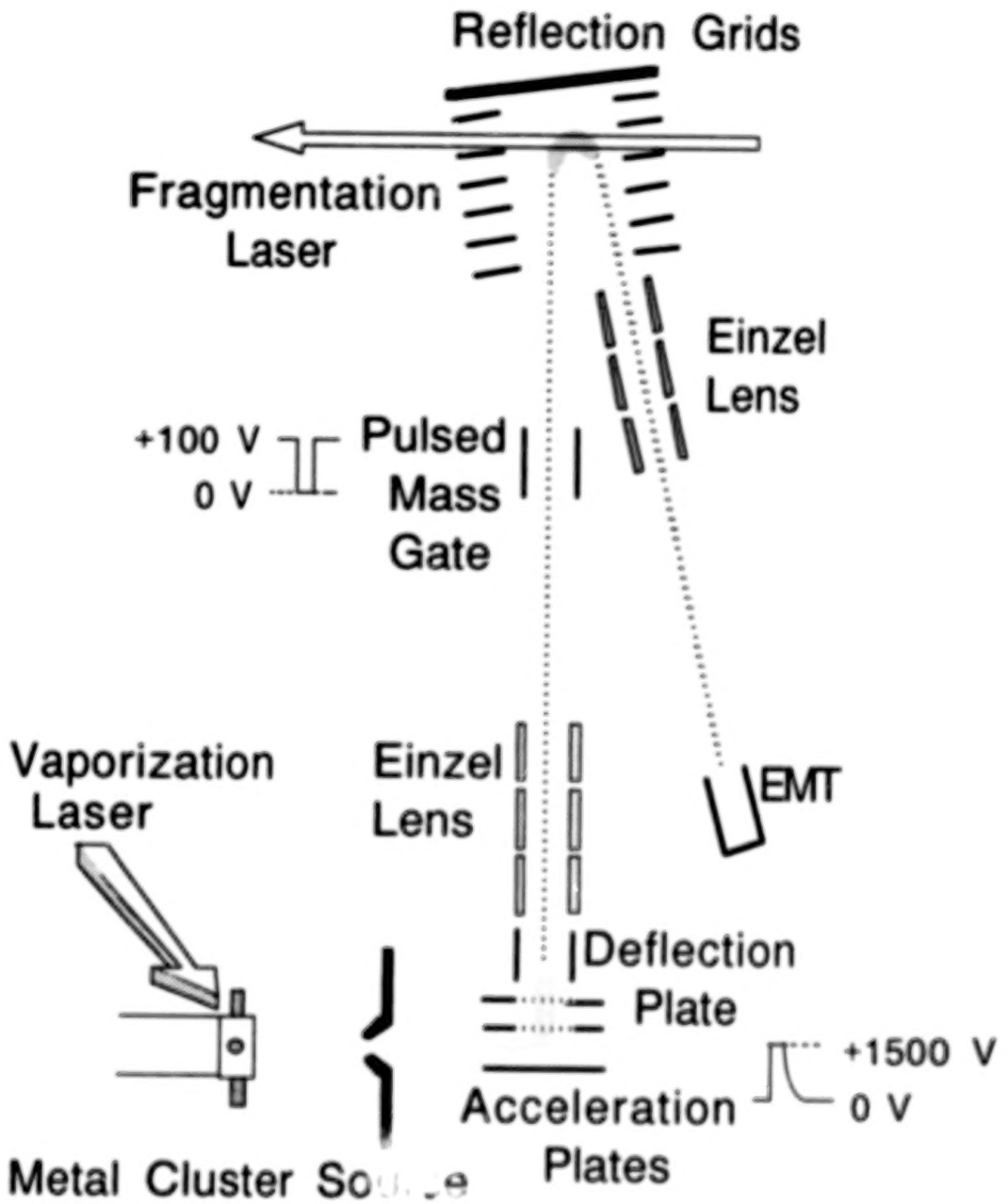

Figure 1. The reflectron mass spectrometer system used for mass selection of cluster particles followed by photodissociation spectroscopy.

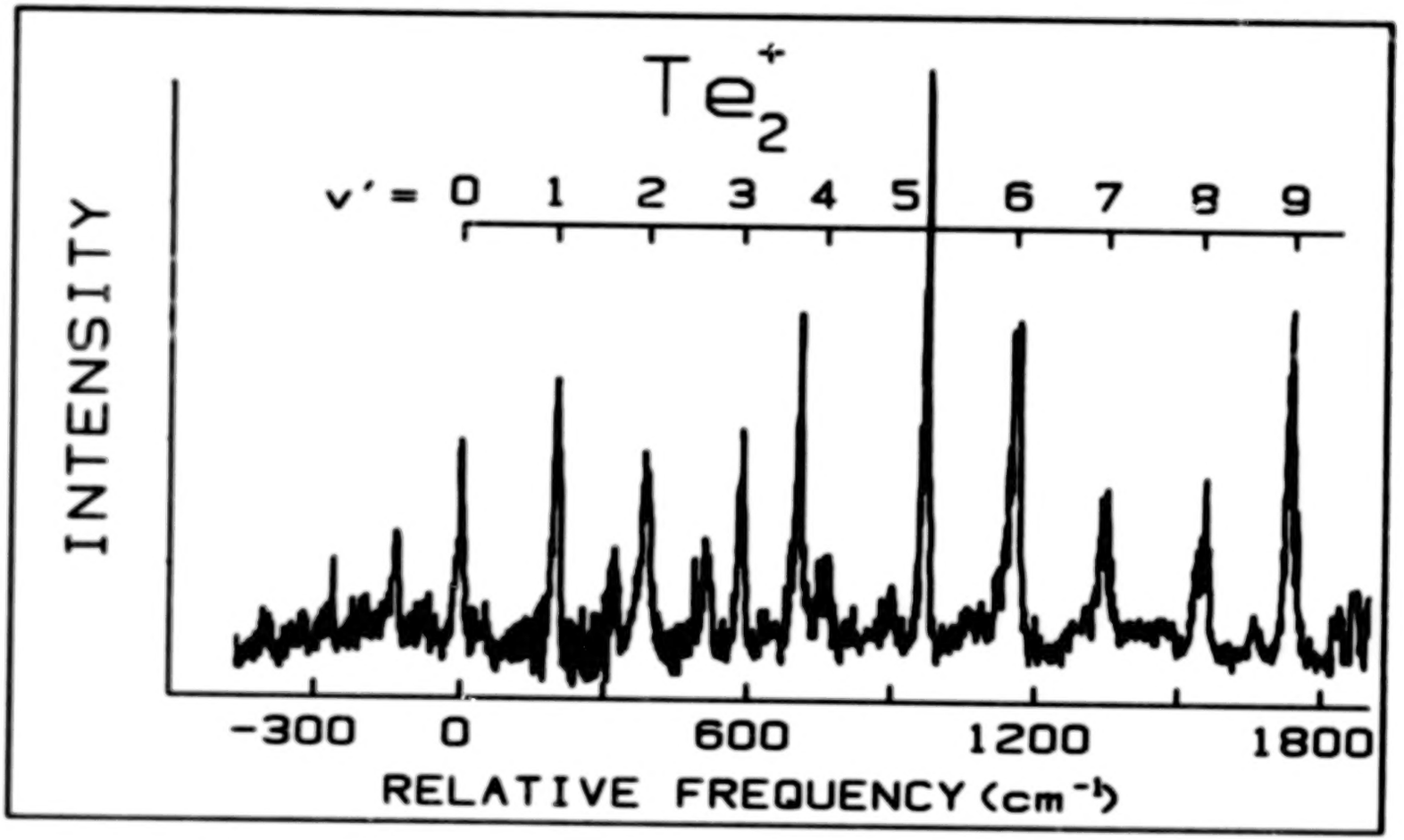

Figure 2. The photodissociation spectrum of Te_2^+ near 670 nm.

FUTURE EXPERIMENTS ON PLANETARY ATMOSPHERIC SPECIES

Ongoing and future experiments in our laboratory will focus on the optical photodissociation spectra of carbon and sulfur atomic cluster cations. There are existing fixed frequency data for carbon cluster cations, but no spectra.[4] Except for our own recent data, there are no photodissociation data for sulphur. Carbon clusters are expected to be important in the formation of dust particles and ice grains in environments such as cometary comas. Elemental molecules of sulfur are expected in the atmosphere of Venus. Similar experiments will focus on ion-molecule complexes of silicon or aluminum with light molecules (e.g. $Al^+C_2H_2$), with which are also likely constituents of cometary comas.

REFERENCES

1. K. LaiHing, R. G. Wheeler, W. L. Wilson and M. A. Duncan, J. Chem. Phys. 87, 3401 (1987).

2. K. LaiHing, P. Y. Cheng, T. G. Taylor, K. F. Willey, M. Peschke and M. A. Duncan, Anal. Chem. 61, 1458 (1989).

3. P. Y. Cheng, K. F. Willey, J. E. Salcido and M. A. Duncan, Int'l. J. Mass Spectrom. Ion Processes, in press.

4. M. E. Geusic, M. F. Jarrold, T. J. McIlrath, R. R. Freeman and W. L. Brown, J. Chem. Phys. 87, 3862 (1987).

N90-26781

STUDY OF POLYOXYMETHYLENE AND ITS SPUTTERED FRAGMENTS-- IMPLICATIONS FOR COMETS

Marla H. Moore* and Toshihiko Tanabe**

*University of Maryland, Dept. of Chem., College Park, MD 20742
**NRC-NASA/GSFC, Code 691, Greenbelt, MD 20771

ABSTRACT

Laboratory mass spectra of sputtered polyoxymethylene, POM, reveals a fragmentation pattern consistent with observed peaks in the PICCA experiment on board the Giotto spacecraft. Both commercially available POM and radiation synthesized POM have been used in our studies. Synthesized POM was identified using infrared absorption spectra after proton irradiation of H_2CO ice on silicate grains at 20K. Laboratory results suggest that similar type sputtering is a possible mechanism for removing species from comet grains.

INTRODUCTION

A complex line of evidence for a form of formaldehyde (H_2CO) in comet Halley came from the interpretation of data from the PICCA instrument on board Giotto. In the inner coma a repeating mass spectral pattern with peak centers at the approximate locations of 45, 61, 75, 91, 105, and 121 amu was detected. Mitchell et al.[1], Huebner and Boice[2], and Huebner[3] suggested the mass spectrum could be fit with the fragmentation pattern of the polymerized form of H_2CO known generically as polyoxymethylene, POM.

The idea that POM could be present in cometary materials is not new. Wickramasinghe[4,5] proposed that H_2CO condenses on interstellar silicate grains as polyoxymethylene and the possibility of this polymer in cometary dust was discussed by Vanysek and Wickramasinghe[6]. Laboratory experiments by Goldanskii et al.[7] showed that irradiation of condensed H_2CO synthesized polyoxymethylene to temperatures below 20K and Goldanskii[8] discussed the possibility of similar radiation synthesis in ices in molecular clouds. In our laboratory experiment radiation synthesized POM was identified by its infrared absorption features.

EXPERIMENTAL RESULTS

We have sputtered POM in vacuum at 300K using 700KeV protons and recorded the mass spectrum. Fragments are observed at 45, 61, 75, 91, 105 121 and 135 amu and these results are compared with the PICCA data in Figure 1. As shown in Table I, these peaks can be assigned to the fragmentation products of POM with an alternating CH_3 or H end group. The 700KeV proton beam current was near

TABLE I: TENTATIVE ASSIGNMENT OF POM FRAGMENTATION PEAKS

m/e	ION$^+$	m/e	ION$^+$
45	$(H_2CO)CH_3$		
61	$(H_2CO)_2H$	60	$(H_2CO)_2$
75	$(H_2CO)_2CH_3$		
91	$(H_2CO)_3H$	89	$(H_2CO)_2HCO$
105	$(H_2CO)_3CH_3$		
121	$(H_2CO)_4H$	119	$(H_2CO)_3HCO$
135	$(H_2CO)_4CH_3$	131&133	unidentified

1.5×10^{-7}amps (corresponding to 2×10^{11} protons/cm^2-sec). In the region of mass 30 the quadrupole mass spectrometer was saturated and the resulting overlaid data in Figure 1 spanned more than 3 log pressure scales in intensity. All data points had the background subtracted automatically and were recorded using the electron multiplier. A 70 eV electron ionizer voltage was used for these experiments.

Sputtering of thin films of commercially available paraformaldehyde (a polyoxymethylene glycol) gave the same results as sputtered POM synthesized in our laboratory. Other peaks recorded in our sputtered spectrum are listed in Table I and two can be attributed to fragments of POM with an attached HCO group.

In contrast, using direct insertion techniques the mass spectrum of solid polyoxymethylene glycol was analyzed by Moller

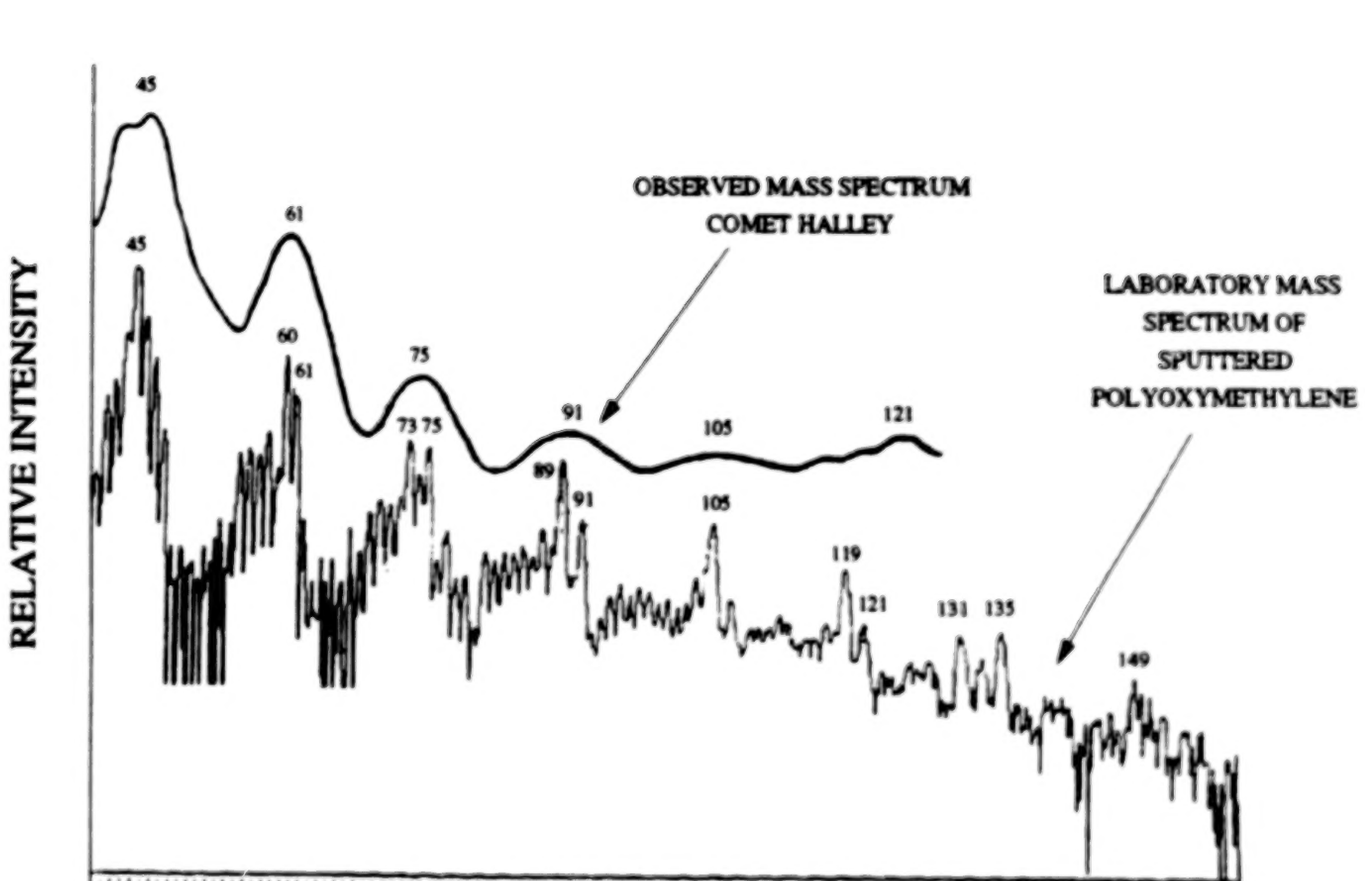

FIGURE 1. The upper curve reproduces the mass spectrum measured by the PICCA instrument on board the GIOTTO spacecraft in the inner coma of comet Halley. This is compared with our laboratory mass spectrum of fragments produced during sputtering polyoxymethylene at 300 K with 700 KeV protons.

and Jackson[9]. At 300K peaks were observed at 47, 61, 77, 91, 107, 121 amu, consistent with a fragmenting polymer with alternating H and OH groups attached. The peaks do not fit the central peak assignments of the PICCA spectrum but could contribute to its width.

Figure 2A shows the infrared spectrum from 2.5um to 25um of an amorphous silicate smoke. It's dominate SiO stretch feature is near 10um, the SiO bend is near 21um. H_2CO gas was condensed onto this smoke at 20K and the resulting ice-silicate was irradiated with 700KeV protons to a total incident dose of 1.5×10^{15} protons/cm^2. Polymerization of formaldehyde occurred at 20K and the POM remained on the silicate when warmed to 300K. The infrared spectrum of the POM-silicate is shown in Figure 2B. The ratio spectrum (POM-silicate/silicate) in Figure 2C reveals the major absorptions of POM on silicate at 8.99um and 10.7um. This sample was subsequently sputtered.

CONCLUSION

Our laboratory results suggest that sputtering of POM is a possible origin of the peaks measured in the PICCA data. Sputtering experiments in which solar wind type ions are used need to be studied since 700KeV protons are not dominate in the inner coma. Each PICCA peak appears to be composed of 3 or more closely spaced masses[1]. Sputtering of POM may contribute to the peak, but other processes such as sublimation may contribute to the width. Also we suggest that other complex non-volatile organic residues may exist on comets and fragments from these may be sputtered from grains in the coma contributing to the observed data. The study of sputtered fragments from other organic residues is currently under investigation.

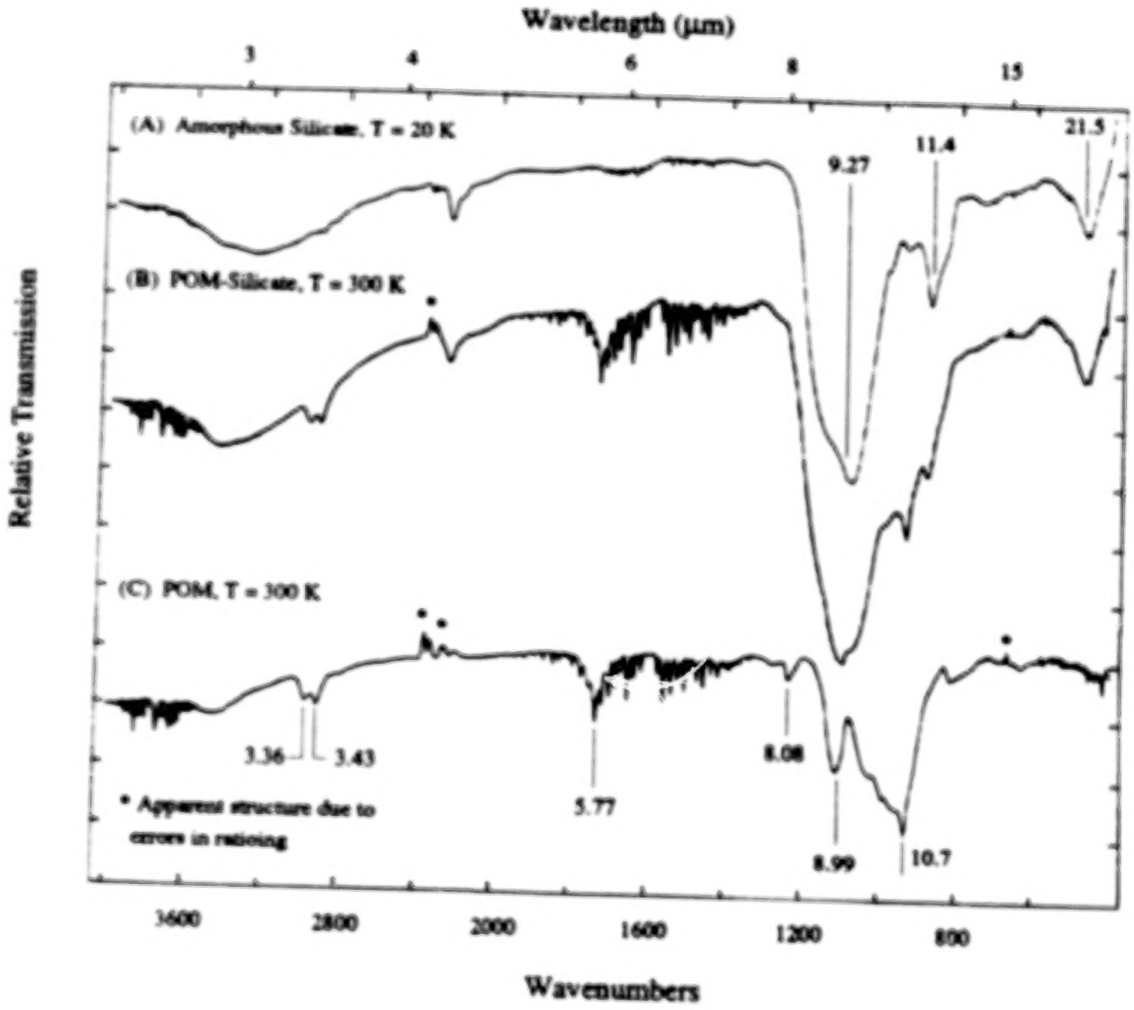

FIGURE 2. (A) Infrared spectrum of amorphous silicate smoke at 20 K. The SiO stretch band is near 10 μm. (B) Formaldehyde ice formed on the silicate smoke was irradiated causing polymerization at 20 K. The resulting POM-silicate spectrum at 300 K is shown. (C) Ratio spectrum, POM-silicate/silicate. Spectral features of POM are revealed allowing identification.

ORIGINAL PAGE IS
OF POOR QUALITY

REFERENCES

[1]D.L.Mitchell, R.P.Lin, K.A.Anderson, D.W.Carlson, D.W.Curtis, A. Korth, H. Reme, J.A.Sauvaud, C. D'Uston, D.A.Mendis, Science **237**, 626 (1987).

[2]W.F.Huebner and D.C.Boice, Ap. J. **320**, L149 (1987).

[3]W.F.Huebner, Science **237**, 628 (1987).

[4]N.C.Wickramasinghe, Nature **252**, 462 (1974).

[5]N.C.Wickramasinghe, M.N.R.A.S. **170**, 11 (1975).

[6]V. Vanysek and N.C. Wickramasinghe, Astrophys. and Sp. Sc. **33**, L19 (1975).

[7]V.I.Goldanskii, M.D.Frank-Kamenetskii, and I.M. Barkalov, Science **182**, 1344 (1973).

[8]V.I.Goldanskii, Nature **279**, 109 (1979).

[9]G. Moller and W.M. Jackson, to be published.

N90-26782

PROTON IRRADIATION OF SIMPLE GAS MIXTURES: INFLUENCE OF IRRADIATION PARAMETERS

NORBERT J. SACK*, R. SCHUSTER, AND A. HOFMANN
Physikalisches Institut der Universität Erlangen, Erwin-Rommel-Strasse 1, D-8520 Erlangen, W-Germany

ABSTRACT

In order to get information about the influence of irradiation parameters on radiolysis processes of astrophysical interest, methane gas targets were irradiated with 6.5 MeV protons at a pressure of 1 bar and room temperature. Yields of higher hydrocarbons like ethane or propane were found by analysis of irradiated gas samples using gas chromatography. The handling of the proton beam was of great experimental importance for determining the irradiation parameters. In a series of experiments current density of the proton beam and total absorbed energy were shown to have a large influence on the yields of produced hydrocarbons. Mechanistic interpretations of the results are given and conclusions are drawn with regard to the chemistry and the simulation of various astrophysical systems.

To improve the understanding of the chemical evolution of planetary atmospheres, many laboratory simulation experiments have been performed which investigate the influence of UV and ionizing radiation on primitive gas mixtures (for references see[1]). However, the physical conditions in the laboratory simulations differ dramatically from those in the simulated systems: e.g., the total irradiation time is many orders of magnitude lower and the flux of ionizing radiation higher. Hence the aim of our investigations was to evaluate the relevance of this latter irradiation parameter and to explain how it influences the chemical reaction newtwork.

We irradiated stationary methane targets at room temperature and atmospheric pressure with 6.5 MeV protons provided by a Tandem - Van de Graaff accelerator. After irradiation the gas targets were analyzed through gas chromatography for higher hydrocarbons like ethane or propane. In order to define exactly the current density of the proton beam (which is proportional to the particle flux), emphasis was given to the handling of the beam: many steering and focusing elements as well as apertures were applied. Measurements

of the current density distribution over the proton beam have shown that the beam current was constant over the define cross section. Experimental details are given in ref. (2).

Current density (power density) was varied between 0.026 $\mu A/cm^2$ (1.5 mW/cm^3) and 28.7 $\mu A/cm^2$ (1640 mW/cm^3); to create the same total absorbed doses the irradiated time was varied between 1.1 sec and 121 min. Strong dependencies of the yield of produced hydrocarbons on the current density have been found and these dependencies differ for different products[2].

To explain these results in terms of a chemical mechanism, one has to consider the principal reaction pathway that leads to the formation of the detected substances. The primary processes are ionizations and excitations of the methane molecules by the high energy protons; this leads to the production of various ions, radicals, and electrons, which itself may cause secondary ionizations. These ions will undergo either ion-molecule reactions or neutralizations. The final products are most likely produced in neutral reactions.

The ion-molecule and neutral reactions can also be classified in another way: some are reactions of reactive species (ions, radicals) with target molecules (methane) like

$$H + CH_4 \rightarrow H_2 + CH_3 \ , \qquad (1)$$

some are reactions between two different reactive species, e.g.,

$$H + C_2H_5 + M \rightarrow C_2H_6 + M \ . \qquad (2)$$

The latter reactions are certainly strongly dependent on the concentration of reactive species and in concurrence to reactions of type (1). Hence it can be stated that the concentration of reactive species (ions, radicals) has considerable influence on the reactions that occur. This density of reactive species is determined by the power density, which was a varied parameter in our experiments. Because the reaction network is complex it is not surprising that different substances show different dependencies of their yields on the varied parameter.

The fluxes of ionizing radiation in the astrophysical systems to which our results shall be applied, are generally very low: e.g., the flux of MeV protons in the atmosphere of Titan is of the order of 10^6 $cm^{-2}sec^{-1}$; the fluxes in our experiments are $(1.6 \cdot 10^{11})$ $cm^{-2}sec^{-1}$ to $(1.8 \cdot 10^{14})$ $cm^{-2}sec^{-1}$. Hence our experimental conditions could perhaps better be applied to auroras or lightening, where very high particle fluxes can occur.

One consequence can be drawn from our experiments which is relevant to the simulation of planetary atmospheres: In most laboratory experiments the particle fluxes of ionizing radiation are by orders of magnitude higher than in the planetary atmosphere. Thereby it seems possible to simulate, for example, 1000 years of the evolution of the planetary atmosphere within some hours in the laboratory, as a similar total energy is deposited. But as our investigations have shown, there are enormous differences in the yields of products already in the small interval of particle flux examined in our experiments. Hence the application of such simulations in a quantitative way to the understanding of the planetary atmospheres is very difficult.

References

[1]N.J. Sack, submitted to Earth, Moon and Planets (1989)

[2]N.J. Sack, R. Schuster, and A. Hofmann, submitted to the Astrophys. J. (1989)

[3]T. Scattergood, P. Lesser, and T. Owen, Nature 274, 100 (1975)

*Present Address:

Department of Nuclear Engineering and Engineering Physics
University of Virginia
Charlottesville, VA 22903-2442

N90-26783

PHOTON SPUTTERING OF H_2O ICES: A PRELIMINARY REPORT

C.Y.ROBERT WU AND D.L. JUDGE
Space Sciences Center and Department of Physics
University of Southern California
Los Angeles, California 90089-1341

ABSTRACT

A preliminary measurement of the total yields of ejected ions and electrons from H_2O ices has been carried out using the He I 584Å resonance line as the incident photon beam. The H_2O ices were prepared at 77K in an ultrahigh vacuum system. The total yield of the ejected ion species and electrons was determined to be 8.8×10^{-5} and 4.2×10^{-4}, respectively.

INTRODUCTION

Sputtering of atoms and molecules from surfaces of cosmic materials is an important process for mass transfer and evolution in a number of astronomical environments, e.g., comets, asteroids, planetary satellites and rings. The excitation sources for sputtering are primarily solar photons, the solar wind, and magnetospheric particles. Experiments on sputtering by energetic ions have been carried out in several laboratories[1-6] and the results have been applied to astrophysical problems.[7] However, this is not the case for solar photon sputtering. In fact, there exists very limited data in the VUV-EUV region.[8] Current theories and model calculations assume that the solar photon energies are directly converted into heat which controls the vaporization of the cosmic material.[9,10] Mass loss due to photon sputtering has not been included since the required data are not available.

We have initiated an experimental program to study solar photon sputtering of molecular ices, such as H_2O ice, NH_3 ice, SO_2 ice, CO_2 ice, etc., from the VUV through the EUV region. The temperature for the ices will be chosen to simulate realistic planetary conditions. We plan to measure the total photon sputtering yield which includes yields for producing ions and neutrals from molecular ices. However, in the initial study we have only measured the total yield of ejected ions and electrons from water ices at the He I 584Å line.

EXPERIMENTAL SETUP AND EXPERIMENTAL PROCEDURES

A schematic diagram of the experimental setup is depicted in Fig.1. Detailed diagrams of the photon flux monitor and the photon-water ice interaction region are shown in Fig.2. The vacuum system consists of an isolation chamber which is pumped by an 80*l*/s turbomolecular pump and an interaction chamber which is pumped by a 25*l*/s VacIon pump. The base pressure of the vacuum system is 2×10^{-8}Torr. A liquid nitrogen dewar system provides a cold finger at 77K which is used for the preparation of water ices. The light source used in this preliminary study was a DC glow discharge which was operated at the optimal conditions for the He I 584Å line.

The photon flux monitor is made of a nickel mesh with 90% optical transmission. The calibrated nickel mesh signal corresponds to 11.7 (±0.4)% of the total photon flux. The photon flux can be constantly monitored in this way since the mesh was permanently installed in the path of the incident photon beam. The ion detector in the interaction region consists of an ion collector wire maintained at a negative potential with respect to the cylindrical cell which surrounds it. The detector has a unity collection efficiency when an appropriate voltage has been applied and has previously been used in our laboratory.[11] This ion detector can be used to detect electrons by simply reversing the voltage polarity of the cylinder and the collector wire. The ion collector was mounted on a bakable linear motion feedthrough. When the water ices were being prepared, the ion detector was retracted to avoid water condensation on the detector surfaces.

The high purity water was provided by Stohler Isotope Chemicals Company. The deposition rate of water vapor onto a quartz substrate was kept constant by immersing the water sample reservoir in an isopropanol-dry ice bath. A thick (several μm) water ice sample was used in the present study.

RESULTS AND DISCUSSION

The electron current from the nickel mesh due to 584Å photons is shown in Fig.3a as a function of collector bias voltage. In the present work a bias voltage of 80 volts in the plateau region was selected for the incident flux measurements, giving an absolute value of 7.89×10^{10} photons/sec.

The ion and electron currents produced by 584Å photon sputtering of water ice at 77K are shown in Fig.3b. Similar to the case of nickel mesh, the measured

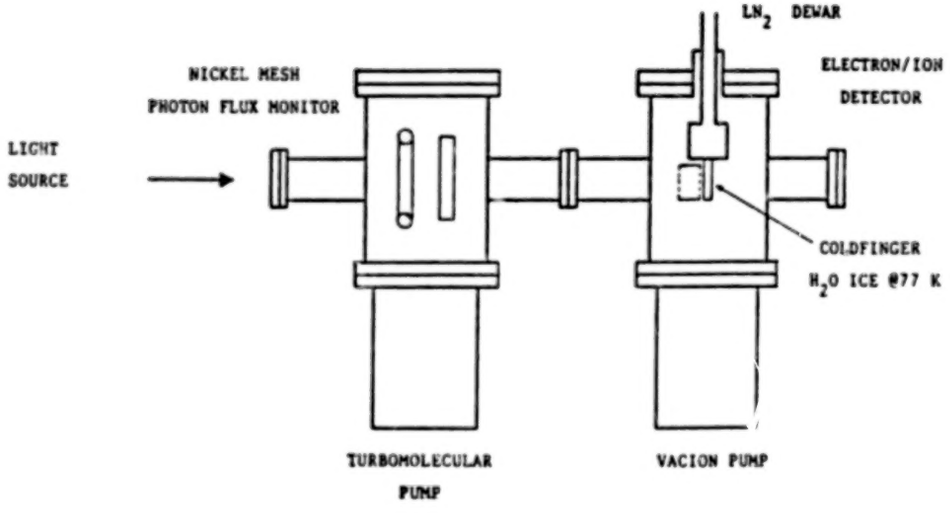

Fig. 1. Schematic diagram of the experimental setup.

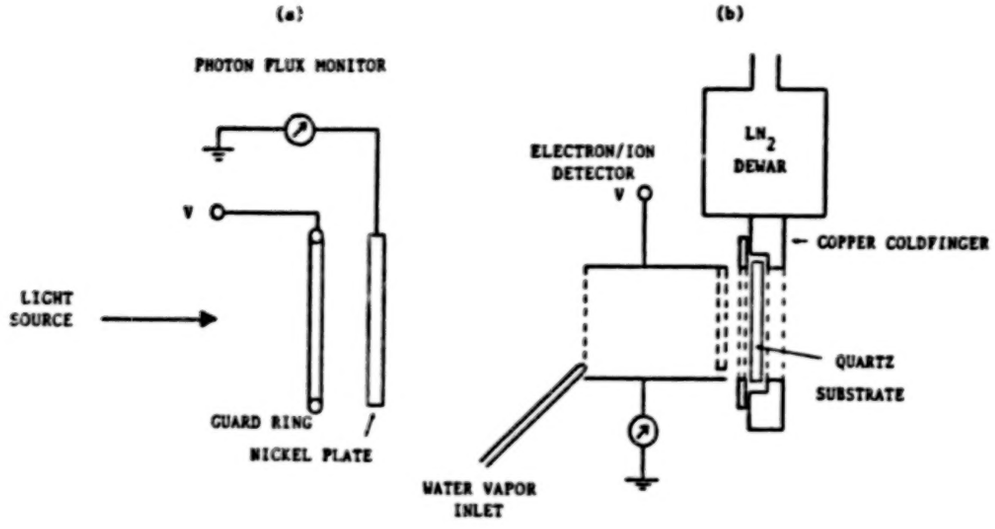

Fig.2. Detailed diagrams for (a) the photon flux monitor and (b) the photon-water ice interaction region.

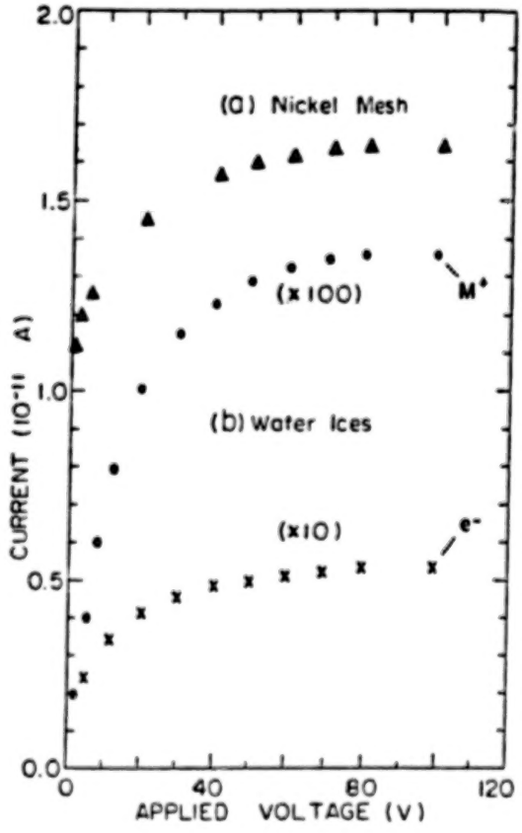

Fig.3. The ion/electron current as a function of the applied repeller voltage.

ion and electron currents approach a plateau at an applied voltage of ~ 70V. The measured quantities at V=80 volts were used to determine the total yields of ejected ions and electrons. As can be seen from Fig.3b, the ion and electron currents are 1.2×10^{-13} and 6.46×10^{-13} ampere, respectively. Knowing the absolute incident photon flux, the total yields of ejected ions and electrons from photon sputtering of H_2O ice at 77K, at a photon wavelength of 584Å, are found to be $8.8(\pm1.1)\times10^{-5}$ and $4.2(\pm0.2)\times10^{-4}$, respectively. The yield of ejected electrons is about a factor of five larger than that of ejected ions. Thus, upon absorbing a 584Å photon the water ice is preferentially left with an excess "ion" after ejection of an electron. The excited ro-vibronic energy of those "ions" may, however, convert into nuclear motion such that the surface binding energy can be overcome resulting in the ejection of ions. In the present case, this probability only amounts to 20%.

The absorption cross section[12] of H_2O vapor at 584Å is $2.18\times10^{-17}cm^2$. If we assume the absorption cross section of water ices is the same as that of water vapor, then the ion sputtering cross section of water ices will be $1.9\times10^{-21}cm^2$ at 584Å.

CONCLUDING REMARKS

In this preliminary report we have demonstrated the feasibility of measuring the total yield of ejected ions and electrons from photon sputtering of water ice at the He I 584Å line. Similar measurements using the NeI 736/743Å lines and others are currently in progress in our laboratory. However, the most difficult measurement will be the total yield of ejected neutral species which can be many orders of magnitude higher[4] than that of the ejected ion species reported here. We have plans to carry out such measurements from water ices and other molecular ices at temperatures to be chosen to simulate realistic planetary conditions.

Acknowledgment - This work was supported by a University of Southern California internal grant.

REFERENCES

1. W.L. Brown, L.J. Lanzerotti, J.M. Poate, and W.M. Augustyniak, Phys. Rev. Lett. 40, 1027 (1978).

2. D.B. Chrisey, J.W. Boring, J.A. Phipps, R.E. Johnson, and W.L. Brown, Nucl. Instr. and Meth. B13, 360 (1986).

3. D.J. Lepoire, B.H. Cooper, C.L. Melcher, and T.A. Tombrello, Rad. Effects 71, 245 (1983).

4. J. Schou, Nucl. Instr. and Meth. B27, 188 (1987).

5. F. Besenbacher, J. Bottiger, O. Graversen, J.L. Hansen, and H. Sorensen, Nucl. Instr. and Meth. 191, 221 (1981).

6. A. Bar-nun, G. Herman, M.L. Rappaport, and Yu. Mekler, Surf. Sci. 150, 143 (1985).

7. J. Klinger, D. Benest, A. Dollfus, and R. Smoluchowski, eds., Ices in the Solar System (Reidel Publishing Co., Boston, 1985).

8. P.K. Haff, A. Eviatar, and G.L. Siscoe, ICARUS 56, 426 (1983).

9. D.A. Mendis, H.L.F. Houpis, and M.L. Marconi, Fund. Cosmic Phys. 10, 1 (1985).

10. L.L. Wilkening, ed., Comets (The University of Arizona Press, Tucson, AZ, (1982).

11. R.W. Carlson, H.S. Ogawa, E. Phillips, and D.L. Judge, Appl. Opt. 23, 2327 (1984).

12. C.Y.R. Wu, and D.L. Judge, J. Chem. Phys. 89, 6275 (1988).

PLENARY REVIEWS

SPECTROSCOPY - A PLENARY REVIEW

KENNETH FOX
The University of Tennessee, Department of Physics and Astronomy,
Knoxville, TN 37996-1200

ABSTRACT

This plenary review of laboratory research on spectroscopy relating to planetary atmospheres will concentrate on the following aspects: science as presented in invited and contributed papers, the importance of this science for planetary atmospheres, and its status with regard to state-of-the-art techniques.

INTRODUCTION

The spectroscopic research reviewed here displays both distinctiveness and connectedness. The spectral wavelengths cover a broad range. The scientific problems of physics and chemistry addressed include states and conditions of microscopic and macroscopic matter, as well as collisions and transformations among them. There are significant interfaces between spectroscopy on the one hand and chemical kinetics, thermodynamics, and charged-particle interactions on the other hand.

REVIEW

Steffes presented an invited review on laboratory measurements of microwave and millimeter-wave properties of constituents in planetary atmospheres. He noted that accurate data is critical for the proper interpretation of radio observations of occultations and continuum or spectral line emissions. He emphasized that experiments under extreme conditions of temperature and pressure characteristic of planetary atmospheres are required. Steffes reviewed instrumentation and techniques for measuring refractivity and absorptivity of atmospheric gases and condensates under planetary conditions simulated in the laboratory. He described an approach to measuring the microwave absorptivity of gaseous sulfuric acid in a

PRECEDING PAGE BLANK NOT FILMED

carbon dioxide atmosphere for studies of Venus. At millimeter wavelengths, the atmospheric system of interest was a mixture of ammonia, hydrogen, and helium relevant to studies of the atmospheres of the outer planets.

Steffes also alluded to several methods for the measurement of absorptivity and refractivity of solids and liquids, equivalent to the measurement of their complex dielectric constants. He noted that the Galileo mission carried a probe with a microwave transmitter to penetrate deep into the atmosphere of Jupiter, creating an opportunity to measure microwave absorption in dense clouds. In order to identify surface constituents on Titan on the basis of their radar reflectivity, it would be necessary to have measurements of their complex dielectric constants in the laboratory.

Steffes described three techniques for the determination of complex dielectric constants. In the first, measurements of refractivity and absorptivity result from changes in bandwidths and spectral frequencies of resonances when resonators are filled with liquids or solids. In the second, where resonances are totally attenuated, materials are placed in an open-circuited coaxial line and a microwave network analyzer measures the complex impedance. In the third, a monopole antenna is placed in a tank containing the material, and its complex dielectric constant is inferred from the change in complex impedance of the antenna from air to immersion in the material.

An alternative approach would be to place a container of liquid material or a slab of solid material on the surface of the flat mirror of a semiconfocal Fabry-Perot resonator to infer a complex dielectric constant from measured changes in resonant frequency and quality factor of the resonator. Steffes plans to utilize this latter technique in laboratory measurements of millimeter-wave properties of potential constituents of clouds on Venus and Jupiter.

Pickett reviewed high-resolution spectroscopy in the microwave and far-infrared spectral regions. He noted that spectroscopy of rotational states in molecules is central to remote sensing techniques in atmospheric sciences and astronomy. New techniques have reached to wavelengths from twenty-five microns to two millimeters and include harmonic generation of microwave sources, infrared laser difference-frequency generation, laser sideband generation, and ultra-high-resolution interferometers.

Technologies for high-resolution submillimeter and far-infrared instrumentation are developing to be important for future planetary observations, with applications in aircraft, balloons, and high-altitude observatories. These capabilities for

measurements of planetary atmospheres require the acquisition of laboratory data suitable for interpreting spectral transition frequencies, intensities, and profiles.

Harmonic generation, an established technique in the far infrared, has recently been made more sensitive by illumination of a diode with microwave power and detection of absorption with harmonics of the microwave source. The new developments include replacement of contact diodes with monolithic Schottky diodes, use of sensitive detectors cooled by liquid helium, and employment of dichroic plates to filter out lower harmonics. These advances have facilitated laboratory studies of molecular spectra such as that of ammonia at 1073 GHz.

Laser difference-frequency generation may be used to cover a broad range of spectral wavelengths in segments of 100 MHz. The accuracy of measurements of positions of spectral lines in the far infrared is limited to about 200 kHz. An extension of coverage of spectral frequency is made possible by combining two infrared photons with a microwave photon.

Laser sidebands were generated by mixing the fixed frequency of a far-infrared laser with a microwave source. The goal of techniques developed by Pickett was to produce a source with accuracy of 100 kHz and power adequate for sensitive spectroscopic measurements. This laser had a very high measured power and a frequency stability of better than 100 kHz per hour. Spectra of ammonia and deuterated water vapor were obtained by this method.

Pickett noted a steady improvement in both user-constructed and commercial interferometers for the far infrared. He indicated that while this technique is limited in resolution by comparison with methods based on lasers, it is nevertheless useful for surveys and for measurements of widths of spectral lines.

Pickett concluded his review with a brief discussion of techniques as to their relative advantages and disadvantages, as well as aspects of their complementarity.

Jennings reviewed high-resolution spectroscopy of planetary molecules with diode lasers and interferometers. The latter technique provides broad spectral coverage and good calibration accuracy, while the former permits increased spectral resolution.

Jennings summarized the atmospheric molecular constituents of planets and their moons in our solar system. He noted that Titan exhibits the greatest variety of molecular features, including condensed phases of complex organics. Jennings emphasized the interactions between observational astronomy and laboratory research in which the complete interpretation of planetary spectra requires knowledge of spectral line frequencies, strengths, and pressure-broadening coefficients as functions of temperature. Astronomical observations included ethane in the atmosphere of

Jupiter, using both a post-disperser coupled to an interferometric spectrometer at the Kitt Peak four-meter telescope, and an infrared heterodyne receiver with a carbon dioxide laser.

Continuing studies of high-resolution molecular spectra in the laboratory have involved a variety of hydrocarbons. Methane, in particular, has been the subject of systematic studies of spectral line frequencies, shifts, and broadening produced by collisions with gases including helium, hydrogen, nitrogen, and argon.

A low-temperature sample cell has been designed, constructed, and operated at temperatures between 50 and 300 K. This system has been utilized to produce spectra of methane, ethylene, ethane, and propane.

Blass, Daunt, Peters, and Weber contributed descriptions of laboratory studies, analyses, and interpretations of infrared spectra of cyanoacetylene, acetylene, and other gaseous hydrocarbons present in planetary atmospheres. This research combined broad-band interferometric spectra and narrow-band spectra obtained with tunable diode lasers, together with some powerful computational techniques.

Observations of the atmospheres of the outer planets and Titan by the infrared interferometric spectrometer aboard the Voyager spacecraft motivated this work. Fundamental vibrational-rotational transitions of cyanoacetylene have been observed in the atmosphere of Titan. Blass et al. reported corresponding experimental results at high resolution and high precision.

Acetylene is present in planetary atmospheres because of the photochemistry of methane there. Understanding features of acetylene at high spectral resolution in the laboratory is a prerequisite to quantitative analyses of the planetary spectra. Several methods were employed to determine spectral line intensities.

Fraser, Pine, and Lafferty presented recent results on the laboratory spectroscopy of van der Waals complexes containing carbon dioxide. These data may be of use in modeling spectra of the atmospheres of Venus and Mars should there be such species present there.

Fraser et al. utilized an optothermal spectrometer based on a color-center laser to obtain sub-Doppler infrared spectra of dimers and trimers of pure carbon dioxide, as well as dimers of the latter with the rare gases neon, argon, and krypton. Moleular beams of these complexes were formed and then repeatedly crossed by the laser beam. Spectra were recorded by monitoring the response of a bolometer, cooled by liquid helium, as a function of spectral frequency of the laser. From the deduced spectroscopic parameters, structures for these complexes have been inferred and van der Waals vibrational frequencies have been estimated.

Spilker has measured microwave spectra of gaseous mixtures of ammonia with hydrogen and helium under conditions of temperatures and pressures relevant to the atmosphere of Jupiter. Such laboratory studies are important to the interpretation of radio astronomical and occultation data from the atmospheres of the outer planets generally.

Spilker has developed a new theoretical formalism to predict ammonia absorptivity over a significant range of conditions. He has utilized this theory for temperatures from 210 to 320 K, total pressures from 1 to 8 atm, and spectral frequencies from 9 to 18 GHz.

Suarez, Chackerian, Valero, and Tarrago reported new values for strengths and broadening coefficients of rovibrational spectral lines of phosphine, deuterated methane, and carbon dioxide. These results are significant for understanding the compositions and dynamics of planetary atmospheres through the use of the corresponding infrared observational astronomy at high spectral resolution.

Suarez et al. measured spectra of phosphine at temperatures between 137 and 294 K in the pure gas and in mixtures with helium. These laboratory measurements yielded broadening coefficients and line intensities from which transition dipole moments were deduced.

Studies of deuterated methane, observed in the atmospheres of the outer planets, are important to understanding not only the formation of the solar system but also the evolution of the cosmos. In order to obtain spectra amenable to analysis, Suarez et al. measured line intensities at temperatures down to 80 K with a high-resolution interferometric spectrometer. They also measured a dependence on temperature of the broadening coefficient in pure carbon dioxide.

Suenram and Lovas have studied microwave spectra of dimers of water vapor and other van der Waals complexes involving carbon dioxide, hydrogen sulfide, nitrogen, carbon monoxide, sulfur dioxide, and ozone. These gaseous species may be present in planetary atmospheres. Their spectra in the laboratory were measured utilizing elements of an interferometric spectrometer, a Fabry-Perot microwave cavity, and a pulsed molecular beam. This instrumentation yielded very narrow line widths and highly accurate spectral line frequencies. Suenram and Lovas summarized results from rotational analyses of weakly bound complexes containing water vapor and/or carbon dioxide gas.

Varanasi presented new acetylene data measured with a tunable diode laser spectrometer and a low-temperature absorption cell. Results in the infrared region included absolute intensities and collision-broadened line widths. The latter were

measured in mixtures with hydrogen, nitrogen, air, helium, and argon at temperatures ranging from 145 to 294 K.

SUMMARY AND CONCLUSIONS

This plenary review has concentrated on those invited and contributed papers within this author's ambit of interest and expertise. The other important and relevant papers have been reviewed separately and independently.

A thread running through many of the invited and contributed papers on spectroscopy has been the replication in the laboratory of conditions present in planetary atmospheres. These conditions include a range of pressures which implicates collisions among molecular and atomic gases, and a range of temperatures from very low to very high relating to a variety of contexts such as the upper atmosphere of Jupiter and the lower atmosphere of Venus, respectively.

There are significant challenges for spectroscopy appropriate to planetary atmospheres. Measurements at the longer wavelengths remain difficult. The application of low-temperature sample cells, even at the shorter wavelengths, is advanced but not yet routine. A theoretical understanding of recent laboratory measurements of phenomena affected by temperatures and pressures, which involves the dynamics of collisions, is in progress.

ACKNOWLEDGMENTS

The author gratefully acknowledges support for this review from the Planetary Atmospheres Program of the Solar System Exploration Division at NASA Headquarters through grant NAGW-125. Support for this Conference generally was also provided by Bowie State University, the NASA Goddard Space Flight Center, and The University of Tennessee.

REFERENCES

Appropriate references for this review are included in each of the invited and contributed papers discussed here.

SPECTROSCOPY AND MOLECULAR DYNAMICS

JOHN E. ALLEN, JR.
NASA/Goddard Space Flight Center
Code 691
Greenbelt, Maryland 20771.

INTRODUCTION

Spectroscopic observations form a substantial portion of the data upon which our understanding of planetary and cometary atmospheres is based. Historically, these observations have been restricted by the transmission properties of the Earth's atmosphere. However, the development of high-altitude and orbiting observatories as well as planetary probes has removed this restriction so that the observational data base now covers a significantly larger portion of the spectrum. New missions that are in various stages of preparation or planning will provide more detailed information in the traditional spectral regions and extend our capabilities to other wavelengths. To be useful in expanding our knowledge of planetary atmospheres and the processes at work in them, it is important that the observations be properly interpreted. This is obvious enough to be axiomatic: an observation without interpretation is just a picture. The necessary insight is provided by models whose complexity and sophistication have increased as our observational capabilities have improved. This trend is expected to continue with the deployment of the Hubble Space Telescope, for example. Besides observational data, models are critically dependent on the availability and quality of relevant laboratory information on fundamental processes which is used as inputs to the model. Without these laboratory data, assumptions must be made that can significantly affect the model results. In fact this suggests a corollary to the axiom above: interpretation without adequate, appropriate supporting data is at best a guess.

A viable, vigorous program in the planetary sciences-indeed in many scientific endeavors undertaken by NASA-requires a proper blend of observations, modeling and laboratory research. It is not uncommon for the level of effort expended and, therefore, resource allocation to be viewed in the linear fashion described above, that is, observations supported by models which are in turn based on laboratory data. However, a relationship that produces a more dynamic, advantageous interaction is illustrated in Fig. 1. Here there is active feedback from one aspect of the program to another. The interplay between models and laboratory research is clear. Models require as inputs certain chemical and physical properties of matter and radiation

and the laboratories respond by supplying this information. Conversely, laboratory measurements may uncover previously unrecognized facts that when incorporated in the models change model predictions. The feedback between observations and models is likewise apparent. Observations provide the data to be modeled and reciprocally models may predict new features or processes to be observed. What is less appreciated is the dynamic between observations and laboratory research. Limits to observational capabilities often prompt laboratory development of new instrumentation, whereas instruments or techniques developed initially for the laboratory may be adapted for use in the field; that is, today's laboratory instrument may well be tomorrow's flight instrument. In the following sections research presented in several invited and contributed papers will be reviewed with an emphasis on the interplay between laboratory research and observations or models.

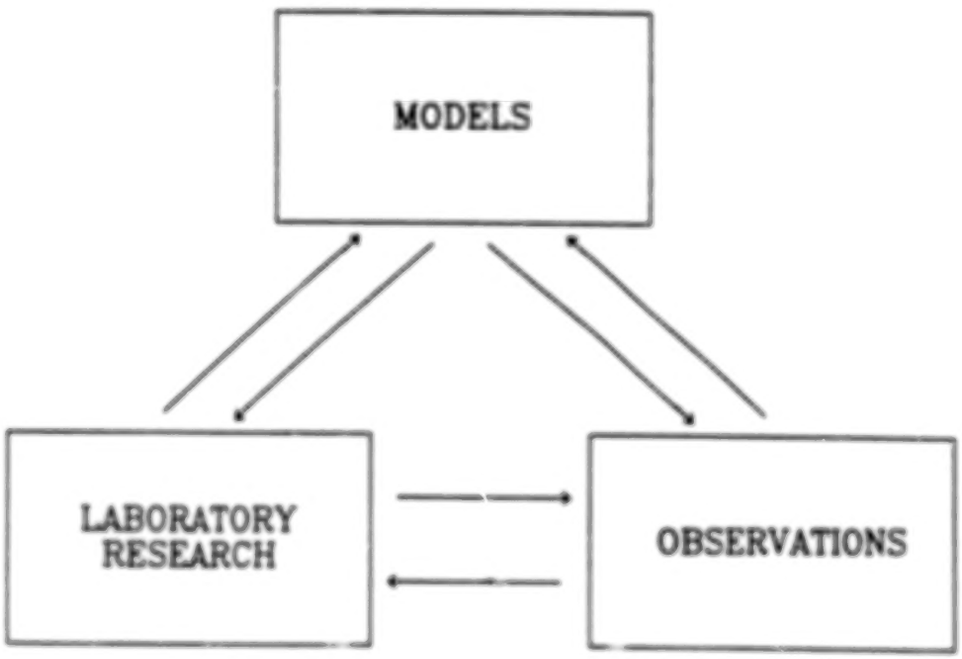

Figure 1: The relationships of components in a balanced program.

SPECTROSCOPY AND PHOTOCHEMISTRY

Molecular absorption in the ultraviolet (UV) and vacuum ultraviolet (VUV) can result in a variety of processes including fluorescence or photodissociation and the understanding of these processes at the microscopic level is vital to the study of planetary atmospheres. For example, observations of fluorescence in these wavelength regions provide an additional method by which to identify trace constituents, and chemical models are critically dependent on accurate measurements of photodissociation parameters, since this process leads to the generation of radicals that drive atmospheric chemistry. This points were made in the review by Judge and Wu, who stressed the need for accurately determined absolute total cross sections, absolute and specific cross sections for fragmentation products and the branching ratios for these products. As Judge and Wu noted, progress in this area has been facilitated by developments in experimental techniques and technology. Besides the availability of user facilities such as synchrotrons, the advancement in laser technology and techniques has had a significant impact on experiments in this spectral region. With laser sources it is now possible to carry out UV and VUV experiments in a conventional laboratory. Several examples of this were illustrated in contributed papers. Using an excimer laser operating at 193 nm, Urdahl et al. examined the photodissociation processes in C_2H_2 that may be relevant to the formation of cometary radicals; information such as this is critical to cometary observations and models. Absorption of one photon produces the radical C_2H and absorption of a subsequent photon by C_2H produces C_2 in a variety of states. The C_2 radical was monitored by direct fluorescence detection and laser-induced fluorescence. Since this dissociation is a two-step process, experiments of this type were not possible before the advent of high-powered lasers. Barts et al. described a laser-based experiment designed to characterize a recently discovered emission from C_2N_2 that may be used to observe this photochemically important molecule which is present in the atmosphere of Titan. Combining these measurements with absorption and photodissociation yield spectra, they were able to determine that heat of formation of CN radicals, an important quantity for chemical models. Both of these experiments used advances in photodetection and demonstrated the power of fluorescence spectroscopy to probe final states, illustrating additional points also made by Judge and Wu.

A recurrent theme of the conference was the need for data obtained at temperatures, pressures and relative abundances appropriate to planetary atmospheres. Much of the data that is available has been taken at room temperature and low pressures which are very different from conditions in planetary atmospheres. Even this information is incomplete and data at other conditions are virtually absent. Parameters at low temperatures cannot be accurately determined by extrapolation of room temperature data, a point that was made in a number of papers. Therefore, it is desirable to make laboratory measurements under the conditions of the planetary atmosphere of interest, e.g., for Venus this may be at high temperatures, while for the outer planets it is at low temperatures. In response to this need Judge and Wu reported photoabsorption cross sections of C_2H_2 taken from 145 nm to 200 nm at 295 K and 155 K; the later temperature corresponds to the C_2H_2 absorbing level in the Jovian atmosphere. They found that the low-temperature cross section values at the absorption peaks increased by 10% to 40%, whereas in the absorption valleys the cross section decreased by as much as 30% in comparison to the measurements at 295 K. They also found that the underlying continuum absorption also decreased somewhat.

As noted by Judge and Wu, requests for temperature-dependent absorption cross sections of PH_3, H_2S, C_2H_2, NH_3 and C_2H_6 were made almost a decade ago by observers who were using data from the International Ultraviolet Explorer to model the albedos of Jupiter and Saturn. In collaboration with one of those observers (Caldwell) the improved C_2H_2 absorption data have been used to reanalyze the UV spectrum of Saturn. This represents an excellent example of the interplays among observations, models and laboratory research. In a contributed paper on this subject, Caldwell et al. pointed out that these lower temperature absorption coefficients are applicable to outer planet atmospheres and employed them together with a new extraction technique to fit the observed albedo of Saturn. The new model produced an albedo maximum at 250 nm in good agreement with previous observational results from the Orbiting Astronomical Observatory; however, there were some very interesting differences with previous models that used room temperature absorption coefficients. Below 200 nm Caldwell et al. found that C_2H_2 alone did not provide a good fit and an additional absorber was needed. Of the species tried, H_2O gave the best results; however, the required abundance of H_2O was reduced by a factor of 2 from previous calculations as consequence of the use of the low-temperature C_2H_2 absorption coefficients. A discrepancy was noted near 160 nm which suggests that another gas may be present and AsH_3 was identified

as a possible candidate, but as Caldwell et al. pointed out there is no relevant laboratory data for this molecule. Verification of this suggestion awaits additional laboratory work.

In a clever application of photoabsorption and coincidence counting techniques, Judge and Wu have also measured the kinetic energy of fragments produced by the photodissociation of H_2 which results in the production of an exited hydrogen atom, a hydrogen ion and an electron. The kinetic energy of atomic fragments can be substantial and therefore important in atmospheric processes. The experiments reported for H_2 indicated that photodissociative ionization plays a role in the nonthermal escape of H atoms from the Earth's atmosphere. Since H_2 is a larger component of outer planet atmospheres, this mechanism may be even more significant there. This then is an example of laboratory research identifying a process that should be incorporated in the models, if these models are to be an accurate representation of planetary atmospheres.

Sputtering of surfaces is an area of research that is crucial to our understanding of various planetary bodies, yet there is very little information available. This is particularly true for photon sputtering, as Judge and Wu indicated. They have initiated experiments to address this problem and a preliminary report on H_2O ices was presented in a companion paper by Wu and Judge. For a more detailed discussion of these results, and sputtering in general, the reader is referred to the review by Lanzerotti. It is suffice to say here that much laboratory work remains to be done in this area before an adequate data base exists to guide the modeling of such phenomena as the processing of cometary nuclei.

SPECTROSCOPY AND ENERGY TRANSFER

The word methane could have preceded the title to this section, since all of the papers reviewed here deal with various aspects of this molecule. This emphasis is not inappropriate, because methane (CH_4) is the third most abundant molecule in the atmospheres of the outer planets and their satellites. Across the spectrum, observations of CH_4 features form the basis for much of our understanding of the dynamics and chemistry of these atmospheres. The ro-vibrational spectroscopy of methane in the infrared has been studied extensively using conventional techniques.

However, some of the features that are regularly observed in planetary atmospheres correspond to overtone-combination bands that lie in the visible to near infrared and are intrinsically very weak. Likewise there are several properties of CH_4, e.g., lack of a permanent dipole moment and spectral congestion, that make acquisition of state-to-state information difficult. Data on energy transfer rates and mechanisms are critical to the development of radiative transfer models or to the interpretation of certain spectral features. As discussed in the previous section, it is important that the information be obtained over the appropriate temperature, pressures range and, in the case of collisional effects, composition.

To acquire this data, it is often necessary to develop or adapt innovative techniques and this portion of the plenary review could have easily been incorporated in the next section. In their invited talk Steinfeld et al. described the principles of one technique, double-resonance spectroscopy, which is finding wider application to problems in spectroscopy and energy transfer. In a typical arrangement a laser pumps a molecule with sufficient energy to saturate a transition. A second source, usually another laser, probes one of the two levels of this transition; hence, it is also referred to as pump-probe spectroscopy. As Steinfeld et al. pointed out, there are two schemes regularly employed and the nature of the information obtained depends on the one used. For a three-level, double-resonance experiment the pump-probe frequencies couple one energy level to two other levels; this is used to simplify spectra. In the four-level version of the experiment the pump and probe radiations excite two pairs of levels that do not share a common level; however, one level in each pair is coupled by a collisional relaxation process. This configuration then provides kinetic information and propensity rules for inelastic collisions. To illustrate these points, Steinfeld et al. discussed the application of the infrared double-resonance technique to the study of spectra and energy transfer in several small ploy atomic molecules-CH_4, SiH_4 and O_3. Their measurements of the state-to-state rotational energy transfer for methane were the first such determinations for a spherical-top molecule and permitted them to develop an exponential energy-gap law to represent these rates. This level of understanding should be particularly useful to modelers, since the experiments result in an expression that can be used to predict rates that have yet to be measured.

In a related paper Halthore et al. cited the lack of adequate measurements for collisional relaxation times or energy transfer rates for the ν_3 and ν_4 levels of CH_4 as an impediment to modeling the 7.8 μm emission feature observed in Jupiter's stratosphere. In the absence of this data it is customary to assume that the

system is in local thermodynamic equilibrium which may not be the case in that environment. To provide these rates, Halthore et al. have undertaken a series of experiments using the pulsed opto-acoustic technique. The data are being acquired over ranges of temperature and pressure and with compositions that simulate planetary atmospheres; consequently, the measurements can be incorporated directly into the models.

Methane absorption bands in the visible and near infrared are major features observed in the spectra of the outer planets and are used as diagnostic tools of atmospheric processes. Despite their importance, interpretation of the observations of these features has been hampered, again by a lack of laboratory data. This dearth of information is due in part to difficulty in acquiring it. Since the transitions are so weak, it is necessary to use long-pathlength cells or more sensitive techniques. Using conventional techniques and long-path cells, Giver et al. have acquired near-infrared spectra at temperatures from 106 K to 297 K and have examined the relative merits of the Malkmus band and exponential sum models to parameterize the spectra. Their conclusion is that the exponential sum model is well suited for regions of strong absorptions, whereas the Malkmus model is more appropriate in regions of weaker absorptions. They cautioned that the procedure can be arbitrary unless care is taken. The weaker absorption features lend themselves to the intracavity laser absorption method discussed by O'Brien and by Lang and Allen. The technique is very sensitive which was demonstrated by Lang and Allen, who applied it to the detection of ambient water vapor in a one-meter path of laboratory air by monitoring weak H_2O combination bands. O'Brien has used the method to measure CH_4 absorption at 619 nm and 682 nm for several different pressures and temperatures. The sensitivity of the technique relaxes requirements on pathlength and cell size which facillitates temperature measurements. As pointed out by O'Brien, the recent development of Ti:sapphire lasers makes it possible to extend the useful spectral range of the technique to 1 μm. Continued progress in the acquisition of temperature-dependent absorption data is crucial to an understanding of the role of CH_4 in outer planet atmospheres.

NEW TECHNIQUES FOR LABORATORY RESEARCH

In some cases the laboratory data that are needed can be obtained using techniques that are by now considered conventional. An example of this was described in a paper by Nava et al., who used resonance fluorescence-flash photolysis to determine the rate constant for the reaction H + GeH_4 which is critical to an understanding of germane chemistry in the Jovian atmosphere. This example also illustrates another point; the chemical compositions of planetary atmospheres are significantly different from that of Earth and, consequently, the chemistry involves the interaction of unusual constituents that can lead to the production of unfamiliar species. In addition, as indicated in the previous section, planetary atmospheres represent extremes in temperature and pressure that may perturb the spectral signals of the species that are being monitored or can result in unusual physical processes. For example, high pressure can give rise to line broadening, line sifts or even induced transitions. The increase in our observational and modeling capabilities and, therefore, our level of understanding of planetary atmospheres requires that new laboratory techniques be developed to obtain the needed data. These points were emphasized in a series of invited and contributed papers that covered a variety of topics.

Two novel techniques designed to provide new or improved information in photochemistry and chemical kinetics were described in an invited talk by Leone. Coupling a photolysis source, e.g., a laser or flashlamp, and a commercial Fourier transform infrared (FTIR) spectrometer, he has developed a method by which to acquire time-resolved emission spectra of radicals. The technique is capable of detecting 10^9 - 10^{11} molecules/cc and is therefore significantly more sensitive than absorption methods. This reduces potential experimental complexities, since long pathlengths or high concentrations are not required. The other technique, time-resolved laser gain-versus-absorption, provides specific but complementary information. Photodissociation can produce an admixture of ground-or excited-state products that can be probed directly, in this case with a tunable, infrared, color-center laser or a tunable, room-temperature, diode laser. By measuring the temporal behavior of the probe laser gain-versus-absorption, Leone and his group have been able to obtain very accurate quantum yields for excited state production. The method has been applied to the dissociation of molecules containing halogen

atoms and accuracies to ± 2% for quantum yields have been achieved; this is an order of magnitude improvement over previous determinations.

Fourier transform spectrometers are being applied to a variety of laboratory research areas and in his talk Leone discussed several of these. As may be surmised from the last section, the photochemistry of C_2H_2 is important to an understanding of outer-planet and perhaps cometary atmospheres. Using the time-resolved FTIR emission method, Leone has investigated the infrared emission spectrum of C_2H formed from the photolysis of C_2H_2 at 193 nm. Recall that this is the intermediate step in the dissociation of C_2H_2 reported by Urdahl et al. and thus these experiments yield insight in the production of C_2 from C_2H_2. Survey scans of C_2H by the FTIR method revealed strong infrared and near-infrared bands associated with the $(\tilde{A}^2\pi)$ electronic state, information that is critical to photochemical models and design of the next generation of observing instruments. The power of the FTIR method in reaction kinetics was illustrated by the example of Cl atoms reacting with the radical C_2H_5. Both atom-radical reactions such as this and radical-radical reactions are difficult to monitor using conventional techniques, but can be studied using newer methods. The kinetics and products of the reaction $N + CH_3$ and related reactions were reported by Nesbitt et al., who studied them using the flow discharge-mass spectrometry method. Their results have significant consequences for models of the atmospheres of Titan and Jupiter. Because quantitative information for these types of reactions is critical to models of planetary atmospheres, it is imperative that newer techniques like those employed by Leone and Nesbitt et al. be developed and applied.

Recall that temperature-dependent studies are necessary for accurate modeling of planetary atmospheres. Most of the apparatus described so far are well suited to cover the upper portion of the required temperature range. In some cases, however, it is desirable to achieve extremely low temperatures; this is critical for the study of dimers. In a novel arrangement Rühl and Vaida used an FTIR spectrometer and laser-based resonance-enhanced multiphoton ionization (REMPI) in conjunction with a free-jet expansion to acquire UV and VUV absorption and emission data for molecules, radicals and clusters at very low temperatures. Compared to the best conventional free-jet absorption techniques, they showed that the FTIR method is fifteen times more sensitive with two orders of magnitude better spectral resolution. Using the REMPI method which combines mass spectrometry and laser-induced photoionization, they obtained spectral data for ClO produced in the dissociation of ClO_2. Since ClO is strongly predissociated, it is not possible to acquire this

information by more conventional methods such as laser-induced fluorescence. Another example of the usefulness of REMPI was presented in a paper by Johnson and Hudgens, who discovered four new electronic states of NH and ND. The photolysis of HN_3 produced NH in the metastable $a^1\Delta$ state which was then monitored using (2+1) REMPI and time-of-flight mass spectrometry; spectra were acquired from 258 nm to 288 nm. These results demonstrate the utility of new methods in monitoring molecules and states that do not lend themselves to conventional techniques. This information may, however, be critical for an understanding of important physical processes or the calculation of fundamental parameters, e.g., cross sections, that are essential for photochemical models.

The use of new spectroscopic techniques to obtain more accurate, temperature-dependent data is not confined to the areas of spectroscopy and photochemistry, but includes thermodynamics as well. One example was discussed by Steffes in his invited talk on microwave and millimeter-wave spectroscopy. Models of observations of the Venutian atmosphere in this spectral region are dependent on accurate laboratory measurements of absorption coefficients for various molecules. In their efforts to supply this information for H_2SO_4, Steffes and his coworkers were hampered by a lack of high-temperature vapor pressure and thermal dissociation data for this molecule. To obtain this information, they adapted their spectroscopic apparatus and developed a new measurement technique. Another example was presented by Masterson et al., who developed a novel thin-film infrared method for measuring vapor pressures at low temperatures. This effort was undertaken in direct response to the needs of modelers, who were attempting to interpret observations of the outer planets and their satellites. When used in conjunction with conventional methods, it is possible to measure vapor pressures over the temperature range appropriate to these bodies. Heretofore, these data did not exist and modelers were forced to extrapolate available high-temperature data using the Clasius-Clapeyron equation. However, as the experiments indicated, the extrapolated values can differ by two orders of magnitude from the measured values. The consequences of these new vapor pressure measurements for C_2H_2 and C_4H_2 were detailed in a paper by Romani. He noted that extrapolation of the previously available vapor pressure data resulted in the model predicting no condensation in the stratosphere of Saturn. In addition to uncertainties in vapor pressures, Romani also discussed the effect that uncertainties in the chemistry can have on model predictions. Again the need for temperature-dependent reaction-rate data was stressed and the consequences of various Arrhenius based extrapolation routines

discussed. Uncertainties in the chemistry such radicals as C_2H can have an order of magnitude effect on the predicted C_4H_2 haze production rate.

CONCLUSION

The invited and contributed papers that have been reviewed here are representative of the breadth of laboratory activities that are necessary for a healthy planetary atmosperes program: spectroscopy, chemical dynamics, photochemistry, thermodynamics and technique development. A common theme throughout the meeting was the need to acquire of this data for temperature and pressure ranges and compositions that are appropriate to the atmosphere being studied. The implications of relevant laboratory data for interpretation of observations was clearly demonstrated in several papers that incorporated some of these data in models. These later papers illustrated the interplay that was suggested in Fig. 1 and that is essential for an in-depth understanding of planetary atmospheres.

In the course of the presentations a number of conclusions were drawn and needs or new areas of research identified. For example, the laboratory spectroscopic data are consistently less complete and lower in quality than the observational data, especially in the UV and VUV spectral regions. This situation is apt to continue with the deployment of sophisticated observatories such as Hubble Space Telescope or the proposed Far Ultraviolet Spectroscopic Explorer. Because the laboratory data are not often taken for conditions encountered in planetary or cometary environments, the data that are available should be carefully considered before being used in models. In some areas the laboratory data are almost nonexistent, due in part to the difficulty in acquiring them. A particularly outstanding gap is the lack of absorption and product channel data for free radicals and ions; this has a profound impact on our ability to realistically model cometary comae. Similar examples maybe cited for other areas: kinetics (hydrocarbon and nitrile chemistries), molecular dynamics (nonLTE effects) and thermodynamics (low-temperature vapor pressures).

A cohesive program in planetary atmospheres would benefit significantly, if there were a central repository for laboratory data and a forum within which to evaluate the data and identify areas for further work. The Ames newsletter provides the spectroscopy community with some of these services; however, for kinetics,

photochemistry or thermodynamics there is nothing comparable. A good example of and effective effort in these later areas is the laboratory data evaluation panel in the NASA Upper Atmosphere Program. Every two years the panel convenes to evaluate the current data base; the information is then summarized in a report that is used extensively by both modelers and laboratory investigators. Activities such as these could easily be incorporated in the existing Planetary Data System. Not only would this serve the planetary atmospheres program directly, but it would have the additional benefit of providing researchers from other areas with a concise summary of needs in planetary science. For example, except for the temperature range of interest some of the reaction chemistry for the atmospheres of outer planets is similar to that in combustion, chemical vapor deposition or terrestrial atmosphere research. These are large programs with very active laboratory research groups that with a little encouragement and easier access to requirements could make meaningful contributions to planetary atmospheres.

Although it is by now a cliche, improvement in laboratory research will require an increase in funding. These funds must be sufficient to provide upgrades in equipment and personnel for existing investigators and attract investigators from other areas, who by the nature of their research can add to the data base. In addition, it is imperative that the allocated funds be protected from use for other aspects of the program. At the conference it was announced the there would be an augmentation to the budget for the upgrade of laboratory equipment; however, at this time that money has been reprogrammed to support other areas. These reprogrammings can have eventually dire consequences for research and analysis. Recall from Fig. 1 that observations, models and laboratory research were related in such a way that they formed a stable triangle. However, the current allocation of funds and hence emphasis is quite different, as illustrated in Fig. 2. Research and analysis, as represented by modeling and laboratory research, constitute a smaller portion of the overall budget than flight programs. This is in part understandable because of the expense associated with flight instruments. However, it must be recognized that as it is presently constituted the program is unstable and continual erosion of the research and analysis portion either by inflation or fund reallocations can only exacerbate this instability. With the dramatic increase in data flow from the new missions that are in progress or planned, it is not inconceivable that unless this problem is addressed NASA could become just an archive for observational data. The problem is particularly critical for planetary science, since NASA has

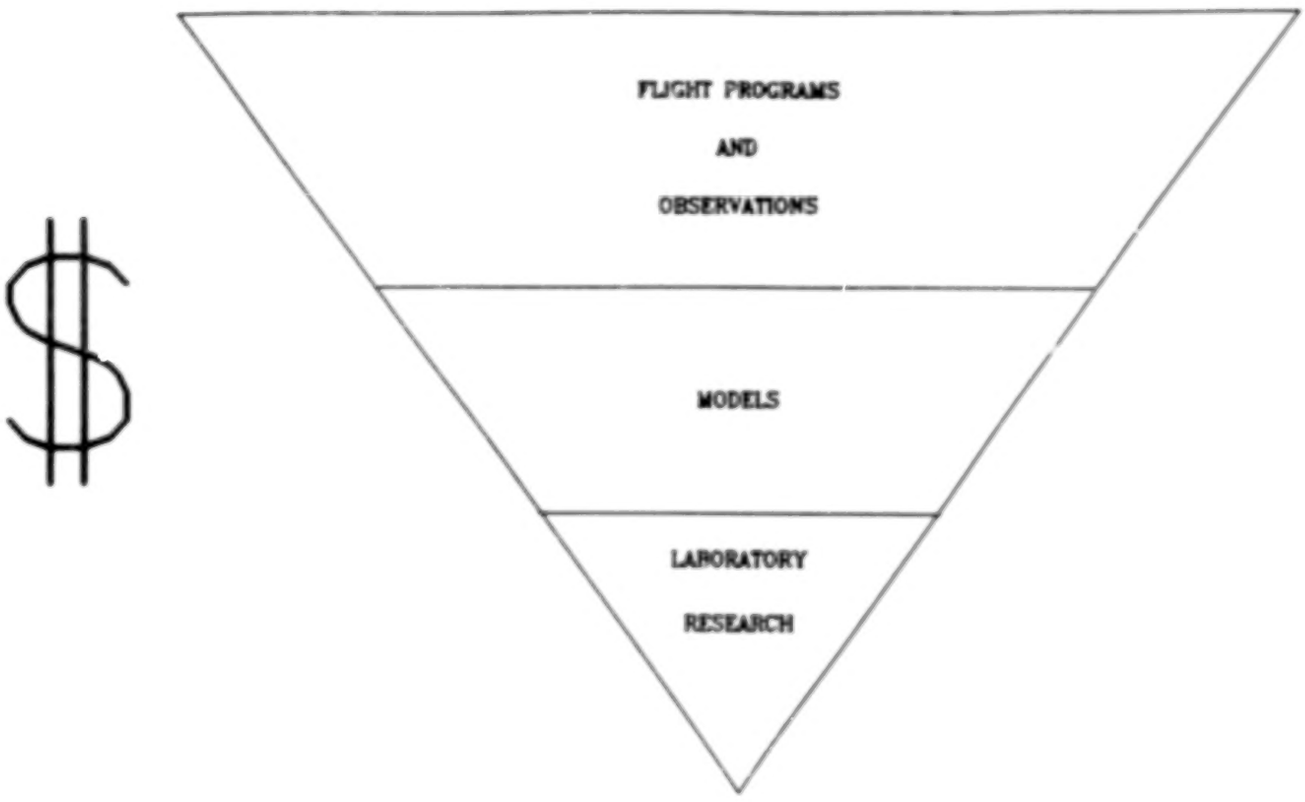

Figure 2: The relationship of components in currently funded programs.

historically been the sole provider for this area of research. It is important that a balanced program be formulated and implemented.

ACKNOWLEDGEMENTS

The author thanks Dr. L.J. Stief for his comments on the manuscript and gratefully acknowledges support form the NASA Planetary Atmospheres Program.

CHEMICAL KINETICS: A PLENARY REVIEW

MARK ALLEN
Earth and Space Sciences Division, Jet Propulsion Laboratory, California Institute of Technology, 4800 Oak Grove Drive, Pasadena, CA 91109 and Division of Geological and Planetary Sciences, California Institute of Technology, Pasadena, CA 91125

ABSTRACT

The quality of chemical models of planetary atmospheres is limited by the availability of measurements from laboratory investigations that are applicable to the physical and chemical conditions of various solar system bodies. A number of key measurements, and techniques that would facilitate in the future valuable laboratory studies, have been reported at this conference. A laboratory program that well supports the NASA solar system exploration effort requires updated equipment for currently funded laboratory investigators and the participation of additional investigators, who may already be funded from other sources for similar studies.

THE ROLE OF LABORATORY STUDIES IN THE SOLAR SYSTEM EXPLORATION PROGRAM

The contribution of laboratory investigations to the NASA solar system exploration program typically is less understood than the respective roles of observations and chemical models. One version of the interrelationship of these various activities is illustrated in figure 1.

The ultimate goal of solar system exploration is an understanding of the natural processes driving the various atmospheres found in the solar system. Since the typical conditions of an extraterrestrial atmosphere are quite different from those of the terrestrial laboratory setting, it is a challenge to develop a chemical model that reproduces available observations of molecular species. An understanding of the chemistry of a planetary atmosphere is also important for understanding the thermal budget of the atmosphere, since molecular species (and photochemically-derived aerosols) regulate the deposition of solar energy (solar heating), its redistribution, and ultimate loss to space. If the chemistry is well established for certain species with sufficiently long chemical lifetimes, these species may serve as tracers of atmospheric dynamics, and observations can be used to map atmospheric motions.

While some insight into natural processes in planetary atmospheres is derived directly from observations, usually observations need to be coupled with a model analysis in order to develop a description of the important processes. Particularly in the effort to determine the important chemical cycles in a planetary atmosphere, observations serve to direct the development of chemical models and serve as a test of

PRECEDING PAGE BLANK NOT FILMED

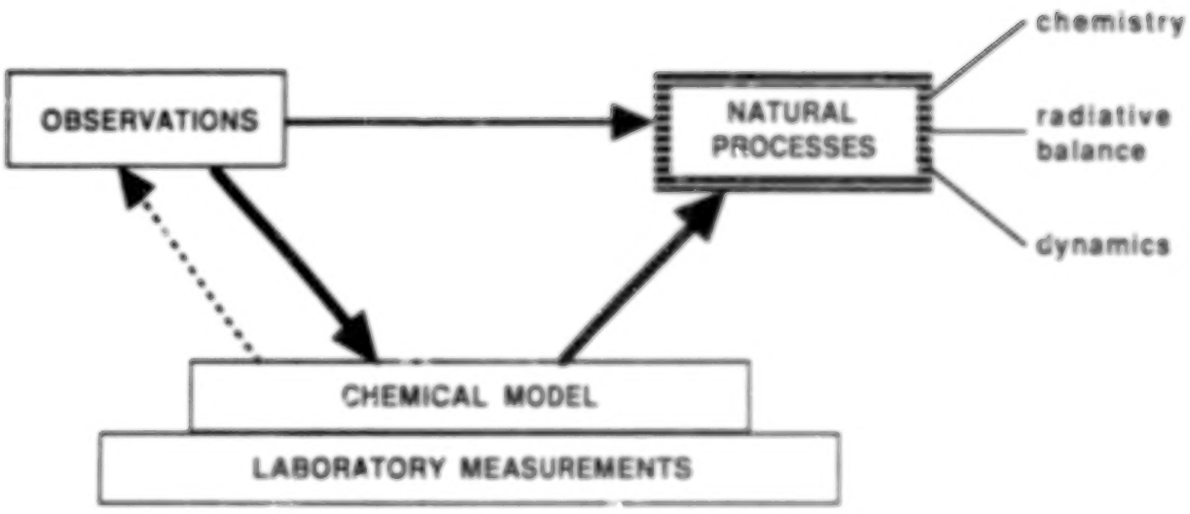

Figure 1. The components of the solar system exploration program.

atmospheric processes (chemistry and transport) incorporated in the chemical model. The chemical model, however, simply incorporates a summary of possible elementary chemical reactions. The model will not be able to reproduce observed atmospheric phenomena, even if the reaction set is correct, if some of the adopted reaction parameters are inaccurate. Thus the laboratory measurement program is the foundation of the model effort. Sometimes, as in the case of identifying the dominant molecular components of cometary ices, the "observations" of parent species are actually the results of a chemical model[1,2], in which the useful information that can be extracted is limited by the quality of the laboratory measurements available for incorporation in the chemical model.

LABORATORY MEASUREMENTS REQUIRED FOR CHEMICAL MODELS OF PLANETARY ATMOSPHERES

In surveying the current state of chemical models, **Yung** and **Fegley** in their respective review talks identified key chemical cycles for which laboratory measurements are needed. **Yung** and **Romani** showed in the specific case of polyyne chemistry the significant sensitivity of model results to the adopted/assumed input parameter values. A vast amount of laboratory research is required to provide chemical models with the parameters needed to attempt to simulate solar system chemistry.

The full set of model parameters, for which laboratory measurements are necessary, are summarized here by general type:

1) Collisional rate constants.

a) TEMPERATURE DEPENDENCE. Typically values reported in the literature are for room temperature. Moreover, hydrocarbon investigations, funded for combustion research, tend to be at even higher temperatures. However, the peak in hydrocarbon reaction rates occurs in the Jupiter atmosphere at 160 K and in the Triton atmosphere at temperatures as cold as 38 K. Therefore laboratory investigations specifically tailored to the physical conditions encountered in the solar system are necessary. In particular, improved theoretical treatments, with corroborating experimental data, of the general temperature dependence of reactions below ~200 K are needed. How accurate are extrapolations to low temperatures using the Arrhenius expression? When does quantum mechanical tunneling become important?

b) PRESSURE DEPENDENCE. The formation of large molecules in planetary atmospheres often is dominated by three-body recombination reactions.[3] The peak formation level in the atmosphere is typically ≤1 mbar. However, again because of the current sources of funding for kinetic measurements, available data are often for pressures no smaller than a few mbar; frequently the pressures are so large that only the high pressure limiting rate constant is reported.

c) NATURE OF THIRD BODY IN RECOMBINATION REACTIONS. Rate constants reported in the literature typically are from experiments utilizing inert gases for the background gas. The measured rate constant can vary quite significantly depending on the identity of the buffer gas. However, in the various atmospheres in the solar system, either H_2, N_2, or CO_2 is the dominant constituent and, as such, there is a need for rate constants measured specifically for these atmospheric compositions.

d) PRODUCT SPECIES. For many reactions for which the rate constants are measured by monitoring the disappearance of a reactant, the identity of the product species is only surmised (often the choice is quite logical). If two or more product channels are energetically possible, the relative yields are rarely known, and modelers typically assume, without real justification, a (democratic) equal distribution among the possible outcomes.

e) HETEROGENEOUS PROCESSES. The level of sophistication of our understanding of planetary atmospheres has evolved to the point that simply considering homogeneous gas-phase processes is not justified. We now know that, in solar system atmospheres, atmosphere-surface and atmosphere-aerosol chemistry are important determinants of gas-phase composition, surface chemical states, and aerosol formation. While current catalysis research focuses on clean, well-characterized surfaces, the planetary context involves much more heterogeneous, amorphous surface and solid states. Both chemical interactions at the gas-solid interface and below the surface (as in the case of processing in the interior of aerosols) will need to be incorporated in future models.

2) Photocross-sections.

a) WAVELENGTH DEPENDENCE. The use of synchrotron light sources has allowed a significant expansion of the wavelength range for which laboratory measurements exist. The long-wavelength tail of the photodissociation spectrum, where the cross-section values are rapidly decreasing, occurs for many molecular species between 1300 and 3000 Å[4]. Since the solar flux increases by a factor of 10^5 from 1300 Å to 3000 Å[5], the longest wavelength, smallest cross-section values still may make a significant contribution to the total photodissociation rate coefficient. Consequently, additional experimental measurements longward of the currently existing data are needed to allow more accurate calculations of key photodissociation rate constants. Rarely available are any cross-sections for transient species, which are crucial for modelling cometary coma species and for the interpretation of many NASA-funded observations.

b) TEMPERATURE DEPENDENCE. See **Judge and Wu** and **Caldwell *et al.*** discussion in a later section.

c) PRODUCT YIELDS. The branching ratios for forming neutral and ion products as a function of wavelength can be rarely found in the current literature. Partly this is a result of the limitations of available techniques for identifying and quantifying product species. For some molecules, the relative neutral and ion yields has been established and, for some species, the ion channels have been

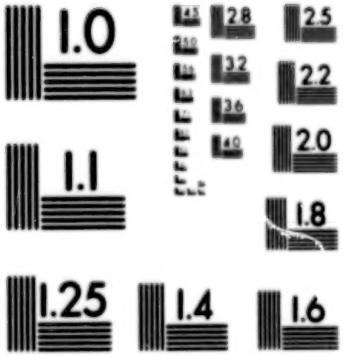

MICROCOPY RESOLUTION TEST CHART
NATIONAL BUREAU OF STANDARDS
STANDARD REFERENCE MATERIAL 1010a
(ANSI and ISO TEST CHART No. 2)

well characterized. The yields of specific neutral fragments, if measured, often are only at specific wavelengths, introducing potentially large uncertainties when models integrate over the full solar spectrum.

3) Ion-electron recombination rate constants.
   a) TEMPERATURE DEPENDENCE. Ionized species are found throughout the solar system in a wide range of physical conditions, such that electron temperatures vary over several orders of magnitude.
   b) PRODUCT YIELDS. There is much controversy surrounding the identity of the products of one of the simplest recombination reactions ($H_3^+ + e$), and nothing is known for most reactions involving more complex molecular ion species.
4) Electron-neutral collisional rate constants.
   a) TEMPERATURE DEPENDENCE. See above discussion.
   b) PRODUCT YIELDS. The formation of ionic and neutral species from electron-neutral collisions may be important in cometary comae.[6]
5) Vapor pressures.

   Romani demonstrated that the profiles derived from model calculations of hydrocarbon formation and condensation are quite sensitive to the input vapor pressure parameters. Laboratory measurements at the low temperature of planetary atmospheres are quite limited.

NEW LABORATORY MEASUREMENTS

Several recent measurements of quantities important for chemical models of solar system atmospheres were reported at the conference. These investigations illustrate the character of laboratory studies that are most valuable for improving chemical models.

The recombination of the CH_3 radical to form C_2H_6 is central to our understanding the presence of C_2H_6 in outer solar system atmospheres.[3] Reported by **Gutman and Slagle**, the measurement of the rate constant for this reaction as a function of both temperature and pressure (in particular, quantifying the temperature dependence of the low pressure limit) is one of the few complete studies available for inclusion in chemical models. (The other complete study that comes to mind is the measurement of the temperature and pressure dependence of rate constant for $H + C_2H_2 \rightarrow C_2H_3$.[7])

Another important reaction in reducing atmospheres is the disproportionation of C_2H_3.[3] **Fahr *et al.*** report the overall rate constant for this reaction and the yields of the various product channels.

In the most recent model of Titan chemistry,[3] the CN bond is formed in the reaction $N + CH_3$ (or CH_2) $\rightarrow HCN + H_2$ (or H), occurring predominantly in the upper atmosphere. The rate constants utilized probably reflected a multi-step reaction sequence that was poorly characterized, the few available laboratory measurements

coming from the literature of the 1950's and 1970's. The temperature-dependent rate constants for the reactions N + CH_3 and N + H_2CN reported by **Nesbitt *et al.*** permit more accurate model simulations of nitrile chemistry in the planetary environment. Characterization of the products of these reactions and measurement of yields are still needed for inclusion in models.

The detections of GeH_4 in the atmospheres of Jupiter[8] and Saturn[9] yield important insights to the coupling between chemistry and transport from the planetary interiors. The reaction H + GeH_4 plays an important role in controlling the abundance of GeH_4. As discussed by **Nava *et al.***, previous measurements of this reaction rate constant vary by more than a factor of 200, so their new study (in agreement with the lower of the two previous values) is of great importance for model descriptions of GeH_4 chemistry.

Few photocross-sections of hydrocarbon species are available for temperatures close to what occur in outer solar system atmospheres. **Judge and Wu** and **Caldwell *et al.*** showed how much the C_2H_2 photocross-sections changed from 295 K to 155 K. Much more data of this kind are needed in order to develop precise models of atmospheric processes.

It is well known that the quantum yield for photodecomposition of C_2H_2 and C_2H_4 is much less than unity. A channel identified only recently is the formation of the transient species vinylidene, H_2CC. **Fahr *et al.*** show that this is the dominant product channel upon absorption of a photon. The subsequent chemistry of $H_2C\,C$ may be important for outer solar system atmospheres.

The need for improved measurements of vapor pressures at the low temperatures found in solar system atmospheres was presented above. Therefore, the results for C_2H_2 reported by **Masterson *et al.*** are particularly valuable and demonstrate the errors existing in older data and extrapolations from higher temperatures.

One laboratory measurement not normally considered in surveys of laboratory studies of value for planetary atmosphere research is the molecular ion-electron recombination rate constant. These rate constants are quite important for modelling the ion chemistry of cometary comae and inferring the abundances of the main "parent" neutral species.[1] These parameters also are important for modelling the ionospheres of planetary atmospheres. The cumulative body of laboratory results (with associated temperature dependences) reported by **Johnsen** provide an important input to chemical models. Needed in the very near future for interpretation of *in situ* ion mass spectrometer data from the recent Giotto flyby of Comet Halley and the upcoming Comet Rendezvous Asteroid Flyby (CRAF) mission are rate constants for electron recombination with large molecular ions.

NEW EXPERIMENTAL TECHNIQUES

A number of laboratory studies were reported at this conference which demonstrated new techniques that can be applied to measurements of parameters needed by chemical models of planetary atmospheres. There are several important reactions between atoms and/or radical molecular species in current chemical models; consequently the presentations of **Gutman and Slagle, Fahr *et al.*,** and **Nesbitt *et al.*** are quite significant. The precise measurement of a reaction rate constant and quantification of the yields for different product channels are facilitated by monitoring the time-dependent disappearance of a radical reactant species and/or the appearance of a transient product species. Various techniques were presented which offered different capabilities (often species-dependent) for such monitoring of the reaction environment: laser gain-vs-absorption spectroscopy and Fourier Transform infrared emission, **Leone**; ultraviolet emission spectroscopy, **Barts *et al.***; photoionization mass spectrometry, **Gutman and Slagle**; resonance enhanced multiphoton ionization, **Johnson and Hudgens** and **Rühl and Vaida**; and multiphoton laser-induced fluorescence, **Urdahl *et al.***

CONCLUSIONS: AN INDIVIDUAL PERSPECTIVE

As discussed earlier, the quality of chemical models of atmospheres in the solar system is limited by the availability of relevant laboratory studies. Since solar system atmospheres typically are quite different from normal laboratory environments, novel techniques will be needed to make measurements of real use to chemical models. Various new laboratory techniques presented at this conference, when applied to making specific measurements of rate constants and cross-sections, hold great promise for expanding the knowledge base on which chemical models rest.

As illustrated by several of the presentations at this conference, the contribution of many laboratory groups currently funded by NASA is limited by the age of their laboratory apparatus. The upcoming funding augmentation for upgrade of laboratory equipment clearly will catalyze expanded studies by groups in the NASA program. However, in addition to the many physical quantities for which no relevant measurements exist, for too few of the most important parameters do more than one measurement exist. As illustrated by the intensive laboratory program in support of the NASA upper atmosphere research program, a quality data base that supports the development of reliable chemical models requires the participation of many groups employing a variety of experimental techniques to generate several, cross-checking, measurements of the important model input parameters. To generate a similar effort for the NASA planetary atmospheres program requires the involvement of additional experimental groups beyond those currently funded by this program. Indeed, many groups already funded by the NASA terrestrial atmosphere program or by other

sources (combustion research, etc.) have the requisite sophisticated techniques for obtaining the measurements required by solar system chemical models. The involvement of these groups through NASA funding of salaries and supplies would effectively enhance the current laboratory program and clearly lead to better chemical models — and understanding — of atmospheres in the solar system.

The funded program of laboratory studies and chemical modelling of planetary atmospheres also would be enhanced by better communication between laboratory and modelling groups. Future International Conferences on Laboratory Research for Planetary Atmospheres certainly will provide important opportunities for interchange among the participants. In addition, a NASA-sponsored electronic forum, taking advantage of presently available technologies, can also facilitate the reporting of new laboratory results and inquiries from modelling groups for specifically-desired data. The Ames spectroscopy newsletter currently provides such a service for that discipline. An electronic forum could expand that interchange to all laboratory disciplines and specifically facilitate the transfer of quantitative information, such as new rate constants to be published and digitized tables of measured cross-sections. Specific benefits to the modelling community include rapid acquisition of newly-measured quantities (eliminating often a multiyear delay between journal submission and appearance of the journal issue in the local institutional library) and in a form most useful for inclusion in chemical models. Existing archival efforts at NIST (either Gaithersburg or JILA) might be effectively tapped to support the NASA laboratory/modelling program.

ACKNOWLEDGEMENTS. The author thanks W. DeMore and Y. Yung for their valuable comments on the manuscript. This work represents one phase of research carried out at the Jet Propulsion Laboratory, under contract to the National Aeronautics and Space Administration. Partial financial support from the Conference is gratefully acknowledged.

[1]M. Allen, M. Delitsky, W. Huntress, Y. Yung, W.-H. Ip, R. Schwenn, H. Rosenbauer, E. Shelley, H. Balsiger, and J. Geiss, Astron. Astrophys. **187**, 502 (1987).

[2]E. K. Jessberger, J. Kissel, and J. Rahe, *Origin and Evolution of Planetary and Satellite Atmospheres*, edited by S. K. Atreya, J. B. Pollack, and M. S. Matthews (University of Arizona Press, Tucson, 1989).

[3]Y. L. Yung, M. Allen, and J. P. Pinto, Astrophys. J. Suppl. Ser. **55**, 465 (1984).

[4]H. Okabe, *Photochemistry of Small Molecules* (Wiley, New York, 1978).

[5]G. Brasseur and S. Solomon, *Aeronomy of the Middle Atmosphere* (D. Reidel, Dordrecht, 1984).

[6]T. E. Cravens, J. U. Kozyra, A. F. Nagy, T. I. Gombosi, and M. Kurtz, J. Geophys. Res. **92**, 7341 (1987).

[7]W. A. Payne and L. J. Stief, J. Chem. Phys. 64, **1150** (1976).

[8]U. Fink, H. P. Larson, and R. R. Treffers, Icarus **34**, 344 (1978).

[9]K. S. Noll, R. F. Knacke, T. R. Geballe, and A. T. Tokunaga, Icarus **75**, 409 (1988).

CHEMICAL THERMODYNAMICS: PLENARY REVIEW

BRUCE FEGLEY, JR.
Abteilung Kosmochemie, Max-Planck-Institut für Chemie (Otto Hahn Institut), Saarstrasse 23, D-6500 Mainz, Federal Republic of Germany

ABSTRACT

The invited and contributed papers dealing with the applications of chemical thermodynamics to planetary atmospheres research are briefly reviewed. The key areas for future applications of chemical thermodynamics research to planetary atmospheres are also described.

REVIEW

Khare and coworkers presented two papers on the optical constants of solid methane and of kerogen. Methane is the most abundant molecule of carbon and hydrogen in the outer solar system and a knowledge of its optical constants in the solid are important for radiative transfer calculations, reflection spectra studies of the surfaces of icy bodies, and for modeling emission in the far infrared and microwave regions. Kerogen is a complex organic solid exemplified by the solvent insoluble carbonaceous material in carbonaceous chondrites. It may also be related to the dark materials observed on some asteroids and outer planet satellites. Again knowledge of its optical constants throughout the visible and IR regions is important for interpretation of spectroscopic data.

Masterson and colleagues presented laboratory measurements of the acetylene C_2H_2 vapor pressure at temperatures of 80 to 188 K. Acetylene is a photolysis product of CH_4 and has been observed in the atmospheres of Jupiter, Saturn, Uranus, Neptune, and Saturn's satellite Titan. Masterson's work extends the literature data base to lower temperatures.

Thompson presented an interesting discussion of the application of solution thermodynamics to multicomponent cryogenic systems such as the N_2-CH_4 and CH_4-C_2H_6 systems believed to be important on Saturn's satellite Titan. He gave a brief introduction to the general thermodynamic concepts, a discussion of the completeness of the existing data base in the literature, and examples of methods of obtaining and evaluating low temperature vapor-liquid phase equilibrium data.

Finally, in my invited paper I described the applications of chemical thermodynamics and chemical kinetics to planetary atmospheres research during the past four decades with an emphasis on chemical equilibrium models and thermochemical kinetics. The need for laboratory measurements of kinetic data important for thermochemical reactions was illustrated by discussing volatile retention reactions in the solar nebula, atmosphere-surface interactions on Venus and Mars, deep mixing in the atmospheres of the gas giant planets, and the origin of the atmospheres of icy satellites.

RECOMMENDATIONS FOR FUTURE WORK

My recommendations for future applications of chemical thermodynamics to planetary atmospheres research are given below. For convenience I have organized this discussion on a planet by planet basis and thus a variety of different topics entailing different types of measurements are discussed together in each section.

Venus

The abundance and vertical distribution of water vapor in the atmosphere of Venus is a longstanding problem which is still incompletely understood. Lewis and Grinspoon have recently proposed that carbonic acid gas H_2CO_3 ($H_2O \cdot CO_2$)is an important water vapor sink in the lower atmosphere of Venus. However essentially no thermodynamic data are actually available for this compound (and the existence of this species is also a matter of dispute). Spectroscopic measurements designed to yield information on the molecular structure and spectroscopic constants are needed to evaluate the thermodynamic properties of H_2CO_3 using statistical mechanics. These data can then be input into theoretical models of the water vapor abundance and vertical profile in the Venus atmosphere.

Chemical interactions between hydrogen halide gases in the atmosphere of Venus and halogen-bearing minerals on the surface of Venus have been proposed to regulate or "buffer" the HCl and HF atmospheric abundances. The proposed chemical equilibrium models invoke equilibria between the gaseous hydrogen halides and simple halide salts (e.g., NaCl, CaF_2, etc.) which are probably unrealistic constituents of the surface of Venus. More realistic equilibria would involve halogen

bearing minerals such as chlorapatite $Ca_5(PO_4)_3Cl$, sodalite $Na_4Al_3Si_3O_{12}Cl$ and marialite $Na_4[AlSi_3O_8]_3Cl$ for which little or no thermodynamic data are available. The necessary laboratory measurements involve low temperature heat capacity measurements below 298 K, high temperature heat content measurements above 298 K, and enthalpy of formation measurements. The latter measurements can be done by a variety of calorimetric techniques.

Earth and Mars

The origin of the D/H ratios on Earth (about 160 ppm) and Mars (about 6 times the terrestrial value according to observations by Owen and colleagues) is still unexplained. The "cosmic" D/H value is only about 20 ppm and enhancement to Earth-like values by homogeneous gas phase isotopic exchange (between HD and H_2O, etc.) in the solar nebula appears to be kinetically inhibited over the lifetime of the solar nebula. Estimates of the rates of catalyzed isotopic exchange indicate that the heterogeneous reactions are still too slow to have proceeded over the lifetime of the nebula. Conventional wisdom is that the Earth-like values are therefore due to the accretion of the icy materials (e.g., from comets) that are already enriched in deuterium, perhaps as a result of ion-molecule exchange reactions in the interstellar medium. However, no data are available on the rates of D/H isotopic exchange catalyzed by either silicate or carbonaceous grains or on possible isotopic exchange effects during organic compound synthesis by Fischer-Tropsch-type (FTT) reactions. Both areas are actually at the interface between thermodynamics and kinetics, but need to be investigated to help provide the explanation for the terrestrial and Martian D/H values.

Gas Giant Planets

A wide variety of problems requiring new thermodynamic data can be identified for the gas giant planets, and I will try to indicate this diversity with a few examples.

Lewis originally proposed a trimodal condensation cloud structure of $NH_3(s)$, $NH_4SH(s)$, and aqueous solution/ice for Jupiter and Saturn. Although detailed cloud condensation models have been calculated by several groups, we still do not

have complete thermodynamic data for $NH_4SH(s)$, one of the three predicted cloud condensates. What is needed in this case are low temperature heat capacity measurements below 298 K, an enthalpy of formation, and vapor pressure data. The heat capacity data will give us an absolute entropy and the Gibbs functions so the vapor pressure data can be analyzed by both the second and third laws of thermodynamics.

The apparent depletion of NH_3 in the 150 - 200 K region of the atmosphere of Uranus by a factor of 100 - 200 times relative to the solar NH_3/H_2 mixing ratio has led to suggestions that NH_3 dissolution in aqueous solution clouds is responsible for the depletion. However, this suggestion has been disputed by other investigators who claim that the solubility of NH_3 in water is insufficient to account for the observed depletion. Some of this controversy is due to the conflicting thermodynamic data on NH_3 solubility used by the different investigators. Furthermore, with the exception of one group who incorrectly extrapolated low temperature solubility data to high temperatures, there has been no consideration of the effects of H_2S and other important solutes on the NH_3 solubility in the aqueous solution clouds. What is needed here is a vapor-liquid equilibrium study of the NH_3-H_2S-H_2O ternary up to the critical point in order to determine the solubilities and vapor pressures of the two solutes. Existing work on this ternary is too limited in scope to be of use and cannot be reliably extrapolated outside the experimental range.

Finally, the deep atmospheres of Uranus and Neptune may contain substantial amounts of water which will form a supercritical fluid capable of dissolving many "rocky" materials. For example, Kennedy and colleagues have reported that at the upper critical endpoint of about 1353 K and 9.7 kb where SiO_2-fluid-melt are in equilibrium, the silica solubility reaches 750 grams per 1 kilogram of fluid. Such behavior has important consequences for the partitioning of "rocky" elements such as P, Ge and As between the interiors and atmospheres of the gas giant planets. Suitably designed high pressure/high temperature phase equilibrium studies are required to map out the behavior of abundant "rocky" materials such as forsterite Mg_2SiO_4, enstatite $MgSiO_3$, troilite FeS, etc. in equilibrium with supercritical water. As a second step, it will also be important to consider the effects of solutes such as NH_3 which Lewis has suggested may enhance the solubility of "rocky" material.

Again a variety of topics that require new thermodynamic data come to mind. The low temperature phase equilibrium studies described by Thompson are clearly important for increasing our understanding of the outer planet satellites. Also, as mentioned in my invited review, in many cases the existing thermodynamic data for clathrates of cosmochemically important volatiles (CO, N_2, CH_4) are incomplete and were obtained under pressure/temperature conditions more appropriate for engineering applications than for the solar nebula. (However these thermodynamic data must also be complemented by studies of the effects of solar UV photons and charged particles on clathrate stabilities and chemical composition).

The origin of the dark material, presumably organic material on some outer planet satellites and (if Halley is typical) on comets also is an important problem which is not receiving the attention it deserves. Organic material on outer solar system bodies (and indeed organic material accreted by the Earth) may have been formed from nebular CO and H_2 via Fischer-Tropsch-type (FTT) reactions which are heterogeneous reactions catalyzed by Fe-bearing materials. These reactions were extensively studied by Anders and colleagues 20 years ago when they synthesized complex organic compounds analogous to those in carbonaceous chondrites. However further experimental studies of FTT reactions have not been pursued since that time. What is needed are quantitative laboratory studies of product yields, product distribution, and formation rates as a function of parameters such as temperature, H_2 pressure, H_2/CO ratio, catalyst type and treatment, etc. These studies have potential applications in many areas of planetary science.

ACKNOWLEDGMENTS

My planetary atmospheres research is currently supported by the Max-Planck-Institut für Chemie. I thank Ken Fox for his patience during the writing of this paper, Diana Quillen for volunteering to do word processing, and Heidi Hansen, Chris Sobon, and the staff and students of the MPI for their help and support.

CHARGED PARTICLE INTERACTIONS

L. J. LANZEROTTI
AT&T Bell Laboratories, Murray Hill, NJ 07974

INTRODUCTION

Studies of the interactions of charged particles with gaseous and solid surfaces have long been associated with the national space research program. The directions and emphases of the laboratory research have changed with time as the space research efforts have evolved. A major area of laboratory investigation has been the determination of the cross sections for light emission of Earth's atmospheric gases under bombardment by electrons and ions with energies characteristic of those in the magnetosphere. The obvious objective has been to obtain an understanding of auroral processes. During the years of detailed analyses of lunar materials returned to the Earth, laboratory studies of the erosion and implantation rates of ions into the lunar regolith was intensely pursued. Studies of the influences of ultraviolet photon fluxes on gases and solids has also been actively pursued.

Charged particles are ubiquitous in the solar wind and in the magnetospheres of the planets, as are the photon fluxes from the sun and from distant stars. As such, it is mandatory that experiments be carried out in order to understand the influences of the radiations on solar system gaseous and solid materials.

A schematic illustration of some of the processes resulting from the stopping of electron and ion fluxes in materials is shown in Fig. 1. Protons, heavier ions, and electrons can produce physical modifications in the material as well as act as a "catalysis", producing chemical changes on the surface and in the interor bulk of the material. The physical modifications include the ejection of electrons and other surface materials from the impacted object. The higher the energy of the incident charged particle, the deeper is the penetration of the primary particle into the material, and thus the deeper can be the modification of the material.

The ejection of electrons and ions from surfaces occurs by electronic processes, in the case of electron, photon, and high energy ions, while lower energy (order few keV and lower) ions can produce ejection by nuclear processes. The modification and injection processes depend upon the energies of the incident radiation, the nature of the material exposed to the radiation, and the temperature (in the case of ices) of the material. For example, for protons incident on stainless steel, the sputtering yield Y (the number of ejected particles per incident ion) has a peak value of $\sim 10^{-2}$ at an incident ion energy of ~ 1 keV. At ~ 1 MeV, $Y \sim 10^{-4}$. This sputtering occurs by nuclear collisions and can be calculated from first principles. About a decade ago, it was discovered that for insulating materials like ices, which can comprise grain materials, and many of the satellites of the outer planets, Y is of the order of one for MeV-energy ions and can reach values as large as 10^2 to 10^3 for incident heavy ions. In this case, the sputtering occurs by electronic processes and is, as yet, not calculable from first principles for a given target material and incident ion.

PRECEDING PAGE BLANK NOT FILMED

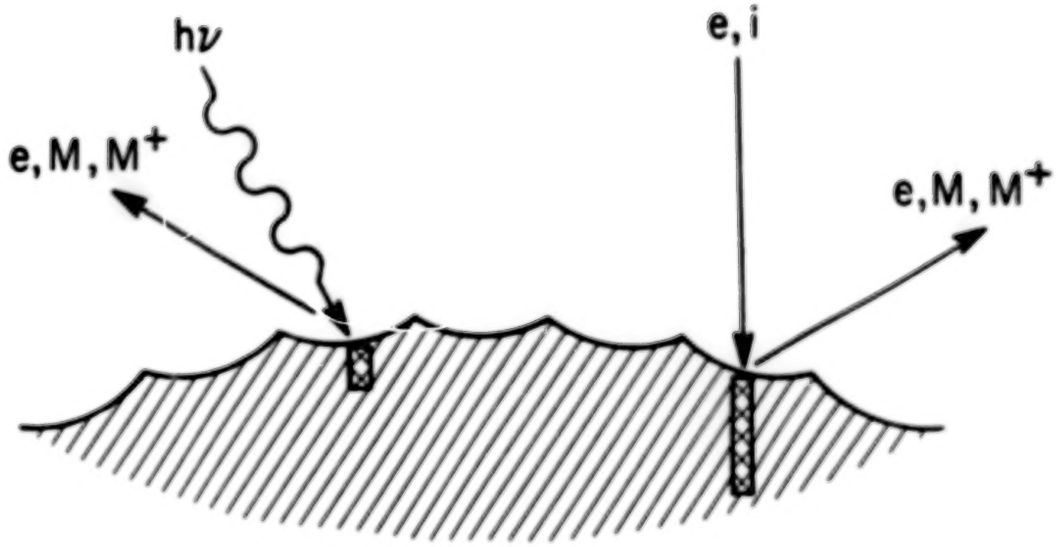

- SURFACE MODIFICATIONS
- SURFACE "CATALYSIS"
- PARTICLE EJECTION (SPUTTERING)

INCIDENT	
e, hν	i
ELECTRONIC	ELECTRONIC NUCLEAR

FIGURE 1

The importance of sputtering and modification of solid materials for planetary atmospheres arises because such radiation-affected materials can be incorporated into the matter which constitutes existing planetary and satellite atmospheres; further, the sputtered matter from a satellite can constitute a portion, or all, of a satellite's atmosphere. (In addition, there are significant planetary "geological" interests in the modifications of surfaces that can occur from particle interactions with the material itself.)

SOLID SURFACES

In this conference, the processes by which charged particles can affect solid surfaces was reviewed by Boring, who also presented a overview of the variety of laboratory data which have been assembled over the last decade. Boring showed that, while a great deal of information exists related to radiation effects on the distinctive ices in the solar system, much work remains to be done in assembling a larger empirical data base of sputtering yields and modification rates and in producing predictive theoretical physical and chemical models.

In addition to the sputtering of surfaces by charged particles, photons, as noted above, can also produce erosion of materials. Little data exist related to the erosion rates of water ice (the primary constituent of many of the satellites of the outer solar system) by incident ultraviolet photon fluxes. At this meeting, some preliminary work on the studies of the erosion of water ice by incident ultraviolet photons was reported by Wu and Judge. They find that the erosion rate for producing H_2O^+ is of the order of 10^{-4}, and that the injection rate for electrons from water ice is of the order of 4×10^{-4}. The experimental capability for detecting the sputtered neutral water atoms does not as yet exist. However, from studies of the charged particle erosion of water ice, it can reasonably be expected that the yield of neutrals is of the order 10^3 to 10^4 (or perhaps even more) times the erosion rate for the water ions. While this laboratory study is just beginning, the potential importance of these results for the outer planets, particularly for the satellites of Saturn and the ring materials, including the E ring, is great.

Another contributed paper related to the effects of charged particles on solid materials was presented by Moore. She investigated the mass spectrum eroded by Mev-energy protons incident on polyoxymethylene (POM) material. She found peaks in the mass spectra very similar to those seen in ions measured by the PICCA instrument on the Soviet Vega spacecraft. The total erosion rate of the POM material has not as yet been measured in order to conclude at what solar radial distance the competition between erosion from solar heating and erosion by charged particles tilts to one or the other process as a dominant mechanism.

An interesting juxtaposition at the meeting was the discussion by Boring of the alterations of icy materials by ions and the discussion by Fegley of the Fisher-Tropsch (F-T) synthesis process on the surfaces of materials, particularly grains. Fegley is interested in the F-T process because grains with products synthesized in the early solar system could become the constituents of the satellites and atmospheres of the outer planets. Considerable discussion centered on the requirements, in many cases, for very clean surfaces for this synthesis process to occur. The very clean surfaces employed in laboratory experiments contrasts sharply with the probably dirty and

irregular surfaces in the interplanetary and interstellar media. An interesting issue in the discussion was that the synthesis can significantly slow after a surface becomes covered with the newly-synthesized material. The question then arises as to whether ion-induced catalysis on surfaces and in the bulk of material might become more relevant than the Fisher-Tropsch synthesis after a surface becomes covered and less able to provide the necessary conditions for the F-T process. These discussions brought out clearly that an understanding of the relevant rates for photon- and ion-induced catalysis effects is very much needed, particularly the relative importances of the two radiation sources in the distant solar system as well as in the early solar nebula. Now that measurements on the Voyager and Pioneer spacecraft have provided the relevant ion fluxes, such comparisons can be done for the present conditions in the solar system.

Another discussion at the meeting concerned the existence or not of clathrates in some of the solar system ices and in the grain materials which comprise comets, icy satellites, and atmospheres of the planets. Furthermore, there are important questions as to the survivability of clathrate structures under radiation bombardment. The "trapping" of methane and other gases in water cages could have been of considerable importance in the early evolution of the solar system. However, given the near 100% probability that ices condensed in the early solar nebula in a sea of plasma, would the formation of clathrates have been possible? In particular, what would the relative rates of formation to destruction of clathrates be in the solar wind of the early solar nebula? A final, most basic, question involves how good the models are for the physical characteristics of the early solar system, in particular the photon and plasma fluxes? What can be learned about possible fluxes from studies of similar G-type stars and stellar winds in the galaxy?

PARTICLE-GAS INTERACTIONS

Trajmar presented a review of the present status of electron impact spectroscopy. He discussed experimental techniques related to electron impact spectroscopic studies of atomic targets and provides in his paper extensive references to laboratory data containing cross-section information for a variety of electron interaction effects. He points out that similar studies of molecular targets largely do not exist and are very complicated. This is an area of laboratory investigation that needs much further pursuit.

Studies of the optical signatures of clusters by use of laser beam techniques was presented in a contributed paper by Duncan. He pointed out that important future work in cluster studies involves the use of photons for the excitation and dissociation, since studies of carbon clusters are important in astrophysical environments. Duncan's paper raises interesting questions that have begun to intrigue planetary and astrophysics researchers: that is, how large does a carbon cluster or silicate cluster have to become before a material can be treated as a bulk material, and therefore a "grain"? It was pointed out in the discussion that even as many as 10^4 carbon atoms, which produce bulk behavior, can actually exist in a "cube" of small facial dimensions. Hence, studies of carbon clusters and their stability under particle and photon radiation, as well as their optical signatures under possible dissociation processes, can be important for astrophysics.

Another particle-gas experimental result was contributed by Sack, who studied the effects of 6.5 MeV protons on methane gas at one bar pressure and at ambient temperatures to produce molecular species. The primary purpose of this study was to examine the influences of high ionization densities on atomic processes by pointing out the differences that might occur in laboratory experiments, with high radiation fluxes, and the actual situation in astronomical regimes where the particles fluxes can be substantially less intense and collective effects are not important. Sack points out that his work can perhaps be relevant for studies of auroral atmosphere conditions.

SUMMARY

Two review papers and four contributed papers were devoted to laboratory studies of photon and charged particle interactions with matter. In addition, one of the review papers by Fegley addressed the issue of catalysis processes on surfaces and their possible importance for planetary atmospheres and satellite materials. The review and contributed papers raised a number of interesting and important questions relevant to the role of charged particle and photon interactions with solar system materials and pointed out the areas where substantially improved, new, and additional measurements are required in order to gain an understanding of planetary observations and to provide constraints for theoretical modelling. It is expected that in the next few years many additional insights will be obtained from laboratory measurements of radiation interactions with matter.

APPENDIX ONE: SPASE REPORT

FOREWORD

In the Spring of 1987, the NASA Planetary Atmospheres Management Operations Working Group (PAMOWG) created a Subgroup on Strategies for Planetary Atmospheres Exploration (SPASE) which was charged with the task of identifying and documenting appropriate areas for augmentation within the Planetary Atmospheres Program. Specifically, SPASE was asked to identify that area of atmospheres research where the need for additional support is particularly urgent, given the present status of the field and of current and planned NASA programs in planetary science.

After much deliberation, the SPASE group concluded that the area of research most in need of augmented support is that of laboratory measurements. The priority of this area is viewed as particularly timely in the interim period between launches of new planetary spacecraft, since it considers the need for laboratory-aided interpretation of existing data sets and anticipates observations from Hubble Space Telescope (HST), Galileo, Magellan, Mars Observer, and the CRAF/Cassini spacecraft. Laboratory studies form one element of the four essential components of a strong planetary program. These four elements are: flight missions, ground based and earth orbital astronomy, laboratory research, and data analysis and numerical modelling. The unanimous view of SPASE is that, in order to maintain a vigorous program in planetary atmospheres research, additional support is urgently needed for both upgrades in laboratory equipment and growth in human resources.

This document presents examples of the kinds of laboratory work identified by SPASE which could lead to notable advances in specific areas of planetary atmospheres research. It is estimated that a level of effort of at least $2M/yr, supporting on the order of 15 laboratory investigations, together with regular topical meetings or conference sessions, could lead to an effective revitalization of this area of research. A suggested plan for implementing a planetary atmospheres laboratory program of this scope is given in this report following a discussion of illustrative science objectives of the proposed initiative. These examples are not intended to be inclusive nor to represent a prioritization, and may include references to published work without formal acknowledgement in the interest of brevity.

PRECEDING PAGE BLANK NOT FILMED

PLANETARY ATMOSPHERES MANAGEMENT OPERATIONS WORKING GROUP

SUBGROUP ON

STRATEGIES FOR PLANETARY ATMOSPHERES EXPLORATION (SPASE)

Sushil K. Atreya
Department of Atmospheric
and Oceanic Science
University of Michigan

Jay Bergstralh
Atmospheres and Cometary
Sciences Section
Jet Propulsion Laboratory

John J. Caldwell
Department of Physics
York University

Kenneth Fox
Department of Physics and Astronomy
University of Tennessee

James F. Kasting
Space Science Division
Ames Research Center

Janet G. Luhmann (co-chair)
Institute of Geophysics
and Planetary Physics
UCLA

Jonathan Lunine
Lunar and Planetary Laboratory
University of Arizona

Daniel J. McCleese (co-chair)
Atmospheres and Cometary
Sciences Section
Jet Propulsion Laboratory

Jurgen Rahe
Planetary Astronomy Program
Solar System Exploration Division
NASA Headquarters

Richard E. Young
Space Science Division
Ames Research Center

I. INTRODUCTION AND OVERVIEW

A. Science Goals

The overall goal of planetary science is to learn about the current state of the solar system and to try to understand its formation and evolution. What physical events led to its formation? How did it and its constituents - planets, atmospheres, satellites, rings - evolve from their primitive states to their present conditions? What can comets tell us about the early history of the solar system? What will this tell us about the existence of other solar systems? What can we learn about the future habitability of our home, the Earth, as it responds to natural and anthropogenically influenced evolutionary processes?

The study of planetary atmospheres is a vital component of this more general research program. NASA's Solar System Exploration Committee (SSEC) has recognized this point in its 1983 report "Planetary Exploration Through the Year 2000-A Core Program". That document lists as primary objectives:

For Venus - Determining "the composition and concentrations of the various photochemically active gases in the 65-135 km altitude region" and investigating "the physical and chemical interaction of the surface with the atmosphere and the composition and formation of atmospheric aerosols"

For Mars - Determining "the distribution, abundance, sources, and sinks of volatile material, including an assessment of the biological potential of the Martian environment now and during past epochs"; establishing the nature of "the interaction of the surface material with the atmosphere and radiation environment"; and exploring "the structure and the general circulation of the Martian atmosphere"

For comets - Determining "the processes that govern the composition and structure of cometary atmospheres"

For Jupiter - Determining "the chemical composition and physical state of its atmosphere"

while the atmospheres of Saturn and its satellite Titan are identified as major targets for our next phase of planetary exploration.

In each of these areas and others selected for emphasis in planetary research and mission planning, supporting laboratory studies are required to glean meaningful information from both spacecraft and ground-based measurements.

B. The Problem

There are important areas of planetary atmospheres research where further progress is severely constrained by lack of supporting laboratory data. Some of these areas are identified in this report. These include: studies of the chemical and thermodynamic stability of the gases that make up planetary and satellite atmospheres (particularly with regard to trace constituents and ionospheric properties which relate to the atmosphere and external influences from sun, solar wind and magnetosphere); studies relating to chemical kinetics, in particular of reaction rates relevant to planetary atmospheres; studies related to the interpretation of the broad variety of spectral data from planetary observations (e.g., high resolution spectra of methane at short wavelengths, and photon spectra of dimers and molecular complexes); and research on the optical and physical properties of condensate aerosols for probing the giant planets.

C. The Solution

We suggest a broadened program of laboratory investigations, including experiments in chemical kinetics, photon and electron spectroscopy, and thermodynamics to fill these important data gaps. This program requires both tools (such as temperature-variable and high pressure absorption gas cells and light sources), and the essential manpower levels of effort for effective use of these tools. An implementation plan is proposed in the final section of this document.

II. PROGRAM OBJECTIVES

Examples of scientific objectives in planetary atmospheres research for the outer planets, terrestrial

planets, and comets which are particularly in need of laboratory studies are outlined here, together with descriptions of the laboratory work required to address those needs.

A. Outer Planets

Jupiter, Saturn, Uranus and Neptune are gaseous down to altitudes where the pressure is 10,000 bars or greater. Their present atmospheric compositions represent the initial endowment of elements, which reflects both solar abundances and enrichment processes which occurred during planetary formation. The enrichment of carbon in the atmospheres of the giant planets, as well as the enhanced heavy element abundances inferred from gravitational moment data, suggests that these bodies formed by accretion of solid cores, followed by gravitational collapse of gas onto these cores and perhaps additional infall of cometary debris.

A number of specific questions concerning the formation of the giant planets can be addressed through observations of their present properties. What is their complete atmospheric inventory of molecules and atoms? The answer ties the inferred heavy element cores to identified atmospheric molecular species. What are the structure and dynamics of the clouds in the Jovian planet atmospheres? This question bears on the abundance of major species and on the mechanisms for heat transport through the regions of these planets which are observable. The diurnal and seasonal effects of sunlight on the planets' energy budgets are revealed most clearly through cloud properties. What is the composition of the upper atmosphere and what physical and photochemical processes are occurring there? This information is required to understand exogenic effects which may affect our interpretation of the internal processes in these planets and our understanding of their internal energy balance.

There are also a number of special scientific problems connected with the satellites of the giant planets which are by-products of the formation of the planets themselves. The large icy satellites may have retained most of their original volatile inventories (e.g., methane and nitrogen), and display a range of physical and chemical processes resulting from the presence of these species. Characterization of the volatile inventories of satellites such as Titan and Triton constrains models of the environment in which they formed and, hence, conditions during the time of giant planet formation. An understanding of the physics and chemistry of atmospheric haze and cloud structures is required to do this, as well as to quantify the seasonal and long-term evolution of the climates on these bodies.

Most of what we know about the giant planet atmospheres is inferred from the interpretation of observations taken with a broad spectrum of remote-sensing techniques, including (ultraviolet, visible, and infrared) spectroscopy and imaging, radiometry, passive radio observations, and radio occultations. As high quality observations from spacecraft have become available, the need for laboratory data to support their interpretation has become essential. Occasionally, the planetary data are far superior to the quality of the laboratory data used to analyze them. This situation is likely to become more acute as highly sophisticated (high spectral and spatial resolution) observations are carried out by experiments connected with new missions such as the Hubble Space Telescope, Mars Observer, Galileo, and CRAF/Cassini as well as from the ground.

Interpretation of infrared, visible and ultraviolet spectra requires high-resolution laboratory spectroscopic data acquired at temperatures and pressures appropriate to solar system atmospheres. Thermodynamic and kinetic data are required to interpret abundance measurements in terms of dynamical and thermochemical processes in atmospheres. Likewise, ionospheric measurements can only be understood correctly when rates and quantum yields of significant reactions have been measured under environmental conditions similar to those encountered in planetary atmospheres. The following subsections describe examples of laboratory experiments and data that are needed for the interpretation of state-of-the-art observations of the atmospheres of the giant planets.

1. Thermodynamical Measurements

Knowledge of the nature of the hazes and of the abundance and stability of methane is crucial for understanding the atmospheric thermal structure on the giant planets. To interpret Voyager photopolarimetry and imaging data properly, saturation vapor pressure measurements of hydrocarbons are required at the low temperatures prevalent in the tropospheres and stratospheres of these planets. The vapor pressure measurements

of the gases need to be carried out not only in equilibrium with their parent ices or liquids, but also in the presence of other gaseous and condensed constituents.

In the tropospheres of the giant planets, interpretation of ground-based and spacecraft observations of condensates of ammonia, ammonium hydrosulfide, hydrogen sulfide, ammonia hydrates, and water depends upon accurate information on vapor pressures and, more generally, on the solid-liquid-vapor phase diagrams of these various substances. Such interpretations include, for example, the inversion of cloud density profiles to derive abundances of the molecular species and to probe convective processes in the troposphere. In turn, these inferences bear on the fundamental issues of elemental abundances and mechanisms of energy transport in the giant planets and place constraints on models of the origin and evolution of these major bodies of the solar system.

In the case of Uranus and Neptune, the presence of an aqueous ocean below a hydrogen-dominated atmosphere requires accurate thermodynamic data on water-hydrogen mixtures at high pressures. Condensation of constituents in the form of clouds or hazes is not limited to Uranus and Neptune, but is equally relevant to Titan and perhaps to Triton and Pluto where compounds also undergo condensation. Much of the thermodynamic data at the appropriate environmental conditions for the nitrogen-methane, ethane-methane, nitrogen-ethane-methane and nitrogen-methane-noble gas systems are either lacking or are highly uncertain. Proper interpretation of ground-based radio observations, and planned Cassini probe investigations of the atmosphere and surface of Titan, depend on these data. The same may be true for upcoming Voyager investigations of Triton.

The more specific thermodynamic investigations mentioned in the following paragraphs are selected to give an indication of the type of laboratory experiments which must be performed to fully utilize planetary data on condensing volatile materials in the outer solar system.

a) Phase relationships in the nitrogen-sulfur system

In the tropospheres of the giant planets, certain volatile species are predicted to condense at high altitudes. Roughly coincident with the upper portion of the predicted water cloud region is a region of ammonium hydrosulfide condensate. This ammonium-hydrosulfide cloud is important for three reasons: (1) it is an indicator of the sulfur abundance in Jupiter and Saturn; (2) it is a possible sink for ammonia (which is inferred to be below the solar abundance based on radio observations); and (3) it is an additional source of cloud material in a region which is often regarded as being occupied solely by water clouds. The last point is critical, because the extent of water clouds in the Jovian troposphere tells us about the elemental oxygen abundance in Jupiter's interior, as well as modes of convection in the troposphere.

Accurate prediction of the extent of the hydrosulfide cloud depends on knowing the vapor pressure in equilibrium with the cloud particles. In this case the necessary quantity is the free energy of formation of ammonium hydrosulfide condensate from gaseous ammonia and hydrogen sulfide. Experimental and theoretical estimates of the free energy vary by a factor of 3, leading to an uncertainty of a factor of 10 in the vapor pressure. This uncertainty will be the limiting factor in analysis and interpretation of Galileo probe data on this cloud region. Interpretation of Galileo probe data with more accurate thermodynamic information would lead to an understanding of the sulfur abundance and of the composition and structure of cloud layers in this complicated region of the troposphere. Accurate thermodynamic measurements would also provide key supporting data for determination of the elemental nitrogen abundance, the true extent of the water cloud, and hence the elemental oxygen abundance. These are key inputs to models of the origin and interior evolution of the giant planets.

What is needed is an experiment to measure the free energy of formation of ammonium hydrosulfide under Jovian temperature and pressure conditions and, more generally, to determine the thermodynamic properties of mixtures of nitrogen-, sulfur-, and oxygen-bearing molecules under conditions similar to those in the Jovian troposphere. Experiments on the thermodynamics of water-ammonia systems under Jovian conditions are also required to determine accurately the vapor pressures over the liquid solutions and the solid hydrates of ammonia.

b) Phase equilibria in the methane-nitrogen-ethane system

The troposphere of Titan is characterized by a modest greenhouse effect driven by nitrogen, methane, and hydrogen gases. Additionally, saturation of methane is predicted at an altitude several kilometers above Titan's surface, and the resulting clouds are predicted to incorporate nitrogen as solution droplets. Closer to the tropopause, solid methane clouds are predicted as the temperature falls below the liquidus for this binary system. The temperatures over which thermodynamic conditions are favorable for cloud formation range from 70 to 90 K; vapor pressures over this range vary by orders of magnitude. It is easy to see that without appropriate laboratory investigations of the solid-liquid-vapor system, the utility of information obtained by both the Cassini probe and ground-based measurements of Titan's atmosphere will be limited.

Models of the surface of Titan predict the presence of an ethane-methane-nitrogen ocean. The ocean and atmosphere are tightly coupled; hence changes in ocean composition change the thermal balance and composition of Titan's atmosphere. The thermodynamics of the ternary system are sufficiently uncertain that they limit the accuracy of models of the evolution of Titan's atmosphere and surface. Uncertainties include mixing in the liquid state and vapor pressures over the liquid and solid-liquid portion of this phase diagram. Understanding of each of these aspects is essential in constructing models of the coupled evolution of Titan's surface and atmosphere, as methane photolysis changes the ocean composition through time. Moreover, the surface of Neptune's satellite Triton may contain both methane and nitrogen in condensed form. Accurate understanding of the phase relationships in these systems at low temperature (< 60 K) is essential for modeling the surface and atmospheric properties from Voyager and ground-based data. The thermodynamic experiment results reported in the literature may not be applicable because they have been affected by very slow approaches to equilibrium (metastability), particularly at lower temperatures. With that understanding, new experiments which measure the solid-liquid, liquid-vapor, and solid-vapor equilibria in the binary and ternary systems of nitrogen, methane, and ethane under conditions appropriate to the surfaces and atmospheres of Titan, Triton, and Pluto need to be carried out. Similarly, the roles of other cryogenic condensates, such as carbon dioxide, carbon monoxide, and noble gases, which may also be present on these outer planet satellites, must be determined with additional thermodynamic data on mixing and solubility in an appropriate environment.

2. Spectroscopic Measurements

Among other things, spectroscopic observations tell us that the atmospheres of the outer planets and some of their satellites are abundant in gaseous methane. The availability of visible overtone spectra of this constituent at low temperatures, over long paths, and at high resolution, ultimately determines our ability to understand clouds and hazes on Jupiter, Saturn, Uranus, Neptune, and Titan. Another example where spectroscopy plays a key role is in determining the surface state (gas, liquid and/or solid) of methane on Triton and Pluto, which is poorly known because of incomplete laboratory data on the near-infrared spectra of condensed phases. There is a strong need for low-temperature (60-200 K) data. Yet another example is that of acetylene, which is the strongest absorber on Jupiter and Saturn, and probably on Uranus and Neptune, and plays an important role in the formation of aerosols in their respective atmospheres. Data at sufficiently low temperatures for the ultraviolet spectral region, corresponding to the high resolution capabilities of the Hubble Space Telescope, are not presently available. In some cases, appropriate laboratory facilities for the relevant experiments may exist, but the necessary data must be secured. Because spectroscopy encompasses such a wide range of observational techniques and scientific problems, it is worthwhile to organize the remainder of this discussion according to the wavelength ranges.

a) Ultraviolet spectroscopy

With the imminent launch of the Hubble Space Telescope, planetary spectra below 200 nm wavelength, with spectral resolution from 10^3 to 10^5, S/N greater than 100, and spatial resolution of order 1 arc sec, will routinely be available. These spectra will be at least an order of magnitude better in each of these characteristics than those obtained with the International Ultraviolet Explorer, for which existing laboratory data are only marginally adequate. To compound the problem, many gases of interest may have "hot bands" that influence room-temperature spectra, but are unimportant at temperatures of planetary interest (150K). Existing laboratory spectra are all at room temperature.

Improved laboratory ultraviolet spectra will be essential in investigations of the stability of methane on the outer planets. Methane is destroyed in outer planet atmospheres by solar ultraviolet photons and charged particles, yet this important trace gas is apparently quite stable. This stability can be studied by investigating the abundance and distribution of methane's photolysis products. A prominent product is C_2H_2, which dominates the absorption spectra of Jupiter and Saturn below 200 nm. In principal, information on both the abundance and altitude distributions of C_2H_2 is contained in the planetary spectra, but our ability to interpret this information is severely limited by the inadequacy of the laboratory data. In particular, since C_2H_2 is known to be one of those constituents having low-lying energy levels which produce infrared "hot bands" at room temperature, a low temperature facility is required for the relevant experiments.

Laboratory spectra are also required to permit the identification of other gases which may be present in much smaller amounts on the outer planets, such as C_2H_4, C_3H_4 and C_4H_2. Spectra of these constituents have similar but not identical band structure. C_6H_6, which is present at Jupiter's poles, has characteristic spectral features near 180 nm. In addition to providing quantitative information on CH_4 stability, these trace molecules are important for understanding the formation of stratospheric polymer hazes (such as polyacetylenes) in the giant planets' stratospheres. While C_2H_2 is regarded as the most probable precursor to planetary haze particles, determining the relative abundances of large molecules such as C_4H_2 (which is linear) and C_6H_6 (which is a ring) is necessary for understanding the microphysical processes by which the polymers form.

Another gas which is important for understanding processes in the atmospheres of the outer planets is CO, which has been detected on Jupiter and Saturn by near-infrared spectroscopy. (CO is also highlighted in a later section on chemical kinetics experients.) Because the continuum opacity in the near-infrared wavelength region is relatively weak, the inferred abundance refers to an integrated line-of-sight down to the troposphere. It is therefore difficult to derive more than a crude vertical distribution of CO from near infrared data.

Knowledge of the vertical distribution of CO is important because there are two possible sources for CO on both planets: internal and external. The external sources include reactions of ionized carbon and oxygen from planetary rings and satellites with neutral atmospheric species. The internal source is upward mixing from the interior. By differentiating between these sources, one can deduce information about non-equilibrium chemistry of the upper atmospheres of the Jovian planets and the efficiency of the vertical mixing processes from the interior. The vertical mixing efficiency has important implications for the entire cloud and haze structure and for the chemical composition of the troposphere. An unambiguous measurement of the stratospheric mixing ratio of CO would clearly distinguish between the alternate models for its source. If it were clear that the concentration in the stratosphere was greater than at lower altitude (as determined from infrared observations), the external source would be indicated.

Ultraviolet planetary spectra are naturally limited to the stratosphere by continuum Rayleigh scattering, which has a λ^{-4} cross-section dependence. Furthermore, CO has a distinctive spectral signature, the Cameron bands, near 200 nm wavelength, that is strong enough to reveal mixing ratios of order 10^{-7} in HST data. Unfortunately, the best laboratory spectra have insufficient spectral resolution and no information on line-broadening by H_2 as opposed to self-broadening by CO. Quantitative interpretation of ultraviolet HST spectral observations, with the objective of establishing the CO vertical distribution on Jupiter and Saturn, thus will require new laboratory data.

b) Near-infrared spectroscopy

Spectroscopic observations of the outer solar system objects, Triton and Pluto, have revealed the presence of methane on both, and possibly nitrogen on Triton. Our knowledge of the state of methane on the surfaces of these bodies relies largely on observations of absorption bands in the near-IR. Analysis of the shapes of these bands can potentially tell us how much methane (or nitrogen) is in gaseous form, what the particle size of the condensed species is, whether liquid is present, and whether different phases are physically and/or chemically mixed. The Voyager Triton encounter in 1989 will provide complementary data, but will only indirectly address the question of how much methane is in the condensed or gaseous phase and how much nitrogen is present. Such analyses are hindered by lack of comprehensive laboratory data for these materials at the appropriate temperatures (40-70K) and in various phases (gas, liquid, solid, fine/coarse grained, mixed/pure). Moderate resolution ($\Delta\lambda/\lambda \approx 1000$) spectra in the near IR (1-5 microns) of mixed and pure candidate surface

materials need to be obtained. Facilities exist, but their cryogenics capabilities require upgrading.

c) Far-IR/microwave spectroscopy

The thermal balance of volatile-rich objects in the outer solar system may be determined by non-polar or weakly-polar materials such as methane, nitrogen and carbon monoxide. These materials may have low emissivities in the far-IR region of the spectrum, where the Planck function peaks for Triton and Pluto, and so significantly raise the surface temperature determined by thermalization with incoming sunlight. Some work has been done on this problem for liquid methane, but there is little information on its solid phases. A laboratory study is needed to determine the far-IR and microwave spectra of condensed methane and nitrogen at low to moderate spectral resolution, from which we could calculate the thermal emissivity of these materials at very low (<60K) temperatures for application to physical models of the surfaces of Triton and Pluto.

A related problem which could also benefit from such a study is the spatial distribution of condensed phases of N_2, CH_4 and also C_2H_6 on the surface of Titan. Global models for condensates on Titan admit the possibility that the condensates are not uniformly distributed over the surface. Throughout most of the electromagnetic spectrum, Titan's atmosphere is sufficiently opaque that it is impossible to observe the surface directly from space. However, in the far-IR and microwave regions, the opacity greatly decreases, and a significant fraction of the net emission to space, as measured by Voyager or by the VLA, comes from the surface. If there are lateral variations in composition, with consequent variations in thermal emissivity, then a microwave sounder flying past Titan could record surface features. A microwave sounder is included in the Cassini orbiter model payload.

d) Visible overtone spectroscopy

High-resolution spectra of the vibration-rotational overtone bands of methane at visible wavelengths have been observed in the atmospheres of Jupiter, Saturn, Uranus, and Neptune. In Jupiter and Saturn, analyses of such bands provide detailed information on the structure and thickness of the ammonia cloud layer in the upper troposphere, since this layer strongly affects the radiative transfer in these bands. For Uranus and Neptune, the data allow the methane abundance to be derived above and below the methane cloud deck.

In order to analyze such data properly, the band and individual line strengths and shapes must be known at temperatures and pressures appropriate to the atmospheres being observed. This information is not currently available to the extent required by the planetary community. Uncertainties in the absorption band strength and shape for the CH_4 translate into poor fits between methane observations and models of haze structure in the upper Jovian troposphere. Advances in this area require the measurement of spectra of the visible and near-IR overtone structure of gaseous methane at high resolution (0.1 cm^{-1}) and low temperature (~70K) for a range of methane and hydrogen pressures. With the addition of such measurements on N_2, laboratory data can also be used to analyze the haze structure in Titan's stratosphere for which the methane data are available.

3. Chemical Kinetics

Knowledge of reaction pathways, rate constants, and quantum yields is critical to our understanding of the composition of the atmospheres of the giant planets and those of Titan and Triton. The giant planet atmospheres are torn between the thermally-induced drive toward thermodynamic equilibrium at great depths and the photochemically-induced drive toward disequilibrium in their uppermost regions. We have not yet been able to observe the chemical consequences of these competing influences, although this situation will be remedied to some degree for Jupiter by the forthcoming Galileo Probe. Clearly, if we are to take full advantage of this mission, it will be necessary to understand as much as possible about the kinetics of photochemical and thermodynamical processes operating in the Jovian atmosphere. Titan's photochemistry is also of interest because Titan is often identified as a natural laboratory for studying some of the photochemical processes that may have been important in the atmosphere of the primitive Earth. Relevant chemical data is to be collected by the Titan probe on the planned Cassini mission. Following is a list of several more specific examples of planetary atmospheres investigations to which additional laboratory kinetic data would contribute significantly.

a) Hydrocarbon photochemistry on Titan

Although the bulk of Titan's substantial atmosphere consists of N_2, the most important gas from a photochemical standpoint is CH_4. The photochemistry of CH_4 begins either with direct photolysis at wavelengths shorter than 1600 Å or with reactions with C_2 and C_2H radicals produced from photolysis of C_2H_2. These processes result in the production of reactive radicals which interact chemically with each other and with other gases in Titan's atmosphere to produce a wide variety of higher hydrocarbons. This organic synthesis process is considered to have at least two important consequences for the evolution and current state of Titan's atmosphere. One of these reactions is hypothesized to have converted a substantial fraction of Titan's original methane endowment into ethane. It has even been suggested that the surface of Titan is covered by an ethane ocean produced in this manner. Other reactions are known to lead to the formation of polyacetylenes. Such compounds are considered as possible precursors to the particles that constitute haze layers on Titan, Jupiter and Saturn. Although the general nature of this hydrocarbon chemistry is known, the details of the reactions involved are often poorly understood. It is especially important to understand the influence of a dominant background gas, such as N_2 for Titan and H_2 for Jupiter and Saturn, on reactions such as the one above. Chemical kinetics laboratory experiments are capable of providing such information.

An additional category of hydrocarbon reactions that require further study involves interactions with oxidizing radicals such as O and OH. The application here is mainly to the atmosphere of early Earth. Would the presence of oxidizing radicals have short-circuited particle formation, or would the early Earth, like Titan, have been enveloped in photochemical smog? The atmosphere during the Archean era (3.8 to 2.5 b.y. ago) may well have been low in O_2 but rich in methane as a result of the activities of methanogens. The photochemistry of such an atmosphere would probably have been dominated by reactions of methane and its by-products with O and OH radicals produced from photolysis of CO_2 and H_2O. Some of these reactions are known from combustion studies, but many still require laboratory analysis.

b) CO - CH_4 interconversion

Carbon monoxide is known to be present in the troposphere of Jupiter and Saturn. Its relatively high abundance is much greater than that which would be expected to prevail at thermodynamic equilibrium. Since there are not enough oxidizing radicals in the troposphere to produce this CO from CH_4, CO must be transported upward from high-temperature regions deep within Jupiter's atmosphere. The presence of CO in the troposphere implies that the rate of vertical transport exceeds the rate at which CO can be reduced to CH_4 by H_2 or other reducing species. The rate of vertical mixing could therefore be inferred if one understood the kinetics of the reduction process. The major pathway is thought to involve a reaction of formaldehyde with molecular hydrogen. Unfortunately, the relevant reaction rates and pathways are not well known. The currently used rate constant gives an implied vertical eddy diffusion coefficient K for the deep Jovian troposphere that is 10^3 times greater than the eddy diffusion coefficient in Earth's troposphere. Such a value is consistent with the value needed to transport heat upward from Jupiter's interior by free convection; however, the uncertainty in the rate constant, which could be improved in the laboratory, corresponds to three orders of magnitude uncertainty in K.

c) Conversion of H^+ to molecular ions

A discrepancy exists between the measured (Voyager radio occultation) and modeled electron concentration profiles at Jupiter and Saturn. The models provide one of the very few means of identifying the ions (as only electron concentrations were measured) and for understanding plasma dynamics and the upper atmospheric energetics of the outer planets. Thus it is important to investigate the reasons for the present discrepancy between the measured and modeled ionospheric structure.

It has been suggested that if the long-lived terminal ion, H^+, were converted to a short-lived molecular ion such as H_3^+ or H_2O^+/H_3O^+, resulting ion concentrations would be much reduced, bringing the measurements into agreement. The rate constants for the conversion of H^+ to H_2^+ and H_2O^+/H_3O^+ are, however, not available because the necessary laboratory experiments have not been done. The conversion rates need to be measured under appropriate planetary (pressure, temperature, auroral energy input) conditions.

B. Terrestrial Planets

At the same time that spacecraft data have greatly increased our knowledge of the terrestrial planet atmospheres, the data have raised new and important questions. For example, although the planets Venus, Earth, and Mars exhibit a number of similarities in terms of bulk composition, density, and in the case of Venus and Earth, size and mass, the present atmospheres are quite different. Understanding the processes by which these atmospheres, that originally may have been similar, evolved to such different states is one of the major questions confronting planetary scientists. An essential part of the problem involves identifying and studying those atmospheric and atmosphere/surface interactions which maintain the present states. To address properly these questions, we need laboratory investigations to understand atmospheric data that we already possess (such as that from the Pioneer Venus Mission) and to interpret the data that we will obtain in the future from projects such as Mars Observer and Mars Rover/Sample Return.

The types of laboratory measurements needed for the interpretation of inner planet data are not subject to the same categorization as are the laboratory measurements for outer planet data. Unlike the atmospheres of the outer planets, the terrestrial planet atmospheres differ markedly in composition, thermal structure, and volatile cycles. Furthermore, they have been more intensively investigated, so that the outstanding science questions are generally at a different level than for the outer planet atmospheres. Therefore, our discussion of the terrestrial planet atmospheres differs from that of the outer planets in that we discuss all types of laboratory measurements which bear on a particular science issue together.

The following subsections discuss specific examples where lack of fundamental knowledge on the radiative, thermodynamic, and chemical properties of various materials and chemical species limits progress in understanding the atmospheres of Venus and Mars, as well as the evolution of the Earth's atmosphere.

1. Sulfur Chemistry in the Venus Clouds

The Venus clouds have an important effect on the radiation budget of the planet and on the composition of its upper atmosphere. The clouds are radiatively active in the infrared, visible, and ultraviolet regions of the spectrum. Because of this, they are also important for understanding the dynamics of the Venus atmosphere, in particular the atmospheric super-rotation and various atmospheric waves.

A major portion of our current knowledge of the dynamic meteorology of Venus is based on UV images of the clouds, such as those from the Pioneer Venus Orbiter. However, the nature and origin of the contrasts in these images is unknown, as are the physical and chemical processes that might be important in producing them. The Venus clouds are known to consist principally of 85% concentrated sulfuric acid. This sulfuric acid is formed by oxidation of SO_2 that diffuses up from the lower atmosphere. The oxidation process is reasonably well understood, largely because of work that has been done in trying to understand acid rain here on Earth. The Venus atmosphere, however, has a much lower oxygen content than does Earth's. Less than 1 ppm of O_2 is present above the level of the cloud tops. This lack of oxygen (and ozone) allows solar ultraviolet radiation in the 200 to 300 nm range to penetrate into the upper cloud layer, initiating a whole new sequence of reactions that produce monatomic sulfur. The sulfur atoms thus formed may recombine with each other to form longer and longer sulfur chains. The thermodynamically stable form of elemental sulfur at low temperatures is S_8, but the Venus atmosphere probably contains a whole suite of gaseous sulfur molecules ranging from S_2 to S_{12}. Chains of five or more sulfur atoms can attach their free ends to form ring molecules. These molecules are considered to be a likely source of the absorption responsible for the UV contrasts. However, to infer the abundances of these elemental sulfur molecules, one needs to know their formation and loss rates. Unfortunately, none of the relevant rate constants is known with sufficient precision. Many of the steps in the S_8 formation sequence have not even been studied. Laboratory experiments involving the relevant sulfur-molecule producing reactions, together with measurements of the photolysis rates of S_8 and other sulfur ring molecules, are thus necessary for deriving the maximum science return from the UV images of Venus clouds.

The photochemistry of sulfur in anoxic atmospheres may have applications to the primitive Earth as well as to Venus. Recent studies suggest that elemental sulfur (and the ring molecules in particular) could have provided an effective screen against solar ultraviolet radiation, thereby facilitating the origin and early evolution of life. The sulfur could have been provided by volcanic outgassing of SO_2 and H_2S. Because the vapor pressure

of elemental sulfur is highly temperature-dependent, a warm surface and a dense CO_2 atmosphere would have been needed for such a screen to have existed. Experiments on the temperature sensitivity of sulfur chemistry will help to put such speculations on more solid footing.

Another key requirement for understanding the Venus cloud system involves an understanding of the chemical equilibrium between the cloud system and its "immediate" precursor gases (H_2SO_4, SO_3, and H_2O). This, in turn, requires the knowledge of the vapor pressure equilibrium conditions for concentrated H_2SO_4 solutions. While a number of laboratory measurements have been made which set upper limits on the partial pressures of gaseous H_2SO_4 and SO_3 surrounding liquid sulfuric acid, no direct measurement of the relative abundances of these constituents has ever been made. Such results would not only make it possible to better model the oxidation process by which SO_2 becomes H_2SO_4 and SO_3, but it would also become possible to recalibrate existing laboratory results for the microwave opacity from saturation abundances of H_2SO_4. This, in turn, would result in more acurate profiles of gaseous H_2SO_4 abundance derived from Pioneer Venus Orbiter radio occultation studies and from Magellan radiometric observations.

2. Water Vapor in the Venus Atmosphere

The determination of the water vapor distribution in the Venus atmosphere is important because water is crucial to the chemistry and physics of the clouds. Furthermore, it affects the radiative balance of the atmosphere, which in turn determines the atmospheric thermal structure and forcing for the general circulation. Based on data from Pioneer Venus and Veneras 11, 12, 13 and 14, it appears that the present water vapor content is between 50 and 100 ppmv near 25 km altitude, but only about 15 ppmv near the planet surface. Cloud level measurements indicate a mixing ratio of about 200 ppmv, decreasing to 30 ppmv above the clouds. There appear to be significant meridional and diurnal variations of water vapor above the clouds, and radiative balance considerations suggest a significant meridional variation in the lower atmosphere as well.

Certain aspects of the above measurements of atmospheric water vapor are extremely puzzling. Foremost is the unusual vertical profile in the H_2O mixing ratio implied by the data, in which the mixing ratio decreases toward the planet surface. Either the planet surface is a sink of water, or water vapor is chemically destroyed in the lower atmosphere. At the same time there must exist a source of water vapor, either higher in the atmosphere or elsewhere on the planet surface. Apart from the vertical profile, there is the question of what would maintain a meridional gradient in water in the lower atmosphere against atmospheric mixing processes. Such a meridional gradient implies sources and/or sinks varying with latitude.

Each of these questions stems originally from spectroscopic determinations of water vapor abundance made by spacecraft descending through the Venus atmosphere, or from radiative balance calculations based on net flux observations from descending spacecraft. A recent reanalysis of Pioneer Venus mass spectrometer data seems to confirm the existence of a vertical gradient in H_2O concentration. Nevertheless, these spectroscopic analyses must be considered uncertain, because the absorption properties of H_2O are not well known under Venus-like conditions. The Venera 11 and 12 measurements of H_2O were based on the analysis of water vapor bands at 0.94 μm and 1.13 μm. Analysis of these two bands for Veneras 11 and 12 yielded very different water vapor profiles. The absorption in the 1.13 μm band evidently implies a constant mixing ratio of H_2O of about 25 ppmv at all levels. The 0.94 μm band gives the inverted vertical profile described above. Synthetic spectra for these different H_2O profiles were matched against the spectra obtained by Veneras 13 and 14 between 0.7 μm and 1.0 μm. These comparisons also seem to indicate an inverted H_2O vertical profile, but it is clear that further laboratory spectroscopy studies are needed to resolve the problems in the interpretation of these combined data sets.

In addition to H_2O distribution, an essential piece of information for models of the greenhouse effect is the accurate knowledge of the opacity of H_2O vapor at visible and infrared wavelengths. Insufficient laboratory spectroscopic data are presently available at the conditions of high temperature and high pressure appropriate to the Venus atmosphere. In particular, more information is needed on CO_2-broadened line shapes and on hot bands not normally observed in Earth's atmosphere. We also need to understand "continuum" H_2O absorption caused by the far spectral wings of individual absorption lines. Better knowledge of infrared absorption by water vapor (and CO_2) should enable us to build realistic models of Venus' past and present climate, and to gain greater understanding of the operation of greenhouse effects in planetary atmospheres.

3. Mars Exploration

In the next decade, the Martian atmosphere will be studied by a series of American and Soviet spacecraft. These spacecraft will carry a new generation of instruments that will greatly increase our understanding of the structure and circulation of the Martian atmosphere, and the Martian climate. Successful analysis of these observations will require an improved understanding of the physical properties of Martian atmospheric materials. Therefore, laboratory studies in support of these missions should be initiated as soon as possible.

Atmospheric dust and condensates such as water ice and CO_2 frost are extremely important components of the Martian atmosphere. Laboratory measurements could provide much-needed information concerning the optical properties of potential Martian dust materials, as well as an improved understanding of the behavior of dust particles and aggregates in the Martian environment. Our understanding of Martian carbon-dioxide frost, which has no terrestrial analog, could especially benefit by new laboratory studies. At present, we do not have a definitive set of measurements of the optical properties of pure CO_2 frost at solar and infrared wavelengths, nor do we understand how surface CO_2 frost deposits behave in the Martian environment. Laboratory studies could also enhance our understanding of processes such as volatile adsorption in the Martian regolith and carbonate formation. Both of these processes may be important in determining the Martian surface pressure over the moderate to long timescales which characterize the planet's "climate."

C. Comets

The origin and evolution of comets are topics of great interest, not only in planetary science, but also in studies of the interstellar medium and of protoplanetary material in the vicinity of young stars. Comets are abundant in the solar system; estimates of their numbers range from 10^{10} to 10^{12}. They are diverse in size, composition, and chemical behavior, and they exhibit a wide range of physicochemical phenomena as they pass near the sun. Only in the last decade, and particularly with the data collected from the spacecraft flybys of Comets P/Halley and P/Giacobini-Zinner, has the range of cometary phenomena become fully recognized.

Laboratory studies play a vital role in understanding various cometary phenomena in the coma and in the dust and gas tails. Cometary phenomena are generally amenable to laboratory experimentation, but relatively little of this work has been done (except for spectroscopy). To describe the role of laboratories in the study of comets, it is most appropriate to divide the discussion into a section on experiments relevant to the nucleus and a section on experiments on cometary gases.

1. The Nature of the Nucleus

Cometary nuclei appear to consist of low-density ices of uncertain composition and structure mixed intimately with more refractory particulate materials. Much of the ice must be water, and much of the refractory material must be silicate mineral grains, but other ices and refractories have also been detected. There are almost no experimental data on the mechanical and thermal properties of fluffy ice and ice/dust structures. This is an area that could significantly benefit from laboratory studies.

The ices in cometary nuclei are thought to have condensed from partially altered interstellar matter prior to and during the protostellar phase of the solar system, so they may be similar to the icy mantles found on interstellar grains in dense molecular clouds. Only recently has the true chemical complexity of interstellar ices been appreciated. In addition to the common components H_2O, NH_3, and CO, new evidence suggests that interstellar ices also contain more complex molecules. These include methyl and methylene groups in molecules like esters, ketones, nitriles, and simple alcohols.

A recent proposal that polycyclic aromatic hydrocarbons are abundant in the interstellar medium suggests that they are also important in the composition of comets. The detection of organic grains in the coma of Comet P/Halley and the emission at 3.4 micrometers in Comets Halley and Wilson are evidence that these materials may indeed be significant. Therefore, ice studies should include investigations of individual condensed volatiles and mixtures, their behavior upon sublimation, the interrelationship with entrained refractory grains, and

the reaction of the mixture to the radiation environment in space.

We need detailed information on optical properties and the complete spectral signatures of ice clathrates, the physicochemical properties and conditions of formation of clathrates, clathrate hydrates, and amorphous mixtures of cosmochemical importance over the range of temperature and pressure relevant to the outer solar system, circumstellar disks, and dense molecular clouds where they are presumed to have formed. Experiments at several laboratories have shown that the vaporization of mixtures of condensed volatiles is a complex phenomenon depending upon species, relative concentrations, and processing conditions (e.g., proton and ultraviolet radiation). To this must be added uncertainties associated with the structure and inclusion of refractory grains and organic matter. In addition, the thermal conductivity of such material and the changes in the core structure with time and temperature need to be determined. It is clear that much laboratory work must be done before we can hope to understand what drives cometary behavior.

Material of lower volatility constitutes the high density component in cometary nuclei, and contributes to the dust ejected during rapid ice sublimation as well as to the build-up of a refractory crust. Silicate grains and unspecified organic grains of high molecular weight are known to occur in the dust coma, and must therefore come from the nuclear ice-refractory mass. Other refractories of unknown composition must also exist in the coma and in the nucleus. The minerals magnetite and laboratory-produced amorphous carbon have been used as likely analog materials in dust models simply because their optical properties are available.

Additional work is needed on the Fischer-Tropsch catalysis of organics on interstellar grains, on the chemistry of ices with inclusions of polycyclic aromatic hydrocarbons, and on the general problems of the origin and evolution of other complex organics in the cometary environment. For example, the peak position of the 3.4-mm emission feature measured in Comets P/Halley and Wilson falls at the high frequency extreme of the normal spectral range for saturated aliphatic hydrocarbons, implying that the CH_2 and CH_3 groups are attached to strongly electronegative groups. Polycyclic aromatic hydrocarbons are very electronegative. Furthermore, complex organics containing these aromatics have exceedingly low vapor pressures and are thus reasonable candidates to consider as part of the non-volatile grain component.

2. The Nature of the Volatile Component

The coma of a comet, the extended atmosphere around the nucleus that occurs during the release of gas and dust, is highly dynamic because of changing insolation (which changes the rate of gas and dust release and the ensuing photochemistry), and hydrodynamical interactions with the solar wind. Owing to the dynamical environment and the fact that the coma consists of dust particles, ice grains, molecules, neutral radicals, atomic species, and molecular ions, the range of physico-chemical phenomena that occur there is enormous. Hydrogen dominates the gas component of the coma, but all of the cosmochemically abundant elements (H, C, N, O, and S) are well represented, as are the most abundant metals.

Three major approaches to analysis of ground-based observations of cometary coma gases are the Haser model, the vectorial model, and chemical models, in order of increasing complexity and (presumably) of reality. The Haser model assumes a simple two (or occasionally three) generation parent molecule and daughter photodissociation product expanding isotropically at constant velocity. It is analytic and easy to use, but it needs laboratory data for the parents and daughters; in some cases the dominant parent is not even known. The vectorial model assumes a range of velocities for the daughter products and is therefore more realistic. The theory is not analytic, however, and it requires that the parent be identified and the dissociation kinetics be understood. Consequently, this theory has been applied successfully only to water. A full chemical model requires simultaneous solution of all the competing chemical reaction equations and therefore requires knowledge of all relevant rate constants, combined with reasonable hydrodynamic and thermodynamic assumptions. This approach has been taken only very rarely because of its uncertainty and complexity. The principal uncertainties lie in the incomplete laboratory data on many constants and in the starting boundary conditions.

A century of spectroscopic work from the Earth and, more recently, from space has given a rather thorough inventory of gas coma constituents. Areas requiring major laboratory work concern the dissociation processes of potential parents and observed radicals, and rates and products of reaction processes occurring among them. These studies must be made at extremely low pressures consistent with actual physical conditions

in the coma.

Dissociation and ionization processes in parent molecules and in dissociation fragments need to be investigated. Photodissociation is the primary process but electron impact phenomena might be important in some circumstances. There are two aspects of such measurements. One is the determination of cross-sections as a function of energy. The other is the determination of dissociation mechanisms or branching ratios when several dissociation channels are possible. For example, in the case of H_2O photodissociation, the relative yields of OH, H_2, and H_2O^+ as a function of wavelength are not known. The details of dissociation of the OH are also unknown. Similar measurements are needed for all known or suspected parent molecules. In addition to these species, investigations of carbon clusters C_2, C_3, C_4 and higher polymers, as well as organic clusters, need to be carried out. C_2 and C_3 are prominent cometary species, and the Giotto ion spectrometer has given evidence for a mixture of possible polymeric species.

Attempts to carry out detailed studies of chemical reactions in the coma are hindered by the limited data on reaction cross-sections, especially for the low pressures within the coma. These are needed for a variety of ion-molecule and radical-radical reactions at temperatures and pressures appropriate to the coma. For spectroscopic analyses as well as for reaction studies, quenching efficiencies should be measured for vibrationally excited species and for metastable electronic states.

III. IMPLEMENTATION/BUDGET

It is proposed that a program of laboratory measurements be supported by an augmentation to the Planetary Atmospheres Program. This opportunity should be open to the scientific community through a NASA Research Announcement (NRA) which contemplates competitive proposals for full peer review.

Research proposals should be invited for support of both laboratory equipment and personnel associated with new projects or enhancements of existing efforts at NASA Centers, Universities and in industry. (It is recognized that an essential level of manpower effort is needed for installation, development and utilization of hardware and for processing, reduction and dissemination of laboratory data.)

The NRA should specify typical areas of research to be funded. These will include, but not be limited to, laboratory studies in thermodynamics, spectroscopy, chemical kinetics, and irradiation effects related to an understanding of planetary atmospheres. Selections will be based upon scientific merit with due regard for balance among the areas of interest and targets of opportunity as determined by NASA's spacecraft missions. Allowance should be made for innovative proposals from the community which are consistent with NASA's goals, and compatible with its budget but not previously recognized by NASA as important areas.

It is expected that this augmentation will fund approximately fifteen efforts in laboratory research at the level of about $100-$150K each for three years. Thus, a program amounting to more than two million dollars per year for an initial period is envisioned, with a corresponding follow-on option.

Balance among the several areas of laboratory research outlined in this report is expected. It is hoped that the actual needs within the community of laboratory scientists, together with the judgments of their peer reviewers, will establish an optimal distribution of funds. As usual, NASA management will assist in effecting a scientifically appropriate and fiscally equitable allocation of resources.

At the outset, workshops and special meetings should be held to highlight requirements and progress relating to laboratory studies for planetary atmospheres. A national meeting involving many members of the Planetary Atmospheres community is planned for calendar 1989; this will serve as an introductory forum for the proposed augmentation. An international meeting is anticipated for calendar 1990; this would both highlight progress and set the stage for the follow-on option.

It is expected that laboratory data facilitated by this program will be made available to the scientific community of users through channels such as scientific journals and communications at professional meetings. In addition, the program will assist in making data available where special circumstances such as length, format, and immediacy require.

APPENDIX TWO: ATTENDEES

APPENDIX TWO: ATTENDEES

Joseph Alexander
National Aeronautics and Space Administration
Headquarters Code E
Washington, DC 20546

John Allen, Jr.
Code 691
National Aeronautics and Space Administration
Goddard Space Flight Center
Greenbelt, MD 20771

Mark Allen
Jet Propulsion Laboratory
MS 183-601
4800 Oak Grove Dr.
Pasadena, CA 91109

E. Arakawa
Oak Ridge National Laboratory
P.O. Box 2008
Oak Ridge, TN 37831-6123

Mohammed Babaki
Laser Chemistry Laboratory
Howard University
Washington, DC 20059

Samuel Barts
Chemistry Department
Howard University
Washington, DC 20059

Johnny Batts
5201 Gallagher Ct.
Baltimore, MD 21212

Jay Bergstralh
National Aeronautics and Space Administration
Headquarters Code EL
Washington, DC 20546

Gordon Bjoraker
National Aeronautics and Space Administration
Goddard Space Flight Center
Code 693.2
Greenbelt, MD 20771

William Blass
Department of Physics and Astronomy
The University of Tennessee
Knoxville, TN 37996-1200

John Boring
Department of Nuclear Engineering
University of Virginia
Charlottesville, VA 22901

John Caldwell
Space Astrophysics Laboratory
Institute for Space and Terrestrial Science
2700 West Steeles
Concord, Ontario L4K3C8
Canada

Michael Casassa
National Institute of Standards and Technology
Building 221 Rm B268
Gaithersburg, MD 20899

Charles Chackerian, Jr.
MS 245-4
National Aeronautics and Space Administration
Ames Research Center
Moffett Field, CA 94035

Regina Cody
Code 691
National Aeronautics and Space Administration
Goddard Space Flight Center
Greenbelt, MD 20771

Michael Duncan
Department of Chemistry
University of Georgia
Athens, GA 30602

Askar Fahr
Chemical Kinetics Division
National Institute of Standards and Technology
222/A260
Gaithersburg, MD 20899

PRECEDING PAGE BLANK NOT FILMED

ATTENDEES

Bruce Fegley, Jr.
Abteilung Kosmochemie
Max-Planck-Institut fur Chemie
(Otto-Hahn-Institut)
Saarstrasse 23
D-6500 Mainz
Federal Republic of Germany

Kenneth Fox
Department of Physics &
Astronomy
The University of Tennessee
Knoxville, TN 37996-1200

Gerald Fraser
Molecular Spectroscopy Division
National Institute of Standards
and Technology
B268 Physics Building
Gaithersburg, MD 20899

Joan Frye
Chemistry Department
Howard University
Washington, DC 20059

Lawrence Giver
MS 245-4
National Aeronautics and Space
Administration
Ames Research Center
Moffett Field, CA 94035

Frederic Glaser
Department of Physics &
Geology
Pan American College
Edinburg, TX 78539

Jacklyn Green
Institute for Astronomy
2680 Woodlawn Dr.
Honolulu, Hawaii 96822

Charles Guilford
Bowie State University
Bowie, MD 20715

David Gutman
Department of Chemistry
201 Maloney Hall
Catholic University of America
620 Michigan Ave., N.E.
Washington, DC 20064

Joshua Halpern
Chemistry Department
Howard University
Washington, DC 20059

Rangasayi Halthore
STX
National Aeronautics and Space
Administration
Goddard Space Flight Center
Code 691
Greenbelt, MD 20771

Jon Hougen
Molecular Spectroscopy Division
National Institute of Standards
and Technology
B268 Physics Building
Gaithersburg, MD 20899

L. Huber
Computer Sciences Corporation
Code 684.9
National Aeronautics and Space
Administration
Greenbelt, MD 20771

Don Jennings
National Aeronautics and Space
Administration
Code 693
Greenbelt, MD 20771

Rainer Johnsen
Department of Physics and
Astronomy
University of Pittsburg
Pittsburg, PA 15260

Robert Johnson
University of Virginia
Thornton Hall
Charlottesville, VA 22901

ATTENDEES

Russell Johnson III
Chemical Kinetics Division
National Institute of Standards
and Technology
Gaithersburg, MD 20899

Darrell Judge
Space Sciences Center
University of Southern
California
University Park
Los Angeles, CA 90089-1341

Bishun Khare
306 Space Sciences Building
Cornell University
Ithaca, NY 14853

Isabelle Kleiner
Molecular Spectroscopy Division
National Institute of Standards
and Technology
B268 Physics Building
Gaithersburg, MD 20899

Walter Lafferty
National Institute of Standards
and Technology
B268 Physics Building
Gaithersburg, MD 20899

Todd Lang
9338 Cherry Hill Rd. #202
College Park, MD 20740

Louis Lanzerotti
P.O. Box 326
New Vernon, NJ 07976

Stephen Leone
Joint Institute for Laboratory
Astrophysics
University of Colorado
Boulder, CO 80309-0440

Frank Lovas
Molecular Spectroscopy Division
National Institute of Standards
and Technology
Gaithersburg, MD 20899

Barry Lutz
Lowell Observatory
1400 West Mars Hill Rd.
Flagstaff, AZ 86001

James Lyons
Bowie State University
Bowie, MD 20715

Julius Mack
7030 Oregon Ave., N.W.
Washington, D.C. 20015

Paul Mahaffy
National Aeronautics and Space
Administration
Headquarters Code ELC
Washington, DC 20546

Christine Masterson
Department of Chemistry &
Biochemistry
University of Maryland
College Park, MD 20742

Dillard Menchan
National Aeronautics and Space
Administration
Goddard Space Flight Center
Code 120.0
Greenbelt, MD 20771

Michael Mickelson
Physics & Astronomy
Department
Denison University
Granville, OH 43023

Marla Moore
Code 691
National Aeronautics and Space
Administration
Goddard Space Flight Center
Greenbelt, MD 20771

Carol Moralejo
Code 691
National Aeronautics and Space
Administration
Goddard Space Flight Center
Greenbelt, MD 20771

ATTENDEES

Thomas Morgan
National Aeronautics and Space Administration
Headquarters Code ELC
Washington, DC 20546

David Nava
Astrochemistry Branch
Code 691
National Aeronautics and Space Administration
Goddard Space Flight Center
Greenbelt, MD 20771

Fred Nesbitt
Code 691
National Aeronautics and Space Administration
Goddard Space Flight Center
Greenbelt, MD 20771

James O'Brien
Department of Chemistry
University of Missouri-St. Louis
St. Louis, MO 63121-4499

Denise Parent
Chemistry Division
Code 6115
Naval Research Laboratory
Washington, DC 20375-5000

Walter Payne, Jr.
Code 691
National Aeronautics and Space Administration
Goddard Space Flight Center
Greenbelt, MD 20771

Herbert Pickett
Jet Propulsion Laboratory
183-601
4800 Oak Grove Dr
Pasadena, CA 91109

Diana Quillen
Bowie State University
P.O. Box 1034
Dunkirk, MD 20754

Jane Rice
Naval Research Laboratory
Code 6110
Washington, DC 20375

Paul Romani
Code 693.2
National Aeronautics and Space Administration
Goddard Space Flight Center
Greenbelt, MD 20771

Eckart Ruhl
Department of Chemistry and Biochemistry
University of Colorado
Box 215
Boulder, CO 80309-0215

Norbert Sack
Department of Nuclear Engineering and Engineering Physics
University of Virginia
Charlottesville, VA 22901

Thomas Spilker
Stanford Center for Radar Astronomy
STAR Laboratory, SEL
Durand Building, Rm 239
Stanford, CA 94305-3551

Paul Steffes
School of Electrical Engineering
Georgia Institute of Technology
Atlanta, GA 30332-3128

Jeffrey Steinfeld
Chemistry Department
Massachusetts Institute of Technology
Mail Code 2/221
Cambridge, MA 02139

Louis Stief
National Aeronautics and Space Administration
Goddard Space Flight Center
Code 691
Greenbelt, MD 20771

ATTENDEES

Carlos Suarez
Space Sciences Division
Code 245-4
National Aeronautics and Space Administration
Ames Research Center
Moffett Field, CA 94035

Richard Suenram
Molecular Spectroscopy Division
National Institute of Standards and Technology
B268 Physics Building
Gaithersburg, MD 20899

W. Reid Thompson
Cornell University
307 Space Science Building
Ithaca, NY 14853

John Townsend
Code 100.0
National Aeronautics and Space Administration
Goddard Space Flight Center
Greenbelt, MD 20771

Sandor Trajmar
Jet Propulsion Laboratory
4800 Oak Grove Dr.
Pasadena, CA 91109

Randall Urdahl
Department of Chemistry
University of California
Davis, CA 95616

Prasad Varanasi
Institute for Atmospheric Sciences
State University of New York
Stony Brook, NY 11794-2300

Richard Wagener
Space Astrophysics Laboratory
Institute for Space and Terrestrial Science
2700 West Steeles
Concord, Ontario L4K3C8
Canada

Alfons Weber
Molecular Spectroscopy Division
National Institute of Standards and Technology
Gaithersburg, MD 20899

John Wilford
New York Times/Science
229 West 43rd St.
New York, NY 10036

C. Y. Robert Wu
Space Sciences Center &
Department of Physics
University of Southern California
Los Angeles, CA 90089-1341

Padma Yanamandra-Fisher
Jet Propulsion Laboratory
Code 183-501
4800 Oak Grove Dr.
Pasaadena, CA 91109

Yuk Yung
Department of Geophysics & Planetary Science
California Institute of Technology
Pasadena, CA 91125

NASA National Aeronautics and Space Administration

Report Documentation Page

1. Report No.	2. Government Accession No.	3. Recipient's Catalog No.
NASA CP-3077		

4. Title and Subtitle

First International Conference on Laboratory Research for Planetary Atmospheres

5. Report Date

May 1990

6. Performing Organization Code

691

7. Author(s)

Kenneth Fox, John E. Allen, Jr., Louis J. Stief, Diana T. Quillen, Editors

8. Performing Organization Report No.

90B00106

10. Work Unit No.

9. Performing Organization Name and Address

Laboratory for Extraterrestrial Physics
NASA/Goddard Space Flight Center
Greenbelt, MD 20771

11. Contract or Grant No.

13. Type of Report and Period Covered

Conference Publication
October 25-27, 1989

12. Sponsoring Agency Name and Address

National Aeronautics and Space Administration
Washington, DC 20546

14. Sponsoring Agency Code

15. Supplementary Notes

K. Fox, University of Tennessee, Knoxville, Tennessee;
J. Allen, Goddard Space Flight Center, Greenbelt, Maryland;
L. Stief, Goddard Space Flight Center, Greenbelt, Maryland;
D. Quillen, Bowie State University, Bowie, Maryland.

16. Abstract

This Report contains the Proceedings of the First International Conference on Laboratory Research for Planetary Atmospheres held at Bowie State University in Bowie, Maryland during 25-27 October 1989. This Conference was organized by Kenneth Fox of The University of Tennessee (chairman), John Allen and Louis Stief of the NASA Goddard Space Flight Center, and Charles Guilford of Bowie State University. The covered areas of research included photon spectroscopy, chemical kinetics, thermodynamics, and charged particle interactions. This Report contains the 12 invited papers, 27 contributed poster papers, and 5 plenary review papers presented at the Conference. A list of attendees and a reprint of the Report of the Subgroup on Strategies for Planetary Atmospheres Exploration (SPASE) are provided in two Appendices.

17. Key Words (Suggested by Author(s))

Spectroscopy
Chemical Kinetics
Thermodynamics
Charged Particle Interactions
Comets
Planetary Atmospheres
Planetary Satellites
Photochemistry

18. Distribution Statement

Unclassified - unlimited

Subject Category 91

19. Security Classif. (of this report)	20. Security Classif. (of this page)	21. No. of pages	22. Price
Unclassified	Unclassified	500	A22